Luminescent Eu^{III} complexes based on phenanthro-imidazole ligands for white LEDs/OLEDs and temperature sensors: Combined experimental and theoretical investigations

Dissertation submitted to the

National Institute of Technology Rourkela

for the degree of

Doctor of Philosophy

in

Department of Chemistry

by

RAJAMOULI BODDULA

October, 2017

DEPARTMENT OF CHEMISTRY,
NATIONAL INSTITUTE OF TECHNOLOGY ROURKELA,
ROURKELA 769008,
ODISHA, INDIA.

Certificate of Examination

11 October, 2017

Roll Number: 512CY6007

Name: Rajamouli Boddula

Title of Dissertation: Luminescent Eu^{III} complexes based on phenanthro-imidazole ligands for white LEDs/OLEDs and temperature sensors: Combined experimental and theoretical investigations

We the below signed, after checking the dissertation mentioned above and the official record book (s) of the student, hereby state our approval of the dissertation submitted in partial fulfillment of the requirements of the degree of Doctor of Philosophy in Department of Chemistry at National Institute of Technology Rourkela. We are satisfied with the volume, quality, correctness, and originality of the work.

Dr. Vaidyanathan Sivakumar
Principal Supervisor

Prof. D. Bisoyi
Member (DSC)

Dr. U. Subuddhi
Member (DSC)

Dr. M. Jana
Member (DSC)

Dr. Raja Shunmugam
Examiner

Prof. S. Chatterjee
Chairman (DSC)

11 October, 2017

Dr. Vaidyanathan Sivakumar
Assistant Professor

Supervisor's Certificate

This is to certify that the work presented in this dissertation entitled Luminescent Eu^{III} complexes based on phenanthro-imidazole ligands for white LEDs/OLEDs and temperature sensors: Combined experimental and theoretical investigations" by "Rajamouli Boddula", Roll Number 512CY6007, is a record of original research carried out by him under my supervision and guidance in partial fulfillment of the requirements of the degree of *Doctor of Philosophy* in *Department of Chemistry*. Neither this dissertation nor any part of it has been submitted for any degree or diploma to any institute or university in India or abroad.

Dr. Vaidyanathan Sivakumar

Dedicated to

My Parents

&

Family

Declaration of Originality

I, **Rajamouli Boddula**, Roll Number 512CY6007 hereby declare that this dissertation entitled ‘‘Luminescent Eu^{III} complexes based on phenanthro-imidazole ligands for white LEDs/OLEDs and temperature sensors: Combined experimental and theoretical investigations" represents my original work carried out as a doctoral student of NIT Rourkela and, to the best of my knowledge, it contains no material previously published or written by another person, nor any material presented for the award of any other degree or diploma of NIT Rourkela or any other institution. Any contribution made to this research by others, with whom I have worked at NIT Rourkela or elsewhere, is explicitly acknowledged in the dissertation. Works of other authors cited in this dissertation have been duly acknowledged under the section "Bibliography". I have also submitted my original research records to the scrutiny committee for evaluation of my dissertation.

I am fully aware that in case of any non-compliance detected in future, the Senate of NIT Rourkela may withdraw the degree awarded to me on the basis of the present dissertation.

11, October 2017

NIT Rourkela *Rajamouli Boddula*

ACKNOWLEDGEMENTS

First, I would like to express my most genuine gratitude; it gives me a great pleasure and words are inadequate to express my deep sense of gratitude to my research supervisor, **Dr. Vaidyanathan Sivakumar** for initiating me in to the enlightening field of organo-metallic lantanide chemistry. I am deeply obliged to him for his inspiring and patient guidance, open discussions, steady support, boundless enthusiasm and friendly attitude. Thanks to his disciplinary supervision, inspiring instruction and generous help, I am able to successfully finish my work in time. The training he has given me has provided insights into the subject and instilled a sense of zeal for experimental research, which would be reflected in all my research endeavours. I am thankful to him for showing keen interest in my professional as well as personal life.

I would like to record my sincere thanks to **Prof. S. Chatterjee** (Head), **Prof. N. Panda** (Ex Head), **Prof. B. G. Mishra (**Ex Head), Department of Chemistry, National Institute of Technology Rourkela for their interest in my work, valuable suggestions and providing me the necessary facilities required to make this program a success.

I express my thanks to Board of Research in Nuclear Sciences (**BRNS**) is an advisory body of the Department of Atomic Energy (**DAE**) and **NIT** Rourkela for the research fellowship and financial support.

My sincere thanks are due to the doctoral committee (DSC) members **Prof.(Ms.) U. Subuddhi**, **Prof.(Ms.) M. Jana**, Department of Chemistry and **Prof. D. K. Bisoyi**, Department of Physics for their valuable suggestions which added value to my work.

I am thankful to **Dr. S. Giri** for initial support for the computational study. I am also grateful to **Dr. V. Subramanian**, CSIR-Central Leather Research Institute, for teaching and supporting the DFT calculations.

I sincerely thank **Prof. V. Krishnan,** IIT Mandi, Himachal Pradesh, India for constant encouragement, persanol discussions and single crystal study. I thank Mr. P. Sood, IIT Mandi for his help in solving the single crystal structure.

I am thankful **Prof. C. K. Jayasankar**, Sri Venkateswara University, Tirupati and **Dr. Deva Prasad Raju** from the same university allowing me to use the PL lifetime measurmetn facility. I woluld like to thank **Mr. C. S. D. Viswanath** for his help during PL lifetime measurement.

My sincere thanks **Dr. Ashish Gupta**, Research Engineer, Samtel Center for Display Technologies (SCDT), IIT Kanpur for his assistance to do photophysical study.

I woluld like to thank **Dr. M. Sarkar**, NISER Bhubaneswar for his kind opportunity to do temperature dependent emission photoluminescence study.

I thank my lab mates **K. Aravind Babu**, **S. Kasturi**, **T. Jairam**, **T. Marikumar** and **Rachna Devi** for their help in all aspects and constant source for joy. My special thanks to **Integrated M.Sc.** students for their help and support.

I would like to thank to all my NIT Rourkela friends for their enjoyable company. I also thank **Pratap Behera, Swagatika Tripathi, Arup Dey and Thirupataiah Boyini** for their help in spectroscopy measurments.

I express sincere thanks to **Mr. Aravind**, Technical Assistant, Department of Ceramic Engineering for DSC-TGA analysis and **Mr. Halder**, Technical Assistant, Department of Bio-Medical Engineering for his help to do FT-IR analysis (NIT Rourkela).

I would like to appreciate **Mr. Abhijeet Mohanty** and **Mr. S. Nayak** (Integrated M.Sc. students) for their contribution to complete my work as much as early.

My special thanks to **C. S. Mohanty**, **Babula Sethi**, **Nityananda Rout**, **R. Kar** due to their office work and help to proced the files as well as documents as early.

I place my deep sense of gratitude to my parents **Bhadraiah** and **Swarupa** for all their entiring efforts in providing me the highest quality of education, love and affection. I will be failing in my duties if I do not acknowledge my wife **A. Mounika** and my brother **B. Sadanandam.**

Rajamouli Boddula

ABSTRACT

The present theis works deals with molecular designing and synthesis of novel class bipolar or ancillary ligand for europium complexes and explore the possibility of using the same in white LEDs, temperature sensor and OLED applications

In **chapter 1,** a general overview of the development of new-generation optical lanthanide based complexes - introduction, literature survey of recent trends and brief objectives of the thesis was discus. In introduction, the basic concepts of the lanthanides, OLED device materials, LEDs applications and ratiometric thermal sensors were discussed. The main aim and importance of the proposed work of the thesis was summarized in this chapter.

In **chapter 2,** four europium complexes ($Eu(TTA)_3Phen$-Ph-Ph, $Eu(TTA)_3Phen$-mCF_3-Ph $Eu(TTA)_3Phen$-pCF_3-Ph and $Eu(TTA)_3Phen$-Fl-Ph) were designed and synthesized. The N1-functionalization of the phenanthro-imidazole ring by phenyl, substituted phenyl moiety (CF_3, electron withdrawing group), fluorene and their influence on photophysical and electrochemical properties of Eu^{III} complexes were determined by experimental and theoretical analyses. Among all the ligands, fluorene functionalized ligand shows white emission in the solid state. All the complexes (in solid and solution) showed the distinctive emission of Eu^{III} ion at 612 nm, due to electric dipole transition ($^5D_0 \rightarrow {}^7F_2$). The absence of ligand emissions (solution, thin film and solid) in the PL emission spectra of Eu^{III} complexes indicate that the efficient energy transfer from ligand to central metal ion (antenna effect), confirmed by DFT, TD-DFT. The HOMO-LUMO levels were determined by CV studies. Eu-complex was doped in PMMA matrix to fabricate the composite film devices ($Eu(TTA)_3Phen$-pCF_3-Ph shown highest quantum yield 78.7 %). The fluorene functionalized ligand integrated with InGaN LED chip (395 nm, forward bias 20 mA) show the potentiality of the ligand and shown white emission. The obtained efficient red emission from the fabricated LEDs (Eu^{III} complexes coated on InGaN-based near UV LED) shown that the currently synthesized complexes could be a potential red component for warm white LEDs.

In **chapter 3**, A new class of bipolar phenanthroimidazole based (N1 functionalization with Ph, mCF_3, pCF_3 and Fl) ligands and their efficient β-diketonate Eu^{III} complexes have been designed, synthesized, characterized successfully and their photophysical, electrochemical properties have also been investigated. All the ligands and complexes show similar UV-Visible absorption behaviour (π - π^*, at ~270, ~360 nm). Photoluminescence emission spectra of Eu-

complexes and its ligands were carried out in solution form as well as in solid and thin film. The PL study indicates that the Eu-complex emits tunable emission due to incomplete/partial energy transfer (white (solution), red (solid)); whereas fluorene decorated Eu-complex shows narrow band red emission with appropriate CIE color gamut. The obtained PL emission clearly indicates that the efficient energy transfer encountered in case of fluorene based complex. The energy transfer mechanism for all the Eu-complexes was proposed based on combined experimental and theoretical study (DFT, TD-DFT). The PL lifetime of the Eu^{III} complexes also supports the PL emission behaviour. The Judd–Ofelt spectral intensity parameters, electrochemical study and absolute QY (mCF_3 based Eu-complex shows better QY of 75.9 %) of the Eu-complexes were also been investigated. White and red LED was fabricated using these complexes with near UV InGaN based LEDs (395 nm).

In **chapter 4**, the efficient β-diketonate red emitting carbazole-based Eu^{III} complexes were synthesized and their photophysical, electrochemical properties were also been investigated. The PL study indicating that the efficient energy transfer from ligand to Eu^{III} metal ion (dominant pathway) with appropriate CIE color gamut and time-dependent density functional theory (TD-DFT) also confirms the identical. The Judd-Ofelt theory to the emissive properties of Eu^{III} complexes was investigated. The $Eu(TTA)_3$Phen-Fl-CBZ complex shown better lifetime was found to be 0.64 ms. The absolute PL quantum yield (QY) of the complexes in solid is found to be 77.3 % and it possesses high thermal decomposition temperature (235°C). The Judd-Ofelt intensity and related parameters were calculated for two complexes. The electrochemical analysis was shown narrow band gap energy (HOMO and LUMO). The PMMA film study of the complexes showed enhanced results than the solution. The fabricated Eu complexes with 395 nm emitted LED (InGaN) chips under 20 mA forward-bias current shown pure red emission and the corresponding CIE color coordinates are x = 0.66, y = 0.33. The obtained pure red emission is superior as compare to that of the solution and solid form of the complexes and the results are shown the presently investigated complexes find potential application in warm white LEDs.

In **chapter 5**, A new diphenylamine (DPA) and carbazole (CBZ) functionalized ancillary ligands coordinated β-diketonate Eu^{III} complexes shown incomplete or complete energy transfer from ligand to Eu^{III} ion. Solvatochromism study of DPA based complex leads to balancing the primary RGB colors to obtain single molecule white emission. The temperature dependent PL study indicates that the DPA based complex could be used as ratiometric temperature sensor

(color changes from blue to yellowish-red via white). In addition, the Eu-complex conjugated with near UV LED shown white emission with 0.34, 0.33 CIE coordinates. In the case of CBZ functionalized bipolar ligand and its corresponding β-diketonate Eu^{III} complex shown efficient energy transfers from the ligand to Eu^{III} center metal ion and emits narrow band red emission with apt CIE color gamut. TD-DFT calculations were performed to know the energies of the singlet (^1S) and triplet (^3T) levels for the bipolar ligand and shown good overlap between the ligand triplet level and Eu^{III} excited level. The PLQY is found to be 44.4 %, whereas the DPA based complex shown comparatively less QY (supports the inefficient energy transfer). HOMO and LUMO energy levels energies (redox reaction) were calculated from the electrochemical analysis for the Eu-complexes. The synthesized Eu^{III} complex was doped in PMMA with different percentage ratio and found to be concentration variation influence on emission intensity and symmetry. The CBZ-Eu-complex conjugated with near UV LED (395 nm) shown red emission with CIE color coordinates of 0.66, 0.33 and could find potential application in white LEDs.

In **chapter 6**, the effect of functionalization of carbazole with spacer in C1 position and fluorine in N1 position in the phenanthroline-imidazole based bipolar ligand has been designed, synthesised, same is utilized to synthesise $Eu(TTA)_3$Phen-Fl-O-CBZ complex and studied their photophysical properties. In addition, phenyl and fluorene functionalization in N1 position of phenanthro-imidazole ring (with alkoxy spacer) and its influence on photophysical properties of their binuclear Eu- complexes were systematically investigated. The mono and binuclear Eu-complexes emission spectra (pure red emission) clearly indicate that the complete energy transfer from ligand (L) to Eu^{III} ion occurs, since there is no emission from ligand was encountered (confirmed by DFT and TD-DFT calculations). It is found that the spacer molecule can decrease the energy gap of HOMO-LUMO energy levels (2.6 eV) with respect to that of without spacer one and increment in the singlet and triplet energy levels was also observed, consequences efficient energy transfer (L to M). The enhanced QY observed by 1% doping with PMMA as compare with other doping concentrations (14.2%). Binuclear Eu show dominant electric dipole transition of Eu^{III} ion ($^5D_0 \rightarrow {}^7F_2$, confirms the Eu^{III} ion in the non-centrosymmetric site). The highest QY (59.5 %, for thin film) obtained for the $Eu_2(TTA)_6$(L2). The binuclear Eu^{III} complexes were combined with InGaN near UV LED, obtained pure red emission with CIE color coordinate values x = 0.65, y = 0.34 and x = 0.66, y = 0.33 for $Eu_2(TTA)_6$(L1) and

$Eu_2(TTA)_6(L2)$, respectively. The obtained results indicate that the synthesized complexes are potential aspirant for light converting devices.

In **chapter 7**, a series of organic chromophores or ancillary ligands (based on phenanthroimidazole) conjugated with triphenylamine or carbazole moieties were designed with and without spacer and studied their excited state photophysical properties by density functional theory and time-dependent density functional theory. The UV absorption analysis shown maxima around λ_{max} 288, which is belongs to the π-π* transition of the ligands. The excited state photophysical properties reveal that the location of the triplet level found among three (1a-f, 2a-f, 3a-f) series 3a-f shown better energy matching with the excited state ($^5D_0$) of Eu^{III} ion and could facilitate the energy transfer from ligand to Eu ion very efficient. In addition, the substituted phenyl moiety (mCF_3 and pCF_3) at N1-position in the phenanthro-imidazole ligand give additional benefits by reducing the triplet energy comparatively with other substitution that leads to efficient energy transfer from L to Eu ion in the complex could be expected. In addition, HOMO and LUMO calculations given lead that some of the designed ligands can also serve as host materials for triplet dopant in OLEDs. The systematic theoretical study is certainly leads to synthesis of best ligand molecules for Eu complexes.

In **chapter 8**, the present works deals with molecular designing and synthesis of novel class bipolar or ancillary ligand for europium complexes and explore the possibility of using the same in white LEDs, temperature sensor and OLED applications. The observations and the conclusions derived from the present investigations are summarized in this chapter.

Keywords: Eu^{III} ion; Energy transfer; White/red emission; LEDs/OLEDs; Sensors; Quantum yield; DFT and TD-DFT

TABLE OF CONTENTS

Chapter 2

Effects of electron withdrawing groups in imidazole-phenanthroline ligands and their influence on photophysical properties of Eu^{III} complexes for white light emitting diodes

Chapter 3

Design and synthesis of new bipolar ligands based on phenanthroimidazole for tunable emissive Eu^{III} complexes: combined experimental and theoretical study

Chapter 4

Carbazole and fluorene functionalized phenanthro-imidazole ancillary ligand based Eu^{III} complexes for leds: detailed photophysical and theoretical study

Chapter 5

Controlled energy transfer from ligand to Eu^{III} ion: A unique strategy to obtain bright white/red light emission and their versatile applications

Chapter 6

Mono and binuclear luminescent Eu^{III} molecular complexes for white light emitting diodes: combined experimental and theoretical study

Chapter 7

Designing of ancillary ligands / organic chromophores and study their excited photophysical properties for Eu^{III} complexes – a theoretical approach

Chapter 8

LIST OF FIGURES

Chapter 2

Chapter 3

Chapter 4

Chapter 5

Chapter 6

Chapter 7

LIST OF TABLES

LIST OF SCHEMES

LIST OF ABBREVIATIONS

Symbol	Abbreviation
E	energy (eV)
Λ	wavelength (nm)
$\bar{\upsilon}$	wavenumber (cm^{-1})
N	frequency (s^{-1} or Hz)
H	Planck's constant
C	speed of light
ΔE	energy gap
δ	Chemical Shift (in ppm)
Φ	Quantum efficiency
Φ_{PL}	Photoluminescence quantum efficiency
FT-IR	Fourier Transform Infrared Spectroscopy
LC-MS	Liquid Chromatograpghy Mass Spectroscopy
CHNS	Carbon Hydrogen Nitrogen Sulphur
UV-Vis	Ultraviolet Visible
PL	Photoluminescence
EL	Electroluminescence
DRS	Diffuse reflectance spectroscopy
FL	Fluorescence
NR	Non-radiative path ways
^1S	Singlet state
^3T	Triplet state
F	Radiative excited state
f*	Excited state
Lm	Luminescence
ET	Energy transfer
BT	Energy back-transfer
IC	Internal conversion
DFT	Density Functional Theory
TD-DFT	Time Dependent Density Functional Theory

ISC	Inter system crossing
XRD	X-Ray Diffraction
PXRD	Powder X-ray diffraction
DSC	Differential Scanning Calorimetry
TGA	Thermogravimetric analysis
^{1}H NMR	Proton Nuclear Magnetic Resonance
^{19}F NMR	Fluorine Nuclear Magnetic Resonance
DEPT	Distortionless Enhancement by Polarization Transfer
D_2O	Deuterium Oxide
TMS	Tetramethylsilane
THF	Tetrahydrofuron
DMSO	Dimethyl sulfoxide
DMF	Dimethylformamide
DCM	Dichloromethane
$CHCl_3$	Chloroform
MeOH	Methanol
ACN	acetonitrile
DMSO-d_6	Deuterated Dimethylsulfoxide
$CHCl_3$-d_6	Deuterated Chloroform
Phen	1, 10- Phenanthroline
CBZ	Carbazole
TPA	Triphenylamine
DPA	Diphenylamine
t-but	Tertiary butyl
OLED	Organic light emitting diode
EQE	External Quantum Efficiency
IQE	Internal Quantum Efficiency
ETL	Electron Transport Layer
HTL	Hole Transport Layer
HBL	Hole Blocking Layer
CBP	4,4'-N,N'-dicarbazolebiphenyl, mCP = 1, 3-N,N'-dicarbazolephenyl

NPB	N,N’-diphenyl-N,N’-bis(1-naphthyl)-1,10- diphenyl-4,4’-diamine
PEDOT:PSS	poly(3,4-ethylene dioxythiophene) poly(styrene sulfonate)
ITO	Indium-tin oxide
BCP	Bathocuproine
Alq_3	Tris-(8-hydroxyquinoline)aluminum
TPBi	2,2′,2"-(1,3,5-Benzinetriyl)-tris(1-phenyl-1-*H* benzimidazole)
PBD	2-(4-biphenyl-yl)-5-(4-tert-butylohenyl)-1,3,4-oxadiazole)
PMPS	Poly(methyl phenylsilane)
PVK	Poly(N-vinylcarbazole)
CNPPP	poly [2-(6’-cyano-6’-methyl-heptyloxy)-1,4 phenylene
TPD	N.N'-diphenyl-N,N'-bis(3-methyl phenyl)-(1,1'-biphenyl)-4,4'diamine
NTSC	National Television System Committee
TLC	Thin-Layer Chromatography
Fl	Fluorene
nBu_4NClO_4	tetrabutylammonium perchlorate
TTA	4,4,4-Trifluoro-1-(2-thienyl)-1,3-butanedione
MHz	Megahertz
CV	Cyclic voltammetry
HOMO	Higher Occupied Molecular Orbitals
LUMO	Lower Occupied Molecular Orbitals
CIE	Commission International de Eclairage

LIST OF PHYSICAL CONSTANTS

Name	Algorithms
Planck's constant (h)	6.626×10^{-27} erg (4.135667516 x 10^{-15} eV*s)
speed of light (C)	299792458 m/s
Π	3.14
Charge of electron (e)	4.80×10^{-10} esu
Energy (E)	hc / λ

Chapter 1

General Introduction

Chapter 1

General Introduction

1. Introduction

Luminescence is the phenomenon in which emission of light occurs when the de-excitation of electrons from the excited state to ground state happens i.e. when an electromagnetic radiation is applied to solid or gaseous materials to excite the molecules and the substance emits photons in the visible region (certain cases infra-red). There are numerous types of luminescence available and they are categorized based on their excitation source (Table 1) [1]. For example, if the biochemical energy is the excitation source then the observed luminescence is called bioluminescence. The source of excitation is used in the suffix for the different type of luminescence.

Table 1.1 Types of luminescence and examples.

S.No.	Type of luminescence	Excitation source	Example
1.	Bioluminescence	Bio-chemical energy	firefly, Photinuspyralis
2.	Cathodoluminescence	Cathode rays (high energy electrons)	Microscope
3.	Chemiluminescence	Chemical reaction energy	luminol + hydrogen peroxide → 3 aminophthalate+ light
4.	Electroluminescence	Applied voltage	OLEDs
5.	Photoluminescence	Photons (UV, Visible)	
6.	Radioluminescence	X-rays, γ rays, etc.	Radium salt
7.	Sonoluminescence	Sound waves	Bubbles in liquid
8.	Thermoluminescence	Thermal stimulation of emission, which is excited by some other means.	Sediment grains
9.	Triboluminescence	Mechanical energy such as grinding, stress, etc.	Diamond

1.1 Fluorescence and Phosphorescence:

Luminescence can be divided into two types of emission i.e fluorescence and phosphorescence based on their excited state lifetime. Fluorescence is the radiative decay of an electron from an excited state to the ground state with same spin multiplicity. It is spin-allowed transition and the lifetime is about 10^{-9} sec. Phosphorescence is also the radiative decay from an excited state (triplet) to the ground state with different spin multiplicity and in general, it is spin-forbidden transition, the lifetime is 10^{-3} to few seconds. Jablonsky diagram was used to explain the process of electronic transitions or the mechanism of photophysical process in the molecules; Jablonsky diagram with lifetime image Figure 1.1. The numerous processes those are available to get the radiative light emission from different sources. Among all the process the fluorescence and phosphorescence are major phenomena, which are majorly depends on the time scale [2-4].

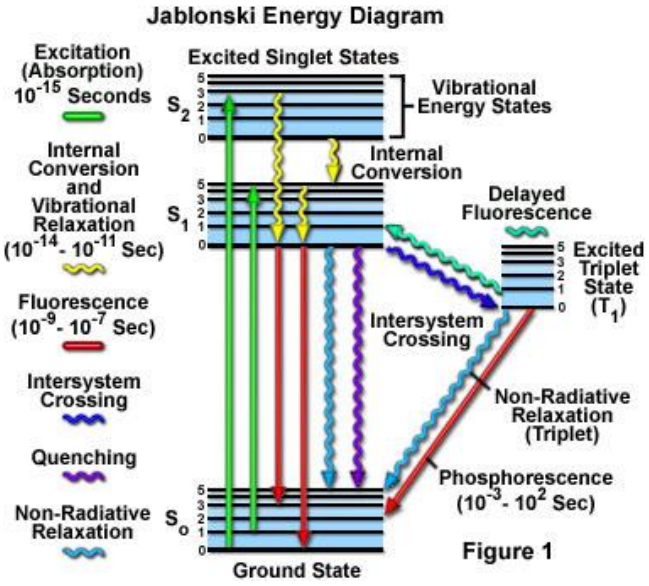

Figure 1.1 Electronic transitions of photophysical process in the molecules (Jablonsky diagram with lifetime).

1.2 Lanthanide luminescence:

In the periodic table, the lanthanide series have fascinating and specific or characteristic light emitting features. Because, the emission spectra of transition-metal complexes and organic dyes are asymmetric and wide-ranging with a huge full width at half maximum (FWHM) is more than 3000 cm^{-1}, due to d-orbitals evolution [6, 7]. But in the case of lanthanides (Ln's), it consists of 4f - 4f electronic transition (Ln contraction), which leads to efficient monochromatic characteristic emission (luminescence), no ligand field interactions are involved in the 4f orbitals of Ln's and hence the emission and excitation lines are very sharp. In Ln series, among 15 elements including lanthanum (La, G. S. $^1S_0$), consists of different valence states (common +3), +2 is the lowest and +4 is the highest valency [8]. The formation compound encountered by reacts Ln with another element; it usually loses three of its outer electrons. It leads tri-positive ions and occasionally develops less stable +2 or +4 ions also [9, 10].

1.3 Classic Dieke Diagram for Lanthanide ions:

The classic Dieke diagram of lanthanide ions is shown in Figure 1.2 [11]. All the lanthanides have multiple energy levels and the emissive excited state is highlighted (thick black color). For example in the case of Eu^{3+} the emissive excited state is $^5D_0$ level. In the diagram one can observe that the many lanthanides emit in the visible spectral windows (example, Dy^{3+} emits in the yellow region, Eu^{3+} emits in the red, Sm^{3+} emits in the orange red etc.,). In addition, other lanthanides such as Ho^{3+}, Er^{3+}, Tm^{3+} and Yb^{3+} are known to emit in the infra red region (applicable to optical communication etc.,). More specifically, lanthanides can have described by two ways, which are fluorescent – praseodymium (Pr, GS. $^3H_4$), neodymium (Nd, GS. $^4I_{9/2}$), holmium (Ho, GS. $^5I_8$), erbium (Er, $^4I_{15/2}$), ytterbium (Yb, NIR region, G. S. $^2F_{7/2}$) and phosphorescence - orange samarium (Sm^{III}, GS. $^6H_{5/2}$), red europium (Eu^{III}, G. S. $^7F_0$), ultraviolet gadolinium (Gd^{III}, GS. $^8S_{7/2}$), green terbium (Tb^{III}, GS. $^7F_6$), yellow dysprosium (Dy^{III}, $^6H_{15/2}$),

blue thulium (Tm^{III}, GS. $^3H_6$) [12-14]. Figure 1.3 indicating the energy levels of the furthermost operational selected Ln metal ions (Ln - Tm, Tb, Dy, Sm and Eu) according to their emission color.

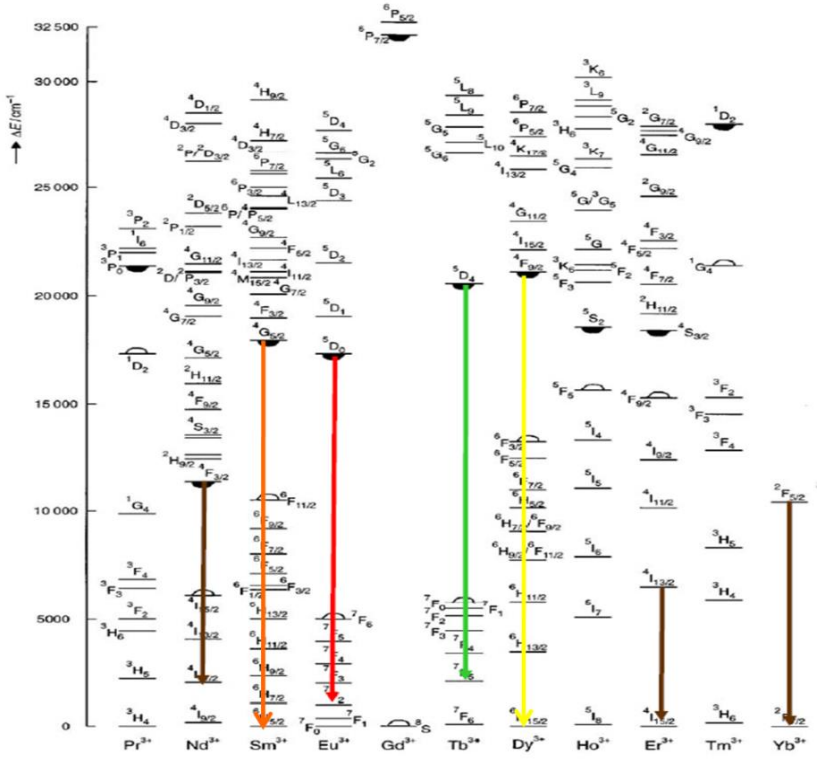

Figure 1.2 Classic Dieke diagram for rare earth ions.

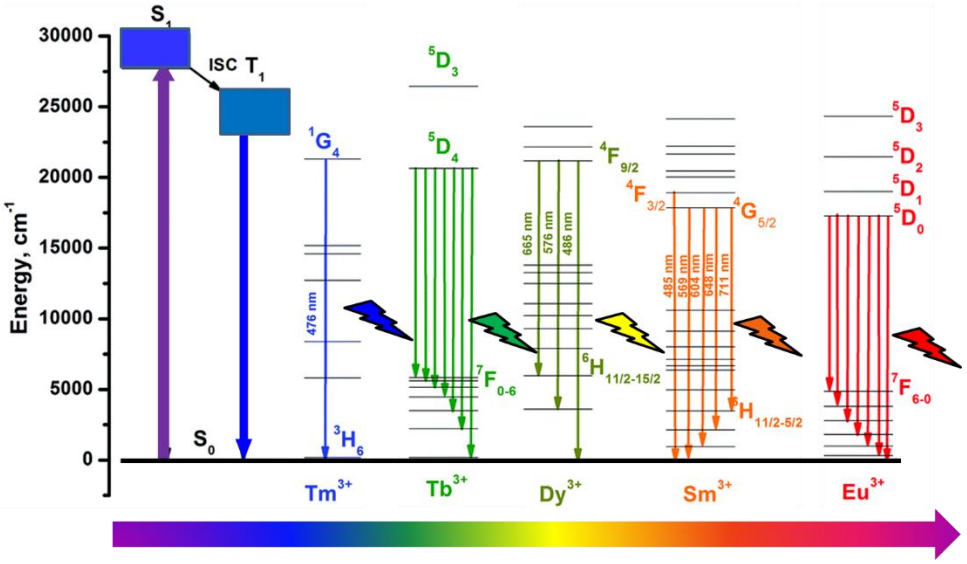

Figure 1.3 The energy levels of the most functioning selected Ln (Ln - Tm, Tb, Dy, Sm and Eu) metal ions according to their emission color.

Ln based complexes are attractive due to their own merits such as unique optical properties (4f-4f and 4f-5d electronic transitions), high quantum yield, long luminescent lifetime (ranging from μs – ms), low long-term toxicity, and structural versatility [15-18]. There are numerous reports documented on luminescent Ln complexes for different applications, such as tunable lasers, plastic optical fiber amplifiers (POFA), multi-color displays, solar energy convertors [19, 20] cathode ray tubes [21] air craft and space shuttles, fluoro-immune assay, biomedical analyses, optical sensor cells [22] sensing reagents of chiral biological substrates and photonic crystals, tissue imaging, medical diagnosis and protein labelling [23-27].

Eu^{III} based complexes are extensively growing attention for medical diagnostics [28, 29], biomarkers [30], electroluminescent materials [31], white LED (environment friendly) [32], materials owing to their simple energy levels of Eu^{III} as well as efficient line like or narrow band red emission. Eu^{III} and Tb^{III} based complexes exhibit numerous appropriate characteristics when associated with that of conventional organic fluorophores; which makes them prominent candidate for the biomedical imaging applications such as long excited state lifetimes (usually in the milliseconds range), large energy shift between absorbed and emitted radiations (in the case of ligand sensitization) and very narrow emission bands. These two effects allow the separation of Ln^{III} luminescence and the short-lived background fluorescence.

1.4 Energy transfer Process:

1.4.1 Photoluminescence Process

When the light energy falls on the material, electrons are excited from ground state to higher energy states of singlet state and it leads to population of ligands singlet state (Figure 1.4). The singlet state electron subsequently decays through intersystem crossing (ISC) to a triplet state. The ISC is a radiationless transition between dissimilar spin states. From triplet state, it leads to the population of emissive *f* excited states via Forster-type dipole-dipole exchange or Dexter mechanism (Figure 1.5) [33].

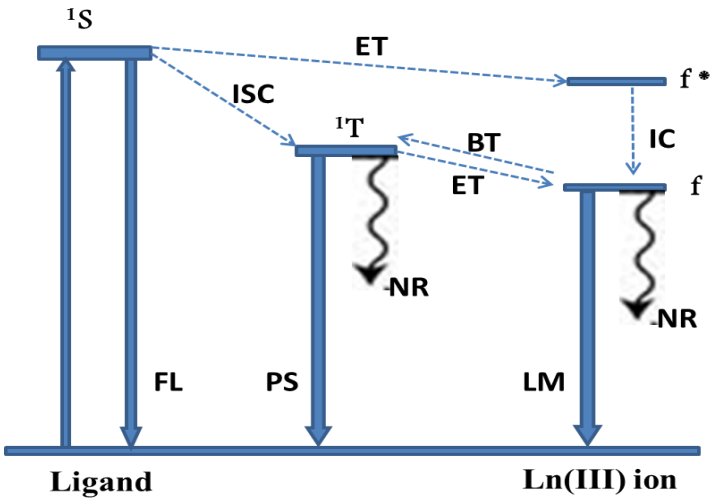

Figure 1.4. Simplified mechanism for emission process ^{1}S = Singlet state, ^{3}T = Triplet state, f = Radiative excited state, f* = Excited state, FL = Fluorescence, PL= Phosphorescence, Lm= Luminescence, NR= Non-radiative path ways, ISC= Inter system crossing, ET = Energy transfer, BT = Energy back-transfer, IC = Internal conversion.

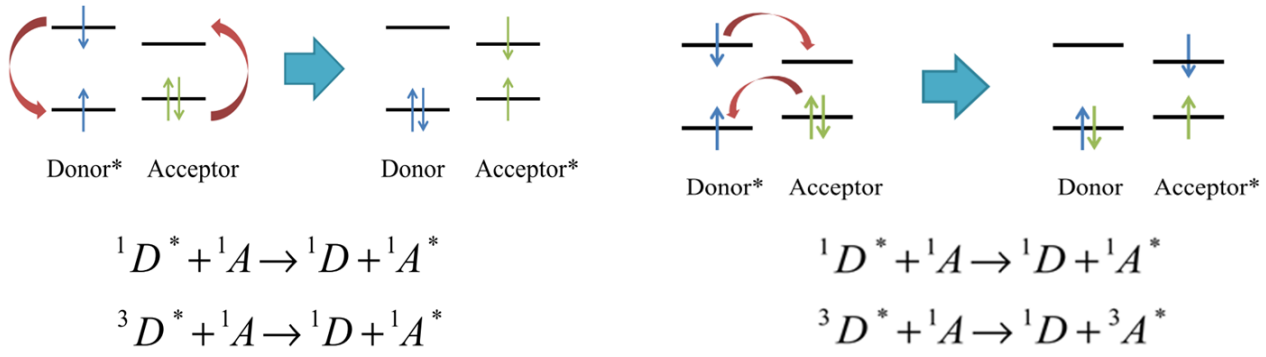

Figure 1.5. Energy transfer mechanism of Donor-Acceptor (Host – Guest).

Finally, the energy comes to ground state with appropriate emission. In the forster-type dipole-dipole exchange mechanism, the columbic interaction is that which arises when the dipole of the excited antenna induces a dipole in the acceptor (Ln). In case of Dexter, an exchange interaction requires a mutual electronic exchange between the antenna and the metal-centre acceptor. In Dexter type mechanism, the energy transfer occurs through the overlapping orbitals of the antenna and the metal ion.

1.5 Why Europium Complex:

It is well documented that the Eu^{III} based complexes are used as ratiometric optical sensors by monitoring two major emission bands, most commonly the magnetic dipole (MD) transition $^5D_0 \rightarrow {}^7F_1$ ($\Delta J = 1$) and electric dipole (ED) transition $^5D_0 \rightarrow {}^7F_2$ ($\Delta J = 2$) bands [34-41]. The MD induced $\Delta J = 1$ transition is relatively insensitive to changes in coordination, whereas the $\Delta J = 2$ and $\Delta J = 4$ transitions are hypersensitive and generally change substantially upon formation of a new complex. Due to their parity forbidden intra-configurational 4f–4f transitions, the Eu^{III} ions feature very low absorption coefficients or oscillator strength and hence their direct photoexcitation is inefficient. It is very much necessary to have sensitizer (organic chromophoric ligands), which can indirectly populate the higher excited level via energy transfer to boost the emission intensity of Eu^{III} ion [42]. The energy transfer or sensitization process usually involves a triplet excited state of a ligand thus requiring efficient intersystem conversion (ISC) in the ligand (facilitated by the heavy metal ion effect) as well as an appropriate alignment of the triplet state energy (T) over that of the accepting lanthanide state(s) (quantum efficiency 100%, theoretically possible) [43].

In addition, ligand to metal (L-to-M) energy transfers embrace the L-to-M charge transfer (LMCT) are analyzed by recent theoretical computations (combined Density Functional Theory (DFT) and Time-dependent density functional theory (TD-DFT) analysis). It is arising because of radiative and nonradiative competitive transitions. The intramolecular energy transfer process by Weissman, [44] Dexter, [45] Crosby *et al.*, [46] were already described in three major ways for typical binary arrangements involving anionic ligands and lanthanide ions. First mechanism is ^1S to higher energy or $^5D_0$ levels through internal conversion (IC), second mechanism is energy transfer to Eu^{III} from triplet (^3T) by ^1S through ISC and third mechanism is direct energy transfer from singlet via mixing of ^1S and ^3T to higher excited Eu^{III} levels. In the case of Eu^{3+}, an optimal energy

gap (ΔE) should be in the range of ~2500–3000 cm^{-1}. Improper alignment of triplet energy to the Eu excited levels (lower ΔE values) would enable back energy transfer and thus reduce sensitization efficiency or possibility of obtaining multiple emissions from ligand as well as metal centre. The exact supportive results were investigated by Latva *et al.,* [43] It is well identified that the Eu^{III} metal ion excited $^5D_0$ energy level located at 17250 cm^{-1} [47]. In addition to that singlet state should be located higher than >24,750 cm^{-1} and triplet state located higher than >19,750 cm^{-1} leads to highly efficient emission and irreversible energy transfer. It is also supported by Reinhoudt's empirical rule, [48]. Energy transfer process from ligand to center Eu^{III} metal ion through ISC process is shown in Figure 1.6.

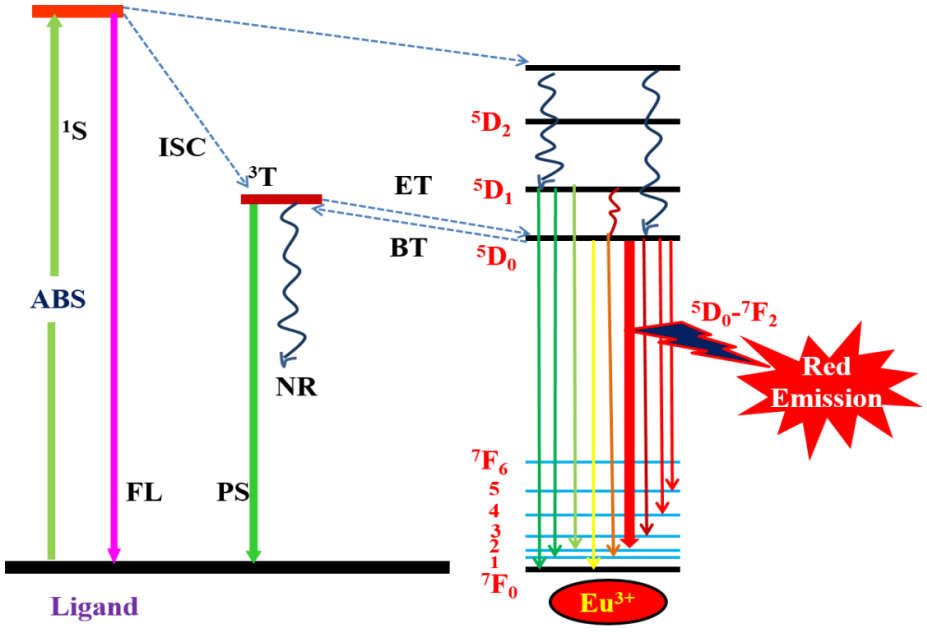

Figure 1.6. Energy transfer process from ligand to center Eu^{III} metal ion through ISC process. ^1S = Singlet state, ^3T = Triplet state, $^5D_{R\ (0,\ 1,\ 2...)}$ = Excited state, FL = Fluorescence, PL= Phosphorescence, NR= Non-radiative path ways, ISC= Inter system crossing, ET = Energy transfer, BT = Energy back-transfer.

Europium complexes are extremely important in organic light emitting diodes and white LEDs as well as ratiometric temperature sensor. The ligand triplet energy levels are responsible for the multiple emissions through incomplete/complete energy transfer process. Solid state lighting (SSL), down converting phosphors or organic fluorophores is essential component and play vital role in converting the LED emission in to white emission [49-51]. Various approaches have been developed for fabricating white LEDs with the aim of producing white emission optimal for the human eye. Current white LED technology relies on either the blue LED combining yellow emitting phosphor or near UV LED with tricolor red, green, blue (RGB) phosphor. The white light attained from the near UV LED conjugated with tricolor phosphor is highly dependent on the color/wavelength convertors, as human eyes are not sensitive to near UV. This method overcomes certain technological figure of merit of the blue LED + yellow phosphor based white LEDs (color rendering index and halo effect). Although there are several organic fluorophores that are capable of emitting individual red-blue-green (RGB) color;

however, white light generated by single molecule (single-component approach) have several advantages than that of simple RGB mixing (multi-component emitters) [52]. The benefit includes improved stability; stable commission International de I'Eclairage (CIE) color coordinates as well as simple fabrication process. White light creation by aggregated induced emission in single organic molecule has also been reported. Iridium-based molecular complex emits white light (all the way from 440 to 800 nm in the spectral window) [53]. By utilizing the sensitizing/energy harvesting capability of Ir^{III} ion to lanthanides, the Ir-Eu dyad was used to release the white light (bluish-green emission from Ir^{III} and red emission from Eu^{III} ion) [53b, c]. Although, generating white emission from the single molecular complex is still a bottleneck.

1.6 Eu-complexes for OLEDs:

Organic light emitting diode device is simple, where the emissive organic molecule sandwich between two electrodes. When the device is forward bias, the electrons injected from cathode (low work function) into LUMO electronic state and holes injected from anode into neighboring HOMO recombine in the middle of the device (emissive layer) leads to form excitons. Finally, it produces light, so called electroluminescence (Figure 1.7), [54, 55]. From the reported articles, mobility of the holes is more in the order as compared to electron mobility [56]. In this case if there is no charge balance, the recombination moves towards anode or cathode with respective voltages, resulting in decrease of the luminescence from emissive layer, unwanted emission by charge combination in the Alq_3 layer [57, 58]. Aziz *et al*., confirmed that the injection of holes into ETL (Alq_3) is the main factor responsible for deficiency of device [59]. Koji Itano *et al*., also observed exciplex formation at the interface of Alq_3 and lower transport potentials of HT materials [60]. For the increasing recombination through charge balance in emissive layer, introduce hole blocking layers (HBL) [61] or electron blocking layers (EBL) [62]. In certain devices HBL acts as both electron transporting (ETL) and hole blocking properties [63]. The position of the branched groups arrangement [64, 65] nature of electron withdrawing groups, sublimation, distance between the ligand and central metal ion (Eu^{III}) within the complex, recrystallization tendencies, phase separation, energy levels of the host and guest molecules (highest occupied molecular orbital (HOMO), lowest unoccupied molecular orbital (LUMO) levels), concentration of organic materials and their size of the layers, addition of layers (thin film) methods, character and nature of Eu^{+3} metal ion complexes (rigidity nature) and resistant oxidation are influencing the carrier charge transportation results manipulating on efficiency [66-71].

To explore the optical and EL properties one need to confirm the study in thin films. To achieve smooth and uniform amorphous thin films, this can be generated by vacuum deposition or spin coated (ink-jet, dry rolling and screen printing), [72-74] amorphous materials are superior. The thickness of the ITO layer and reactive index are responsible for the external coupling efficiency. For the efficient carrier injection, hole and electron layer with a low HOMO or high LUMO level are suitable [75]. The absorption energy of the guest is less than that of emission energy of host material, leading to increase in the emission efficiency of the guest. Most of the devices are made by vacuum thermal evaporation and it is satisfactory by excellent ambipolar CBP host matrix and TPD, NPB are hole-transporting moieties. Alq_3 is good electron-transporting moiety. PVK and PFO are spin coated host mediums (including PBD), PEDOT:PSS

(hole-injecting) and PVK (hole-transporting layer) are hole related moieties. BCP act as bifunctional emission layer in the device. As the formation of excitons in the device is 25 % singlet and 75% triplet (by theoretical prediction) and harvesting the triplet excitons to the ground state is attractive research task. It is necessary to have heavy metal ion as the triplet emission to the ground state is restricted, according to spin selection rule. Ln containing molecular complexes are able to give 100% internal QE (IQE) by harvesting the unwanted excited triplet excitons to the ground state and the same is shown Figure 1.7, right. The IQE can be calculated by the following equation. The QY (Φ) is the ratio of emitted to absorbed photons and reflects the efficiency of the emission process, [76].

Electroluminescence $(\eta_{el}) = \eta_{int} X \eta_{ex}$. The IQE ($\eta_{int}$) of an electroluminescent device is the ratio of formed photons to injected charges which combine to form excitons. Internal QE $(\eta_{in}) = x \Phi_{fl} \eta_{r}$. Here, η_r = fraction of injected charge carriers that form excitons, x = fraction of charge carrier recombination that form singlet excitons, Φ_{fl} = photoluminescence efficiency of dye and $\eta_{ex=}$ external quantum efficiency.

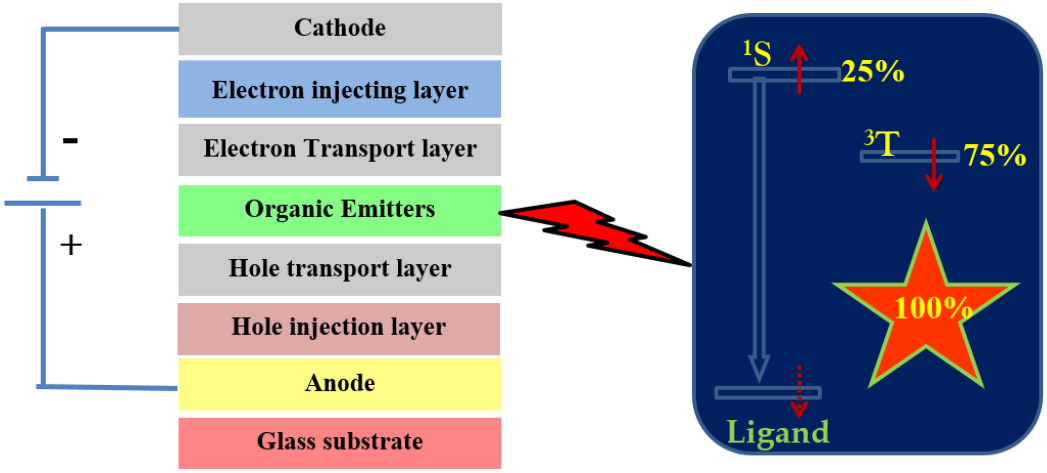

Figure 1.7 Electroluminescence emission from the OLED device (left) and the utilization of ^{1}S and ^{3}T for 100% IQE (right).

1.6.1 TTA and Phen based Eu-complexes for OLEDs:

The two or three (frequently) β-diketone bidentate anionic ligands occupies the coordination site of the Eu^{III} ion and addition to that one or two neutral ligands (bi, tri or tetra) occupies to full fill the coordination sphere of the complex (coordination number ranging from 8 to 10). The first binary Eu^{III} complex was made $Eu(TTA)_3$ and after that $Eu(DBM)_3$ was reported. Based on the popular anionic antenna's, we styled in different ways to undertand better way the Eu luminescence and their use in OLEDs. The β-diketone bidentate ligands were separated according to TTA and DBM including the TPPO core resources. Figure 1.8 presents the TTA based antennas for OLED applications.

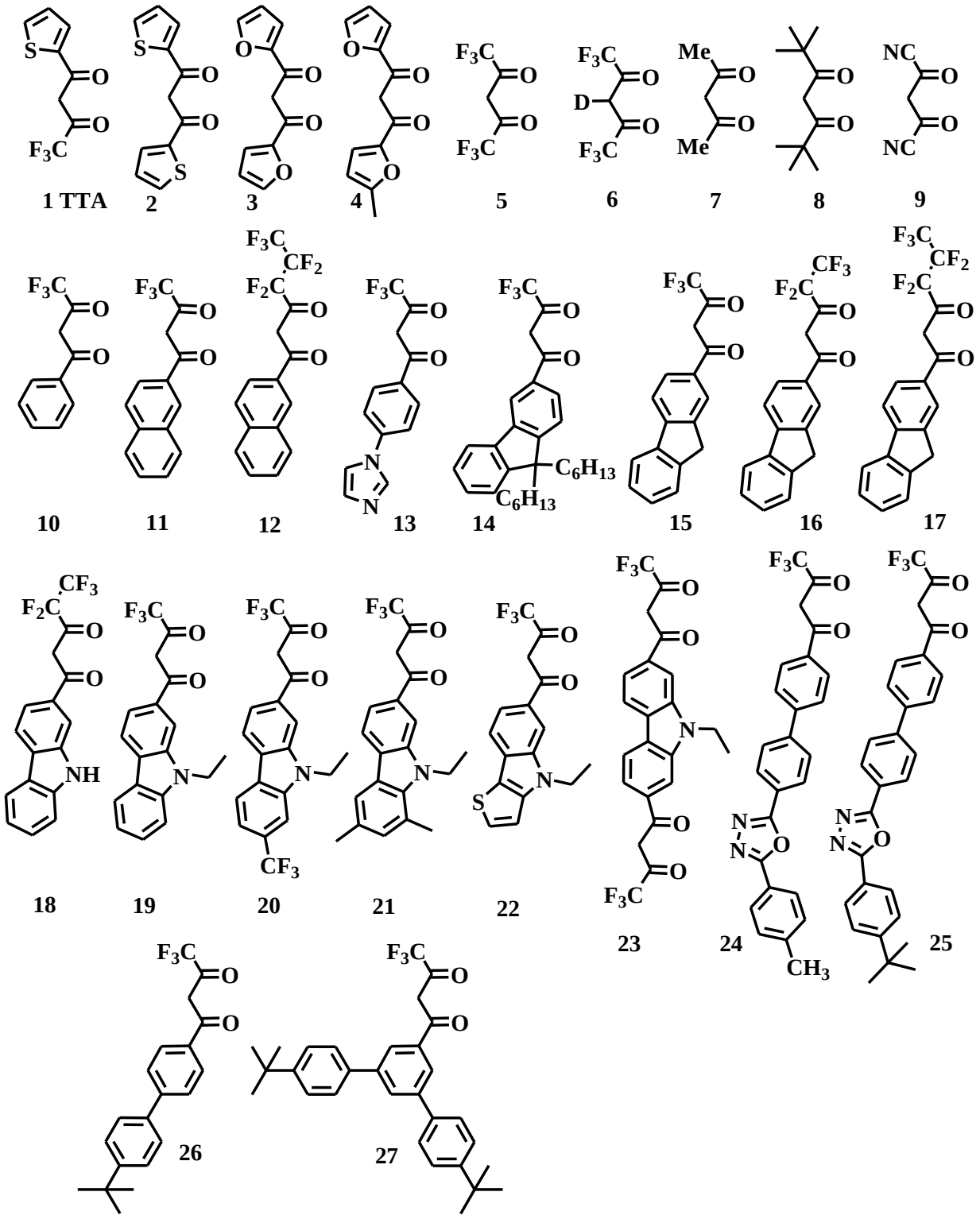

Figure 1.8. The β-diketonate (TTA based) anionic antenna's for Eu^{III} complexes.

1.6.2 TTA as anionic ligand:

J. Kido *et al.*, and Y. Okamoto were introduced Eu^{III} metal ion with TTA based EL device. Eu complex **AA** have non-volatile nature. So the PMPS and Eu are spin coated and PBD was made by vacuum deposition. The device configuration is glass substrate / ITO / PMPS doped with (20 wt %) **AA** (600 A^o) / PBD (600 A^o) / Mg (100 A^o) /Ag (1500 A^o) and observed red emission with turn-on voltage (TOV) 12 V, maximum intensity of 0.3 cd / m^2 at 18 V, [77, 78]. After their invention, the same complex with connected Phen was taken in different device structures and made improvement towards high efficiency. Takada *et al.*, designed a micro cavity structure with using SiO_2 / TiO_2 bilayers. Device fabrication is SiO_2 / TiO_2 bilayers / ITO / TPD / **AB** / Alq_3 / Mg : Ag. A planer microcavity is constituted by dielectric reflector and the Mg Ag metal electrode, when operated under DC drive voltage, observed sharply directed emission from the europium complex [79].

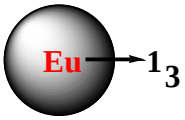

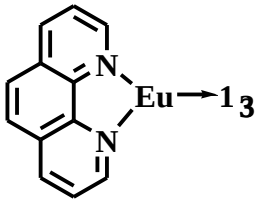

AA: $Eu(TTA)_3$ **AB: $Eu(TTA)_3Phen$**

Sano and co-workers, [80] are studied same Eu-complex to improve the electroluminescence using co-deposition method for complex doped in host material (1AZM-Hex) in emission layer. From the device with only HTL or ETL, no emission observed because of poor transporting property in the solid state but in the case of both layer device shows maximum luminescence 7 Cd m^{-2} (16 V, 125 mA cm^{-2}). Introduction of host material in the device with only HTL in different wt% of Eu-complex, 5 wt% shows red emission and it is better than both layer device. The device structure is ITO / TPD / 1AZM-Hex : **AB** / Mg In (10:1, 2000 A^0) and a maximum luminance of 137 cd / m^2 at 200 mA cm^{-2}.

Sano *et al.*, [81] also studied the EL properties of the **AB**. The synthesized **AB** is an emitting layer with red emission in the El organic light emitting diodes. Organic layer is vacuum deposited and the device structure is glass substrate/ ITO / TPD / **AB** /Mg:In. Eu complex PL wavelength is 614 nm. The device PL originates transition between energy levels of the Eu^{III} ion and not shows emission effectively, because of lower EL efficiency. Observed luminescence is very poor at 100 cd m-^{2}.

Adachi and co-workers, [82] reported based on energy transfer process in the device. The host material (CBP) was doped with Eu-complex **(AB)** in different concentrations. Device structure is ITO / TPD (50 nm) / CBP : **AB** (1%) (20 nm) / BCP (10 nm) / Alq_3 (30 nm) / Mg : Ag (10:1, 100 nm) achieve a maximum external EL quantum efficiency (η) of 1.4% at a current density of 0.4 mA / cm^2 and maximum luminescence 505 cd / m^2 at 12 V and 100 mA cm^{-2}. A significant decrease of QE was observed with increasing current along with increase in CBP host emission due to triplet-triplet annihilation on CBP molecules following back transfer from TTA, because of near resonance of TTA and CBP triplet state. From this, conclusion was made that the direct trapping of electrons and holes and subsequent formation of the excitons occurs on the dopant, leading to high QE at low current densities. It was further, analyzed by Y. Ohmoria *et.*

al., [83] by fabricating single layer based ITO / **AB** : PVK / Mg : In device. The emission peak perceived from Eu compound and PVK at 610 nm and 420 nm, respectively. Ratio of emission peak intensity is decreased with an increasing of Eu concentration and at >0.01 mol% of concentration red emission was observed. From energy band diagram, formed excitons are transferred successfully to Eu-complex from PVK host.

1.6.3 TTA modification

In 1998, Keizou okada *et.al*., [84] a novel complex-**AC** was introduced as a emitting layer between HTL and cathode (sandwiched type) in organic EL device and the device structure is Glass substrate/ ITO (sheet resistance 10 Ω/square / TPD (600 A^o) / **AC** (600 A^o) / Al : Li (99 : 1) (2000 A^o). Bright red emission with maximum luminescence 34.3 cd / m^2 at 12 V and current density 25.7 mA / cm^2 and the organic layer was vaccum deposited. The identical PL spectra and EL spectra suggested no interaction between TPD layer and Eu complex and recombination at Eu-complex layer. In the same year Okada *et.al.,* [85] substituted methyl group in complex-**AC** **(**$Eu(MDFP)_3(phen)$, **AD**) (MDFP=5-methyl-l,3-di-(2-furyl)-l,3-propanedione, phen= 1,10-phenanthroline). Device structure is glass substrate / ITO / TPD (600A^o) / **AD** (600 A^o) / Al: Li (99:1) (2000 A^o), and showed max. luminescence 32.0 cd m^{-2} at 9 V and 25.7 mA cm^{-2}.

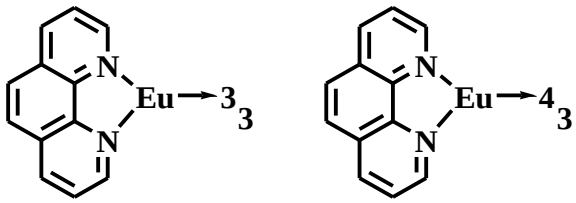

AC: $Eu(DFP)_3(Phen)$ AD: $Eu(MDFP)_3(Phen)$

Zhang *et al.*, [86] introduced Eu-complex layer with PVK and PBD (30 wt %) blend in the device in different doping concentrations (0.2 - 8 %) to achieve the hole and electrons in the device equal at active (emissive) layer. The emission originates from the PVK : PBD host is decrease with increasing dopant concentration. Around 8 % was completely disappeared; it means high efficiency energy transfer from complex, **AG** to host system. Due to the large site-isolation effect, the dendritic phenylene (polyphenylene) functionalized europium complex shows an enhanced EL efficiency. This polyphenylene groups are decrease self-quenching of europium complex compare to other two and it observed by PLQE. The general configuration of device of Eu-complexes (X = **AE, AF and AG**) is ITO/PEDOT:PSS (150 nm)/ PVK:30 wt % PBD : X Eu-complex (75 nm)/ Ba (4 nm)/ Al; (200 nm). The charge trapping in the doping system is observed, it was confirmed by increasing turn-on voltage with increasing doping concentration. The highest EQE and maximum luminescence was observed for complexes, **AE, AF and AG** are 0.22, 0.34, 0.42 % and 166, 272, 277 cd / m^2, respectively at 0.2 wt % doping concentration with red emission. When the introducing of TBPI is as a HBL in the device with Eu- complex (0.5%), observed EQE, luminous efficiency and max. luminescence are 0.72, 0.79, 1.90; 0.78, 1.93, 2.01 and 332, 640, 319, respectively.

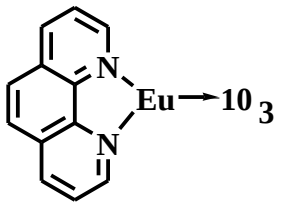

AE: Eu(TPD)$_3$Phen

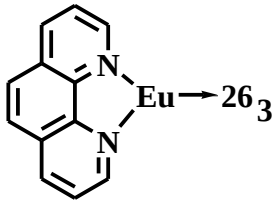

AF: Eu(Ph-TPD)$_3$Phen

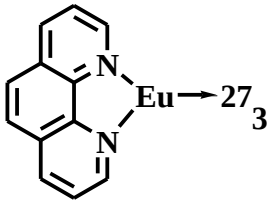

AG: Eu(G1-Ph-TPD)$_3$Phen

The absorption energy of the guest (G) is lesser than that of emission energy of host (H) material. Based on this M. Uekawn *et.al* (1997), [87] synthesized different groups and introduced **AB**, **AH**, and **AI**. PL emission was greater for **AI**, (370 nm) than other **AB**, (343 nm) and **AH**, (351 nm) with of comparing the spectral overlap between **AI** and TPD emission. The absorption peak of **AI** complex shows at lower energy with respect to emission energy of the host due to energy transfer to **AI** complex, from TPD (HTL) higher than that of **AB** and **AH** complexes.

Gong, *et al.,* [88] introduced two novel carbazole based Eu^{III} complexes, **AJ** and **AK**. (2-(4'4'4'-trifluoro-1'3' - dioxobutyl)-carbazole (2-TFDBC) and 2,7-bis(4'4'4'-trifluoro-1'3' - dioxobutyl)-carbazole (2,7-BTFDBC)). Both the complexes have best decomposition temperatures (> 361 °C). The expanded π-conjugation leads to red shift in the complex excitation band (towards visible region). The obtained high color purity was almost reached NTSC standards with Commission internationale de L'Eclairage (CIE) coor-dinates of (0.68, 0.32). **AJ** shown relatively high PLQE (28%) than rest of the complex (10%) and which is due to reduced Eu–Eu distance in dinulear structures.

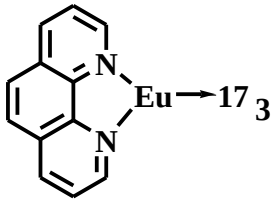

AH: Eu(FIHA)$_3$Phen

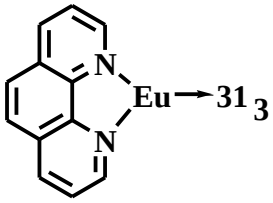

AI: Eu(DNM)$_3$Phen

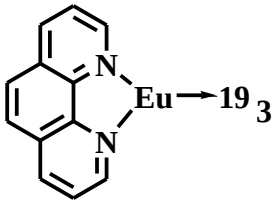

AJ: Eu(2-TFDBC)$_3$Phen

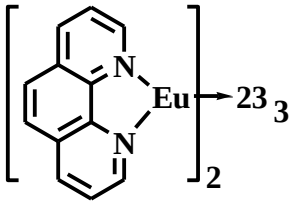

AK: Eu$_2$(2,7-BTFDBC)$_3$(Phen)$_2$

The fluorination is a feasible way of increasing emission efficiency via reduction of vibrational deactivation from their associated high energy oscillators. It can also explain as curbed C-H vibration by fluorination. In the case of the complex **AM** and **AL** have showed low device efficiencies. However, the complex **AN** was showed enhanced PLQY, which is almost reached to 34%, [89-91].

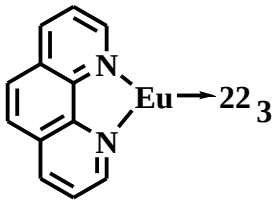

AL: Eu(22)$_3$Phen

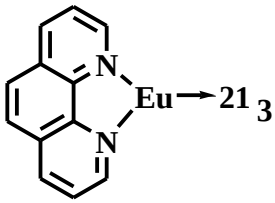

AM: Eu(21)$_3$Phen

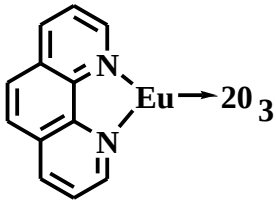

AN: Eu(ETFMCTFBD)$_3$Phen

As we know that the pyridine, imidazole and 1,3,4-oxadiazole (OXD) are strong electron-transporting capable moieties. Utilizing these materials for Eu^{III} complexes to modify the BTA to improve sensitizability of the ligands as well as thermal and luminescent enactment; proposed a similar type of complexes **AO**, **AP,** and **AQ** [92-94]. The introducing conjugate extension hetero cyclic groups by Gong and co-workers are shown bathochromic shift in the absorption spectra. These Eu^{III} complexes have PLQY is 14-18%. Europium ternary complex coated onto an ~395 nm-emitting InGaN chip and achieved red emission with appropriate CIE chromaticity coordinates. The complex **AO** exhibited a ligand-sensitized luminescence process (antenna effect) and light-emitting diode with an improved PE of 0.53 lm W^{-1}. **AO**, **AP** and **AQ** are shown CIE (0.66, 0.33). In addition to achieve the good efficiency and stability for the complexes, $Eu(TPBDTFA)_2(TPATFA)Phen$, $Eu(MEP)_3Phen$ and $Eu(MEP)_3$ are synthesized by mixing of different ratios of two β-diketonates. The complex **AR** was shown good thermal stability. and however, it is less compared to that of mixing of different ratios of two β-diketonate complexes. Introducing the carbazole moiety in the ligand enlarged the π-conjugated system of the ligand as well as enhanced the Eu^{III} complexes luminescent intensity.

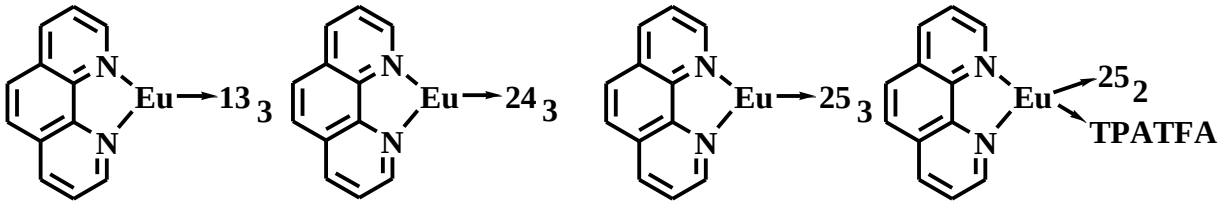

AO:Eu(IDTFBD)$_3$Phen **AP:Eu(MPBDTFA)$_3$Phen** **AQ:Eu(TPBDTFA)$_3$Phen** **AR:Eu(TPBDTFA)$_2$(TPATFA)Phen**

1.6.4 Modification of Phen:

Pei Sun *et.al.,* introduced PyPhen, MPP, DPPz, MDPz, DDPz and BDPz ligands with $Eu(TTA)_3$ moiety (**AS, AT, AU, AV, AW** and **AX**), [95-97]. Which are developed for high sensitizability and electroactivity for luminescent Eu^{III} complexes. Li *et al.*, worked additionally on the same by computational resources (DFT) and analyzed the small sized ligands can undergo ligan to metal energy transfer efficiently. It leads to higher ^1S and ^3T levels. It is strictly follow by **AB**, **AS** and **AT** complexes through the empirical rule that the excited energy transfer (EET) must be larger than 0.43 eV and excited inter-system crossing (EISC) must be larger than 0.62 eV. Rest of the complexes was shown low efficiency due to mismatching of the energy levels.

It is also found that the contribution of fused pyrazine rings considerably reduced the LUMOs of the complexes (−2.8 to −3.0 eV). Device general structure is ITO/ TPD (or) NPB (50 nm) / Eu : CBP (1.7 - 7.6 %) (30 nm) / BCP (20 – 30 nm) / Alq_3 (25 – 35 nm) / Mg : Ag. Compare to all Eu-complexes, **AX** exhibits 550 nm strong emission; 612 nm weak emission from center metal Eu^{III} ion and strong emission is closed to free BDPz. It is proposed that intramolecular energy transfer from ligand to Eu metal ion seems incomplete in the complex. **AS** : CBP at 2.6 % exhibits luminescence (L)1309 cd m^{-2} with less EQE (η_{ext}), but at 7.6% exhibits 757 cd m^{-2} with EQE 1.15% and current efficiency 2.16 cd A^{-1}. **AT** : CBP at 1.7 % exhibits 1256 cd m^{-2} with EQE 1%. **AU** : CBP at 2% exhibits 2046 cd m^{-2} with less EQE, but at 4.5% exhibits 1670 cd m^{-2} with EQE 2.05% and **AW** : CBP at 2 % given 1528 cd m^{-2} with less EQE, at 5 % given 1248 cd m^{-2} with improved EQE 1.24 %. Author observed, by improving the concentration of dopant, **AT** and EQE are changing different way (unmatchable). The relative

HOMO and LUMO energy levels of the materials that are used in the device structure [NPB/Eu:CBP/BCP/Alq] is shown in Figure 1.9.

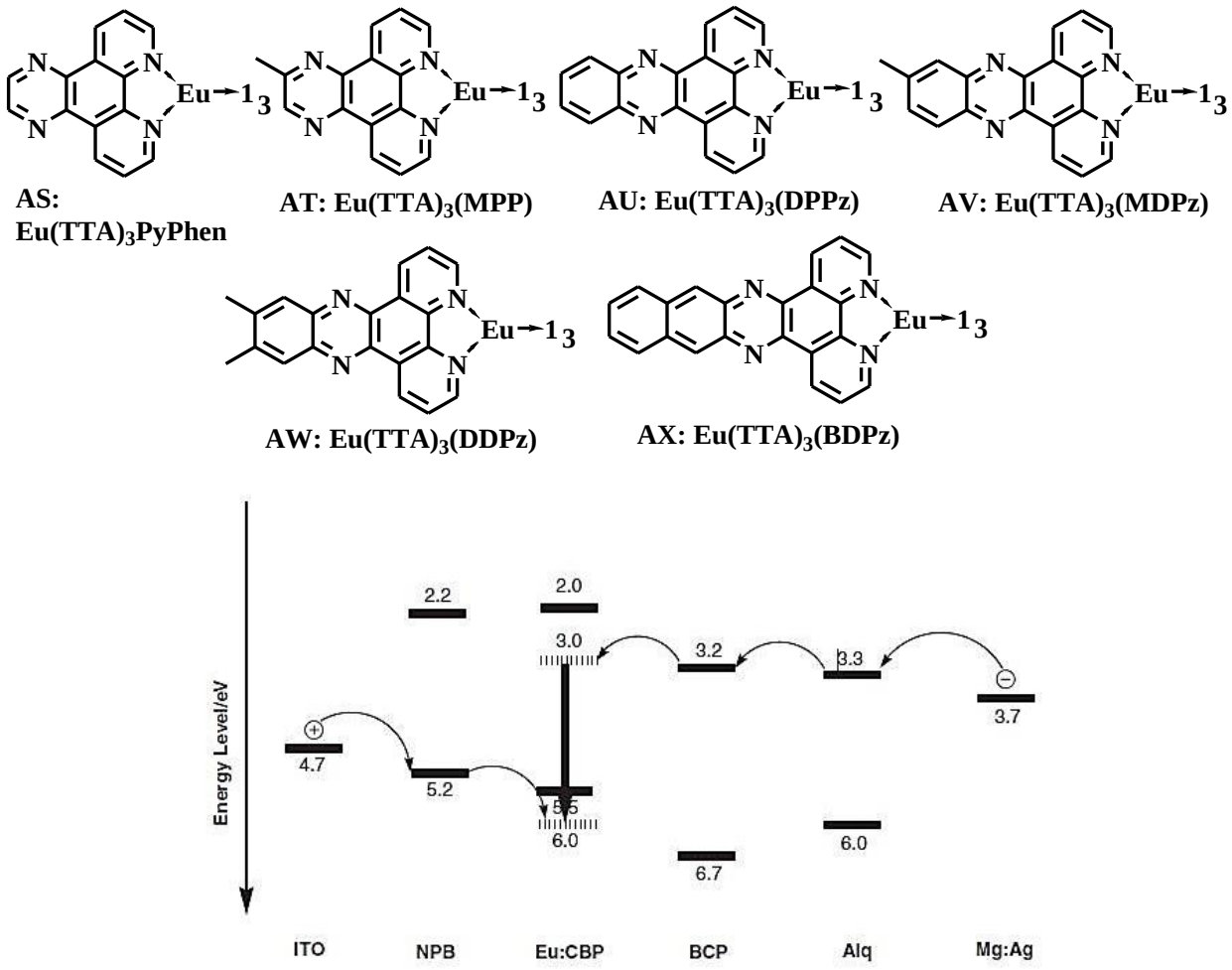

Figure 1.9 The relative HOMO/LUMO energy levels of device structure [NPB/Eu:CBP/BCP/Alq].

The above structure related Eu^{III} complexes were introduced by utilizing an indole-fused PyPhen based ligand **BB** [98]. The complex consisted bipolar structure that combines electron-donating indole and electron-withdrawing pyrazine moieties. Addition to the same indole-fused ligand moiety was replaced by thiadiazole for Eu^{III} complex ($Eu(TTA)_3(TDAP)$, **BC**) [99] as an extended the conjugation of 1,10-phenanthroline was introduced by Pereira *et al.*, in 2011. Incorporation made as electron-deficient five-membered thiadiazole ring to enhance the electron-injection ability of the ligand. The fabricated bilayer device is ITO / NPB / CBP : **BC** / Al. The HOMO and LUMO of BC were located at −5.7 and −2.6 eV, respectively.

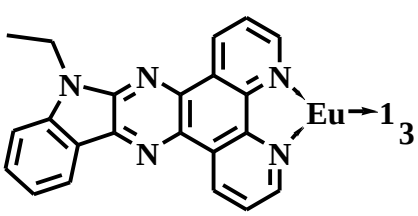

BB: Eu(TTA)$_3$DIQ-Et

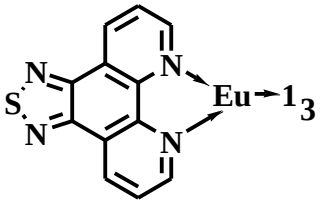

BC: Eu(TTA)$_3$TDAP

The Phen was substituted with different types of electron withdrawing and electron donating groups. The overview of a chlorine-substituted group shown improved EL performance compared to that of a nitryl substitution. The increased significant EL efficiency by reduction of the energy loss was initiated by light hydrogen atom vibration. The devices structures are, ITO / TPD / CBP : **AB** / BCP / Alq_3 / LiF / Al, η_c: 1.73 cd A^{-1}, ITO / TPD / CBP : **BD** / BCP / Alq_3 / LiF / Al, η_c: 2.34 cd A^{-1}, ITO / TPD / CBP : **BE** / BCP / Alq_3 / LiF / Al, η_c: 0.98 cd A^{-1}, [141]. Fang and Ma also introduced methyl substituted Phen, trivalent Eu^{III} complex **BG** into ITO/ TPD (40 nm) / Eu complex: CBP (1%, 30 nm) / BCP (20 nm) / Alq_3 (30 nm) / LiF (1 nm) / Al (100 nm) device. Observed max. luminance up to 800 cd/m^2 at drive voltage 24.5V, an external quantum efficiency of 4.3%, current efficiency of 4.7 cd/A, and power efficiency of 1.6 lm/W and at the brightness of 100 cd/m^2, the quantum efficiency reaches 2.2% (2.3 cd/A). The EL QE decreases with increasing current, recombination of long-lived triplet excitons cause luminescence. The same explained by the help of triplet-triplet annihilation on CBP molecules following back transfer from TTA due to the neighboring resonance, [100, 101].

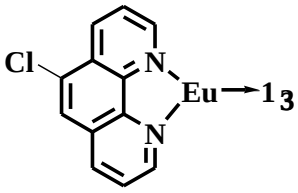

BD: Eu(TTA)$_3$ClPhen

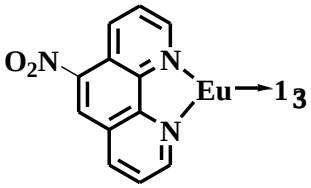

BE: Eu(TTA)$_3$NPhen

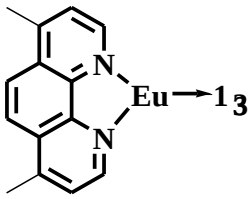

BF: Eu(TTA)$_3$DmPhen

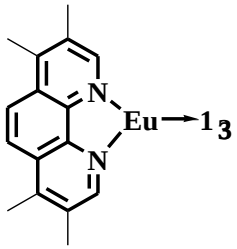

BG: Eu(TTA)$_3$TmPhen

4, 7- positon substituted Phen by carbazole moieties were introduced by Zucchi and co-workers [102] for Eu^{3+} complex, **BH**. The energy transfer from the ^{3}T level of ligand to Eu^{III} metal ion was well suited for the LMET process. Which is supported by the ligand broadened absorption in the range of 300-400 nm did not lead the change of the ^{3}T state (21,000 cm^{-1}). The bulky nature of neutral ligand was providing the protection for excited Eu^{3+} from quenching as well as improve the long emission lifetimes (0.66 and 0.80 ms in acetonitrile solutions and films, respectively). It leads to high PLQE (80%) in a poly(methyl methacrylate)(PMMA).

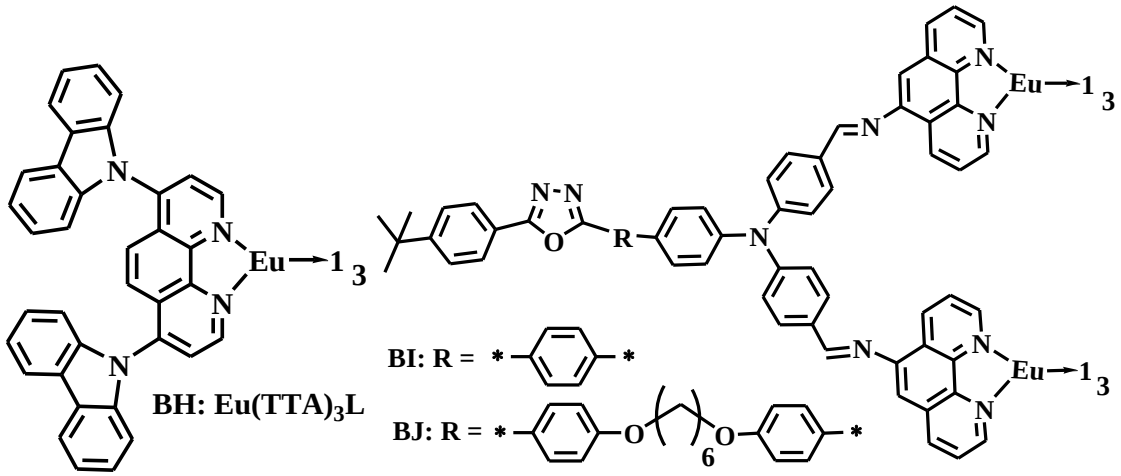

Utilizing the both hole-transporting triphenylamine (TPA) and electron-transporting oxadiazole (OXD) based two novel bipolar-transporting binuclear Eu^{III} complexes were reported (**BI** and **BJ**) [103]. Both have separated by spacer moiety (hexyl linker) to arrest the conjugation. Fully conjugated complex was shown high thermal stability with a decomposition temperature of 304 °C (higher than that of non-conjugated complex). The structure of single-layer PLEDs were fabricated is ITO / PEDOT:PSS (50 nm) / PVK - PBD (30 wt %) : europium(III) complex (70 nm) / LiF (0.5 nm) / Al (150 nm). The emitting layer consists host matrix of the PVK-PBD blend, the weight ratio of PBD is 30 % and doping weight vary from 1, 2, 4 to 8 wt for europium(III) complexes concentration. **BI** The molecular complex have good carrier injection and transporting abilities and the fabricated device shown luminance up to 296 cd m^{-2} at low turn-on voltage of 8.5 V.

1.6.5 Both TTA and Phen modification:

In 1999, Keizou okada, *et. al*.; synthesised a novel Eu based **BK** as an essential component layer in double and triple layer EL devices by vacuum deposit in technique. Triple layer EL device is higher luminesence than that of double layer device due to the introduction of ETL (Alq_3).

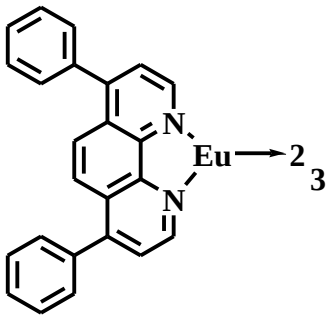

BK: Eu $(DTP)_3$(Dipphen)

Device fabrication was followed in the following manner glass substrate/ITO / TPD (600 A^o) / **BK** (500 A^o) / Alq_3 (200 A^o) / Al : Li (99:1)(2000 A^o). The turn-on voltage is <5, max. luminescence is 450 cd / m^2 at 15 V and current density 200 mA / cm^2. Decrease in luminescence was observed > 16v. This is because of existence of dark sports created between Eu layer and

Al-Li interface due to the humidity and presence of Oxygen. Decreasing of emissive layer (300 A^o) thickness appears a broad peak at 535 nm coming from Alq_3 (500 A^o). It states that the energy transfers from Eu-layer to Alq_3. It is shown better improvement when compare to that of oxygen consisted antenna complex **(AC).**

1.7 Eu complexes for white LEDs:

Recently, Eu complex gained much attention due to their emerging technological applications such as SSL (essential component as a red emitting phosphor for near UV or blue LED based warm white LEDs). By combining the Eu complex with inorganic color convertors the white light emission can be realised. For example, the hybrid white LEDs could be fabricated by combining the phosphors in a polymer matrix, the same is placed in the top of LED chip and by integrating the light from LED chip and emission from phosphor could produce white light (shown in Figure 1.10).

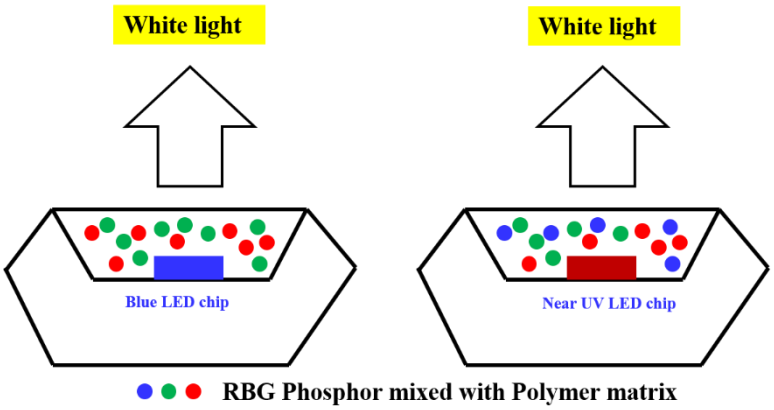

Figure 1.10 Structure of white LED based on near UV LED chip

The molecular structure which are used in this section are summarised in Figure 1.11, 1.13, 1.15, 1.16. Lee *et al.*, has fabricated hybrid white LED by combining $SrAl_2O_4:Eu^{2+}$ (for green (520 nm) emission) and $Sr_4Al_{14}O_{25}:Eu^{2+}$ (for blue (490 nm) emission) and new organic Eu metal complex, $Eu(BTFA)_3phen$ (for red (614 nm) emission, complex-1). The fabricated white LED electroluminescence spectrum shows typical RBG emission and the CIE values (0.321, 0.365) are better than that of the typical commercial Nichia white-light LED (0.297, 0.297). It is worth to note that the preliminary lifetime test indicated that the phosphor is robust, showing no degradation over a period of 100 h, [104].

Several Eu based complexes (complex 1-6 along with 3 phosphine based Eu complexes) were taken and studied their photoluminescence properties for white LEDs. Among all the complexes, phosphine oxide based β-diketone Eu complex (given below) shown better luminescence quantum yield. Eu complex (described below) integrated with near UV LED given intense red light with luminous intensity was over 200 mcd (20 mA) and these type complexes (fluorescence compounds) are promising for application in warm white LEDs, [105].

N. J. Xiang *et al.*, designed and synthesised novel Eu^{III} tetrabasic complex, $Eu(TPBDTFA)_2(TPATFA)Phen$ (complex-7) for white LED applications. The complex-7 exhibits bright red emission due to the $^5D_0 \rightarrow {}^7F_J$ transitions of Eu^{III} ions with appropriate CIE (Commission International de l'Eclairage, International Commission on Illumination)

chromaticity coordinates (x = 0.64, y = 0.35) under λ_{exc} = 230–470 nm. The luminescence QY for the complex-7 is 0.126 and the decomposition temperature is found to be high (383.4 °C) from thermogravimetric analysis (TGA). An intense red-emitting LED was fabricated by combining the mono-phosphor (complex-7) with a ~395 nm emitting InGaN chip [106].

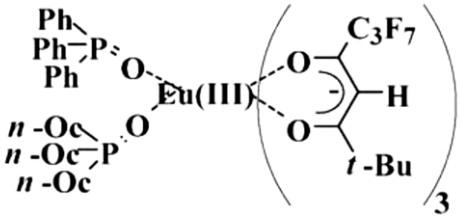

Figure 1.11 The molecular structure of Eu-complex.

Pei He *et al.*, reported an efficient red-emitting Eu^{III} organometallic complex $Eu(ECTFBD)_3phen$ (complex-8), where ECTFBD was 1-(9-ethyl-9H-carbazol-3-yl)-4,4,4-trifluorobutane-1,3-dione and phen was 1,10-phenanthroline. Combined spectroscopic and thermogravimetric analysis reveals that the complex-8 exhibits a high thermal stability and excellent photoluminescence properties. Ligand-sensitized luminescence was observed due to the energy match between the triplet level of ligand and Eu excited ($^5D_0$) levels. A bright red LED was fabricated based on InGaN chip and the CIE coordinates (x = 0.65, y = 0.320) are close to the NTSC values for red with high CRI value, [107].

Similarly the complex-9 $Eu_2(BTFBDEC)_3(phen)_2$ (BTFBDEC is 3,6-bis(4,4,4-trifluoro-1,3-Butyldiketone)-9-ethyl-carbazole and phen is 1,10-phenanthroline) also possess good thermal and photoluminescence properties with good absorption near UV region. Hence it is possible use the same in near UV based white LEDs. An intense red-LED was fabricated by combining complex-9 with a ~395 nm emitting InGaN chip [108].

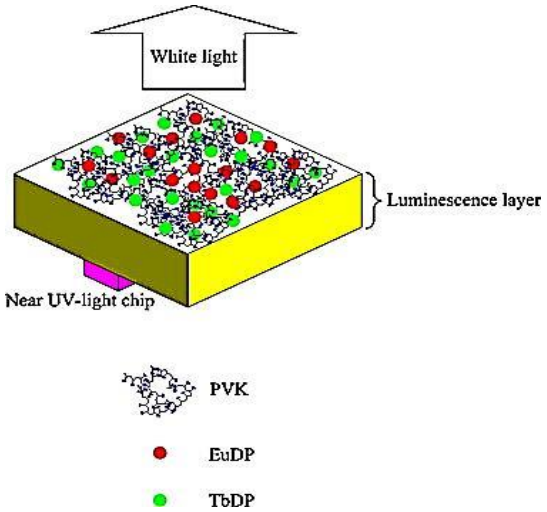

Figure 1.12 The model of ultraviolet-excited white LEDs.

White light emitting Complex: Terbium and/or Europium β-diketonate complex with different ratio doping was done in the poly(N-vinylcarbazole) (PVK) matrix and studied their photoluminescence properties. The various energy transfer process involved in these doping

systems well analyzed. Inter-molecular energy transfer from PVK to $Tb(DBM)_3Phen$(TbDP) and $Eu(DBM)_3Phen$(EuDP), and from TbDP to EuDP exists in the present systems. By simply adjusting the dopant mixing ratio and excitation of wavelength one can tune the emission color and further optimizing the dopant concentration white light was realized (shown below, Figure 1.12) [109].

S. Liu *et al.,* in 2009 reported quadruple stranded dinuclear Eu^{III} complex $Na_2[Eu_2(dbt)_4]$ (complex-10), where H_2dbt - 2,8-bis(4;,4',4'-trifluoro-1',3'-dioxobutyl)-dibenzothiophene. The complex show typical ED transitions of Eu^{3+} ion with QE of 23%. The LED were fabricated by amalgamation of a 395 nm-emitting InGaN chip with the complex-10 as a red emitting phosphor while an original LED without phosphor and an LED with $Y_2O_2S:Eu^{3+}$ were also made for comparison. The emission spectra of the InGaN–complex-10 LEDs show red emission, whereas the original InGaN LED without phosphor shows near UV emission under 20 mA forward bias. The dependence of the CIE chromaticity coordinates of the fabricated LEDs on the mass ratio of the complex to the silicone also been investigated. The results show that the mass ratios of complex to the silicone are 1:5, 1:10, 1:20, the CIE chromaticity coordinates of the fabricated LEDs are (x = 0.6224, y = 0.3238), (x = 0.5322, y = 0.2701), (x = 0.4997, y = 0.2471), respectively. The CIE chromaticity coordinates of LED of the mass ratio of $Y_2O_2S:Eu^{3+}$ to silicone (1:1) are (x = 0.4033, y = 0.1871). The efficiency of the original LED without phosphor or with $Y_2O_2S:Eu^{3+}$ were only 0.39 and 0.20 lm/W, though, the efficiency of the fabricated LEDs with the complex-10 attain 1.55, 1.86, 2.18 lm/W, [110].

Due to their structural advantage the ligand namely 2-(4,4,4-trifluoro-1,3-dioxobutyl)-dibenzothiophene (Hdbt) was synthesized and used for the Eu-complex (complex-11) further evaluated for the white LED applications. The ligand structural advantages are (1) It contains a β-diketone unit, which could coordinate successfully to Eu^{3+} ions to form a stable Eu^{III} complex; (2) Dibenzothiophene unit has a suitable - conjugated system and could absorb the NUV energy effectively and then transfer it to the Eu^{3+} ion; (3) It has no absorption in the blue and green emission range. The complex efficiently emits red emission due to ED transition and absorption in the near UV region. The complex was used to fabricate the red LED (integrated with ∼395 nm-emitting InGaN chip) and found the LED device's CIE chromaticity coordinates are x = 0.5835, y = 0.2857, and the luminescence efficiency is 1.29 lm/w, [111].

Carbazole - based *β*-diketonates with different alkyl substituents (CH_3, C_2H_5, C_3H_7, C_5H_{11}) at N-position in the carbazole ring was synthesised and used the same for making ternary Eu^{III} complex with phen (complex similar to 12a but the N-1 position of the ligand should be different CH_3, C_2H_5, C_3H_7, C_5H_{11}. The complexes show good thermal stability (decomposition temperature > 300°C), which is very much suitable for LED applications. Efficient energy transfer from ligand to metal ion was observed due to location of the triplet level of ligands are higher than that of Eu^{III} $^5D_0$ levels. Even though all the complexes show red emission, however the emission intensity is found to be decreasing in the following order the emission intensity is $Eu(N\text{-}C2)_3Phen$ > $Eu(N\text{-}C3)_3Phen$ > $Eu(N\text{-}C5)_3Phen$ > $Eu(N\text{-}C1)_3Phen$. By using these complexes bright red LED was fabricated and this study clearly indicates that the complexes can be used as a red component for fabrication of NUV-based white LEDs [112].

The functionalization in the 2- or 2, 7-postiion in the carbazole ring (2-(4,4,4-trifluoro-1,3-dioxobutyl)-carbazole (2-TFDBC) and 2,7-bis(4,4,4-trifluoro-1,3-dioxobutyl)-carbazole (2,7-BTFDBC)) was carried out in order to enhance the visible light absorption (with extended π conjugation). The same was used to metallate the Eu^{3+} ion and made two Eu^{III} ternary complexes $Eu(2\text{-}TFDBC)_3$phen and $Eu_2(2,7\text{-}BTFDBC)_3(phen)_2$ (complex–12a) to use in the white LED

based on blue InGaN chip. The QY of the Eu complex is mainly depends on the location of the triplet level of the ligands and these ligands show higher triplet energy levels than that of the Eu^{III} $^5D_0$ levels. The complexes emit bright red color in the region of 615 nm with blue ray excitation and make potential candidate for the white LEDs [113].

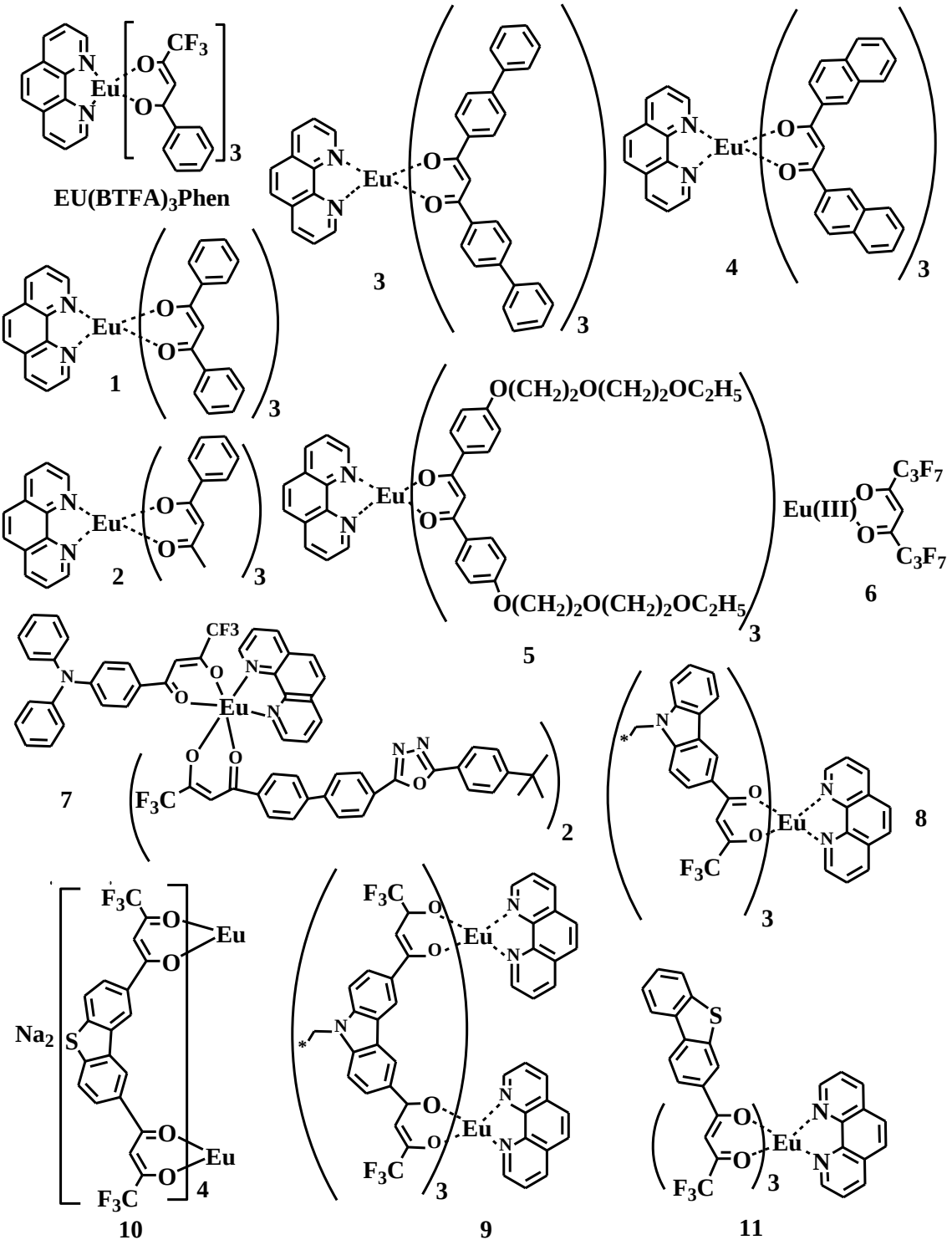

Figure 1.13. The molecular structure of complex 1 - 11

P. He *et al.*, in 2010 synthesized carbazole functionalized β-diketone (TTA based) ligand for the novel Eu^{III} ternary complex $Eu(EMOCTFBD)_3phen$ (complex–12b) EMOCTFBD - 1-(9-ethyl-7-methoxyl-9*H*-carbazol-2-yl)-4,4,4-trifluorobutane-1,3-dione and phen - 1,10-phenanthroline). The methoxy moiety introduction significantly extends to blue region and intensifying the absorption intensity. The complex emits bright red emission due to antenna effect. The decomposition temperature of $Eu(EMOCTFBD)_3phen$ is found to be 338.3 °C, which is good enough for luminescence applications. The fabricated red LED using this complex integrated with ~ 460 nm-emitting InGaN chip emits bright red color (Figure 1.14) [114].

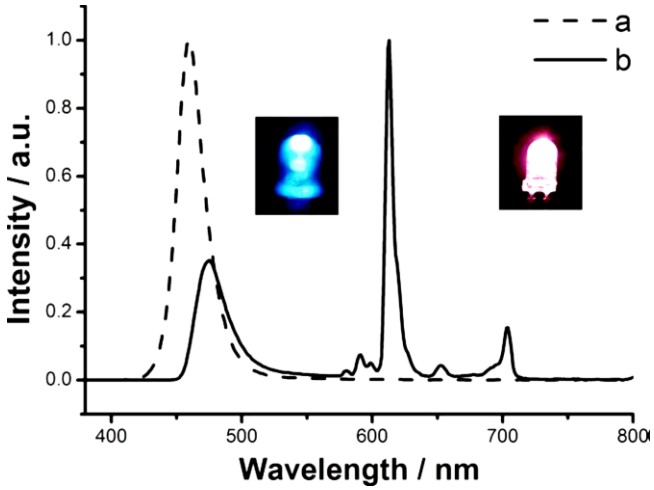

Figure 1.14. Emission spectra and the photographs of the original InGaN LED without phosphor (a and left) and the LED with $Eu(EMOCTFBD)_3phen$ (b and right) under excitation of 20 mA forward bias. Insert: photographs of the lighting LEDs.

Wang *et al.*, designed and synthesised two new multinuclear Eu^{III} complexes, $[Eu(AFTFBD)_3]_2$(1,4-bmb) and $[Eu(AFTFBD)_3]_3$(tmb) (complex-13), where HAFTFBD was 2-acetylfluorene-4,4,4-trifluorobutane-1,3-dione, 1,4-bmb was 1,4-bis[2-(2'-pyridyl)benzimidazolyl]benzene and tmb was 1,3,5-tris[2-(2'-pyridyl)benzimidazolyl] benzene. Red luminescence of Eu^{3+} ion due to the $^5D_0$–^7F_J (J = 0–4) transitions under 395 nm-light excitation was observed for all the Eu-complexes. The fabricated LED (coating the selected complex-13 onto ~395 nm-emitting InGaN chips) shows bright red light with appropriate CIE color coordinates. The complex-13 is found to be promising candidates as red component for application in fabrication of near UV-based white LEDs [115].

Trivalent europium complex (complex-14), was synthesized, and studied their photoluminescence properties. Fortunately the complex have broad excitation band in the near UV spectral range and complex emits bright red emission due to the $^5D_0 \rightarrow {}^7F_J$ transitions of Eu^{III} ions. The luminescence QY for the complex-14 is 0.17 and complex show high thermal stability (confirms from thermogravimetric analysis decomposition temperature of 344°C). An intense red light-emitting diode was fabricated by combining the complex-14 with a ~395 nm-emitting InGaN chip, [116].

β-diketone based Eu complex (complex-15, $(Eu(IDTFBD)_3phen$ HIDTFBD = 4-imidazol-4,4,4-trifluorobutane-1,3-dione) was designed for white LED applications. The complex-15 was characterized by IR, UV–visible, thermogravimetric analysis (TGA) and photoluminescence (PL) spectroscopy. The complex exhibited a strong and wide excitation band between 320 and

420 nm (due to the formation of a big π-conjugated system). The complex-15 exhibits strong red emission of Eu^{3+} ion due to the $^5D_0 \rightarrow {}^7F_J$ (J=0–4) transitions with near UV excitation and the corresponding Gd^{3+} complex help the triplet energy of the ligand was measured and it is higher than that of Eu^{3+} excited levels. Finally, a bright red light emitting diode was fabricated by coating the complex-15 onto a ~395 nm-emitting InGaN chip, efficiency of the fabricated LED is 0.531 lm/W, much higher than that of the original LED without phosphor (0.33 lm/W). The LED exhibited appropriate CIE chromaticity coordinates in red area, [117].

The design and synthesis of a novel indane based β-diketone with trifluorobutane in the contraposition, 5-acetylindane-4,4,4-trifluorobutane-1,3-dione (HAITFBD) and its Eu^{III} ternary complex, $Eu(AITFBD)_3$phen were reported. The complex-16 was characterized by spectroscopic and thermogravimetric analysis and the complex-16 shows high thermal stability, wide and strong excitation bands from 300 nm to 425 nm when monitored at 611 nm (synchronize well with InGaN chips emission). The complex exhibits intense red emission under excitation of near UV light with CIE chromaticity coordinates are calculated as x = 0.63 and y = 0.34. Efficient antenna effect expected due to the lowest triplet state energy of the primary ligand AITFBD (17,730 cm^{-1}), which is higher than that of the lowest excitation state energy level of the central Eu^{III} ion, $^5D_0$. Finally, a bright red light-emitting diode was fabricated with combining the complex-16 with 380 nm-emitting InGaN chip, the efficiency of the fabricated LED is 0.51 lm/W, more than twice of the original LED without phosphor (0.23 lm/W). The results indicate that the red phosphor is potential for near UV based white LEDs [118].

H. Wang *et al.,* synthesized a novel indane based β-diketone ligand for ternary Eu^{III} complex (complex-17). The ligand, 5-Acetylindane-4,4,4-trifluorobutane-1,3-dione (HAITFBD) was synthesized through the Claisen condensation reaction from the ketone and ester. The complex excitation band observed in a wide spectral range (300–425 nm), this could be attributed that the availability of the good and extended π-conjugated system in the complex. A strong and narrow Eu^{3+} red emission was observed at ~611 nm with 380 nm excitation, by exciting ligand absorption, the characteristic emission from Eu^{3+} ions was observed (no emission from ligand). This clearly indicates that the effective intermolecular energy transfer from the coordinated ligands to the luminescent central Eu^{3+} ions in the complex occurs [119]. By integrating the $Eu(AITFBD)_3$phen complex with an ~380 nm-emitting InGaN chip show bright red LED [120].

Guang Shao *et al.*, reported a new Eu^{III} ternary complex based on a fluorinated β-diketonate ligand and 1,10-phenanthroline as an ancillary ligand and assessed as a candidate for white LEDs. The complex-18 exhibits a high decomposition temperature (316 °C) and good absorption in the near UV region. The complex exhibits an efficient energy transfer pathway from the ligands to the central Eu^{3+} ion due to energy level matching. An intense red-emitting LED was obtained by coating the complex-18 on to a 395 nm-emitting InGaN chip. The results reveal that the energy transfer from the InGaN chip to the complex is very effective and it can be suitable candidate for white LEDs [121].

G. Shao et al., synthesized six Eu^{III} ternary complexes (complex-19a-f) using different β-diketonate ligands (antenna) and 1,10-phenanthroline as an ancillary ligand. The ligand to metal CT band could be possible as the calculated triplet energy level values are above the $^5D_0$ level of Eu^{3+} ion (lowest triplet state levels of ligands 2a–f could be calculated by the shortest wavelength of the phosphorescence peaks, which are about 19,267 cm^{-1} (519 nm), 18,975 cm^{-1} (527 nm), 19,230 cm^{-1} (520 nm), 20,366 cm^{-1} (491 nm), 18,248 cm^{-1} (548 nm) and 19,723 cm^{-1} (507 nm), respectively. Bright red light-emitting diodes (LEDs) were then fabricated by coating

the complexes onto 395 nm-emitting InGaN chips. The light emission from the InGaN chips could be completely absorbed in the spectra of LEDs [122].

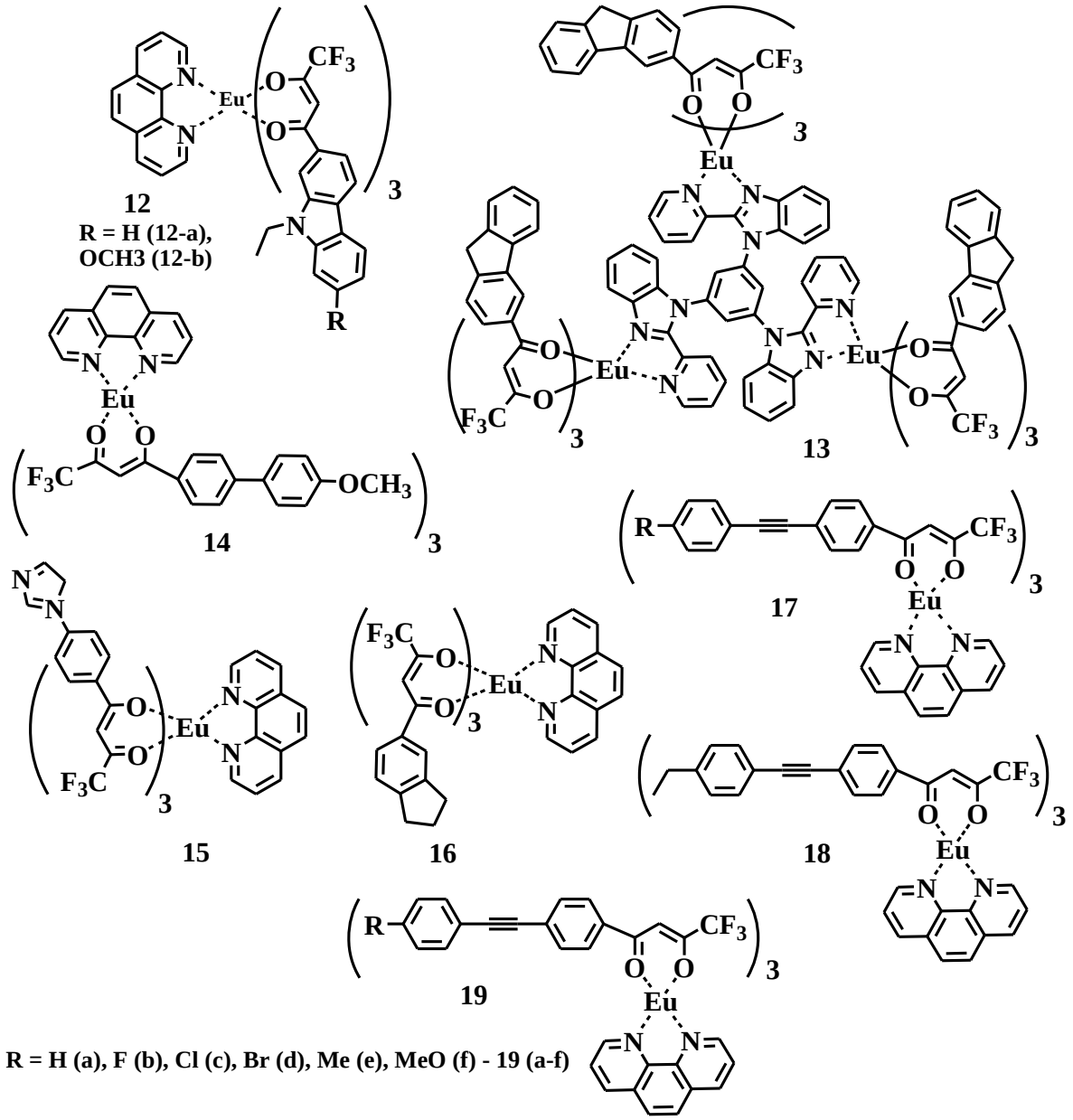

Figure 1.15 The molecular structure of complex 12 – 19

The complex [Eu(DBM)$_3$(Phen)] is one of the renowned red-emitting Eu^{3+}-based molecular phosphors with high quantum yield. However due to their low absorption in the visible region (blue region) restricts their application as a red phosphor in white LEDs. Recently, taking all the advantage of the ligand DBM and Phen, Zhengliang Wang *et al.*, designed additional ligand 2,7-bis(4'4'4'-trifluoro-1,3-dioxobutyl)-(9-ethyl-9H-carbazole) (2,7-BTFDBC), with extended π conjugation (facilitate the blue absorption) for the Eu-complex (complex-20). It is evident from the PL emission and excitation spectra of the synthesized complexes that all the complexes efficiently excited with blue light and emit bright red emission

(ED transition, confirms the LMCT). The $[Eu_2(2,7\text{-BTFDBC})(DBM)_4(Phen)_2]$ was to fabricate single red LED with combining with a ~460 nm-emitting GaN chip [123].

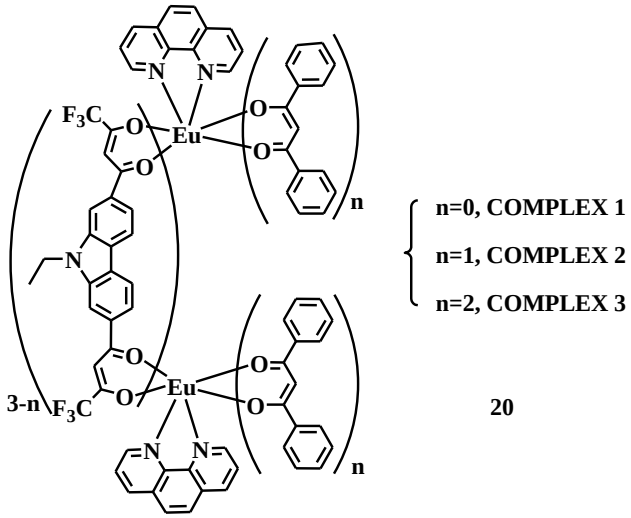

Figure 1.16 The molecular structure of complex-20

1.8 Eu-complexes for ratiometric temperature sensor:

It is well accepted that the temperature is the most important physical property and is frequently required to be measured in scientific research and in industrial applications [124, 125]. There are two types of common luminescent temperature sensors: (i) inorganic phosphors, that include chromium phosphors (i.e., alexandrite) and lanthanum oxysulfides (i.e., La_2O_2S:Eu) and (ii) organic molecules ~e.g., rhodamine B base dyes). Europium chelates are considered organic, luminescent-based temperature sensors [126]. Temperature-dependent luminescence is a well-known phenomenon which has been exploited to develop luminescent thermometers based on molecular complexes and their nanoparticles. [127-131]. It has diverse benefits over other conventional thermometers because of their fast response, high sensitivity, non-invasive operation (temperature distributions in biological tissues (e.g., in tumors), the medium of interest is observed remotely, eg, infrared and luminescence thermography), and inertness to strong electric or magnetic fields. The temperature-dependent lanthanide emission is a key feature for developing new ratiometric temperature sensors, as the emission PL intensity or wavelength and lifetime (the classification luminescent sensor is given in Figure 1.17) is conjugated or reflected with the temperature. [132].

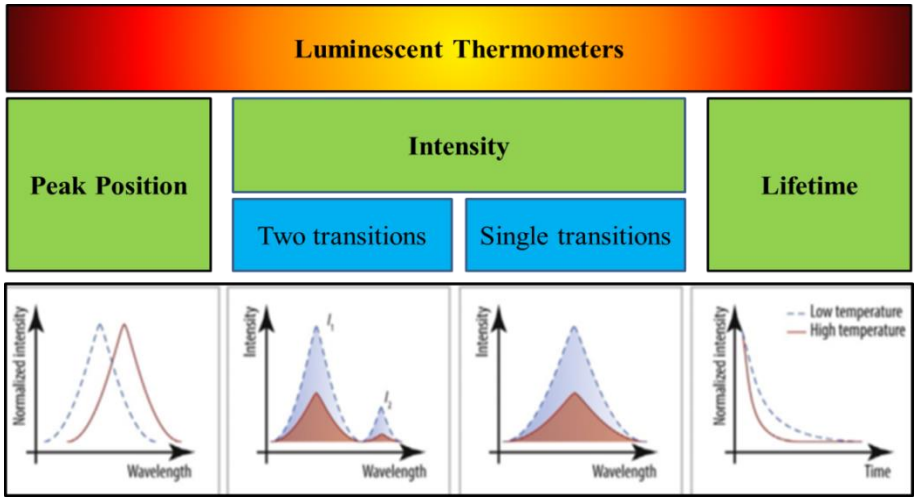

Figure 1.17 Luminescent thermometers classification [126].

PL emission intensity measurements are more straightforward and readily carried out as compared to PL lifetime measurements. Organo-lanthanide complexes are shown potent in terms temperature of sensing and imaging, since the emission bands are strong and sharp (FWHM is as small as small ~10 -20 nm) and lifetimes from several hundred microseconds (μs) to several milliseconds (ms). In addition, lanthanide luminescence is scarcely quenched by oxygen and different emitting centers or multiple luminescent active centre can cover the entire electromagnetic spectrum, ranging from UV (eg, Gd^{3+}) to IR (eg, Er^{3+}, Yb^{3+}, Nd^{3+}); thus, it is practically promising to design on-demand luminescent probes for diverse applications.

Numerous research efforts yields a huge number of lanthanide (especially Ln^{3+}) based molecular thermometers covering temperatures from the cryogenic (T<100 K) to the physiological (298–323 K) ranges, involving generally, ligand-to-Tb^{3+}, ligand-to-Eu^{3+}, and Tb^{3+}-to-Eu^{3+} energy transfer and exhibiting the distinctive $^5D_4 \rightarrow {}^7F_5$ (Tb^{3+}) and $^5D_0 \rightarrow {}^7F_2$ (Eu^{3+}) transitions. Recently, thermometer behaviour was identified, involving lanthanide chelate complexes [133-135], metal-organic frameworks (MOFs) [136-139], upconverting NPs (UCNPs) [140, 141] and downshifting nanomaterials [142, 143]. Most of the emissive temperature sensors that are currently in use are based on only one type of emission core (lanthanide ion). However, their precision is easily prejudiced by the light source intensity, excitation power, and the drifts of the optoelectronic system and/or on lifetime which requires a relatively long time and the computational treatment [144]. Recently, Pioneered work executed by Carlos et al., to discover a more robust and reliable luminescent thermometers based on two luminescent transitions approach based on molecular coordination compounds and nanoparticles [145]. The other approach is to manipulate the ligand and lanthanide emission in a single molecular complex system. The ligand and lanthanide emission can be modulated by increasing or decreasing the temperature.

The europium beta diketonate temperature sensitivity mechanism is based on thermal quenching; the major contribution is from the thermal deactivation of 5*D*1 and 5*D*0 Eu excited energy levels. Deactivation process involves the coupling of the electronic energy level to the environment through molecular vibration energy levels and it is recognized to a nonradiative process [146]. Thermal deactivation of the $^5D_1$ to the $^5D_0$ level can also play a vital role. It is generally believed that the thermal deactivation of ligand energy levels prior to transferring the

energy to the Eu excited states to have a negligible role. It is well documented by several research groups that the tris ligating chelates show larger temperature dependence (shorter lifetime) than tetrakis chelates. The addition of a fourth ligand or a Lewis base could minimizes the radiationless deactivation process (generally believed) and produces temperature insensitive chelates. It is worth to note that the tris chelate Eu complexes are very hard to obtain in a pure form, mostly due to the highly favoured formation of a tetrakis form [147].

Gamal E. Khalil et al., synthesised several Eu containing β-diketone complexes and evaluated the temperature sensitivities of europium chelate sensor films as a function of the following variables: (i) nature and number of ligands, (ii) the carrier polymers, and (iii) concentration ratio (Eu-chelate vs polymer). The main focus is to study the emission intensity, photodegradation and PL lifetime. [148]. The accurate temperature sensing can be achieved once the chelator is dispersed in a polymer matrix via their decay lifetime. Their lifetime as a function of temperature depends on three factors or variables that were mentioned earlier. Various tris and tetrakis Eu-chelates are used to study ligand effects, while the polymers FIB, polycarbonate, and Teflon© are used to analyze matrix effects. The study indicates that the higher concentrations loading give rise to shorter lifetimes and higher temperature sensitivities.

Strongly fluorescent and highly photo-stable europium-(III) *β*-diketonate based complexes are found to be new optical temperature probe and it can simultaneously sense both temperature and oxygen [149]. Organo-lanthanide complexes based Eu^{III} and Tb^{III} were synthesized and shown green, red emission (bright emission and small FWHM), respectively. The Tb containing complexes show PL lifetimes in the order of almost 1 ms at RT, good color purity, and high relative PLQY. Due to their photophysical properties makes them excellent probes for sensing temperature through PL lifetime measurement. In addition, the Eu and Tb containing complexes were incorporated into various polymer matrices to give sensor films for use as temperature-sensitive paints (TSPs). Among the complexes, Eu^{III} complexes have the advantage as compare to Tb^{III} complexes, since the complex can effectively excited by purple LEDs (λ_{max} = 405 nm). All the Eu and Tb based TSPs show good temperature sensitive and especially the Tb based complexes show temperature-lifetime sensitivities of −13.8 μs per °C and − 9.2 μs per °C, respectively. Assuming a precision of ± 1 μs in the determination of lifetime, this will enable temperature to be determined with a precision of around ± 0.1 °C and is the highest one reported so far for lanthanide complexes [150]

New potential luminescent thermo-sensitive molecular probes were reported by Balamurugan *et al*., based on the π-conjugated polymer–Eu^{3+} ion complexes. Efficient photosensitizers based on carboxylic acid functionalized segmented π-conjugated polymers having chromophores (oligophenylenevinylene (OPV)) in the poly(ethyleneoxide) or polymethylene backbones were custom designed, synthesized for Eu^{3+} ions. These π-conjugated polymer–Eu^{III} ion complex emissions are found to be sensitive to temperature and reversible 'turn-on' or 'turn-off' luminescent switches behaviour in solution as well as in solid state was observed. The experimental photoluminescent decay studies discovered that the red-emission from the excited $^5D_0$ level of Eu^{III} ion is highly sensitive to temperature which leads to make them use as a optical switches. The observed lifetime decay rate constants followed a typical Arrhenius trend over a wide range of temperature (having similar activation energies). The luminescent on–off process with variation of temperature is highly depends on the nature as well as length of the segmented polymer chain that tied the OPV optical chromophores. The oligomer–Eu^{3+} ion complex emission were found to be non-thermosensitive, given a lead for the segmented π-conjugated polymer ligand structure for the probes based on Eu^{III} ion complexes

(Figure 1.18). The present strategy opens up new concept and molecular design principles for π-conjugated polymer–lanthanide ion complexes as potential candidates for temperature sensitive luminescent molecular probes [151].

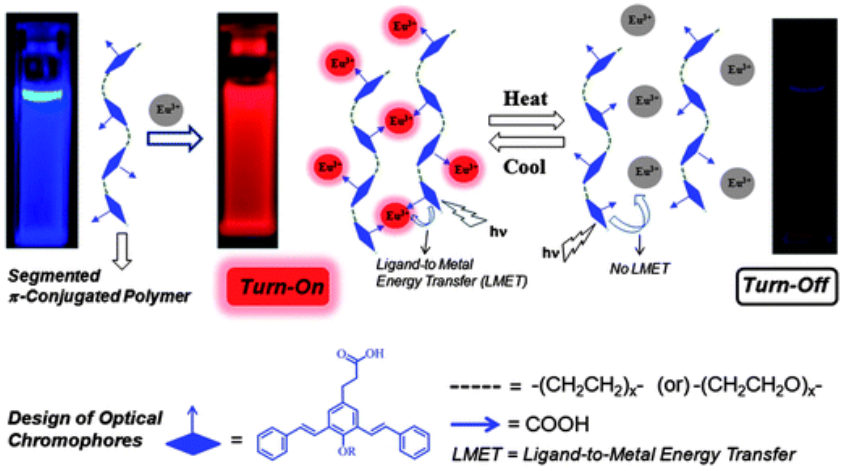

Figure 1.18 Approach for thermo-sensitive π-conjugated polymer–Eu^{III} ion complexes and their turn-on and turn-off switching pathways.

Tianren Wang and co-workers reported the fascinating multi-colored photoluminescent and white-light-emitting hybrid composite by simple supramolecular co-assembly of organoclay, sensitizer as well as Ln^{3+} in aqueous medium at RT (Figure 1.19). The luminescent hybrid composites (powder and transparent film) were prepared by simply mixing organic sensitizer, aminoclay (AC), and lanthanide (Ln^{3+}) in aqueous solution. The tuning of emission color can be achieved by adjusting the molar ratio of Eu^{3+} to Tb^{3+} in the hybrid composite, excitation wavelength, and the temperature. White emission with satisfied CIE color coordinates was achieved. The linear relationship was achieved in the temperature range from 78 K to 288 K for emission intensity ratio of Tb^{3+} ($^5D_4 \rightarrow {}^7F_5$) transition and electric dipole $^5D_0 \rightarrow {}^7F_2$ transition of Eu^{3+} in the hybrid composite containing both Eu^{3+} and Tb^{3+} ions. The obtained unique characteristics make the Eu^{3+} and Tb^{3+} ions containing hybrid composites appropriate for optoelectronic devices (thermosensors and white light LED) [152].

Figure 1.19 Images of luminescent materials with tunable emission colors under 254 nm UV lamp illumination and luminescent films on quartz substrate

Polyfluorene derivative complexed with a europium ion was synthesised and their thermochromism was interpreted by using photophysical properties (Figure 1.20). The pyridine

sites of poly(9,9′-dihexylfluorene-diyl-*alt*-3,5-bipyridinevinylene) act as a coordinating site for Eu ion. The complex integrated with polyfluorene show distinct temperature dependent PL emission color tuning (strong red emission at low temperatures (170–260 K, due to Eu^{3+} ion) and a blue color at higher ones (280–330 K, due to fluorene)), this can be easily visualized by naked eye [153].

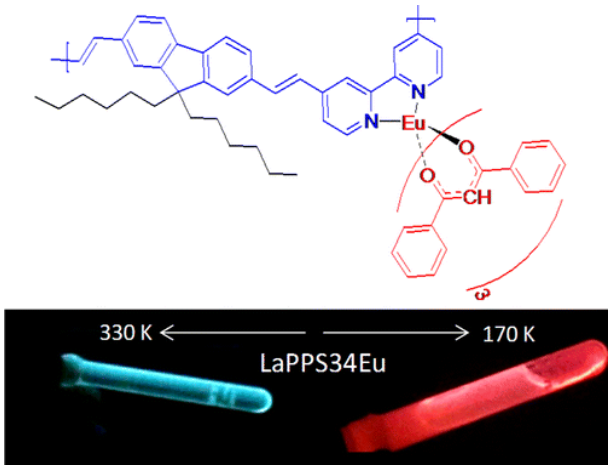

Figure 1.20 The chemical structure of polyfluorene integrated with Eu complex and thermochromism behaviour (color tuning)

Shen *et al.*, reported the hybrid lanthanide complex as a ratiometric sensor [154]. The hybrid system consist of two type of luminescent centre (Eu^{III} and Tb^{III}) with two types of organic ligands, Ad and BPDC (Ad = adeninate, BPDC = biphenyl-4,4'-dicarboxylate). The fluorescent sensing properties of Ad/$Tb_{0.999}Eu_{0.001}$/BPDC complex studied in details and compared the results with those of $Tb_{0.999}Eu_{0.001}$/BPDC with a single ligand. The ratiometric temperature sensing characteristics of the hybrid complex show that the emission color will change from green–yellow to red from 100 K to 300 K, because of energy transfer between Tb^{3+} to Eu^{3+} in the hybrid complex.

Lanthanide-based organic–inorganic hybrid was synthesised by doping the lanthanide^{III}–hexafluoroacetylacetone complex into LAPONITER. The co-doped Eu^{3+} and Tb^{3+},hybrid materials show temperature-dependent luminescence with high sensitivity and stability over a temperature range of 197 K to 287 K, which made it a candidate for ratiometric and colorimetric luminescent thermos-sensors. The PL emission intensity ratio of the $^5D_4 \rightarrow {}^7F_5$ transition (Tb^{3+}) to the $^5D_0 \rightarrow {}^7F_2$ transition (Eu^{3+}) of the hybrid material containing both Eu^{3+} and Tb^{3+} can be linearly related to temperature in the range from 197 K to 287 K (temperature sensitivity: 1.107% per K), which will be an appealing alternative for in situ and real time detection of temperature in many special areas [155].

1.9 Objectives of the present study:

The main aim of the proposed project is to design and synthesis of efficient red emitting molecular complexes based on Eu^{III} with ambipolar ligands. Since most of the red organic-luminophores, currently in use, do not show a good compromise between device efficiency and color purity because of the nature of the red emitters (efficient and bright-dopants are not red enough, and vice-versa). In addition, dual characteristic emissive Eu-complexes to be explored as active component for white LEDs and ratiometric sensors.

1. The main aim of the thesis work is to design and synthesis of bidentate ligand based on phenanthro-imidazole with (capable of the hole transporting group) triphenylamine and carbazole in the C1 – substitution and N1-position with various aromatic groups (phenyl, substituted phenyl and fluorene) for Eu^{III} complexes and investigate their photophysical properties.
2. Binuclear Eu-complexes to be explored to enrich the photoluminescence quantum yield (PLQY).
3. Structural (single crystal X-ray diffraction as well as geometry optimization by theoretical calculations) and photophysical properties of the synthesized ligands and europium complexes to be investigated by various spectroscopic techniques (IR, NMR, ESI-Mass, Elemental analysis, UV-vis, PL).
4. The energy transfer mechanism from ligand to europium to be investigated for the synthesized complexes by using both experimental and density functional theory (DFT), time-dependent density functional theory (TD-DFT).
5. To explore the dual emissive characteristic Eu^{III} complexes for temperature sensors and develop single component white emissive Eu-complexes for white LEDs.
6. The theoretical approach to be used to design various bidentate ligands for Eu^{III} complexes and study their excited state photophysics by combined DFT and TD-DFT.

1.10 References:

[1] K. D. Gundermann, Encyclopedia britannica school and library subscribers, *Luminescence Physics,* 2011 (http://www.britannica.com/science/luminescence).

[1] W. Li, X. D. Xin, S. Y. Feng, Y. Liu, J. Zhang, B. A. Yang and Y. J. Li, *Luminescence*, 2014, **29**, 810–817.

[2] F. Geist, A. Jackel and F. R. Winter, *Dalton Trans.*, 2015, **44**, 3974–3987.

[3] F. Geist, A. Jackel and F. R. Winter, *Inorg. Chem*., 2015, **54**, 10946−10957.

[4] N. Siraj, B. El-Zahab, S. Hamdan, T. E. Karam, L. H. Haber, M. Li, S. O. Fakayode, S. Das, B. Valle, R. M. Strongin, G. Patonay, H. O. Sintim, G. A. Baker, A. Powe, M. Lowry, J. O. Karolin, G. D. Chris and M. W. Isiah, *Anal. Chem.*, 2016, **88**, 170–202.

[5] J. P. Duan, P. P. Sun and C. H. Cheng, *Advances in Technology of Materials and Materials Processing*, 2014, **6**, 95-102.

[6] A. Vogler and H. Kunkely, *Inorganica Chimica Acta.,* 2006, **359**, 4130–4138.

[7] R. L. Morss, *Inorganica Chimica Acta*., 1984, **94**, 31.

[8] W. Centennial, Coordination chemistry of the lanthanide elements–one hundred years of development and understanding, 1967**, 62**, Chapter 21, pp. 306–317.

[9] D. Parker, R. S. Dickins, H. Puschmann, C. Crossland and J. A. K. Howard, *Chem. Rev*., 2002, **102**, 1977−2010.

[10] G. H. Dieke, Spectra and energy levels of rare earth ions in crystals, Interscience Publishers, New York, 1968.

[11] R. Deng, J. Yu, H. Zhang, L. Zhou, Z. Peng, Z. Li and Z. Guo, *Chemical Physics Letters.*, 2007, **443,** 258–263.

[12] S. Petoud, G. Muller, G. Moore Evan, J. Xu, J. Sokolnicki, J. P. Riehl, U. N. Le, S. M. Cohen and K. N. Raymond, *J. Am. Chem. Soc*., 2007, **129**, 77–83.

[13] M. Hu, D. Ma, C. Liu, J. Wang, Z. Zhang and L. Meng, *J. Mater. Chem. C*., 2016, **4,** 6975-6981.

[14] G. Blasse, B. C. Grabmaier, Luminescent materials, springer-verlag publications, 1994.

[15] J. C. G. Bunzli and S. V. Eliseeva, *J. Rare Earth.*, 2012, **28**, 824.

[16] J. C. G. Bunzli and A. S. Chauvin, in Handbook on the physics and chemistry of rare earths, ed. J. C. G. Bunzli and V. K. Pecharski, Elsevier Science Publishers, Amsterdam, 2014, **44**, pp. 169–281.

[17] X. Huang, S. Han, W. Huang and X. Liu, *Chem. Soc. Rev.*, 2013, **42**, 173–201.

[18] H. Liang, Q. Zhang, Z. Zheng, H. Ming, Z. Li, J. Xu, B. Chen and H. Zhao, *Optics Letters*, 2004, **29**, 477–479.

[19] J. Hwan Oh, H. M. Song, Y. K. Eom, J. H. Ryu, M. J. Ju and H. K. Kim, *Bull. Korean Chem. Soc.*, 2011, **32**, 2743.

[20] D. A. Atwood and J. Wiley & Sons, The rare earth elements: fundamentals and applications, *science*., 2013, pp. 696.

[21] F. Piccinelli, M. Bettinelli, A. Melchior, C. Grazioli and M. Tolazzi, *Dalton Trans.*, 2015, **44**, 182.

[22] X. Zhou, X. Zhao, Y. Wang, B. Wu, J. Shen, L. Li and Q. Li, *Inorg. Chem.*, 2014, **53**, 12275–12282.

[23] J. Feng and H. Zhang, *Chem. Soc. Rev.*, 2013, **42**, 387.

[24] E. Yablonovitch, Photonic crystals: semiconductors of light, *scientific American inc*, 2001, **47.**

[25] J. A. Peters, C. A. M. Vijverberg, A. P. G. Kieboom and H. van. Bekkum, *Tetrahedron Letters*, 1983, **24,** 3141-3144.
[26] G. A. Molander, *Chem. Rev*., 1992, **92**, 29–68.
[27] W. M. Momani, Z. A. Taha, A. M. Ajlouni, Q. M. Abu Shaqra and M. A. Zouby, *Asian Pac J Trop Biomed*., 2013, **3,** 367–370.
[28] G. Han, Y. Deng, J. Sun, J. Ling and Z. Shen, *Exp Ther Med.*, 2015, **9**, 1561–1566.
[29] C. Yang, J. Xu, Y. Zhang, Y. Li, J. Zheng, L. Liang and M. Lu, *J. Mater. Chem. C*, 2013, **1**, 4885–4901.
[30] J. C. G. Bunzli, *Chem. Rev.*, 2010, **110**, 2729–2755.
[31] G. Shao, H. Yu, N. Zhang, Y. He, K. Feng, X. Yang, R. Cao and M. Gong, *Phys. Chem. Chem. Phys*., 2014, **16**, 695–702.
[32] M. H. Ho, Y. S. Wu, S. W. Wen, M. T. Lee and T. M. Chen, *Appl. phys. Lett.*, 2006, **89**, 252903.
[33] J. Kido, M. Kimura and K. Nagai, *Science*, 1995, **267**, 1332.
[34] J. Kido, W. Ikeda, M. Kimura and K. Nagai, *Jpn. J. Appl. Phys.*, 1996, 35, L394.
[35] D. Bera, L. Qian, T. K. Tseng and P. H. Holloway, *Materials*, 2010, **3**, 2260-2345.
[36] J. Huang, M. Pfeiffer, A. Werner, J. Blochwitz, K. Leo and S. Liu, *Appl. Phys. Lett.*, 2002, **80**, 139-141.
[37] M. Sun, H. Xin, K. Z. Wang, Y. A. Zhang, L. P. Jin and C. H. Huang, *Chem. Commun.*, 2003, 702–703.
[38] K. Binnemans, *Coord. Chem. Rev.*, 2015, **295**, 1–45.
[39] E. J. New, D. Parker, D. G. Smith and J. W. Walton, *Curr. Opin. Chem. Biol.*, 2010, **14**, 238–246.
[40] J. Hammell, L. Buttarazzi, C. H. Huang and J. R. Morrow, *Inorg. Chem.*, 2011, **50,** 4857–4867.
[41] C. Yang, L. M. Fu, Y. Wang, J. P. Zhang, W. T. Wong, X. C. Ai, Y. F. Qiao, B. S. Zou and L. L. Gui, *Angew. Chem. Int. Ed.*, 2004, **43**, 5010–5013.
[42] M. Latva, H. Takalo, V. M. Mukkala, C. Matachescu, J. C. Rodriguez-Ubis and J. Kankare, *J. Lumin.*, 1997, **75**, 149–169.
[43] H. Xu, Q. Sun, Z. An, Y. Wei and X. Liu, *Coord. Chem. Rev.*, 2015, 293–294, 228–249.
[44] D. L. Dexter, *J. Chem. Phys*., 1953, **21**, 836–850.
[45] G. A. Crosby, R. E. Whan and R. M. Alire, *J. Chem. Phys.*, 1961, **34**, 743–748.
[46] N. M. Baek, Y. H. Kim, D. H. Lee, K. D. Seo and H. K. Kim, *Bull. Korean Chem. Soc.*, 2009, **30**, 1153.
[47] L. Armelao, S. Quici, F. Barigelletti, G. Accorsi, G. Bottaro, M. Cavazzini and E. Tondello, *Coord. Chem. Rev*., 2010, **254**, 487–505.
[48] J. Y. Tsao, M. H. Crawford, M. E. Coltrin, A. J. Fischer, D. D. Koleske, G. S. Subramania, G. T. Wang, J. J. Wierer and R. F. Karlicek, *Adv. Opt. Mater.*, 2014, **2**, 803–809.
[49] Z. Xia and A. Meijerink, *Chem. Soc. Rev.*, 2017, **46**, 275–299.
[50] N. J. Findlay, J. Bruckbauer, A. R. Inigo, B. Breig, S. Arumugam, D. J. Wallis, R. W. Martin and P. J. Skabara, *Adv. Mater.*, 2014, **26**, 7290–7294.
[51] J. B. H. Kwon, H. S. Jang, H. S. Yoo, S. W. Kim, D. S. Kang, S. Maeng, D. S. Jang, H. Kim and D. Y. Jeon, *J. Mater. Chem.*, 2011, **21**, 12812.
[52] (a) H. J. Bolink, F. D. Angelis, E. Baranoff, C. Klein, S. Fantacci, E. Coronado, M. Sessolo, K. Kalyanasundaram, M. Gratzel and Md. K. Nazeeruddin, *Chem. Commun.*, 2009,

4672; (b) P. Coppo, M. Duati, V. N. Kozhevnikov, J. W. Hofstraat and L. De Cola, *Angew. Chem. Int. Ed.*, 2005, **44**, 1806; (c) D. Sykes, I. S. Tidmarsh, A. Barbieri, I. V. Sazanovich, J. A. Weinstein and M. D. Ward, *Inorg. Chem.*, 2011, **50**, 11323.

[53] W. Y. Wong and C. L. Hoa, *J. Mater. Chem.*, 2009, **19**, 4457–4482.

[54] M. A. Katkova and M. N. Bochkarev, *Dalton Trans.*, 2010, **39**, 6599–6612.

[55] H. Chishio, T. Hiroshi, H. Hisahiro and K. Tadashi, *Appl. phys. Let.*, 1992, **60**, 1220.

[56] G. Umberto, P. Mariacecilia, F. Christelle, B. Chiara, P. William and D. Silvia, *J. Phys. Chem. C*, 2009, **113**, 2290–2295.

[57] S. S. Lee, D. Ko, C. H. Chung and S. M. Cho, *Synthetic Metals*, 2002, **128**, 51–55.

[58] A. A. Hany, D. P. Zoran, N. X. Hu, A. M. Hor and X. Gu, *Science*, 1999, **283**, 1900-1902.

[59] I. Koji, O. Hiromitsu and S. Yasuhiko, *Appl. Phys. Lett.*, 1998**,** **72**, 636.

[60] Q. Xin, W. L. Li, G. B. Che, W. M. Su, X. Y. Sun, B. Chu and B. Li, *Appl. Phys. Lett.*, 2006, **89**, 223521–223524.

[61] J. S. Park, J. W. Lee, Y. M. Kim, S. J. Bae, J. Jang, J. K. Kim and B. K. Ju, *Journal of the Electrochemical Society*, 2005, **152**, H196-H199.

[62] J. Wang, R. Wang, J. Yang, Z. Zheng, D. Michael, T. C. Carducci, N. Peyghambarian and E. J. Ghassan, *J. Am. Chem. Soc.*, 2001, **123**, 6179.

[63] A. P. Kulkarni, C. J. Tonzola, A. Babel and S. A. Jenekhe, *Chem. Mater.*, 2004, **16**, 4556–4573.

[64] D. Wagner, S. T. Hoffmann, U. Heinemeyer, I. Munster, A. Kohler and P. Strohriegl, *Chem. Mater.*, 2013, **25**, 3758–3765.

[65] J. Huang, T. Watanabe, K. Ueno and Y. Yang, *Adv. Mater*., 2007, **19**, 739–743.

[66] S. B. Unnat, P. Evgueni, S. James, W. H. Swensen, H. J. Chen, J. Daniel, B. E. Gaspar, A. B. Gnade, P. Padma and A. O. Mohammad, *Appl. Phys. Lett*., 2009, **95**, 233304.

[67] J. P. Duan, S. Pei and C. H. Cheng, *Adv. mater*, 2003, **15**, 224–228.

[68] R. L. White, *J. Appl. Phys.*, 1969, **40**, 1061.

[69] G. Zhiqiang, C. S. Lee, I. Bello, S. T. Lee, R. M. Chen, T. Y. Luh, J. Shi and C. W. Tang, *Appl. Phys. Lett.*, 1999, **74**, 865.

[70] Y. Wu and W. Zhu, *Chem. Soc. Rev*., 2013, **42,** 2039–2058.

[71] W. Zeng, H. Wu, C. Zhang, F. Huang, J. Peng, W. Yang and C. Cao, *Adv. Mater.*, 2007, **19**, 810–814.

[72] C. L. Ho and W. Y. Wong, *Coord. Chem. Rev.*, 2013, **257**, 1614–1649.

[73] G. M. Farinola and R. Ragni, *Chem. Soc. Rev.*, 201, **40**, 33467–33482.

[74] P. Amitava, *Chem. Mater*, 2002, **14**, 4044–4048.

[75] H. Xu, R. Chen, Q. Sun, W. Lai, Q. Su, W. Huang and X. Liu, *Chem. Soc. Rev.*, 2014, **43**, 3259–3302.

[76] J. Kido, K. Nagai and Y. Okamoto, *J. Alloy Compd.*, 1993, **192**, 30–33.

[77] J. Kido, K. Nagai, Y. Okamoto and T. Skotheim, *Chem. Lett.*, 1991, **20**, 1267–1270.

[78] T. Noriyuki, T. Tetsuo and S. Shogo, *Jpn. J. Appl. Phys*., 1994, **33,** L863-L866.

[79] S. Takeshi, F. Masayuki, F. Takanori, H. Yuji, S. Kenichi and K. Kazuhiko, *Jpn. J. Appl. Phys*., 1995, **34,** 1883-1887.

[80] S. Takeshi, N. yoshitaka, H. Yuji, T. Hisakazu, U. Tatsuro and S. Kenichi, *J. Mater. Chem*., 2000, **10**, 157–161.

[81] C. Adachi, M. A. Baldo and S. R. Forrest, *J. Appl. Phys*., 2000, **87**, 8049.

[82] O. Yutaka, K. Hirotake, S. Takumi, U. Hiroshi and Y. Katsumi, *Thin Solid Films*, 2001, **393**, 407–411.
[83] O. Keizou, U. Mesahiro, Y. F. Wang, T. M. Chen and T. Nakaya, *Chemistry Letters*, 1998, 801-802.
[84] O. Keizou, Y. F. Wang and N. Tadao, *Synthetic Metals*, 1998, **97**, 113-116.
[85] Y. Zhang, W. Lei, L. I. Chun, W. J. Zeng, H. H. Shi and C. Yong, *Chin. Phys. Lett.*, 2007, **24,** 1376.
[86] M. Uekawn, Y. Miyamoto, H. Ikeda, K. Kaifu and T. Nakaya, *Synthetic Metals*, I997, **91**, 259–262.
[87] P. He, H. H. Wang, S. G. Liu, J. X. Shi, G. Wang and M. L. Gong, *Inorg. Chem*., 2009, **48**, 11382–11387.
[88] P. He, H. H. Wang, S. G. Liu, J. X. Shi, G. Wang and M. L. Gong, *Appl. Phys*., 2010, **99**, 757–762.
[89] S. G. Liu, R. K. Pan, X. P. Zhou, X. L. Wen, Y. Z. Chen, S. Wang and X. B. Shi, *Inorg. Chim. Acta*., 2013, **395**, 119–123.
[90] S. G. Liu, W. Y. Su, R. K. Pan, X. P. Zhou, X. L. Wen, Y. Z. Chen, S. Wang and X. B. Shi, *Spectrochim. Acta A*., 2013, **103**, 417–422.
[91] H. Wang, P. He, H. Yan, J. Shi and M. Gong, *Inorg. Chem. Commun*., 2011, **14**, 1183–1185.
[92] N. J. Xiang, L. M. Leung, S. K. So and M. L. Gong, *Spectrochim. Acta A.*, 2006, **65**, 907–911.
[93] N. Xiang, Y. Xu, Z. Wang, X. Wang, L. M. Leung, J. Wang, Q. Su and M. Gong, *Spectrochim. Acta A*., 2008, **69**, 1150–1153.
[94] P. P. Sun, J. P. Duan, J. J. Lih and C. H. Cheng, *Adv. Funct. Mater.*, 2003, **13**, 683–691.
[95] P. P. Sun, J. P. Duan, H. T. Shih and C. H. Cheng, *Applied Physics Letters*, 2002, **81**, 792.
[96] X. N. Li, Z. J. Wu, Z. J. Si, Z. Liang, X. J. Liu and H. J. Zhang, *Phys. Chem. Chem .Phys*., 2009, **11**, 9687–9695.
[97] J. Sun, G. Hu, Q. She, Z. Zuo and L. Guo, *Spectrochim. Acta A*., 2012, **91**, 192–197.
[98] A. Pereira, G. Conte, H. Gallardo, C. Zucco, W. G. Quirino, C. Legnani, M. Cremona and I. H. Bechtold, *J. Soc. Inf. Disp*., 2011, **19**, 793–797.
[99] J. Fang, H. You, J. Gao, W. Lu and D. Ma, *J. Lumin.*, 2007, **124**, 157–161.
[100] J. Fang and D. Ma, *Appl. Phys. Lett*., 2003, **83**, 4041.
[101] G. Zucchi, V. Murugesan, D. Tondelier, D. Aldakov, T. Jeon, F. Yang, P. Thuery, M. Ephritikhine and Geffroy, *Inorg. Chem*., 2011, **50,** 4851–4856.
[102] Y. Liu, K. Chen, K. Xing, Y. Wan, H. Jiang, X. Deng, M. Zhu and W. Zhu, *Tetrahedron*., 2013, **69,** 4679–4686.
[103] K. M. Lee, K. W. Cheah, B. L. An, M. L. Gong and Y. L. Liu, *Appl. Phys., A*, 2005, **80**, 337.
[104] H. Iwanaga, A. Amano, F. Aiga, K. Harada and M. Oguchi, *Journal of Alloys and Compounds*, 2006, **408–412**, 921–925.
[105] N. J. Xiang, L. M. Leung, S. K. So, J. Wang, Q. Su and M. L. Gong, 2008, **69**, 1150-1153.
[106] P. He, H. Wang, S. Liu, W. Hu, J. Shi, G. Wang and M. Gong, *Journal of The Electrochemical Society*, 2009, **156**, E46-E49.

[107] P. He, H. Wang, S. Liu, J. Shi, G. Wang and M. Gong, *Electrochemical and Solid-State Letters*, 2009, **12**, B61-B64.
[108] Y. Luo, Q. Yan, Z. Zhang, X. Yu, W. Wu, W. Su and Q. Zhang, *J. Photochem. Photobiol. A*, 2009, **206**, 102–108.
[109] S. Liu, P. He, H. Wang, J. Shi and M. Gong, *Inorg. Chem. Commun.*, 2009, **12**, 506–508.
[110] S. G. Liu, M. L. Gong, S. Wang and X. M. Tan, *Spectrochimica Acta Part A*, 2009, **74**, 731–734.
[111] P. He, H. Wang, S. Liu, J. Shi, G. Wang and M. Gong, *J. Phys. Chem. A*, 2009, **113**, 12885–12890.
[112] A. W. Freeman, M. Urvory and M. E. Criswell, *Inorg. Chem*., 2009, **48**, 11382–11387.
[113] P. He, H. H. Wang, H. G. Yan, W. Hu, J. X. Shi and M. L. Gong, *Dalton Trans.*, 2010, **39**, 8919–8924.
[114] H. Wang, P. He, S. Liu, J. Shi and M. Gong, *Inorg. Chem. Commun.*, 2010, **13**, 145–148.
[115] Z. Wang, N. Xiang, Q. Wang, G. Zhang and M. Gong, *J. Lumin.*, 2010, **130**, 35–37.
[116] H. Wang, P. He, H. Yan, J. Shi and M. Gong, *Inorg. Chem. Commun.*, 2011, **14**, 1183–1185.
[117] H. Wang, P. Hea, H. Yana and M. Gong, *Sensors and Actuators B*, 2011, **156**, 6–11.
[118] N. Sabbatini, M. Guardingli and J. M. Lehn, *Coord. Chem. Rev.*, 1993, **123**, 201–228.
[119] G. Shao, Y. Li, K. Feng, F. Gan and M. Gong, *Sensors and Actuators B*, 2012, **173**, 692–697.
[120] G. Shao, N. Zhang, D. Lin, K. Feng, R. Cao and M. Gong, *J. Lumin.*, 2013, **138**, 195–200.
[121] G. Shao, H. Yu, N. Zhang, Y. He, K. Feng, X. Yang, R. Cao and M. Gong, *Phys. Chem. Chem. Phys.*, 2014, **16,** 695-702.
[122] Z. Wang, H. Yang, P. He, Y. He, J. Zhao and H. Tang, *Dalton Trans*., 2016, **45**, 2839.
[123] J. S. Yagoobi, *Rev. Sci. Instrum.*, 1991, 62, 249– 250.
[124] X. Wang, Q. Liu, Y. Bu, C. S. Liu, T. Liu and X. Yan, *RSC Adv*., 2015, **5**, 86219.
[125] C. D. S. Brites, A. Millan and L. D. Carlos, Handbook on the physics and chemistry of rare earths, 2016, 49, pp. 339–427.
[126] K. Binnemans, *Chem. Rev*., 2009, **109**, 4283.
[127] L. D. Carlos, R. A. S. Ferreira, V. Z. Bermudez, B. J. Lopez and P. Escribano, *Chem. Soc. Rev*., 2011, **40**, 536.
[128] H. Peng, M. I. J. Stich, J. Yu, L. N. Sun, L. H. Fischer and O. S. Wolfbeis, *Adv. Mater.*, 2010, **22**, 716.
[129] F. Vetrone, R. Naccache, A. Zamarron, A. J. Fuente, F. S. Rodriguez, L. M. Maestro, E. M. Rodriguez, D. Jaque, J. G. Sole and J. A. Capobianco, *ACS Nano*, 2010, **4**, 3254.
[130] L. N. Sun, J. Yu, H. Peng, J. Z. Zhang, L. Y. Shi and O. S. Wolfbeis, *J. Phys. Chem. C*, 2010, **114**, 12642.
[131] X. D. Wang, O. S. Wolfbeis and R. J. Meier, *Chem. Soc. Rev.*, 2013, **42**, 7834–7869.
[132] C. D. S. Brites, P. P. Lima, N. J. O. Silva, A. Millan, V. S. Amaral, F. Palacio and L. D. Carlos, *Adv. Mater*., 2010, **22**, 4499–4504.
[133] H. Peng, M. I. Stich, J. Yu, L. N. Sun, L. H. Fischer and O. S. Wolfbeis, *Adv. Mater.*, 2010, **22**, 716–719.
[134] S. Uchiyama, A. P. Silva and K. Iwai, *J. Chem. Educ.*, 2006, **83**, 720–727.

[135] A. Cadiau, C. D. S. Brites, P. M. F. J. Costa, R. A. S. Ferreira, J. Rocha and L. D. Carlos, *ACS Nano*, 2013, **7**, 7213–7218.
[136] Y. Cui, F. Zhu, B. Chen and G. Qian, *Chem. Commun.*, 2015, **51**, 7420–7431.
[137] L. Li, Y. Zhu, X. Zhou, C. D. S. Brites, D. Ananias, Z. Lin, F. A. A. Paz, J. Rocha, W. Huang and L. D. Carlos, *Adv. Funct. Mater.*, 2016, **26**, 8677–8684.
[138] V. Lojpur, M. G. Nikolic and M. D. Dramicanin, *J. Appl. Phys.*, 2014, **115**, 203106.
[139] O. A. Savchuk, P. Haro-Gonzalez, J. J. Carvajal, D. Jaque, J. Massons, M. Aguilo and F. Diaz, *Nanoscale*, 2014, **6**, 9727–9733.
[140] F. Vetrone, R. Naccache, A. Zamarron, J. Fuente, F. S. Rodriguez, L. M. Maestro, E. M. Rodriguez, D. Jaque, J. G. Sol and J. A. Capobianco, *ACS Nano*, 2010, **4**, 3254–3258.
[141] S. Balabhadra, M. L. Debasu, C. D. Brites, L. A. Nunes, O. L. Malta, J. Rocha, M. Bettinelli and L. D. Carlos, *Nanoscale*, 2015, **7**, 17261–17267.
[142] U. Rocha, K. U. Kumar, C. Jacinto, I. Villa, F. S. Rodriguez, M. C. I. Cruz, A. Juarranz, E. Carrasco, F. C. Veggel, E. Bovero, J. G. Sol and D. Jaque, *Small*, 2014, **10**, 1141–1154.
[143] Y. J. Cui, H. Xu, Y. F. Yue, Z. Y. Guo, J. C. Yu, Z. X. Chen, J. K. Gao, Y. Yang, G. D. Qian and B. L. Chen, *J. Am. Chem. Soc.*, 2012, **134**, 3979–3982.
[144] C. D. S. Brites, P. P. Lima, N. J. O. Silva, A. Millan, V. S. Amaral, F. Palacio and L. D. Carlos, *Adv. Mater.*, 2010, **22**, 4499.
[145] (a) M. L. Bhaumik, *J. Chem. Phys.*, 1964, **40**, 3711, 1; (b) S. I. Weissman, *J. Chem. Phys.*, 1942, **10**, 214.
[146] M. Kleinerman, R. J. Hovey and D. O. Hoffman, *J. Chem. Phys.*, 1964, **41**, 4009.
[147] G. E. Khalil, K. Lau, G. D. Phelan, B. Carlson, M. Gouterman, J. B. Callis and L. R. Dalton, *Rev. Sci. Instrum.*, 2004, **75**, 192–206.
[148] S. M. Borisov and O. S. Wolfbeis, *Anal. Chem.*, 2006, **78**, 5094–5101.
[149] J. Yu, L. Sun, H. Pengac and M. I. J. Stich, *J. Mater. Chem.*, 2010, **20**, 6975–6981.
[150] A. Balamurugan, M. L. P. Reddy and M. Jayakannan, *J. Mater. Chem. A*, 2013, **1,** 2256–2266.
[151] T. Wang, P. Li and H. Li, *ACS Appl. Mater. Interfaces*, 2014, **6,** 12915–12921.
[152] D. A. Turchetti, R. A. Domingues, C. Zanlorenzi, B. Nowacki, T. D. Z. Atvars and L. C. Akcelrud, *J. Phys. Chem. C*, 2014, **118**, 30079–30086.
[153] X. Shen, Y. Lu and B. Yan, *Eur. J. Inorg. Chem.*, 2015, **6**, 916–919.
[154] Q. Xu, Z. Li, Y. Wang and H. Li, *Photochem. Photobiol. Sci.*, 2016, **15**, 405–411.

Chapter 2

Effects of electron withdrawing groups in imidazole-phenanthroline ligands and their influence on photophysical properties of Eu^{III} complexes for white light emitting diodes

Abstract

Four europium complexes ($Eu(TTA)_3Phen$-Ph-Ph, $Eu(TTA)_3Phen$-mCF_3-Ph $Eu(TTA)_3Phen$-pCF_3-Ph and $Eu(TTA)_3Phen$-Fl-Ph) were designed and synthesized. The N1-functionalization of the phenanthro-imidazole ring by phenyl, substituted phenyl moiety (CF_3, electron withdrawing group), fluorene and their influence on photophysical and electrochemical properties of Eu^{III} complexes were determined by experimental and theoretical analyses. Among all the ligands, fluorene functionalized ligand shows white emission in the solid state. All the complexes (in solid and solution) showed the distinctive red emission of Eu^{III} ion at 612 nm, due to electric dipole transition ($^5D_0 \rightarrow {}^7F_2$). The absence of ligand emissions (solution, thin film and solid) in the PL emission spectra of Eu^{III} complexes indicate that the efficient energy transfer from ligand to central metal ion (antenna effect), confirmed by DFT, TD-DFT. The HOMO-LUMO levels were determined by cyclic volmmetry studies. The Eu-complex was doped in a PMMA matrix to fabricate the composite film devices ($Eu(TTA)_3Phen$-pCF_3-Ph shown highest quantum yield 78.7 %). The fluorene functionalized ligand was integrated with InGaN LED chip (395 nm, forward bias 20 mA) showed the potentiality of the ligand and shown white emission. The obtained efficient red emission from the fabricated LEDs (Eu^{III} complexes coated on InGaN-based near UV LED) shown that the currently synthesized complexes could be a potential red component for warm white LEDs.

Key words: Eu^{III} complex; PMMA matrix; Energy transfer; Red; White LED

2.1 Introduction:

Organo-lanthanide complexes have received significant attention in recent years, due to their potential application in a variety of fields including analytical techniques, display technology (LEDs/OLEDs), bio-imaging, single molecular magnets, data storage and transfer, metallogel technology [1-5]. Their luminescent features are of special importance, such as sharp line like emissions, long luminescence lifetimes; large stokes shifts, delayed phosphorescence, high fluorescent quantum efficiency, good stability and tunable photophysical properties [6-8]. The Ln's have a unique emission spectrum arising from the Laporte forbidden 4f - 4f electronic transition, which is also responsible for their poor absorption (low oscillator strength) [9]. However, according to Weismann *et al.*, the emission of the metal ions can be enhanced by the introduction of highly sensitive chromophores (energy harvesters) with suitable singlet and triplet energy levels (antennae effect), which can feed the higher energy levels of the Ln ions (to counter the low absorption) [10]. Among the entire Ln's, the europium-based complexes have proved to be efficient red emitters with several scopes of improvement that the demand further probing into the currently existing notions regarding the subject. Aromatic β-diketo compounds have been reported to be an important class of energy harvesters for the Eu^{III} complexes [11, 12]. Most of the Eu-based complexes are reported by using imidazole as a core moiety. The substituted imidazole (N1 position) was reported to have stronger PL emission compared to that of their unsubstituted (alkyl) counterparts [13]. Fluorination of the ligands leads to decrease in the triplet energy state, which facilitates the efficient energy transfer from ligand to central metal ion. The low vibrational frequency of the C-F bond can lower the vibrational quenching in the complex and enhance the PL quantum efficiency [14, 15]. In addition, to facilitate the energy transfer from ligand excited state to Eu^{III} metal ion, suitable excited states are required and ligand triplet level plays a significant role [16, 17].

Smart lighting technology based on solid state lighting (SSL) has proven to be potential (owing to their significant power saving, environmental friendliness, longer lifetime, higher luminous efficiency and brightness) in reducing the global lighting energy use by nearly one half and subsidize significantly to our world's climate change solutions [18]. In SSL, down converting phosphors or organic fluorophores are essential component and play vital role in converting the LED emission into white emission [19–25]. Various approaches have been developed for fabricating white LEDs with the aim of producing white light emission that is optimal for the human eye. Current white LED technology relies on either the blue LED combining yellow emitting phosphor or near UV LED with tricolor phosphor (blue, green, red (RGB). The white light attained from the near ultraviolet (UV) LED conjugated with tricolor phosphor is highly dependence on the color/wavelength convertors, as human eyes are not sensitive to near UV. This method overcome certain technological figure of merit of the blue LED + yellow phosphor based white LEDs such as color rendering index as well as the halo effect.

2.2. Effects of electron withdrawing groups in phenanthro-imidazole ligands and their influence on photophysical properties of Eu^{III} complexes:

2.2.1 Outline of the present study:

Recently, Eu^{III} based molecular complexes gained much attention due to their emerging technological application in warm white LEDs. Several studies were reported on

photoluminescence properties of Eu^{III} complexes and the complexes were conjugated with InGaN (395 nm or 465 nm) chip to produce either red or combining with other emitters to produce white emission [26].

In this chapter, design and synthesis of three new ancillary ligands (Phen-Ph-Ph (1L) (1,2-diphenyl-1H-imidazo[4,5-f][1,10]phenanthroline), Phen-mCF_3-Ph (2L) (1-(3-(trifluoromethyl)phenyl)-2-phenyl-1H-imidazo[4,5-f][1,10]phenanthroline), Phen-pCF_3-Ph (3L) (1-(4-(trifluoromethyl)phenyl)-2-phenyl-1H-imidazo[4,5-f][1,10]phenanthroline)), and their corresponding Eu^{III}-complexes ($Eu(TTA)_3$Phen-Ph-Ph (1-Eu), $Eu(TTA)_3$Phen-mCF_3-Ph (2-Eu) and $Eu(TTA)_3$Phen-pCF_3-Ph (3-Eu)) (Figure 2.1) for white LEDs was systematically investigated. In details, the substitution effect at N1 (mCF_3-Ph, pCF_3-Ph, Ph) and C1 (Ph) position of the imidazole core moiety and their influence on photophysical properties of Eu^{III} complexes were examined. Each of the ligands contains a phenanthroline fragment, substituted aniline, and a phenyl fragment. TTA has gained a choice over other β-diketo complexes, because of the presence of the halogen moieties, it is well documented that the presence of halogen in the structure can reduce the vibrational quenching effect and prolong the PL lifetime of the emitting complexes [27-30].

The photophysical and electrochemical studies (UV, PL spectroscopy and cyclic voltammetry) were carried out for all the ligands and their respective Eu-complexes. Their HOMO-LUMO energy levels were also calculated using density functional theory (DFT) and time-dependent density functional theory (TD-DFT) calculations [30-34]. To understand the mechanism of energy transfer between the ligands and the central metal ion, the singlet and triplet energy levels of the ligands were also calculated. The observations were compared to understand the effects of substitution of different functional groups in the derivative of the phenanthroline ligand, knowledge of which will allow a higher degree of control on the properties of the Eu-complexes to be synthesized. To show the potential use of the presently synthesized ligands as well as Eu-complexes, the compounds were integrated with near UV emitting InGaN LEDs to fabricate red or white LEDs.

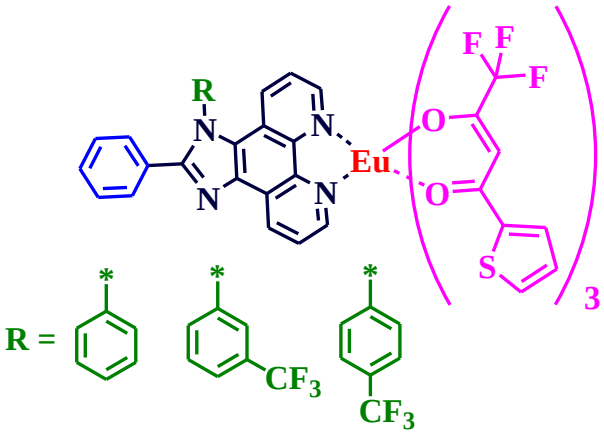

R = Ph, $Eu(TTA)_3$Phen-Ph-Ph
R = mCF_3, $Eu(TTA)_3$Phen-mCF_3-Ph
R = pCF_3, $Eu(TTA)_3$Phen-pCF_3-Ph

Figure 2.1 Chemical structures of the Eu^{III} complexes with respective substitutions.

2.2.2 Experimental Section:

2.2.2.1 Materials:

All the commercially obtained chemicals were used directly without any further modifications unless stated otherwise. 4,4,4-Trifluoro-1-(2-thienyl)-1,3-butanedione (TTA, 99.99%), tetrabutylammonium perchlorate (n-Bu_4NClO_4, 99.9%) electrolyte were purchased from Sigma-Aldrich chemicals company. Europium (III) oxide (99.99%), 1, 10-Phenanthroline, aniline and benzaldehyde were purchased from Alfa Aesar and 4-(trifluoromethyl)benzenamine, 3-(trifluoromethyl)benzenamine were purchased from Avra chemicals. Thin layer chromatography with silica gel 60 F_{254} Aluminium plates (Merk) was used to monitor the reactions. Column chromatography was conducted using 100-200 mesh silica to get the pure compound. All the reactions were carried in inert nitrogen atmosphere.

2.2.2.2 Measurement:

Nuclear magnetic resonance (^{1}H-, ^{13}C-, ^{19}F NMR) spectra were recorded with an AV 400 Avance-III 400 MHz Fourier Transform nuclear magnetic resonance (FT-NMR) Spectrometer Bruker Biospin International, Switzerland, in deuterated chloroform($CDCl_3$) or dimethyl sulfoxide solution (based on the solubility nature). Chemical shifts were estimated relative to the tetramethylsilane (TMS) standard reference. Fourier Transform Infrared (FT-IR) spectra were recorded with a Perkin Elmer, USA/ RX-I FTIR spectrophotometer and elemental analyses were measured by Elementar Analysen Systeme, Germany/Vario EL spectrometer. The mass spectra were recorded by LC–MS (Perkin–Elmer, USA/Flexer SQ 300 M). A single crystal of ligands, a suitable crystal was selected and structures were performed on a Supernova, Dual, Cu at zero, Eos diffractometer. The crystal was kept at 293(2) K during data collection. Using Olex2 [35], the structure was solved with the ShelXS [36] structure solution program using Direct Methods and refined with the ShelXL refinement package using Least Squares minimisation.

2.2.2.3 Photophysical properties:

Absorption analysis was done by using the UV-Visible spectrometer (Shimadzu Corporation, Japan or UV-2450 Perkin Elmer, USA/Lamda 25 and Lamda Perkin Elmer) for a solution and solid form diffuse reflectance spectra (DRS). The PL excitation and emission spectrum in both solid and solution phase for all the samples were recorded with a Horiba Jobin Yvon, USA/Fluoromax 4P spectrophotometer with a 150W xenon lamp as an excitation source. Thin films were prepared by a spin coating method using a spin NXG P1A instrument and measured the PL by spectrofluorimetry. The PL quantum yield (PLQY) of the complex in the form of a solution, a thin film (with a different ratio (PMMA Vs Eu-complexes) and solid were measured with Edinburgh spectrofluorometer FS5, integrating sphere S30. A lifetime of the Eu^{III} complexes and ligands were measured at 298 K with Edinburgh Instruments FLS 980 based on the time correlated single photon counting technology upon the excitation at a suitable wavelength for ligands and complexes, respectively. A pulsed xenon lamp was used as the excitation source and the signals were detected with a photomultiplier. The triplet energy of the ligand was measured with the corresponding Gd-complex at 77 k and liquid nitrogen quartz Dewar was used to record the phosphorescence spectra of the ligand with FLS920 spectrofluorimeter (Edinburgh Instruments Ltd., UK).

2.2.2.4 Electrochemical and theoretical analysis:

Cyclic voltammetry was carried out using AUTOLAB 302N Modular potentiostat at room temperature in N, N-dimethylformamide (DMF) with glass-carbon rod as working, Pt wire as auxiliary and Ag/AgCl wire as reference electrodes. Bu_4NClO_4 (0.1 M) in DMF was used as the supporting electrolyte and scan rate was maintained as 100 mV s^{-1}. All the ligand structures were optimized using density functional theory (DFT) and their respective theoretical UV-Vis spectra were computed using B3LYP/6-31(G) level of theory. The ground state geometry of the ligand structures was confirmed and the ligands were excited vertically to estimate the first excited state using time-dependent DFT (TD-DFT). The same procedure was followed to obtain the triplet excited states from which PL spectra of the compounds were derived. The HOMO and LUMO levels were also been calculated.

2.2.2.5 Synthesis:

The synthesis scheme of the ligands and their corresponding complexes are shown in Scheme 2.1. Europium(III) chloride was synthesized from the Europium(III) oxide through a reported process [37]. The product was then subjected to treatment with alcoholic solution of TTA (3 eq.) in presence of 1N sodium hydroxide solution (3.1 eq.) to get $Eu(TTA)_3(H_2O)_2$. The 1,10-Phenanthroline-5,6-dione was synthesized from 1,10-Phenanthroline by previous reported procedure [38a-b]. The ligand, 1L synthesized by well reported procedure [38c-e].

The Eu^{III} complex was doped with polymethyl methacrylate (PMMA) in 0.1, 0.5 and 1% ratio (PMMA : Eu^{III} = 99.9 : 0.1, 99.95 : 0.5, 99 : 1 in mg and pure complex) by using tetrahydrofuron solution with spin coated by three stages were at 500 (20 sec), 1500 (40 sec) and 2000 rpm (60 sec), respectively. The prepared thin films were kept under vacuum at 50 °C for 3 hrs to get excess solvent evaporation.

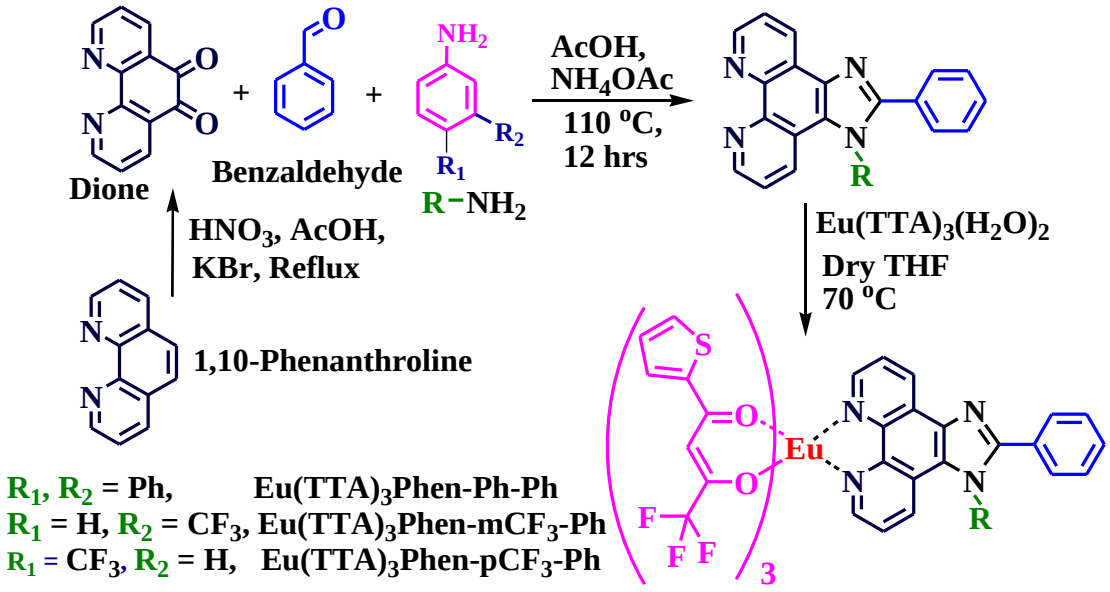

Scheme 2.1 Synthesis scheme for the ligands and the respective complexes.

2.2.2.5.1 ***Synthesis of 1,2-diphenyl-1H-imidazo[4,5-f][1,10]phenanthroline (1L)*****:**

To a stirred solution of 1,10-phenanthroline-5,6-dione (1.0 g, 4.762 mmol) in acetic acid, aniline (0.44 g, 4.762 mmol) and benzaldehyde (0.5 g, 4.762 mmol) were added turn wise followed by ammonium acetate (3.7g, 47.62 mmol) and stirred for 12 hours at 110 °C under nitrogen atmosphere. The reaction was monitored with TLC (MeOH : DCM = 1 : 9). The product was neutralised with ammonium hydroxide solution and extracted with DCM followed by drying with sodium sulphate. It was then concentrated and purified through column chromatography using silica bed (100-200 mesh) with 5% MeOH in DCM as the eluent. The purified product was dissolved in minimal amount of THF and excess amount of hexane was added to it. The solid was allowed to settle down and then the solvent was decanted. The above process was repeated till a fine powder like sediment was obtained. ^{1}H NMR (400 MHz, $CDCl_3$): δ (in ppm) 9.22 (dd, 1 H, *J*= 2Hz, *J*= 1.6 Hz), 9.16 (dd, 1 H, *J*= 1.6 Hz, *J*= 2 Hz), 9.09 (dd, 1 H, *J*= 1.6 Hz, *J*= 1.6 Hz), 7.96 (d, 1 H, *J*= 7.6 Hz), 7.83-7.74 (m, 4 H), 7.53-7.51 (m, 2 H), 7.43-7.34 (m, 6 H). ^{13}C NMR (100 MHz, $CDCl_3$): δ (in ppm) 151.9, 148.7, 147.6, 144.4, 143.9, 138.1, 138.0 135.9, 131.7, 130.6, 129.1, 129.0, 128.9, 128.0, 127.0, 126.4, 126.0, 125.4, 123.4, 123.2, 122.3, 121.7, 120.2, 119.0, 115.9; FT-IR (ν_{str} in cm^{-1}): 3022.2, 2921.2, 1672.0, 1601.4, 1558.7, 1502.1, 1456.8, 1380.1, 1332.2, 1298.1, 1264.4, 1168.1, 1117.0, 1069.2, 1029.3, 805.5, 74.6, 703.6.

2.2.2.5.2 ***Synthesis of 1-(3-(trifluoromethyl)phenyl)-2-phenyl-1H-imidazo[4,5-f][1,10]phenanthroline (2L)****:*

The above procedure was followed for synthesis of Phen-mCF_3-Ph. ^{1}H NMR (400 MHz, $CDCl_3$): δ (in ppm) 9.20 (dd, 1 H, *J*= 1.6 Hz, *J*= 1.6 Hz), 9.165 (dd, 1 H, *J*= 2 Hz, *J*= 1.6 Hz), 9.06 (dd, 1 H, *J*= 1.6 Hz, J= 2 Hz), 9.77 (dd, 1 H, *J*= 4.4 Hz, *J*= 4.4 Hz), 7.69-7.61 (m, 3 H), 7.59 (dd, 2 H, *J*= 2.8 Hz, *J*= 2 Hz), 7.56-7.53 (m, 2 H), 7.30-7.39 (m, 4 H). ^{13}C NMR (100 MHz, $CDCl_3$): δ (in ppm) 151.7, 148.5, 147.4, 144.4, 143.8, 137.4, 135.6, 130.0, 129.9, 129.7, 129.3, 128.8, 128.2, 127.8, 127.5, 126.3, 123.4, 123.0, 121.6, 119.3; FT-IR (ν_{str} in cm^{-1}): 1690.9, 1604.0, 1539.7, 1509.5, 1449.1, 1415.1, 1354.6, 1305.5, 1248.8, 1230.0, 11392.2, 1143.1, 1059.9, 927.7, 787.9, 719.9, 640.6.

2.2.2.5.3 ***Synthesis of 1-(4-(trifluoromethyl)phenyl)-2-phenyl-1H-imidazo[4,5-f][1,10]phenanthroline (3L):***

The same procedure was followed for the synthesis of Phen-pCF_3-Ph. ^{1}H NMR (400 MHz, $CDCl_3$): δ (in ppm) 9.12 (dd, 1 H, *J*=2 Hz, *J*= 1.6 Hz), 9.13 (dd, 1 H, *J*= 1.6 Hz, *J*= 1.6 Hz), 9.07 (dd, 1 H, *J*= 1.6 Hz, *J*= 1.6 Hz), 7.91 (d, 2 H, *J*= 8.4 Hz), 7.79-7.75 (m, 1 H), 7.70 (d, 2 H, *J*= 8.4 Hz), 7.52-7.50 (m, 2 H), 7.42-7.31 (m, 5 H). ^{13}C NMR (100 MHz, $CDCl_3$): δ (in ppm) 151. 75, 149.78, 148.74, 147.61, 144.43, 143.89, 141.49, 140.62, 135.96, 135.42, 135.34, 132.01, 131.68, 131.35, 130.06, 129.11, 129.00, 128.88, 128.07, 127.09, 127.05, 125.97, 124.26, 123.34, 123.12, 122.53, 121.70, 121.56, 118.92); FT-IR (ν_{str} in cm^{-1}): 3011.58, 1592.33, 1495.55, 1468.65, 1451.41, 1235.52, 1293.95, 1181.06, 1129.29, 1072.85, 735.28.

2.2.2.5.4 ***Synthesis of Eu(TTA)$_3$Phen-Ph-Ph:***

In a round-bottom flask, a solution of $Eu(TTA)_3(H_2O)_2$ (0.230 g, 0.27 mmol) in dry THF (15 mL) was taken and to its mixture of Phen-Ph-Ph ligand in THF was added. The mixture was

then stirred for 6 hours at 60 °C in nitrogen atmosphere. It was concentrated and then dissolved in minimum amount of THF. To the solution excess of hexane was added and powder type sediment was obtained. The solvent layer was then decanted and the sediment was dried. The same procedure was repeated several times and obtained final complex in pure powder form. FT-IR (ν in cm^{-1}): 1693.4, 1604.4, 1537.4, 1531.1, 1448.3, 1413.8, 108.6, 1192.2, 141.7, 1064.8, 934.3, 861.6, 852.5, 808.0, 786.4, 721.6, 641.1; Elemental analysis: Anal. Calc. for $C_{49}H_{28}EuF_9N_4O_6S_3$, C, 49.54; H, 2.38; N, 4.72; S, 8.10; found C 49.75, H 2.52, N 4.74, S 8.06.

2.2.2.5.5 *Synthesis of $Eu(TTA)_3Phen\text{-}mCF_3\text{-}Ph$:*

The complex was synthesised in the above mentioned procedure using Phen-mCF_3-Ph as the ligand. FT-IR (ν in cm^{-1}): 1690.9, 1604.0, 1539.7, 1509.5, 1449.1, 1415.1, 1354.6, 1305.5, 1248.8, 1230.0, 1139.2, 1143.1, 1059.9, 927.7, 787.9, 719.9, 640.6; Elemental analysis: Anal. Calc. for $C_{50}H_{27}EuF_{12}N_4O_6S_3$, C, 47.82; H, 2.17; N, 4.46; S, 7.66 (%); found C 47.65, H 2.29, N 4.74, S 7.76 (%).

2.2.2.5.6 *Synthesisi of $Eu(TTA)_3Phen\text{-}pCF_3\text{-}Ph$:*

The complex was synthesized in the previously described steps using Phen-pCF_3-Ph as the ligand instead of aniline as in the first case. FT-IR (ν in cm^{-1}): 1689.8, 1603.5, 1537.2, 1449.5, 1411.4, 1304.6, 1190.2, 1140.7, 1064.4, 938.6, 789.8. 723.2, 641.8; Elemental analysis: Anal. Calc. for $C_{50}H_{27}EuF_{12}N_4O_6S_3$, C, 47.82; H, 2.17; N, 4.46; S, 7.66 (%); found C 47.55, H 2.32, N 4.74, S 7.69 (%).

2.2.3 Results and discussions:

2.2.3.1 Characterization:

All the synthesized ligands and their corresponding complexes were confirmed by different spectroscopic methods (NMR, FT-IR) and Elemental analysis. The NMR data for the ligands (1L, 2L and 3L) are shown in Figure 2.S1 to S3**.** 1L and 3L crystal structures were confirmed by singe crystal X-ray diffraction analysis. The photophysical study of the Eu^{III} complexes and ligands were characterized, by UV-Vis absorption, DRS and PL analyses. The electrochemical and theoretical analyses were also been performed to gain more information regarding the energy levels.

2.2.3.1.1 FT-IR and Single crystal XRD analysis:

The FT-IR analyses were performed to confirm the ligand-metal coordination. The functional group spectral analyses of the ligand were shown in Figure 2.2 (left) and Figure 2.2 (right). The peak appears for the ligands (1L, 2L, and 3L) at ~1671, 1665 and 1590 cm^{-1} were attributed to C=N stretching frequency. However, in the complexes, the same was shifted to ~1600 cm^{-1} spectral region and this evidences that the Eu-complex has formed. In addition, the C=O stretching frequency of the complexes was also changed from ~1608 (without coordination) to ~1690 cm^{-1} (with coordination). It is also evidence that the ligands were coordinated with the Eu^{III} metal ion.

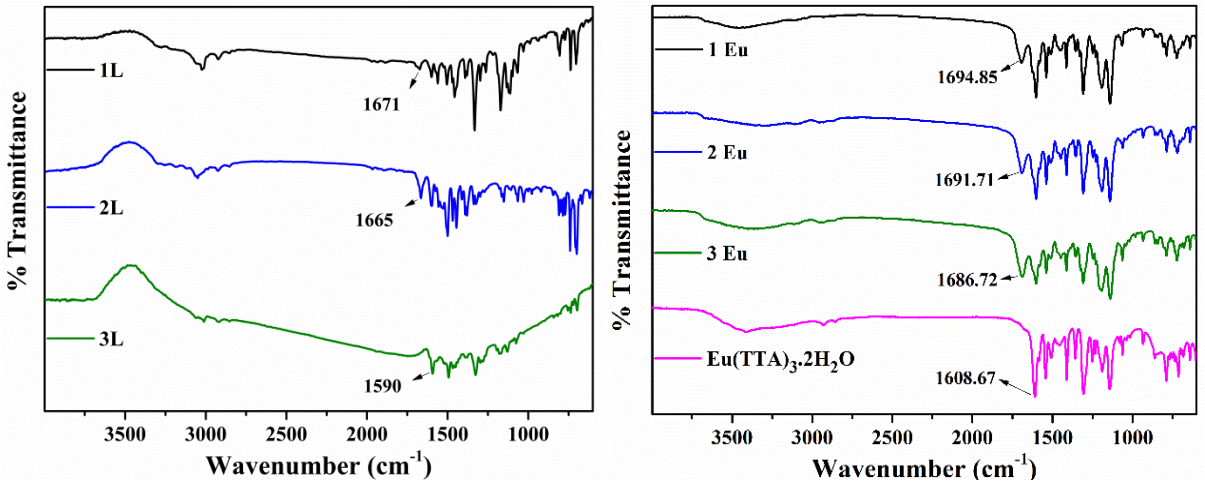

Figure 2.2 The FT-IR spectra of the ligands with their functional groups (left), The FT-IR spectra of the Eu^{III} complexes with their functional groups and its comparison with $Eu(TTT)_3.2H_2O$ (right).

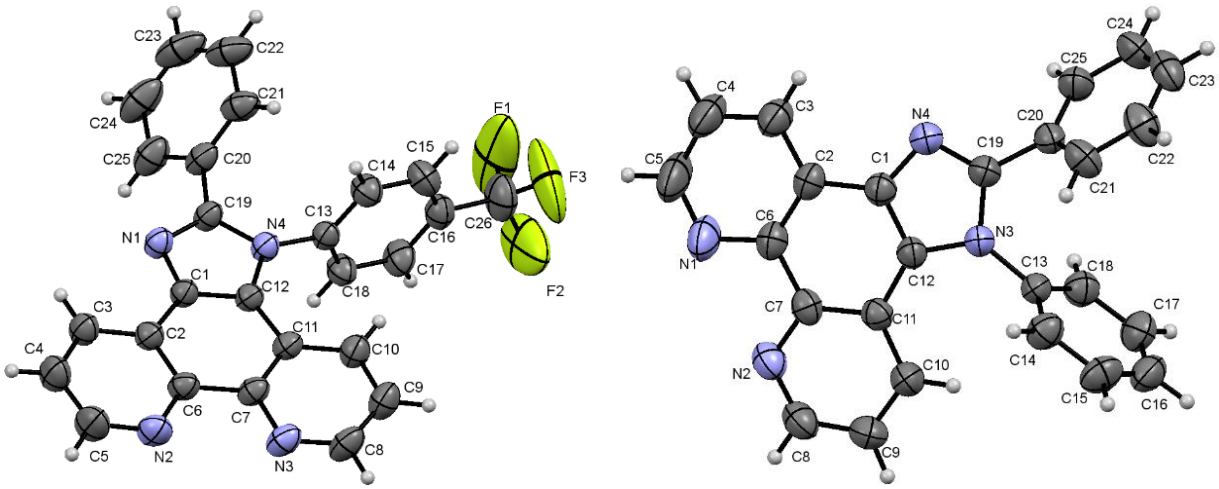

Figure 2.3 Single crystal XRD structures of Phen-pCF_3-Ph (CCDC 1535216) and Phen-Ph-Ph (CCDC 1535217) (blue: Nitrogen, Black: Carbon, White: Hydrogen, yellow: Fluorine).

The fine crystals of ligands, 1L and 3L were isolated from ethanol solution. The single crystal X-ray analysis of the ligands, 1L and 3L, were performed and structurally characterized (ORTEP diagram, Figure 2.3. The obtained single crystal structures of the ligands as well as obtained optimized structures from the computational study showed a similar arrangement of atoms. It clearly indicates that the outcomes obtained from the theoretical analysis are prominent. The structure-refinement parameters of the ligands (1L, 3L) were shown in Table 2.1.

Table 2.1. Crystal data and structure-refinement parameters of Phen-Ph-Ph and Phen-pCF_3-Ph.

Phen-pCF_3-Ph		**Phen-Ph-Ph**	
Empirical formula	$C_{26}H_{15}F_3N_4$	Empirical formula	$C_{25}H_{16}N_4$
Formula weight	440.42	Formula weight	372.42
Temperature/K	293(2)	Temperature/K	293(2)

Crystal system	monoclinic	Crystal system	triclinic
Space group	$P2_1/c$	Space group	P-1
a/Å	8.3313(9)	a/Å	8.8714(8)
b/Å	12.5035(13)	b/Å	10.1323(10)
c/Å	19.8612(18)	c/Å	11.8936(11)
α/°	90.00	α/°	100.266(8)
β/°	93.365(9)	β/°	110.428(8)
γ/°	90.00	γ/°	102.530(8)
Volume/$Å^3$	2065.4(4)	Volume/$Å^3$	939.55(15)
Z	4	Z	2
$\rho_{calc}g/cm^3$	1.416	$\rho_{calc}g/cm^3$	1.316
μ/mm^{-1}	0.105	μ/mm^{-1}	0.080
F(000)	904.0	F(000)	388.0
Crystal size/mm^3	0.401 × 0.342 × 0.249	Crystal size/mm^3	0.43 × 0.197 × 0.161
Radiation	MoKα (λ = 0.71073)	Radiation	MoKα (λ = 0.71073)
2θ range for data collection/°	3.86 to 56.38	2θ range for data collection/°	3.8 to 56.3
Index ranges	$-8 \le h \le 10$, $-16 \le k \le 12$, $-19 \le l \le 26$	Index ranges	$-10 \le h \le 11$, $-13 \le k \le 12$, $-14 \le l \le 7$
Reflections collected	6946	Reflections collected	5698
Independent reflections	4476 [R_{int} = 0.0182, R_{sigma} = 0.0335]	Independent reflections	4043 [R_{int} = 0.0199, R_{sigma} = 0.0445]
Data/restraints/parameters	4476/0/298	Data/restraints/parameters	4043/0/262
Goodness-of-fit on F^2	1.063	Goodness-of-fit on F^2	1.090
Final R indexes [I>=2σ (I)]	R_1 = 0.0738, wR_2 = 0.2022	Final R indexes [I>=2σ (I)]	R_1 = 0.0617, wR_2 = 0.1559
Final R indexes [all data]	R_1 = 0.0937, wR_2 = 0.2224	Final R indexes [all data]	R_1 = 0.0879, wR_2 = 0.1776
Largest diff. peak/hole / e $Å^{-3}$	0.58/-0.51	Largest diff. peak/hole / e $Å^{-3}$	0.18/-0.28

2.2.3.2 Photophysical Studies:

2.2.3.2.1 UV-Vis spectroscopy and diffuse reflectance spectroscopy (DRS):

Ultraviolet **(**UV)-Vis absorption studies for the ligands and the Eu-complexes were measured in chloroform ($CHCl_3$) solution, solid as well as thin film. The normalized UV-Visible absorption spectra of the ligands and their corresponding complexes in solution are given in Figure 2.4. All the ligands were shown absorption maxima (λ_{max}) at 271 nm. The peak in the 270 nm regions can be attributed to the $\pi \rightarrow \pi^*$ transition of aromatic moieties present in the ligand structure. In the complexes, along with the maxima in 270 nm regions, two other peaks have also been observed in the spectrum (~296 nm and 340 nm). Since the 340 nm peaks are characteristic of $Eu(TTA)_3$, so the presence of this peak in the complex can be confirmed the presence of $Eu(TTA)_3$ [39]. Also the appearance of the peak at 272 nm in the complexes confirms that the

ligands were coordinated to the central metal ion. To further understand, the obtained UV spectral absorption, the same analysis was carried out by using computational calculation (both gas phase as well as the solution). The obtained results are supporting the experimental findings (Figure 2.5).

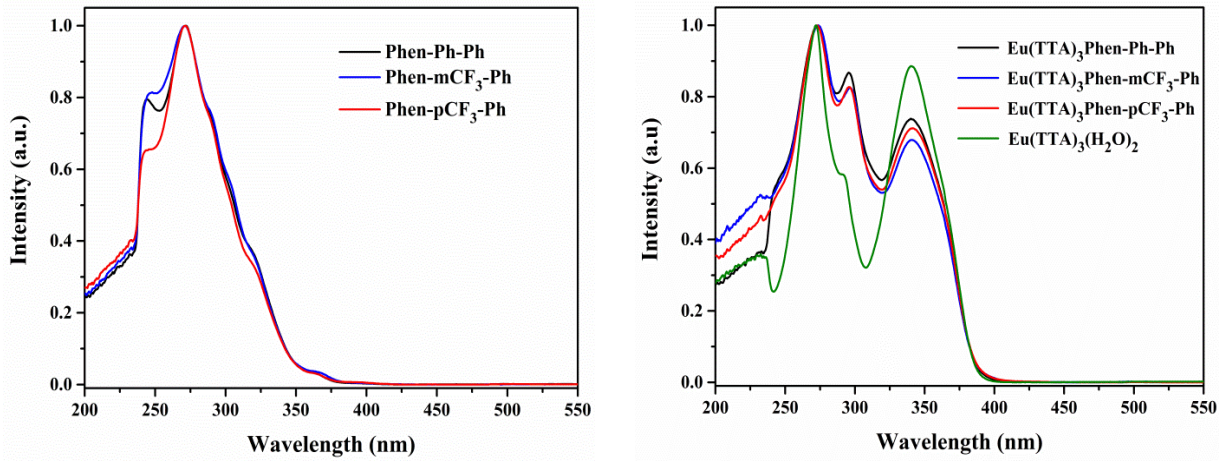

Figure 2.4 The UV-absorption spectra of the ligands (left) and corresponding Eu^{III} complexes (right).

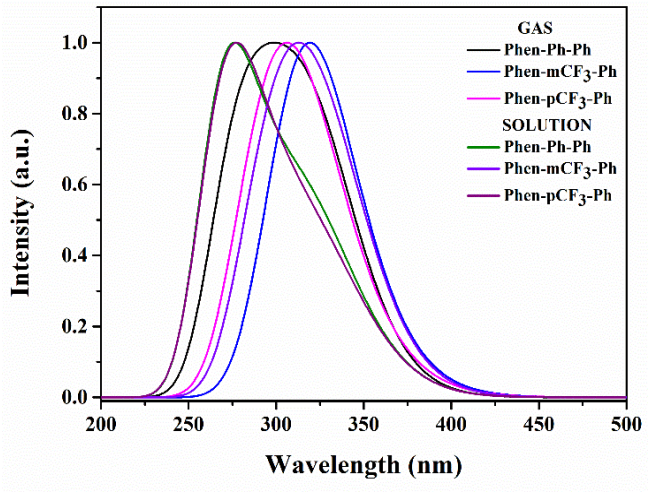

Figure 2.5 The theoretical UV spectra of the ligands in gas phase and DCM solution.

In order to find the optical band gap of the ligands and the complexes, the DRS of the ligands, as well as solids were also carried out. The optical band gaps were calculated for all the compounds by converting the DRS data (Figure 2.6 (left, right)) into Kubelka-Munk function by using the equation 2.1 [40]. The acquired spectrum is converted to Kubelka-Munk function ($\alpha = F(R_\infty)$).

$$\alpha h\nu = A(h\nu - Eg)^n \qquad \ldots\ldots\ldots\ldots (2.1)$$

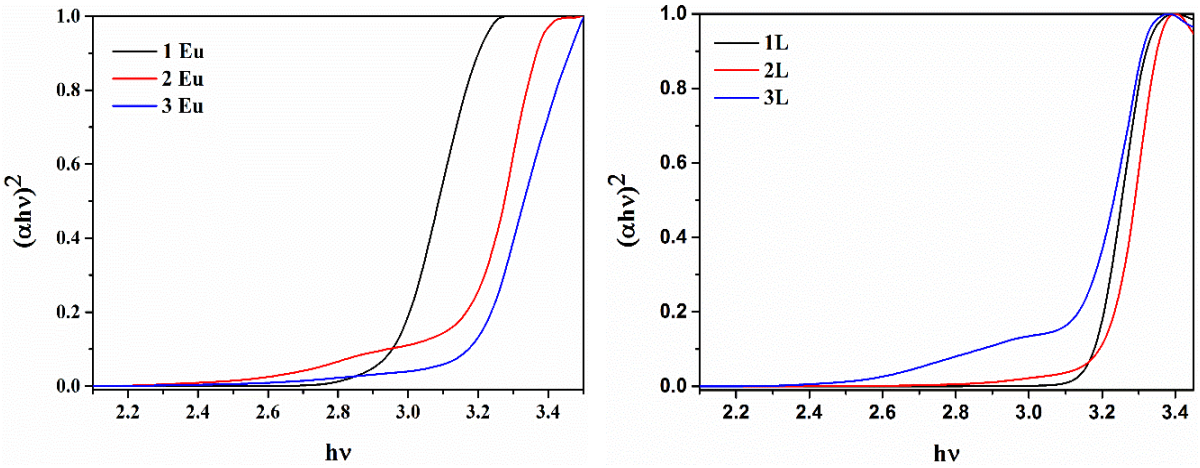

Figure 2.6 The band gap of the Eu-complexes (left) and ligands (right) by diffuse reflectance spectra (DRS).

2.2.3.2.2 Photoluminescence (PL):

The emission of the Eu^{III} complex purely depends on the ligand emission (1L, 2L, 3L) or TTA excited energy levels, because of its forbidden nature of the 4f-4f electronic transition. The solution PL emission studies were carried out for the currently synthesized complexes and the ligands, in solid phase as well as chloroform solution. The PL study of the ligands indicate that all the ligands (1L, 2L and 3L) emit blue photons with the emission maximum (λ_{max}) at 403, 407 and 403 nm under 328, 338 and 328 nm excitation, respectively (Figure 2.7, left). Similar observation was made for ligand emission (~445 nm) in solid state with ~340 nm excitation (Figure 2.7, right). However, both excitation and emission spectra of the ligands were shown little broad and shift towards red region (bathochromic shift) as compare to that of the excitation and emission in the solution. This could be attributed that the aggregation of the ligands in the solid state. The sharp intense red emission was obtained for the Eu^{III} complexes when the blue emitting ligands were coordinated with the Eu^{III} metal ion.

All the synthesized complexes showed a dominant emission peak around 612 nm when excited with a wavelength of 372, 370 and 372 nm for 1Eu, 2Eu, and 3Eu, respectively in solution form (Figure 2.8, left). The obtained intensive emission peak at 612 nm corresponds to the electric dipole transition of Eu^{III} ($^5D_0$-$^7F_2$). Similarly, the complex in the solid state also was shown intense red emission at 612 nm under 275, 365 and 375 nm excitation, respectively (Figure 2.8, right). Foremost, the absence of several bands in excitation spectra of the complexes in the region from 350 to 580 nm ((due to Eu^{III}) (364, 394, 415, 465 and 534 nm corresponds to $^7F_0 \rightarrow {}^5D_4$, $^7F_0 \rightarrow {}^5L_6$, $^7F_0 \rightarrow {}^5D_3$, $^7F_0 \rightarrow {}^5D_2$ and $^7F_0 \rightarrow {}^5D_1$, respectively)) indicating that the efficient energy transfer from ligand to centre Eu^{III} metal ion.

In addition, the absence of ligand emission in the spectral range from 400–550 nm, clearly indicating complete energy transfer. Along with 612 nm emission peak, there are several other emission peaks at 582, 592, (612), 652 and 703 nm ($^5D_0$-$^7F_0$, $^5D_0$-$^7F_1$, ($^5D_0$-$^7F_2$), $^5D_0$-$^7F_3$ and $^5D_0$-$^7F_4$) were observed, this is due to 4f - 4f electronic transitions of the Eu^{III} ion. The observed emission line at ~582 nm is due to $^5D_0$-$^7F_0$ transition indicates that all Eu^{III} ions in the complex crystal structure, occupy a site of the same symmetry and experience the similar crystal field perturbation in the complex. Peaks at 580 and 652 nm are weak forbidden both in magnetic and electric dipole systems. The observed dominant electric dipole (ED) transitions at 612 nm

indicate Eu^{III} ion occupies the non-center of the symmetric site and it is dependent on the coordinate environment (local site) of Eu^{III} ion.

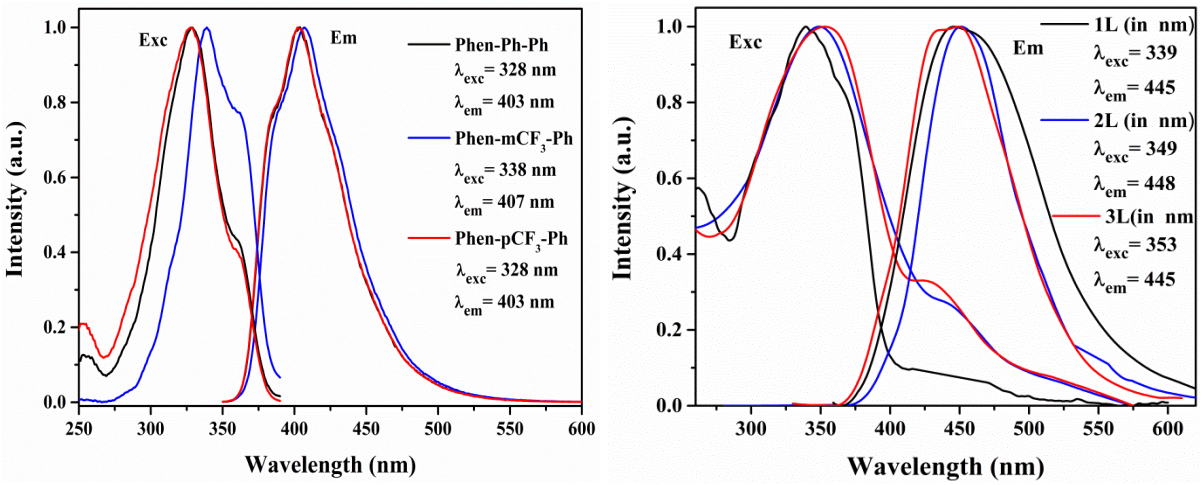

Figure 2.7 The PL excitation and emission spectra of ligands, 1L, 2Land 3L in solution (left) and solid form (right).

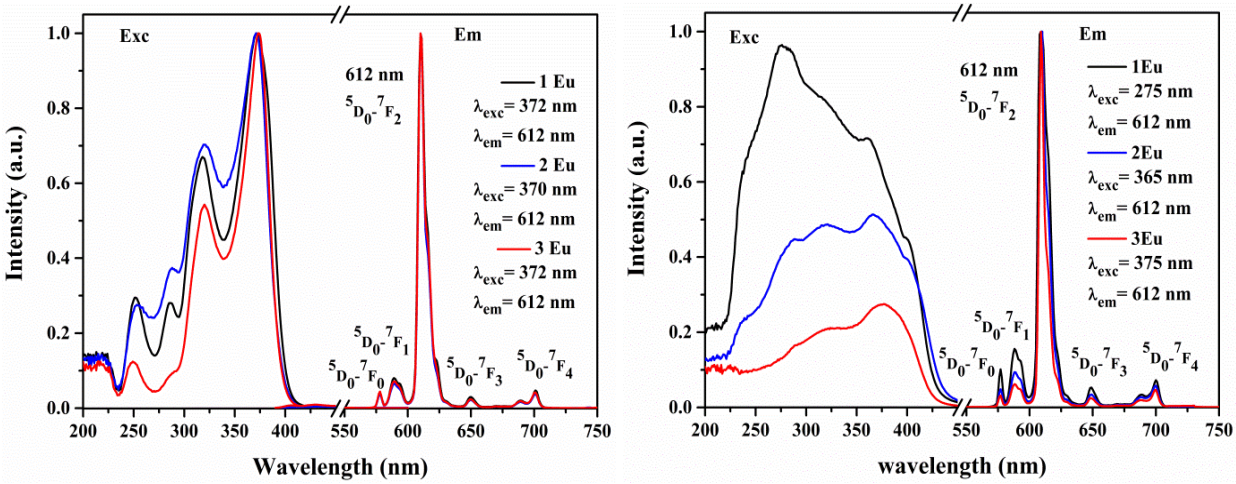

Figure 2.8 The PL excitation and emission spectra of the complexes in solution (left) and solid form (right).

The emission intensity ratio between ED and MD transition is a very important parameter and the value signifies the covalent environment or non-centrosymmetric location of Eu^{III} ion in the crystal structure. From the complex emission spectra, the asymmetric ratio was determined for each of them by calculating the ratio between the intensities of $^5D_0$-$^7F_1$ and $^5D_0$-$^7F_2$ emissions. The intensity ratio (I_2/I_1) of the Eu^{III} complex, 1Eu, 2Eu and 3Eu shown 12.5, 13.9 and 15.2 in solution, respectively. Similarly, the solid showed 6.4, 10.6 and 15.7, respectively. The results are given in Table 2.2 and prove that the complexes are sufficiently asymmetric in nature, which is a desirable property in photoluminescent and electroluminescent materials. It is clear that the Eu^{III} ion and ligand have strong coordination interaction. The details of the intensity ratio of solution and solid were shown in Table 2.ST1. The full width at half maximum (FWHM) of the complexes, 1Eu, 2Eu, and 3Eu was showed 7.3, 5.9 and 6.0 nm in solution; 10.6, 8.0 and 4.9 nm in solid. The solid form of 3Eu shown less FWHM value and 1Eu was shown broad peak

emission, which is ~10 nm. The FWHM of the emission lines are more important since it decides the overall efficiency of the light converting devices (white LEDs) [41].

Table 2.2 Absorption, excitation and emission of the ligands and the corresponding complexes in solution as well as solid.

S. No.	Compound	λ_{abs} (nm)[a,b]		λ_{ex} (nm)[a,c]	λ_{em} (nm)[a,d]	I_2/I_1 (a/e)	FWHM (a/e)
		solution		solid			
1.	**Phen-Ph-Ph**	244, 271, 317	328, 360	339	403, 445[e]	NA	NA
2.	**Phen-mCF_3-Ph**	246, 271, 317	338, 360	349	407, 448[e]	NA	NA
3.	**Phen-pCF_3-Ph**	243, 271, 316	328, 357	353	403, 445[e]	NA	NA
4.	**Eu(TTA)$_3$Phen-Ph-Ph**	296, 340, 342	251, 286, 319, 372	275, 319, 363	612	12.5/ 6.4	7.3/ 10.6
5.	**Eu(TTA)$_3$Phen-mCF_3-Ph**	296, 340, 272	253, 287, 320, 370	287, 319, 367	612	13.9/ 10.6	5.9/ 8.0
6.	**Eu(TTA)$_3$Phen-pCF_3-Ph**	296, 341, 272	248, 286, 319, 372	321, 375	612	15.2/ 15.7	6.0/ 4.9

[a] measured in chloroform solution at 298 K, [b]absorption peaks from the UV-Vis absorption spectra. [c]excitation peaks from PL monitoring emission. [d]emission peaks from photoluminescence emission spectra. [e]emission from PL in solid form. NA = Not applicable

In order to obtain high-efficiency red emission from Eu^{III} ion, it is very much essential to realize the energy transfer between singlet ($^1\pi\pi^*$) and triplet ($^3\pi\pi^*$) energy levels of ligand and subsequent triplet ($^3\pi\pi^*$) to $^5D_0$ level energy transfer to get characteristic red emission from Eu^{III} metal ion. It is well identified that the Eu^{III} metal ion, excited ($^5D_0$) energy level located at 17500 cm^{-1} [42]. Latva *et al.,* investigation explains the difference between ligand triplet ($^3\pi\pi^*$) and the Eu excited state ($^5D_0$) should be > 2500 cm^{-1} [43]. Therefore, considering these facts, one should keep in the mind while designing the ligand electronic structure for Eu-complex. The ligand should have triplet energy level higher than that of $^5D_0$ level of Eu^{III} ion. In accumulation, singlet state should be located higher than >25,000 cm^{-1} and triplet state located higher than >20,000 cm^{-1}. Therefore, in the present study, the singlet and triplet energy state values were calculated by theoretical analysis (DFT and TD-DFT). 1L, 2L and 3L were shown singlet and triplet energy levels at 29,140 (3.61 eV), 29,269 (3.62 eV), 29,342 (3.63 eV) and 22,639 (2.80 eV), 22,607 (2.80 eV), 22,615 (2.80 eV) cm^{-1}, respectively (Figure 2.9). The reported TTA ligand moiety located at around 25,164 (3.12 eV) and 18,954 cm^{-1} (2.35 eV) [44].

The triplet state energy level is higher than that of $^5D_0$ energy level of the Eu^{III} complex (around 3373 cm^{-1}) and it is clearly indicating that the energy gap (ΔE) between triplet state of the ligands and $^5D_0$ energy level of Eu^{III} ion is optimum, which facilitates the energy transfer from ligand to Eu^{III} ion. In addition, energy transfer mechanism of complex, one need to consider the TTA excited singlet and triplet state and it can act as a transitional state between the singlet to triplet excited states of the ligand and triplet excited state to the excited $^5D_0$ level of Eu^{III} ion, respectively. Because the energy gap between ligand triplet state and $^5D_0$ level of Eu^{III} ion was sufficiently more. Thus, one can argue that the energy transfer from ligand triplet state to Eu^{III} metal ion excited level occurs through TTA triplet state. It is well known that the effective energy transfer process from donor to acceptor occurs when there is an effective overlap between the emission spectrum of the donor as well as the absorption spectrum of the acceptor. In order to further understand the energy transfer from the excited energy of the ligand singlet level to TTA moiety (singlet state), we have experimentally found that the overlap of the absorption spectrum

of TTA and the ligand emission spectrum (Figure 2.S4). It is clear that ligand excited energy can transfer to TTA [45]. In addition, the digital images of the complexes as well ligands were shown in Figure 2.10.

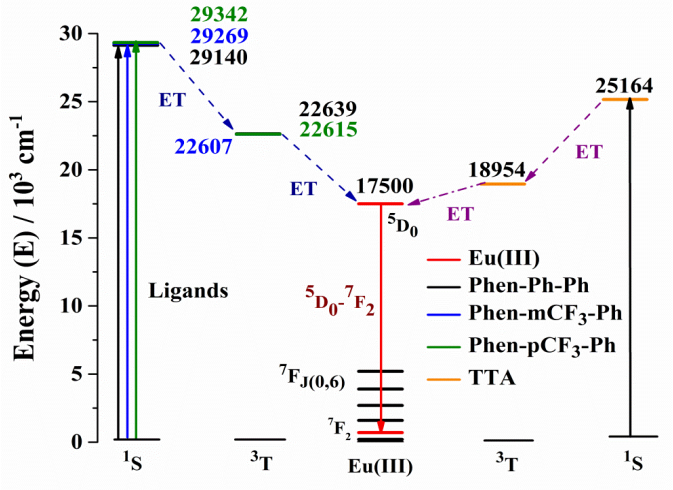

Figure 2.9 Schematic representation of the photophysical process of the Eu^{III} complex via singlet and triplet energy levels of the ligand a TTA and the term states of the Eu^{III} metal ion.

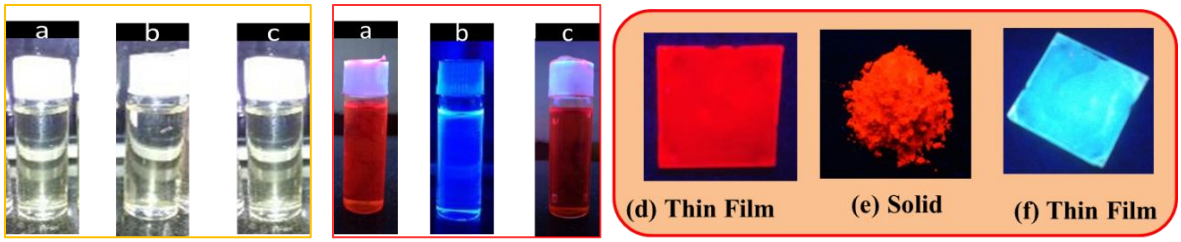

Figure 2.10 Synthesised Eu^{III} complex, ligand and $Eu(TTA)_3$ under normal light, a, b, c (left) and under UV lamp (right) in solution a, b, c; respectively. Thin film of (d) $Eu(TTA)_3$Phen-R-Ph (3 complexes), solid of (e) Phen-R-Ph (3 ligands) and thin film of (f) ligands.

2.2.3.2.3 Photoluminescence quantum yield (PLQY):

The quantum yield of the complexes was calculated using an integrating sphere for both solid samples and complex in chloroform solutions. The absolute quantum yield (φ, QE) (integration sphere) of the complex calculated by the following formulae (2.2 and 2.3) [46].

$$\varphi = \frac{L_0(\lambda) - L_i(\lambda)}{L_0(\lambda)} \quad \text{..... (2.2)}$$

$$\eta = \frac{E_i(\lambda) - (1-\varphi)E_0(\lambda)}{E_0(\lambda)\varphi} \quad \text{..... (2.3)}$$

Where, $L_0(\lambda)$ is the integrated excitation profile (sample is directly excited by the incident beam) and $L_i(\lambda)$ are the integrated excitation profile attained from the empty integrated sphere. $E_0(\lambda)$ is the integrated luminescence of powder caused by direct excitation and Ei(λ) is indirect illumination from the sphere, respectively. The calculated QY of the complexes, 1Eu, 2Eu, and 3Eu are 23.6, 26.5 and 16.3 % in solution, respectively. In the case of solid complexes QY showed is 33.5, 39.4 and 36.5 % for 1Eu, 2Eu, and 3Eu, respectively. The highest observed

quantum yield for 2Eu in solid phase was 26.5 % whereas, that in the chloroform solution was 39.4 %. In addition, fluorination of the ligands (2L and 3L) showed a slight decrease in the triplet energy state compare to that of without fluorinated ligand, which facilitates the efficient energy transfer from ligand to central metal ion. The measured QY results are tabulated in Table 2.4.

2.2.3.2.4 Judd-Ofelt parameters and lifetime analysis:

The Judd-Ofelt parameters for the Eu^{III} complexes were calculated form the PL emission spectra and it is well reported [47-49]. Judd-Ofelt parameters are necessary to know in order to have an idea about the covalent (strong/weak) nature of the complexes. To archive, the faster Eu^{III} radiative rates, design asymmetrical Eu^{III} complexes with larger Ω_2 are preferable. The calculation of experimental intensity parameters Ω_J (J = 2 and 4) was done for $^5D_0 \rightarrow {}^7F_2$ and $^5D_0 \rightarrow {}^7F_4$ transition by keeping $^5D_0 \rightarrow {}^7F_1$ as a reference. The relation between radiative emission rate and integrated emission intensity is given by equation 2.4:

$$\frac{A_{0-2,4}}{A_{0-1}} = \frac{I_{0-2,4}}{I_{0-1}} \frac{h\vartheta_{0-1}}{h\vartheta_{0-2,4}} \quad \text{..... (2.4)}$$

where I_{0-J} represents the area under the spectral curve and $h\upsilon_{0-J}$ is the energy corresponding to the $^5D_0 \rightarrow {}^7F_J$ (J = 1, 2, 4) transition of Eu^{III}. The magnetic dipole radiative transition rate A_{0-1} was taken to be 50 s^{-1} for present calculations. Hence the electric dipole transition probability can be obtained from the above relation. The forced electric dipole transitions $^5D_0 \rightarrow {}^7F_2$ and $^5D_0 \rightarrow {}^7F_4$ as a function of Judd–Ofelt intensity parameter is formulated as (equation 2.5):

$$A_{0-J} = \frac{64\pi^4(\vartheta_{0-2,4})^2}{3hc^3} \frac{1}{4\pi\epsilon_0} \sum_{J=1,2} \chi \left\langle {}^5D_0 \middle| U_J \middle| {}^7F_2 \right\rangle^2 \quad \text{..... (2.5)}$$

Where v is the Lorentz local field correction factor which is a function of refractive index n = 2.02 of the host and is given by the relation $\chi = n\,(n^2 + 9)^2/9$. $\left\langle {}^5D_0 \middle| U_J \middle| {}^7F_2 \right\rangle^2$ are the square reduced matrix elements, independent of the chemical environment of the Eu^{III} ion. The values of non-zero square reduced matrix $\left\langle {}^5D_0 \middle| U_J \middle| {}^7F_2 \right\rangle^2$ = 0.0032 for $^5D_0 \rightarrow {}^7F_2$ transition and $\left\langle {}^5D_0 \middle| U_J \middle| {}^7F_4 \right\rangle^2$ = 0.0023 for $^5D_0 \rightarrow {}^7F_4$ transition were taken for the present calculations. The Judd-Ofelt parameters (Ω_2, Ω_4 values) of the complexes, 1Eu, 2Eu, and 3Eu are interpreted in Table 2.4. From the obtained Ω_{0-2} value, one can agree that the 2Eu and 3Eu complexes are having more covalent character. It could be expected that the presence of $-CF_3$ group in the complexes (2Eu and 3Eu).

Luminescence decay curves of the Eu^{III} complexes $^5D_0$ excited state were measured at 298 K and under 360 nm excitation source (Figure 2.11). The lifetime data of the ligands and the respective complexes were fitted with the single exponential function given by the equation, $I(t) = I_0 + A_1 \exp\left(\frac{-t}{\tau}\right)$; where A_1 is the scalar quantity obtained from the curve fitting of the complex, t is time in mille second, $I_0 = 0$ is the offset value and τ is the decay time value for the exponential component. However, some of the complexes in solid, thin film and most of the ligands are best fitted with the bi-exponential curve and details are inferred in Table 2.3.

The lifetime of the complexes and the ligands were calculated both in solid phase as well as in solution (different solvents). It was observed that the longer lifetimes were obtained in dichloromethane, acetone, and dimethyl sulfoxide solutions for the complexes 1Eu, 2Eu, and 3Eu, respectively. It indicates that the complexes in DCM, acetone, and DMSO have less non-radiative transitions pathway. The observed order for three complexes were: 1Eu: Acetone >

dichloromethane (DCM) > dimethyl sulfoxide (DMSO) > Toluene > Chloroform ($CHCl_3$) > Tetrahydrofuran (THF) > Solid > dimethylformamide (DMF); 2Eu: DCM > Acetone > DMSO > Toluene > $CHCl_3$ > THF > Solid > DMF; and 3Eu: DMSO > Acetone > Toluene > DCM=$CHCl_3$ > THF > DMF > Solid, respectively. Very less lifetime observed in the case of the Eu complexes in the solid phase. It could be expected that the close packing of the molecules in the solid state leads to non-radiative relaxation via vibrionic coupling than that of the solution [50].

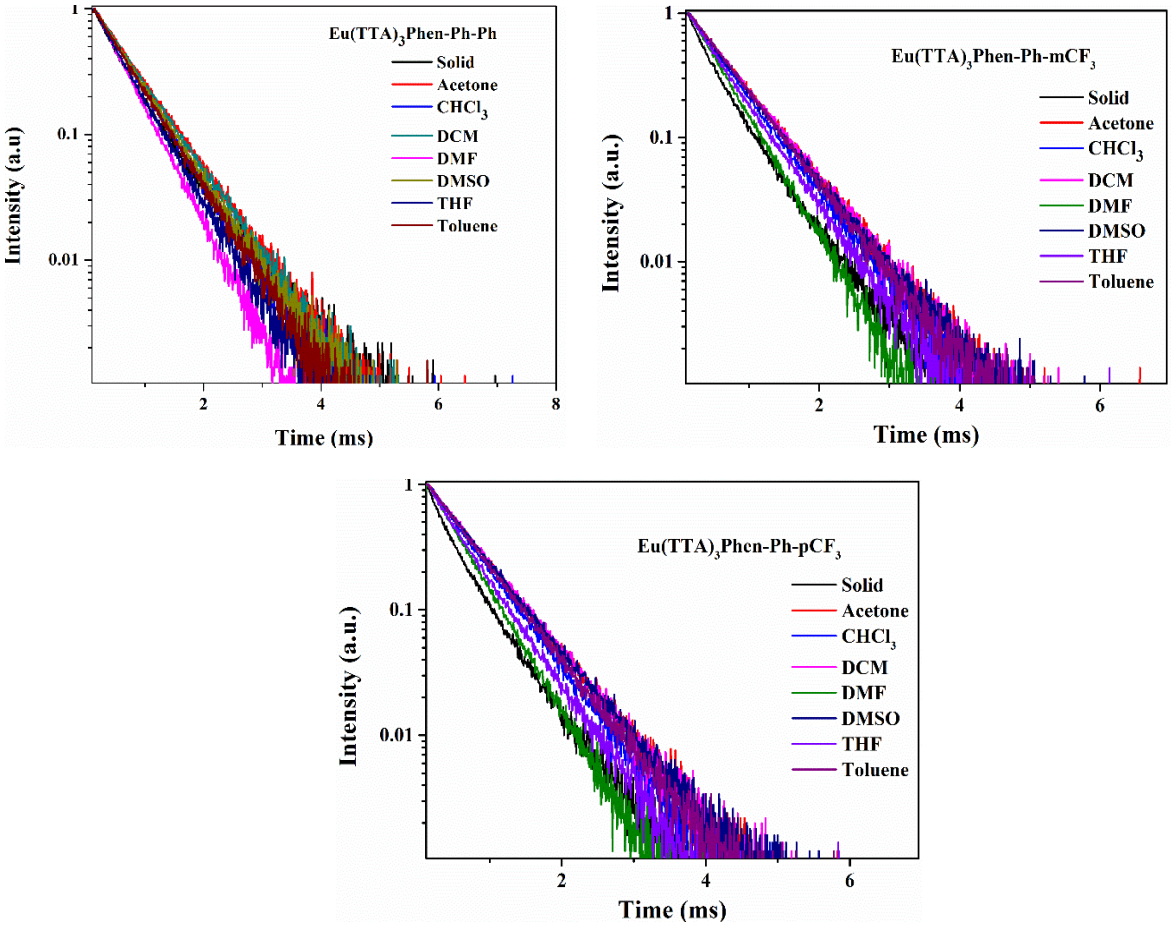

Figure 2.11 The lifetime of the complexes, 1Eu, 2Eu and 3Eu in different solvents.

The lifetime of the ligands, 1l, 2L and 3L are showed in Figure 2.S5 to 2.S7, respectively. The obtained ligand lifetime out comes was also shown the longer lifetimes in dichloromethane, acetone and dimethyl sulfoxide. In addition, the PMMA matrix thin film of the complexes shown improved lifetime and found to be highest lifetime is 0.665 ms (0.1 %) for 2Eu complex (Figure S11-13). When the concentration increasing from 0.1 to 1 %, the lifetime was also increased and afterwards lifetime was reduced. It may be due to the presence of Eu^{III} ions close packing in the concentrated thin film (leads to concentration quenching) [51] of the complexes and leads to non-radiative enhancement via decreasing the lifetime.

Table 2.3 Lifetime of the complexes and ligands in solution and solid phase.

S. No.	Compound	Lifetime (in ms)							
		Solid	Acetone	$CHCl_3$	DCM	DMF	DMSO	THF	Toluene
1	1Eu	0.500[a]	0.648	0.573	0.632	0.479	0.597	0.513	0.580
2	2Eu	0.466[a]	0.609	0.555	0.612	0.453	0.592	0.506	0.587
3	3Eu	0.416[a]	0.596	0.548	0.548	0.449	0.598	0.49	0.574
4	1L[a]	0.002	0.0024	0.0019	0.0019	0.0028	0.0026	0.0018	0.0025
5	2L[a]	0.0019	0.0018	0.0019	0.0021	0.0019	0.0038	0.0019	0.0025
6	3L[a]	0.0017	0.0022	0.0019	0.0024	0.002	0.002	0.0019	0.0021

[a]Bi-exponential fitting. Luminescence intensity could be described by the sum of two exponential decay components from $I(t) = A_1\exp(-\frac{t}{\tau_1}) + A_2\exp(-\frac{t}{\tau_2})$, Here, τ_1 and τ_2 are short- and long-decay components, A_1 and A_2 are fitting constants. The average lifetime τ is $=(\frac{A_1\tau_1^2 + A_2\tau_2^2}{A_1\tau_1 + A_2\tau_2})$.

To understand further, the overall quantum yield ($\Phi_{overall}$) (Eqn. 2.6) was calculated and other lifetime parameters also been calculated for Eu^{III} complexes. The $\Phi_{overall}$ obtained under ligand excitation and it depends on two essential parameters. The primary one, efficiency of energy transfer from the ligand to the Eu^{III} ion (Φ_{sens}), and another one is the intrinsic quantum yield (Φ upon direct excitation into the f level) [52, 45b].

$$\Phi_{overall} = \Phi_{sens}\,\Phi_{Ln} \quad \ldots\ldots\ldots\ldots\ldots\ldots\ldots (2.6)$$

The intrinsic quantum yield (Φ_{Ln}) of the Eu^{3+} ion can calculate with τ_{obs} and τ_{rad} lifetime, the equation (2.7) followed as

$$\Phi_{Ln} = \left(\frac{A_{RAD}}{A_{RAD} + A_{NR}}\right) = \frac{\tau_{obs}}{\tau_{RAD}} \quad \ldots\ldots\ldots\ldots\ldots\ldots\ldots (2.7)$$

The radiative lifetime (τ_{RAD}) can be calculated by corrected emission spectrum according to using equation 2.8. It is assuming that the energy of the $^5D_0 \rightarrow {}^7F_1$ (MD) transition and its oscillator strength are constant. Here, I_{TOT}/I_{MD} is the ratio of the total area of the corrected Eu^{III} emission spectrum to the area of the $^5D_0$ - $^7F_1$ band, $A_{MD,0}$ (14.65 s^{-1}) represents the spontaneous emission probability of the $^5D_0$ - $^7F_1$ transition (in vacuo), and n is the refractive index of the medium. An average index of refraction (1.5) was employed in the calculation [53].

$$A_{RAD} = \left(\frac{1}{\tau_{RAD}}\right) = A_{MD,0}\,n^3\,\left(\frac{I_{TOT}}{I_{MD}}\right) \quad \ldots\ldots\ldots\ldots\ldots\ldots\ldots (2.8)$$

From the relative areas of the $^5D_0$–^7F_J emission transitions (which associates with the already predicted J–O theory) of Eu^{3+} ion is used to determine the experimental branching ratio ($\beta_{1\text{-}3}$). In general, the efficiency of the energy transfer from the ligand to Eu^{III} ion can be predicated by the obtained intrinsic quantum yield (Φ_{Ln}) and energy transfer efficiency (Φ_{sen}). The calculated value for the presently studied complex indicates that the currently studied ancillary ligand is an efficient sensitizer for the Eu^{3+} ion. All the calculated parameters are tabulated in Table 2.4. In addition, the calculated experimental branching ratios ($\beta_{1\text{-}3}$) of the complexes were also investigated in Table 2.ST2.

2.2.3.2.5 PMMA film study of Eu^{III} complexes and CIE color coordinates:

The PL emission of the complexes in solution, as well as solid, was studied. In addition, thin film analysis by using PMMA as a matrix in different ratio with Eu complex to fabricate the composite film devices. It is well-known that the PMMA can easily prepared polymer (excellent

optical quality) and cost effective. It was observed that all the three complexes as the concentration were increased (0.1 to 5 through 0.5 and 1), there was an increase in the intensity of the $^5D_0$-$^7F_1$ transition, thus signaling activation of magnetic dipole transitions and at the same time splitting of $^5D_0$-$^7F_2$ peak is also observed (at 5 %). This can be attributed to the aforementioned reason (Figure 2.12). In addition, the calculated I_2/I_1 asymmetric ratio values are decreasing with increasing the concentration of Eu-complex in the thin film. The corresponding FWHM (nm) showed increasing with increasing the concentration (in all the complexes).

Obtained results one can conclude that the concentration inversely proportional to intensity ratio values and proportional to the FWHM. The highest intensity ratio is found to be ~9 and highest FWHM is ~17 nm. The calculated intensity ratio as well FWHM outcomes are interpreted in the Table S2. Further, absolute QY of the composite film devices (0.1, 0.5, 1 and 5 %) of the complexes (1Eu, 2Eu, and 3Eu coated with PMMA film) was measured, shown for 1Eu is 58.6% (1%), 2Eu is 63.8 (0.5%) and 78.7% (5%), respectively. The fluorinated bipolar ligand containing complexes were shown highest QY as compared to that of free fluorinated Eu-complex (1Eu). The obtained results are suggesting that the 1 and 5 % Eu complex doping is suitable, whereas the increasing concentration of Eu-complex in PMMA matrix leads to energy transfer between the Eu^{III} ions themselves through as a non-radiative process, instead of to reach the ground state (radiative). The obtained results from the lifetime of thin films were also supporting the same.

Table 2.4 The J-O parameters (Ω_2 and Ω_4), Radiative (A_{RAD}) and nonradiative (A_{NR}) decay rates, $^5D_0$ lifetime (t_{obs}), intrinsic quantum yield (Φ_{Ln}), energy transfer efficiency (Φ_{sen}) and overall quantum yield ($\Phi_{overall}$) for complexes.

S. No.	Compound	Ω_2	Ω_4	A_{RAD}	A_{NR}	τ_{obs}	τ_{RAD}	Φ_{Ln}	Φ_{Sen}	$\Phi_{Overall}$
		(10^{-20} cm^2)		(S^{-1})	(S^{-1})	(ms)	(ms)	(%)	(%)	(%)
1.	**1Eu, Solution**			728.7	101	0.573	1.37	41.75	80.2	33.5
2.	**Solid**	3.64	0.34	408.1	159	0.500	2.45	20.4	11.7	23.6
3.	**Thin film, 0.1%**			313.7	128	0.627	3.19	19.7	10.5	20.6
4.	**0.5 %**			349.0	131	0.604	2.86	21.0	19.0	40.1
5.	**1 %**			257.4	130	0.642	3.88	16.8	34.7	58.6
6.	**5 %**			199.6	150	0.587	5.02	11.7	--.--	--.--
7.	**2Eu, Solution**			888.5	913	0.555	1.12	49.31	79.9	39.4
8.	**Solid**	6.02	0.46	610.6	154	0.466	1.64	28.4	93.2	26.5
9.	**Thin film, 0.1%**			323.0	118	0.665	3.09	21.4	15.3	32.8
10.	**0.5 %**			261.8	138	0.610	3.81	16.01	23.6	37.8
11.	**1 %**			260.8	132	0.634	3.83	16.6	38.4	63.8
12.	**5 %**			211.2	141	0.615	4.73	13.0	--.--	--.--
13.	**3Eu, Solution**			810.3	101	0.548	1.23	44.4	82.1	36.5
14.	**Solid**	8.96	0.58	852.3	155	0.416	1.17	35.6	45.8	16.3
15.	**Thin film, 0.1%**			351.3	129	0.609	2.84	21.5	13.6	29.2
16.	**0.5 %**			225.1	136	0.631	4.44	14.2	37.1	52.7
17.	**1 %**			318.1	133	0.608	3.14	19.3	23.2	44.9
18.	**5 %**			206.4	149	0.587	4.84	12.1	64.8	78.7

The highest QY was obtained for thin film than in the solution state, indicate that the fluorination could reduce the non-radiative energy migration in the complex and thus it leads to higher QY in a thin film. In addition, the PPMA matrix can reduce the collisional quenching of

the ligand triplet state in the polymer matrix leads to enhance the QY. In other words, the long chain of the PMMA and rigidity may lead to near the donor and acceptor in the Eu-complex through efficient inter molecular energy transfer. Similar results also been documented, in highly fluorinated carbazole substituted β-diketonate ligand consisted Eu-complexes shown photoluminescence quantum yields 79-84 % (thin film) [54a]. Further, it is also comparable with the reported luminescent β-diketonate europium complexes doped in PMMA matrixes [54b-d].

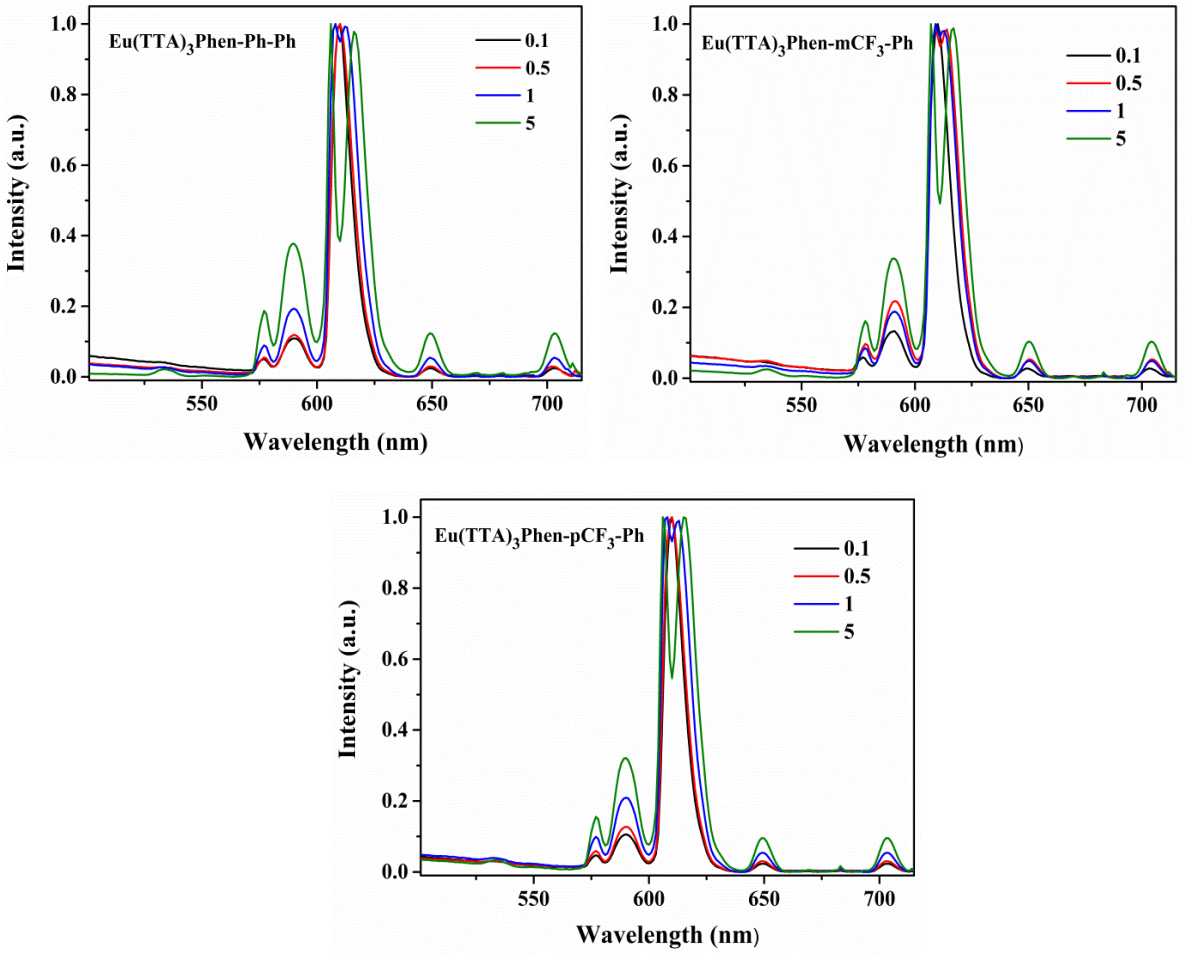

Figure 2.12 The PL emission spectra of the complexes, 1Eu, 2Eu and 3Eu in a thin film by using PMMA matrix.

The CIE color coordinates were calculated using a MATLAB software package from the emission spectral data of both the solid and solution phase of the samples. The calculated results are given in Figure 2.13 (screen shot of the absolute QY measurement is given in Figure 2.S9). The detailed investigation of CIE for the ligands and complexes in solution as well as solid were given in Table 2.ST4 to 2.ST7. It can be seen that all the ligands have emission in the blue region, whereas the complexes all emit in the red region in both solution and solid state. When the concentration increasing, the CIE value moves towards pure red emission in spectra. However, a thin film of the all the complexes shown red emission and the corresponding CIE color coordinates are also confirmed the same. In addition, the values are well matched with the NTSC standard values and the calculated CIE values for all the thin films (different Eu complex ratio) are tabulated in Table 2.ST3.

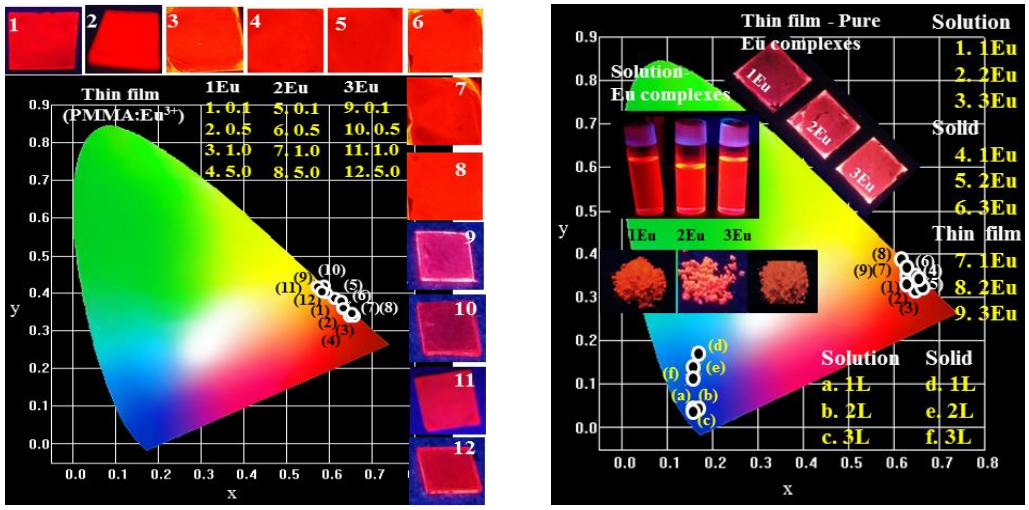

Figure 2.13 The calculated CIE color coordinates of Eu^{III} complexes in PMMA matrix (inset thin film digital images under UV light, left), and ligands and respective complexes in solution, solid and thin film (inset digital images of solution, solid and thin film under UV light (365 nm) (right)).

2.2.3.3 Electrochemical properties:

The cyclic voltammetry (CV) analysis was carried for the ligands and their respective complexes. The potential Vs. current curves of the ligands and the complexes is provided in Figure 2.14. The onset potentials (E_{onset}) of the complexes can be utilized further to calculate their HOMO and LUMO energy levels with the formula (2.9 and 2.10): [55]

$$E_{HOMO} = -(E_{Onset}^{Ox} + 4.4)eV \quad \ldots\ldots\ldots\ldots\ldots\ldots\ldots (2.9)$$

$$E_{LUMO} = -\left(E_{Onset}^{Red} + 4.4\right)eV \quad \ldots\ldots\ldots\ldots\ldots\ldots\ldots (2.10)$$

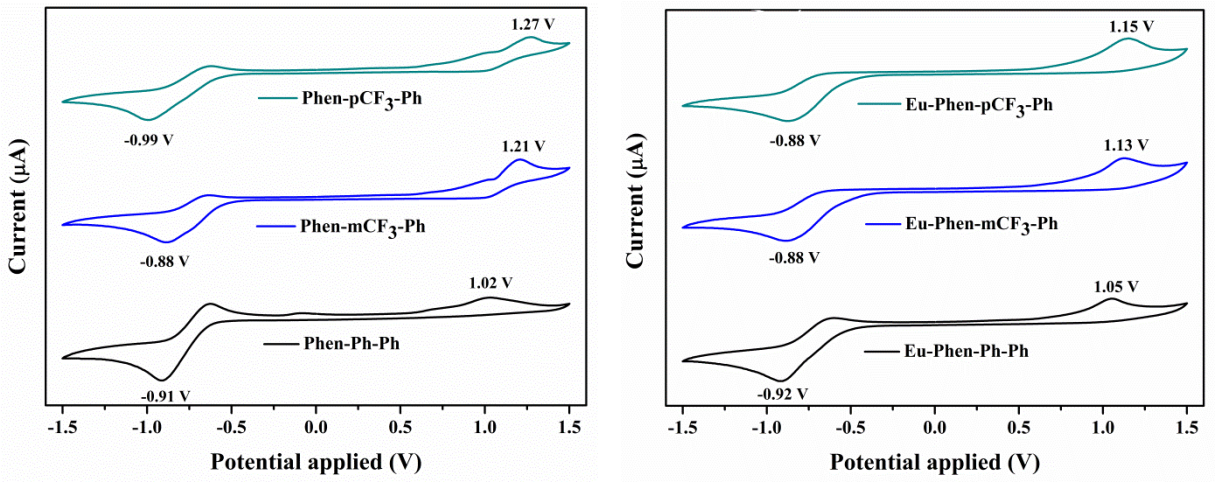

Figure 2.14 The Cyclic voltammetry plot of the ligands (left) and the corresponding complexes (right).

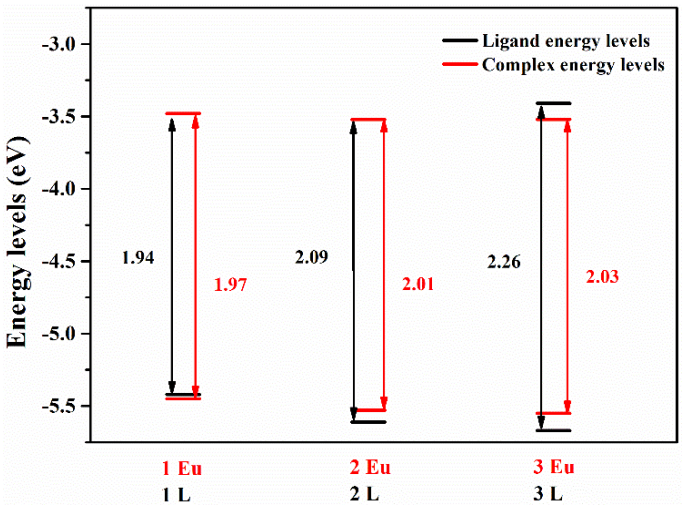

Figure 2.15 The energy levels of the complex and corresponding ligands.

The results are given in Table 2.5 and the relative levels of the HOMO and LUMO of the corresponding complexes and ligands are given in a pictorial view (Figure 2.15). The currently studied complexes follow each redox reaction involves a reversible one-electron transfer and it is responsible by the phenanthromidazole (phen and imidazole) as well as fluorine moieties. The obtained HOMO and LUMO levels of the complex and ligands are shown less variation. The complexes have a lower HOMO level compared to that of the ligands which prove that the ligands were coordinated. Also, a lower band gap on the complex indicates towards the bathochromic shift in the emission of the complex as compared to that of the ligands. The calculated energy gap of the complexes is showed at ~2.0 eV, which is the best association to obtain the red emission.

Table 2.5 Onset oxidation and reduction potentials of the ligands and complexes.

S. No.	Compound	$Voltage_{onset}^{Ox}$ (V) (E_{HOMO} (eV))	$Voltage_{onset}^{Red}$ (V) (E_{LUMO} (eV))	Energy gap (eV)	Wavelength (nm)
1.	**Phen-Ph-Ph**	1.016 (-5.42)	-0.916 (-3.48)	1.94	639
2.	**Phen-mCF_3-Ph**	1.208 (-5.61)	-0.889 (-3.52)	2.09	593
3.	**Phen-pCF_3-Ph**	1.271 (-5.67)	-0.992 (-3.41)	2.26	548
4.	**Eu(TTA)$_3$Phen-Ph-Ph**	1.051 (-5.45)	-0.916 (-3.48)	1.97	629
5.	**Eu(TTA)$_3$Phen-mCF_3-Ph**	1.127 (-5.53)	-0.884 (-3.52)	2.01	616
6.	**Eu(TTA)$_3$Phen-pCF_3-Ph**	1.152 (-5.55)	-0.878 (-3.52)	2.03	610

2.2.3.4 Theoretical Calculations:

The ligand structures were first optimized in the gas phase using DFT and Becke three-parameter Lee-Yang-Parr (B3LYP) form for exchange-correlation potential and 6-31G (d, p) basis set [56, 30]. All the structures were found to be in the minima of the potential energy surface as the normal mode of frequencies are all positive. After that, the UV−Vis spectra calculations were performed using time-dependent density functional theory (TD-DFT) with gas phase optimized geometries. Taking into consideration that the geometry of the molecule might

change in solvent phase the optimization of the geometries under solvent phase has also been carried out. We found that there is no such prominent change in the geometries of the molecule.

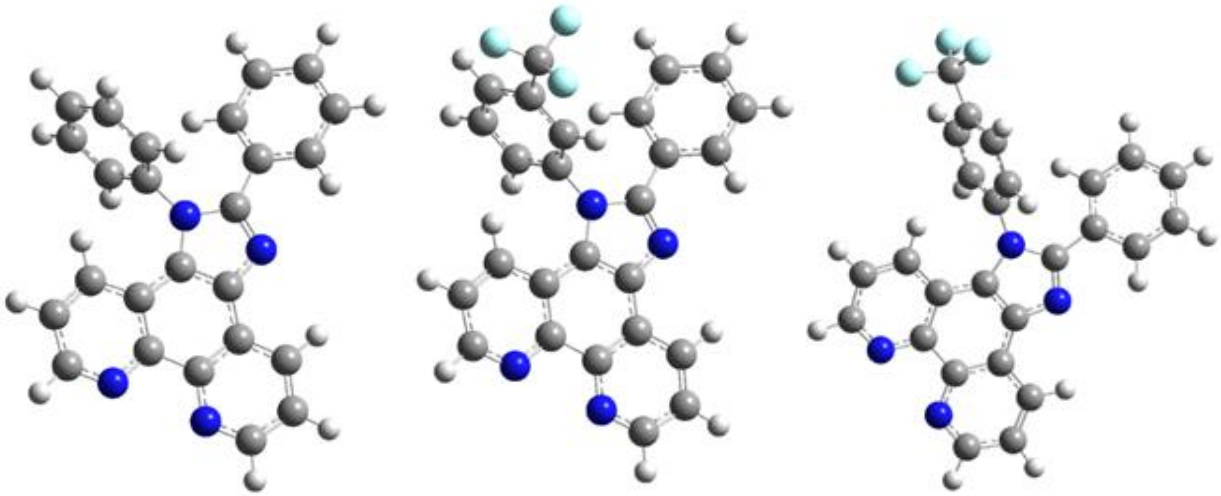

Figure 2.16 Optimized structures of the ligands 1L, 2L, and 3L.

All calculations were carried out using Gaussian09 W and Gaussian view suite of programs. Optimized geometries of the ligands are given in Figure 2.16. Their corresponding frontier orbital energies and gas phase UV-Vis spectral wavelengths are tabulated in Table 2.ST8. The frontier orbital (LUMO+1 to HOMO-1) diagrams also been provided in Table 2.6

Table 2.6 The HOMO-LUMO and HOMO-1, LUMO+1 diagram of the ligands

	Phen-Ph-Ph	**Phen-mCF_3-Ph**	**Phen-pCF_3-Ph**
LUMO+1	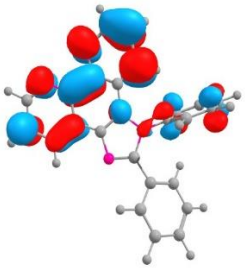	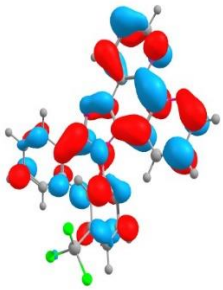	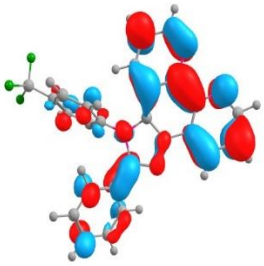
LUMO	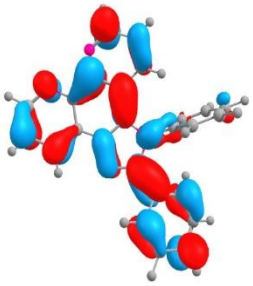	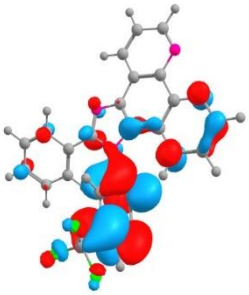	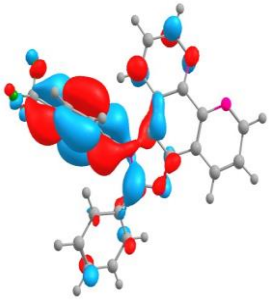

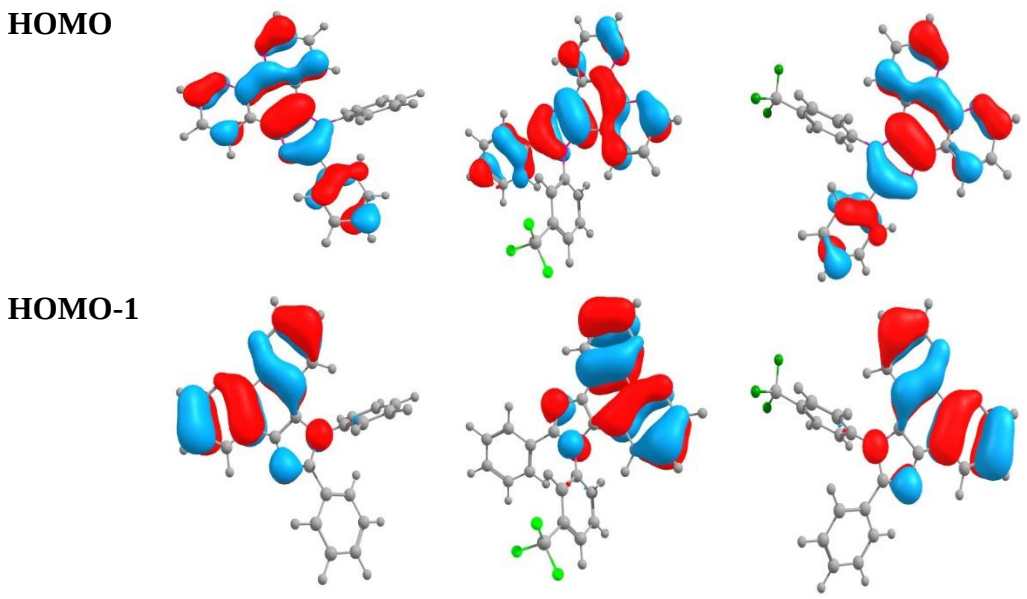

2.2.3.5 Fabrication of LED using Eu complexes:

Based on the red emission of the complexes in solid as well as in the thin film, it was taken initiation to do the realistic application for the complex. Part of that, fabrication of LED by using these complexes was established. InGaN-based LED chip (395 nm – UV light) conjugated with the presently synthesized complex in different ratios (Figure 2.17) and obtained emission spectrum with 20 mA as a forward bias. It extreme, the complexes in 1:10 and 1:50 (Eu: PMMA) mass ratio shown red emission. The CIE color coordinates are, x = 0.65, y = 0.34 (1:10), x = 0.65, y = 0.34 (1:50); x = 0.64, y = 0.35 (1:10), x = 0.65, y = 0.34 (1:50) and x = 0.65, y = 0.34 (1:10), x = 0.65, y = 0.34 (1:50) for 1Eu, 2Eu and 3Eu (Figure 2.17, right). The calculated outcomes were approximately satisfactory values of NTSC standards. The excitation source from LED was mostly utilized by complex for 2Eu than remaining complexes. The calculated CIE of the 3Eu was shown a slight deviation from the red emission and shown pinkish-red emission in the CIE spectra. However, all the complexes are shown red emission and indicating that the synthesized complexes are potential red materials.

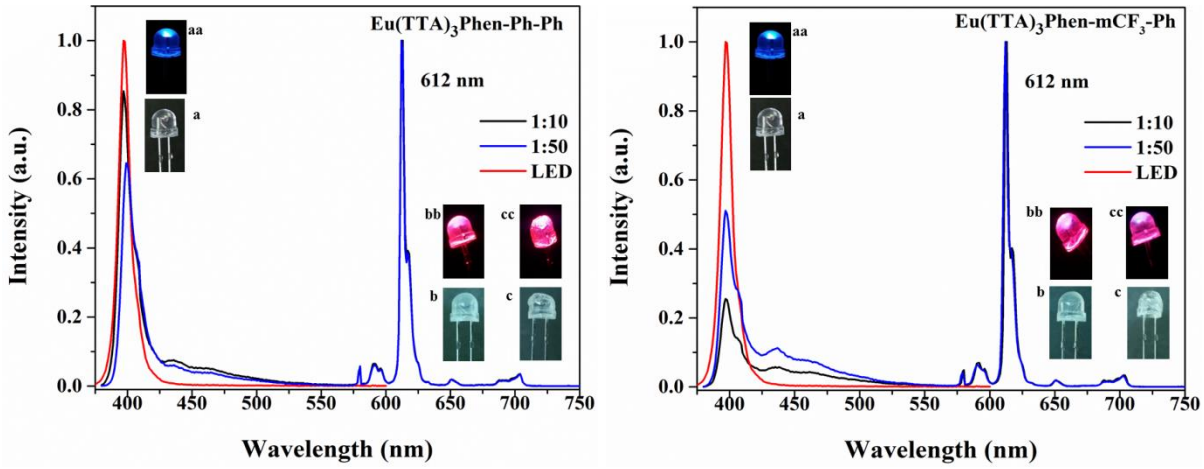

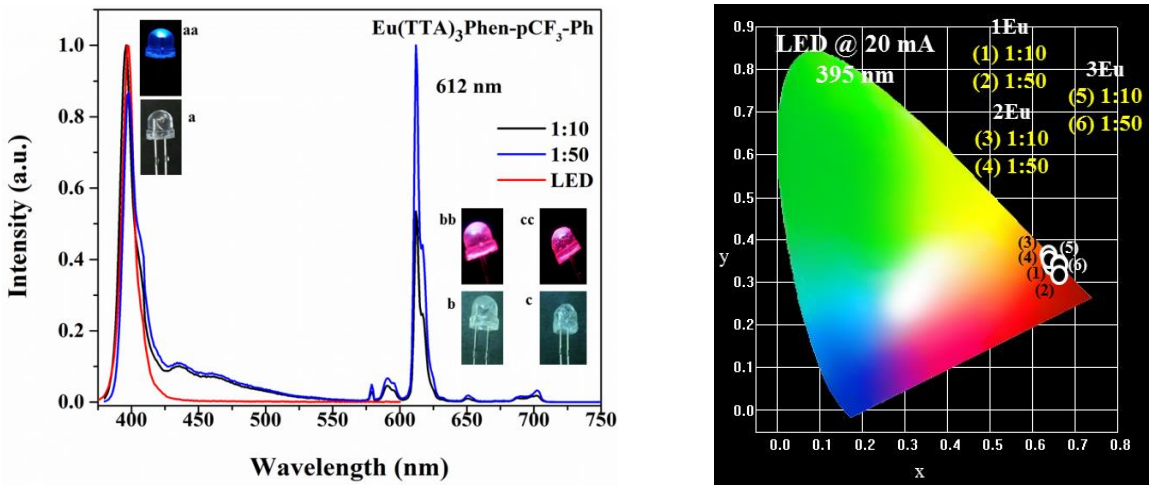

Figure 2.17 The emission spectra of the Eu^{III} complex with coated on the InGaN (395 nm) emitted LED chip. In inset **a** is the original 395 nm emitted LED chip, **aa** is under forward bias. **b** is coated with Eu^{III} complex and **bb** is with a forward bias, respectively. The calculated CIE color coordinates for complex coated LED's (right side down).

2.3 White light emissive ancillary ligand and their Eu^{III} complex:

2.3.1 Outline of the present study:

As mentioned in the previous part of this chapter that the Eu complexes find potential applications in the white LEDs. White LEDs based on multiple emitters conjugated with either near UV or blue LEDs can be problematic as the device is very complicated, and the controlling of color balance is difficult. It is also difficult to attain continuous visible spectrum over the wide range of wavelengths that can serve as a natural and human-friendly lighting source. Thus, most of the problems that are encountered can be evaded by using single-phase white-emitting phosphors/fluorophores with higher luminous output and brilliant color rendering index [56].

Since, single molecule white emission in lanthanide coordination complex is scarcely reported [57-59], research on designing and synthesizing new white emissive lanthanide complexes are attractive research task. Designing of white light emitting lanthanide complex relies on twofold strategy: first the lanthanide ions should provide a set of kinetically labile coordination geometries and show a red luminescence from Ln^{III} (Ln^{III} = Eu^{III}, Pr^{III} and Sm^{III}) emissive center. The second one is to design ancillary ligand that could act as a bridge between the triplet level of ligand and the excited level of Ln^{III} ion (indirectly help in a population of emissive Ln^{III} centre). Ligand to metal energy transfer (LMCT) process is highly dependent on the design principle of the ligand.

Here, we introduce the strategy to achieve white-light-emission from the single molecular complex by incorporating polyaromantic chromophores in the Eu complex that are capable of emitting in the bluish-yellow region and simultaneously sensitize red emissive center, Eu^{III}, through incomplete or partial energy transfer. White emission from single molecular complex achieved by combining a bluish-yellow emitter (ligand/excimer) and a Eu^{III} red sensitized emission. The detailed investigation of photophysical, electrochemical properties and theoretical analysis were performed for the newly synthesized ligand as well as the Eu complex. The

energy transfer mechanism was proposed based on the combined experimental and theoretical studies. The presently synthesized ligand and the respective Eu^{III} complex are shown in Figure. 2.18.

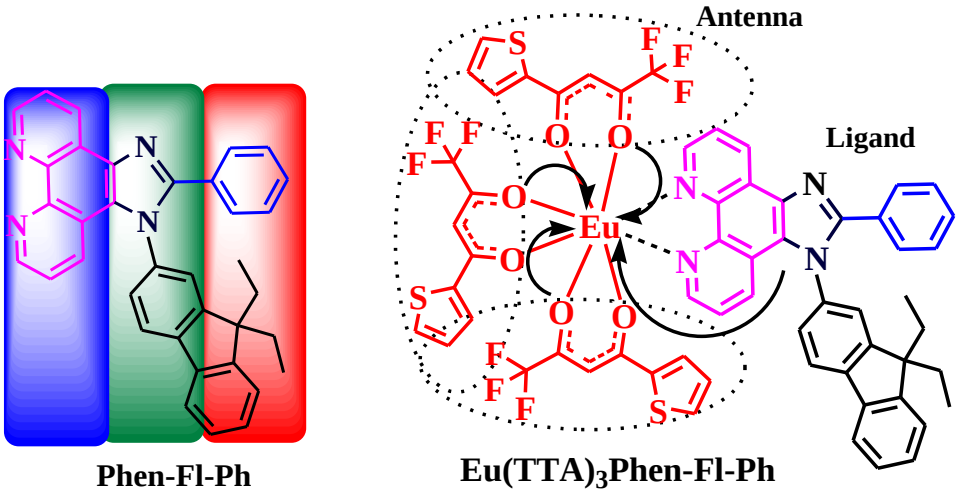

Figure 2.18 Structure of the synthesized ligand and respective Eu^{III} complex, the pictorial view of energy transfer shown with arrows.

2.3.2 Experimental:

2.3.2.1 Materials:

The chemicals obtained through commercial means were used without any modification unless otherwise stated. Fluorene (Fl 99.9%), was purchased from Sigma-Aldrich chemicals, details are given in previous part experimental section 2.2.2.1.

2.3.2.2 Measurement:

The details are given in previous measurement section 2.2.2.

2.3.2.3 Synthesis:

An inert nitrogen atmosphere was maintained for all the reactions. The $Eu(TTA)_3 \cdot 2H_2O$ and 1,10-phenanthroline-5, 6-dione synthesis explained in section 2.2.2.3. A reported literature procedure was used to synthesize fluorene compound [38a].

2.3.2.3.1 Synthesis of 9,9-diethyl-2-nitro-9H-fluorene (1-1):

Into a clean two neck round bottom flask poured 1-1 (0.2 g, 0.899 mmol) and added acetic acid (1.6 mL) solution at RT. This mixture was heated to 50 ^{o}C then added nitric acid (0.2 g, 5.411 mmol) drop wise. The resulting mixture was stirred for 24 hrs at 70 ^{o}C and the progress of the reaction was monitored by TLC (1:9 EtoAc: Hexane, Rf is 0.5). RM was cooled to RT and poured into water then basified with diluted sodium hydroxide solution up to pH 7 (neutral), extracted with ethyl acetate combined organic layer was washed with brine followed by dried with anhydrous sodium sulphate, solvent was evaporated to get crude compound. This was washed with hexane and diethyl ether simultaneously to get 1-2 (220 mg, 91%) with brick

yellow color solid. ^{1}H-NMR Data (400 MHz, $CdCl_3$): δ (in ppm) 8.29 (dd, 1H), 8.21 (d, 1H), 7.82-7.80 (m, 2H), 7.47-7.39 (m, 3H), 2.14-2.07 (m, 4H) and 0.32 (t, 6H). ^{13}C-NMR Data ($CdCl_3$, 100 MHz): δ (in ppm) 151.5, 151.1, 148.0, 147.1, 139.1, 129.2, 127.4, 123.3, 121.1, 119.7, 118.3, 56.71, 32.5 and 8.39.

2.3.2.3.2 Synthesis of 9,9-diethyl-9H-fluoren-2-amine (1-2):

To a stirred solution of 1-2 (200 mg, 0.749 mmol) in ethanol (15 mL) added hydrazine monohydrate (0.5 mL) at RT. Then palladium on carbon (Pd/C, 10% w/w) (0.05 g) was added under nitrogen atmosphere and resulting mixture was refluxed (85 ^{o}C) for 10 hrs. The progress of the reaction was monitored by TLC (EtOAc: Hexane 2:8, Rf-0.6, ninhydrin active) and RM was filtered through celite bed followed by concentrated to get 190 mg of 1-3 crude compound. This was purified with column chromatography by using silica gel (100-200 mash). The compound eluted with 8% ethyl acetate in pet ether and solvent concentrated to get 160 mg (90%) 1-3 pure compound with pale brown color. ^{1}H-NMR Data (400 MHz, $CdCl_3$): δ (in ppm) 7.60 (d, 1H), 7.54-7.51 (m, 1H), 7.34-7.29 (m, 2H), 7.25 (d, 1H), 6.70-6.68 (m, 2H), 3.63 (bs, 2H), 2.06-1.95 (m, 4H) and 0.37 (t, 6H). ^{13}C-NMR Data ($CdCl_3$, 100 MHz): δ (in ppm) 151.7, 148.8, 141.9, 132.7, 126.9, 125.5, 122.6, 120.3, 118.2, 113.8, 109.7, 55.7, 32.8, 8.4

2.3.2.3.3 *Synthesis of 1-(9,9-diethyl-9H-fluoren-2-yl)-2-phenyl-1H-imidazo[4,5-f][1,10]phenanthroline*:

9,9-diethyl-9H-fluoren-2-amine (0.13 g, 4.762 mmol) and benzaldehyde (0.5 g, 4.762 mmol) were added turn wise to a stirred solution of 1,10-phenanthroline-5,6-dione (1.0 g, 4.762 mmol) in acetic acid, followed by ammonium acetate (3.7g, 47.62 mmol) and the mixture was stirred for 12 hours at 110°C under nitrogen atmosphere. The reaction was monitored by TLC (MeOH : DCM = 1:9). The product was then neutralized with ammonium hydroxide solution followed by extraction with DCM and drying with sodium sulphate. The product was then concentrated and purified by column chromatography using silica bed (100-200 mesh) with 5% MeOH in DCM as the eluent. The purified product was dissolved in minimal amount of THF and an excess amount of hexane was added to it. The solid was allowed to settle down and then the solvent was decanted. The above process was repeated till a fine powder like sediment was obtained. Elemental Analysis: Anal. Calc. for. $C_{36}H_{28}N_4$; C, 83.69; H, 5.46; N, 10.84 %, Found: C, 83.58; H, 5.40; N, 10.91 %. ^{1}H-NMR (400 MHz, $CDCl_3$): δ (in ppm) 9.22 (dd, J = 4.4 Hz, 1H), 9.19 (dd, J = 8.2 Hz, 1H), 9.06 (dd, J = 4 Hz, 1H), 7.94 (d, J = 8 Hz, 1H), 7.8 (d, J = 5.6 Hz, 1H), 7.78 (dd, J = 7.8 Hz, 1H), 7.69 - 7.658 (m, 3H), 7.65 - 7.41 (m, 5H), 7.34 - 7.24 (m, 4H), 2.11 - 1.98 (m, 4H), 0.447 (t, J = 7.2 Hz, 3H), 0.280 (t, J = 7.2 Hz, 3H). ^{13}C NMR ($CDCl_3$, 100 MHz): δ (in ppm) 151.9, 149.6, 148.4, 147.4, 144, 143.7, 139, 135, 130, 129, 128, 127, 126.8, 123, 122, 121, 120, 119, 56.24, 32.4, 7.96.

2.3.2.3.4 *Synthesis of $Eu(TTA)_3$Phen-Fl-Ph*:

In a round-bottom flask, solution of $Eu(TTA)_3.2H_2O$ (0.230 g, 0.27 mmol) in dry THF (15 mL) was taken and to it the Phen-Fl-Ph ligand was added. The mixture was then stirred for 6 hours at 60°C in a nitrogen atmosphere after which it was concentrated and dissolved in minimum amount of THF. To the solution excess of hexane was added and powder type sediment was obtained. The solvent layer was then decanted and the powder was dried.

Elemental Analysis: Anal. Calc. for. $C_{60}H_{40}EuF_9N_4O_6S_3$; C, 54.10; H, 3.03; N, 4.21; S, 7.22 %, Found: C, 53.98.; H, 2.99; N, 4.31; S, 7.25 %.

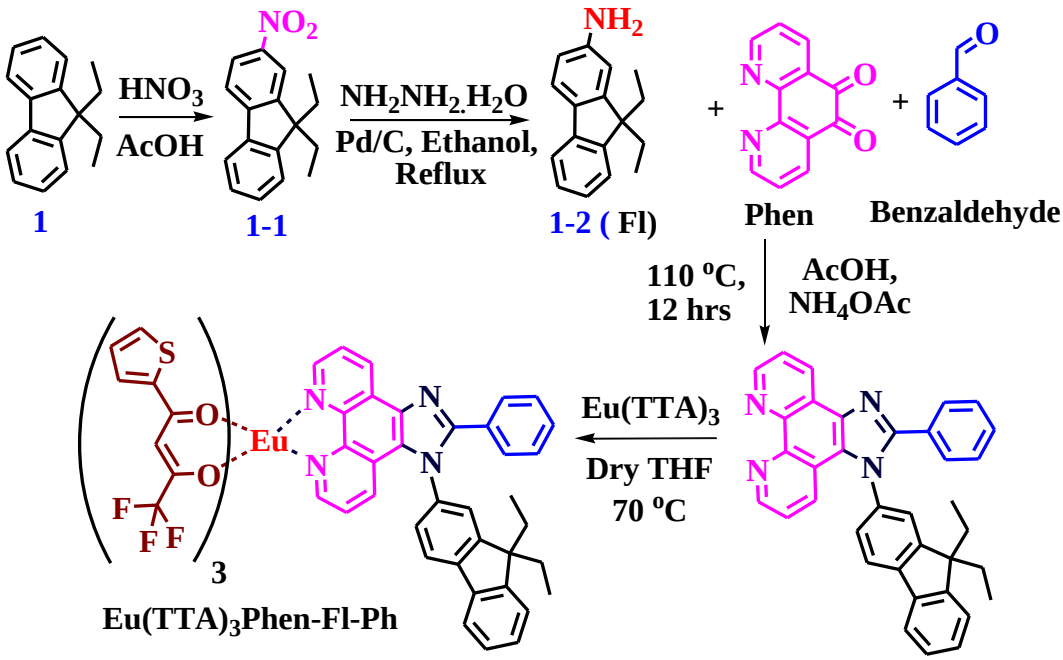

Scheme 2.2 The synthetic route for the preparation of Eu^{III} complex.

2.3.2.4 FT-IR analysis:

The synthesized ligand and its corresponding complex were characterized by FT-IR analysis. The ligand was shown a peak at around 1606 cm^{-1} (attributed to the C=N stretching frequency) and the complex shown 1688 and 1595 cm^{-1} (attributed to the C=O and C=N stretching frequency), respectively. The changing of C=N starching frequency of the ligand in the Eu-complex indicates that the ligand is coordinated with the Eu^{III} metal ion. In addition, it was also further confirmed by the FT-IR analysis of $Eu(TTA)_3$ complex. The $Eu(TTA)_3$ complex shown a peak at 1609 cm^{-1}, due to C=O stretching frequency, the same peak was shifted to 1688 cm^{-1} in the Eu^{III}-complex and it clearly indicates that the coordinated water molecule in the $Eu(TTA)_3$ complex was replaced by the phenanthroimidazole ligand. The FT-IR spectra of the ligand and complex comparison with $Eu(TTA)_3$ was shown in Figure 2.19.

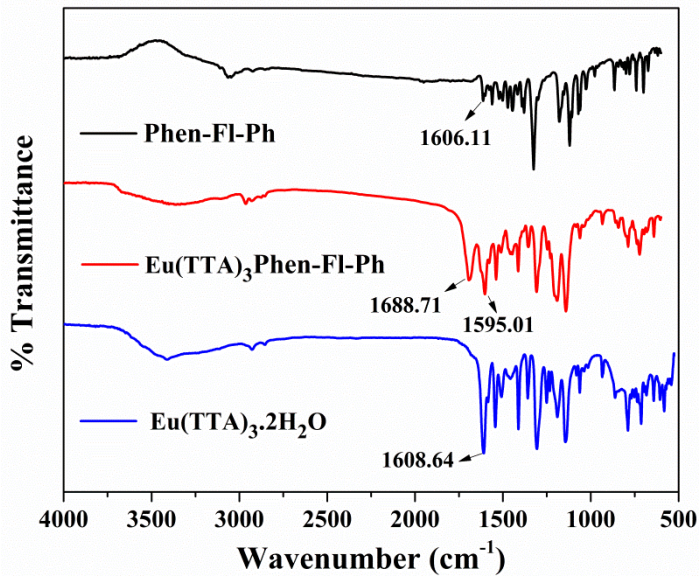

Figure 2.19 The FT-IR analysis of the complex and ligand as well as comparison with $Eu(TTT)_3.2H_2O$.

2.3.3 Results and Discussion:

The ligand was synthesized and coordinated with $Eu(TTA)_3$ complex. The ligand as well as the complex was characterized by NMR (Figure 2.S8-2.S10), FT-IR (Figure 2.S11 and S12) and elemental analysis. The photophysical, electrochemical and theoretical analysis were also been carried out. The synthetic scheme of the ligand and complex was given in the Scheme 2.2.

2.3.3.1 Photophysical Study:

2.3.3.1.1 UV-Vis Spectroscopic analysis:

The UV-Visible spectra of Phen-Fl-Ph and the corresponding complex, $Eu(TTA)_3$Phen-Fl-Ph, were measured in chloroform solution ($1x10^{-4}$ mol/L) and shown in Figure 2.20 (left). In the absorption spectra, identical peaks from $Eu(TTA)_3$Phen-Fl-Ph complex and $Eu(TTA)_3$ at 297 nm and 340 nm was observed and it can be attributed to $\pi \rightarrow \pi^*$ of the ligand molecules. It is also worth to note that the $Eu(TTA)_3$ presence in the synthesized Eu complex. Similarly, the ligand absorption peaks appear in the complex, it also further indicates that the ligand coordinated with the Eu metal ion in the complex. The peak in the UV region (200 to 300 nm) with peaking wavelength at 270 nm, usually attributed to the $\pi \rightarrow \pi^*$ transitions of aromatic moieties present in the ligands and complex. The obtained absorption spectral analysis was interpreted in Table 2.7. The UV-absorption spectra of the ligands were calculated in gas and solution from the theoretical calculation and shown in Figure 2.20 (right). The peak maximum of the ligand shown at ~280 nm and it is similar to that of the obtained from experimental UV-absorption analysis. In addition, we also calculated the energy gap of the ligand and Eu-complex from diffuse reflectance spectra (DRS) by using Kubelka-Munk function ($\alpha = F(R_\infty)$, equation 2.1) [60]. The energy gap from UV-absorption spectra of the ligand and the complex was shown in Figure 2.21.

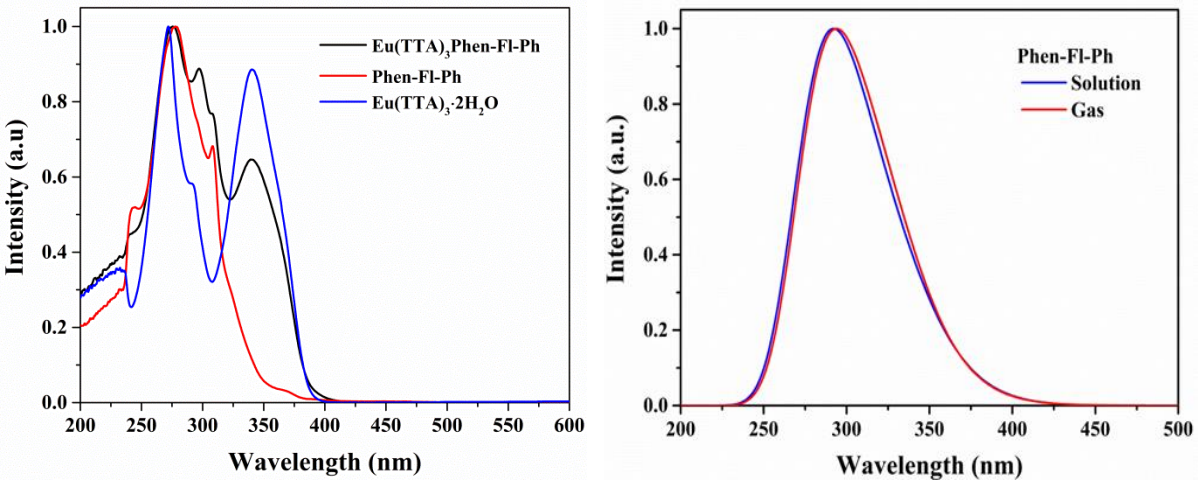

Figure 2.20 UV-Vis absorption spectra of the Eu-complex and the ligand in chloroform solution (left), The theoretical UV spectra of the ligand obtained through DFT calculations (right).

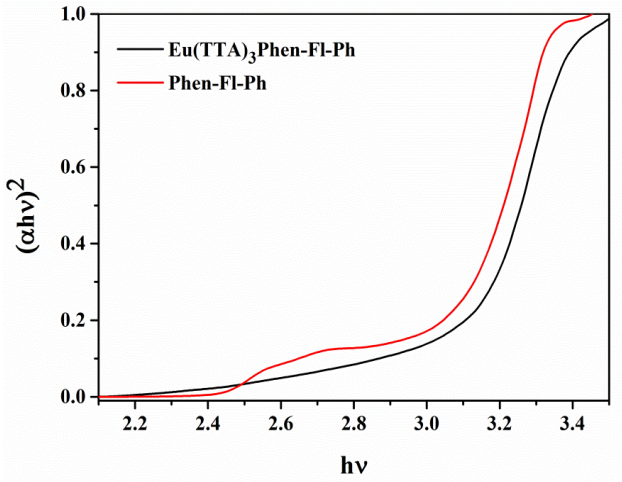

Figure 2.21 The UV-absorption spectra of the ligand and the complex in solid state (diffused reflectance spectra, DRS).

Table 2.7 The UV-absorption and PL emission data of synthesized Eu^{III} complexes and ligands.

S. No.	Compound name	UV λ_{max} (abs) [nm] Solution (a) (b)	λ_{ex} (d) [nm]	PL λ_{em} (a) [nm]	FWHM (a) [nm]
1.	**$Eu(TTA)_3$Phen-Fl-Ph**	276, 296, 340	249, 322, 374	579, 592, 612, 652, 702	7.01 / 9.18(c)
2.	**Phen-Fl-Ph**	243, 276, 308	252, 330, 370	400 / 419,442,540 (c)	--.--
3.	**$Eu(TTA)_3(H_2O)_2$**	273, 340	275, 340	580, 592, 612, 652, 703	--.--

[a] measured in chloroform solution at 298 K, [b] absorption peaks from the UV-absorption spectra, [c] emission from solid PL, [d] wavelengths are taken to get the emission of ligands and Eu^{III} complexes.

2.3.3.1.2 Photoluminescence Spectroscopy:

Photoluminescence excitation and emission spectral analyses are very much necessary to understand the energy transfer process like fluorescence and phosphorescence emission in the presently studied ligand as well as the complex. In the present study, the PL excitation and emission of the ligand and the corresponding Eu^{III} complex in the solid phase, thin film phase and chloroform solution was executed. The excitation spectrum of the ligand is identical with the absorption spectrum of the ligand (Figure 2.20). The emission spectrum shows blue emission under 330 nm excitation (Figure 2.22, left), whereas the solid phase of the ligand shows broad emission covering whole visible spectrum (white emission) (Figure 2.22, right, the inset shows the commission international de l'éclairage (CIE) color coordinates with value).

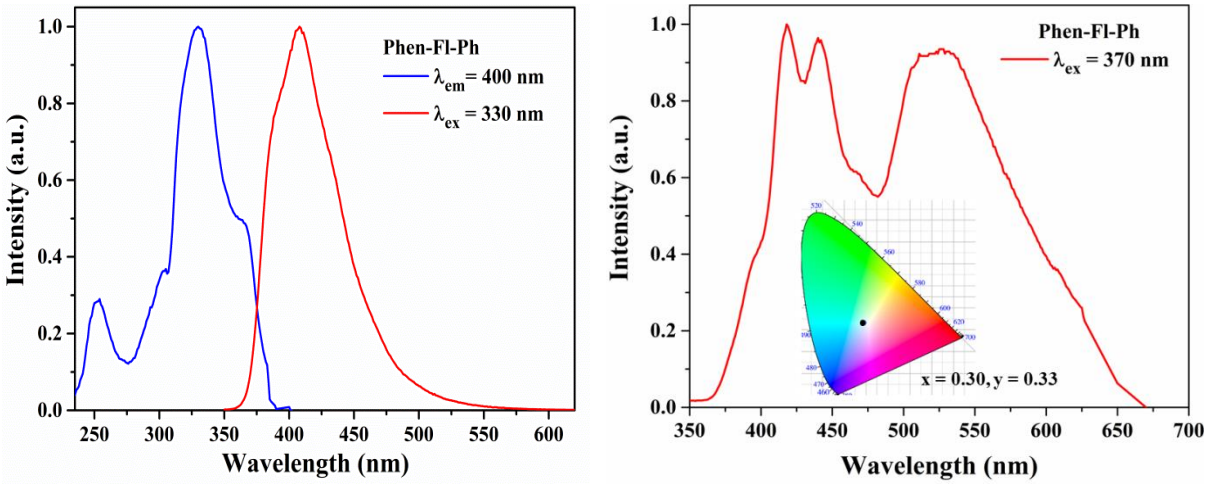

Figure 2.22 The PL excitation and emission spectra of the ligand in chloroform solution (left) and solid phase, in inset shown respective CIE color coordinate (right).

2.3.3.1.3 Solvatochromism:

The solvatochromism is necessary to understand solvent-dependent emission of the ligand. The emission of the ligand was performed under different solvents such as toluene, dichlorobenzene (DCM), tetrahydrofuron (THF), acetone, ethylacetate (EtOAc), chloroform ($CHCl_3$), methanol (MeOH), dimethylformamide (DMF), and dimethylsulphoxide (DMSO) and measured their stocks' shift values. The obtained results of ligands (from emission spectra) interpreted in terms of Lippert-mataga equation. Based on the increasing the polarity of the solvent, there is a shift observed towards high wavelength and shown red / batho chromic shift. The obtained results and calculations are incorporated in the Table 2.S9. The following equations of Lippert−Mataga describes the solvatochromic Stokes shift $\Delta\bar{\nu}$ (expressed in wavenumbers) as a function of the change of the dipole moment $\Delta\mu_{ge} = \mu_e - \mu_g$ of the dye. The several solvents are performed by equation 2.11 and 2.12 with dissimilar dielectric constants (ε) and refractive indices (n) and by plotting $\Delta\bar{\nu}$ as a function of Δf [61, 62].

$$\Delta\bar{\nu} = \frac{2\Delta f}{4\pi\epsilon_0 hca^3}(\mu_e - \mu_g) + \text{constant} \qquad \text{…….. 2.11}$$

$$f(\epsilon) = \frac{f(\epsilon-1)}{f(2\epsilon+1)} \text{ and } f(n^2) = \frac{(n^2-1)}{(2n^2+1)} \qquad \text{…..…… 2.12}$$

$\Delta\bar{\nu} = \Delta\bar{\nu}_{abs} - \Delta\bar{\nu}_{em}$ is the solvatochromic shift (in cm^{-1}) between the maxima of absorption and fluorescence emission [$\Delta\bar{\nu}_{abs} = 1/\lambda_{abs}$ (max), $\Delta\bar{\nu}_{em} = 1/\lambda_{em}$ (max)], *h* is Planck's constant, c is the velocity of light, ε_0 is the permittivity of vacuum (signifies the radius of the cavity in which the solute resides), μ_e, μ_g are dipolemoments in the excited and ground states. Figure 2.23 indicating that the linear relationship [correlation coefficient r = 0.72] of the Stokes shift plotting $\Delta\bar{\nu}$ verses Δf for the 9 solvents of the ligand.

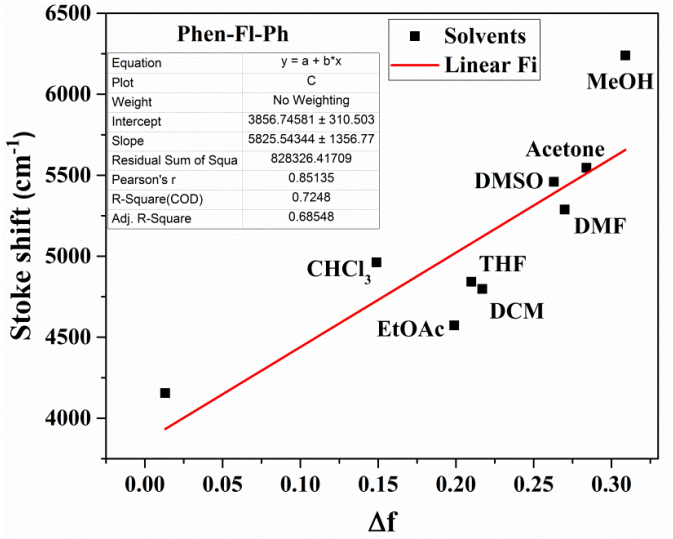

Figure 2.23 Stokes shift $\Delta\bar{\nu}$ of Phen-Fl-Ph versus the Lippert solvent parameter $\Delta f = f(\varepsilon) - f(n^2)$ and the straight line represents the linear fit to the 9 data points.

The emission maximum of the ligand is observed at ~400 nm (blue emission). The PL excitation and emission spectra of the ligand in different solvent were shown in Figure 2.24. Among all solvents, methanol solution was shown distinguished emission behavior and almost covering the entire visible region from 390 – 600 nm, further analysis is necessary to understand the same. One can argue that the present of O-H group in the solvent can make hydrogen bonding with ligand moieties that may lead to aggregation and shift as well as broaden the emission band towards the red region. However, in the case of solid also we have observed the similar trend (broad emission with peak splitting (419, 442 nm) in the blue region and maxima at 540 nm under 370 nm as excitation source) (Figure 2.24, right). The covering of entire visible spectrum (blue, green and red) of ligand in solid state was shown extremely white emission with CIE color coordinates value x = 0.30, y = 0.33, respectively. In general, the emission bands of the ligands in the solid state appear obviously red-shifted, the observed red shift emission is attributed that the aggregation of ligands in the solid state. The CIE chromaticity coordinates of the ligand in different solvents was interpreted in Figure 2.25, left and respective CIE values are shown in Table 2.ST11.

In addition, to understand further the ligand white emission, the PL emission spectrum in different excitation wavelength ranging from 300 - 400 nm was recorded. Increasing with the excitation wavelength, the emission maxima of the ligand was further shifted to the higher wavelength (from 530 to 548 nm) and resulting white to yellow emission (Figure 2.26, left). The emission spectra of the ligand in solid form and the respective CIE color coordinates were shown in Figure 2.26, right. Since the ligand shown tunable emission ranging from white to yellow (confirm CIE color coordinates Figure 2.24, right), it can find potential applications as

wavelength dependent sensor applications. Thus, the observed white emission (covering the entire visible spectral window) from the ligand could utilize them in the light converting molecular devices such as white LEDs, OLEDs. The CIE color coordinates for the ligand in different excitation source from 300-400 nm are shown in Table 2.ST11.

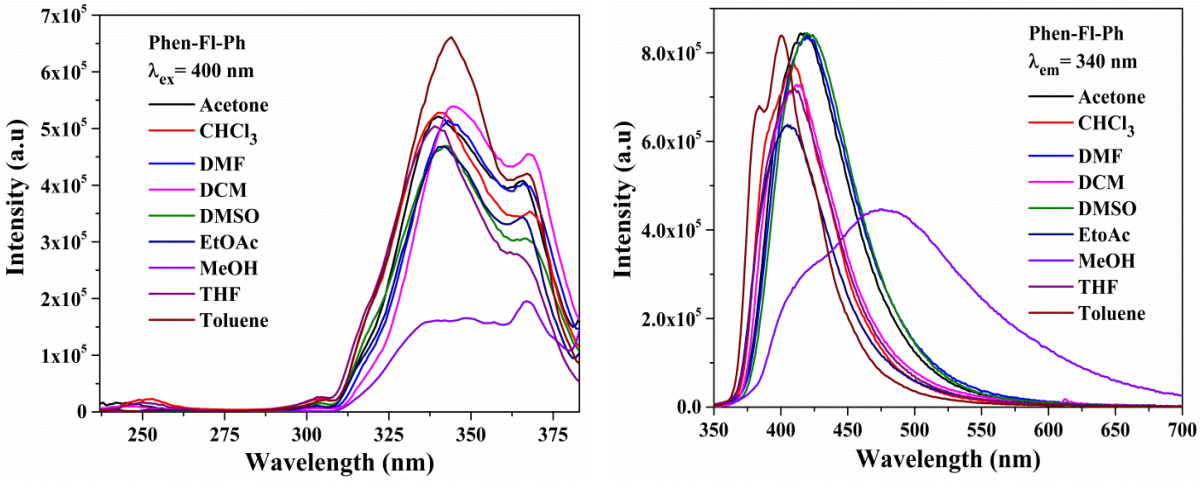

Figure 2.24 The PL excitation (left) and emission spectra (right) of the ligand in chloroform solution.

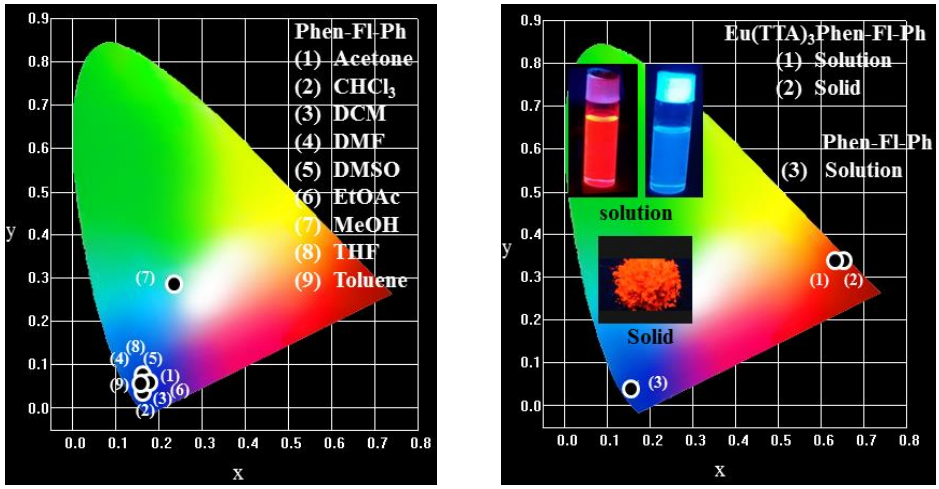

Figure 2.25 The CIE color coordinates of PL emission spectra for the ligand in solution (left) and ligand as well as respective complex in chloroform solution and solid (right).

It is also worth to note that the diphenyl factionalized Phen-Fl-Ph shows sky blue emission in the CIE color coordinates x = 0.16, y = 0.19 [38a]. Though numerous strong emissive organic chromophores or dyes in solution were documented, in most of the cases strong quenching of fluorescence occurs due to molecular aggregation and intermolecular interaction in the solid state [64]. Therefore, the currently synthesized white emissive neutral ligand in the solid state is very attractive and of prodigious significance in the display devices and other applications. White emission can be realized by the complimentary emission from the two similar or dissimilar organic chromophores (host-guest system). Nevertheless, mixing of similar or dissimilar emitting materials (largely distinct molecular structure) could cause micro-

segregation that affects the device operation [65]. Hence, the design strategy one needs to restrict by functionalizing the main chromophoric π-conjugated main framework that is capable of exhibiting multicolor emission [66].

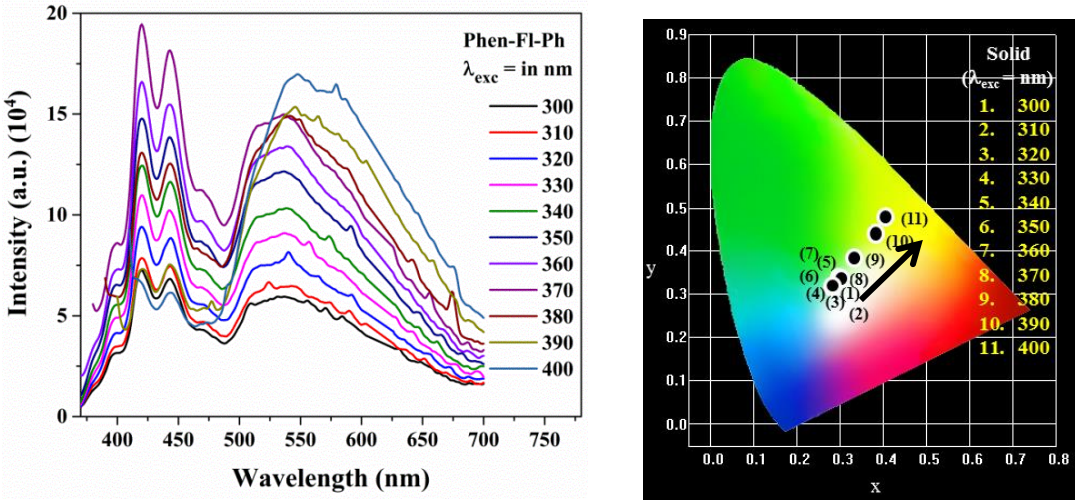

Figure 2.26 The PL emission spectra of the ligand in different excitation source from 300-400 nm in the solid phase (left) and their respective CIE color coordinates.

The ligand coordinated Eu^{III} complex was excited with 375 (solution) and 360 nm (solid) and achieved red emission with sharp maxima at 612 nm in both the solution and solid form (Figure 2.25). The calculated CIE color coordinates for the ligand and the complex in solution and a solid phase in Figure 2.25, right; the corresponding CIE values are incorporated in Table 2.ST12. This is attributed to the allowed electric dipole transition of $^5D_0 \rightarrow {}^7F_2$. In the PL emission spectra there is no emission was observed in the region of 400 - 500 nm region (where the ligand emission can appear) and it clearly indicates that the complete energy transfer arising from ligand to Eu^{III} metal ion in the complex. In addition, it is also worth to note that the higher excited level emission also been quenched or deactivated to the higher first excited level of Eu^{III} ion ($^5D_0$). The deactivation of a Eu^{III} complex of the excited state of $^5D_0$ to the ground states levels ^7F_J (J=0−4) gives distinctive Eu^{III} emission bands at around 581, 593, 614, 654, and 702 nm. The excitation spectrum was recorded by monitoring the $^5D_0$-$^7F_2$ transition of Eu^{III} emission line (electric dipole transition, ED) and shown in Figure 2.27.

In addition, minor peaks at 581, 593, 654, and 702 nm also been observed and are attributed to $^5D_0 \rightarrow {}^7F_0$, $D_0 \rightarrow {}^7F_1$, $D_0 \rightarrow {}^7F_3$, and $D_0 \rightarrow {}^7F_4$, respectively. The peak at 581 nm is induced magnetic dipole (MD) transition and it can only observe when the Eu^{III} ion presents in the C_n, C_{nv} and C_s symmetry in the structure [66, 67]. This transition is exactingly forbidden according to the standard Judd–Ofelt (J-O) theory. The intensity of the magnetic dipole transition (MD) at 593 nm is independent of Eu^{III} local site environment in the Eu^{III} complex. The intensity of this transition is considered to be constant and it is used to calibrate the intensity of Eu^{III} luminescence spectra. The high intensive peak at 612 nm is a hypersensitive transition and its intensity strongly dependent on local environment around the Eu ion in the complex. This hypersensitive transition used as a measure of the asymmetry of the Eu^{III} site. The peak at 654 nm is forbidden nature transition and 702 nm is intensity dependent on environment, but no hypersensitivity in the complex.

The PL spectra of the ligand and complex emission spectra in chloroform solution and combined emission of the complex in solution, solid are shown in Figure 2.S13. The calculated asymmetric ratio of the complex in solution and solid was shown 8.36 and 13.5, respectively. The intensity of the complex in solid showed better than the solution. However, the full width at half maximum of the complex in solution (7.01) found to be narrow emission than solid (9.18). The PL properties were tabulated in Table 2.7. The intensity ratio (intensities of $^5D_0$-$^7F_1$ and $^5D_0$-$^7F_2$) of the complex in $CHCl_3$ solution and solid was shown 13.8 and 8.7, respectively.

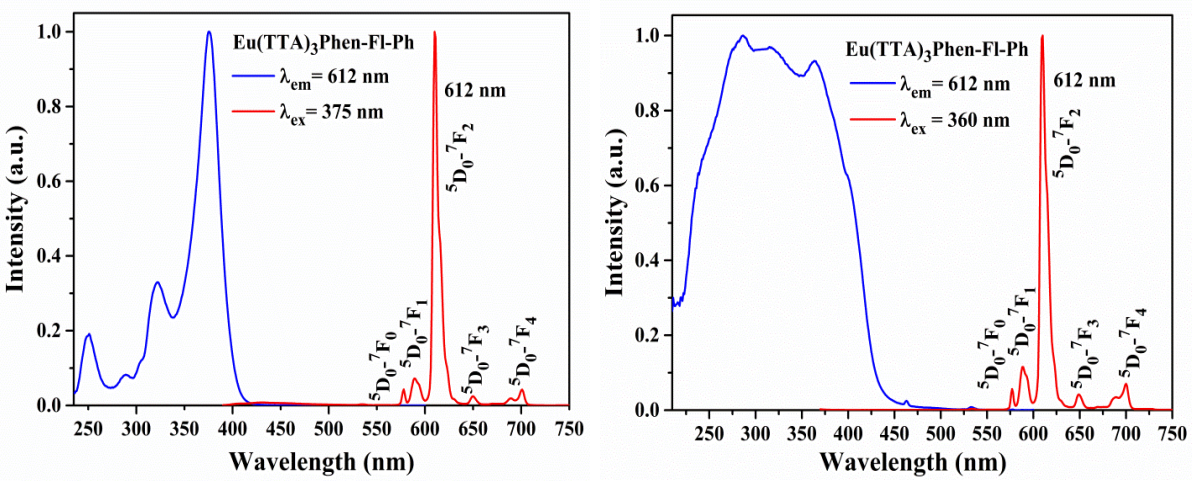

Figure 2.27 The PL excitation and emission spectra of the complex in chloroform solution (left) and solid phase (right).

In addition, to understand the PL emission of the complex, (i.e) energy transfer from ligand to the Eu^{III} excited state of $^5D_0$ level, we have calculated singlet and triplet energy level energies of the ligand by using DFT and TD-DFT calculations. Singlet and triplet energy levels are located at 28923 and 22623 cm^{-1}, respectively (Figure 2.28, left). The optimized structure of the ligand molecule was also shown in Figure 2.28, right. Furthered, we also estimated and compared the calculated triplet energy of the ligand by measuring the phosphorescence emission spectra of the Gd^{III} complex at 77 K and found to be 20619 cm^{-1} (2.55 eV, 486 nm, Figure 2.S14). The experimentally obtained values are nearly matching with the value obtained from theoretical calculations. It is well known that the TTA energy levels are located at 25164 (singlet) and 18954 cm^{-1} (triplet). The Eu^{III} metal ion $^5D_0$ level located at 17,500 cm^{-1} and other energy levels are also presented ($^5D_3$ (24,800 cm^{-1}), $^5D_2$ (21,500 cm^{-1}), and $^5D_1$ (19,100 cm^{-1}), but the radiative transition can appear from the lowest energy level of the Eu^{III} metal ion ($^5D_0$). The obtained results are clearly indicating that the efficient energy transfer occurring from ligand excited state of triplet to the excited level of $^5D_0$ of the Eu^{III} metal ion. It was clear that from the PL emission analysis of the complex. Furthered, it was also supported by the Leva *et al.*, investigations ($\Delta E = E(T_1) - E(^5D_0)$ is 2500 - 4000 cm^{-1}; singlet above 25,000 (3.09 eV) and triplet above 20,000 cm^{-1} (2.47 eV)) [43]. It is indicating that there is no back energy transfer (no emission in the rage of 400 to 500 nm) from Eu^{III} excited levels ($^5D_0$ or $^5D_1$ levels) to triplet level of ligand molecules. Based on the energy level location, one can argue that the energy transfer can occur from TTA triplet energy level to Eu^{III} metal ion. It means TTA can act as a transitional state between the singlet to triplet excited states of the ligand and triplet excited state to the excited $^5D_0$ level of Eu^{III} ion, respectively.

Generally, to get the efficient energy transfer between donor and acceptor, an effective overlap between the emission spectrum of the donor as well as the absorption spectrum of the acceptor is highly necessary. Based on these criteria, we have experimentally found that the overlap of the absorption spectrum of TTA and the ligand emission spectrum in the region of 370 – 450 nm and the same is shown in Figure 2.S14, right [45, 68]. The obtained results are showed that the synthesized ligand have potential to get efficient energy transfer and ligand calculated excited state energy levels are suitable for a Eu^{III} metal ion to get efficient red emission. The singlet state of the currently synthesized ligand has slightly less energy (~400 cm^{-1}) as compared with that of different N1 functionalization such as phenyl, meta-trifluoro phenyl and para-trifuoro phenyl. However, the triplet state of the ligands is not much influenced. These outcomes can suggest that the singlet level can transfer the energy efficiently then the different N1 functionalization. Hence, the obtained QY of the complex reached from 1.83 (lowest) to 57.3 (highest) % (detailed explained in the QY part).

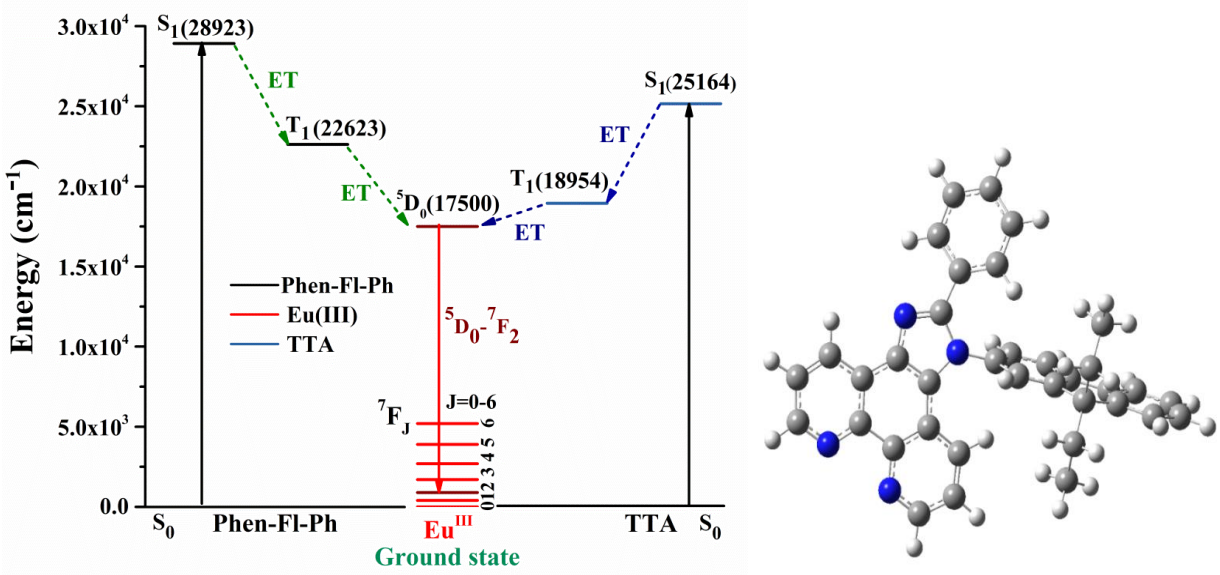

Figure 2.28 Schematic diagram for the energy transfer process from ligand to Eu^{III} ion in the Eu^{III} complex (left) and optimized structure of the ligand molecule (right).

2.3.3.1.4 Poly methyl methacrylate (PMMA) film of ligand and Eu^{III} complex and Commission internationale de l'éclairage (CIE) Chromaticity coordinates:

The synthesized bipolar ligand and complex has imbedded in PMMA film with a different ratio, to show the potentiality of the complex for molecular light converting devices. The excitation (Figure 2.29, left) and emission spectra (Figure 2.29, right) are shown in Figure 2.26. The emission spectra of the ligand were shown in the region of blue in 0.1 to 5 % ratio. Their CIE color coordinates are shown x = 0.20, y = 0.18 (0.1 %), x = 0.20, y = 0.20 (0.5 %); x = 0.20, y = 0.19 (1 %), and x = 0.20, y = 0.19 (5 %), respectively. However, in the case of the pure thin film of the ligand shown yellowish green emission and the CIE value is x = 0.30, y = 0.43. The ligand coordinated Eu^{III} complex shown red emission with CIE values are x = 0.66, y = 0.34 (0.1 %), x = 0.66, y = 0.34 (0.5 %); x = 0.66, y = 0.34 (1 %), and x = 0.65, y = 0.34 (5 %), respectively. In addition, the calculated FWHM (nm) shown for complex is 11.4, 14.0, 14.0, 17.9 nm and their intensity ratios are 3.49, 2.68, 3.19, 2.60 for 0.1, 0.5, 1, 5 %, respectively.

Increasing of FWHM was observed in the emission spectral lines, with increasing the concentration of the complex in the film. Compare to the solution and solid state emission, the asymmetric ratio of the thin film of the complex shown less and shown FWHM more. The CIE coordinates for the ligand and their corresponding complex in the different ration of concentration in the thin film shown in Figure 2.330. The ligand and corresponding Eu^{III} complex CIE color coordinate values in the thin film are shown in Table 2.ST13.

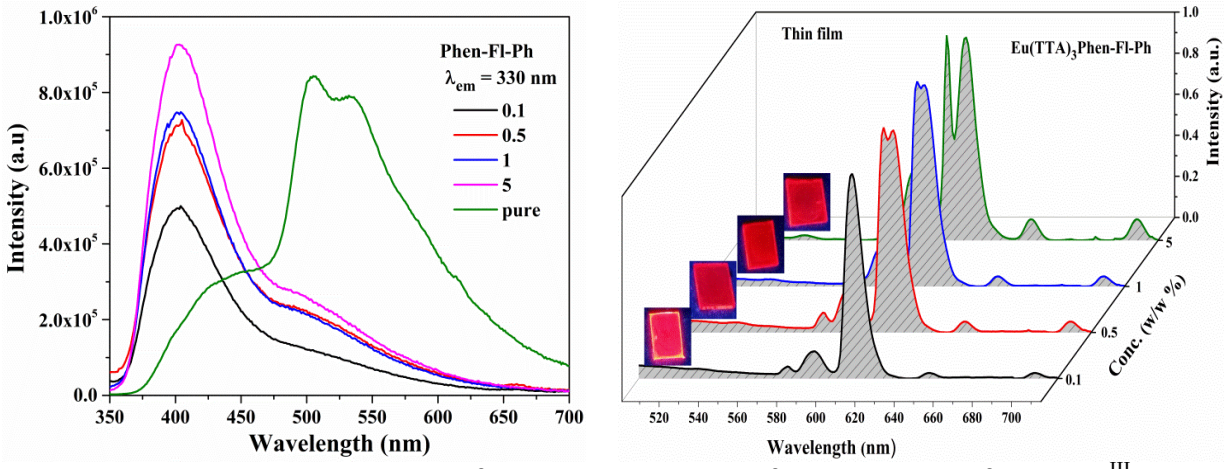

Figure 2.29 The PMMA doped thin films emission spectra for the ligand (left) and Eu^{III} complex (right) in different dopant concentration (onset respective digital images).

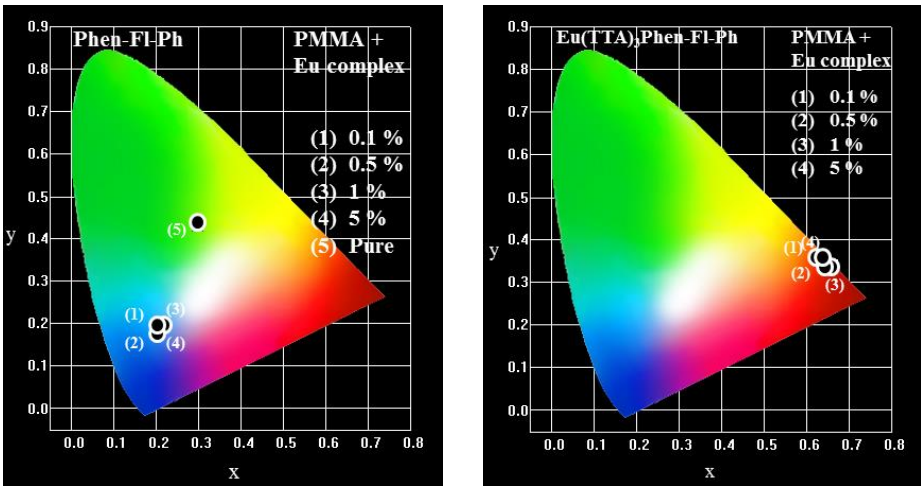

Figure 2.30 CIE coordinates for the ligand (left) and their corresponding complex (right) in the different ration of concentration in thin film.

2.3.3.1.5 Photoluminescence quantum yield:

The absolute quantum yield of the ligand and Eu-complex were calculated in the form of a solution and solid. The absolute quantum efficiency (measured by integration sphere) of the complex as well as ligand was calculated by the following formulae, the quantum efficiency (φ) can be obtained (by using equation 2.2 and 2.3). The absolute quantum efficiency of the complex was carried out in solution (chloroform) as well as solid and the obtained values are 35.8 and 23.9 %, respectively. The calculated absolute QY of the ligand in solution (chloroform) and solid

are found to be 6.27 and 1.83 %, respectively. In addition, to understand the furthered ligand emission in different solution; it was analyzed in acetonitrile, dichloromethane, DMF, DMSO, EtOAc, THF and toluene and found to be 16.7, 12.7, 22.7, 23.2, 12.3, 23.2 and 10.3 %, respectively. It is very familiar that the PMMA can easily prepared polymer (outstanding optical quality) and cost effective. The QE of the complex by doping with PMMA also were calculated and found those to be 26.6 (0.1%), 57.3 (0.5%) and 43.5 (1%), respectively. The obtained thin film results are indicating that the reducing the quantum efficiency by doping with an excess of the complex with PMMA. So, the 1% doping of complex with PMMA is suitable to get the efficient energy transfer and it leads to highest QY of the complex. Decreasing of the QY with increasing the complex concentration in the thin film is expecting due to energy transfer between the Eu^{III} ions themselves through as a non-radiative process, instead of reach to the ground state (radiative transition). The highest QY found to be in the thin film as compared with a solution and solid state. It is known that the near location (matching) of the donor and acceptor energy levels leads to efficient energy transfer. Similarly, when the complex doped with PMMA; the PPMA matrix can reduce the collisional quenching of the ligand triplet state in the polymer matrix and the long chain of the PMMA as well as rigidity may lead to close the donor and acceptor in the Eu-complex through efficient inter molecular energy transfer.

2.3.3.1.6 Judd-Ofelt (J–O) spectral parameters and PL Lifetime analysis:

As mentioned in the previous section, the Judd-Ofelt (J-O) parameters [47-49] are one of the most important intensity constituents and it is calculated from the emission spectra which highlight the radiative properties of the Eu^{III} in the host matrixes. The transitions of Eu^{III} from $^5D_0 \rightarrow {}^7F_J$ (J = 2, 4, and 6) are allowed according to the transition selection rules and in electronic-dipole nature. However, the Ω_6 intensity parameter was not determined, as the $^5D_0 \rightarrow {}^7F_6$ emission in this system could not be detected and recorded (long range effects). Judd–Ofelt intensity parameters provide the necessary information regarding local structure and bonding in the vicinity of lanthanide ions in the structure. The intensity parameter, Ω_2 ($^5D_0 \rightarrow {}^7F_2$) of the complex is more sensitive to the site symmetry and it reveals the covalent bonding environment between Eu^{III} ion and surrounding ligand moiety in the Eu-complex. It also states about the symmetry around the Eu^{III} ions, higher the value of Ω_2 parameter higher the amount of asymmetry. The calculation of experimental intensity parameters Ω_J (J = 2 and 4) was done for $^5D_0 \rightarrow {}^7F_2$ and $^5D_0 \rightarrow {}^7F_4$ transition by keeping $^5D_0 \rightarrow {}^7F_1$ as a reference. The relation between radiative emission rate and integrated emission intensity is given in equation 2.4:

The electric dipole transition probability can be obtained from equation 2.4. The forced electric dipole transitions $^5D_0 \rightarrow {}^7F_2$ and $^5D_0 \rightarrow {}^7F_4$ as a function of Judd–Ofelt intensity parameter is formulated and given in equation 2.5. The Ω_2 and Ω_4 parameters for the complexes were calculated to be 1.40 and 0.25, respectively. Higher value of Ω_2 parameter than that of Ω_4 indicates the probability of $^5D_0 \rightarrow {}^7F_2$ transition is indeed dominating. The large value of Ω_2 for the Eu^{III} complex proposes an enriched covalency and strengthening of the $Eu^{3+} – O^{2-}$ bond with high energy and shorter bond length. The detail spectral intensity parameters are tabulated in Table 2.9.

Decay curves of luminescence of the Eu^{III} complex $^5D_0$ excited state were measured at 298 K and under 360 nm excitation source (Figure 2.31). The lifetime of the complex and ligand was calculated in different solutions as well as in solid phase. The obtained decay values of the complexes were best fitted with the single exponential fitting and their ligands were fitted with bi exponential fitting. The single exponential task is given by the equation $I(t) = I_0 +$

A_1 exp $\left(\frac{-t}{\tau}\right)$, where I_0 = 0 is the offset value, A_1 is the scalar quantity (observed from curve fitting), t is the time in ms/μs and τ is the decay time value for the exponential module. The calculated lifetime of the complex is 0.433 ms in solid. In addition, it was also calculated lifetime of the ligand in solid form with different excitation source from 300-420 nm (Figure 2.S15). In case of solution variations were observed lifetime followed in the trend as DMSO (0.62) > acetone (0.60) ≥ DCM (0.60) > toluene (0.57) > $CHCl_3$ (0.55) > THF (0.48) > DMF (0.46) > solid (0.44 ms) at 360 nm. The calculated lifetime of the ligand was found to be higher in DMSO solution ($2.66x10^{-3}$ ms).

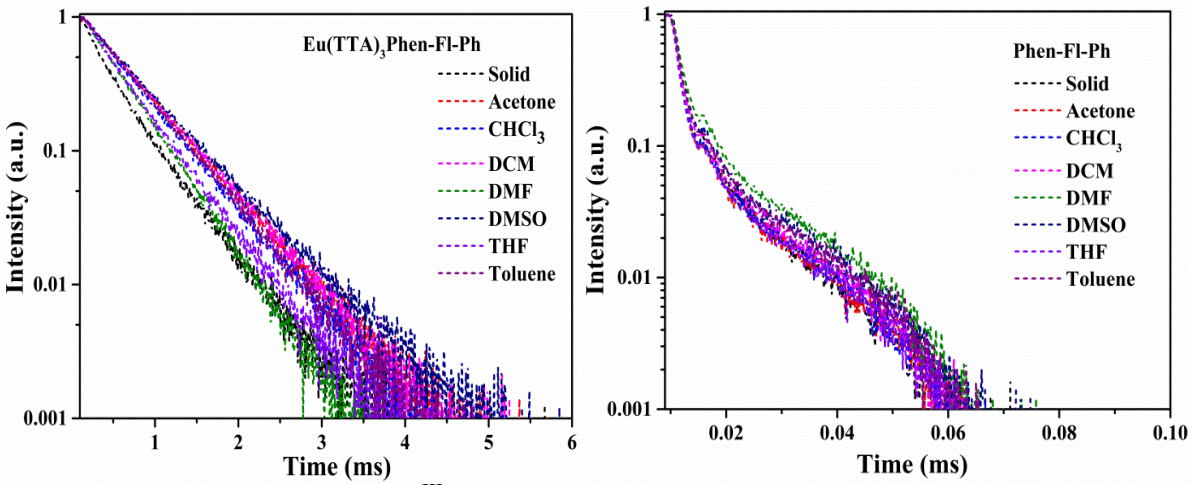

Figure 2.31 The lifetime of the Eu^{III} complex (left) and ligand (right) in different solvents and in the form of solid.

Table 2.8 Calculated luminescence lifetimes (τ_{obs}) and intensity parameters of ligands and corresponding Eu^{III} complexes.

S. No.	Compound	Lifetime (in ms)							
		Solid	Acetone	$CHCl_3$	DCM	DMF	DMSO	THF	Toluene
1.	$Eu(TTA)_3$Phen-Fl-Ph	0.433	0.602	0.557	0.601	0.462	0.625	0.480	0.575
2.	Phen-Fl-Ph (10^{-3} ms) [a]	1.66	1.91	1.95	2.13	2.68	2.66	1.93	2.56

[a]bi-exponential fitting was followed. Luminescence intensity could be described by the sum of two exponential decay components from $I(t) = A_1\exp(-\frac{t}{\tau_1}) + A_2\exp(-\frac{t}{\tau_2})$, Here, τ_1 and τ_2 are short- and long-decay components, A_1 and A_2 are fitting constants. The average lifetime τ is $=(\frac{A_1\tau_1^2 + A_2\tau_2^2}{A_1\tau_1 + A_2\tau_2})$.

The calculated lifetime values are incorporated in the Table 2.8. As compared with the solid, lifetime of the solution is higher and also it is found to be higher in DMSO in both case of ligand and complex. It could be expected that the close packing of the molecules in the solid state leads to non-radiative relaxation via vibrionic coupling than that of the solution [50]. Commonly, the excited state lifetime of $^5D_0$ (Eu^{III}) level is usually comparatively long (μs to ms scale) [69, 70], and which is depends on energy transfer process and it can effect by high frequency vibrational oscillators such as O−H, N−H, and C−H. the obtained results are indicating that the vibrational oscillators frequency is less in DMSO and leads to high lifetime

value. In addition, it was analyzed lifetime of the thin film of the complexes in different ratio (0.1, 0.5, 1 and 5 %) and the observed lifetime is 0.65 (0.1 %), 0.64 (0.5 %), 0.60 (1 %) and 0.57 (5 %), respectively. The observed decay analysis of the thin film of the complex indicates that the increasing the concentration of the Eu^{III} complex leads to decrease lifetime and it is also being reflected from the QY analysis of thin film. The obtained results were tabulated in the Table 2.10.

The overall quantum yield ($\Phi_{overall}$) of the Eu^{III} complex can be obtained by using equation 2.6. The $\Phi_{overall}$ is depends on the two factors such as first one is the efficiency with which the ligands transfer energy onto the Eu^{III} ion, Φ_{sens}, and the second is the intrinsic quantum yield (Φ_{LN}) [71-73]. The intrinsic quantum yield ($\Phi_{Ln)}$ of the Eu^{3+} ion calculated by using equation 2.7. The radiative lifetime (τ_{RAD}) can be calculated by using equation 2.8. Assumption was made that the energy of the MD transition ($^5D_0 \rightarrow {}^7F_1$) and its oscillator strength are constant. Here, $A_{MD,0}$ (14.65 s^{-1}) represents the spontaneous emission probability of the $^5D_0$ - $^7F_1$ transition (vacuo), n is the refractive index of the medium, I_{TOT}/I_{MD} is the ratio of the total area of the corrected Eu^{III} emission spectrum to the area of the $^5D_0$ - $^7F_1$ band and index of refraction equal to 1.5 (average) was taken in the calculation [74, 52a]. From the relative areas of the $^5D_0$–^7F_J emission transitions of Eu^{III} ion is used to predict the experimental branching ratio ($\beta_{1\text{-}3}$). The efficiency of the energy transfer from the ligand levels to Eu^{III} ion can be predicated by the found intrinsic quantum yield (Φ_{Ln}) and energy transfer efficiency (Φ_{sen}). The calculated value of the complex indicates that the currently studied ancillary ligand is an efficient sensitizer for Eu^{III} ion in the presently synthesized complex. All the calculated parameters are tabulated in Table 2.9 and Table 2.10.

Table 2.9 Intensity ratio (I_2/I_1), J-O parameters (Ω_2 and Ω_4) and their experimental branching ratios ($\beta_{1\text{-}3}$) of the complex.

S. No.	$Eu(TTA)_3Phen$-Fl- Ph	I_2/I_1	Ω_2 (10^{-20} cm^2)	Ω_4 (10^{-20} cm^2)	σ_1	σ_2	σ_3	β_1	β_2	β_3
1.	**Solid**	8.36	1.40	0.25	0.559	5.324	0.415	9.69	83.27	70.29
2.	**Thin film, 0.1%**	3.49	5.90	2.89	0.369	5.15	0.372	18.32	66.16	15.52
3.	**0.5 %**	2.68	4.48	2.34	0.419	3.417	0.277	22.45	62.15	15.40
4.	**1 %**	3.19	5.39	3.02	0.419	1.822	0.464	19.35	63.68	16.96
5.	**5 %**	2.60	4.27	2.45	0.488	5.179	0.493	22.76	60.96	16.27

Table 2.10 The Radiative (A_{RAD}) and nonradiative (A_{NR}) decay rates, $^5D_0$ lifetime (t_{obs}), intrinsic quantum yield (Φ_{Ln}), energy transfer efficiency (Φ_{sen}) and overall quantum yield ($\Phi_{overall}$) for the complex.

S. No.	$Eu(TTA)_3Phen$-Fl-Ph	A_{RAD} (S^{-1})	A_{NR} (S^{-1})	τ_{obs} (ms)	τ_{RAD} (ms)	Φ_{Ln} (%)	Φ_{Sen} (%)	$\Phi_{Overall}$ (%)
1.	**Solid**	515.96	179	0.433	1.94	22.34	18.46	12.1
2.	**Thin film, 0.1%**	180.61	125	0.653	3.66	17.87	15	26.6
3.	**0.5 %**	222.71	132	0.643	4.49	14.32	25	57.3
4.	**1 %**	258.29	139	0.606	3.87	15.65	35.97	43.5
5.	**5 %**	219.67	153	0.573	4.55	12.59	--.--	--.--

2.3.3.2 Electrochemical analysis:

To comprehend the redox potentials of the ligand and the corresponding complex, we have measured cyclic voltammetry (CV) analysis. Since the redox potentials gives the LUMO and HOMO of the same, respectively. The obtained cyclic voltammetry data for the complex and the ligand was given in Figure 2.32. From the onset potential curves the HOMO and LUMO levels were calculated by using equation 2.9 and 2.10. As can be observed from the cyclic voltammogram, there has been a slight increase in the onset potential for oxidation and the vice versa for a reduction in case of the complex as compared to the ligand. This can be an indication towards the formation of the expected metal complex. The energy gap of the ligand (1.93 eV) found to be less as compared to that of the complex (2.36 eV). The obtained narrow band gap is suitable to get the red emission from the complex. The reasonable difference of the band gap of the ligand and complex from the cyclic voltammetry analysis and UV absorption analysis provoked as to repeat the experiment and found the same results which are incorporated in Table 2.11.

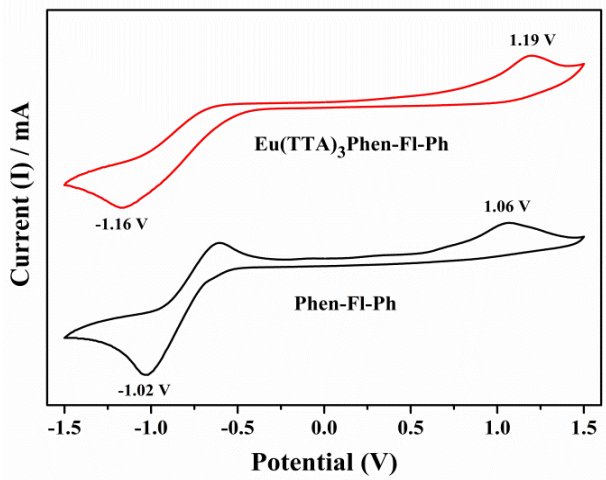

Figure 2.32 The cyclic voltammetry plot for the complex and the ligand.

Table 2.11 Electrochemical properties of the ligands and respective Eu^{III}-complexes.

S. No.	Compound Name	Voltage$^{Oxi}_{onset}$ [V] (E_{HOMO} [eV])	Voltage$^{Red}_{onset}$ [V] (E_{LUMO} [eV])	$\lambda_{onset,}$ [nm] (a)	Band gap/Energy gap E_g^{Opt}, [eV] (b)
1.	**Phen-Fl-Ph**	1.066 (-5.46)	-1.030 (-3.37)	536.7	2.31 (1.93)
2.	**$Eu(TTA)_3$Phen -Fl-Ph**	1.189 (-5.59)	-1.169 (-3.23)	399.9	3.10 (2.36)

E_{red}^{onset}= the onset reduction potentials, E_{Oxd}^{onset}= the onset oxidation potentials, E_g = band gap, E_g = E_{LUMO} − E_{HOMO}. (a) Calculated from the optical absorption (DRS spectra), (b) Calculated the onset wavelength of optical absorption (onset) in the solid-state film (DRS spectra). The energy differences (HOMO and LUMO) values calculated by cyclic voltammogram are mentioned in the bracket.

2.3.3.3 Theoretical Calculations (Density functional theory (DFT) calculations):

The theoretical calculations were made for the ligand and Frontier orbital (LUMO+1 to HOMO-1) were tabulated in Table 2.12. To cognize the phenomena with the help of theoretical calculation, the ligand was optimized first in the gas phase using DFT and Becke three parameter

Lee-Yang-Parr (B3LYP) form for exchange-correlation potential and 6-31G (d, p) basis set [75,76]. The structure was found to be in the minima of the potential energy surface as the normal mode of frequency is positive. Optimized ligand ground state electrons were excited vertically to obtain the excited energy levels. Subsequently, the UV−Vis spectral calculation was also performed by time dependent density functional theory (TD-DFT) with gas phase and solution. All the calculations were carried out using Gaussian09 W and Gauss View suite of programs. Computed vertical transitions and their oscillator strengths as well as respective configurations were incorporated in Table 2.13. The electron density of HOMO of the ligand was located on the phenanthroimidazole moiety and LUMO was located on Fluorene moiety.

Table 2.12 The HOMO-LUMO and HOMO-1, LUMO+1 energy levels of the ligand.

Phen-Fl-Ph			
HOMO	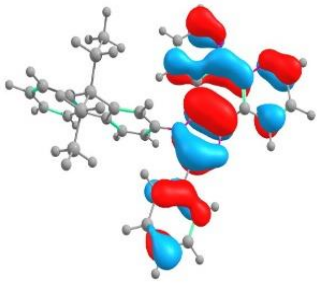	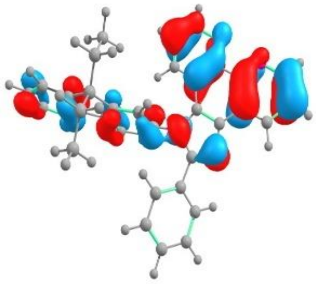	**HOMO-1**
LUMO	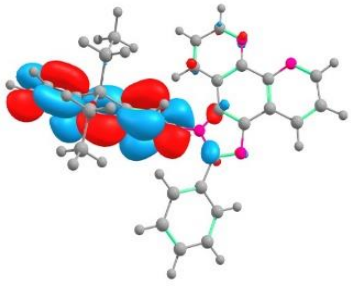	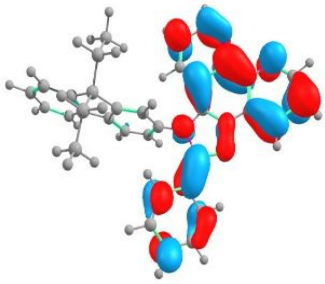	**LUMO+1**

Table 2.13 Computed vertical transitions and their oscillator strengths and configurations[a]

Compound Phen-Fl-Ph	**State**	**Energy (eV)**	**λ_{max} nm**	***f***	**Configuration**
Singlet	Gas	3.4889	355.53	0.0160	HOMO → LUMO (69.8%)
		3.8878	318.91	0.2960	HOMO-1 → LUMO+1 (13.43%)
					HOMO → LUMO+1 (38.58%)
					HOMO → LUMO+2 (53.51%)
		4.2602	291.03	0.2113	HOMO-2 → LUMO (18.93%)
					HOMO-1 → LUMO (64.40%)
					HOMO → LUMO+4 (14.6%)
		4.3907	282.3	0.3529	HOMO-2 → LUMO (50.35%)
	DCM	3.586	345.75	0.0736	HOMO → LUMO (66.76%)
		3.8055	325.80	0.2664	HOMO-2 → LUMO (16.7%)
					HOMO → LUMO (16.10%)
					HOMO → LUMO+1 (65.64%)
		4.0891	303.21	0.1272	HOMO-4 → LUMO (11.98%)
					HOMO → LUMO+3 (45.69%)

		4.1643	297.73	0.2887	HOMO-4 → LUMO (19.33%) HOMO-1 → LUMO+1 (56.42%) HOMO → LUMO+3 (30.41%)
		4.4051	281.45	0.5844	HOMO-4 → LUMO+1 (15.43%) HOMO-2 → LUMO+1 (17.73%) HOMO-1 →LUMO+2 (61.77%)
Triplet	Gas	2.4679	447.94	-	HOMO-6 → LUMO+4 (10.88%) HOMO-1 → LUMO+2 (13.91%) HOMO → LUMO (22.10%) HOMO →LUMO+1 (45.96%) HOMO →LUMO+2 (36.73%)
	DCM	2.8055	441.93	-	HOMO-2 → LUMO (17.89%) HOMO → LUMO (31.14%) HOMO → LUMO+1 (50.67%)

[a]Orbital contributions below 10% are omitted.

2.3.3.4 Fabrication of LED with Ligand and Eu complex:

The ligand and the complex were conjugated with the LED, InGaN-based LED chip (395 nm, near UV light) in a different ratio of the ligand/complex to do the realistic application and obtained emission spectrum with 20 mA as a forward bias is shown in Figure 2.33. The ligand was shown in solution form as well as the thin film as blue emission and solid shown almost white emission. However, ligand with LED was shown blueish green (x = 0.26, y = 0.36; 1-10) and sky blue (x = 0.20, 0.29; 1-50) emission, respectively. The Eu^{III} complex conjugated LED was shown red emission with CIE are x = 0.65, y = 0.34 (1-10) and x = 0.66, y = 0.34, respectively.

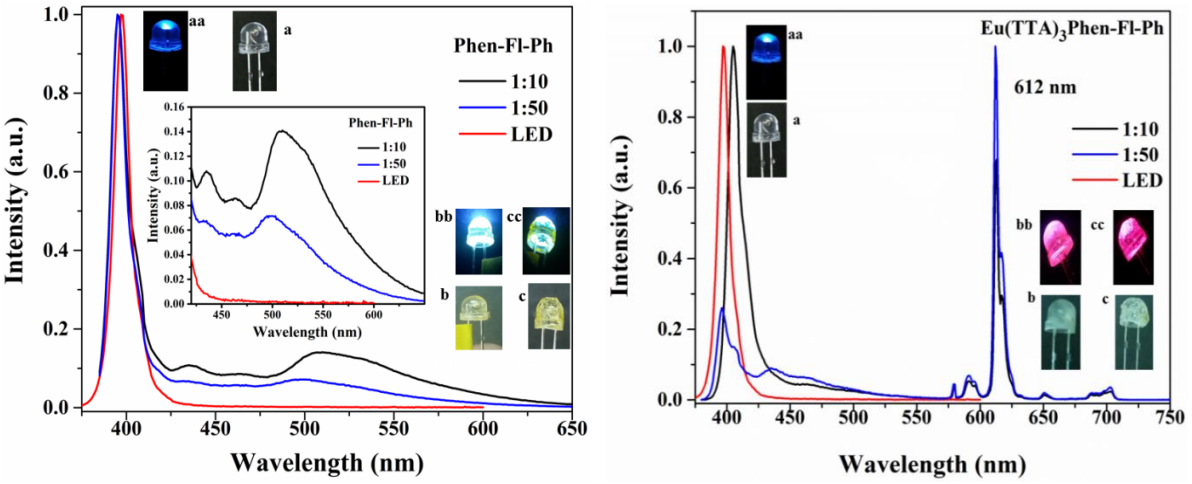

Figure 2.33 The spectra's of ligand and complex coated on the 395 nm emitted LED chip at 20 mA forward bias in 1-10 and 1-50 ratio. Left: the ligand emission and shown in onset emission of a ligand for clarity. Right: Eu^{III} complex emission. In inset **a** is the original 395 nm emitted LED chip, **aa** is under forward bias. **b** (1:10), **c** (1:50) is coated with L/Eu^{III} complex and **bb** is with a forward bias, respectively.

The CIE color coordinates of the ligand and the corresponding complex were shown in Figure 2.34, left. The calculated outcomes were satisfactory values of NTSC standards (x = 0.66, y = 0.33) for red emission. The excitation source from LED was mostly utilized by complex for 1-10 ratios.

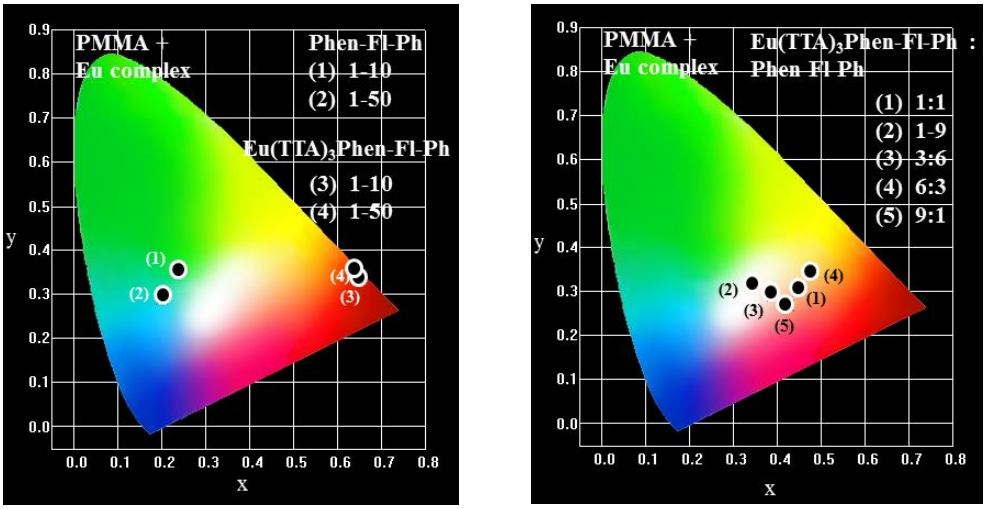

Figure 2.34 The CIE spectra of ligand and complex coated on the 395 nm emitted LED chip at 20 mA forward bias in 1-10 and 1-50 ratio (left) and CIE of mixing of different ratio of Eu^{III} complex and ligand.

However, the complex was shown red emission and indicating that the synthesized complex is potential red materials. To explain the LED emission from the ligand and Eu^{III} complex as well as to get the white light LED emission, efforts have been made to conjugate the mixing of Eu^{III} complex and ligand in different ratios (Figure 2.35). Since, the emission of the ligand is overlapped with the excitation lines of Eu^{III} ion which could help to excite the Eu^{III} ions by resonance energy transfer (host-guest or sensitizer acceptor concept).

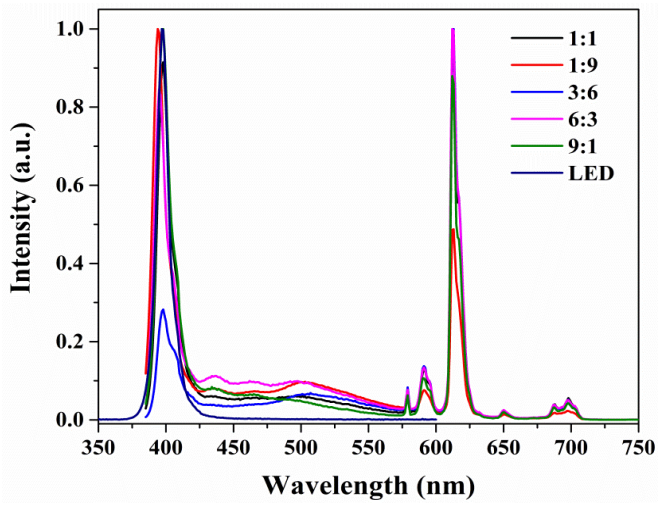

Figure 2.35 The emission of the LED conjugated with Eu^{III} complex and ligand mixing in different ratio.

The excited energy of the ligand triplet level can feed efficiently to the Eu excited levels. The ratio of the complex and ligand with 1: 9 was shown white light emission with corresponding CIE color coordinate is x = 0.34, y = 0.32. The CIE of the remained ratio of the complex and ligand were incorporated in the Figure 2.32, right.

2.4 Summary and conclusion:

The designed ancillary ligands were synthesized and two of them structurally characterized. Their corresponding Eu-complexes were also been synthesized successfully and studied their photophysical properties syatamatically. The excited energy of the ligand is fully transferring to the Eu-metal ion in the complexes, 1Eu, 2Eu, and 3Eu confirmed from the PL emission analysis. However, fluorene integrated with phenthroimazolde show white light emission and the corresponding mono nuclear Eu^{III} complex tris-β-diketones shown red emission. The QY of the complex, 2Eu was shown higher value (39.4 %) indicating that the presence of m-CF_3 leads to improve the efficiency and $Eu(TTA)_3$Phen-pCF_3-Ph showed 78.7 % (thin film). The analysis from the InGaN-based LED (395 nm) also supported the same. The consumption of the emission from the source is higher in m-CF_3 connected complex than remained complexes. The calculated CIE color coordinates for the complexes are shown bright red emission in solution, solid, thin film, and LEDs. These are indicating that the fluorine moieties could reduce the non-radiative transition and leads to enhancement in the red emission. The white emissive fluorene based ligand combined with near UV LED show yellowish green emission with CIE color coordinates of x = 0.26, y = 0.36 (1-10) and sky blue, x = 0.20, y = 0.29 (1-50), whereas the Eu complex integrated with near UV LED show red color emission with CIE color coordinates of x = 0.66, y = 0.34, respectively. White emission from LED was obtained from the mixing of ligand and the complex (host guest system) combined with near UV LED. This work demonstrates that the potential usage of the ligand and the complex can give complement color to produce white emission. The prominent results are indicating that the synthesized complexes are efficient and applications to novel organic Eu^{III} devices, like organic liquid lasers, plastic lasers, and optical fibers.

2.5 References:

[1] (a) S. Reineke, F. Lindner, G. Schwartz, N. Seidler, K. Walzer, B. Lussem and K. Leo, *Nature*, 2009, **459**, 234; (b) A. H. Shelton, I. V. Sazanovich, J. A. Weinstein and M. D. Ward, *Chem. Commun.*, 2012, **48**, 2749; (c) S. Liu, P. He, H. Wang, J. Shi and M. Gong, *Inorg. Chem. Commun.* 2009, **12**, 506–508; (d) J. Andrez, G. Bozoklu, G. Nocton, J. Pecaut, R. Scopelliti, L. Dubois and M. Mazzanti, *Chem. Eur. J.*, 2015, **21**, 15188–15200.

[2] C. W. Tang and S. A. VanSlyke, *Appl. Phys. Lett.*, 1987, **51**, 913.

[3] (a) L. M. Zhang and B. Li, *J. Lumin.*, 2009, **129,** 1304; (b) H. Xu, Q. Sun, Z. An, Y. Wei and X. Liu, *Coord. Chem. Rev.*, 2015, **293–294**, 228–249.

[4] P. Z. Qin, C. G. Niu, M. Ruan, G. M. Zenga and X. Y. Wanga, *Analyst*, 2010, **135**, 2144–2149.

[5] D. E. Barry, D. F. Caffrey and T. Gunnlaugsson, *Chem. Soc. Rev.*, 2016, **45**, 3244–3274.

[6] (a) Y. J. Fu, T. K. S. Wong, Y. K. Yan, G. M. Wang and X. Hu, *Thin Solid Films*, 2002, **417**, 78-84; (b) D. B. Ambili Raj, B. Francis, M. L. P. Reddy, R. R. Butorac, V. M. Lynch and A. H. Cowley, *Inorg. Chem.*, 2010, **49**, 9055–9063.

[7] I. Hemmila and V. Laitala, *J. Fluoresc.*, 2005, **15**, 529.

[8] E. Moretti, L. Bellotto, M. Basile, C. Malba, F. Enrichi, A. Benedetti and S. Polizzi, *Mater. Chem. Phys.*, 2013, **142**, 445- 452.

[9] (a) P. Hanninen and H. Harma, Lanthanide luminescence, Springer series on fluorescence, 2011, pp 1-45; (b) S. Comby and J. C. G. Bunzli, in Handbook on the physics and chemistry of rare earths, ed. J. C. G. Bunzli, K. A. Gschneidner Jr and V. K. Pecharsky, *Elsevier*, 2007, pp 217–470.

[10] (a) S. I. Weissman, *J. Chem. Phys.*, 1942, **10**, 214–217; (b) Koen Binnemans, *Coord. Chem. Rev.*, 2015, **295**, 1–45.

[11] K. Binnemans, *Chem. Rev.*, 2009, **109**, 4283–4374.

[12] C. Piguet and J.-C. G. Bunzli, *Chem. Soc. Rev.*, 1999, **28**, 347.

[13] B. Zuqiang, G. Deqing, G. Min, X. Hao, L. Fuyou, H. Chunhui, W. Kezhi and J. Linpei, *Science in China Ser. B Chemistry*, 2004, **47**, 326–334.

[14] Y. Zheng, J. Lin, Y. Liang, Q. Lin, Y. Yu, Q. Meng, Y. Zhou, S. Wang, H. Wang and H. Zhang, *J. Mater. Chem.*, 2001, **11**, 2615–2619.

[15] (a) Ana de Bettencourt-Dias, *Dalton trans.*, 2007, 2229-2241; (b) C. Yang, L. M. Fu, Y. Wang, J. P. Zhang, W. T. Wong, X. C. Ai, Y. F. Qiao, B. S. Zou and L. L. Gui, *Angew. Chem. Int. Ed.*, 2004, **43**, 5010–5013.

[16] (a) A. D'Aleo, F. Pointillart, L. Ouahab, C. Andraud and O. Maury, *Coord. Chem. Rev.*, 2012, **256**, 1604–1620; (b) A. D'Aleo, A. Picot, A. Beeby, J. A. G. Williams, B. Le Guennic, C. Andraud and O. Maury, *Inorg. Chem.*, 2008, **47**, 10258−10268; (c) A. D'Aleo, E. G. Moore, G. Szigethy, J. Xu and K. N. Raymond, *Inorg. Chem.*, 2009, **48**, 9316–9324; (d) F. J. Steemers, W. Verboom, D. N. Reinhoudt, E. B. V. Tol and J. W. Verhoeven, *J. Am. Chem. Soc.*, 1995, **117**, 9408–9414.

[17] (a) G. F. de Sa, O. L. Malta , C. de Mello Donega, A. M. Simas, R. L. Longo, P. A. Santa-Cruz and E. F. da Silva Jr, *Coord. Chem. Rev.*, 2000, **196**, 165–195; (b) J. H. S. K. Monteiro, Ana de Bettencourt-Dias and F. A. Sigoli, *Inorg. Chem.*, 2017, **56**, 709−712.

[18] J. Y. Tsao, M. H. Crawford, M. E. Coltrin, A. J. Fischer, D. D. Koleske, G. S. Subramania, G. T. Wang, J. J. Wierer and R. F. Karlicek, *Adv. Opt. Mater.*, 2014, **2**, 803–809.

[19] Z. Xia and A. Meijerink, *Chem. Soc. Rev.*, 2017, **46**, 275–299.
[20] K. Singh and S. Vaidyanathan, *Chemistry Select.,* 2017, **1**, 5448–5462.
[21] K. Singh and S. Vaidyanathan, *RSC Advances.,* 2016, **6**, 98652–98662.
[22] H. J. Yu, K. Park, W. Chung, J. Kim, B. H. Chun and S. H. Kim, *Polymer Journal.*, 2009, 41, 1076–1079.
[23] N. J. Findlay, J. Bruckbauer, A. R. Inigo, B. Breig, S. Arumugam, D. J. Wallis, R. W. Martin and P. J. Skabara, *Adv. Mater.*, 2014, **26**, 7290–7294.
[24] A. B. Kajjam, S. Giri and S. Vaidyanathan, *Mater. Chem. Front.*, 2017, **1**, 572–572.
[25] A. Luridiana, G. Pretta, D. Chiriu, C. M. Carbonaro, R. Corpino, F. Secci, A. Frongia, L. Stagi and P. C. Ricci, *RSC Adv.*, 2016, **6**, 22111–22120.
[26] (a) P. He, H. Wang, S. Liu, W. Hu, J. Shi, G. Wang and M. Gongz, *Journal of The Electrochemical Society*, 2009, **156**, E46–E49; (b) Y. Luo, Q. Yan, Z. Zhang, X. Yu, W. Wu, W. Su and Q. Zhang, *J. Photochem. Photobiol. A*, 2009, **206**, 102–108; (c) P. He, H. Wang, S. Liu, J. Shi, G. Wang and M. Gong, *J. Phys. Chem. A*, 2009, **113**, 12885–12890; (d) H. Wang, P. He, S. Liu, J. Shi and M. Gong, *Inorg. Chem. Commun.*, 2010, **13**, 145–148.
[27] Z. Zheng, Q. Dong, L. Gou, J. H. Su and J. Huang, *J. Mater. Chem. C*, 2014, **2**, 9858.
[28] M. L. Bhaumik, *J. Chem. Phys.*, 1964, **40**, 3711.
[29] W. M. Watson, R. P. Zerger, J. T. Yardley and G. D. Stucky, *Inorg. Chem.*, 1975, **14**, 2675.
[30] C. Freund, W. Porzio, U. Giovanella, F. Vignali, M. Pasini, S. Destri , A. Mech , S. D. Pietro, L. D. Bari and P. Mineo, *Inorg. Chem.*, 2011, **50**, 5417–5429.
[31] (a) A. Becke, *J. Chem. Phys.*, 1993, **98**, 5648; (b) C. Lee, W. Yang and R. G. Parr, *Phys. Rev. B*, 1988, **37**, 785–789.
[32] R. Bauernschmitt and R. Ahlrichs, *Chem. Phys. Lett.*, 1996, **256**, 454−464.
[33] M. J. Frisch, G. W. Trucks, H. B. Schlegel, G. E. Scuseria, M. A. Robb, J. R. Cheeseman, G. Scalmani, V. Barone, B. Mennucci, G. A. Petersson, H. Nakatsuji, M. Caricato, X. Li, H. P. Hratchian, A. F. Izmaylov, J. Bloino, G. Zheng, J. L. Sonnenberg, M. Hada, M. Ehara, K. Toyota, R. Fukuda, J. Hasegawa, M. Ishida, T. Nakajima, Y. Honda, O. Kitao, H. Nakai, T. Vreven, J. A. Montgomery, Jr., J. E. Peralta, F. Ogliaro, M. Bearpark, J. J. Heyd, E. Brothers, K. N. Kudin, V. N. Staroverov, R. Kobayashi, J. Normand, K. Raghavachari, A. Rendell, J. C. Burant, S. S. Iyengar, J. Tomasi, M. Cossi, N. Rega, J. M. Millam, M. Klene, J. E. Knox, J. B. Cross, V. Bakken, C. Adamo, J. Jaramillo R. Gomperts, R. E. Stratmann, O. Yazyev, A. J. Austin, R. Cammi, C. Pomelli, J. W. Ochterski, R. L. Martin, K. Morokuma, V. G. Zakrzewski, G. A. Voth, P. Salvador, J. J. Dannenberg, S. Dapprich, A. D. Daniels, Ö. Farkas, J. B. Foresman, J. V. Ortiz, J. Cioslowski and D. J. Fox, Gaussian 09, Revision A.1, Gaussian, Inc., Wallingford CT, 2009.
[34] (a) J. Tomasi, B. Mennucci and R. Cammi, *Chem. Rev.*, 2005, **105**, 2999−3093; (b) I. Gupta, S. Das, H. R. Bhat, N. Balsukuri, P. C. Jha, Y. Hisamune, M. Ishida, H. Furuta and S. Mori, *Inorg. Chem. Front.,* 2017, DOI: 10.1039/C6QI00558F.
[35] O. V. Dolomanov, L. J. Bourhis, R. J. Gildea, J. A. K. Howard and H. Puschmann, *J. Appl. Cryst.*, 2009, **42**, 339–341.
[36] G. M. Sheldrick, *Acta Cryst.*, 2008, **A 64**, 112−122.
[37] (a) X. Zhou, X. Zhao, Y. Wang, B. Wu, J. Shen, L. Li and Q. Li, *Inorg. Chem.*, 2014, **53**, 12275–12282; (b) L. R. Melby, N. J. Rose, E. Abramsonan and J. C. Caris, *J. Am. Chem. Soc.*, 1964, **86**, 5117–5125.

[38] (a) B. Rajamouli, P. Sood, S. Giri, V. Krishnan and V. Sivakumar, *Eur. J. Inorg. Chem.*, 2016, **24**, 3900–3911; (b) B. Rajamouli and V. Sivakumar, *New J. Chem.*, 2017, **41**, 1017-1027; (c) K. Qiu, Y. Liu, H. Huang, C. Liu, H. Zhu, Y. Chen, L. Ji and H. Chao, *Dalton Trans*., 2016, **45**, 16144; (d) J. Liu, Y. Chen, G. Li, P. Zhang, C. Jin, L. Zeng, L. Ji and H. Chao, *Biomaterials*, 2015, **56,** 140-153; (e) C. Jin, J. Liu, Y. Chen, L. Zeng, R. Guan, C. Ouyang, L. Ji and H. Chao, *Chem. Eur. J.*, 2015, **21**, 12000–12010.

[39] H. Zhang, S. Wang, Y. Li, B. Zhang, C. Du, X. Wan and Y. Chen, *Tetrahedron*, 2009, **65**, 4455–4463.

[40] Ebraheem and A. El-Saied, *Materials Sciences and Applications*, 2013, **4**, 324–329.

[41] V. Sivakumar and U. V. Varadaraju, *J. Electrochem. Soc.*, 2005, 152, H168–H171.

[42] (a) M. Shi, F. Li, T. Yi, D. Zhang, H. Hu and C. Huang, *Inorganic chemistry*, 2005, **44**, 8929−8936; (b) T. Li, W. Shang, F. Zhang, L. Mao, C. Tang, M. Song, C. Du and Y. Wu, *Engineering*, 2011, **3**, 301−311.

[43] M. Latva, H. Takalo, V. M. Mukkala, C. Matachescu, J. C. Rodriguez-Ubis and J. Kankare, *J. Lumin.*, 1997, **75**, 149–169.

[44] H. Xu, H. L. Wang, X. H. Zhu, K. Yin, G. Y. Zhong, X. Y. Hou and W. Huang, *J. Phys. Chem. B*, 2006, **110**, 3023–3029.

[45] (a) A. Balamurugan, M. L. P. Reddy and M. Jayakannan, *J. Mater. Chem. A*, 2013, **1**, 2256; (b) A. R. Ramya, S. Varughese, M. L. P. Reddy, *Dalton Trans.*, 2014, **43**, 10940.

[46] J. C. de Mello, H. F. Wittmann and R. H. Friend, *Adv. Mater.*, 1997, **9**, 230–232.

[47] G. S. Oflet, *J Chem. Phys.*, 1962, **37**, 511–520.

[48] B. R. Judd, *Phys. Rev.*, 1962, **127**, 750.

[49] S. Kasturi and V. Sivakumar, *Chemistry Select*, 2016, **1**, 5448–5462.

[50] G. R. Choppin and D. R. Peterman, *Coord. Chemical Reviews*, 1998, **174**, 283−299.

[51] (a) J. Kido, K. Nagai and Y. Ohashi, *Chem. Lett.*, 1990, 657–660; (b) Y. Okamoto, *Makromol. Chem., Macromol. Symp.*, 1992, **59**, 83–98; (c) C. Adachi, M. A. Baldo and S. R. Forrest, *J. Appl. Phys*., 2000, **87**, 8049; (d) C. Tao, X. Yuan, Q. Yin, H. Yan, W. Ni, L. Yan and L. Zhang, *J Mater Sci: Mater Electron*, 2016, **27**, 5715–5722.

[52] (a) A. R. Ramya, M. L. P. Reddy, A. H. Cowley and K. V. Vasudevan, *Inorg. Chem*. 2010, **49**, 2407; (b) M. Xiao and P. R. Selvin, *J. Am. Chem. Soc.*, 2001, **123**, 7067; (*c*) B. Rajamouli, C. S. D. Viswanath, S. Giri, C. K. Jayasankar and V. Sivakumar, *New J. Chem.*, 2017, **41**, 3112–3123.

[53] (a) S. Quici, M. Cavazzini, G. Marzanni, G. Accorsi, N. Armaroli, B. Ventura and F. Barigelletti, *Inorg. Chem.*, 2005, **44**, 529; (b) Y. H. Kim, N. S. Baek and H. K. Kim, *Chem. Phys. Chem.*, 2006, **7**, 213; (c) S. Comby, D. Imbert, C. Anne-Sophie, J. C. G. Bunzli, L. J. Charbonniere and R. F. Ziessel, *Inorg. Chem.*, 2004, **43**, 7369.

[54] (a) D. B. Ambili Raj, B. Francis, M. L. P. Reddy, R. R. Butorac, V. M. Lynch and A. H. Cowley, *Inorg. Chem.*, 2010, **49**, 9055–9063; (b) O. Moudam, B. C. Rowan, M. Alamiry, P. Richardson, B. S. Richards, A. C. Jones and N. Robertson, *Chem. Commun.*, 2009, 6649–6651; (c) Y. Hasegawa, H. Kawai, K. Nakamura, N. Yasuda, Y. Wada and S. Yanagida, *J. Alloys Compd.*, 2006, **408**, 669–674; (d) N. Wartenberg, O. Raccurt, D. Imbert, M. Mazzantic and E. Bourgeat-Lami, *J. Mater. Chem. C*, 2013, **1**, 2061–2068.

[55] D. M. de Leeuw, M. M. J. Simenon, A. R. Brown and R. E. F. Einerhand, *Synth. Met.*, 1997, **87**, 53–59.

[56] M. Shang, C. Li and J. Lin, *Chem. Soc. Rev.*, 2014, **43**, 1372–1386.

[57] P. Coppo, M. Duati, V. N. Kozhevnikov, J. W. Hofstraat and L. De Cola, *Angew Chem Int Ed.*, 2005, **44**, 1806–1810.
[58] A. H. Shelton, I. V. Sazanovich, J. A. Weinstein and M. D. Ward, *Chem comm.*, 2012, **48**, 2749–2751.
[59] N. K. Al-Rasbi, H. Adams and F. E. O. Suliman, *Dyes and Pigments.*, 2014,**104**, 83–88.
[60] K. Singh and S. Vaidyanathan, *RSC Advances.*, 2016, **6**, 98652–98662
[61] N. Mataga, Y. Kaifu and M. Koizumi, *Bull. Chem. Soc. Jpn.*, 1956, **29**, 465−470.
[62] A. Filarowski, M. Kluba, K. C. Boczula, A. Koll, A. Kochel, L. Pandey, W. M. D. Borggraeve, M. V. D. Auweraer, J. Catalanc and N. Boens, *Photochem. Photobiol. Sci.*, 2010, **9**, 996–1008.
[63] Masaki Shimizu and Tamejiro Hiyama, *Chem. Asian J.*, 2010, **5**, 1516–1531.
[64] B. W. D'Andrade and S. R. Forrest, *Adv. Mater.*, 2004, **16**, 1585–1595.
[65] E. Kim and S. B. Park, *Chem. Asian J.*, 2009, **4**, 1646–1658.
[66] K. Binnemans, *Coord. Chem. Rev.*, 2015, **295**, 1–45.
[67] S. Han, W. Huang and X. Liu, *Chem. Soc. Rev.*, 2013, **42**, 173–201.
[68] H. Xu, Q. Sun, Z. An, Y. Wei and X. Liu, *Coord. Chem. Rev.*, 2015, **293–294**, 228–249.
[69] E. G. Moore, A. P. S. Samuel and K. N. Raymond, *Acc. Chem. Res.*, 2009, **42**, 542−552.
[70] D. Parker, R. S. Dickins, H. Puschmann, C. Crossland, and J. A. K. Howard, *Chem. Rev.*, 2002, **102**, 1977−2010.
[71] S. Quici, M. Cavazzini, G. Marzanni, G. Accorsi, N. Armaroli, B. Ventura and F. Barigelletti, *Inorg. Chem.*, 2005, **44**, 529–537.
[72] Y. H. Kim, N. S. Baek and H. K. Kim, *Chem. Phys. Chem.*, 2006, **7**, 213–221.
[73] S. Comby, D. Imbert, C. Anne-Sophie, J. C. G. Bunzli, L. J. Charbonniere and R. F. Ziessel, *Inorg. Chem.*, 2004, **43**, 7369–7379.
[74] N. B. D. Lima, S. M. C. Gonçalves, S. A. Júnior and A. M. Simas, *Scientific Reports.*, 2013, **3**, 2395.
[75] S. Yoo, X. C. Zeng and S. S. Xantheas, *J. Chem. Phys.*, 2009, **130**, 221102.
[76] B. Komjati, A. Urai, S. Hosztafi, J. Kokosi, B. Kovats, J. Nagy and P. Horvath, *Spectrochimica Acta Part A: Molecular and Biomolecular Spectroscopy*, 2016, **155**, 95–102.

Chapter 3

Design and synthesis of new bipolar ligands based on phenanthroimidazole for tunable emissive Eu^{III} complexes: combined experimental and theoretical study

Abstract

A new class of bipolar phenanthroimidazole based (N1 functionalization with Ph, mCF_3, pCF_3 and Fl) ligands and their efficient β-diketonate Eu^{III} complexes have been designed, synthesized, characterized successfully and their photophysical, electrochemical properties have also been investigated. All the ligands and complexes show similar UV-Visible absorption behaviour (π - π*, at ~270, ~360 nm). Photoluminescence emission spectra of Eu-complexes and its ligands were carried out in solution form as well as in solid and thin film. The PL study indicates that the Eu-complex emits tunable emission due to incomplete/partial energy transfer (white (solution), red (solid)), whereas fluorene decorated Eu-complex shows narrow band red emission with appropriate CIE color gamut. The obtained PL emission clearly indicates that the efficient energy transfer encountered in case of fluorene based complex. The energy transfer mechanism for all the Eu-complexes was proposed based on combined experimental and theoretical study (DFT, TD-DFT). The PL lifetime of the Eu^{III} complexes also supports the PL emission behaviour. The Judd–Ofelt spectral intensity parameters, electrochemical study and absolute QY (mCF_3 based Eu-complex shows better QY of 75.9 %) of the Eu-complexes were also been investigated. White and red LED was fabricated using these complexes with near UV InGaN based LEDs (395 nm).

Keywords: Eu^{III} ion; white emission; Fluorene; Energy transfer

3.1 Introduction:

Light emitting lanthanide (Ln) based molecular complexes are considered as a new class of EL molecular materials for phosphorescent based OLED devices due to their line like emission characteristics and other eminent properties like large Stokes shifts, long luminescence lifetime as well as phosphorescent emission [1, 2]. The Ln emission arises specifically from the 4f - 4f electronic transition. In organo-Ln complexes the excitation energy of the ligand (antenna) is efficiently transferred to the central metal ion via triplet state of ligand and produce different emission colors. Among all the Ln ions, europium (Eu) based complexes have gained considerable attention to generate efficient red emitters [3, 4]. The Eu^{III} ion excited states cannot be directly populated efficiently as it violates both spin and Laporte selection rule (forbidden transition). Thus, the oscillator strength of the absorption band is very weak and restricted for practical applications. Hence, the Eu excitation levels need to be indirectly populated via ligand absorption that can populate the Eu excited state manifold by energy transfer (ET). In general, the electrically excited electrons are produce 25% singlet and 75% triplet state excitons and it is well documented. Hence, the efficiency is limited to 25% (singlet) according to spin statistics and it means that only the singlet excitons can recombine to produce light. However, there is a possibility of harvesting both singlet and triplet state excitons to ground state by the introduction of heavy metal ions and the theoretical internal quantum efficiency can be expected to reach up to 100% [5]. The presence of Ln metal ion facilitates the energy transfer from the singlet to triplet states through inter system crossing (ISC) and subsequently the emission arises from the 4*f*- levels of Ln ions. The sharp emission bands of Ln ions are suitable for full color displays. Nevertheless, in terms of practical applications the performance of Ln-ions is still unsatisfactory.

Most of the devices are unable to produce efficient characteristic red emission due to inefficient energy transfer from ligand to central Eu^{III} metal ion, as well as poor carrier (hole / electron) transporting properties in the device. In addition, the matrix vibration through nonradiative pathways leads to luminescence quenching and subsequent decrease in quantum efficiency (QE) [6, 7]. In accordance with the energy band gap law, generating efficient red emitters is intrinsically more difficult [8]. For the period of the device operation, phase separation occurs between the host and guest by usual doping methods. To avoid such problems, an alternative method has been proposed that the charge transporting groups could be linked to the Ln complexes by covalent bonding [9, 10]. Most of the holes transporting materials reported are derived from aromatic amines (arylamine units) [11, 12]. The aryl amine moieties are attached to the emissive materials and the same is expected to improve the hole injection/transporting properties of the emissive materials. Eu^{III} complexes with triphenylamine (TPA)/carbazole (CBZ) as a hole transporting, phenanthroline (Phen) as an electron transporting and Dibenzoylmethane (DBM) as an antenna fragments have been documented [13, 14]. However, focused research is still necessary in proactive design of Ln complexes, in order to improve the quantum efficiency of the Ln complex as well as the color purity. Further, it is also essential to understand the energy transfer between singlet ($^1\pi\pi^*$) and triplet ($^3\pi\pi^*$) energy levels of ligand and subsequent triplet (π-π^*) to $^5D_0$ level energy transfer to get characteristic red emission from Eu^{III} metal ion. Since, the ligand excited levels were responsible for red or white emission (complete or partial energy transfer). Numerous researches were executed to obtain single white light emissive organometallic complex to use in smart displays [15, 16]. However, lanthanide based single molecular white emission complexes scarcely reported [17-19] and research on design of organic chromophore that can facilitate partial energy transfer in the Eu complexes is fascinating.

3.2 TPA functionalized new bipolar ligands for white emissive Eu^{III} complex:

3.2.1 Outline of the present study:

The Previous chapter, the synthesized Eu-complexes with phenyl-phenanthroimidazole (N^1 functionalization with Ph, mCF_3, pCF_3, Fl) ancillary ligands show efficient energy transfer from ligand to Eu^{III} ion. In the current study, electron rich and capable of hole transporting diphenylamine moiety was introduced phenyl-phenanthroimidazole (N1 functionalization with Ph, phenyl ring with mCF_3, pCF_3, Fl) ligand backbone and use the same to make ternary Eu-complexes. In the current discussion was made in two parts and first session / part explaining the N1-functionalization with Ph, mCF_3, pCF_3 and second session / part explained polyaromatic moiety such as fluorene was introduced in the N1 positon of phenanthroimidazole and used to synthesis corresponding Eu-complex.

The designed and synthesized three new bipolar ligands, named as Phen-Ph-TPA (1L, N,N-diphenyl-4-(1-phenyl-1H-imidazo[4,5-f][1,10]phenanthrolin-2-yl)benzenamine), Phen-mCF_3-TPA (2L, 4-(1-(3-(trifluoromethyl)phenyl)-1H-imidazo[4,5-f][1,10]phenanthrolin-2-yl)-N,N-diphenylbenzenamine) and Phen-pCF_3-TPA (3L, 4-(1-(4-(trifluoromethyl)phenyl)-1H-imidazo[4,5-f][1,10]phenanthrolin-2-yl)-N,N-diphenylbenzenamine) and their corresponding complexes are $Eu(TTA)_3$Phen-Ph-TPA (1Eu), $Eu(TTA)_3$Phen-mCF_3-TPA (2Eu), $Eu(TTA)_3$Phen-pCF_3-TPA (3Eu) and respectively. As mentioned in the previous chapter that the fluorination on the ligand can induce the energy level modulation (used to match the lanthanide emissive levels) and reduce the non-radiative energy migration (help to enhance the internal quantum efficiency). The synthesized bipolar ligand and its corresponding Eu^{III} complex structures are represented in Figure 3.1.

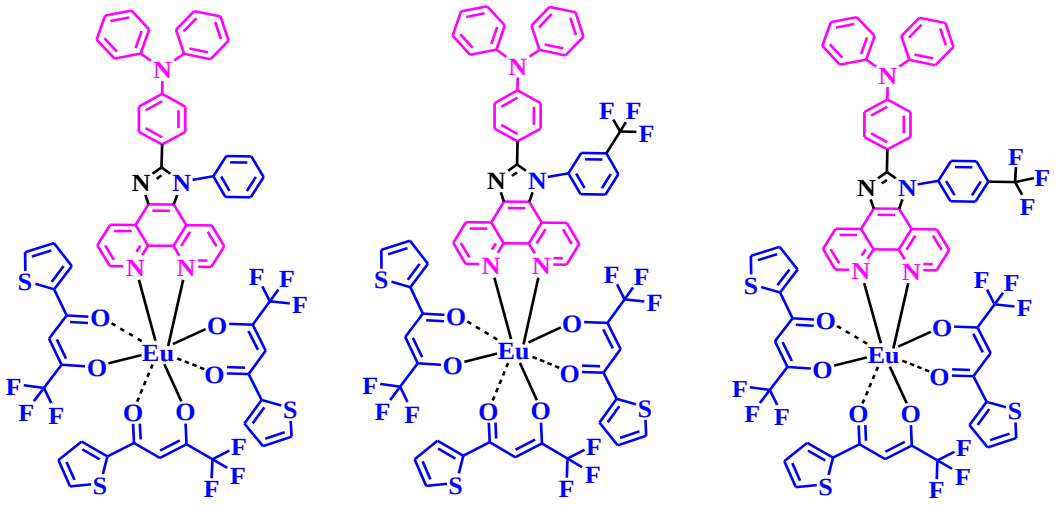

Figure 3.1 Designed structures of Eu-complexes.

3.2.2 Experimental section:

3.2.2.1 General information for synthesis:

The details of starting materials for the synthesis and electrolyte materials used in the CV were included in the previous Chapter 2. (2.2.2, Experimental section). Diphenylamine (DPA) was purchased from the Sigma-Aldrich.

3.2.2.2 Measurements:

The detailed characterization techniques that are used for the characterization of ligands and respective complexes were mentioned in the previous Chapter 2 (2.2.2, Experimental section). DSC-TGA (thermal decomposition) was performed by using Netzsch, Germany, STA449C/4/MFC/G.

3.2.2.3 Synthesis:

The compounds aldehyde [20], and 1,10-phenanthroline-5,6-dione [21], were synthesized by reported literatures. The metal complex tris(thenoyltrifluoroacetone) europium(III) ($Eu(tta)_3(H_2O)_2$) was synthesized by using the well-known method, the details are given in the previous chapter (synthesis 2.2.2.5). The synthetic scheme of the ligands and complexes were shown in Scheme 3.1.

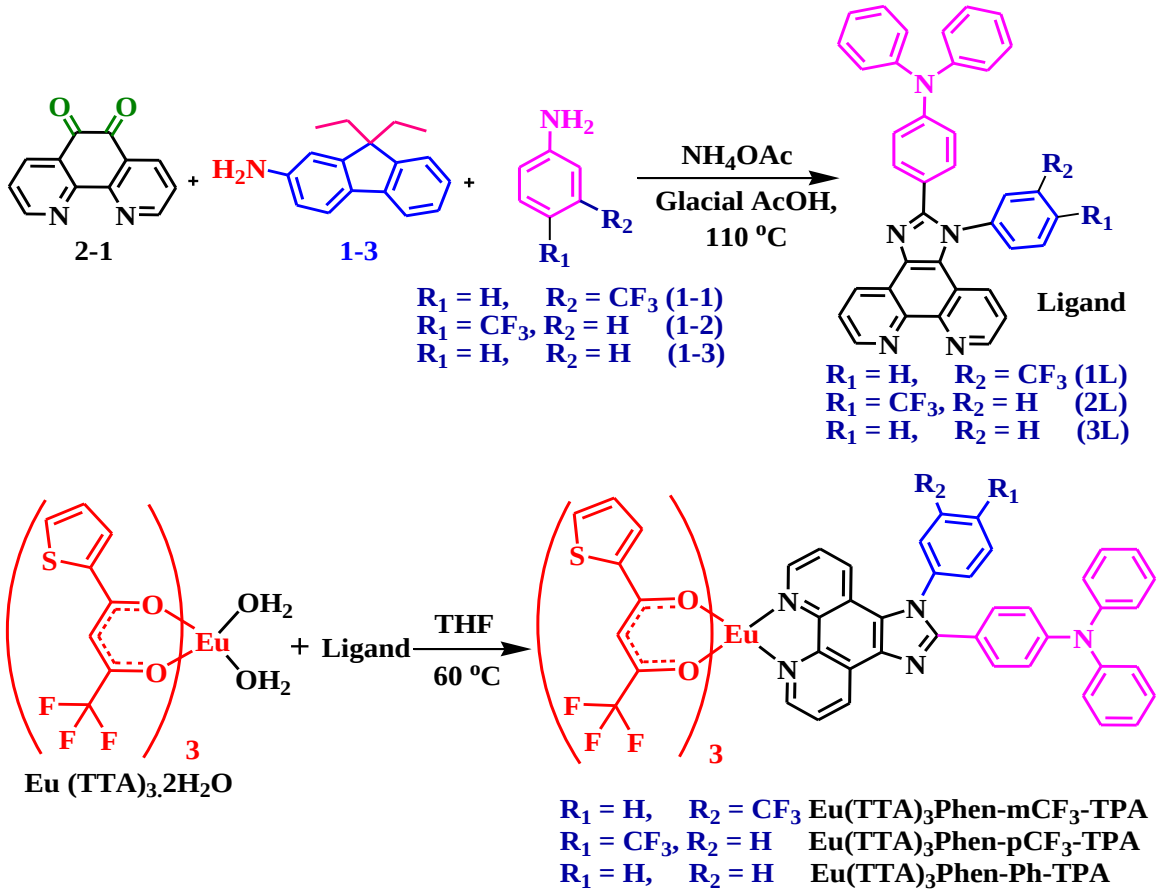

Scheme 3.1 Synthetic route of CBZ attached triphenyl functionalized ligand and the corresponding β diketonate Eu^{III} ternary complex.

3.2.2.3.1 Synthesis of *N,N-diphenyl-4-(1-phenyl-1H-imidazo[4,5-f][1,10]phenanthrolin-2-yl)benzenamine*) *(1l, Phen-Ph-TPA):*

The similar synthetic procedure was already discussed in the Chapter 2 (synthesis 2.2.2.5) procedure was followed for the synthesis of Phen-Ph-TPA and get the 1.33 g compound 2L (52.0 %) solid. ^{1}H-NMR Data (400 MHz, $CDCl_3$): δ (ppm): 9.19 (dd, *J* = 2 Hz, *J* = 2 Hz,1H), 9.15 (dd, *J* = 2 Hz, *J* = 2 Hz, 1H), 9.04 (dd, *J* = 1.6 Hz, *J* = 1.5 Hz, 1H), 7.67 (m, 1H), 7.57 (m, 3H), 7.45 (d, J = 2 Hz, 2H), 7.42 (m, 3H), 7.28 (m, 5H), 7.04 (m, 6H), 6.8 (d, *J* = 6.8 Hz, 2H). ^{13}C-NMR Data ($CDCl_3$, 100 MHz): δ (ppm) 151.6, 148.4, 148.3, 147.2, 146.5, 144.2, 143.8, 137.7, 135.6, 130.0, 129.8, 129.4, 128.8, 128.3, 127.3, 126.2, 124.7, 123.4, 123.2, 122.9, 122.1, 121.5, 121.1, 119.3. Elemental Analysis: Anal. Calc. for. $C_{37}H_{25}N_5$; C, 82.35; H, 4.67; N, 12.98 %, Found: C, 82.30; H, 4.61; N, 12.99%. EI-MS: m/z exp (calc). 539.63 m/z found 541.33 $[M + H]^+$. FT-IR (KBr, ν in cm^{-1}): 3419, 3055, 3034, 1589, 1525, 1491, 1465, 1442, 1391, 1378, 1313, 1290, 1281, 1191, 1181, 1151, 1120, 1073, 1063, 1031, 975, 933, 900, 858, 838, 831, 812, 799, 782, 760, 744, 698, 670, 638, 618.

3.2.2.3.2 *Synthesis of (4-(1-(3-(trifluoromethyl)phenyl)-1H imidazo[4,5f][1,10] phenanthroline-2-yl)-n,n-diphenylbenzenamine (2L, Phen-mCF$_3$-TPA):*

The above mentioned (2.2.2.5) procedure was followed for the synthesis of Phen-MCF_3-TPA. After minimum amount of THF solution and an excess of hexane solvent, the pale yellow color solid was formed. After settled of solid, decant and repeated this process three more times and get 1.54 g compound 1L (55.0 %) solid. ^{1}H-NMR Data (400 MHz, $CDCl_3$): δ (ppm): 9.19 (dd, *J* = 1.2 Hz, 1H), 9.12 (dd, *J* = 1.6 Hz, *J* = 1.2 Hz, 1H), 9.05 (dd, *J* = 1.6 Hz, *J* = 1.2 Hz, 1H), 7.95 (d, *J* = 4 Hz, 1H), 7.79 (m, 4H), 7.39 (dd, *J* =1.6 Hz, *J* =1.6 Hz, 1H), 7.30 (m, 7H), 7.08 (m, 6H), 6.97 (d, *J* = 8.8 Hz, 2H). ^{13}C-NMR Data ($CDCl_3$, 100 MHz): δ (ppm): 151.8, 148.6, 147.4, 146.4, 144.2, 144.7, 138.3, 135.9, 132.7, 132.3, 131.9, 130.6, 130.1, 129.6, 128.9, 126.9, 126.4, 126.4, 125.7, 125.5, 125.4, 124.7, 123.3, 123.2, 123.1, 121.6, 121.3, 121.2, 118.9. Elemental Analysis: Anal. Calc. for. $C_{38}H_{24}F_3N_5$; C, 75.11; H, 3.98; N, 11.53%, Found: C, 75.06; H, 3.95; N, 11.56 %. EI-MS: m/z exp (calc). 607.63, m/z found 608.36 $[M + H]^+$. FT-IR (KBr, ν in cm^{-1}): 3421, 3012, 1592, 1490, 1467, 1451, 1388, 1377, 1327, 1298, 1280, 1176, 1129, 1073, 1031, 897, 842, 807, 756, 736, 721, 693, 618.

3.2.2.3.3 *Synthesis of 4-(1-(4-(trifluoromethyl)phenyl)-1H-imidazo[4,5-f][1,10] phenanthroline-2-yl)-n,n-diphenylbenzenamine) (3L, Phen-pCF$_3$-TPA):*

The similar synthetic procedure was already discussed in the Chapter 2 (2.2.2.5) procedure was followed for the synthesis of Phen-pCF_3-TPA and get the 1.51 g compound 2L (54.0 %) solid. ^{1}H-NMR Data (400 MHz, $CDCl_3$): δ (ppm): 9.21 (dd, *J* = 2 Hz, *J* = 1.6 Hz, 1H), 9.46 (dd, *J* = 1.6 Hz, *J* = 2 Hz, 1H), 9.07 (dd, *J* = 1.6 Hz, *J* = 1.6 Hz, 1H), 7.94 (d, *J* = 8.4 Hz, 2H), 7.45 (m, 3H), 7.34 (m, 8H), 7.05 (m, 6H), 6.96 (d, *J* = 2 Hz, 2H). ^{13}C-NMR Data ($CDCl_3$, 100 MHz): δ (ppm): 151.7, 149.8, 148.6, 148.6, 147.4, 146.3, 144.3, 143.8, 140.9, 136.0, 130.1, 129.5, 129.0, 128.9, 127.1, 127.1, 127.0, 125.9, 124.8, 123.4, 123.3, 123.1, 122.5, 121.7, 121.3, 121.9, 118.9. Elemental Analysis: Anal. Calc. for. $C_{38}H_{24}F_3N_5$; C, 75.11; H, 3.98; N, 11.53 %, Found: C, 75.05; H, 3.92; N, 11.58 %. EI-MS: m/z exp (calc). 607.63, m/z found 609.35 [M +

H]$^+$. FT-IR (KBr, ν in cm^{-1}): 3449, 3319, 3059, 3040, 1591, 1514, 1491, 1468, 1441, 1417, 1379, 1321, 1294, 1271, 1166, 1132, 1120, 1066, 1058, 1028, 977, 881, 836, 807, 757, 738, 618.

3.2.2.3.4 *Synthesis of Eu(TTA)$_3$Phen-Ph-TPA*:

The similar synthetic procedure was already discussed in the Chapter 2 (2.2.2.5) procedure was followed for the synthesis of Eu(TTA)$_3$Phen-Ph-TPA**.** The obtained product was dissolved in minimum amount of THF and added an excess of hexane to get a solid product (repeated several times) and get pale yellow color solid with 120 mg (50.0 %). Elemental Analysis: Anal. Calc. for. $C_{61}H_{37}EuF_9N_5O_6S_3$; C, 54.07; H, 2.75; N, 5.17; S, 7.10 %; Found: C, 53.98; H, 2.70; N, 5.20; S, 7.05 %. EI-MS: m/z exp (calc). 1355.12, m/z found 1354.62 [M - H]$^+$. FT-IR (KBr, ν in cm^{-1}): 3406, 3088, 2955, 2927, 2870, 1598, 1537, 1509, 1494, 1469, 1447, 1411, 1349, 1306, 1244, 1230, 1187, 1140, 1061, 934, 858, 840, 786, 721, 695, 637.

3.2.2.3.5 *Synthesis of Eu(TTA)$_3$Phen-mCF$_3$-TPA:*

The similar synthetic procedure was already discussed in the Chapter 2 (2.2.2.5) procedure was followed for the synthesis of Eu(TTA)$_3$Phen-mCF$_3$-TPA**.** The obtained product was dissolved in minimum amount of THF and added an excess of hexane to get a solid product (repeated several times) and get pale yellow color solid with 713 mg (60.1 %). Elemental Analysis: Anal. Calc. for. $C_{62}H_{36}EuF_{12}N_5O_6S_3$; C, 52.33; H, 2.55; N, 4.92; S, 6.76 %; Found: C, 52.30; H, 2.51; N, 4.98; S, 6.79 %. EI-MS: m/z exp (calc). 1423.12, m/z found 1444.53 [M + Na]$^+$. FT-IR (KBr, ν in cm^{-1}): 3419, 3092, 1693, 1598, 1537, 1511, 1493, 1445, 1413, 1329, 1303, 1190, 1193, 1066, 931, 837, 808, 786, 720, 698, 640.

3.2.2.3.6 *Synthesis of Eu(TTA)$_3$Phen-pCF$_3$-TPA:*

The similar synthetic procedure was already discussed in the Chapter 2 (2.2.2.5) procedure was followed for the synthesis of Eu(TTA)$_3$Phen-pCF$_3$-TPA**.** The obtained product was dissolved in minimum amount of THF and added an excess of hexane to get a solid product (repeated several times) and get pale yellow color solid with 689 mg (58.0 %). Elemental Analysis: Anal. Calc. for. $C_{62}H_{36}EuF_{12}N_5O_6S_3$; C, 52.33, H, 2.55; N, 4.92; S, 6.76 %; Found: C, 52.29; H, 2.51; N, 4.95; S, 6.79 %. EI-MS: m/z exp (calc). 1423.12, m/z found 1422.51 [M - H]$^+$. FT-IR (KBr, ν in cm^{-1}): 3441, 2926, 1691, 1606, 1536, 1470, 1444, 1411, 1322, 1307, 1248, 1230, 1193, 1138, 1064, 1402, 983, 957, 935, 861, 839, 787, 758, 735, 721, 690, 676, 639.

3.2.3 Results and Discussion:

3.2.3.1 Characterization of the complex:

The synthesis method for Eu^{III} complex is summarized in Scheme 3.1. The compounds are characterized by nuclear magnetic resonance spectroscopy (^{1}H, ^{13}C and ^{19}F NMR, Figure 3.S1 – 3.S10), Fourier transforms infrared spectroscopy (FT-IR) Mass (Figure 3.S11 - 3.S13) and elemental analysis. All the measurements were done at room temperature.

3.2.3.1.1 FT-Infrared spectroscopy:

The FT-IR of synthesized ligands and their corresponding Eu^{III} complexes was measured in the range of 500 - 4000 cm^{-1} at room temperature and shown in Figure 3.2. The strong carbonyl (C=O) stretching frequency of the $Eu(TTA)_3(H_2O)_2$ complex shown at 1610 cm^{-1}, whereas the same peak for the 1Eu, 2Eu and 3Eu complexes, shown at 1598, 1693 and 1691 cm^{-1}. The peak carbonyl (C=O) stretching frequency shifted in the complex indicates that the β-diketonate ($Eu(TTA)_3(H_2O)_2$) compound coordinated with the neutral ligand. In addition, the vibration frequency due to C=N appears at ~1593 cm^{-1} for free ligands 1L, 2L and 3L, respectively. All the above strategies are suggesting that the Eu^{III} metal ion was coordinated with neutral ligands.

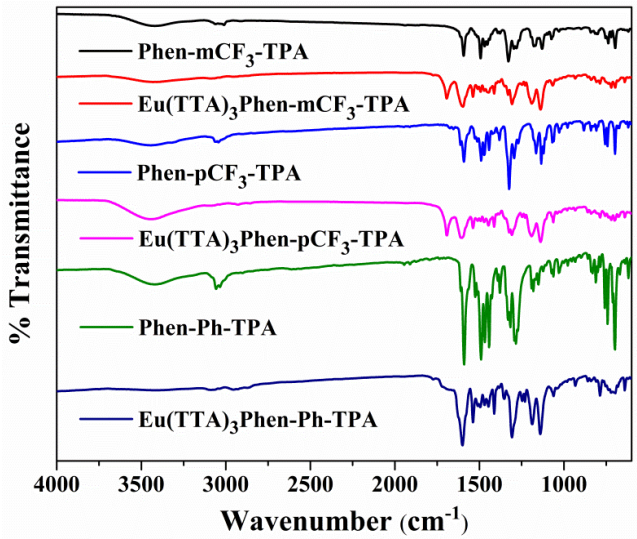

Figure 3.2 The FT-IR analysis of the ligands and their respective complexes.

3.2.3.2 Photophysical properties:

3.2.3.2.1 UV-Visible absorption and DRS studies:

The UV-Visible absorption spectra of the synthesized ligands (1L, 2L and 3L) and their respective complexes were characterized in solution (chloroform solution conc. 1.0 × 10^{-4} mol L^{-1}) and solid (Figure 3.3). The UV absorption of the ligands was shown at ~245, ~263, ~289 and ~360 nm. In case of complexes were shown at ~242, ~260, ~290 and ~350 nm. The observed peaks at ~260 and ~350 nm are attributed to the π→π* transitions of aromatic moieties present in the ligand. In addition, it was also analysed by theoretically (gas and solvent phase) and the results are supporting the experimental findings (Figure 3.4 left). The peak maxima of the $Eu(TTA)_3(H_2O)_2$ shown at 275, 340 nm, which are reflecting in the Eu-complexes (1Eu, 2Eu and 3Eu). These observations are indicating that the Eu-complex was coordinated with the $Eu(TTA)_3$. The absorption analysis was interpreted in Table 3.1. The band gaps for all the ligands as well as their corresponding Eu-complexes (Table 3.4) were calculated by using the DRS with the help of kubelka-munk function (Figure 3.4, right) [22, 23]. The obtained data from the DRS was converted to Kubelka-Munk function and α is substituted with $F(R_\infty)$ ($\alpha = F(R_\infty)$) and the equation 2.1 is used for energy gap calculation (Table 3.5).

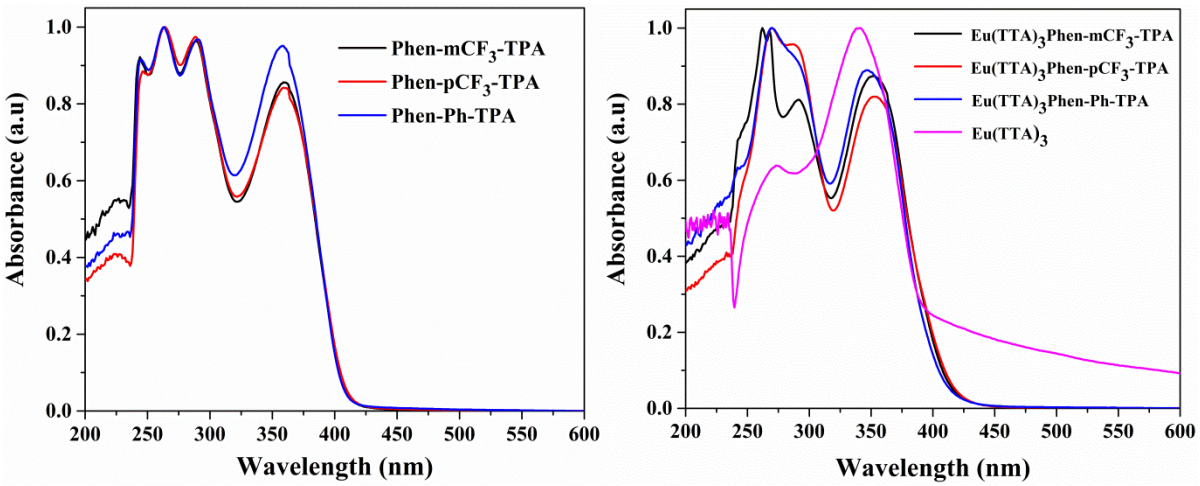

Figure 3.3 The UV-Vis absorption spectra of ligands (left) and respective $Eu(TTA)_3Phen$-mCF_3/p-CF_3/Ph-TPA (right) in chloroform solution.

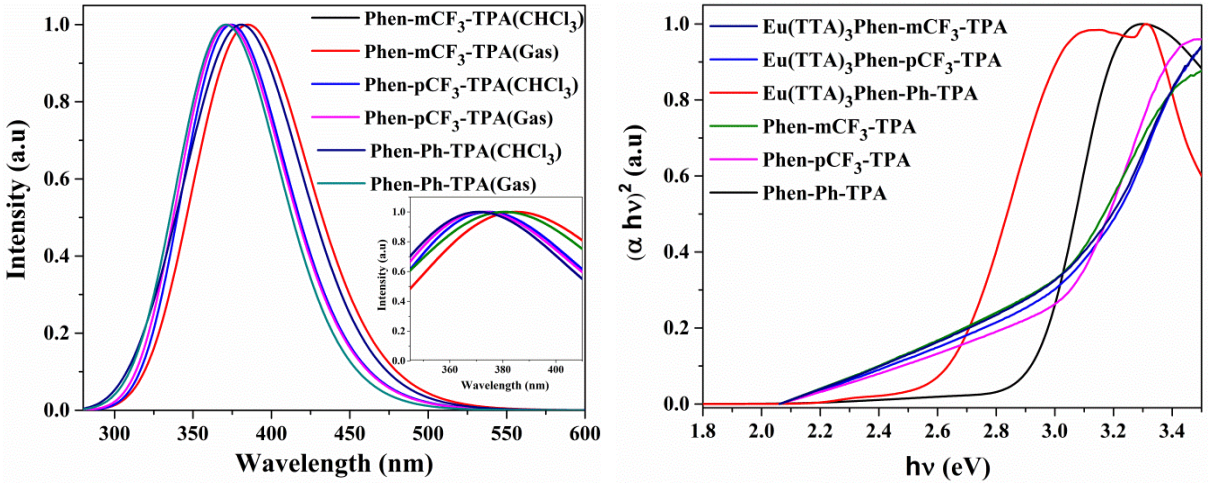

Figure 3.4 The UV-Vis absorption spectra of ligands (left) by theoretical and energy gap of the ligands and complexes by DRS (right).

3.2.3.2.2 Photoluminescence (PL) and Solvatochromism studies:

The PL emission spectra of the Eu-complexes and their ligands were measured in solution and solid phase. The ligand, 1L, 2L and 3L was shown emission at 435, 432 and 435 nm, in solution under 389, 366 and 389 nm excitation, respectively (Figure 3.5, left). In case of solid showed peak maxima at 453, 509 and 469 nm under 398, 386 and 394 nm excitation, respectively. The PL emission of the ligands was shown in the region of the blue in solution. However, in case of solid state the emission was shifted towards higher wavelength (red shift) with broadening of band. The observed red shift in solid state (Figure 3.5, right) is expected because of well-known phenomena aggregation [24, 25]. Further in order to understand the polarity dependent ligand emission in the solution, the emission spectrum was recorded for all the 1L, 2L and 3L ligands in different solvents, such as acetone, acetonitrile (ACN), chloroform ($CHCl_3$), dichloromethane (DCM), dimethylformamide (DMF), dimethyl sulfoxide (DMSO), ethyl acetate (EtOAc), methanol (MeOH), tetrahydrofuran (THF) and toluene (Figure 3.6-3.8).

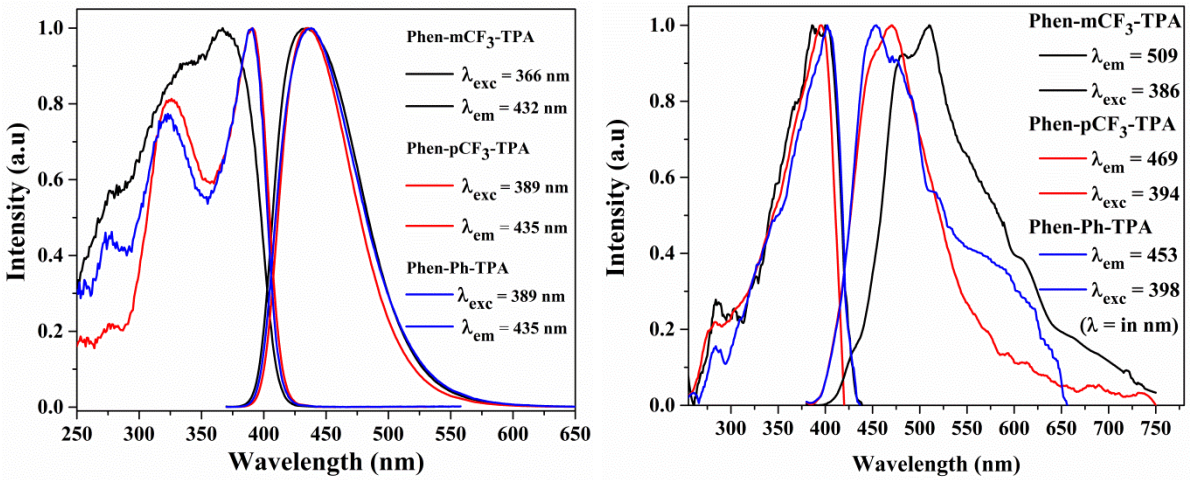

Figure 3.5 The PL excitation and emission spectra of the ligands, 1L, 2L and 3L in chloroform (left) and solid (right).

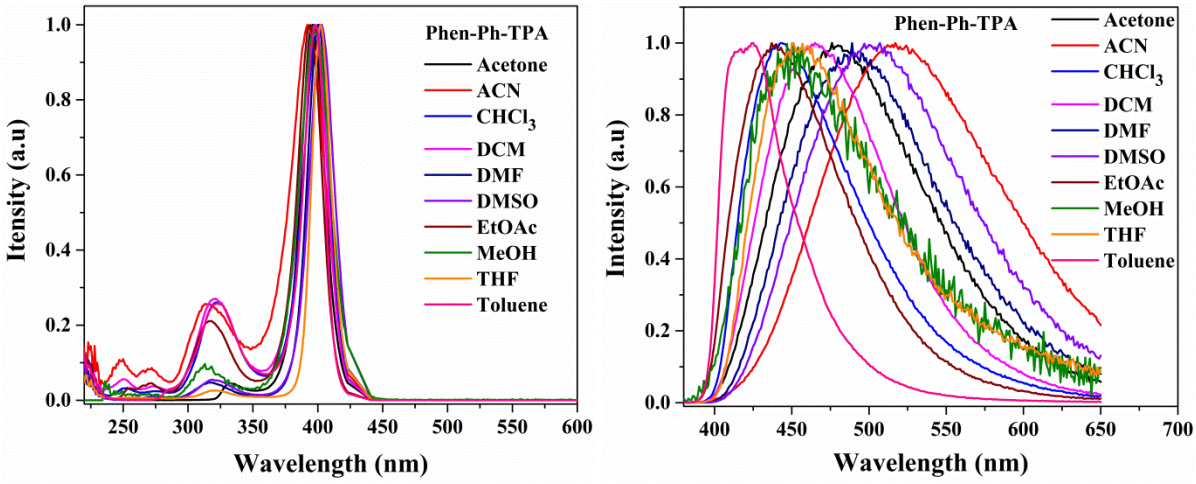

Figure 3.6 The PL excitation (left) and emission (right) spectra of the ligand (3L) in different solvents.

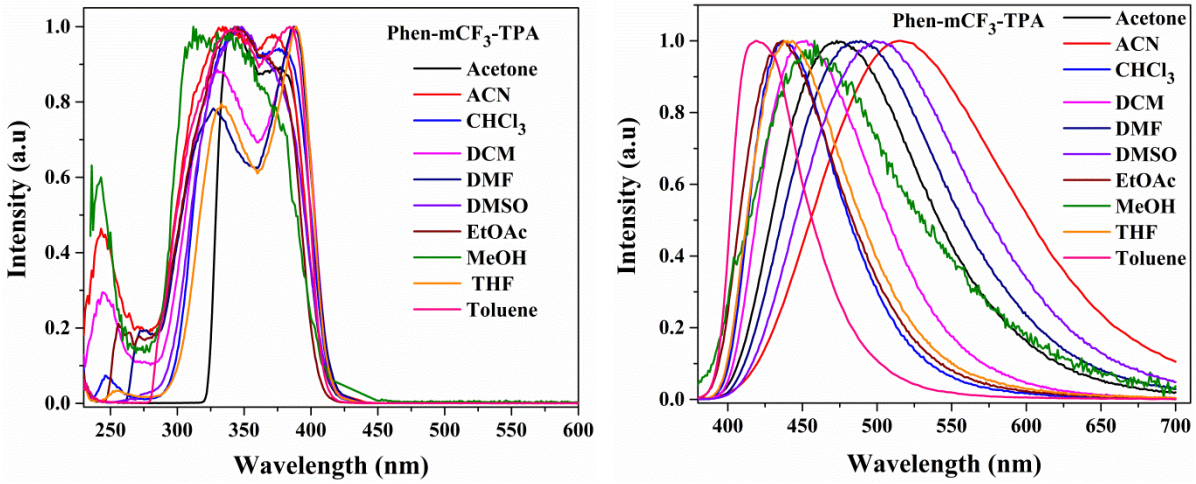

Figure 3.7 The PL excitation (left) and emission (right) spectra of the ligand (1L) in different solvents.

Table 3.1 The UV-absorption and PL emission data of synthesized ligands as well as Eu^{III} complexes.

S. No.	Compound name	UV λ_{max} (abs) [nm] Solution (a)(b)	PL λ_{ex} (a)/(d) [nm]	PL λ_{em} (a)/(e) [nm]	I_2/I_1 ratio	FWHM
1.	**$Eu(TTA)_3$Phen-Ph-TPA**	242, 268, 290, 346	330, 366/ 348, 376, 421	579, 592, 612, 652, 701	16.9/ 17.79	3.33/ 5.13
2.	**$Eu(TTA)_3$Phen-mCF_3-TPA**	243, 261, 291, 352	324, 380/ 349, 376, 406	580, 591, 612, 651, 702	10.5/ 16.73	4.16/ 8.77
3.	**$Eu(TTA)_3$Phen-pCF_3-TPA**	244, 268, 289, 353	318, 400/ 348, 414	581, 592, 612, 655, 701	12.6/ 9.11	6.16/ 5.44
4.	**Phen-Ph-TPA**	243, 263, 289, 357	276, 322, 389/ 398	435/453	NA	NA
5.	**Phen-mCF_3-TPA**	243, 263, 289, 360	274, 335, 366/ 386	432/509	NA	NA
6.	**Phen-pCF_3-TPA**	245, 263, 288, 360	274, 324, 389/ 394	435/469	NA	NA
7.	**$Eu(TTA)_3(H_2O)_2$**	273, 340	--.--	580, 592, 612, 652,703		

[a] measured in $CHCl_3$ solution at 298 K, [b] from the UV-absorption spectra, [c] from solid PL, [d] PL excitation spectra of ligands and Eu^{III} complexes, [e] The PL emission in solid.

The ligands showed emission in the region of 424-518 nm, the peak maxima is highly dependent on the solvents that are used. The trend followed as ACN (518) > DMSO (501) > DMF (489) > acetone (479) > DCM (463) > THF (457) > MeOH (451) > $CHCl_3$ (443) > EtOAc (438) > toluene (424) at excitation ~395 nm (Figure 3.6). The ligand 2L was shown ACN (515) > DMSO (500) > DMF (487) > acetone (473) > MeOH (455) > DCM (450) > THF (441) > $CHCl_3$ ≅ EtOAc (437) > toluene (419) at excitation ~375 nm (Figure 3.7). Similarly the ligand 3L also was shown ACN (516) > DMSO (497) > DMF (484) > acetone (465) > MeOH (462) > DCM (450) > THF (444) > $CHCl_3$ (439) > EtOAc (436) > toluene (422) under excitation at 385 nm (Figure 3.8). All the ligands showed similar trend from ACN (high wavelength) to toluene (less wavelength. These obtained results are indicating that the observed emission maxima shifting towards higher wavelength with increasing the polarity of the solvent. It clearly indicates that the solvent plays a major role to shift the emission from the blue to yellow emission (due to the polarity dependent excited state stabilization).

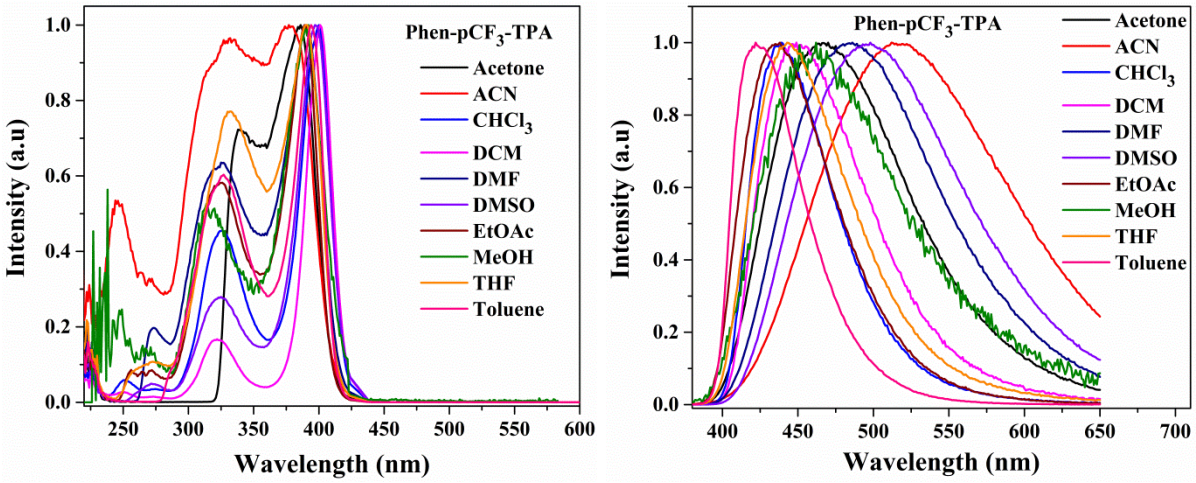

Figure 3.8 The PL excitation (left) and emission (right) spectra of the ligand (2L) in different solvents.

The ligand coordinated Eu-complexes, 1Eu, 2Eu and 3Eu was shown characteristic intense emission at 612 nm ($^5D_0$-$^7F_2$) in solution under 366, 386 and 400 nm excitation, respectively (Figure 3.9, left). In addition with characteristic Eu emission, the Eu-complex emission spectra also consist of broad band in the region of 400-580 nm, which is belongs to ligand emission. Due to the present of both ligand and Eu^{III} emission, the color of the complex under UV lamp shown yellowish red emission (deviated from pure red emission). As mentioned in the previous chapter that the Eu-complex emission peaks was attributed to the intraconfigurational 4f-4f ($^5D_0 \rightarrow {}^7F_J$ (J = 0 - 4)) electronic transitions. Not surprisingly the emission spectrum contain bands at ~579, ~592, 612, ~652 and ~702 nm and these are corresponding to f-f transitions of $^5D_0 \rightarrow {}^7F_0$, $^5D_0 \rightarrow {}^7F_1$, $^5D_0 \rightarrow {}^7F_2$, $^5D_0 \rightarrow {}^7F_3$ and $^5D_0 \rightarrow {}^7F_4$, respectively [26].

In general, the Eu-complex emission spectra give two major transitions, which are electric dipole (ED, hypersensitive transition, appears or dominates when the Eu ion located in the non-centrosymmetric site) and magnetic-dipole (MD, dominates when the Eu ion located in the centrosymmetric site). In the presently studied complexes, the single emission peak at 579 nm ($^5D_0 \rightarrow {}^7F_0$ transition) in the spectra indicates that the all Eu^{III} ions occupy a site with the same symmetry. The emission at 579, 652 nm ($^5D_0 \rightarrow {}^7F_0$, $^5D_0 \rightarrow {}^7F_3$) are forbidden both in magnetic and electric dipole systems and which are weak. The important band at 592 nm emission is not strong enough, because of magnetic character ($^5D_0 \rightarrow {}^7F_1$) is independent of the coordinate environment. Hence, it was taken major peak for calculate the Judd-Ofelt parameters. Among all the Eu^{III} ion emission peaks, $^5D_0 \rightarrow {}^7F_2$ transition at 612 nm is most intense and it is belongs to ED transition. The high intensive peak clearly indicates that the Eu^{III} occupies site without inversion centre in the presently stuided Eu-complexes. Similar emission behaviour was encountered in the case of solid, intense emission peak at 612 nm was observed without ligand emission (which is observed in the Eu-complexes in solution) in the region of 400-580 nm (Figure 3.9, right), which clearly indicates that the energy transfer between the ligand and Eu^{III} metal ion is efficient.

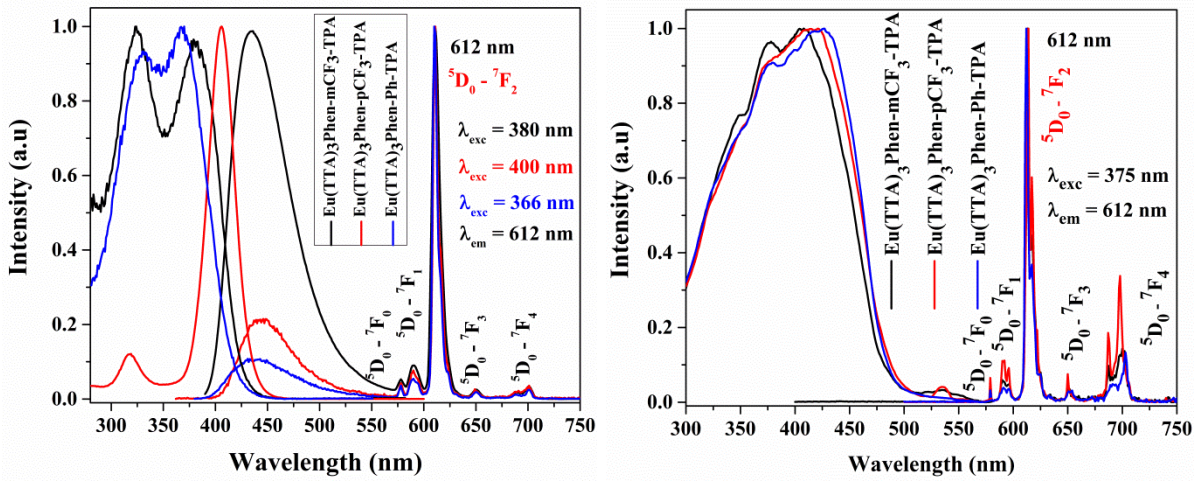

Figure 3.9 The PL excitation and emission spectra of the Eu^{III} complex in solution form, thin film, and solid phase.

3.2.3.2.3 Asymmetric ratio of Eu-complexes:

As mentioned in the previous chapter, the intensity or asymmetric ratio of the ED transition ($^5D_0 \rightarrow {}^7F_2$) and the MD transition ($^5D_0 \rightarrow {}^7F_0$) of Eu complexes is the measure of symmetry around the Eu^{III} ion in the complex. In the presently studied complexes also the same has been calculated and analysed. The I_2/I_1 ($I_{5D0\text{-}7F2}/I_{5D0\text{-}7F1}$) ratio of the 1Eu, 2Eu and 3Eu complexes was found to be 16.9, 10.5 and 12.6 in solution, respectively. However, in case of solid state emission was shown 17.79, 16.73 and 9.11 for 1Eu, 2Eu and 3Eu complexes, respectively. The presently studied Eu-complexes are shown high intensity (asymmetric) ratio which clearly indicates that the Eu metal ion occupies non-centrosymmetric site. The calculated narrow full width at half maximum (FWHM) for the solution and solid for 1Eu, 2Eu and 3Eu found to be 3.33, 4.16, 6.16 and 5.13, 8.77, 5.44 nm, respectively.

3.1.3.2.4 Solvent dependant Emission study of Eu-complexes:

In addition to understand the Eu-complex emission behaviour in solvents, the emission of Eu-complexes was measured in different solvents such as acetone, ACN, $CHCl_3$, DCM, DMF, DMSO, EtOAc, MeOH, THF and toluene. The ligand emission in the Eu-complex was observed significantly high while polarity of the solvent increased. However, the maximum intensity of the ligand emission from the complex observed in mostly in THF, $CHCl_3$ and DMF solvents (Figure 3.10. 3.11, 3.12 and the corresponding CIE color coordinate diagram depicted). The ligand emission (400-550 nm) is responsible for the blue to greenish yellow, whereas the 612 nm red emission is responsible for the Eu^{III} emission. In general, production of white emission requires three primary colours such as blue (B), green (G) and red (R). By careful balancing of these three colors are necessary to achieve the white emission with CIE value x = 0.33, y = 0.33 [15-19]. The ligands show broad emission in the polar solvent (DMF, DMSO), which is covering visible region (400-600 nm) and it leads to greenish yellow emission.

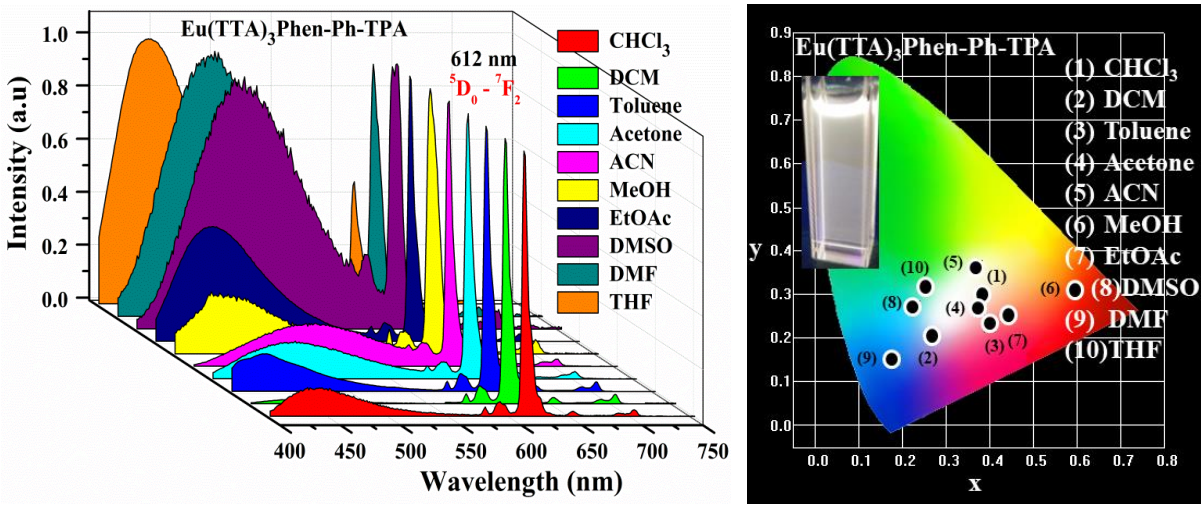

Figure 3.10 The PL emission spectra of $Eu(TTA)_3$Phen-Ph-TPA under 360 nm excitation under different solvents (left) and correspondiong CIE color coordinates (right).

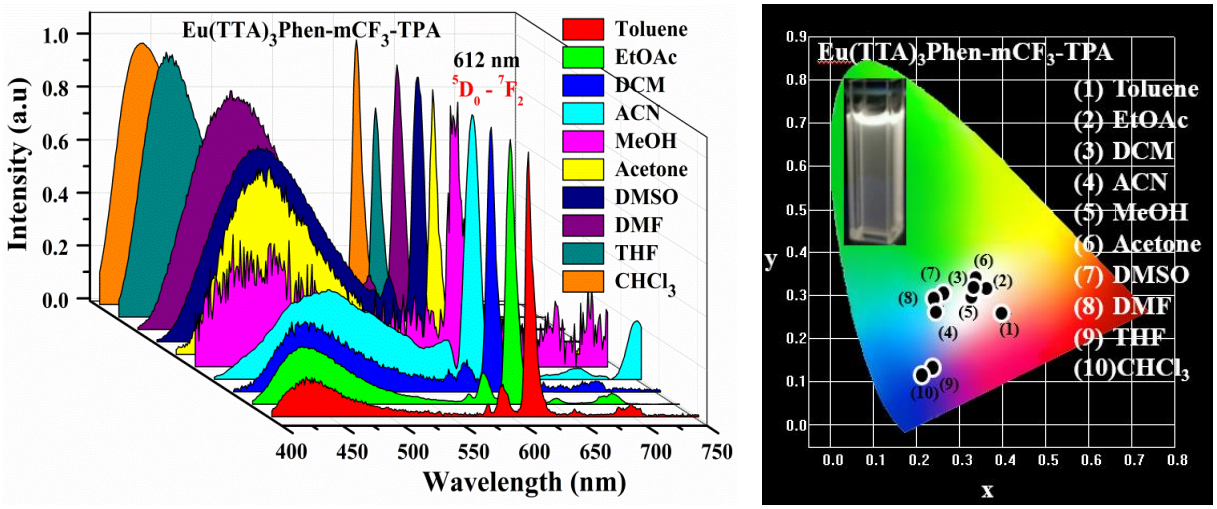

Figure 3.11 The PL emission spectra of $Eu(TTA)_3Phen\text{-}mCF_3\text{-}TPA$ under 360 nm excitation under different solvents (left) and correspondiong CIE color coordinates (right).

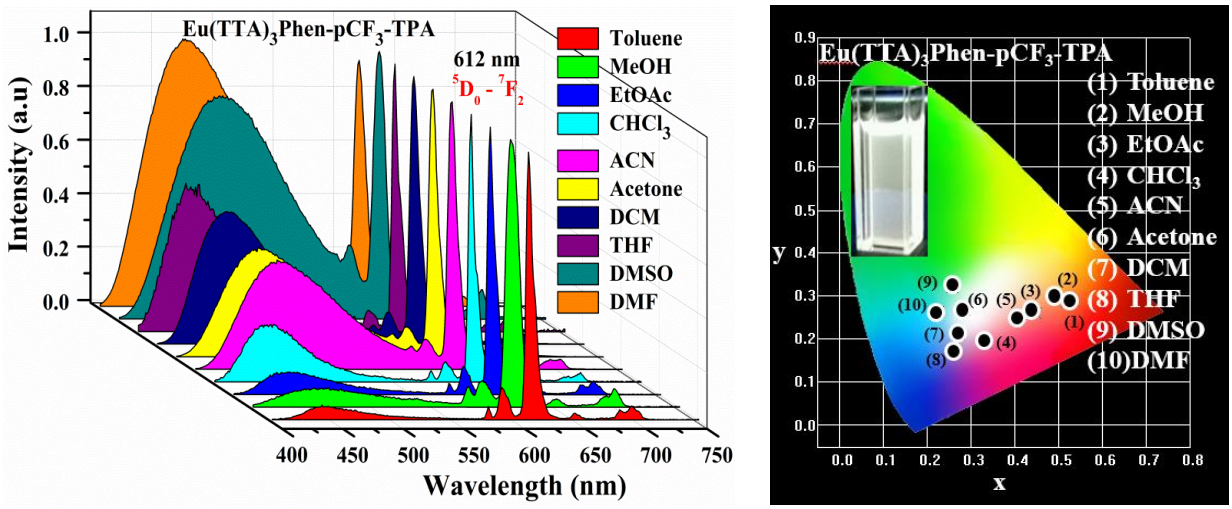

Figure 3.12 The PL emission spectra of $Eu(TTA)_3Phen\text{-}pCF_3\text{-}TPA$ under 360 nm excitation under different solvents (left) and correspondiong CIE (right).

Based on these criteria, the presently studied complexes also were verified the above strategy to get white emission, since both ligand and Eu emission (with intensity variation) were encountered in the emission spectra of the complexes in different solvents. The emission in different solvent analysis made to achieve the white light emission from the Eu-complexes in DMSO, DMF solution. Remaining solutions were tunable emission behaviour rather than white emission, due to improper balancing of the RGB colours.

3.2.3.2.5 Temperature dependent PL study of Eu-complexes for ratiometric temperature sensor:

Temperature-dependent luminescence is a well-known phenomenon which has been exploited to develop luminescent thermometers based on lanthanide molecular complexes [27, 28]. It has diverse benefits over other conventional thermometers because of their fast response, high sensitivity, non-invasive operation (temperature distributions in biological tissues (e.g., in tumors), the medium of interest is observed remotely, eg, infrared and luminescence thermography), and inertness to strong electric or magnetic fields. The temperature-dependent lanthanide emission is a key feature for developing new ratiometric temperature sensors, as the emission PL intensity or wavelength and lifetime is conjugated or reflected with the temperature. Since, in the presently studied complexes shown dual emissive behaviour, the temperature dependent PL study was executed to explore the possibility of using this as a ratiometric temperature sensor.

The temperature dependent emission of the complexes in DMSO solution from 293 – 423 K under different excitation wavelength (330, 360 and 390 nm) and their corresponding CIE color coordination are shown in Figure 3.13 to 3.21. In $Eu(TTA)_3Phen$-Ph-TPA complex, the ligand emission was increased with increasing the temperature from 293 – 423 K. In $Eu(TTA)_3Phen$-Ph-TPA complex due to ligand enhancement, emission band shifted from yellow to near blue region and the same was reflected in the CIE color coordinates (Figure 3.13, 3.14, 3.15). However, in the case of 390 nm excitation ligand emission was fully dominated than that of Eu^{III} ion emission, which leads to greenish yellow emission in the spectrum (Figure 3.15).

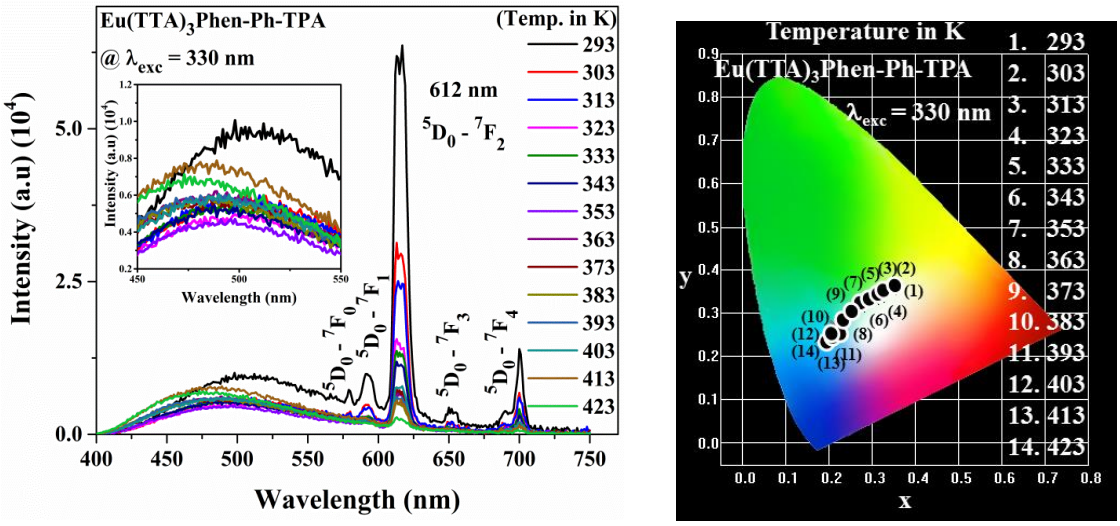

Figure 3.13 The PL emission spectra of $Eu(TTA)_3Phen$-Ph-TPA at 293-423 K under 330 nm excitation (left) and correspondiong CIE color coordinates (right).

In similar way, $Eu(TTA)_3Phen$-mCF_3-TPA was shown ligand emission, however the emission intensity depends on the temperature (Figure 3.16, 3.17, 3.18). Ligand emission in the complex slightly decreases up to 343 K and increased maximum at 423 K. From the emission and the CIE color coordinates, it is observed that the emission shifting from yellow to sky blue region via white region (emission). Under 390 nm excitation, the

complex shown intensive ligand emission along with red emission, however the color purity in the CIE color coordinateds shown in the green region. The third $Eu(TTA)_3Phen$-pCF_3-TPA complex shown increses of ligand emission from 293 K to 423 K (Figure 3.19, 3.20, 3.21). Ligand emission in the complex slightly decreases up to 343 K and increased maximum at 423 K. The CIE color coordinates was shown emission shifting from the yellow to sky blue region through white emission. Intensive ligand emission shown at 390 nm excitation and emission in CIE color coordinates located at bluish green region.

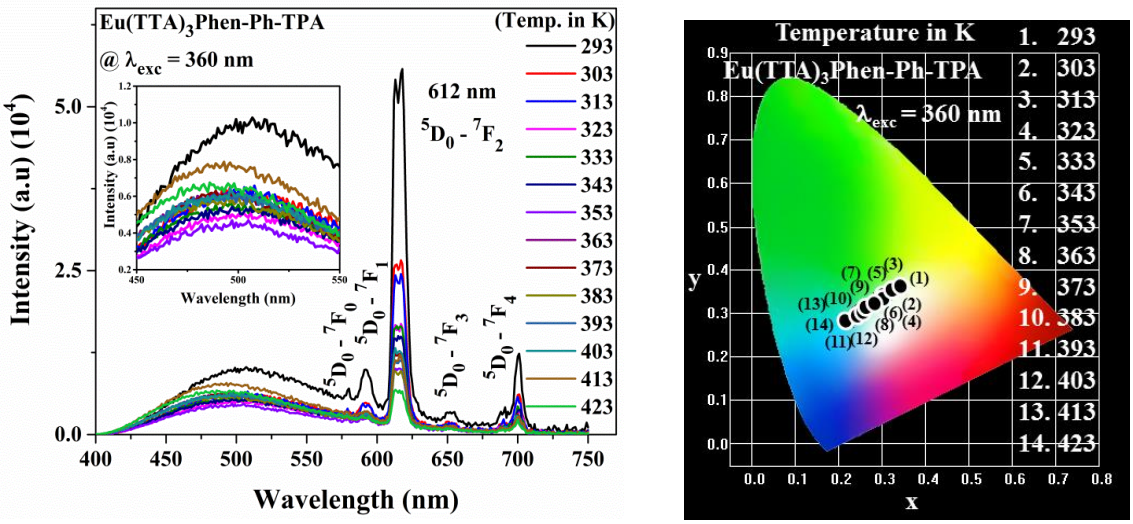

Figure 3.14 The PL emission spectra of $Eu(TTA)_3Phen$-Ph-TPA at 293-423 K under 360 nm excitation (left) and correspondiong CIE color coordinates (right).

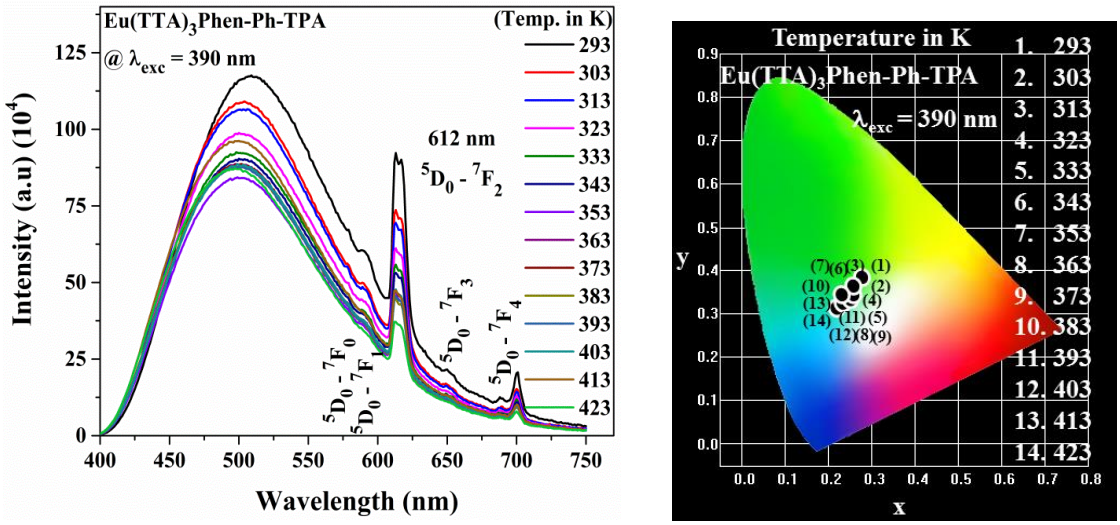

Figure 3.15 The PL emission spectra of $Eu(TTA)_3Phen$-Ph-TPA at 293-423 K under 390 nm excitation (left) and correspondiong CIE color coordinates (right).

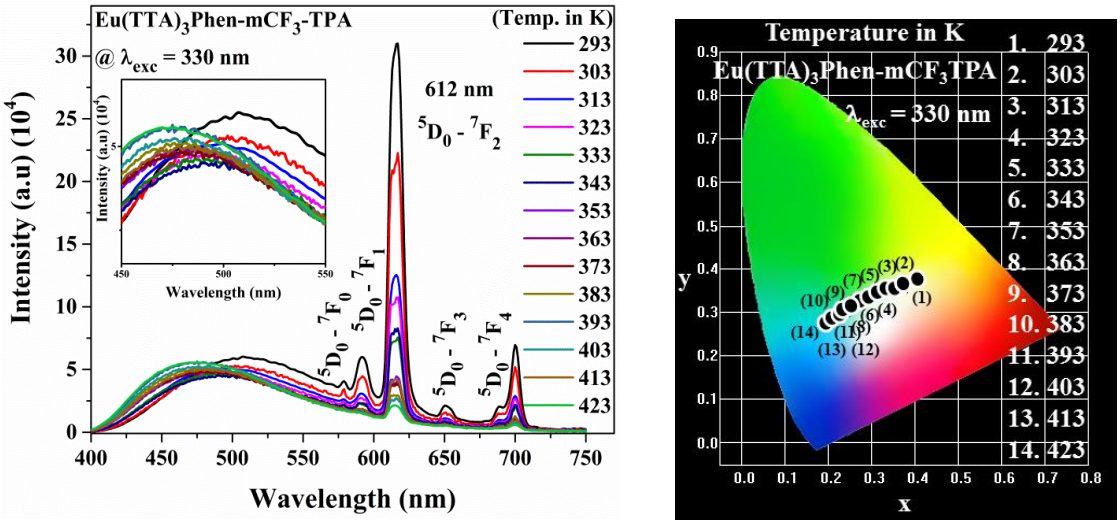

Figure 3.16 The PL emission spectra of Eu(TTA)$_3$Phen-mCF$_3$-TPA at 293-423 K under 330 nm excitation (left) and correspondiong CIE color coordinates (right).

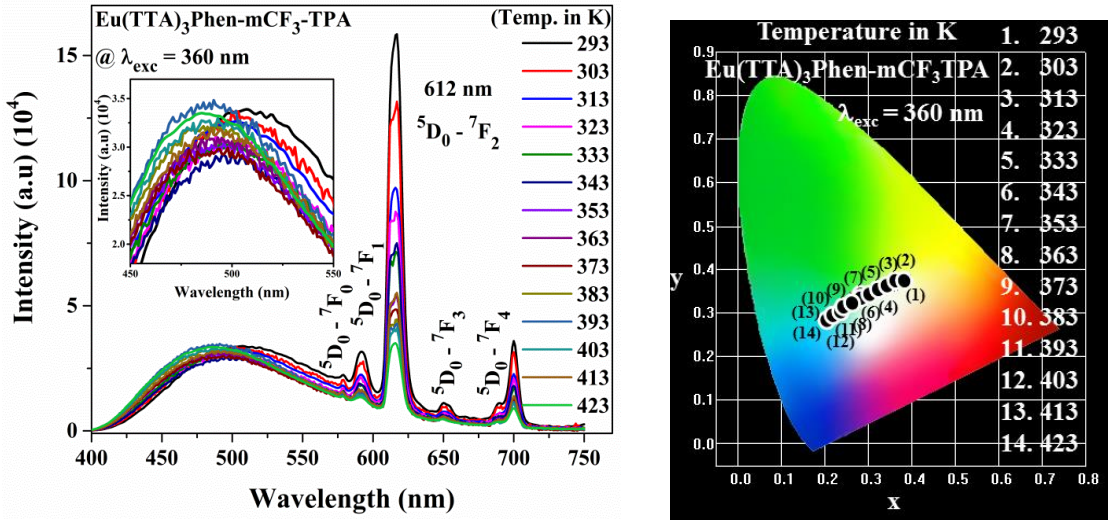

Figure 3.17 The PL emission spectra of Eu(TTA)$_3$Phen-mCF$_3$-TPA at 293-423 K under 360 nm excitation (left) and correspondiong CIE color coordinates (right).

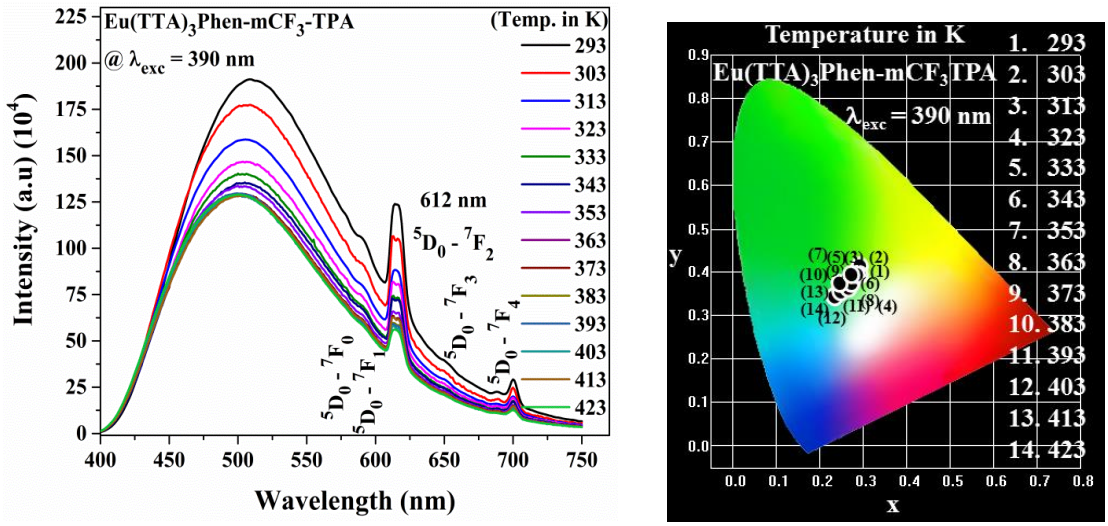

Figure 3.18 The PL emission spectra of Eu(TTA)$_3$Phen-mCF$_3$-TPA at 293-423 K under 390 nm excitation (left) and correspondiong CIE color coordinates (right).

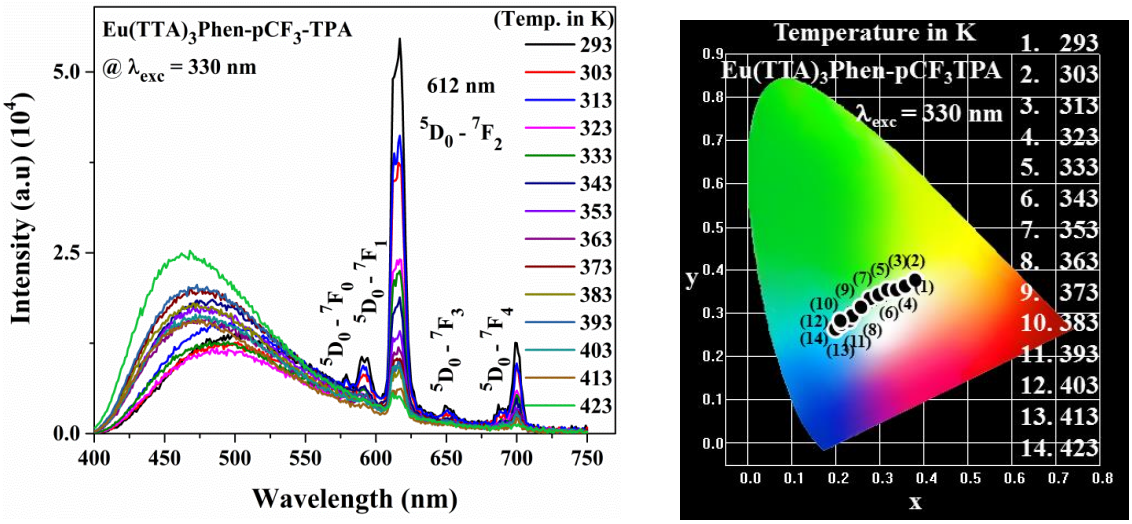

Figure 3.19 The PL emission spectra of Eu(TTA)$_3$Phen-pCF$_3$-TPA at 293-423 K under 330 nm excitation (left) and correspondiong CIE color coordinates (right).

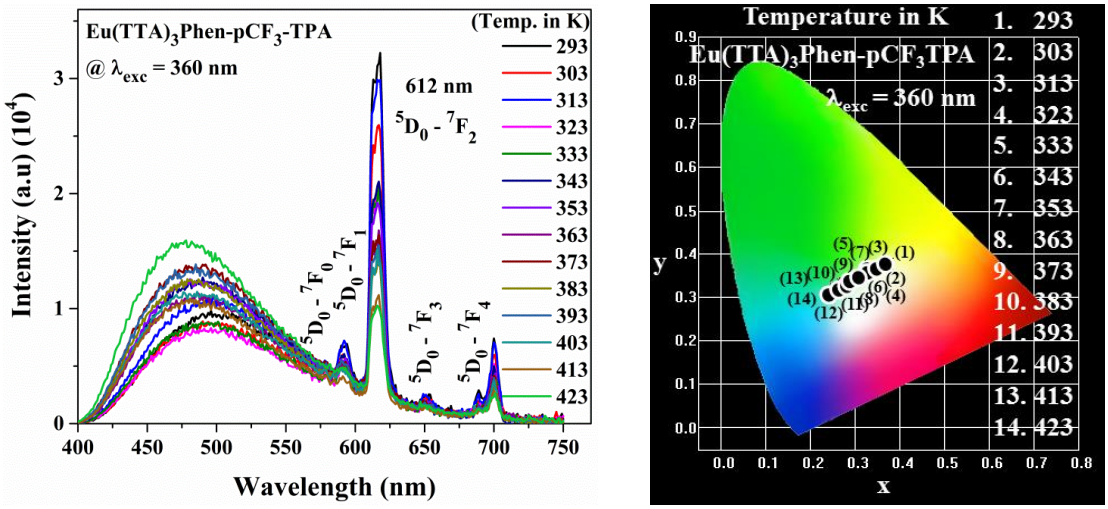

Figure 3.20 The PL emission spectra of $Eu(TTA)_3Phen\text{-}pCF_3\text{-}TPA$ at 293-423 K under 360 nm excitation (left) and correspondiong CIE color coordinates (right).

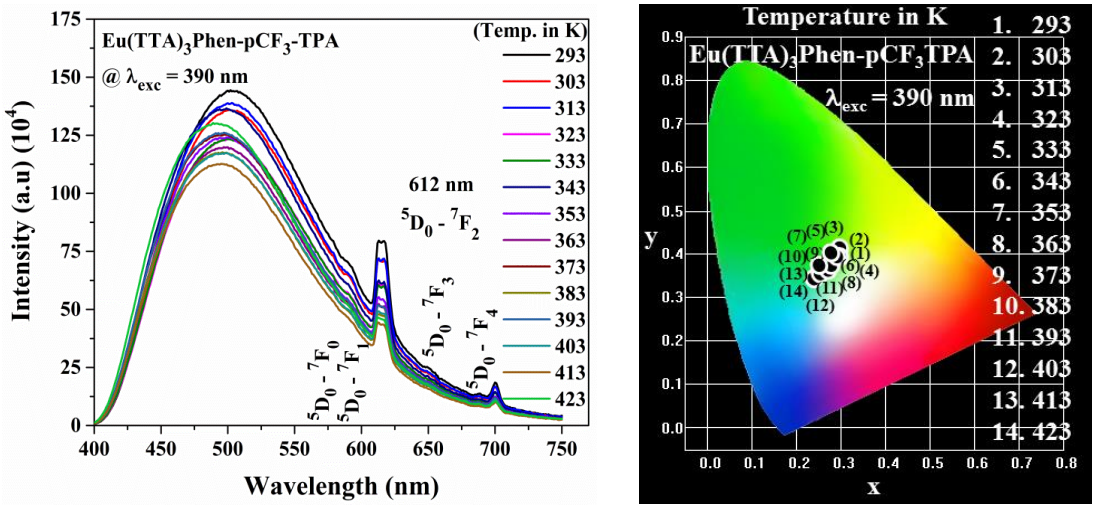

Figure 3.21 The PL emission spectra of $Eu(TTA)_3Phen\text{-}pCF_3\text{-}TPA$ at 293-423 K under 390 nm excitation (left) and correspondiong CIE color coordinates (right).

3.2.3.2.6 Energy transfer mechanism:

Further to understand the ligand emission from the Eu-complex requires, knowing the exact energy transfer pathway in the complex. Since the dual emission characteristics (contributed by both ligand and Eu^{III} ion) of the complex originates from ligand as well as Eu^{III} excited levels. Understanding of the excited level locations is very important to propose the energy transfer mechanism in the presently studied complexes. Theoretical studies were performed for the presently synthesized ligands to explain the phenomena in detailed. The singlet and triplet energies of the exited energy levels were calculated by using DFT and TD-DFT analysis. The singlet energy level of 1L, 2L and 3L ligands were located at 25,575 (3.17 eV), 25,598 (3.16 eV) and 25,469 (3.17 eV), respectively. The triplet levels are located at 20,850 (2.58 eV), 20,844 (2.58 eV) and 20,807 (2.58 eV), respectively (Figure 3.22). It is well known

that the TTA energy levels are located at 25,164 (singlet) and 18,954 (triplet) [29]. The $^5D_0$ excited state energy level of the Eu^{III} metal ion located at the 17,500 cm^{-1} [30, 31]. The obtained results are indicating that the presence of triplet level is ~20,800 cm^{-1} and it can leads the energy back transfer, results emission from the ligand in the emission spectrum along with 612 nm. It was also supported from the PL emission spectra of the complexes in solution. The triplet energy level of the ligand was calculated by phosphorescence emission spectra at 77 K with respective Gd^{III}-complex (Figure 3.23). The obtained results are shown similar to that of the theretical findings. The obtained results are in good contract with Letva *et al.*, investigations that the energy difference (ΔE should be in the range of 2500 - 4000 cm^{-1}) [32]. It can be concluded from the results obtained that the energy transfer is occurring from the triplet level to excited state of Eu^{III} metal ion [33].

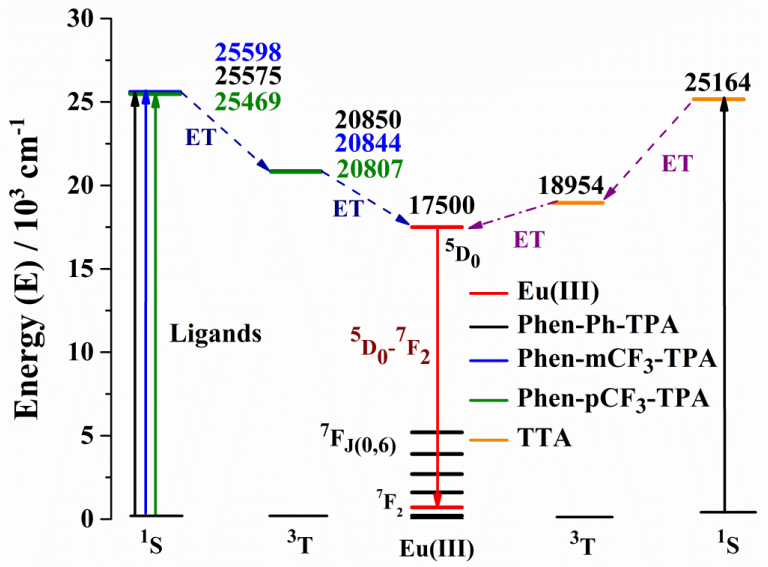

Figure 3.22 The energy transfer diagram for the complexes and energy transfer from ligand as well TTA to the Eu^{3+} ion.

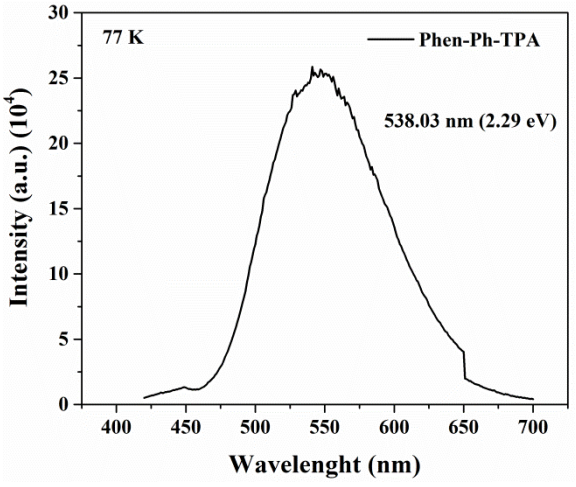

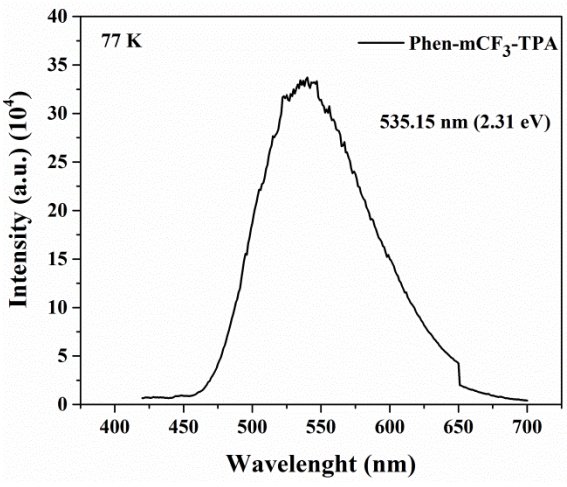

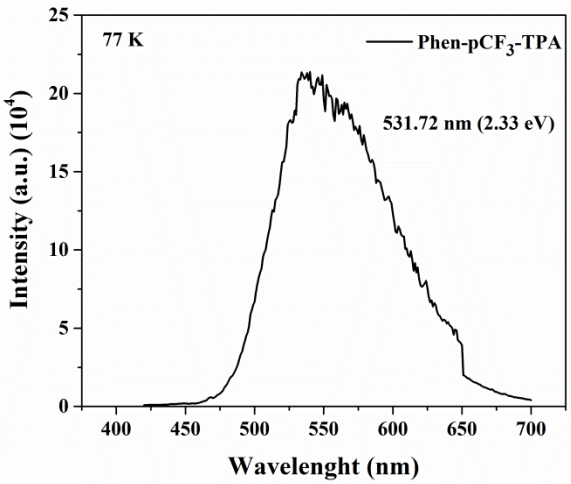

Figure 3.23 The phosphorescence emission spectra of the ligand measured at 77 K with respective Gd^{III}-complex and calculated triplet energy level.

3.2.3.2.7 Photoluminescence quantum yield (PLQY) and PL lifetime:

As mentioned in the previous chapter, by using equation 2.2 and 2.3, the quantum efficiency (φ) can be obtained. The PLQY of the complexes were measured in solution and solid phase. The quantum yield of the complexes 1Eu, 2Eu and 3Eu shown 6.6, 6.24 and 24 % in solid; 10.4, 25.3 and 25.2 % in solution phase, respectively. Among all complexes, the QY found to be in mCF_3 and pCF_3 consisted Eu-complexes shown better value. It indicates that the fluorination leads to increase the efficiency than the free fluorination Eu-complex. Furthered, the quantum yield of the complexes 1Eu, 2Eu and 3Eu were incorporated on the glass substrate (thin film – pure Eu-complex) are shown 9.42, 4.21 and 4.09, respectively.

In order to understand the excited state properties, the PL lifetime of the complexes were measured. The lifetime data was fitted with the single exponential function by following given equation, $I(t) = I_0 + A_1 \exp\left(\frac{-t}{\tau}\right)$; where A_1 is the scalar quantity obtained from the curve fitting, t is the time in ms, $I_0 = 0$ is the offset value and τ is the decay time value for the exponential component. Lifetime for the complexes luminescence decay curves of the $^5D_0$ excited state were measured at 298 K by monitoring the most intense 612 nm emission line ($^5D_0 \rightarrow {}^7F_2$) of the Eu-ion center under 360 nm excitation. The lifetime of the 1Eu, 2Eu and 3Eu complexes in the solid state calculated and the values are 0.32, 0.30 and 0.51 ms, respectively. In addition, to understand the solvent influence; the lifetime was also investigated in various solvents (acetone, $CHCl_3$, DCM, DMF, DMSO, THF, toluene), with different solvent polarity. The most of the solvents are followed single exponential decay, whereas the PL lifetime of the solid followed bi-exponential decay fitting (Figure 3.24, 3.25, 3.26).

The luminescent lifetime values (τ) of Eu^{III}-complexes 1Eu, 2Eu and 3Eu found to be highest is ~0.53 ms (in $CHCl_3$ solution). It indicates that the non-radiative relaxation in the both the state (solution and solid) having slight lifetime variation (0.51/0.53 ms). The lifetime of the ligands is also calculated and found to be ~1.7×10^{-3} ms in solution. In solution, the quenching of lifetime is due to non-radiative relaxation via vibronic coupling

and it is less in the case of the $CHCl_3$ solution. It could be attributed that the C-H vibrational oscillators frequency is less compare to that of O-H and N-H.

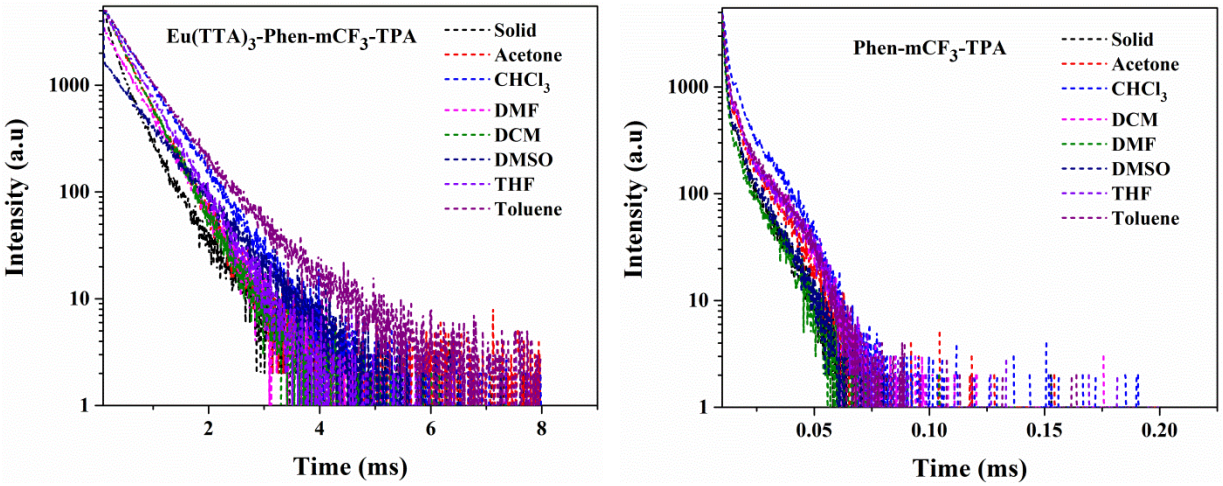

Figure 3.24 The lifetime of the Eu^{III} complex (1Eu, left) and ligand (1L, right) in different solvents and in the form of solid.

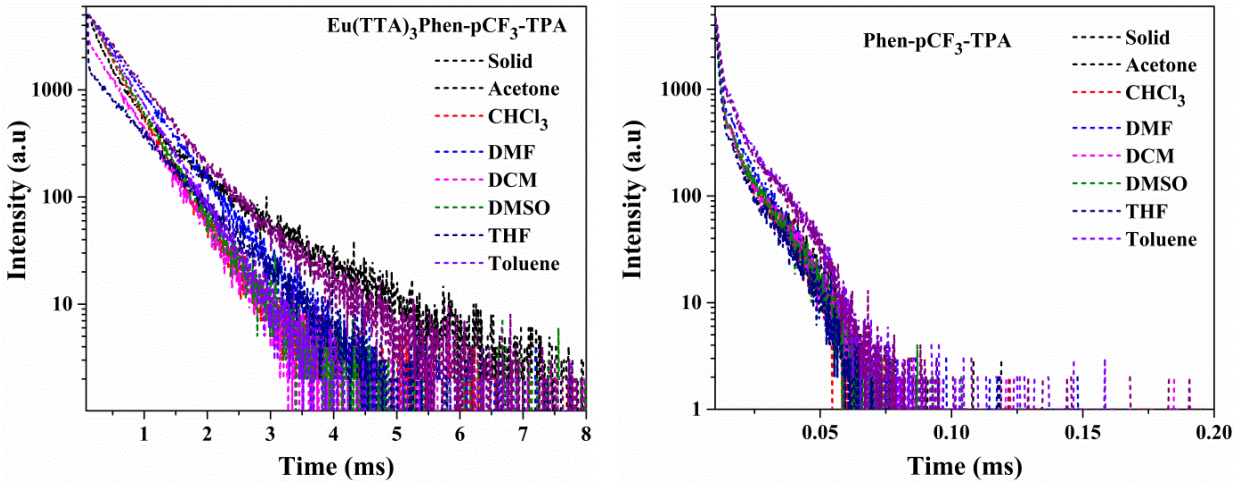

Figure 3.25 The lifetime of the Eu^{III} complex (2Eu, left) and ligand (2L, right) in different solvents and in the form of solid.

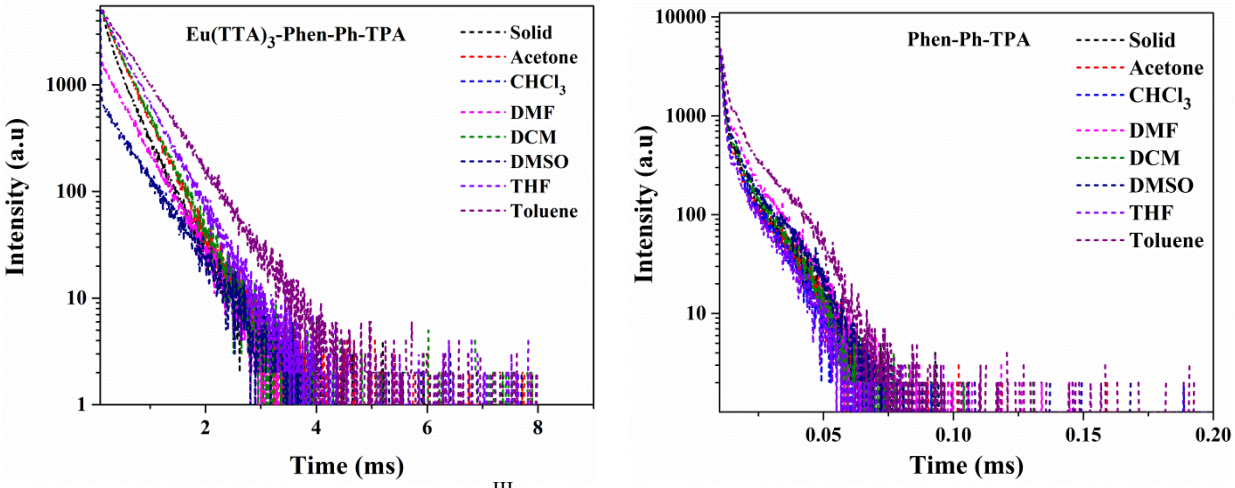

Figure 3.26 The lifetime of the Eu^{III} complex (3Eu, left) and ligand (3L, right) in different solvents and in the form of solid.

3.2.3.2.8 Judd-Ofelt (J-O) spectral parameters for Eu-complexes:

The detailed J-O spectral parameter calculations were explained in Chapter 2, section 2.2.3.2.4). The calculated Judd-Ofelt (J-O) parameters of the complexes showed Ω_2 and Ω_4 are 4.31 and 1.40; 2.87 and 1.00; 1.57 and 1.24, respectively. The obtained value of intensity parameter, Ω_2 ($^5D_0 \rightarrow {}^7F_2$) is more sensitive to the symmetry and reveals covalent bonding environment between Eu^{III} ion and the surrounding ligand moiety in the presently studied Eu-complexes.

In addition, the radiative (A_{RAD}), nonradiative (A_{NR}) decay rates, $^5D_0$ lifetime (t_{obs}), intrinsic quantum yield (Φ_{Ln}), energy transfer efficiency (Φ_{sen}) and overall quantum yield ($\Phi_{overall}$) for complexes were also been calculated. The experimental branching ratios and cross section ($\sigma_{1\text{-}4}$) parameters are calculated. All the calculated parameters are tabulated in Table 3.2 and Table 3.3. The highest sensitization for the complex 2Eu shown 66.35 %, which is clearly indicating that the pCF_3 consisted complex leads to enhance the sensitization. It is also reflecting in in case of QY of the 2Eu.

Table 3.2 J-O parameters (Ω_2 and Ω_4) and their experimental branching ratios ($\beta_{1\text{-}3}$) of the complex.

S. No.	Complex name	σ_1	σ_2	σ_4	Ω_2	Ω_4	β_1	β_2	β_3
					(10^{-20} cm^2)				
1.	**$Eu(TTA)_3$Phen-Ph-TPA**	0.293	2.13	0.032	4.31	1.402	3.21	83.76	12.99
2.	**$Eu(TTA)_3$Phen-mCF_3-TPA**	0.353	1.142	0.042	2.878	1.001	4.70	81.62	13.68
3.	**$Eu(TTA)_3$Phen-pCF_3-TPA**	0.607	5.88	0.113	1.579	1.243	7.07	67.02	25.90

Table 3.3 The Radiative (A_{RAD}) and nonradiative (A_{NR}) decay rates, $^5D_0$ lifetime (t_{obs}), intrinsic quantum yield (Φ_{Ln}), energy transfer efficiency (Φ_{sen}) and overall quantum yield ($\Phi_{overall}$) for complex.

S. No.	Complex name	A_{RAD} (S^{-1})	A_{NR} (S^{-1})	τ_{obs} (ms)	τ_{RAD} (ms)	Φ_{Ln} (%)	Φ_{Sen} (%)	$\Phi_{Overall}$ (%)
1.	**$Eu(TTA)_3Phen\text{-}mCF_3\text{-}TPA$**	1062.8	224	0.303	0.94	32.23	19.36	6.24
2.	**$Eu(TTA)_3Phen\text{-}pCF_3\text{-}TPA$**	706.34	125	0.510	1.41	36.17	66.35	24.0
3	**$Eu(TTA)_3Phen\text{-}Ph\text{-}TPA$**	1554.3	155	0321	0.64	50.1	13.17	6.6

3.2.3.3 Electrochemical Properties:

The cyclic voltammetry analysis has an important role for redox properties and it help to understand the energy levels (HOMO and LUMO) of the Eu^{III}-complex and ligand. The Eu^{III}-complex onset oxidation potential found to for 1Eu, 2Eu and 3Eu are 1.33, 1.25 and 1.53, respectively (Fig. 3.27). The reduction potentials data and their band gap was listed in Table 3.4. The HOMO and LUMO energy levels were calculated by using equation 2.9 and 2.10.

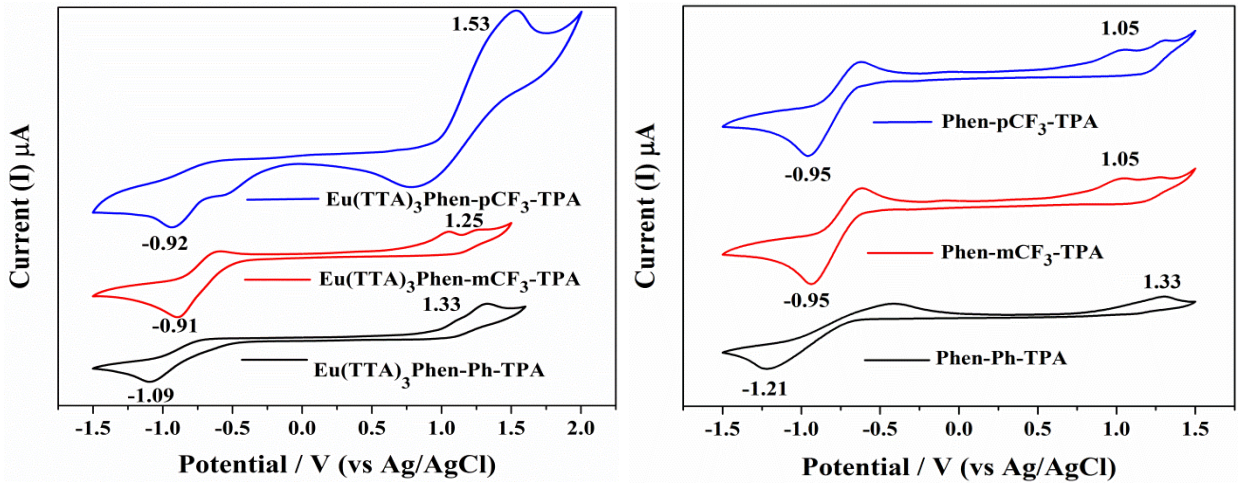

Figure 3.27 Cyclic voltammogram of ligands and its corresponding Eu^{III}-complexes.

Table 3.4 Electrochemical properties of the ligands and respective Eu^{III}-complexes.

S. No.	Compound Name	$Voltage^{Oxi}_{onset}$ [V] (E_{HOMO} [eV])	$Voltage^{Red}_{onset}$ [V] (E_{LUMO} [eV])	λ_{onset}, [nm] (a)	Bandgap/Energy gap E_g^{Opt}, [eV] (b)
1.	**$Eu(TTA)_3Phen\text{-}Ph\text{-}TPA$**	1.33 (- 5.73)	-1.09 (-3.31)	467	2.65 (2.42)
2.	**$Eu(TTA)_3Phen\text{-}mCF_3\text{-}TPA$**	1.25 (-5.65)	-0.91 (-3.49)	453	2.73 (2.16)
3.	**$Eu(TTA)_3Phen\text{-}pCF_3\text{-}TPA$**	1.53 (-5.93)	-0.92 (-3.48)	467	2.65 (2.45)
4.	**Phen-Ph-TPA**	1.30 (-5.70)	-1.21 (-3.19)	439	2.82 (2.51)
5.	**Phen-mCF_3-TPA**	1.28 (-5.68)	-0.93 (-3.46)	421	2.93 (2.22)
6.	**Phen-pCF_3-TPA**	1.04 (-5.44)	-0.96 (-3.43)	424	2.92 (2.01)

(a) Calculated from the optical absorption (DRS spectra), (b) Calculated the onset wavelength of optical absorption (onset) in solid-state film (DRS spectra). The energy differences (HOMO and LUMO) values calculated by cyclic voltammogram are mentioned in bracket.

The HOMO and LUMO energy level of the Eu^{III}-complexes 1Eu, 2Eu and 3Eu are found to be -5.73 and -3.31 eV; -5.65 and -3.08; -5.93 and -3.88, respectively. Eu^{III}-complex projected energy gap >2.5 eV. The ligands energy gap was found to be almost higher than that of the Eu-complexes. The calculated energy gap from the optical absorption was matched with the cyclic voltammetry analysis. Each redox reaction involves a reversible one-electron transfer, and each is attributed to a ligand-based redox process in the complex.

3.2.3.4 Theoretical calculations:

To understand the obtained results of HOMO and LUMO of the ligands, it was analysed by theoretical calculations such as DFT and TD-DFT analysis (frame work using B3LYP/6-31G (d, p) level of theory) [34, 35]. The optimized structure of ligands (Phen-mCF_3-TPA, Phen-pCF_3-TPA and Phen-Ph-TPA) was incorporated in Figure 3.28. The HOMO and LUMO energy levels of the ligands molecular orbitals shown in Table 3.5. The HOMO and LUMO energy levels of the ligands with their respective band gaps as well as singlet and triplet energy levels were incorporated in the Table 3.6 and it is harmonized with the experimental findings. The electron density in the HOMO of ligands were located on phenanthroline moiety and in LUMO located on Phenanthroimidazole and slightly on phenyl ring. In case of Phen-Ph-TPA shown electron density mostly transferred on TPA moiety. It is expecting due to the absence of fluorine in the ligand. In addition, computed vertical transitions and their oscillator strengths and configurations were incorporated in the Table 3.7, 3.8 and 3.9.

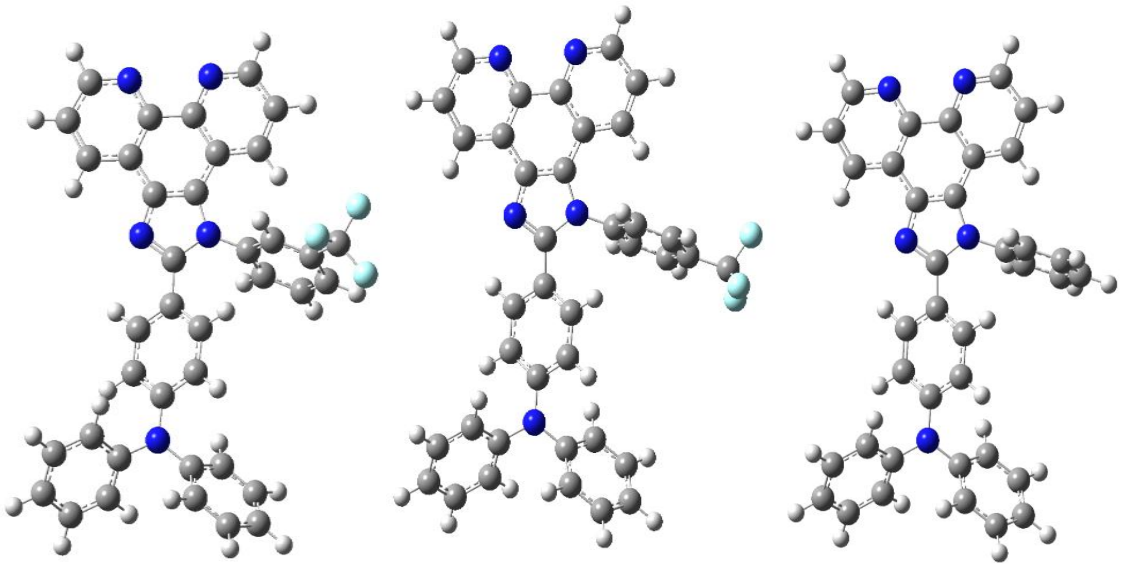

Figure 3.28 Optimized structures of ligands (Phen-mCF_3-TPA, Phen-pCF_3-TPA and Phen-Ph-TPA)

Table 3.5 The HOMO and LUMO orbital diagrams of the ligands.

	Phen-mCF$_3$-TPA	**Phen-pCF$_3$-TPA**	**Phen-Ph-TPA**
LUMO+1	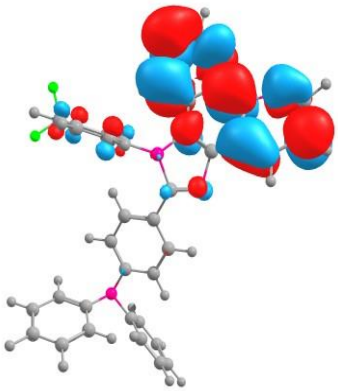	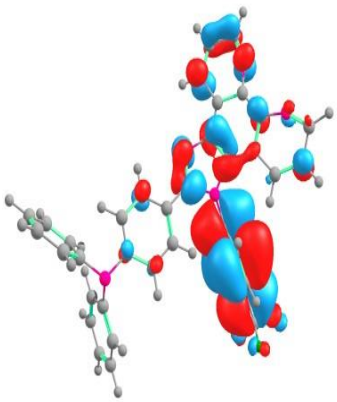	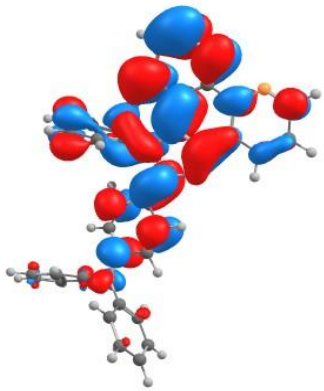
LUMO	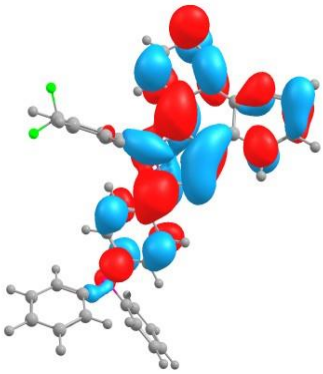	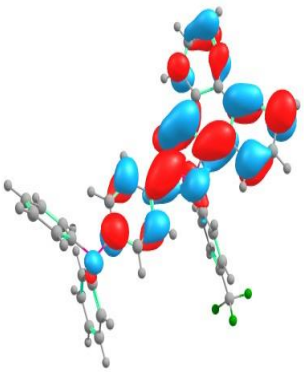	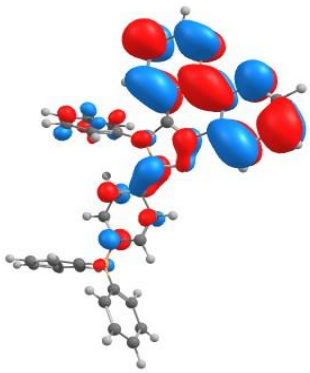
HOMO	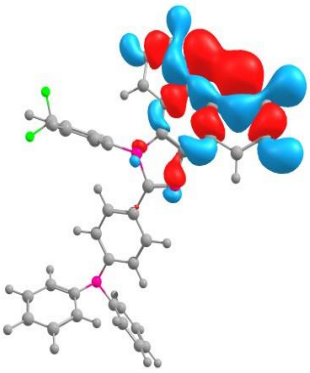	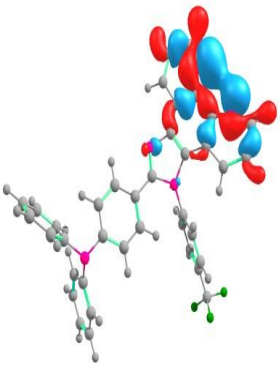	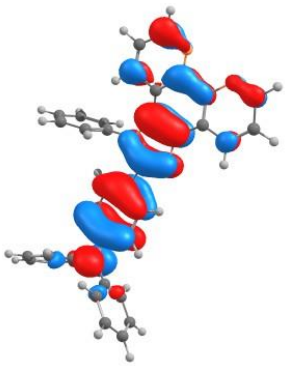
HOMO-1	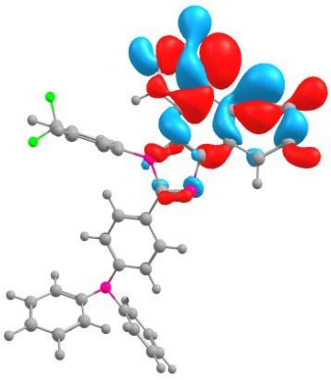	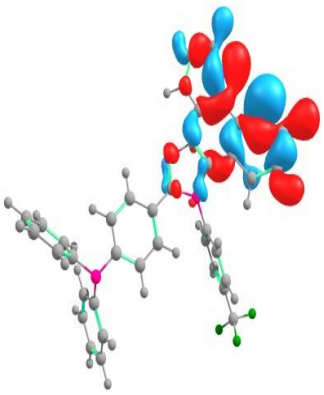	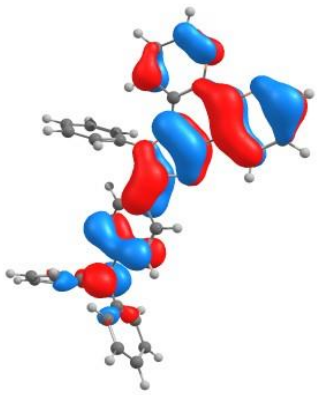

Table 3.6 The HOMO and LUMO energy levels of the ligands with their respective band gaps as well as singlet and triplet energy levels.

Molecule	HOMO	HOMO-1	LUMO	LUMO+1	E_g	S1	T1
	in electron volts (eV)						
1L	-5.065	-5.799	-1.404	-1.375	3.661	3.17	2.58
2L	-5.066	-5.872	-1.528	-1.305	3.538	3.16	2.58
3L	-4.966	-5.689	-1.223	-1.129	3.743	3.17	2.58
Eu^{III} metal ion	--.--	--.--	--.--	--.--	--.--	$^5D_0$ level = 2.17	

Table 3.7 Computed vertical transitions and their oscillator strengths and configurations[a]

Phen-Ph-TPA	State	Energy (eV)	λ_{max} nm	*f*	Configuration
Singlet	Gas	3.3200	373	0.8208	HOMO → LUMO (69.47%)
		3.6457	340.09	0.100	HOMO → LUMO+3 (68.37%)
	DCM	3.1709	391	0.5969	HOMO → LUMO (66.76%)
					HOMO→ LUMO+1 (17.60%)
		3.2908	376.75	0.3244	HOMO → LUMO+1 (65.99%)
					HOMO → LUMO+2 (11.80%)
		3.6167	342.81	0.2296	HOMO → LUMO+3 (67.64%)
Triplet	Gas	2.5835	479.9	-	HOMO-1 → LUMO (19.0%)
					HOMO → LUMO (58.80%)
	DCM	2.5851	479	-	HOMO-1 → LUMO (13.41%)
					HOMO-1 → LUMO+1 (19.04%)
					HOMO → LUMO (36.65%)
					HOMO → LUMO+1 (40.52%)
					HOMO → LUMO+3 (20.94%)

[a]Orbital contributions below 10% are omitted.

Table 3.8 Computed vertical transitions and their oscillator strengths and configurations[a]

Phen-mCF_3-TPA	State	Energy (eV)	λ_{max} nm	*f*	Configuration
Singlet	Gas	3.1771	390.25	0.019	HOMO → LUMO (68.25%)
		3.2368	383.04	0.3283	HOMO → LUMO (11.62%)
					HOMO → LUMO+1 (67.62%)
					HOMO → LUMO+3 (18.16%)
		3.3716	367.73	0.4266	HOMO → LUMO+2 (67.29%)
	DCM	3.1737	390.66	0.6536	HOMO → LUMO (64.81%)
		3.2594	380.39	0.1905	HOMO → LUMO+1 (64.30%)
Triplet	Gas	2.5792	480.71	-	HOMO-1 → LUMO (10.83%)
					HOMO-1 → LUMO+1 (15.67%)
					HOMO-1 → LUMO+3 (10.46%)
					HOMO →LUMO (26.79%)

					HOMO →LUMO+1 (45.71%)
	DCM	2.5844	479.73	-	HOMO-1 → LUMO (13.98%)
					HOMO-1 → LUMO+1 (19.31%)
					HOMO → LUMO (36.66%)
					HOMO → LUMO+1 (44.53%)
					HOMO → LUMO+3 (15.67%)
					HOMO → LUMO+4 (14.17%)

[a]Orbital contributions below 10% are omitted.

Table 3.9 Computed vertical transitions and their oscillator strengths and configurations[a]

Phen-pCF$_3$-TPA	**State**	**Energy (eV)**	**λ_{max} nm**	***f***	**Configuration**
Singlet	Gas	3.0513	405.67	0.0834	HOMO → LUMO (69.45%)
		3.373	371.51	0.5742	HOMO → LUMO+1 (68.84%)
		3.3759	367.26	0.1780	HOMO → LUMO+2 (67.65%)
	DCM	3.1578	392.63	0.6917	HOMO → LUMO (60.8%)
					HOMO → LUMO+1 (33.08%)
					HOMO → LUMO+3 (10.30%)
		3.4311	361.36	0.2351	HOMO → LUMO+2 (67.83%)
Triplet	Gas	2.5705	482.34	-	HOMO-1 → LUMO (13.49%)
					HOMO-1 → LUMO+1 (12.65%)
					HOMO → LUMO (36.66%)
					HOMO →LUMO+1 (38.99%)
					HOMO →LUMO+2 (27.21%)
					HOMO →LUMO+3 (10.63%)
					HOMO →LUMO+4 (13.15%)
	DCM	2.5798	480.60	-	HOMO-1 → LUMO (15.74%)
					HOMO-1 → LUMO+1 (16.21%)
					HOMO → LUMO (41.13%)
					HOMO →LUMO+1 (37.12%)
					HOMO →LUMO+3 (19.10%)

[a]Orbital contributions below 10% are omitted.

3.2.3.5 CIE Chromaticity coordinates:

The CIE color coordinates of the ligands and their Eu-complexes were calculated from the emission data's with the help of MATLAB software (Figure 3.29). The ligands 1L, 2L and 3L CIE color coordinates in solid shown x = 0.24, y = 0.26, x = 0.29, y = 0.41 and x = 0.19, y = 0.22, respectively; in solution shown x = 0.15, y = 0.09; x = 0.15, y = 0.08 and x = 0.15, y = 0.07, respectively. The ligand coordinated Eu-complexes 1Eu, 2Eu and 3Eu were shown x = 0.66, y = 0.33, x = 0.65, y = 0.33 and x = 0.66, y = 0.33 solution; x = 0.40, y = 0.23, x = 0.23, y = 0.13 and x = 0.37, y = 0.19 (solid), respectively. The ligands were largely deviated from solution (blue region) to solid (sky blue to green region). These outcomes were also supporting from the PL emission spectral analysis of solution and solid (aggregation). In case of complexes, the similar trend was obtained and deviating from the red (solid) to bluish pink (solution). It is due to the presence of ligand emission in the Eu-complex. However, Eu-complexes in solid state exhibited red color in

the CIE gamut color space and matching to National Television System Committee (NTSC) standards.

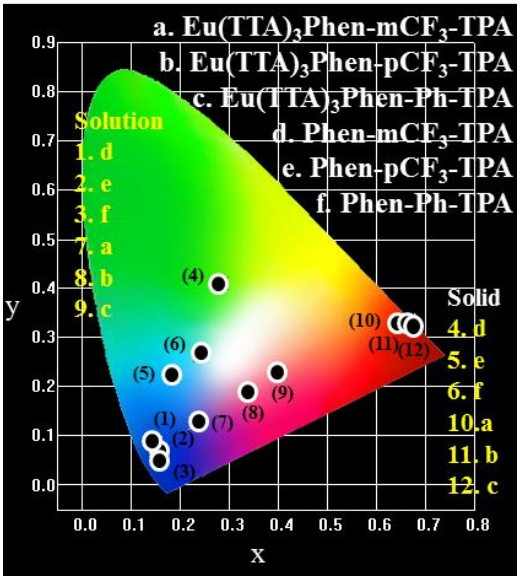

Figure 3.29 The CIE chromaticity coordinates for complexes and ligands in solution as well as solid phase.

3.2.3.6 PMMA film of Eu^{III} complex:

Apart from PL emission study in solution and solid, thin film emission study also been executed. The complexes were incorporated in PMMA matrix in different ratio (0.1, 0.5, 1% of Eu-complex) and studied the emission behaviour (Figure 3.30, their digital photographs under 365 nm shown in the inset). The calculated CIE color coordinates of the complexes are shows good color saturation. The intensity of the Eu^{III} metal ion at 612 nm emission peak is enhanced by increasing the concentration level of the Eu-complex in the PMMA matrix. The calculated CIE color coordinates and their respective intensity parameters were interpreted in the Table 3.10. Thin film of the naked film of the complexes was shown orange red emission. The thin film PL study indicates that the emission from the ligand is negligible and fully dominated by Eu^{III} (612 nm, ED transition) emission. These results are convincingly supports the ligand energy fully transferring to the Eu^{III} metal ion in the presently studied Eu-complexes.

In addition, it was also observed that the intensity ratio (I_2/I_1) decreasing with the increasing of the concentration of the Eu-complex in the PMMA matrix. It is signifying that the concentration of the Eu^{III} complex is influencing the asymmetric ratio. In addition, the calculated QY of the complexes 1Eu, 2Eu and 3Eu are shown at 0.1 % are 31.8, 62.9 and 43.9 %; at 0.5 % shown 53.7, 48.8 and 75.9 %, at 1.0 % shown 63.4, 58.3 and 54.3 %, respectively. The complex 2Eu shown QY increment up to 0.5 % after the QY reduces. This indicates that the quenching of the red emission occurs at above 1 % of complex. However, rest of the complexes was shown no such type of quenching behaviour. As compared with the pure thin film of the complexes, PMMA doped complexes gained high QY yield and reached from 31.8 to 75.9 %. These results were indicates that the complex with doping in PMMA was best advantage for practical applications.

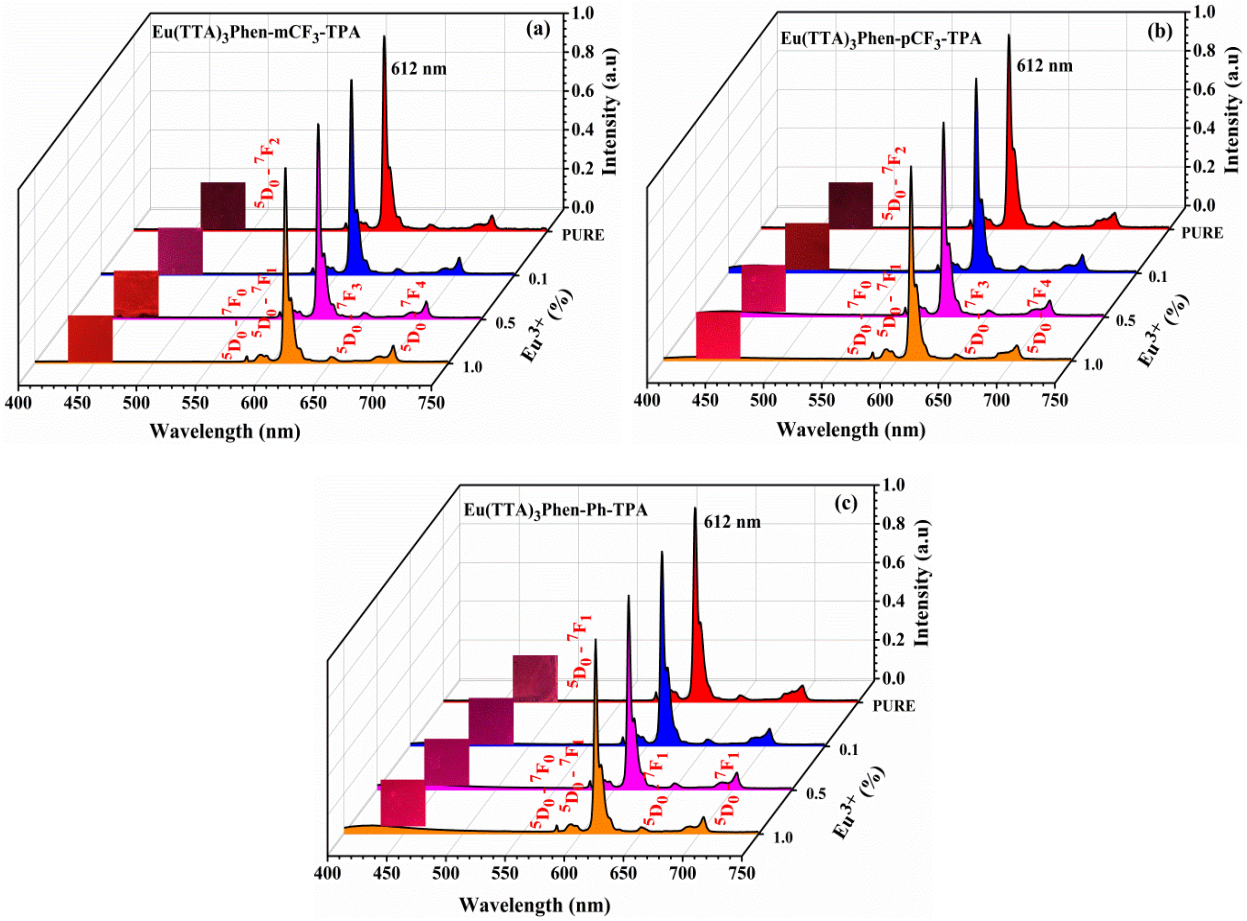

Figure 3.30 The emission spectra of the Eu^{III} complexes doped with PMMA in different percentage ratio (a,b,c) and its thin film patterns were shown. d is CIE color coordinates of the thin film of the complexes in different ratios.

Table 3.10 The calculated CIE color coordinates of the thin film of the complexes in different ratios and their intensity ratios.

		$Eu(TTA)_3Phen$-Ph-TPA	**$Eu(TTA)_3Phen$-pCF_3-TPA**	**$Eu(TTA)_3Phen$-mCF_3-TPA**
I_2/I_1 (% of Eu^{3+})		24.42 (PURE) 21.23 (0.1) 19.58 (0.5) 17.81 (1.0)	23.06 (PURE) 27.11 (0.1) 18.56 (0.5) 22.65 (1.0)	20.12 (PURE) 25.27 (0.1) 27.11 (0.5) 26.91 (1.0)
CIE	**x**	0.54 (PURE) 0.58 (0.1) 0.61 (0.5) 0.66 (1.0)	0.56 (PURE) 0.65 (0.1) 0.65 (0.5) 0.55 (1.0)	0.61 (PURE) 0.66 (0.1) 0.66 (0.5) 0.64 (1.0)
	y	0.27 (PURE) 0.29 (0.1) 0.31 (0.5) 0.33 (1.0)	0.28 (PURE) 0.33 (0.1) 0.33 (0.5) 0.28 (1.0)	0.31 (PURE) 0.33 (0.1) 0.33 (0.5) 0.33 (1.0)

3.2.3.7 Fabrication of LED with Eu complexes:

Light-emitting diodes were fabricated by using combination of a 395 nm emitting InGaN LED chip with the complexes in different ratios such 1:10 and 1:50 (Eu^{III} complex : PMMA). The emission of the original naked InGaN LED with 395 nm chip and emission from the complexes under 20 mA forward-bias current was shown in Figure 3.31. The excitation source from 395 nm emitting LED was fully absorbed by the complexes and among all 2Eu shown better source utilization. Most of the complexes were shown red and pinkish-red emission from the LED. Complex 2Eu shown pinkish red in case of 1-50 ratio is due to the presence of ligand emission in the Eu-complex. However, red emission observed in case of 1-10 ratio and it is due to the ligand emission in complex have less intensive than 1-50 ratio of LED emission. The calculated CIE color coordinates of the complexes shown for 1Eu is x = 0.52, y = 0.30 (1:10); x = 0.50, y = 0.30 (1:50); 2Eu is x = 0.55, y = 0.30 (1:10); x = 0.48, y = 0.28 (1:50) and 3Eu is x = 0.52, y = 0.29 (1:10); x = 0.57, y = 0.30 (1:50), respectively. In addition, the CIE of the obtained results are interpreted in the Figure 3.31.

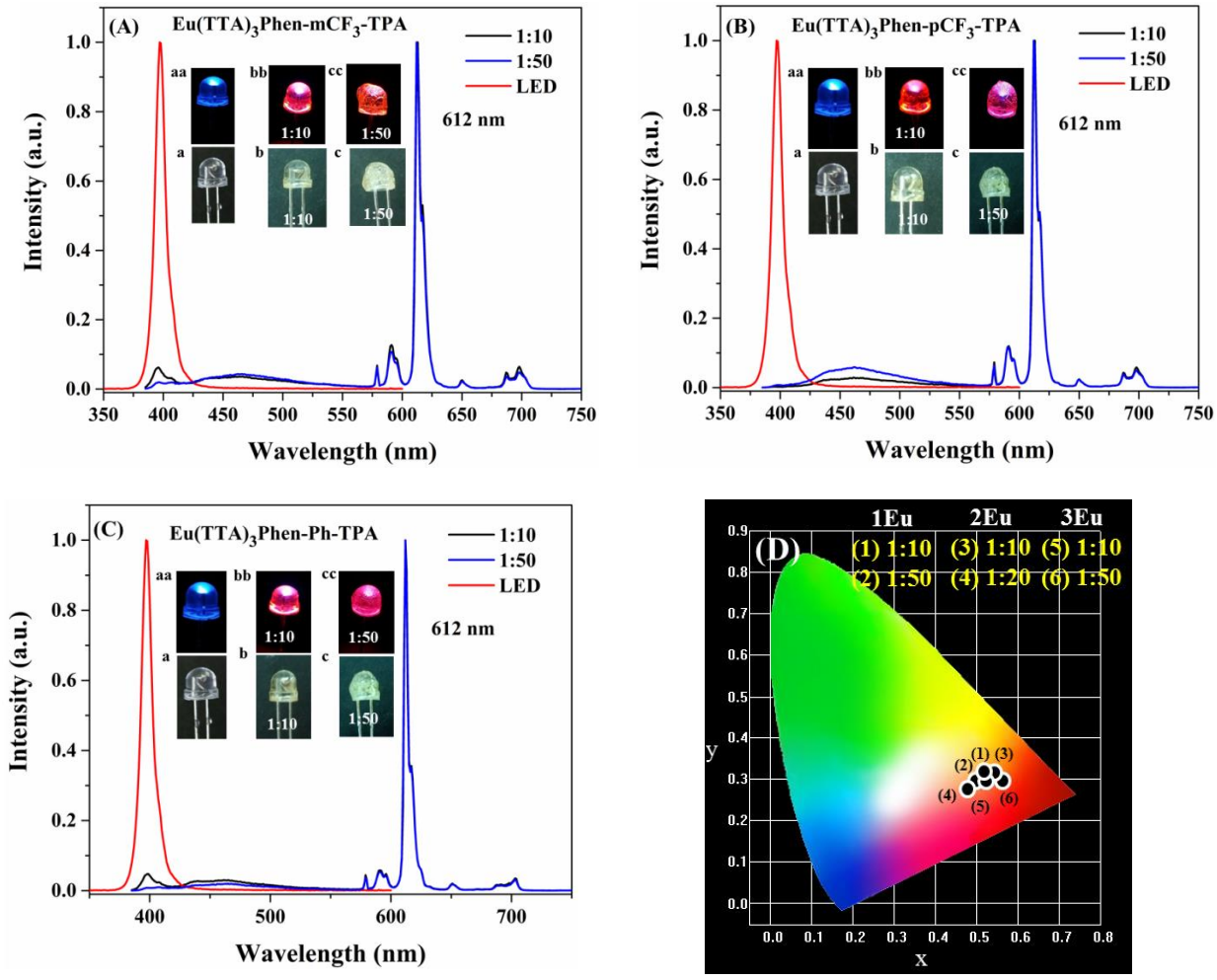

Figure 3.31 The spectra's **A**, **B** and **C** are Eu^{III} complexes coated on the 395 nm emitted LED chip. In inset **a** is the original 365 nm emitted LED chip, **aa** is under forward bias. **b** and **c** are coated with Eu^{III} complexes and **bb** and **cc** are with forward bias, respectively. The CIE color coordinates of the Eu-complexes shown in D.

3.3 Fluorene decorated phenthro-imadaole bidentate ligand for ternary mono nuclear Eu^{III} molecular complex: synthesis, photophysical, electrochemical and theoretical study:

3.3.1 Outline of the present study:

In the previous section, N1 functionalization by phenyl and substituted phenyl (mCF_3 and pCF_3) of phenthro-imadaole was synthesised and used the same for the synthesis of Eu^{III} complexes. The photophysical studies reveal that the complexes can efficiently emit white in solution and red in solid. In the part, resent study, N1 functionalization by polyaromatic ring containing fluorene was introduced in the phenthro-imadazole backbone (triphenylamine-phenanthroline-fluorene, Phen-Fl-TPA) and used for the synthesis of an efficient red emitting Eu^{III} complex ($Eu(TTA)_3$Phen-Fl-TPA, Phen-Fl-TPA = 4-(1-(9,9-diethyl-9H-fluoren-2-yl)-1H-imidazo[4,5-f][1,10]phenanthrolin-2-yl)-N,N-diphenylbenzenamine, TTA = Thenoyltrifluoroacetone. Incorporation of TPA (hole-transporting), Phen (electron-transporting) and fluorene fragments into one molecule could be advantage: the fluorene has strong π-π* absorption is photochemically and thermally stable and it is expected that it can also improve the morphological stability of the Eu^{III}-phosphors. The second one is the enhancement in the hole transporting properties may be anticipated by the attached TPA group, which prevents the crystallization of complexes. In addition, it protects the metal radiating states (light-harvesting unit), as well as increases the solubility in common organic solvents and thermal stability of the complex [36, 37]. Phen acts as an electron transporting moiety and is also co-operative in increasing the thermal stability of Eu^{III} complex. Thenoyltrifluoroacetone (TTA) as well as fluorene acts as an antenna that harvest energy efficiently to Eu^{III} central metal ion. It is well documented that the presence of halogen can decrease the vibrational quenching and increase the decay time at room temperature (RT) [38, 39]. It is very much intended that the designed ligand can act as a dual characteristic, that is bipolar nature and antenna for the Eu^{III} complex and the structure of the ligand and complex is represented in Figure 3.32.

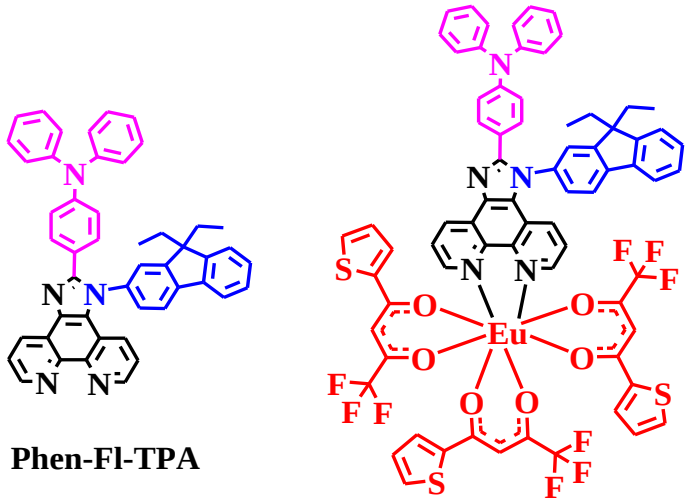

Figure 3.32 Chemical structures of bipolar ligand and the corresponding Eu^{III} complex.

3.3.2 Experimental:

3.3.2.1 General Information for synthesis:

The general information related to synthesis was mentioned in Chapter 2, experimental section 2.2.2.

3.3.2.2 Measurements:

Details are given in previous measurement section in Chapter 2 (2.2.2).

3.3.2.3 Synthesis:

The detailed synthesis of the ligand and complexes were given in 3.1.2.3 and the compounds were confirmed by ^{1}H NMR, CHNS and FT-IR analysis (Figure 3.S13 and 3.S16).

3.3.2.3.1 *Synthesis of N-(4-(1-(9,9-diethyl-9H-fluoren-7-yl)-1H-imidazo[4,5-f][1,10]phenanthrolin-2-yl)-N,N-diphenylbenzenamine (Phen-Fl-TPA)*:

Fl (0.169 g, 0.714 mmol) was added to a stirred solution of TPA-CHO (0.194 g, 0.714 mmol) in glacial acetic acid (15 mL) at room temperature. To this reaction mixture subsequently ammonium acetate (0.274 g, 3.571 mmol) and Dione (0.150 g, 0.714 mmol) were added. Then resulting mixture was stirred for 12 hrs at 110 °C. The progress of the reaction was monitored by TLC (MeOH in Chloroform 1:9, Rf-0.2). The RM was poured into minimum amount of water and then ammonium hydroxide solution was added. Then the formed solid was filtered and dissolved in dichloromethane, followed by dried with anhydrous sodium sulphate and the solvent was evaporated to get 200 mg crude compound. The resultant compound was purified with column chromatography by using silica gel (100-200 mesh), eluent with 5% methanol in chloroform and the solvent was evaporated and dissolved in minimum amount of THF solution added excess of hexane solvent, the pale brown color solid was formed. After settling of solid, decanted and repeated this process three more times to obtain Phen-Fl-TPA, 260 mg (53.3%) with pale brown color solid. The spectra were mentioned in Figure S5 and Figure S6. ^{1}H-NMR Data (400 MHz, $CdCl_3$): δ 9.21-9.17 (m, 2H), 9.03 (dd, 1H), 7.97 (d, 1H), 7.87-7.84 (m, 1H), 7.75-7.80 (m, 1H), 7.63-7.56 (m,2H), 7.53 (d, 2H), 7.48-7.42 (m, 4H), 7.25-7.21 (m, 5H), 7.07-7.03 (m, 5H), 6.93 (d, 2H), 2.12-2.06 (m, 4H), 0.42 (t, 3H), 0.28 (t, 3H). ^{13}C-NMR Data (100 MHz, $CdCl_3$): δ 152.5, 152.0, 150.2, 148.8, 147.7, 147.0, 144.7, 144.3, 143.6, 139.9, 136.6, 136.0, 130.56, 130.0, 129.6, 129.3, 128.4, 127.9, 127.5, 127.3, 126.8, 125.7, 125.0, 123.9, 123.6, 123.4, 123.2, 123.0, 122.8, 121.8, 121.3, 120.4, 119.9, 56.7, 32.7, 8.3. EI-mass: m/z 684.23 (M^{+}+1).

3.3.2.3.2 *Synthesis of $Eu(TTA)_3$Phen-Fl-TPA*:

Taken a 100 mL two neck round bottom flask with nitrogen containing balloon contained adaptor and poured $Eu(TTA)_3 \cdot 2H_2O$ (124 mg, 0.146 mmol, 1 eq) dissolved in dry tetrahydrofuron (THF) (5 mL). The ligand (100 mg, 0.146 mmol, 1 eq) dissolved in THF (10 mL) and added to the stirred solution of reaction mixture and then stirred for 12 hrs at room temperature. The resulting mixture was concentrated and dissolved in minimum amount of THF and added excess of hexane to get solid product. After settling of solid, it was decanted and the

process was repeated it another two times and dried to get pale yellow color solid with 150 mg (68.4%). Elemental analysis: Anal. Calc. for $C_{72}H_{49}EuF_9N_5O_6S_3$: C, 57.68; H, 3.29; N, 4.67; S, 6.42. Found: C, 57.55; H, 3.72; N, 4.74; S, 6.76%. EI-mass: m/z 1498.4 (M^+-1).

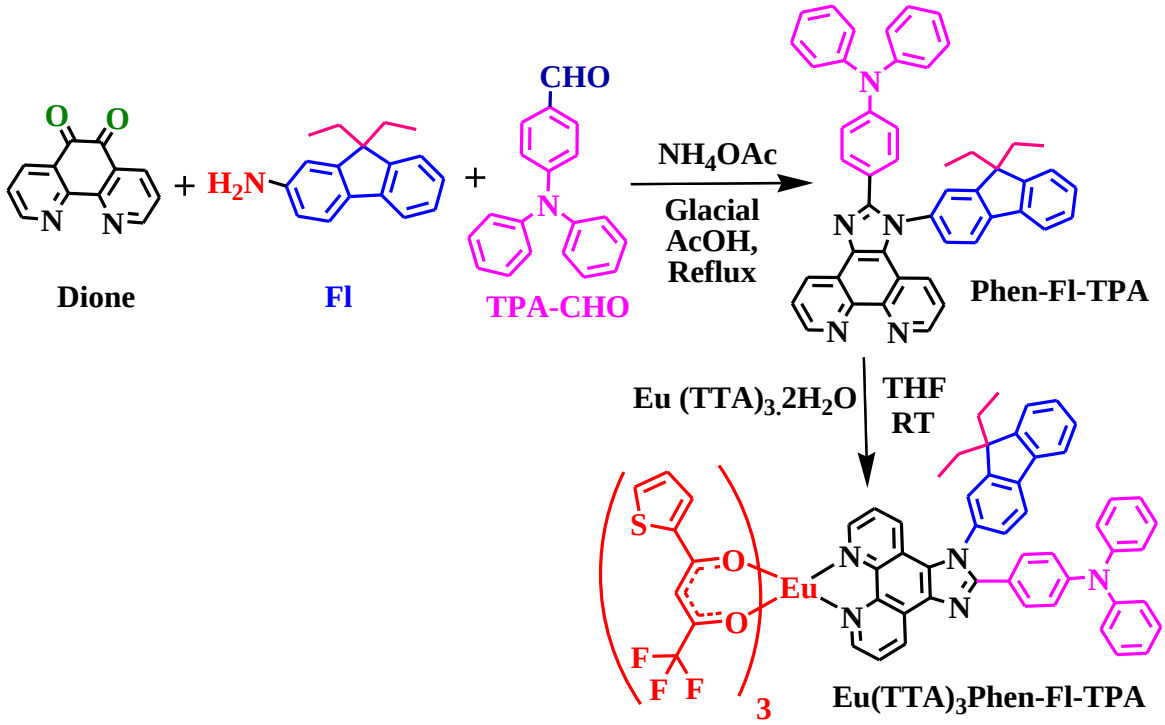

Scheme 3.2 Synthetic route of triphenyl functionalized ligand and their corresponding β-diketonate Eu^{III} ternary complex.

3.3.3 Results and Discussion:

3.3.3.1 Characterization of the complex:

The method of Eu^{III} complex synthesis is summarized in Scheme 3.2. The compounds were characterized by NMR (^1H and ^{13}C NMR; Figure 3.S14, S15), Mass spectroscopy, FTIR and Elemental analysis. All the measurements were done at room temperature (RT). Both the ligand and Eu^{III} complex showed good solubility in common organic solvents (dichlorobenzene (DCM), tetrahydrofuron (THF), chloroform ($CHCl_3$), methanol (MeOH), dimethylformamide (DMF) and acetonitrile (ACN) and toluene).

3.3.3.1.1 FT-Infrared spectroscopy and Power X-ray diffraction (PXRD) study:

The FT-IR spectra of ligand and its corresponding Eu^{III} complex were measured in the range of 500 - 4000 cm^{-1} (Figure 3.33, left). The observed strong carbonyl (C=O) stretching frequency at 1609 cm^{-1} for the $Eu(TTA)_3.2H_2O$ complex is shifted to 1595 cm^{-1} for the Eu^{III} complex. These changes are the indirect evidence that the β-diketonate ($Eu(TTA)_3$) compound coordinated with the neutral ligand and the C=N bond is converted into a structure of C=N–Eu-O bond. The vibrational frequency due to C=N appears at 1588 cm^{-1} for the ligand and the same is shifted to 1534 cm^{-1} for the ligand coordinated with Eu^{III} ion. These results are suggesting that

the N atom in ligand also coordinates with $Eu(TTA)_3$ [40]. All other major vibrational frequencies are listed out in Table 3.11.

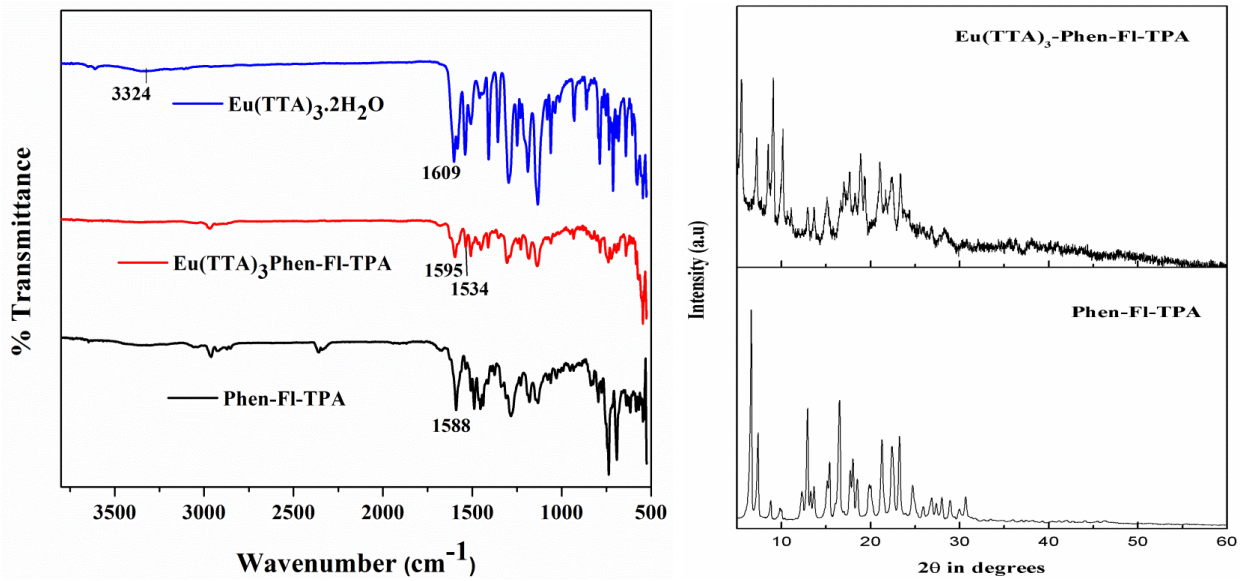

Figure 3.33 FT-IR spectra of the ligand, $Eu(TTA)_3 \cdot 2H_2O$ and Eu^{III}-complex (left); the PXRD of ligand and corresponding Eu^{III} complex (right).

Table 3.11 The major Infrared frequencies (wavenumber in cm^{-1}) at room temperature for free ligand, corresponding Eu^{III} complex, and $Eu(TTA)_3 \cdot 2H_2O$.

S. No.	Compound	ν (C=O) (Wavenumber in cm^{-1})	ν (C=N)	ν (C-N)	ν (C-F)	ν (C-CF_3)	ν (C-H) (phen)
1	**$Eu(TTA)_3$Phen-Fl-TPA**	1595	1534	1287	1306	1136	785, 731
2	**Phen-Fl-TPA**	--.--	1588	1283	--.--	--.--	833, 733
3	**$Eu(TTA)_3 \cdot 2H_2O$**	1609	--.--	--.--	1296	1133	--.--

The PXRD diffraction studies have been carried out, in order to evaluate the crystalline or amorphous nature of the ligand and its corresponding Eu^{III} complex (Figure 3.33, right). The PXRD pattern of the ligand shows crystalline nature, however the Eu^{III}complex diffraction shows amorphous structure. It is also worth to note that the interplanar distances (d) of Eu^{III} complex are shifted to higher value as compared to that of the ligand. It is also documented that the d-values are large for $Ln(DBM)_3$ (Ln = La, Tb and Eu) as compared to that of HDBM ligand [41]. The stimulated powder pattern (mercury software) of the single crystal was well matching with the PXRD data of ligand.

3.3.3.1.2 Thermal Properties:

DSC-TG analysis was carried out (under nitrogen atmosphere and the heating rate was maintained 10 °C for min^{-1}) to find the thermal stability and glass transition temperature of the ligand and their corresponding Eu^{III} complex. The TG analyses showed that the thermal decomposition occurs above 250 °C for both ligand and Eu^{III} complex (Figure 3.34).

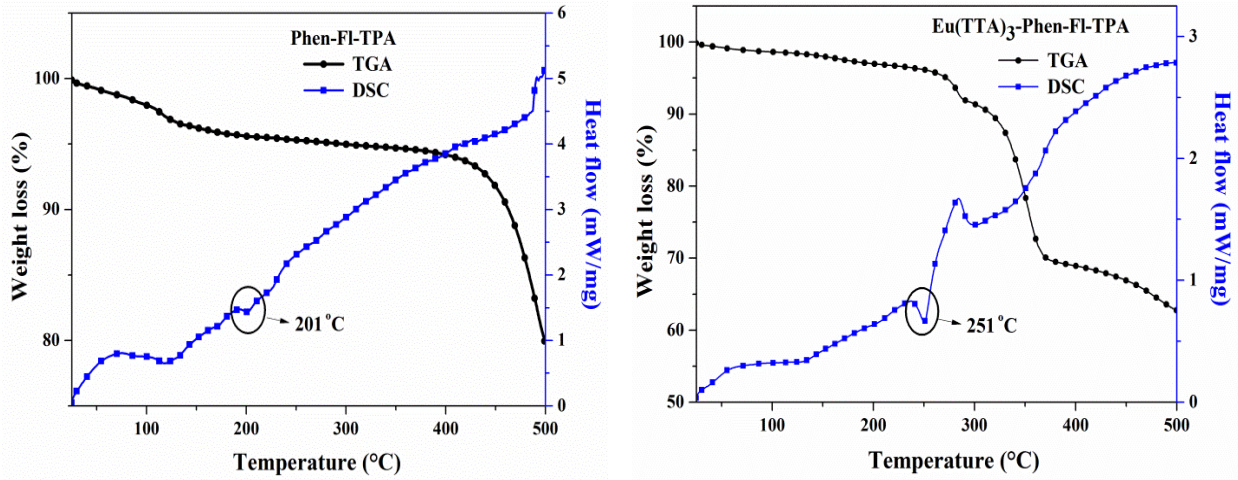

Figure 3.34 DSC-TG analysis curves for the ligand (left) and Eu^{III} complex (right).

The 10% weight loss was observed for ligand and its Eu^{III} complex at 462 and 317 °C, respectively. The observed high thermal decomposition temperature for Eu^{III} complex is similar to that of the related documented β-diketonate coordinated Eu^{III} complexes ($Eu(DBM)_3IPD$–PPO, $Eu(AITFBD)_3phen$ and $Eu(DBM)_3(DPPZ)$ (5 wt%)) [42, 43]. It is also worth to note that the thermal decomposition temperature of the Eu complex is higher than that of DBM (dibenzoylmethanate) coordinated Eu^{III} complex ($Eu(DBM)_3IPD$) [44]. It clearly signifies that the currently synthesized red emitting Eu^{III} complex is promising candidates for further investigations. $Eu(TTA)_3$Phen-Fl-TPA complex shown three stages of thermal decompositions and the corresponding temperatures are 278 (range 270-301 °C, minor), 319 (range 304-392°C, major) and 449 °C. The thermal decomposition temperature of ligand Phen-Fl-TPA (>400 °C) is higher than that of the corresponding Eu^{III} metal complex.

More importantly, the second stage where there is a major weight loss started at 304 °C, completed at 392 °C and reached the largest rate at 319 °C. This is attributed to the elimination and/or decomposition of ligand fragments such as TTA moiety, TPA and fluorene groups in the Eu^{III} complex [45, 46]. The DSC curve showed specific heat or glass transition temperature of the ligand and Eu^{III} complex at 201 and 251°C, respectively. This was due to the sample undergoing a change in heat capacity; no formal phase change was observed. The transition from amorphous to crystalline solid is observed at 283 °C. This is happens because the molecules may obtain enough freedom of motion to spontaneously arrange themselves into a crystalline form at some point which is known as the crystallization temperature. These DSC-TG results are suggesting that the $Eu(TTA)_3$Phen-Fl-TPA complex have high thermal decomposition temparature (> 250 °C).

3.3.3.1.3 Structural Characterization:

The crystal data and structure refinement parameters are presented in Table 3.12. The structure of the ligand is mentioned in Figure 3.35. The TPA consisted N atom bonded phenyl groups are placed in different plane (out of 3, 3 are dissimilar). The obtained ground state optimized structure of Phen-Fl-TPA ligand and its single crystal structure were well matching (Figure 3.35). The bond lengths and bond angles from the single crystal XRD data of Phen-Fl-TPA ligand are shown in Table 3.ST3 and 3.ST4. It is worth to note that the several attempts

which were made for growing single crystal of Eu complex in different solvents and mixtures / combination of solvents have failed.

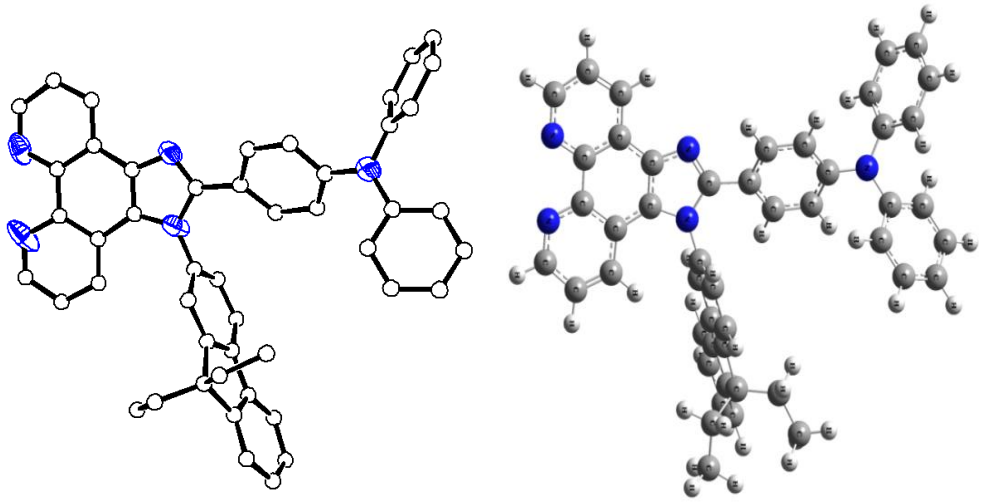

Figure 3.35 ORTEP molecular structure of Phen-Fl-TPA (50% probability ellipsoids; H atoms and cocrystallized solvent molecules are omitted). Heteroatom: N, blue [CCDC 1450296] (left), The ground state optimized structure (right).

Table 3.12 Crystal data and structure refinement parameters of ligand.

Parameter	Phen-Fl-TPA
Empirical formula	$C_{48}H_{37}N_5$
Formula weight	683.83
Temperature/K	293(2)
Crystal system	triclinic
Space group	P-1
a/Å	11.1077(5)
b/Å	11.9637(6)
c/Å	15.1543(8)
α/°	95.659(4)
β/°	91.562(4)
γ/°	110.298(5)
Volume/Å^3	1875.50(16)
Z	2
ρ_{calc}g/cm^3	1.211
μ/mm^{-1}	0.072
F(000)	720.0
Crystal size/mm^3	0.224 × 0.193 × 0.066
Radiation	MoKα (λ = 0.71073)
2Θ range for data collection/°	3.66 to 56.64
Index ranges	$-14 \le h \le 7$, $-13 \le k \le 15$, $-19 \le l \le 19$
Reflections collected	10584
Independent reflections	8028 [R_{int} = 0.0219, R_{sigma} = 0.0704]
Data/restraints/parameters	8028/0/480

Goodness-of-fit on F^2	1.045
Final R indexes [I>=2σ (I)]	R_1 = 0.0795, wR_2 = 0.1650
Final R indexes [all data]	R_1 = 0.1590, wR_2 = 0.1980
Largest diff. peak/hole / e $Å^{-3}$	0.20/-0.20

3.3.3.2 Photophysical properties:

3.3.3.2.1 UV-Visible absorption and DRS studies:

The UV-Visible absorption spectra of ligand Phen-Fl-TPA, $Eu(TTA)_3$ and Eu-complex were carried out in solution (chloroform solution conc. 1.0×10^{-5} mol L^{-1}), thin film and in the solid phase are shown in Figure 3.36 (right). The absorption spectrum of ligand shows absorption band from 250 to 420 nm with λ_{max} values of 358 and 279 nm, these bands are attributed to the $\pi \rightarrow \pi^*$ transitions. The theoretically calculated UV-spectra in gas/solution phase also support the experimental findings (Figure 3.36 (left)). The absorption spectra of the starting materials (TTA, TAP, Phenathroaline and fluorene-alkyl) have also been given for reference in Figure 3.S16. Similarly the europium complex also showed the peak maxima values at 343 and 275 nm, while in the case of $Eu(TTA)_3$, the peak maxima values at 340 and 273 nm, respectively.

The Eu^{III} complex absorptions are very similar to that of the ligand as well as $Eu(TTA)_3$ and the results are tabulated in Table 3.14. The comparative study of absorption spectra of the Eu^{III} complex of solid, solution and thin film (the observed flat absorption in the spectrum from 430 nm to 800 nm is due to an instrumental artefact) have been made, and absorption maximum shift to longer wavelength for solid phase as compared to that of the complex in solution and thin film. The observed bathochromic shift in the absorption spectra is due to the aggregation of the complex in the solid phase [24, 25]. As mentioned in the previous section that the band gap were calculated for all the compounds by converting the UV-Visible data into Kubelka-Munk function [22, 23]. The acquired spectrum was converted to Kubelka-Munk function ($\alpha = F(R_\infty)$, equation 2.1).

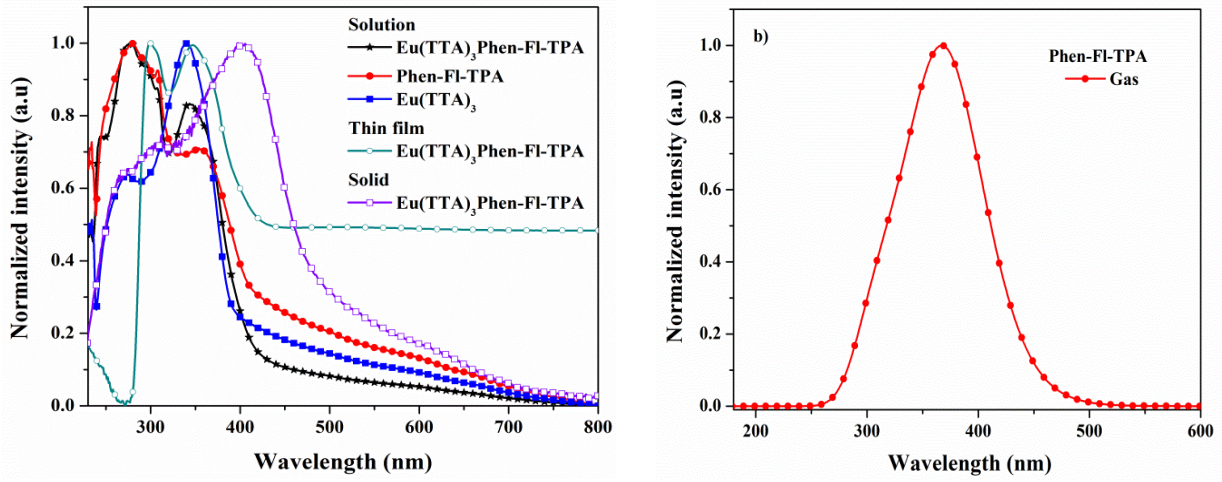

Figure 3.36 The UV-Vis absorption spectra of a) $Eu(TTA)_3$Phen-Fl-TPA comparison study in solution, thin film as well as in solid (left). b) The Phen-Fl-TPA ligand absorption spectra theoretically calculated (right).

3.3.3.4.2 Photoluminescence studies:

The radiative emission is dependent upon on the population of ligand triplet state as well as the excited state of the Eu^{III} complex energy levels. When the ligand is excited, the excited energy of the ligand is transferred to the Eu^{III} excited states and the emission occurs from lowest excited state ($^5D_0$ level) of Eu^{III} ion with different colors, but the intensity of the red and orange emission (electric or magnetic dipole transition) is depends on the local site symmetry of Eu^{III} ion present in the complex. The excitation and emission spectra were recorded for the ligand and its Eu^{III} metal complex in solution, thin film and solid. The ligand, Phen-Fl-TPA emission spectrum shows emission at around 443 nm (Figure 3.37a) under 280, 294, 305 and 365 nm excitation wavelengths in solution. The PL excitation spectrum shows multiple absorption in the near UV region (325 and 397 nm), under the monitoring emission wavelength 443 nm. In the case of solid phase, the ligand shows blue emission (456 nm) under different (280, 305, 332, 365 nm) excitation, whereas the excitation spectrum shows broad absorption in the near UV region (332 and 365 nm) under the emission monitoring wavelength 456 nm (Figure 3.37b).

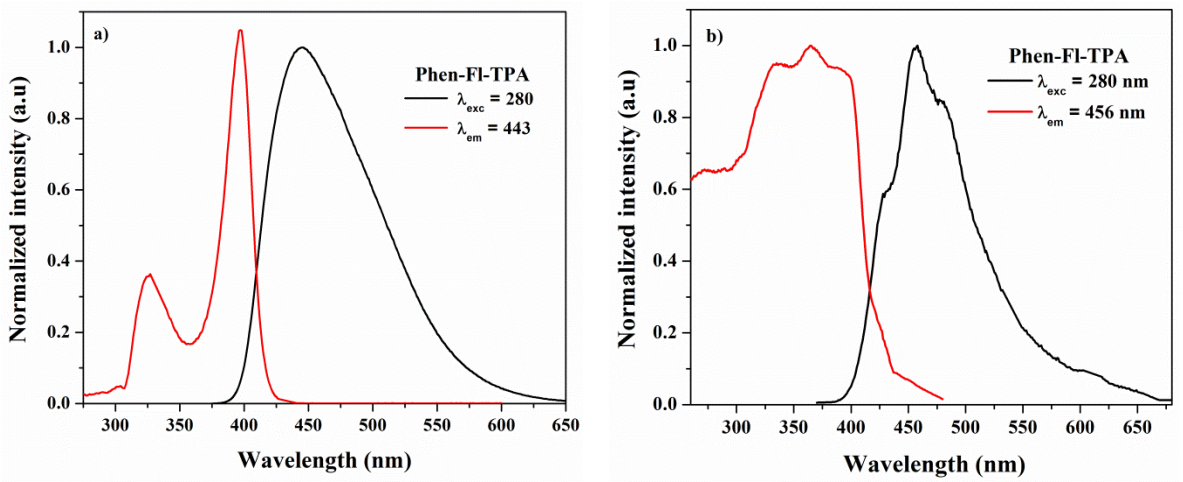

Figure 3.37 The PL excitation and emission spectra of Phen-Fl-TPA in (a) chloroform solution and (b) solid phase.

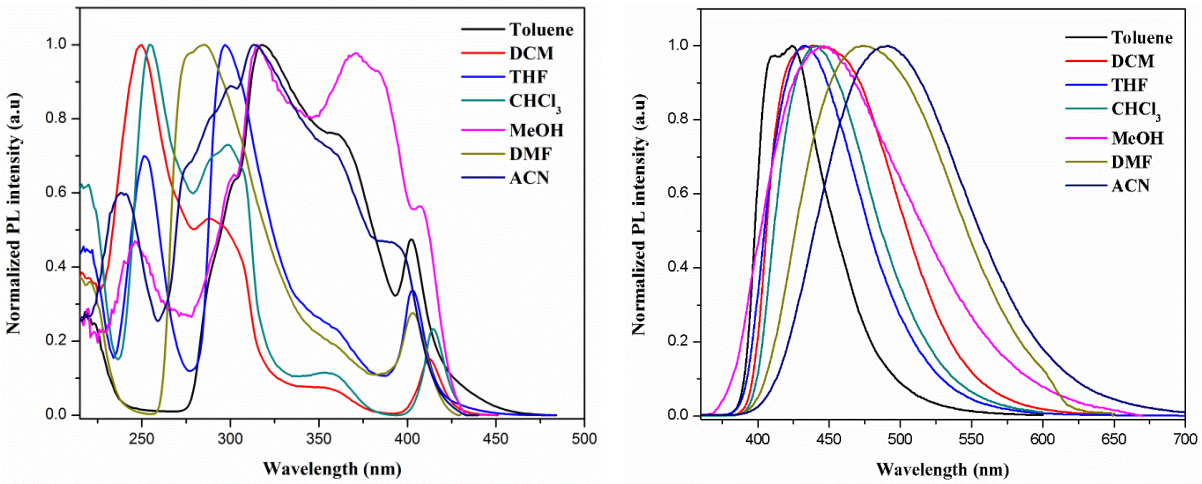

Figure 3.38 The solvent effect of Phen-Fl-TPA of PL in different solvents.

To understand further the solvent effect, further the solvatochromism studies were carried out (details mentioned in the previous section**:** 2.3.3.1.3). The ligand emission was monitored in different solvents, and the emission of solvent-dependent aggregation was observed. The emission shifted from 420 to 490 nm by changing from toluene to ACN, Figure 3.38. Stoke's shift $\Delta\bar{\nu}$ of Phen-Fl-TPA versus the Lippert solvent parameter $\Delta f = f(\varepsilon) - f(n^2)$. The numbers refer to the solvents in Table 3.13. The straight line represents the best linear fit to the 7 data points (Figure 3.39). There is close to linear relationship [correlation coefficient $R^2 = 0.1869$, slope = $(6.598) \times 10^3\ cm^{-1}$, intercept = $(1.526) \times 10^3\ cm^{-1}$.

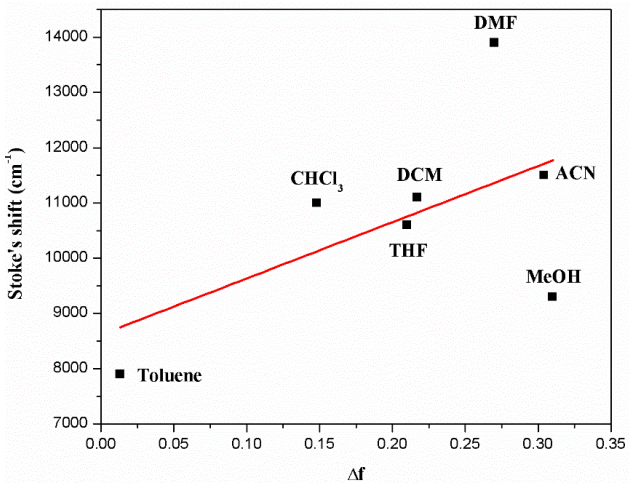

Figure 3.39 Stoke's shift $\Delta\bar{\nu}$ of Phen-Fl-TPA versus the Lippert solvent parameter $\Delta f = f(\varepsilon) - f(n^2)$. The straight line represents the best linear fit to the 7 data points.

Table 3.13 PL spectral data of ligand in various solvents

S.No.	Solvent	λ_{abs} (max) in nm	λ_{em} (max) in nm	Stoke's shift ($\Delta\bar{\nu}$) in cm^{-1}
1	**Toluene**	318	424	7900
2	**DCM**	291	430	11100
3	**THF**	297	434	10600
4	**$CHCl_3$**	298	443	11000
5	**MeOH**	315	446	9300
6	**DMF**	286	475	13900
7	**ACN**	314	491	11500

The excitation and emission spectra of Eu-complex is shown in Figure 3.40. The broad absorption band (due to ligand π - π^* electronic transition) was observed for $Eu(TTA)_3$ Phen-Fl-TPA in solution with peaking wavelength 405 nm. However, the excitation (at 394 and 465 nm) due to Eu^{III} was not clearly observed due to the overlap with ligand absorption band. The emission spectrum (Figure 3.40a) shows red emission at 612 nm, irrespective of the excitation wavelength (275, 296, 343 and 358 nm) for solution. The emission comparison of Eu^{III} complex and $Eu(TTA)_3$ is showed similar emission peaks (~612 nm). It is also equally important that the Eu complex solid PL emission characteristics study. The Eu^{III} complex shows red emission under 280, 365 nm excitation wavelength (Figure 7b) with appropriate CIE color coordinates in solid phase (Figure 3.40b). The Eu^{III} complex in solution, solid and thin film (spin coated on a glass substrate), show characteristic emission peaks, due to the intra-configurational $^5D_0$ - ^7F_J (J = 0 - 4)

electronic transitions. When the ligand emission wavelength is used to excite the Eu^{III} complex, emissions appear at 580, 592, 612, 652 and 703 nm, due to 4f - 4f electronic transitions of Eu^{III} ion ($^5D_0$-$^7F_0$, $^5D_0$-$^7F_1$, $^5D_0$-$^7F_2$, $^5D_0$-$^7F_3$ and $^5D_0$-$^7F_4$). It is indirect evidence that the energy transfer occurs from the ligand to Eu central metal ion.

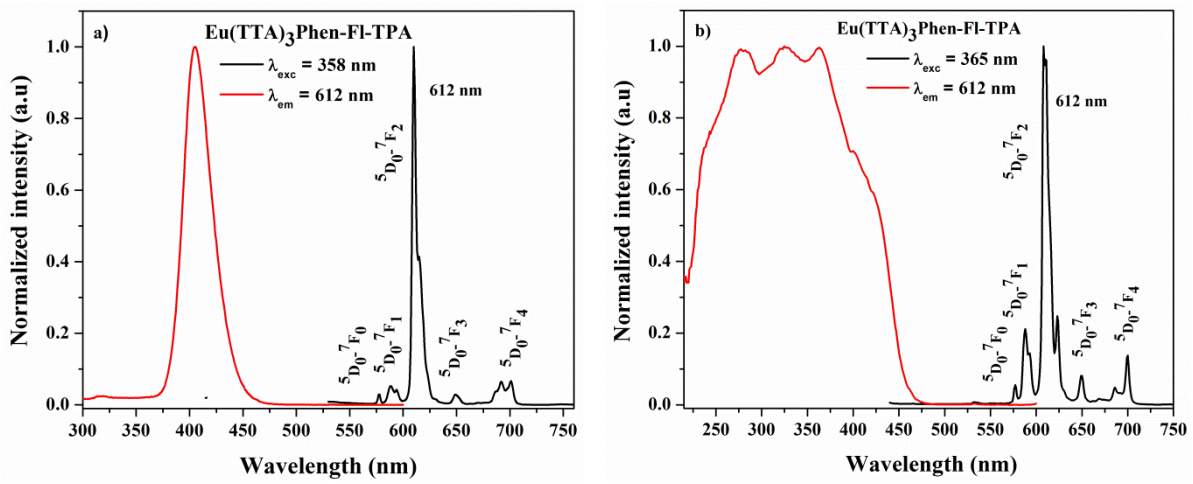

Figure 3.40 The PL excitation (left) and emission (right) spectra of $Eu(TTA)_3$Phen-Fl-TPA complex in a) chloroform solution (conc. 1.0×10^{-5} mol L^{-1}), b) solid phase.

The Eu^{III} complex exhibits characteristic red emission from the center metal ion under 358 nm excitation. The observed emission line at ~580 nm (single peak) due to $^5D_0$-$^7F_0$ transition indicates that all Eu^{III} ions in the structure occupy a site of the same symmetry and experience the similar crystal field perturbation. The emission lines at around 580 and 652 nm are weak and their corresponding $^5D_0$-$^7F_0$, $^5D_0$-$^7F_3$ transitions are forbidden both in magnetic and electric dipole systems [26]. The emission intensity of the magnetic dipole (MD) transitions ($^5D_0$-$^7F_1$) intensity, when Eu^{III} ion occupies center of symmetric site and this MD transition is independent of the coordinate environment. The most intense induced electronic dipole transition $^5D_0$ - $^7F_2$ is observed at 612 nm and the intensity is very sensitive to the local chemical environment of Eu^{III} ion. The Eu^{III} ion in the complex has stronger interactions with its local ligand environment, the local environment of the Eu ion sense to be more non-symmetrical. In the present study, the intensity of the electric dipole transition is more intense.

Table 3.14 The UV-absorption and PL emission data of synthesized Eu^{III} complex and ligand.

S.No.	Compound	λ_{max} (abs) (nm)		λ_{ex} [a]	λ_{em} [a d]	PL QY
		Solution[a b]	Thin film[c]	(nm)	(nm)	(%)
1	**$Eu(TTA)_3$Phen-Fl-TPA**	275, 296, 306, 343	299, 346	275, 296, 343, 358	580, 592, 612, 652, 702	34.1
2	**Phen-Fl-TPA**	279, 295, 307, 358	--.--	280, 294, 305, 325, 365	443	--.--
3	**$Eu(TTA)_3$**	273, 340	--.--	275, 340	580, 592, 612, 652, 703	--.--

[a] measured in chloroform solution at 298 K, [b]absorption peaks from the UV-Vis absorption spectra. [c]emission peaks from photoluminescence emission spectra.

The europium ion site symmetry or asymmetric ratio was calculated from the integration emission intensity ratio of the $^5D_0$-$^7F_2$ transition to $^5D_0$-$^7F_1$ transition (I_2/I_1).[31,32] The intensity ratio (I_2/I_1) of the Eu^{III} complex in solution, thin film and solid are 18.2, 9.35 and 4.88, respectively. These ratios are also indicating that the Eu^{III} ion occupied non-center of symmetry site and it is very much clear that Eu^{III} ion and ligand have strong coordination interaction. The calculated intensity ratio (I_2/I_1) of $Eu(TTA)_3$ was around 11.5. The Eu^{III} complex in solution was showed high intensity ratio than $Eu(TTA)_3$. The comparative PL emission study of the complex in solution, thin film and solid phase have been executed and these were showed similar results with 612 nm intensive emission peak. A small change in emission spectral wavelength was observed between solution, thin film and solid emission spectra which is negligible. These results are conclude that the energy transfer from the ligand to central Eu^{III} metal ion is efficient in $Eu(TTA)_3$Phen-Fl-TPA.

3.3.3.2.3 Energy transfer mechanism:

As mentioned in the previous section that to further understand the energy transfer between singlet ($^1\pi\pi^*$) and triplet ($^3\pi\pi^*$) energy levels of ligand as well as resultant red emission from Eu^{III} metal ion by means of triplet ($^3\pi\pi^*$) to $^5D_0$ level energy transfer one need to know the exact location of the excited levels. The theoretical calculations were performed to calculate the singlet and triplet energy state values by DFT and TD-DFT. The energy transfer mechanism and the structural representation for energy transfer from fluorene and TTA to Eu^{III} ion is shown in Figure 3.41a, b. The theoretical data of the Phen-Fl-TPA, Show the singlet and triplet energy levels are shown at 25,624 (3.17 eV) and 20,873 cm^{-1} (2.58 eV), respectively. It is also documented that the singlet and triplet energy level of the TTA are located at around 25,164 (3.12 eV) and 18,954 cm^{-1} (2.35 eV) [27]. In present study, the synthesized Eu^{III} complex shows red emission due to efficient energy transfer from both the bidentate ligand as well as TTA to center metal ion. As mentioned earlier the Eu^{III} metal ion excited $^5D_0$ energy level is located at 17,500 cm^{-1} [28, 29].

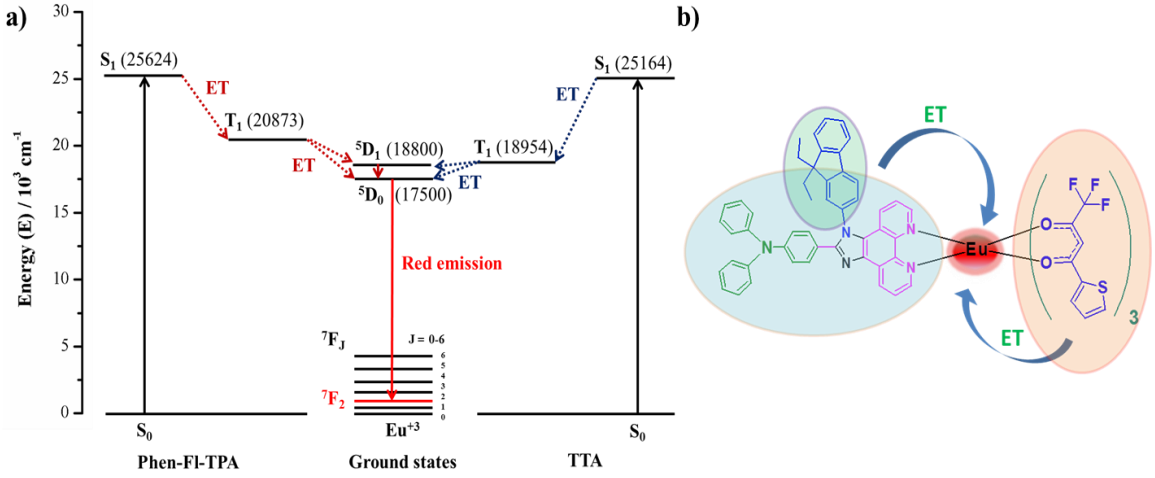

Figure 3.41 a) Schematic diagram for ligand to Eu^{III} center metal ion energy transfer mechanism (S = singlet, T = triplet, ET = energy transfer (dotted arrow is non-radiative, $\rightarrow$ is radiative). b) energy transfer from fluorene and TTA moiety to Eu^{III} metal ion.

The triplet state energy level is higher than that of $^5D_0$ energy level of the Eu^{III} complex (around 3,373 cm^{-1}) and it is clearly indicating that the energy gap (ΔE) between triplet state of the ligand and $^5D_0$ energy level of Eu^{III} ion, facilitates the energy transfer from the ligand to Eu^{III} ion. These results are also supportive according to the Latva *et al.*, investigations (difference between ligand ($^3\pi\pi^*$) and the Eu excited state ($^5D_0$) should be > 2,500 cm^{-1}) [30]. In addition, singlet state should be located higher than >25,000 cm^{-1} and triplet state located higher than 20,000 cm^{-1}. These details are indicating that the efficient energy transfer occurs from the ligand triplet excited state to $^5D_0$ excited level of Eu^{III} ion. Finally, it reaches to the ground state as a radiative red emission ($^5D_0$-$^7F_2$). It Is also supported by Reinhoudt's empirical rule [31]. In addition, in this energy transfer mechanism TTA excited singlet and triplet state can act as a transitional state between the singlet to triplet excited states of the ligand and the triplet excited state to excited $^5D_0$ level of Eu^{III} ion, respectively. The results are suggesting that these moieties are potential components to achieve red emission with high luminescence efficiency.

The ligand, $Eu(TTA)_3$ and $Eu(TTA)_3$Phen-Fl-TPA under normal light and UV-lamp (365 nm), Figure 3.42. Ligand and Eu^{III} complex shows blue and red color, respectively. The Eu^{III} complex under UV-light in the form of thin film and solid phase are mentioned.

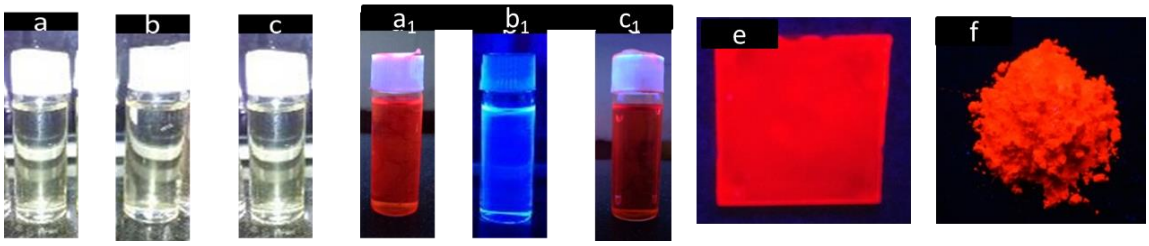

Figure 3.42 Under normal light (a) $Eu(TTA)_3$Phen-Fl-TPA (b) Phen-Fl-TPA (c) $Eu(TTA)_3$ and under UV (365 nm) lamp a_1, b_1, c_1 as well as thin film (e) and solid phase (f).

3.3.3.2.4 Photoluminescence quantum yield:

As mentioned in the previous chapter, by using equation 2.2 and 2.3, the quantum yield (φ) can be obtained. The absolute PLQY was measured in chloroform solution. The obtained PLQY is supporting the efficient energy transfer from ligand to center Eu^{III} metal ion. The PLQY of the $Eu(TTA)_3$Phen-Fl-TPA showed 34.1 % upon excitation at 358 nm. The encouraging results are due to the presence of chromophore (amines and fluorene) groups which directly involved for the sensitization process for the Eu^{III} ion in complex. Hui Xu *et al*., [47] experimental results are also suggesting that the introduction of chromophores can improve the PL properties of the complexes is cause steric effects and decrease intra molecular energy transfer efficiently. The gained QY is nearer to the $Eu(TTA)_3$Phen in DMF (36.5%) [48]. In addition, the obtained QY is higher than that of the related DBM coordinated Eu^{III} complexes [$Eu(DBM)_3LN$ (N = 1-3)] [49]. This result was matching with some of the TTA associated aryl phosphine oxide Eu^{III} complexes ([$Eu(TTA)_3(TMOADPO)_2$, $Eu(TTA)_3(EtCzDPO)_2$ and $Eu(TTA)_3(PhCzDPO)_2$) [50].

3.3.3.2.5 Lifetime and Jodd-Ofelt investigations:

Lifetime decay curve analysis of Eu^{III} complex and ligand is represented in the Figure 3.43. The measured data was fitted with the single exponential function given by the equation

$I(t) = I_0 + A_1 \exp\left(\frac{-t}{\tau}\right)$, where A_1 is the scalar quantity obtained from the curve fitting, $I_0 = 0$ is the offset value, t is the time in ms and τ is the decay time value for the exponential component. In order to better understand the luminescent properties of the Eu complex in the $CHCl_3$ solution and solid state, luminescence decay curves of the $^5D_0$ excited state were measured at 298 K by monitoring the most intense emission lines ($^5D_0 \rightarrow {}^7F_2$) of the Eu-ion center at 612 nm, and under 360 nm excitation. In addition, to further understand the solvent effect, the lifetime was investigated in various solvents (Acetone, DCM, DMF, THF) with different polarity. The exhibited mono exponential behavior of Eu^{III} complex is indicative of the presence of a single chemical environment around the europium ion. The luminescent lifetime values (τ) of $Eu(TTA)_3$Phen-Fl-TPA and respective ligand (Phen-Fl-TPA) were found to be 0.53 ms and 5.93 x 10^{-3} ms (in $CHCl_3$ solution), and 0.66 ms and 1.38 x 10^{-3} ms (in solid state), respectively. Lifetime of the Eu^{III} complex in solid was higher than that of $CHCl_3$ solution, which is due to reduce the non-radiative transitions in solid phase. The lifetime changes were observed in different solvents and shown decreased in the order of DMF (0.46) > THF (0.42) > DCM (0.38) > Acetone (0.37) (Table 3.15).

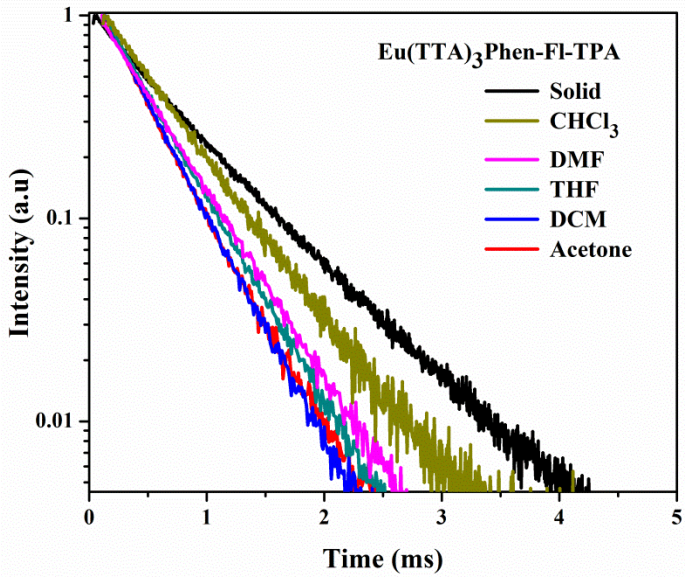

Figure 3.43 Decay curves of luminescence of $Eu(TTA)_3$Phen-Fl-TPA at 612 nm in $CHCl_3$ and Solid.

Table 3.15 Observed luminescence lifetimes τ_{obs} and intensity parameters of synthesized Eu^{III} complex and corresponding ligand.

S. No.	Compound	Intensity parameters (10^{-20} cm^2)		τ / ms [a]					
		Ω_2	Ω_4	Solid	$CHCl_3$	DMF	THF	DCM	Acetone
1	**$Eu(TTA)_3$Phen-Fl-TPA**	3.36	0.44	0.66	0.54	0.46	0.42	0.38	0.37
2	**Phen-Fl-TPA (10^{-3} ms)**	---.--	--.--	1.38	5.93	4.23	4.47	2.79	4.26

[a] The decay curves were found to be mono-exponential for the β-diketonate europium(III) complex and its ligand.

The interaction parameters of ligand fields are given by the Judd–Ofelt parameters Ω_λ (where λ = 2, 4 and 6). Among all transitions of Eu^{III} ion, the $^5D_0 \rightarrow {}^7F_{0,3,5}$ transitions are forbidden, both in magnetic and electric dipole systems ($S_{(ED)}$ and $S_{(MD)}$ = zero). From these intensity parameters, the Ω_2 ($^5D_0 \rightarrow {}^7F_2$) was found to be more sensitive to the symmetry and the hypersensitive ratio (R) reveal similar physical implication of the symmetric/asymmetric and covalent/ionic bonding environment between Eu^{III} ion and the surrounding ligand moiety [51, 52]. The intensity parameter Ω_4 ($^5D_0 \rightarrow {}^7F_2$) is less sensitive to the coordination sphere than Ω_2 and its value reflects the chemical environment rigidity surrounding the Eu^{III} ion. The $^5D_0$ to $^7F_1$ (J=1) transition is the isolated magnetic dipole transition and has no electric dipole involvement, which is practically independent of the ion's chemical environment and henceforward can be used as a reference for estimation of J–O intensity parameters. The experimental intensity parameters (Ω_2 and Ω_4) for typical Eu^{III} complex was determined from the emission spectra, based on the $^5D_0 \rightarrow {}^7F_2$ and $^5D_0 \rightarrow {}^7F_4$ electronic transitions (Table 3.15). The transition $^5D_0 \rightarrow {}^7F_6$ transition is not observed experimentally, thus the experimental Ω_6 parameter cannot be predictable. The details of the J-O parameter calculations have been mentioned in Chapter 2 (2.2.3.2.4).

3.3.3.3 Electrochemical Properties:

The redox properties of Eu^{III}-complex and ligand are considerable importance, since they give the foremost information about the HOMO and LUMO energy of the molecules/compounds. The ligand onset potential is 1.34 eV and the corresponding Eu^{III} complex onset potential is 1.25 eV, respectively (Figure 3.44). The details of reduction wave with onset potentials data's are listed in Table 3.16. The HOMO and LUMO energy levels were calculated by using equation 2.9 and 2.10. HOMO and LUMO energy levels of the Eu^{III} complex are -5.65 and -2.87 eV; ligand is -5.74 and -2.81 eV, respectively. The Eu^{III} complex demonstrated energy gap around 2.8 eV and ligand is around 2.9 eV. The ligand can be used as a host, owing to their HOMO-LUMO values which are almost similar to the host materials like CBP [53]. In addition, the energy gap of Eu^{III} complex is lesser than ligand.

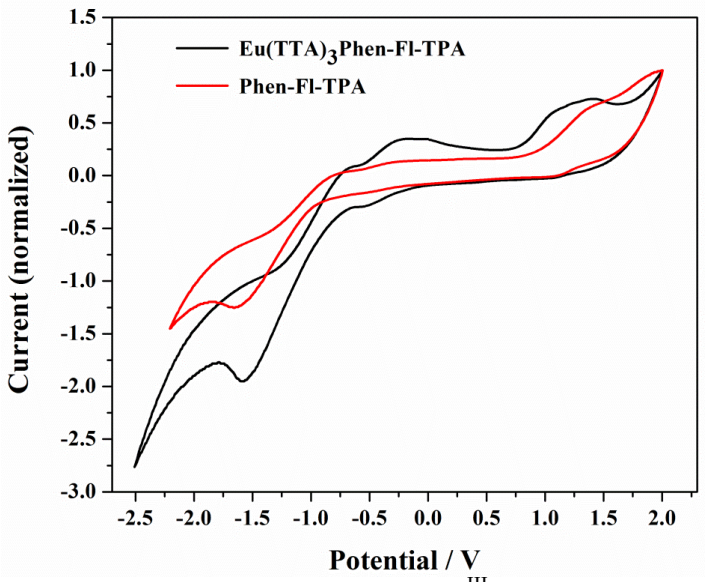

Figure 3.44 Cyclic voltammogram of Eu^{III} -complex and ligand.

The band gaps which are calculated from DRS spectra are almost matching with the cyclic voltammogram results. For ligand, the calculated HOMO – LUMO energy by DFT frame work using B3LYP/6-31G (d, p) level of theory were equivalent to CV analysis shown in Figure 3.45. However, the narrow energy gap of the Eu^{III} complex is a better sign further application. As far as we know, the LUMO and HOMO energy levels reported so for TTA and phenanthroline consisted Eu^{III} -complex ($Eu(TTA)_3Phen$) are positioned at -3.1 and -6.3 eV with respect to the vaccum level [53]. Compared with $Eu(TTA)_3Phen$, our complex showed increment in the E_{HOMO} value about 0.42 eV. This is one of the interesting results for TTA and Phen consisting Eu^{III} complexes. In addition, the energy gap of the europium complex is close to related TTA coordinated Eu complexes ($Eu(TTA)_3L$ (L=PyPhen, MPP, DPPz, MDPz and DDPz).

Table 3.16 Electrochemical properties of the Eu^{III} complex and ligand.

S. No.	Compound	$Voltage^{Oxi}_{onset}$ (V) (E_{HOMO} (eV))	$Voltage^{Red}_{onset}$ (V) (E_{LUMO} (eV))	λ_{onset}, (nm)	Energy gap E_g^{Opt}, (eV)[a]
1	$Eu(TTA)_3Phen$-Fl-TPA	1.25 (-5.65)	-1.53 (-2.87)	441	2.81 (2.78)
2	Phen-Fl-TPA	1.34 (-5.74)	-1.59 (-2.81)	421	2.94 (2.93)

[a]Calculated the onset wavelength of optical absorption (λ_{onset}) in solid-state film (DRS spectra). In bracket, mentioned their energy difference (HOMO and LUMO) value calculated by cyclic voltammogram.

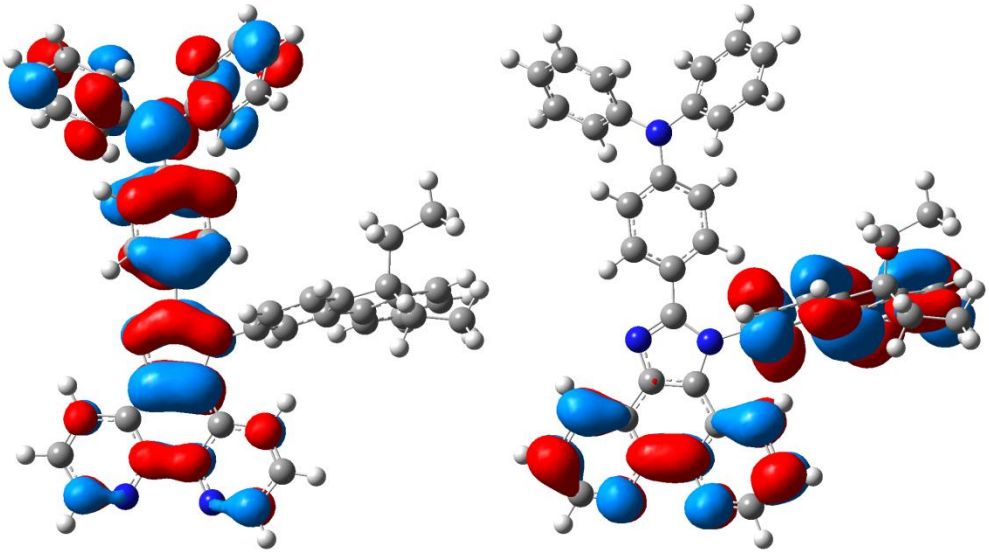

Figure 3.45 the calculated HOMO – LUMO (left – right) energy orbitals by density functional theory (DFT) frame work using B3LYP/6-31(G) level of theory of Phen-Fl-TPA.

3.3.3.4 CIE Chromaticity coordinates:

The Commission International de Eclairage (CIE) chromaticity coordinates were calculated in solution for both ligand and Eu^{III} complex from emission spectral data's (λ_{ex} = 358 nm). Figure 3.46 shows the calculated CIE color coordinates are x = 0.62 and y = 0.36 ($Eu(TTA)_3Phen$-Fl-TPA), x = 0.16 and y = 0.17 (Phen-Fl-TPA), x = 0.66 and y = 0.33 $Eu(TTA)_3$. The calculated CIE values for the solid samples are given in Figure 3.46 (right). Eu^{III} complex exhibited red color in the CIE gamut color space.

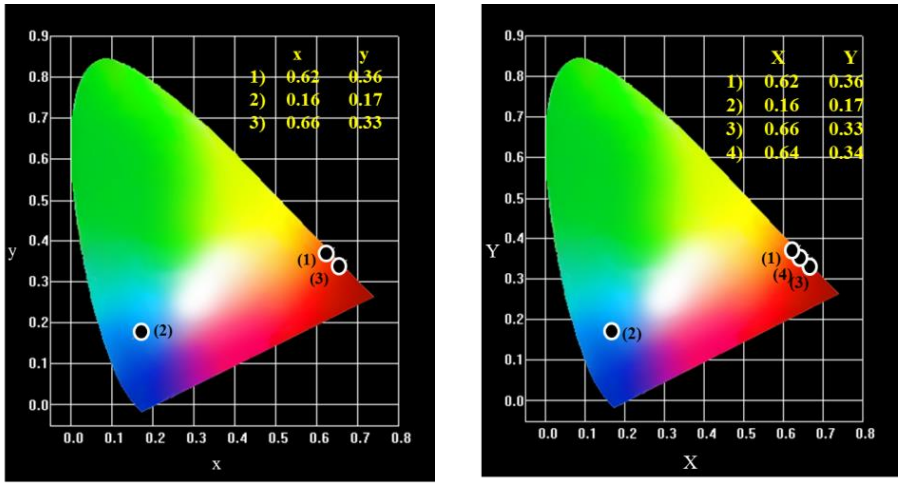

Figure 3.46 The CIE chromaticity coordinates for 1) $Eu(TTA)_3Phen$-Fl-TPA, 2) Phen-Fl-TPA and 3) $Eu(TTA)_3$ (left) solid samples CIE chromaticity coordinates (right).

3.4 Summary and Conclusion:

In conclusion, successful incorporation of Ph, mCF_3, pCF_3 and Fl moiety in phenanthroimidazole ligands were achieved and their efficient β-diketonate Eu^{III} complexes have been synthesized, spectroscopically characterized. The photophysical, electrochemical properties have been investigated, to know the effect of the substitution in the ligand. All the ligands and complexes show similar UV-Visible absorption behaviour (π - π*, at ~270, ~360 nm). DFT calculations were supportive of the experimental outcomes. Eu-complexes and its ligands PL study were carried out in solution form as well as in solid and thin film. The study indicates that the Eu-complex emits tunable emission due to incomplete/partial energy transfer (white (solution), red (solid)), whereas fluorene decorated Eu-complex shows narrow band red emission with appropriate CIE color gamut. The calculated asymmetric ratio (I_2/I_1) clearly indicates that the Eu^{III} ion located in the non-centro symmetric site or the local chemical environment is asymmetric in nature. The obtained PL emission clearly indicates that the efficient energy transfer encountered in case of fluorene based complex. The energy transfer mechanism for all the Eu-complexes was proposed based on combined experimental and theoretical study (DFT, TD-DFT). The PL lifetime of the Eu^{III} complexes also supports the emission behaviour. The calculated band gap of the complex by DRS and CV are almost similar. The Judd–Ofelt spectral intensity parameters, electrochemical study and absolute QY (mCF_3 based Eu-complex shows better QY of 75.9 %) of the Eu-complexes were also been investigated. White and red LED was fabricated using these complexes with near UV LEDs (395 nm). These promising properties are suggesting that the synthesized Eu^{III} molecular complex is potential red emitters for white LEDs and can be used a ratiometric temperature sensor.

3.5 References:

(1) J. Kido and Y. Okamato, *Chem. Rev*., 2002, **102**, 2357–2368.
(2) I. Hemmila and V. Laitala, *J. Fluoresc.,* 2005, **15**, 529.
(3) C. Adachi, M. A. Baldo and S. R. Forrest, *J. Appl. Phys.*, 2000, **87**, 8049.
(4) S. V. Eliseeva and J. C. G. Bunzli, *Chem. Soc. Rev.,* 2010, **39,** 189–227.
(5) C. Adachi, M. A. Baldo, M. E. Thompson and S.R. Forrest, *J. Appl. Phys*., 2001, **90,** 5048.
(6) J. Fang, H. You, J. Gao and D. Ma, *Chem. Phys. Lett.,* 2004, **392,** 11–16.
(7) H. Aziz, Z. D. Popovic, N. X. Hu, A. M. Hor, and G. Xu, *Science*, 1999, **283**, 1900.
(8) S. Comby and J. C. G. Bunzli, in Handbook on the Physics and Chemistry of Rare Earths, ed. J. C. G. Bunzli, K. A. Gschneidner Jr and V. K. Pecharsky, Elsevier, 2007, pp 217–470.
(9) Y. Zheng, F. Cardinali, N. Armaroli and G. Accorsi, *Eur. J. Inorg. Chem.* 2008, 2075–2080.
(10) J. F. Wang, R. Y. Wang, J. Yang, Z. P. Zheng, M. D. Carducci, T. Cayou, N. Peyghambarian and G. E. Jabbour, *J. Am. Chem. Soc.*, 2001, **123,** 6179–6180.
(11) H. Xu, K. Yin and W. Huang, *J. Phys. Chem., C* 2010, **114**, 1674–1683.
(12) N. M. Shavaleev, S. V. Eliseeva, R. Scopelliti and J. C. G. Bunzl, *Inorg. Chem.,* 2010, **49,** 3927–3936.
(13) M. Sun, H. Xin, K. Z. Wang, Y. A. Zhang, L. P. Jin and C. H. Huang, *Chem. Commun.*, 2003, 702–703.
(14) M. Guan, Z. Q. Bian, F. Y. Li, H. Xin and C. H. Huang, *New J. Chem.*, 2003, **27,** 1731–1734.
(15) H. J. Bolink, F. D. Angelis, E. Baranoff, C. Klein, S. Fantacci, E. Coronado, M. Sessolo, K. Kalyanasundaram, M. Gratzel and Md. K. Nazeeruddin, *Chem. Commun.*, 2009, 4672.
(16) (a) P. Coppo, M. Duati, V. N. Kozhevnikov, J. W. Hofstraat and L. De Cola, *Angew. Chem. Int. Ed.*, 2005, **44**, 1806; (b) D. Sykes, I. S. Tidmarsh, A. Barbieri, I. V. Sazanovich, J. A. Weinstein and M. D. Ward, *Inorg. Chem.*, 2011, **50**, 11323.
(17) (a) A. Kar, S. Kundu and A. Patra, *RSC Adv.*, 2012, **2**, 4879; (b) R. Wang, J. Peng, F. Qiu, Y. Yang and Z. Xie, *Chem. Commun*., 2009, 6723; (c) G. He, D. Guo, C. He, X. Zhang, X. Zhao and C. Duan, *Angew. Chem. Int. Ed.*, 2009, **48**, 6132.
(18) A. H. Shelton, I. V. Sazanovich, J. A. Weinstein and M. D. Ward, *Chem. Commun.*, 2012, **48**, 2749.
(19) J. Zhang, H. Li, P. Chen, W. Sun, T. Gao and P. Yan, *J. Mater. Chem. C*, 2015, **3**, 1799.
(20) (a) L. Ji, Q. Fang, M. Yuan, Z. Liu, Y. Shen and H. Chen, *Organic letters*, 2010, **12**, 5192; (b) Z. Ning, Z. Chen, Q. Zhang, Y. Yan, S. Qian, Y. Cao and H. Tian, *Adv. Funct. Mater*., 2007, **17**, 3799.
(21) B. Rajamouli, P. Sood, S. Giri, V. Krishnan and V. Sivakumar, *Eur. J. Inorg. Chem.,* 2016, **24**, 3900–3911.
(22) S. Ebraheem and A. El-Saied, *Materials Sciences and Applications,* 2013, **4,** 324–329.
(23) M. Dongol, *Egypt. J. Sol.* 2002, **25**, 33–47.
(24) A. V. Kharchevaa, A. V. Ivanovb, N. E. Borisovab, T. P. Kaminskayaa, S. V. Patsaeva, V. V. Popova and V. I. Yuzhakov, *Proc. of SPIE*, 2014, 9448.
(25) T. Li, W. Shang, F. Zhang, L. Mao, C. Tang, M. Song, C. Du and Y. Wu, *Engineering* 2011, **3,** 301–311.
(26) J. P. Martins, P. Martin-Ramos, C. Coya, M. Ramos Silva, M. E. S. Eusebio, A. D. Andres, A. L. Alvarez and J. Martin-Gil, *J. Lumin.,* 2015, **159,** 17–25.
(27) K. Binnemans, *Chem. Rev.,* 2009, **109**, 4283.

(28) L. D Carlos, R. A. S. Ferreira, V. Z. Bermudez, B. J. Lopez and P. Escribano, *Chem. Soc. Rev.,* 2011, **40,** 536,
(29) H. Xu, H. L. Wang, X. H. Zhu, K. Yin, G. Y. Zhong, X. Y. Hou and W. Huang, *J. Phys. Chem. B,* 2006, **110,** 3023–3029.
(30) M. Shi, F. Li, T. Yi, D. Zhang, H. Hu and C. Huang, *Inorg. Chem.,* 2005, **44,** 8929–8936.
(31) T. Li, W. Shang, F. Zhang, L. Mao, C. Tang, M. Song, C. Du and Y. Wu, *Engineering* 2011, **3,** 301–311.
(32) M. Latva, H. Takalo, V. M. Mukkala, C. Matachescu, J. C. Rodriguez-Ubis and J. Kankare, *J. Lumin.,* 1997, **75,** 149–169.
(33) F. J. Steemers, W. Verboom, D. N. Reinhoudt, E. B. V. Tol and J. W. Verhoeven, *J. Am. Chem. Soc.,* 1995, **117,** 9408–9414.
(34) C. L. Xiao, C. Z. Wang, L. Mei, X. R. Zhang, N. Wall, Y. L. Zhao, Z. F. Chai and W. Q. Shi, *Dalton Trans.,* 2015, **44,** 14376.
(35) N. V. D. Brande, G. V. Lier, F. D. Pieve, G. V. Assche, B. V. Mele, F. D. Proft, and P. Geerlings, *RSC Adv.,* 2014, **4,** 52658–52667.
(36) Y. Zheng, F. Cardinali, N. Armaroli and G. Accorsi, *Eur. J. Inorg. Chem.,* 2008, 2075–2080.
(37) M. R. Robinson, M. B. Regan and G. C. Bazan, *Chem. Commun.,* 2000, 1645–1646.
(38) Y. Zheng, J. Lin, Y. Liang, Q. Lin, Y. Yu, Q. Meng, Y. Zhou, S. Wang, H. Wang and H. Zhang, *J. Mater. Chem.,* 2001, **11,** 2615–2619.
(39) C. R. De Silva, R. Wang and Z. Zheng, *Polyhedron,* 2006, **25,** 3449–3455.
(40) J. Bao, H. Tian and R. Tang, *Inorg. Chim. Acta.,* 2013, **401,** 19–23.
(41) J. Ts. Zaharieva, M. M. Milanova, N. Vasilev, B. Morgenstern and D. S. Todorovsky, *Bulgarian Chemical Communications,* 2011, **43**, 558–562.
(42) Y. Liu , Y. Wang, J. He, Q. Mei, K. Chen, J. Cui, C. Li, M. Zhu, J. Peng, W. Zhu and Y. Cao, *Organic Electronics,* 2012, **13,** 1038–1043.
(43) H. Wang, P. He, H. Yan and M. Gong, *Sensors and Actuators B,* 2011, **156**, 6–11.
(44) L. Yingkui, *J. Lumin.,* 2012, **132**, 2102–2108.
(45) Y. Liu, Y. Wang, H. Guo, M. Zhu, C. Li, J. Peng, W. Zhu and Y. Cao, *J. Phys. Chem. C,* 2011, **115**, 4209–4216.
(46) D. F. Parra, A. Mucciolo, D. G. Duarte, H. F. Brito and A. B. Lugao, *J. Appl. Polym. Sci.,* 2006, **100**, 406–412.
(47) H. Xu, K. Yin and W. Huang, *Chem. Eur. J.,* 2007, **13**, 10281–10293.
(48) F. R. G. Silva, J. F. S. Menezes, G. B. Rocha, S. Alves, H. F. Brito, R. L. Longo and O. L. Malta, *J. Alloys Compd.,* 2000, **303–304**, 364–370.
(49) B. Zuqiang, G. Deqing, G. Min, X. Hao, L. Fuyou, H. Chunhui, W. Kezhi and J. Linpei, *Science in China Ser. B Chemistry*, 2004, **47,** 326–334.
(50) H. Xu, K. Yin and W. Huang, *J. Phys. Chem., C* 2010, **114**, 1674–1683.
(51) S. J. L. Ribeiro, R. E. O. Diniz, Y. Messaddeq, L. A. Nunes and M. A. Aegerter, *Chem. Phys. Lett.,* 1994, **220,** 214.
(52) H. Ahrens, M. Wollenhaupt, P. Froebel, L. Jun, K. Barner, G. S. Sun and R. Braunstein, *J. Lumin.,* 1999, **82,** 77.
(53) N. V. D. Brande, G. V. Lier, F. D. Pieve, G. V. Assche, B. V. Mele, F. D. Proft and P. Geerlings, *RSC Adv.,* 2014, 4, 52658–52667.

Chapter 4

Carbazole and fluorene functionalized phenanthro-imidazole ancillary ligand based Eu^{III} complexes for LEDs: detailed photophysical and theoretical study

Abstract

The efficient β-diketonate red emitting carbazole-based Eu^{III} complexes were synthesized and their photophysical, electrochemical properties were also been investigated. The PL study indicating that the efficient energy transfer from ligand to Eu^{III} metal ion (dominant pathway) with appropriate CIE color gamut and time-dependent density functional theory (TD-DFT) also confirms the identical. The Judd-Ofelt theory to the emissive properties of Eu^{III} complexes was investigated. The $Eu(TTA)_3$Phen-Fl-CBZ complex shown better lifetime was found to be 0.64 ms. The absolute PL quantum yield (QY) of the complexes in solid is found to be 77.3 % and it possesses high thermal decomposition temperature (235°C). The Judd-Ofelt intensity and related parameters were calculated for two complexes. The electrochemical analysis was shown narrow band gap energy (HOMO and LUMO). The PMMA film study of the complexes showed enhanced results than the solution. The fabricated Eu complexes with 395 nm emitted LED (InGaN) chips under 20 mA forward-bias current shown pure red emission and the corresponding CIE color coordinates are x = 0.66, y = 0.33. The obtained pure red emission is superior as compare to that of the solution and solid form of the complexes and the results are shown the presently investigated complexes find potential application in warm white LEDs.

Keywords: carbazole (CBZ); t-butyl CBZ; luminescence; energy transfer; warm white LED

4.1 Introduction:

The red emitting based europium (Eu) molecular complexes have gained ample attention for display technology and red, green and blue (RGB) utilities for lighting and smart display applications. The emergent global energy disaster and the novel utilities are demanding high energy efficient lighting systems which can reduce the energy consumption. Solid state lighting (SSL) based white LEDs are shown less energy consumption than the traditional lighting sources. However, warm white LEDs need a pure red component (full width at half maximum (FWHM) as small as possible to gain enhanced external output) in the white LED spectrum. To accomplish the same visible light (near UV to blue) excited red emitting Eu complexes as a red phosphor materials gained much attention [1-4]. It is well-known that the non-center of symmetry and highly distorted structure favors the electric dipole transition character of the Eu^{III} complex leads to sharp high intensive red emission. In addition europium, other lanthanides such as samarium (Sm) and praseodymium (Pr) also known to show orange-red emission arises from 4f - 4f electronic transition [5-9]. However, to get the pure red emission among the lanthanides; Eu metal ion with distorted local structure is applicable due to its outstanding properties like large Stokes shifts, long luminescence lifetime and its phosphorescent emission character [10, 11]. The efficient direct population of Eu^{III} ion excited states is not possible, since the oscillator strength of the absorption band is very weak and requires indirect population via antenna/ligand absorption that can populate the Eu excited state assorted by energy transfer [12, 13]. It leads to get up to 100% internal quantum efficiency [14].

The arylamine moieties or hetero cyclic compounds are attractive emissive resources towards to get the characteristic bright red emission with a less full width half maximum and also same is expected to improve the hole injection/transporting properties of the emissive materials in the light emitting device [15, 16]. It is well documented that the carbazole (CBZ, hole), phenanthroline (Phen, electron) are best transporting moieties and dibenzoylmethane (DBM) as an antenna. The inclusion of these moieties in the ligand structure (imidazole, oxadiazole, triazole and phospheneoxide as a core), different LED's and OLED's were constructed to produce the high efficient bright red emission with high quantum efficiency [17-21]. Even though obtained outcome results of devices were not satisfactory to achieve the desired efficiency. The good carrier transporting properties (less mobility of electrons than holes) of these complexes was one of the major reasons to get promising results. However, still focused research is necessary in the proactive design of Ln complex, in order to improve the charge balance leads to improve the quantum efficiency as well as the color purity of the device. In addition, it is also essential to understand that the energy transfer process between ligand triplet ($^3\pi\pi^*$) to $^5D_0$ level of Eu^{III} metal ion to achieve the pure bright red emission.

4.2 Carbazole and fluorene functionalized phenanthro-imidazole ancillary ligand based Eu^{III} complexes for LEDs:

4.2.1 Outline of the present study:

It is well accepted that the inclusion of charge transporting moieties in the emissive materials will certainly improve the overall quantum yield and device performance of the OLEDs. In addition, incorporation or functionalization of multi chromophoric group in the back bone of the emissive complexes will increase the absorptions strength as well as extend the absorption edge towards near UV to blue region, where the LED emission occurs. In the

previous chapter, using phenyl (Ph), triphenylamine (TPA) decorated phenanthro-imadazole ligands can lead to efficient Eu complexes [22, 23]. The further increment of the internal quantum efficiency of the bipolar ligand is highly necessary to obtain highly efficient Eu complexes. In this study, we have used CBZ as a functional moiety to enhance the luminescence efficiency as well as the charge transporting properties in the device. In the current study, CBZ and Phen based consequences were made by using 2-thenoyltrifluoroacetone (TTA) as an antenna named were $Eu(TTA)_3$Phen-Fl-CBZ (1Eu) and $Eu(TTA)_3$Phen-Fl-CBZ-t-But (2Eu) with novel bipolar ligands Phen-Fl-CBZ (2-(4-(9H-carbazol-9-yl)phenyl)-1-(9,9-diethyl-9H-fluoren-2-yl)-1H-imidazo[4,5-f][1,10]phenanthroline, 1L) and Phen-Fl-CBZ-t-But (2-(4-(3,6-di-tert-butyl-9H-carbazol-9-yl)phenyl)-1-(9,9-diethyl-9H-fluoren-2-yl)-1H-imidazo[4,5f][1,10] phenanthroline, 2L). The inclusion of the bulky t-butyl groups expecting to reduce self-quenching and phase separation in the device, it leads to the longer lifetime operations [24, 25].

TTA acts as efficient energy transfer to Eu^{III} central metal ion and it may increase the decay time by decrease the vibrational quenching. It is very much anticipated that the designed ligand can act as a dual characteristic, that bipolar nature and antenna for the presently designed Eu^{III} complexes (Figure 4.1). The ancillary ligand was optimized by using theoretical model (DFT calculation). The energy level location (singlet and triplet levels) also been calculated by using TD-DFT, which is used to analyze the energy transfer process from ligand to Eu^{III} metal ion in the complexes. In order to show the potentiality of the currently synthesized complexes, efforts have been made to fabricate red LED conjugated with commercially available near-UV LEDs. The characteristic sharp red emitting Eu^{III} complexes were obtained from the fabricated LEDs (complex conjugated with UV-Visible InGaN LED chip (395 nm)). The corresponding CIE (Commission International de Eclairage) color coordinates were calculated, which are well matched with National Television Standard Committee (NTSC) standards.

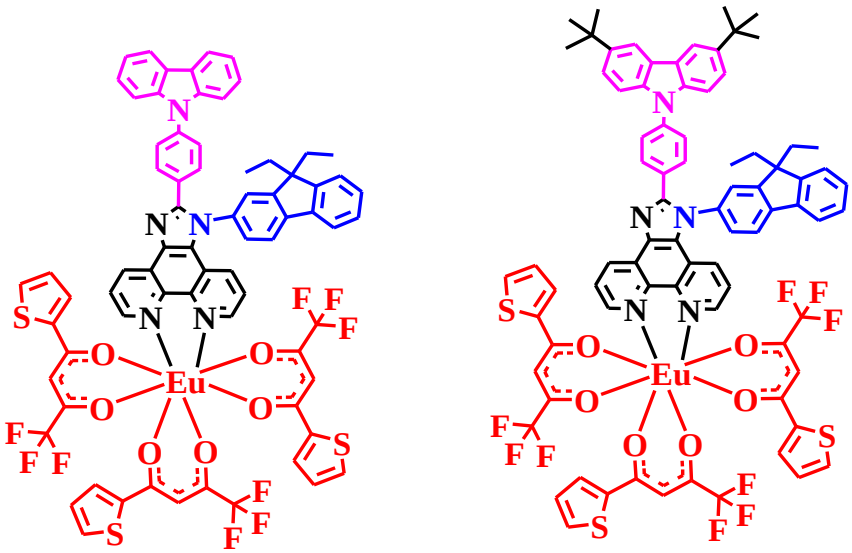

$Eu(TTA)_3$Phen-Fl-CBZ (1Eu) **$Eu(TTA)_3$Phen-Fl-t-but CBZ (2Eu)**

Figure 4.1 Chemical structures of bipolar ligands connected Eu^{III} complexes.

4.2.1 Experimental:

4.2.1.1 General Information for synthesis:

The details of starting materials for the synthesis and electrolyte materials used in the CV were included in Chapter 2. (Experimental section). Carbazole (CBZ) was purchased from the Sigma-Aldrich.

4.2.1.2 Measurements:

The detailed characterization techniques that are used for the characterization of ligands and respective complexes were mentioned in Chapter 2. (Experimental section).

4.2.1.3 Preparation of PMMA thin film with complexes:

The Eu^{III} complex was doped with PMMA in 0.1, 0.5 and 1% ratio (PMMA : Eu^{III} = 99.99 : 0.1, 99.95 : 0.5, 99 : 1 in mg) by using chloroform solution with spin coated by two stages were at 500 (20 sec) and 2000 rpm (30 sec), respectively. The prepared thin films were kept under vacuum at 50 °C for 3hrs to get excess solvent evaporation.

4.2.1.4 Synthesis:

The compounds 9,9-diethyl-9H-fluoren-2-amine (1-3), 1,10-phenanthroline-5,6-dione (2-1) and tris(thenoyltrifluoroacetone)europium(III) ($Eu(TTA)_3 \cdot 2H_2O$) were synthesized according to previous reported procedures [22]. 3,6-di-tert-butyl-9H-carbazole synthesized by well-known friedel craft alkylation method [28].

4.2.1.4.1 *Synthesis of 4-(9H-carbazol-9-yl)benzaldehyde (CBZ-Ph-CHO (3-2))*:

In a 250 mL round bottom flask, carbazole (8 gm, 47.84 mmol), potassium carbonate (13.2 gm, 95.68 mmol) copper (0.30 gm, 4.78 mmol) 18 – crown – 6 (0.18 gm, 1.43 mmol) and 4-bromo benzaldehyde (10.6 gm, 57.41 mmol) were refluxed in 1,2-dichlorobenzene (50 mL) for 48 hrs, under nitrogen atmosphere at 170 °C. The inorganic components were filter off while hot and then the solvent was evaporated. The crude product was purified by column chromatography on silica (EtOAc: pet ether = 1:9, v/v, Rf-6) to afford the product as yellow powder with 11 gm (yield: 85.2 %). ^{1}H-NMR Data (DMSO-d_6, 400 MHz): δ 10.13 (s, 1H), 8.28 (d, 2H), 8.21 (dd, 2H), 7.92 (d, 2H), 7.53 (d, 2H), 7.47 (t, 2H), 7.35 (t, 2H).

4.2.1.4.2 Synthesis of *4-(3,6-di-tert-butyl-9H-carbazol-9-yl)benzaldehyde (t-but CBZ-Ph-CHO (3-3))*:

The similar reaction procedure was adopted as above CBZ-Ph-CHO. The product as pale brown powder with 65.5% yield. ^{1}H-NMR Data ($CDCl_3$, 400 MHz): δ 10.11 (s, 1H), 8.15-8.11 (m, 4H), 7.80 (d, 2H), 7.52-7.46 (m, 4H), 1.487 (s, 18H). ^{13}C NMR data (100 MHz, $CDCl_3$): δ 191.0, 143.9, 138.3, 134.1, 131.3, 126.2, 124.0, 123.9, 116.4, 109.3, 34.7, 31.9.

4.2.1.4.3 *Synthesis of 2-(4-(9H-carbazol-9-yl)phenyl)-1-(9,9-diethyl-9H-fluoren-2-yl)-1H-imidazo[4,5-f][1,10]phenanthroline (Phen-Fl-CBZ, 1L (4))*:

1-3 (0.124 g, 0.523 mmol) was added to a stirred solution of 3-2 (0.128 g, 0.476 mmol) in glacial acetic acid (10 mL) at room temperature. To this reaction mixture subsequently ammonium acetate (0.366 g, 4.762 mmol) and 2-1 (0.100 g, 0.476 mmol) were added. Then resulting mixture was stirred for 12 hrs at 110 °C. The progress of the reaction was monitored by TLC (MeOH in Chloroform 1:9, Rf-0.25). The RM was poured into the minimum amount of water and then ammonium hydroxide solution was added. Then the formed solid was filtered and dissolved in dichloromethane, followed by dried with anhydrous sodium sulphate and the solvent was evaporated to get 0.20 g crude compound. The resultant crude compound was purified with column chromatography by using silica gel (100-200 mesh), eluent with 2% methanol in chloroform and the solvent was evaporated and dissolved in minimum amount of THF solution added an excess of hexane, the pale brown color solid was formed. After settling the solid decanted and repeated this process three more times to obtain compound-4 (Phen-Fl-TPA) 260 mg (53.3%) as a pale brown color solid. ^{1}H-NMR Data (400 MHz, $CDCl_3$): δ 9.24-9.19 (m, 2H), 9.07 (dd, 1H), 8.10 (d, 2H), 8.02 (d, 1H), 7.94 (dd, 2H), 7.87 (dd, 1H), 7.80 (dd, 2H), 7.66-7.62 (m, 2H), 7.57-7.52 (m, 3H), 7.47-7.47-7.40 (m, 3H), 7.37-7.36 (m, 4H), 7.34-7.26 (m, 4H), 2.15-2.05 (m, 4H), 0.45 (t, 3H), 0.32 (t, 3H). ^{13}C NMR data (100 MHz, $CDCl_3$): δ 150.1, 149.1, 148.1, 145.0, 144.4, 143.9, 140.4, 139.8, 138.6, 136.3, 136.2, 130.7, 130.5, 128.8, 128.6, 128.1, 127.5, 127.3, 126.6, 126.0, 124.0, 123.6, 123.5, 123.2, 123.1, 122.0, 121.5, 120.5, 120.3, 120.2, 120.2, 119.9, 109.6, 56.8, 32.9, 32.6, 8.48, 8.41. EI-MS: m/z exp (calc). 681.83, m/z found 682.29 $[M + H]^+$.

4.2.1.4.4 *Synthesis of (2-(4-(3,6-di-tert-butyl-9H-carbazol-9-yl)phenyl)-1-(9,9-diethyl-9H-fluoren-2-yl)-1H-imidazo[4,5-f][1,10] phenanthroline) (Phen-Fl-t-but CBZ, 2L (5))*:

Reaction procedure was adopted for synthesis of Phen-Fl-CBZ. ^{1}H-NMR Data (400 MHz, $CDCl_3$): δ 9.24-9.21 (m, 2H), 9.07 (d, 1H), 8.11 (d, 2H), 8.03 (d, 1H), 7.93-7.90 (m, 3H), 7.83-7.80 (m, 1H), 7.67-7.62 (m, 4H), 7.58 (d, 2H), 7.53-7.40 (m, 5H), 7.32-7.25 (m, 2H), 2.10-2.08 (m, 4H), 1.45 (s, 18H), 0.45 (t, 3H), 0.34 (t, 3H). ^{13}C NMR data (100 MHz, $CDCl_3$): δ 162.7, 152.4, 151.3, 150.3, 149.0, 148.1, 144.5, 143.5, 140.2, 138.4, 136.7, 135.6, 131.3, 130.1, 128.8, 128.2, 127.6, 127.3, 126.1, 124.2, 123.8, 123.5, 122.7, 122.2, 121.3, 119.9, 117.2, 109.3, 56.8, 36.2, 35.2, 34.9, 32.2, 8.76, 8.63. EI-MS: m/z exp (calc). 794.04, m/z found 794.46 $[M + H]^+$.

4.2.1.4.5 *Synthesis of $Eu(TTA)_3$Phen-Fl-CBZ (1Eu)*:

Taken a 50 mL two neck round bottom flask with nitrogen containing balloon contained adaptor and poured $Eu(TTA)_3.2H_2O$ (250 mg, 0.293 mmol, 1eq) dissolved in dry tetrahydrofuran (THF) (5 mL). The compound Phen-Fl-CBZ (200 mg, 0.293 mmol, 1eq) dissolved in THF (10 mL) and added to stirred solution of the reaction mixture (RM) then stirred for 12 hrs at room temperature. The resulting mixture was concentrated and dissolved in minimum amount of THF and added an excess of hexane to get a solid product. After settled of solid, decant and repeated it another two times and dried to get pale yellow color solid with 269 mg (60.1%). EI-MS: m/z exp (calc). 1497.32, m/z found 1499.14 $[M + H]^+$. Elemental analysis: Anal. Calc. for.

$C_{72}H_{47}EuF_9N_5O_6S_3$; C, 57.75; H, 3.16; N, 4.68; S, 6.42, Found: C, 57.79; H, 3.20; N, 4.62; S, 6.39 %.

4.2.1.4.6 Synthesis of Eu(TTA)$_3$Phen-Fl-t-but CBZ (2Eu):

Reaction procedure was adopted for the synthesis of Eu(TTA)$_3$Phen-Fl-CBZ. EI-MS: m/z exp (calc). 1609.53, m/z found 1627.97 $[M + H_2O]^+$. Elemental analysis: Anal. Calc. for. $C_{80}H_{63}EuF_9N_5O_6S_3$; C, 59.70; H, 3.95; N, 4.35; S, 5.98, Found: C, 59.74; H, 3.99; N, 4.36; S, 5.97 %.

4.2.2 Results and Discussion:

4.2.2.1 Characterization of the complex:

The process of Eu^{III} complexes synthesis was precise in Scheme 4.1 The compound was characterized by nuclear magnetic resonance spectroscopy (^1H and ^{13}C NMR) (Figure 4.S1- 4. S6), Mass spectrometry (LC-MS) (Figure 4.S7-4.S8), Fourier transform infrared spectroscopy (FT-IR) and elemental analysis and all the measurements were done at room temperature (RT).

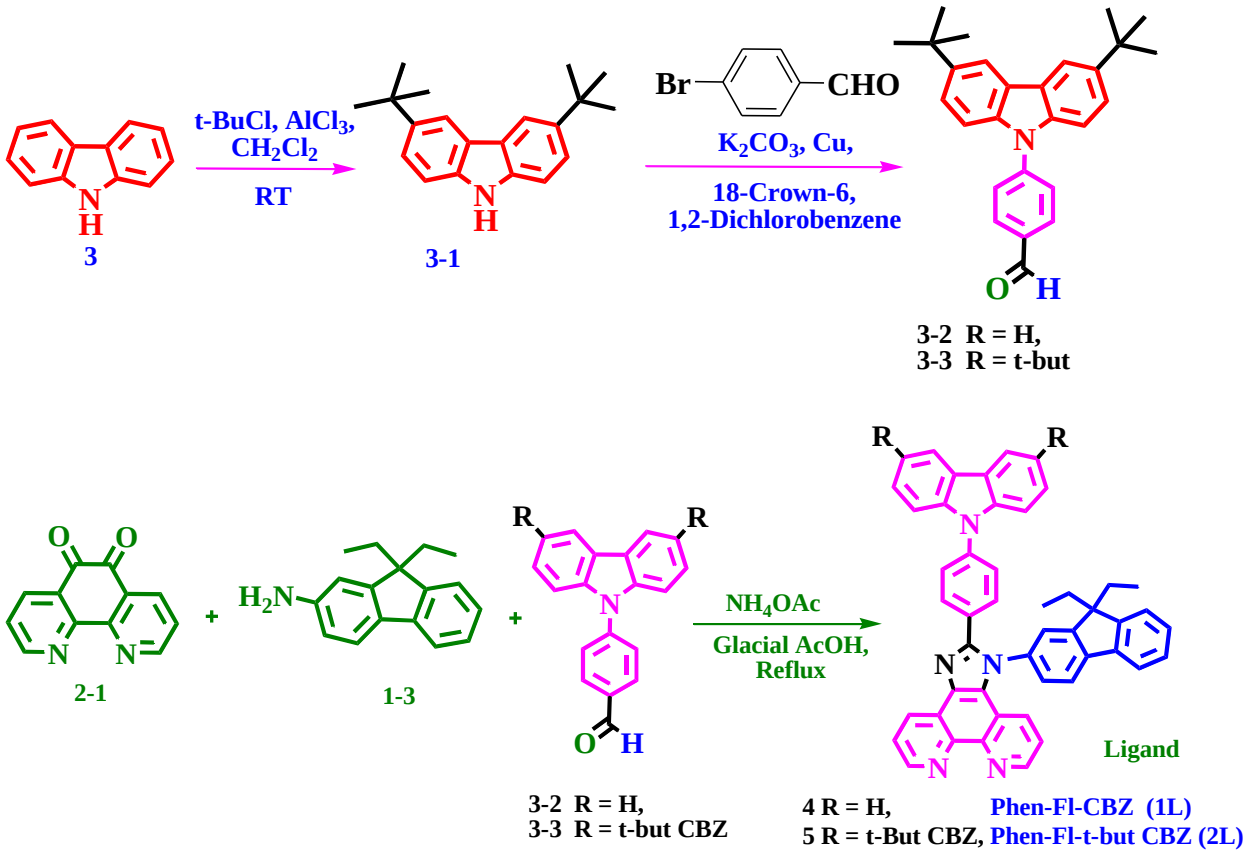

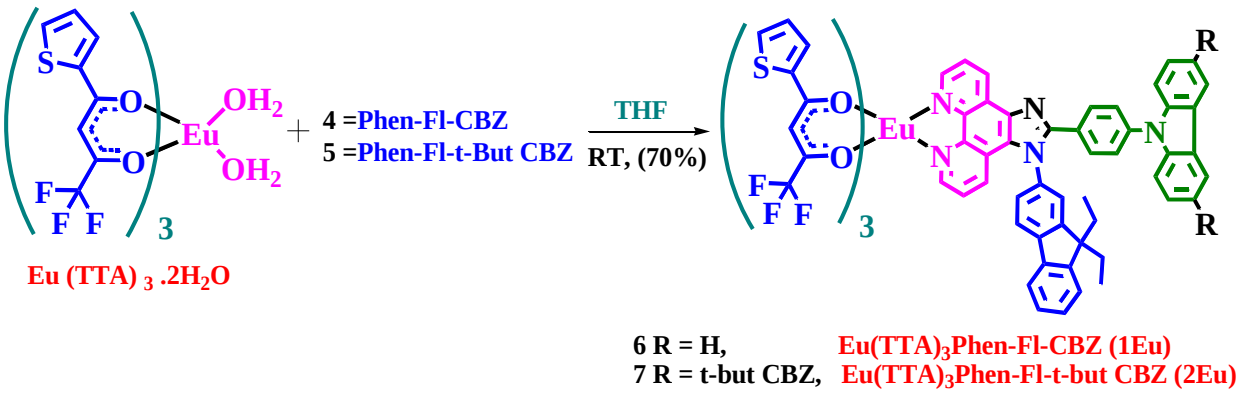

Scheme 4.1 Synthetic route of carbazole functionalized ligands and their corresponding β-diketonate Eu^{III} ternary complexes.

4.2.2.2 FT-Infrared spectroscopy:

The FT-IR spectrum of ligand and its corresponding Eu^{III} complexes were measured in the range of 500 - 4000 cm^{-1} (Figure 4.2). The observed strong carbonyl (C=O) stretching frequency at 1611 cm^{-1} for the $Eu(TTA)_3.2H_2O$ complex is shifted further to 1599 and 1598 cm^{-1} for the 1Eu and 2Eu complexes, respectively.

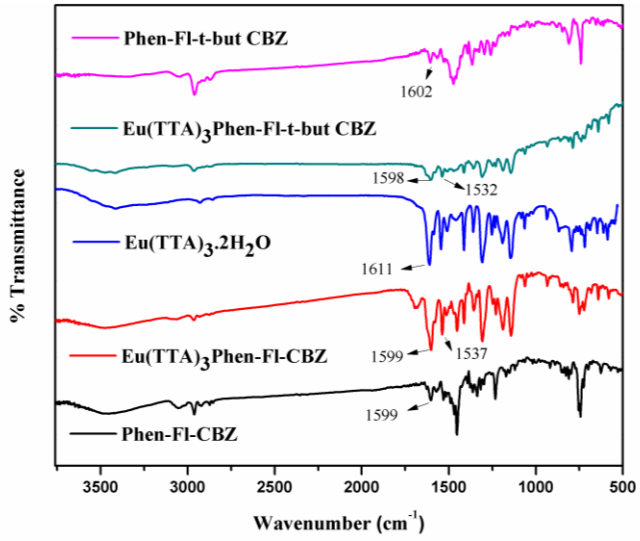

Figure 4.2 FT-IR spectra of the ligands and their corresponding Eu^{III} complexes.

The change obtained from FT-IR spectra are the concluding evidence that the β-diketonate ($Eu(TTA)_3.2H_2O$) compound coordinated with the neutral ligand. The results that the C=N bond is converted into a structure of C=N–Eu-O bond. The vibration frequency due to C=N appears at 1599 and 1602 cm^{-1} for the Phen-Fl-CBZ and Phen-Fl-t-but CBZ were shifted to 1537 and 1532 cm^{-1} for the ligand coordinated Eu^{III} complex, respectively. These outcomes are signifying that the N atom in the ligand also coordinates with $Eu(TTA)_3$. The other stretching vibrational frequencies were also suggesting the same and tabulated in Table 4.1.

Table 4.1 The major infrared frequencies (wavenumber in cm^{-1}) at room temperature for free ligands, corresponding Eu^{III} complexes, and $Eu(TTA)_3.2H_2O$.

S. No.	Compound	ν (C=O)	ν (C=N)	ν (C-N)	ν (C-F)	ν(C-CF_3)	ν (C-H) (phen)
		(Wavenumber in cm^{-1})					
1.	**$Eu(TTA)_3$Phen-Fl-CBZ**	1599	1537	1229	1306	1141	751
2.	**$Eu(TTA)_3$Phen-Fl-t-but CBZ**	1598	1532	1246	1308	1142	811, 738
3.	**Phen-Fl-CBZ**	--.--	1599	1232	--.--	--.--	743
4.	**Phen-Fl-t-but CBZ**	--.--	1602	1256	--.--	--.--	809, 741
5.	**$Eu(TTA)_3.2H_2O$**	1609	--.--	--.--	1296	1133	--.--

4.2.2.3 Thermal Properties and PXRD analysis:

The DSC-TGA of europium complexes and the bipolar ligands were measured under a nitrogen atmosphere at the range of ambient temperature to 800°C (Figure 4.3). The TG analyses showed that the gradual thermal decomposition occurs for ligands and its Eu^{III} complexes are due to the presence of ternary molecules. The ligands 1L and 2L showed major thermal decomposition at 440 and 410 °C, respectively. Thermal decomposition of $Eu(TTA)_3$Phen-Fl-CBZ complex shown in three stage thermal degradation is 253, 308 and 435. However, $Eu(TTA)_3$Phen-Fl-t-but CBZ shown different than foremost Eu^{III} complex was 235, 262, 326, and 457 °C. It was expected due to the presence of t-butyl groups on carbazole and their 10% weight loss are shown around at 265, 235 °C for Eu^{III} complexes, respectively.

The ligand high thermal stability is due to presence of percentage (%) of the carbon bonds are more and additionally, C-C bond is stronger. Gradual decreasing of the decomposition/weight loss of Eu^{III} complexes below 200 °C is attributed to the elimination of the coordinated water and solvent molecules. However, the Eu^{III} complexes consisted metal (Eu) ligand coordination bonds (3 moiety's of TTA and 1 moiety of Phen-Fl-CBZ/Phen-Fl-t-but CBZ) and leads to first major decomposition at 235-268 °C with maxima at ~253 °C (8.19 %) ($Eu(TTA)_3$Phen-Fl-CBZ) and 247-272 °C with maxima at ~260 °C (19.94 %) ($Eu(TTA)_3$Phen-Fl-t-but CBZ), respectively; which is attributed to the elimination of the TTA molecules from the Eu-complex. Similarly the immediate decomposition also belongs to the same and observed at 282-346 °C with maxima at ~308 °C ($Eu(TTA)_3$Phen-Fl-CBZ) and 290-357 °C with maxima at ~323 °C ($Eu(TTA)_3$Phen-Fl-t-but CBZ), respectively. It indicates that the TTA decomposition happens in the range of 235 to >350 °C. The similar results were observed from the reported literature [29, 30].

The final decomposition in the range of 378-476 °C with maxima at ~435 °C ($Eu(TTA)_3$Phen-Fl-CBZ) and 392-503 °C with maxima at ~441 °C ($Eu(TTA)_3$Phen-Fl-CBZ), respectively; which is attributed to the elimination or decomposition of ligand fragments such as CBZ/t-but CBZ, Phenanthroline and fluorene groups in the Eu^{III} complex [31, 32]. These results are suggesting that the Eu complexes have less thermal decomposition. However, all the Eu^{III} complexes are shown thermal decomposition above 235°C, which is good for further analysis.

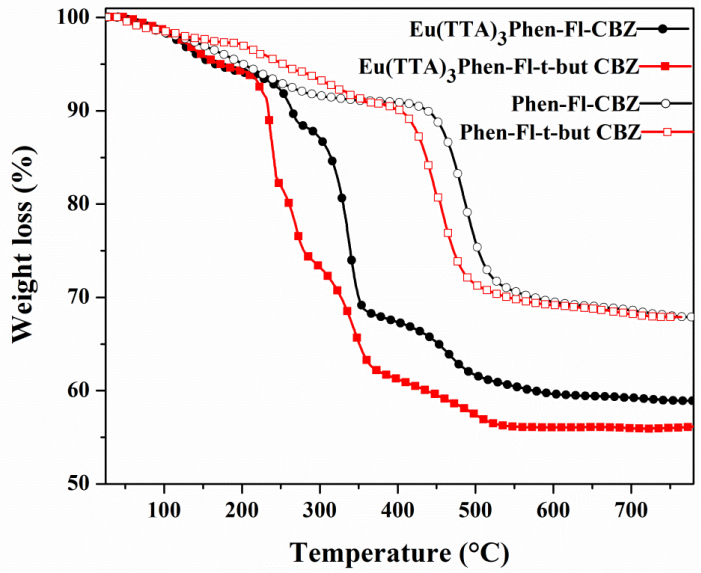

Figure 4.3 TG analysis curves for the ligands and Eu^{III} complexes.

The DSC curve showed specific heat or glass transition temperature of the ligands is 387 and 367 °C, respectively. The corresponding Eu^{III} complexes showed glass transition temperature at 283 and 262 °C, respectively (Figure 4.4, left). These DSC-TG results are suggesting that the Eu complexes have a good thermal decomposition (> 235 °C) with high glass transition temperatures, which is good for device fabrication. The T_g of the europium complexes were observed almost where the peak maxima to minima of the decomposition occurs in TGA curve (temp range 235-275 °C). The complexes are expected to change phase in the above mentioned temperature range. Thus, it might be reflecting in the DSC curves (highlighted in the DSC) and T_g peaks of the complexes are almost observed at decomposition point of the europium complexes. In the DSC, the hump was observed before the T_g peaks, which was negligible effect in the DSC. It might be expected due to elimination of the coordinated water and solvent molecules and TGA curves were also reflecting the same scenario.

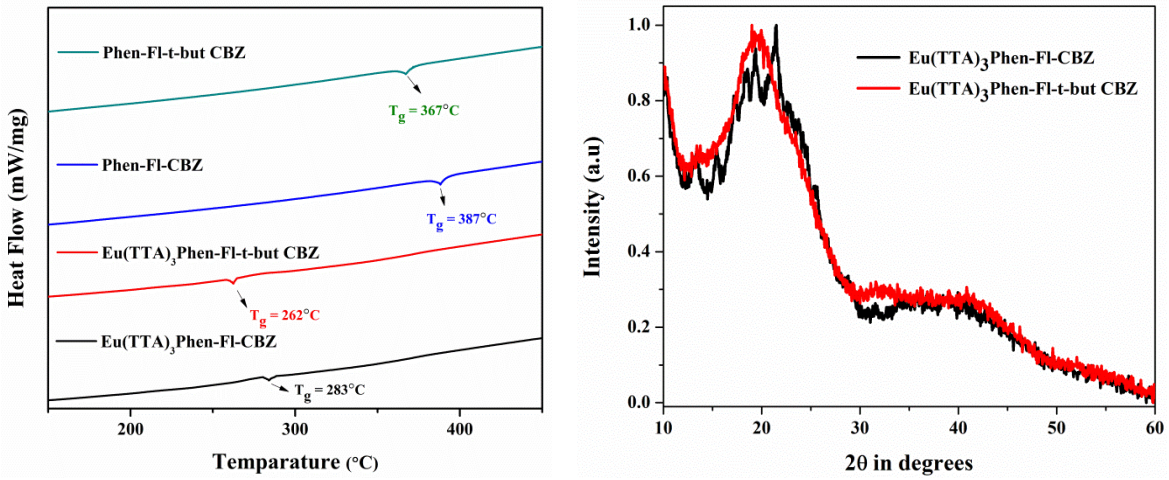

Figure 4.4 DSC analysis curves for the ligands and corresponding Eu^{III} complexes (left). The PXRD of the Eu^{III} complexes (right).

The powder x-ray diffraction (PXRD) analysis of the complexes was studied to understand the nature of the complexes as well as ligands to carry forward to further application. The both Eu^{III} complexes were shown amorphous nature and the same is shown in pictorial view in Figure 4.4, right. In addition, PXRD of the ligands are also measured and shown in Figure 4.S9. The ligand, Phen-Fl-CBZ was shown crystalline nature compare to that of rest of the ligand. It is also compared with already reported crystal data of the ligand, Phen-Fl-TPA (Figure 4.S9, left). A similar type of peaks with different intensity as well as slight shifting was observed. It might be expected that the presence of CBZ instead of TPA in the presently studied ligand. It is also noted that the interplanar distances (d) of Eu^{III} complexes are shifted to a lower value as compared to that of respective ligands.

4.2.2.4 Photophysical properties:

4.2.2.4.1 UV-Visible absorption and DRS studies:

The UV-visible absorption spectra of synthesized ligands, its Eu-complexes and $Eu(TTA)_3$ were carried out in solution (chloroform solution conc. 1.0×10^{-4} mol L^{-1}), and in the solid state (Figure 4.5). The UV-Visible absorption study of ligands shows absorption from 250 to 400 nm with λ_{max} 341, 280, 246 nm, these bands are due to $\pi \rightarrow \pi^*$ transitions of the ligands (TTA, L). The Eu^{III} complexes were shown similar peaks of the ligand as well as $Eu(TTA)_3$. The UV-visible reflectance spectra of the solid sample of ligands and corresponding Eu^{III} complexes are shown in Figure 4.5 right.

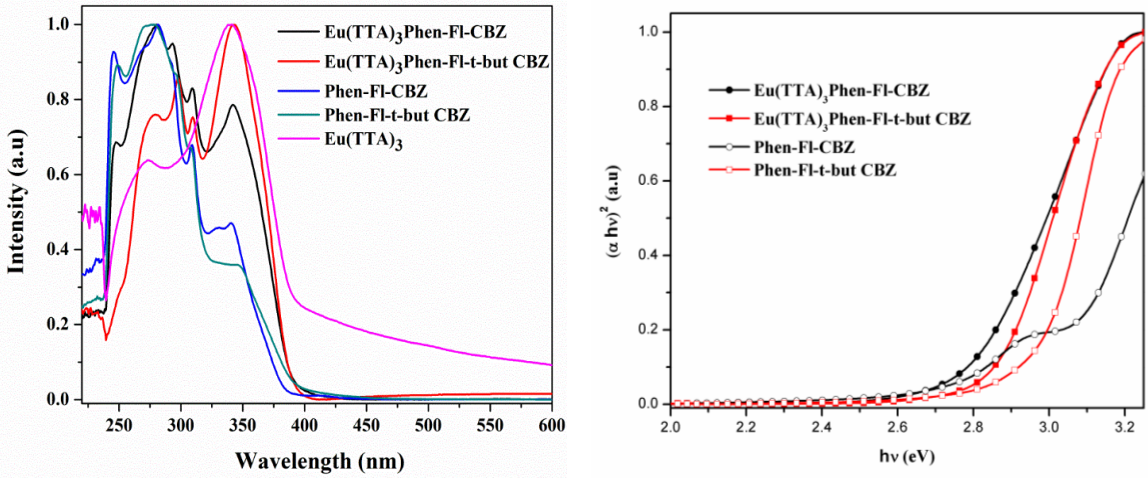

Figure 4.5 The UV-Vis absorption spectra of ligands and respective Eu^{III} complexes in chloroform solution (left), The diffuse reflectance spectra of the solid sample of ligands and corresponding Eu^{III} complexes (right).

4.2.2.4.2 Photoluminescence studies:

The photoluminescence (PL) emission spectra of ligands and their respective complexes were studied in solution (chloroform) as well as solid. The ligands 1L and 2L were excited with 365 nm to achieve the blue emission at 410 and 413 in solution; 449 and 463 in solid (Figure 4.6). Ligands in the solution shown vary with ligands in solid, which is shifted towards higher

wavelength. This was due to the aggregation. The corresponding $Eu(TTA)_3$Phen-Fl-CBZ and $Eu(TTA)_3$Phen-Fl-t-but CBZ complexes were excited with different wavelengths (365, 405 and 365, 410 nm) shown in Figure 4.7. Eu-complexes exhibit $^5D_0$-^7F_J (J=0 -4) transitions of the Eu^{III} ion. Both the Eu-complexes were shown intensive characteristic red emission at 612 nm. It is due to the intra-configurational $^5D_0$ -^7F_J (J = 0 - 4) electronic transitions.

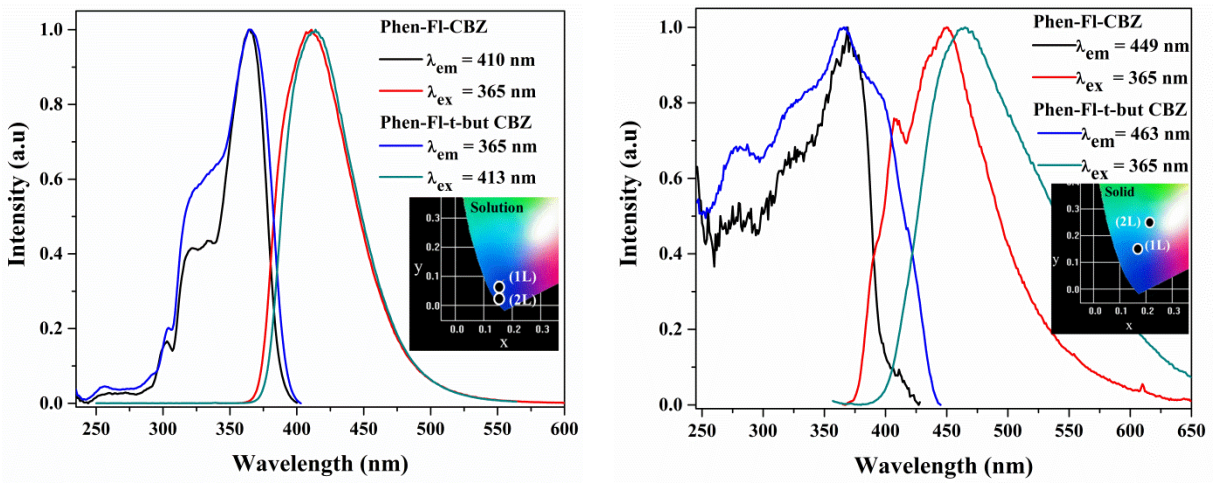

Figure 4.6 Excitation and emission spectra of the ligands in solution (left) and solid (right).

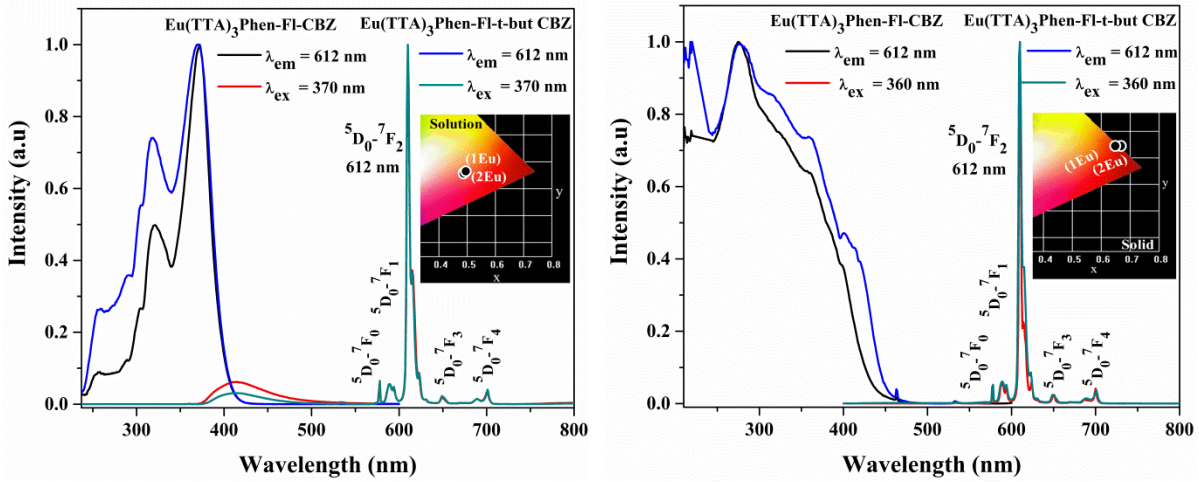

Figure 4.7 The PL excitation and emission spectra of Eu^{III} complexes $Eu(TTA)_3$Phen-Fl-CBZ, $Eu(TTA)_3$Phen-Fl-t-but CBZ in solution (left) and solid (right).

It was observed that the minor emission in the blue region and which belongs to the ligand. However, dominated red emission was observed from the solid emission of the Eu^{III} complexes (ligand emission completely disappears). When the ligand emission wavelength is used to excite the Eu^{III} complex, the emission appears with different wavelengths were at 580, 592, 612, 652 and 703 nm, due to 4f - 4f electronic transitions of Eu^{III} ion ($^5D_0$-$^7F_0$, $^5D_0$-$^7F_1$, $^5D_0$-$^7F_2$, $^5D_0$-$^7F_3$ and $^5D_0$-$^7F_4$). It is clearly indicating that the energy transfer occurs from the ligand to Eu central metal ion in the complex. The emission peak at ~580 nm observed due to $^5D_0$-$^7F_0$ transition. The emission peaks at around 580 and 652 nm are weak and these were attributed to

$^5D_0$-$^7F_0$, $^5D_0$-$^7F_3$ transitions are forbidden both in magnetic and electric dipole systems. The magnetic dipole (MD, strong emission) transition ($^5D_0$-$^7F_1$) indicates that the Eu ion occupies the center of symmetric site and it is independent of the coordinate environment. The intense induced electric dipole transition observed at 612 nm was sensitive to the local chemical environment of Eu ion. The absorption and emission peaks in solution and solid were retained in Table 4.2.

The synthesized europium complexes were shown red emission under UV-light (365 nm) and their corresponding ligands were shown blue emission at the same wavelength. The pictorial view (digital photographs) of the emissions was shown in Figure 4.8. The site symmetry or asymmetric ratio of Eu^{III} ion was calculated from the ratio of the $^5D_0$-$^7F_2$ transition to $^5D_0$-$^7F_1$ transition (I_2/I_1) emission intensity. The intensity ratio of the 1Eu and 2Eu complexes shown in solution was 18.5 and 17.8, respectively. The solid was shown 18.5 and 16.1, respectively. Both the Eu^{III} complexes were shown better ratio and which was improved compared with that of reported TPA based Eu^{III} complex. The integrated intensity ratios were indicating that the Eu^{III} ion occupied non-center of symmetry site and which reveals strong coordination interaction of Eu^{III} ion with surrounding ligand environment. The full width half maximum (FWHM) of the complexes, 1Eu and 2Eu are in solution shown below 5 nm (4.5 and 4.2 nm) and in solid also shown the same (4 and 5 nm), respectively. It indicates that the obtained pure narrow emissions are red efficient for finest applications.

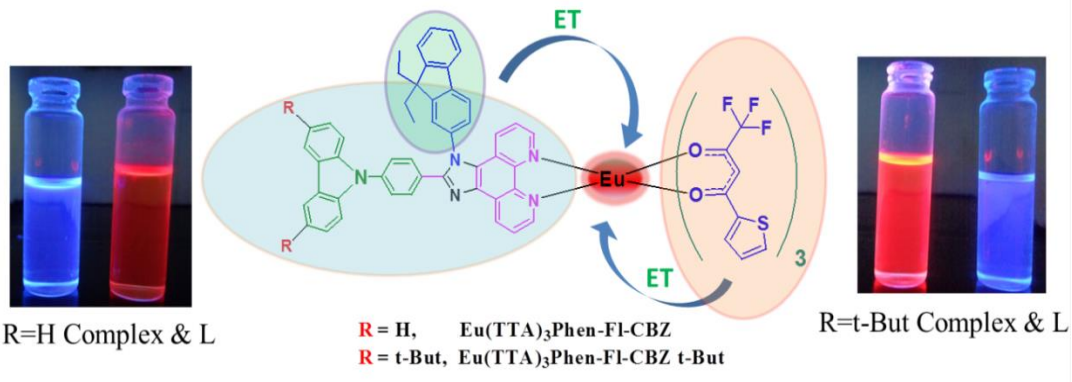

Figure 4.8 The emission color of the ligands and Eu^{III} complexes in solution, ligand and TTA energy transfer (ET) to Eu^{III} metal ion

Table 4.2 The UV-absorption and PL emission data of synthesized Eu^{III} complex and ligand.

S. No.	Compound	λ_{max} (abs) (nm) Solution[a b]	Solid[c]	λ_{ex} [a] (nm)	λ_{em} [a d] (nm)	PL QY (%)
1.	**$Eu(TTA)_3$Phen-Fl-CBZ**	246, 280, 309, 341	370	275, 360, 317, 370[d]	581, 589, 612, 652, 703	60.1
2.	**$Eu(TTA)_3$Phen-Fl-t-but CBZ**	245, 279, 309, 341	370	275, 360, 317, 370[d]	581, 589, 612, 652, 703	50
3.	**Phen-Fl-CBZ**	245, 281, 341	350	365, 317	410, 449[d]	--.--
4.	**Phen-Fl-t-but CBZ**	247, 279, 348	350	365, 317	413, 463[d]	--.--
3	**$Eu(TTA)_3.2H_2O$**	273, 340	--.--	275, 340	580, 592, 612, 652, 703	--.--

[a] measured in chloroform solution at 298 K, [b]absorption peaks from the UV-Vis absorption spectra. [c]emission peaks from photoluminescence emission spectra. [d]solid sample

To better understand the PL emission study of the Eu^{III} complexes, it was calculated the singlet ($^1\pi\pi^*$) and triplet ($^3\pi\pi^*$) energy states by DFT and TD-DFT. The energy transfer mechanism from ligand to Eu^{III} metal ion and structural representation for energy transfer from TTA to Eu^{III} ion is shown in Figure 4.9. The theoretically calculated singlet and triplet energy levels of the 1Eu and 2Eu are shown at 27,212 (3.37 eV), 21,704 (2.69) and 26,728 (3.31), 21,896 cm^{-1} (2.71), respectively. It is known that the singlet and triplet energy level of the TTA located at around 25,164 (3.12 eV) and 18,954 cm^{-1} (2.35 eV) [34]. It is well recognized that the Eu^{III} metal ion excited $^5D_0$ energy level located at 17500 cm^{-1} [34, 35]. In current observation, the synthesized Eu^{III} complex shows red emission because of efficient energy transfer from both the bidentate ligand as well as TTA to center metal ion. These results were satisfying the Latva *et al.,* investigations [36]. The triplet state energy level of the 1Eu and 2Eu is higher than (4,204 and 4,396 cm^{-1}) that of $^5D_0$ energy level. It means T_1 located at higher than 20,000 cm^{-1}. These results indicating that the efficient energy transfer facilitating between triplet state of the ligand to $^5D_0$ energy level of Eu^{III} ion. In the other hand, fully energy transfers of solid form of Eu^{III} complexes are expected might be a change of prominent triplet energy level.

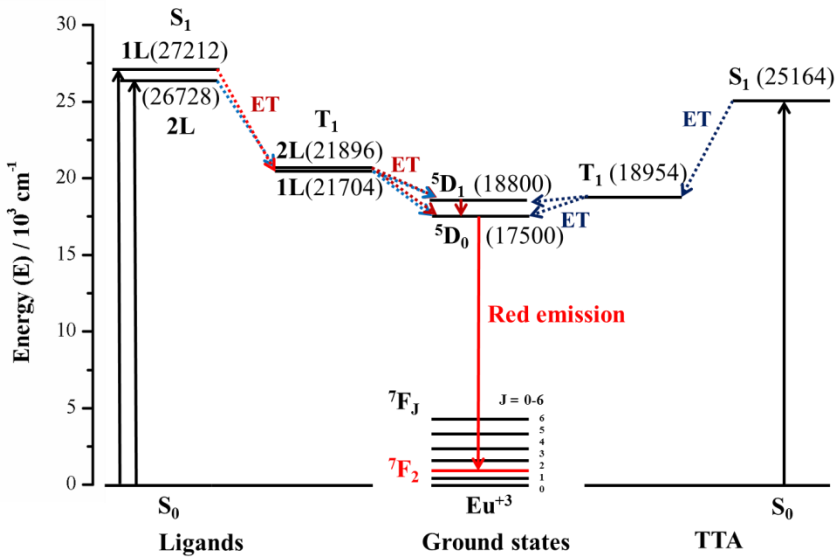

Figure 4.9 Representation illustration of ligands to Eu^{III} center metal ion energy transfer mechanism (S = singlet, T = triplet, ET = energy transfer (darted line is non-radiative)).

4.2.2.4.3 Photoluminescence quantum efficiency:

PLQY was measured in chloroform solution by using quinine sulfate as a reference in 1M H_2SO_4 (φ = 54.6%) at room temperature [37]. The obtained PLQY is supporting the efficient energy transfer from ligand to center Eu^{III} metal ion. Overall quantum yields of the Eu^{III} complexes were calculated according to the well-known equation (4.1),

$$\varphi_{overall} = \frac{n^2 A_{ref} I}{n_{ref}^2 A I_{ref}} \varphi_{ref} \qquad \text{..... (4.1)}$$

Here, n is the refractive index of solvent, A is an area of the emission spectrum, I is an absorbance at the excitation wavelength, $\varphi_{overall}$ is the quantum yield of the sample and φ_{ref} is the quantum yield of the standard quinine sulfate solution, respectively. The PLQY of the 1Eu and 2Eu was shown 60.1 and 50 % upon excitation at 358 nm. The obtained results are due to

directly involvement of chromophore (amines and fluorene) groups in the sensitization process for the Eu ion in Eu^{III} complexes. These outcomes were better than TPA based Eu^{III} complex [22]. It is an indirect indication that the CBZ were increasing radiative pathway by reducing non-radiative transition. In addition, we also measured the absolute QY of the complex and details can be found in the reported literature [23]. The absolute QY is found (in the solid phase) to be 72.4 and 77.3 % under 330 nm excitation for 1Eu and 2Eu, respectively (Figure 4.10). The obtained results are extremely good and found more than earlier reported TPA and carbazole based complexes [22, 23, 43].

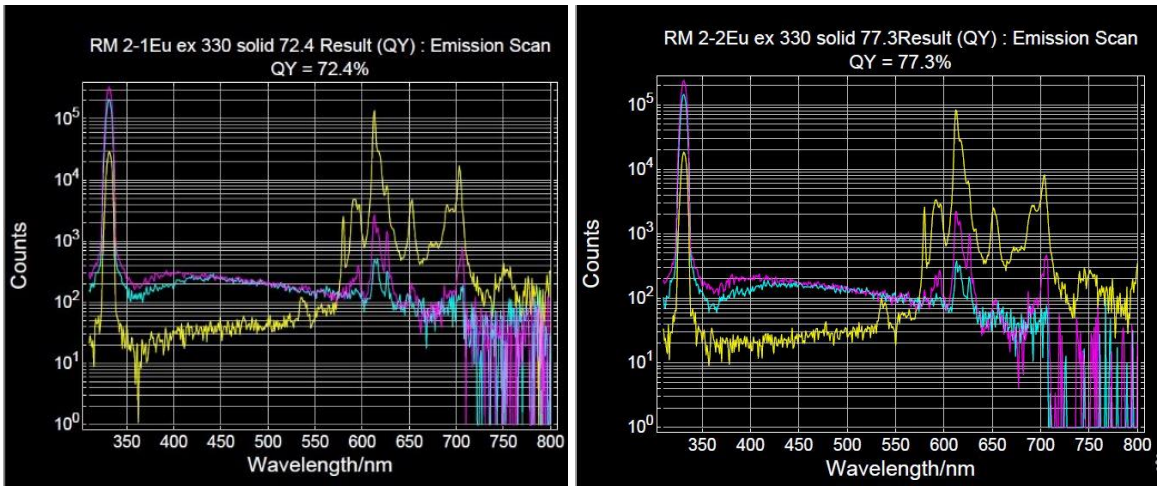

Figure 4.10 The PLQY of the complex, $Eu(TTA)_3Phen$-Fl-CBZ. (Yellow: direct, pink: indirect and sky-blue: reference) (left), PLQY of the complex, $Eu(TTA)_3Phen$-Fl-t-but CBZ. (Yellow: direct, pink: indirect and sky-blue: reference) (right).

4.2.2.4.4 Lifetime and Jodd-Ofelt investigations:

The PL Lifetime data of Eu^{III} complexes and ligands were obtained and best fitted with the single exponential function given by the equation $I(t) = I_0 + A_1 \exp\left(\frac{-t}{\tau}\right)$. Where A_1 is the scalar quantity obtained from the fitting curve, $I_0 = 0$ is the offset value, t is the time in ms and τ is the decay time value for the exponential component. The luminescence decay curves of the $^5D_0$ excited state were measured at 298 K by monitoring the most intense emission lines ($^5D_0 \rightarrow {}^7F_2$) of the Eu-ion center at 612 nm, and under at 360 nm excitation. The demonstrated mono-exponential performance of Eu^{III} complex, indicative that the europium ion presence in a single chemical environment. To understand furthered its solvent effect compared with solid, the lifetime was investigated in various solvents (Acetone, $CHCl_3$, DCM, DMF and THF) and the obtained results were shown in Figure 4.11.

In general, the excited state lifetime of the $^5D_0$ (Eu^{III}) level is typically long (ms to ms scale) and caused by enable energy transfer to high frequency vibrational oscillators (O–H, N–H, and C–H). The luminescent lifetime values (τ) of $Eu(TTA)_3Phen$-Fl-CBZ and $Eu(TTA)_3Phen$-Fl-t-but CBZ were found to be 0.64 (solid) > 0.58 (Acetone) > 0.57 (DCM) > 0.52 ($CHCl_3$) > 0.51 (THF) > 0.45 (DMF) and 0.61 (Acetone) > 0.60 (DCM) > 0.59 ($CHCl_3$) > 0.55 (THF) > 0.48 (DMF) > 0.40 (solid). Lifetime of the solid $Eu(TTA)_3Phen$-Fl-CBZ was found to be higher than that of other Eu^{III} (2Eu) complex, which is due to reduce the non-radiative transitions in the solid

as compare to that of 2Eu solid. To support the same it could be expected that the existence of t-butyl groups influence to increase the non-radiative emission channels. However, in the case of 2Eu highest lifetime found to be in acetone (DCM, $CHCl_3$ also same). It is because of the presence of O–H, N–H group's frequency vibrational oscillation is higher than that of C–H vibrational oscillators. In addition, lifetimes of the ligands were also calculated and all obtained results were tabulated in Table 4.3.

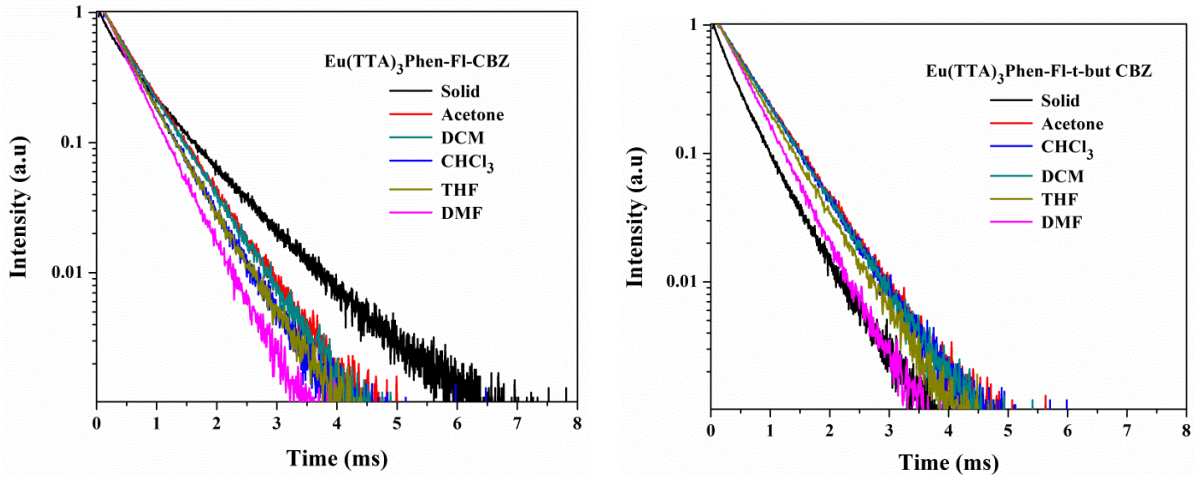

Figure 4.11 Decay curves of $Eu(TTA)_3$Phen-Fl-CBZ (left) and $Eu(TTA)_3$Phen-Fl-t-but CBZ (right) at 360 nm in different solutions and solid.

The spectral intensity parameters of the Eu^{III} complexes are given by the Judd–Ofelt parameters Ω_λ (where λ = 2, 4 and 6). Among all transitions of Eu^{III} ion, the $^5D_0 \rightarrow {}^7F_{0,3,5}$ transitions are forbidden ($S_{(ED)}$ and $S_{(MD)}$ = zero) and the Ω_2 ($^5D_0 \rightarrow {}^7F_2$) electric dipole transition is allowed, which is more sensitive to the symmetry [38, 39]. The detailed calculations are reported elsewhere [40] as well as in Chapter 2. The intensity parameter Ω_4 ($^5D_0 \rightarrow {}^7F_2$) is less sensitive to the coordination sphere than Ω_2. The $^5D_0$ to $^7F_1$ (J=1) transition has no electric dipole involvement; it is isolated magnetic dipole transition and hence forward can be used as a reference for estimation of J–O intensity parameters. The calculated Ω_2 value (Table. 4.3) shown the Eu^{III} ion is located in the complex in the highly covalent environment.

Table 4.3 Observed luminescence lifetimes (τ_{obs}) and intensity parameters of synthesized Eu^{III} complexes and corresponding ligands

S. No.	Compound	Intensity parameters (10^{-20} cm^2)		τ / ms [a]					
		Ω_2	Ω_4	Solid	Acetone	$CHCl_3$	DCM	DMF	THF
1.	**$Eu(TTA)_3$Phen-Fl-CBZ**	12.0	0.95	0.64	0.58	0.52	0.57	0.45	0.51
2.	**$Eu(TTA)_3$Phen-Fl-t-but CBZ**	13.5	1.1	0.40	0.61	0.59	0.60	0.48	0.55
3.	**Phen-Fl-CBZ (10^{-3} ms)**	--.--	--.--	2.53	3.13	1.81	3.54	3.80	7.58
4.	**Phen-Fl-t-but CBZ (10^{-3} ms)**	---.--	--.--	1.38	5.93	4.23	4.47	2.79	4.26

[a] The decay curves with mono-exponential

The overall quantum yield ($\Phi_{overall}$) (equation 4) of the Eu^{III} complexes obtained under ligand excitation and it depends on two essential parameters, which are the efficiency with which the ligands transfer energy onto the Eu^{III} ion (Φ_{sens}), and the intrinsic quantum yield (Φ_{LN}) and the quantum yield upon direct excitation into the f level, which is [15, 41, 42].

$$\Phi_{overall} = \Phi_{sens}\, \Phi_{Ln} \quad \text{……..... (4)}$$

The intrinsic quantum yield ($\Phi_{Ln)}$ calculated by the following equation (5) for the Eu^{III} ion. The radiative lifetime (τ_{RAD}) of the complexes can be calculated by the equation 6 and assume that the energy of the $^5D_0 \rightarrow {}^7F_1$ transition (MD) as well as its oscillator strength was constant. Here, the considering the $A_{MD,0}$ (14.65 s^{-1}) represents the spontaneous emission probability of the $^5D_0$ - $^7F_1$ transition (vacuo), and n is the refractive index of the medium. An average index of refraction equal to 1.5 was employed in the calculation [43].

$$\Phi_{Ln} = \left(\frac{A_{RAD}}{A_{RAD} + A_{NR}}\right) = \frac{\tau_{obs}}{\tau_{RAD}} \quad \text{…….. (5)}$$

$$A_{RAD} = \left(\frac{1}{\tau_{RAD}}\right) = A_{MD,0} n^3 \left(\frac{I_{TOT}}{I_{MD}}\right) \quad \text{…..…….. (6)}$$

The obtained intrinsic quantum yield (Φ_{Ln}), energy transfer efficiency (Φ_{sen}) and lifetime analysis indicates that the currently studied ligand is efficient sensitizer for Eu^{3+} ion in both the complexes. In addition, the Φ_{sen} of the 1Eu is higher than that of the 2Eu. However, an obtained result indicates that the both complexes are potential components. All the calculated parameters are tabulated in Table 4.4.

Table 4.4 The radiative (A_{RAD}) and nonradiative (A_{NR}) decay rates, $^5D_0$ lifetime (t_{obs}), intrinsic quantum yield (Φ_{Ln}), energy transfer efficiency (Φ_{sen}) and overall quantum yield ($\Phi_{overall}$) for complex.

S. No.	Complex name	A_{RAD} (S^{-1})	A_{NR} (S^{-1})	τ_{obs} (ms)	τ_{RAD} (ms)	Φ_{Ln} (%)	Φ_{Sen} (%)	$\Phi_{Overall}$ (%)
1.	**$Eu(TTA)_3$Phen-Fl-CBZ**	1137.1	191	0.64	0.729	87.7	82.5	72.4
2.	**$Eu(TTA)_3$Phen-Fl-t-but CBZ**	1078.1	142	0.40	0.927	43.1	17.9	77.3

4.2.2.5 Electrochemical Properties

The electrochemical analysis was the takeaway for synthesized ligands and their corresponding europium complexes. Redox properties of Eu^{III} complexes and ligand molecule are considerable important because it gives results about the HOMO and LUMO energy of the molecules/compounds. The details of oxidation and reduction with onset potentials data's are listed in Table 4.5. The HOMO and LUMO energy levels were calculated by using well-known equation 2.8 and 2.9. [44] The oxidation and reduction potentials of t-but CBZ was shown less compare to the rest of the Eu^{III} complex. Low band gap of the complexes are superior suitable candidates for future applications. The obtained redox potentials were shown in Figure 4.12. In addition, it is also calculated the onset wavelength of optical absorption (onset) in the solid-state (DRS spectra) and the results were well matched with electrochemical analysis. The comparison of HOMO-LUMO energy gap of ligands and complexes are shown in Figure 4.13.

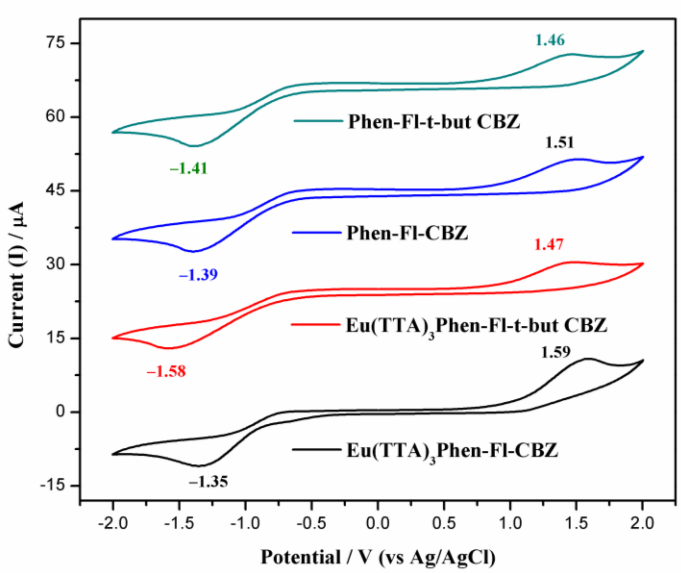

Figure 4.12 Cyclic voltamogram of Eu^{III} complexes and their ligands.

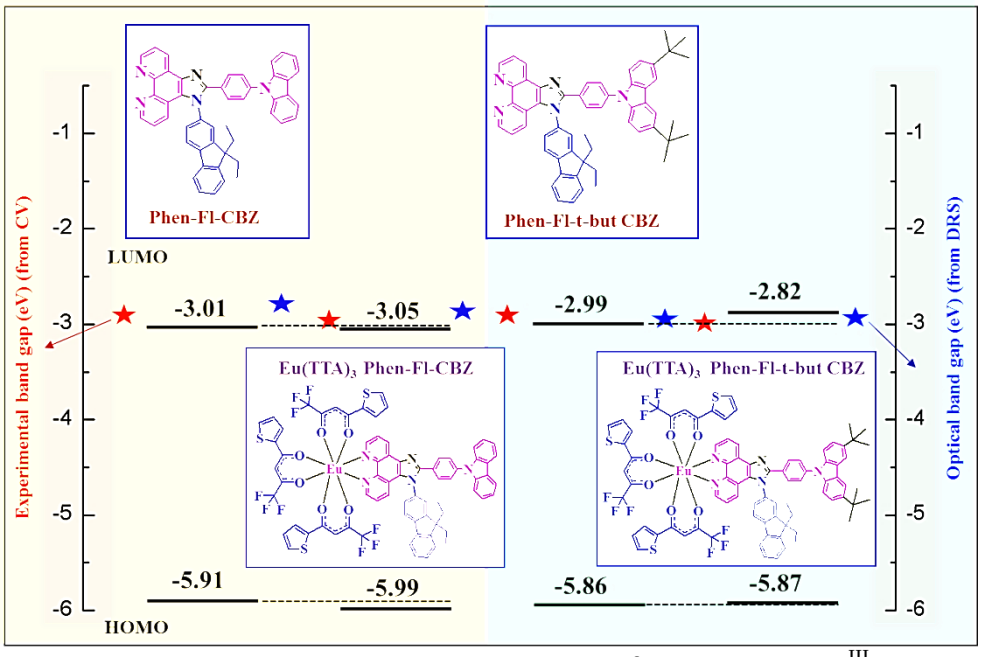

Figure 4.13 HOMO – LUMO energy gap diagram of Ligands and Eu^{III} complexes.

Table 4.5 Electrochemical properties of the Eu^{III} complexes and ligands

S. No.	Compounds	$Voltage^{Oxi}_{onset}$ (V) (E_{HOMO} (eV))	$Voltage^{Red}_{onset}$ (V) (E_{LUMO} (eV))	$\lambda_{onset,}$ (nm)	Energy gap E_g^{Opt}, (eV) (a)
1	**$Eu(TTA)_3$Phen-Fl-CBZ**	1.59 (-5.99)	-1.35 (-3.05)	444	2.80 (2.94)
2	**$Eu(TTA)_3$Phen-Fl-t-but CBZ**	1.47(-5.87)	-1.58 (-2.82)	434	2.86 (3.05)
3	**Phen-Fl-CBZ**	1.51 (-5.91)	-1.39 (-3.01)	419	2.70 (2.90)
4	**Phen-Fl-t-but CBZ**	1.46 (-5.86)	-1.41 (-2.99)	459	2.96 (2.87)

a) Calculated the onset wavelength of optical absorption in the solid-state film (DRS spectra). In bracket mentioned their energy differences (HOMO and LUMO) values calculated by CV.

4.2.2.6 DFT and TD-DFT Calculation:

The details of DFT and TD-DFT methodology and basic set was used for this study are given in section (Chapter 2, 3.3 theoretical calculation). The optimized structures of the ligands were depicted in Figure 4.14. The calculated FMO diagrams of ligands were shown in Table 4.6. The calculated energy gaps for the ligands are showed ~3 eV. The calculated HOMO and LUMO of the ligands results are shown similar to that of cyclic voltammetry analysis (Table 4.7). Locality of the electron density for HOMO of the ligand 1L was shown on CBZ and partially on phenanthroline moiety. It is due to the presence of CBZ as electron rich moiety in the structure. In LUMO, electron density located on the fluorene and partially located towards the Phenanthroline. The fluorine moiety is generally electron rich but it is connected with the electron deficient imidazole molecule. Hence, the electron cloud might be fulling towards imidazole group.

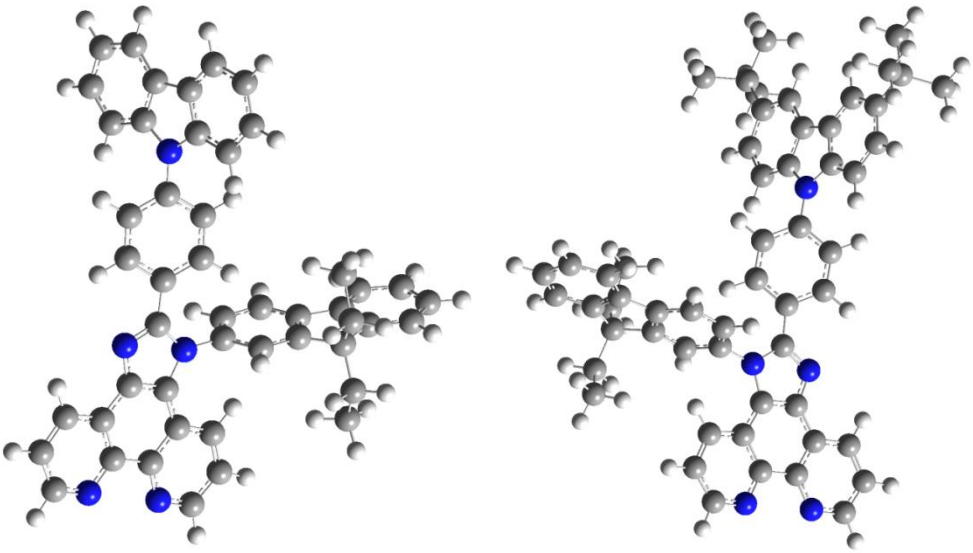

Figure 4.14 The optimized structures of the ligands Phen-Fl-CBZ (left) and Phen-Fl-t-but CBZ (right)

Table 4.6 The calculated HOMO – LUMO (top-down) energy orbitals by density functional theory (DFT) frame work using B3LYP/6-31(G) level of theory of ligands.

	Phen-Fl-CBZ	
HOMO-1	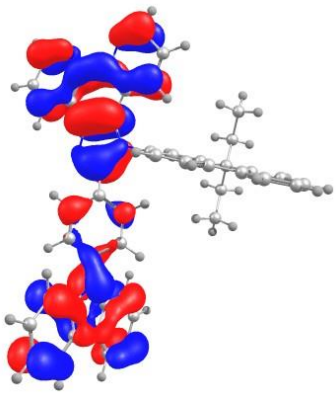	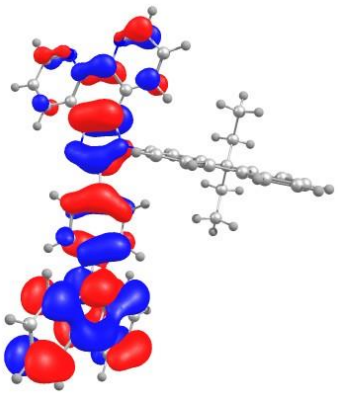 **HOMO**

LUMO+1 **LUMO**

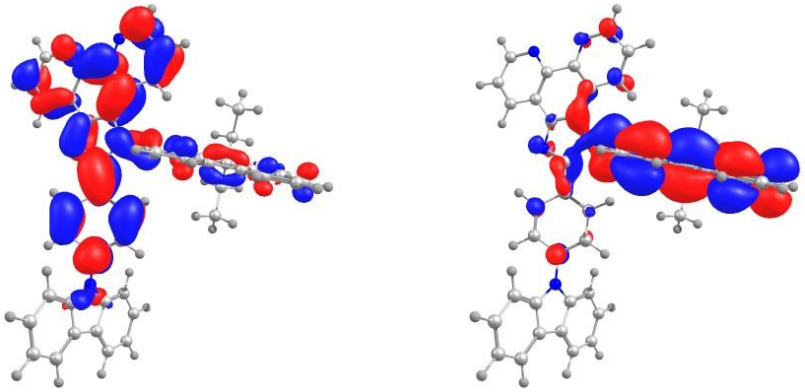

Phen-Fl-t-but CBZ

HOMO-1 **HOMO**

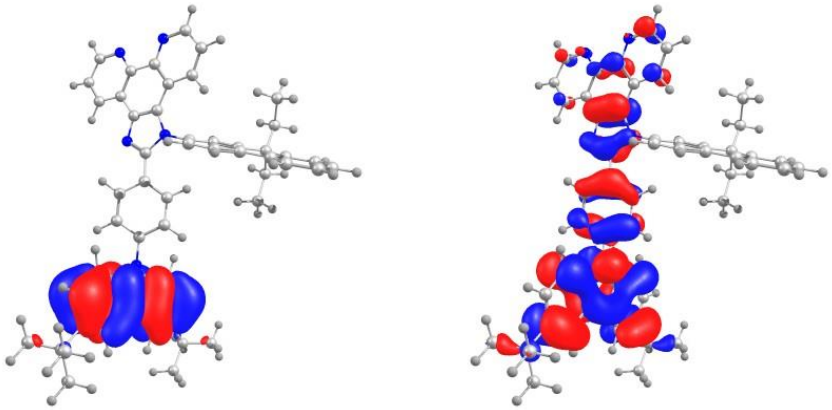

LUMO+1 **LUMO**

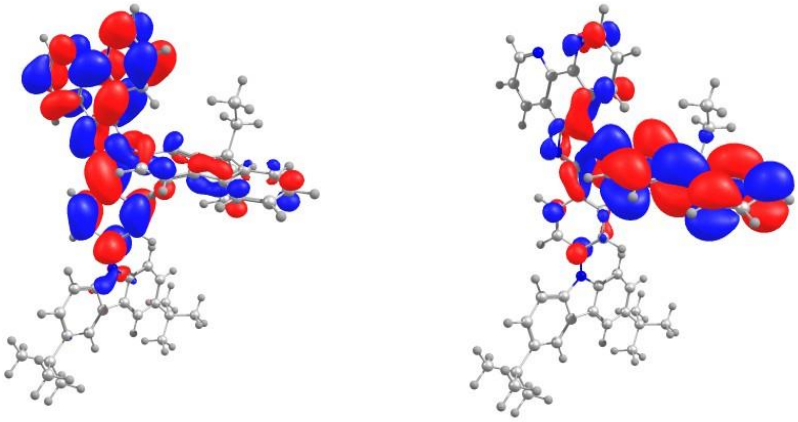

The obtained results show electron cloud absence in unoccupied molecular orbital shown on LUMO. The similar observations are also found for the 2L ligand (t-but CBZ functionalized ligand). The computed vertical transitions and there oscillator strengths and configuration of ligands (CBZ and t-but CBZ) are tabulated in Table 4.8 and 4.9.

Table 4.7 The HOMO and LUMO energy levels of the ligands with their respective band gaps and calculated singlet and triplet energy levels.

Molecule	HOMO	HOMO-1	LUMO	LUMO+1	E_g	S1	T1
	in electron volts (eV)						
Phen-Fl-CBZ	-5.02	-5.71	-1.52	-1.39	3.75	3.37	2.69
Phen-Fl-t-but CBZ	-5.17	-5.63	-1.51	-1.32	3.66	3.31	2.71
Eu^{III} metal ion	--.--	--.--	--.--	--.--	--.--	$^5D_0$ level = 2.17	

Table 4.8 The computed vertical transitions and there oscillator strengths and configuration of CBZ ligand.

Compound	State	Energy (eV)	λ_{max} nm	*f*	Configuration
Phen-Fl-CBZ	Gas	3.3276	355.53	0.1136	HOMO → LUMO (68.67%)
					HOMO-1 → LUMO (12.55%)
Singlet		3.889	318.80	0.1632	HOMO1→LUMO+1(50.46%)
					HOMO-1→LUMO+3(10.25%)
					HOMO → LUMO+3 (39.66%)
					HOMO → LUMO+4 (11.65%)
					HOMO → LUMO+5 (10.91%)
	DCM	3.3738	367.49	0.7253	HOMO → LUMO (67.58%)
					HOMO → LUMO+1 (10.79%)
					HOMO → LUMO+3 (11.26%)
		3.8796	319.58	0.2632	HOMO-1 → LUMO (50.49%)
					HOMO-1 → LUMO+3 (13.18%)
					HOMO → LUMO+1 (11.71%)
					HOMO → LUMO+3 (38.28%)
Triplet	Gas	2.6557	466.86	-	HOMO-1→LUMO (14.47%)
					HOMO-1→LUMO+1 (29.10%)
					HOMO → LUMO (22.88%)
					HOMO →LUMO+1 (48.10%)
	DCM	2.6915	460.66	-	HOMO-4 → LUMO (11.31%)
					HOMO-1 → LUMO (19.15%)
					HOMO-1 → LUMO+1 (16.76%)
					HOMO → LUMO (46.83%)
					HOMO → LUMO+1 (22.93%)
					HOMO → LUMO+2 (12.05%)

Table 4.9 The computed vertical transitions and there oscillator strengths and configuration of and t-but CBZ ligand.

Compound	State	Energy (eV)	λ_{max} nm	*f*	Configuration
Phen-Fl-t-but CBZ	Gas	3.2555	380.84	0.1573	HOMO-2 → LUMO (10.98%)
					HOMO → LUMO (68.56%)
Singlet		3.3965	365.04	0.4777	HOMO → LUMO+1 (67.42%)
		3.8902	318.71	0. 1341	HOMO-2 → LUMO+1 (54.55%)
					HOMO → LUMO+5 (24.48%)

	DCM	3.3138	374.14	0.6714	HOMO → LUMO (65.09%) HOMO → LUMO+1 (19.34%) HOMO → LUMO+3 (13.87%)
		3.8222	324.38	0.1540	HOMO-2 → LUMO (60.38%) HOMO → LUMO+1 (17.14%) HOMO → LUMO+2 (14.85%)
		3.8949	318.32	0.1536	HOMO-2 → LUMO (13.48%) HOMO-2 → LUMO+1 (14.96%)
Triplet	Gas	2.6812	462.42	-	HOMO-2 → LUMO (19.63%) HOMO-2 → LUMO+1 (30.94%) HOMO → LUMO (25.39%) HOMO →LUMO+1 (40.91%)
	DCM	2.7147	456.71	-	HOMO-4 → LUMO (11.82%) HOMO-2 → LUMO (33.49%) HOMO-2 → LUMO+1 (20.74%) HOMO-2 → LUMO+2 (12.76%) HOMO → LUMO (40.88%) HOMO → LUMO+1 (22.78%) HOMO → LUMO+2 (14.83%)

4.2.2.7 PMMA thin film study and CIE chromaticity coordinates:

To understand the emission of the Eu^{III} complexes in thin film, the complexes also been doped with the PMMA matrix in different mass ratio (0.1, 0.5, 1 and 5 %). Preparation of PMMA thin film with complexes was discussed in section 4.33. The corresponding PL emission spectra as well as digital photographs are shown in Figure 4.15. The intensity of the complexes with PMMA was increased compare to that of undoped Eu-complex. In addition, it is observed that the increase the percentage of Eu^{III} complex with increase the intensity. However, the complex with 5% doping is showed better red emission. The calculated CIE coordinates are for 1Eu, 0.1 %, x = 0.53, y = 0.43; 0.5 %, x = 0.55, y = 0.42; 1 %, x = 0.53, y = 0.43 and 5 %, x = 0.60, y = 0.38 and their asymmetric intensity ratio of (I_2/I_1) shown 6.34, 5.24, 4.84 and 3.98, respectively. Similarly, calculated CIE coordinates are for 2Eu, 0.1 %, x = 0.55, y = 0.42; 0.5 %, x = 0.55, y = 0.42; 1 %, x = 0.61, y = 0.37 and 5 %, x = 0.60, y = 0.39 and their asymmetric intensity ratio of (I_2/I_1) shown 5.98, 6.03, 9.06 and 2.86, respectively. In addition, the FWHM of the complexes, 1Eu and 2Eu (0.1, 0.5, 1, 5%) are calculated and found to be 11.0, 13.0, 13.1, 18.2 and 11.1, 12.2, 10.4, 18.4, respectively. FWHM of the complexes with doping was increases with concentration of the Eu^{III} complex increment. It indicates that the PMMA matrix doping is responsible to increase the FWHM. In addition, un-doped films as well as solution and solid are shown less FWHM (< 5 nm).

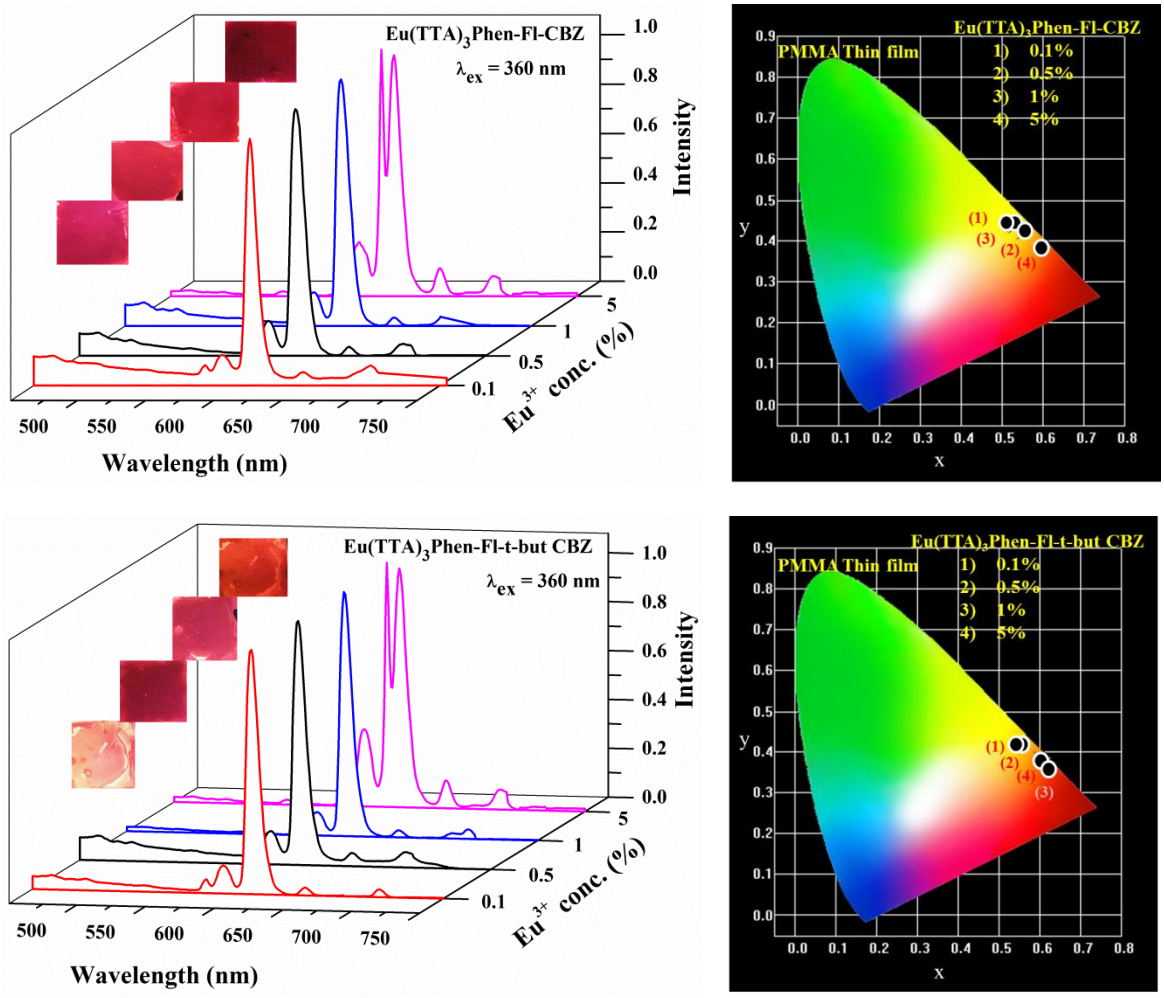

Figure 4.15 The Eu^{III} complex doped with PMMA (different percentage ratio) as well as their thin film patterns (left) and its CIE color coordinates (right).

CIE chromaticity coordinates were calculated from emission the spectral data's (λ_{ex}=360 nm) for CBZ and t-but CBZ functionalization Eu^{III} complexes (Figure 4.16, left). The ligands 1L and 2L shown CIE coordinates were x = 0.17, y = 0.15 and x = 0.21, y = 0.25 in solid; x = 0.15, y = 0.04 and x = 0.15, y = 0.02 in solution, respectively. The corresponding 1Eu and 2Eu shows the calculated CIE color coordinates were x = 0.65, y = 0.34 and x = 0.64, y = 0.34 in solid; x = 0.50, y = 0.26 and x = 0.50, y = 0.26 in solution, respectively. The obtained CIE values of the Eu^{III} complexes were indicating in the region of red and ligands were shown deep blue coordinates. The Eu^{III} complexes in solution are shown deviation from the solid color coordinates and which solid results are close to the NTSC standards. The presence of small spectral quantity of the ligand emission along with Eu^{III} metal ion in Eu^{III} complexes in solution is deviating from pure red emission. However, there is no such type of observation (from ligand) in complexes and pure red emission was observed in solid form. So, solid forms of the complexes are better materials to achieve the efficient red emission.

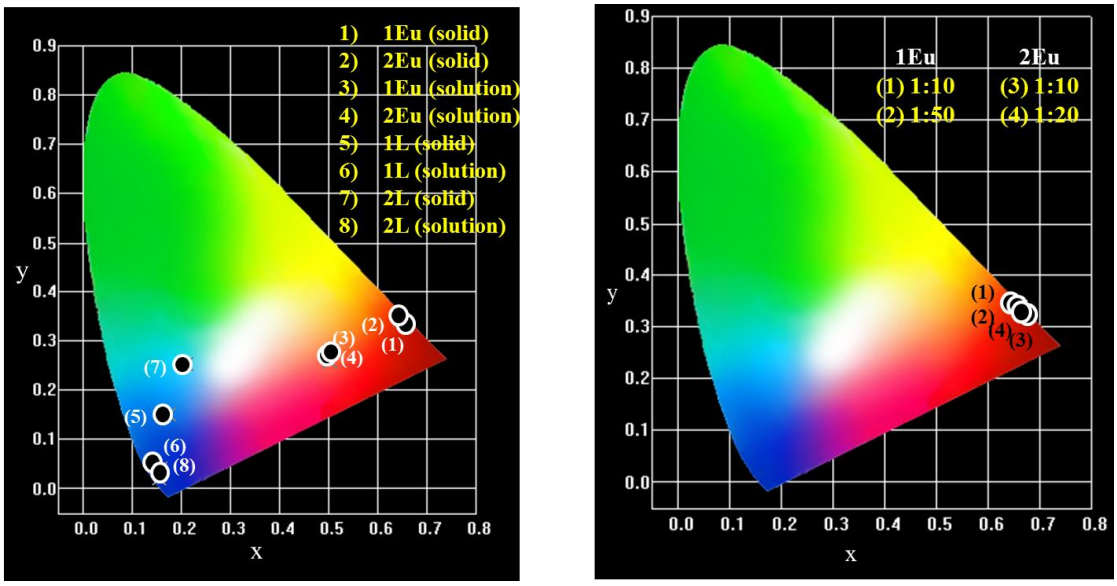

Figure 4.16 The CIE chromaticity coordinates for ligands and respective Eu^{III} complexes in solution as well as solid (left) and CIE for the Eu^{III} complexes coated on the 395 nm emitted LED chip (right).

4.2.2.8 LED fabrication with Eu^{III} complexes:

Light-emitting diodes were fabricated by using a permutation of a 395 nm emitting InGaN chip with the Eu^{III} complexes in different proportions are 1:10 and 1:50 (Eu^{III} complex: PMMA). After coating the complexes in LEDs, the same was dried for 6 hr at afar ambient temperature (40 ^{0}C). The original InGaN LED with 395 nm chip and emission from the complexes under 20 mA forward-bias current as well as in normal were shown in Figure 4.17. The emission peak in the range of 395 nm is almost reduced except 2Eu (1:10). It indicates that the 1Eu complex transfer's their excitation energy to emission center and fully excitation was consumed by the Eu complex. However, in the case of 2Eu, 1:50 shown fully observed excitation source compare to that of 1:10. It could be expected that the presence of Eu^{III} ions are more in 1:10 concentration (% of Eu^{III} ion is high). The both 1Eu and 2Eu complexes are shown sharp intensive red emission. The same was also confirmed by chromaticity coordinates and satisfying the NTSC standard values for red emission. The CIE color coordinates shown for 1Eu is x = 0.65, y = 0.34 (1:10); x = 0.66, y = 0.34 (1:50) and 2Eu is x = 0.66, y = 0.33 (1:10); x = 0.66, y = 0.33 (1:50), respectively. The pictorial view of the CIE color coordinates for Eu complexes coated LED with forward bias are shown in Figure 4.16, right. We have calculated luminescence efficiency of the LEDs with and without coating the Eu^{III} complexes. The efficiency of the original LED (395 nm from the InGaN chip) without Eu^{III} complex is found to be only ~0.22 lm W^{-1}. After, the fabricated LED with Eu^{III} complexes, 1Eu and 2Eu showed a higher efficiency of 1.12 and 0.9 lm W^{-1}.

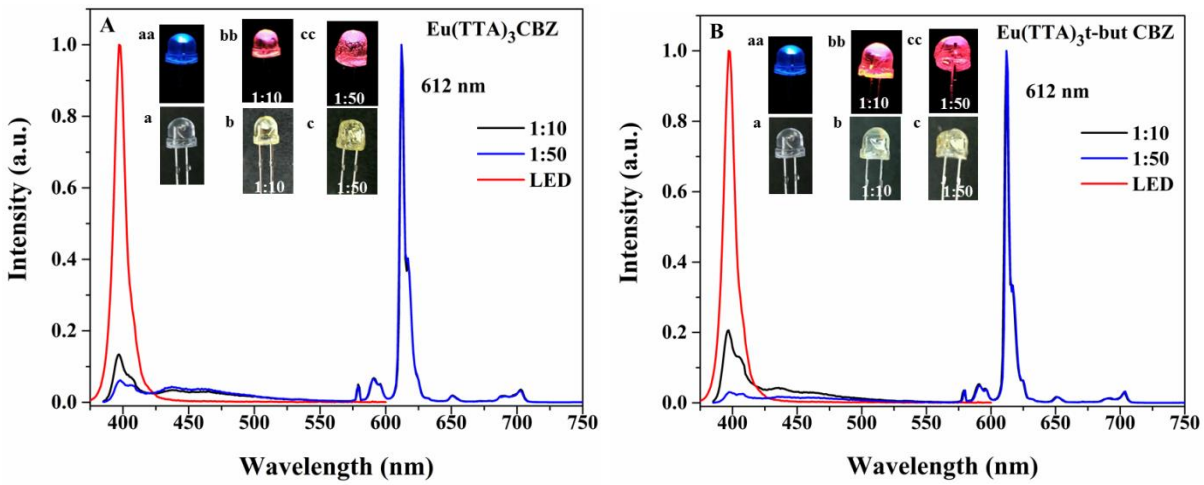

Figure 4.17 The spectra's **A** and **B** are red emitting synthesized Eu^{III} complexes coated on the 395 nm emitted LED chip. In inset **a** is the original 365 nm emitted LED chip and **aa** is under forward bias. **b** and **c** are coated with Eu^{III} complexes and **bb** and **cc** are with forward bias, respectively.

4.3 Summary and Conclusion:

Two bipolar ligands and their corresponding Eu^{III} complexes were designed and successfully synthesized. DSC-TGA showed good thermal stability and decomposition, which is good for furthered solicitations and good glass transition temperature as well. The PL analysis indicates that all complexes showed pure red emission at around 612 nm, which is due to electric dipole transition of Eu^{III} ion present in the complex. In addition, there is no ligand emission in complex which clearly indicates that the complete energy transfer from the ligand to Eu^{III} metal ion occurs. To support the same, the energy transfer mechanism by computational study (DFT and TD-DFT) also been executed. The obtained absolute QY found to be superior (77.3%) to that of the reported complexes. The Judd–Ofelt theory to the emissive properties of Eu^{III} complexes were investigated and the lifetime found better in $Eu(TTA)_3$Phen-Fl-CBZ complex was to be 0.64 ms. The calculated HOMO-LUMO band gap of the complexes was good for furthered analysis. The fabricated red LED (Eu complexes with 395 nm emitted LED) shown pure red emission and the CIE color coordinates are x = 0.66, y = 0.33. The obtained results indicating that the presently studied complexes may potential application in white LEDs.

4.4 References:

[1] G. Shaoa, Y. Li, K. Feng, F. Gana and M. Gong, *Sensors and Actuators B.,* 2012**, 173,** 692–697.

[2] G. Shao, H. Yu, N. Zhang, Y. He, K. Feng, X. Yang, R. Cao and M. Gong, *Phys. Chem. Chem. Phys*., 2014, **16**, 695–702.

[3] Z. Wang, H. Yang, P. He, Y. He, J. Zhao and H. Tang, *Dalton Trans*., 2016, **45**, 2839–2844.

[4] S. Liu, P. He, H. Wang, J. Shi and M. Gong, *Inorg. Chem. Commun.,* 2009, **12**, 506–508.

[5] N. M. Shavaleev, S. V. Eliseeva, R. Scopelliti, and J–C. G. Bunzli, *Chem. Eur. J.*, 2009, **15**, 10790–10802.

[6] J. Kido, K. Nagai and Y. Ohashi, *Chem. Lett.,* 1990, 657.

[7] C. W. Tang and S. A. VanSlyke, *Appl. Phys. Lett.,* 1987, **51**, 913.

[8] Y. Zheng, L. Fu, Y. Zhou, J. Yu, Y. Yu, S. Wang and H. Zhang, *J. Mater. Chem.,* 2002, **12**, 919–923.

[9] R. Reyes, M. Cremona, E. E. S. Teotonio, H. F. Brito and O. L. Malta, *Chem. Phys. Lett.,* 2004, **396**, 54–58.

[10] S. Petoud, S. M. Cohen, J-C. G. Bunzli and K. N. Raymond, *J. Am. Chem. Soc.,* 2003, **125**, 13324−13325.

[11] L. Armelao, S. Quici, F. Barigelletti, G. Accorsi, G. Bottaro, M. Cavazzini and E. Tondello, *Coord. Chem. Rev.,* 2010, **254**, 487−505.

[12] E. G. Moore, A. P. S. Samuel and K. N. Raymond, *Acc. Chem. Res.,* 2009, **42**, 542−552.

[13] F. F. Chen, Z. Q. Chen, Z. Q. Bian and C. H. Huang, *Coord. Chem. Rev.,* 2010, **254**, 991−1010.

[14] H. Xu, Q. Sun, Z. An, Y. Wei and X. Liu, *Coord. Chem. Rev.,* 2015, **293–294**, 228–249.

[15] A. R. Ramya, M. L. P. Reddy, A. H. Cowley and K. V. Vasudevan, *Inorg. Chem.,* 2010, **49**, 2407−2415.

[16] S. Biju, D. B. A. Raj, M. L. P. Reddy and B. M. Kariuki, *Inorg. Chem.,* 2006, **45**, 10651−10660.

[17] M. Sun, H. Xin, K. Z. Wang, Y. A. Zhang, L. P. Jin and C. H. Huang, *Chem. Commun.,* 2003, 702–703.

[18] M. Guan, Z. Q. Bian, F. Y. Li, H. Xin and C. H. Huang, *New J. Chem.,* 2003, **27**, 1731–1734.

[19] C. J. Xu, J. T. Wan and B. G. Li, *Dyes and Pigments*, 2013, **98**, 493–498.

[20] A-D. B. Dias, *Dalton Trans.,* 2007, **22**, 2229.

[21] G. Hughes and M. R. Bryce, *J. Mater. Chem.,* 2005, **15**, 94.

[22] B. Rajamouli, P. Sood, S. Giri, V. Krishnan and V. Sivakumar, *Eur. J. Inorg. Chem.,* 2016, **24**, 3900–3911.

[23] B. Rajamouli, Rachna Devi, A. Mohanty, V. Krishnan and V. Sivakumar, Sensors and Actuators, 2017 (submitted).

[24] J. Liu, J–S. Miao and H–B. Wu, *Luminescence*, 2015, **30**, 393–396.

[25] M. R. Robinson, J. C. Ostrowski, G. C. Bazan and M. D. McGehee, *Adv. Mater.,* 2003, **15**, 1547–1551.

[26] F. Gutierrez, C. Rabbe, R. Poteau and J. P. Daudey, *J. Phys. Chem. A,* 2005, **109**, 4325–4330.

[27] M. M. Nolasco, P. D. Vaz and L. D. Carlos, *New J. Chem.,* 2011, **35**, 2435–2441.

[28] F. C. Teng, X. Yang, C. Yuan, C. Li, R. Chen, H. Tian, S. Li, A. Hagfeldt and L. Sun, *Org. Lett.*, 2009, **11**, 5542–5545.
[29] C. Yang, S. Liu, J. Xu, Y. Li, M. Shang, L. Lei, G. Wang, J. He, X. Wang and M. Lu, *Polym. Chem.*, 2016, **7**, 1147–1157.
[30] H. Xu, K. Yin and W. Huang, *J. Phys. Chem. C,* 2010, **114**, 1674–1683.
[31] Y. Liu, Y. Wang, H. Guo, M. Zhu, C. Li, J. Peng, W. Zhu and Y. Cao, *J. Phys. Chem. C,* 2011, **115**, 4209–4216.
[32] D. F. Parra, A. Mucciolo, D. G. Duarte, H. F. Brito and A. B. Lugao, *J. Appl. Polym. Sci.*, 2006, **100**, 406–412.
[33] H. Xu, H. L. Wang, X. H. Zhu, K. Yin, G. Y. Zhong, X. Y. Hou and W. Huang, *J. Phys. Chem. B,* 2006, **110**, 3023−3029.
[34] Z. Ahmed and K. Iftikhar, *Inorg. Chim. Acta*, 2012, **392**, 165–176.
[35] T. Li, W. Shang, F. Zhang, L. Mao, C. Tang, M. Song, C. Du and Y. Wu, *Engineering*, 2011, **3**, 301–311.
[36] M. Latva, H. Takalo, V. M. Mukkala, C. Matachescu, J. C. Rodriguez-Ubis, and J. Kankare, *J. Lumin.*, 1997, **75**, 149–169.
[37] M. Shi, F. Y. Li, T. Yi, D. Q. Zhang, H. M. Hu and C. H. Huang, *Inorg. Chem.*, 2005, **44**, 8929.
[38] V. Divya, R. O. Freire and M. L. P. Reddy, *Dalton Trans.*, 2011, **40**, 3257–3268.
[39] L. Zhou and B. Yan, *J. Phys. Chem. Solids,* 2008, **69**, 2877.
[40] S. Kasturi and V. Sivakumar, *Chemistry select,* 2016, **1**, 5448–5462.
[41] S. Quici, M. Cavazzini, G. Marzanni, G. Accorsi, N. Armaroli, B. Ventura and F. Barigelletti, *Inorg. Chem.*, 2005, **44**, 529.
[42] Y. H. Kim, N. S. Baek and H. K. Kim, *Chem. Phys. Chem.*, 2006, **7**, 213.
[43] B. Rajamouli, C. S. D. Viswanath, S. Giri, C. K. Jayasankar and V. Sivakumar, *New J. Chem.*, 2017, **41**, 3112-3123.
[44] F. C. Teng, X. Yang, C. Yuan, C. Li, R. Chen, H. Tian, S. Li, A. Hagfeldt and L. Sun, *Org. Lett.*, 2009, **11**, 5542–5545.

Chapter 5

Controlled energy transfer from ligand to Eu^{III} ion: A unique strategy to obtain bright white/red light emission and their versatile applications

Abstract

A new diphenylamine (DPA) and carbazole (CBZ) functionalized ancillary ligands coordinated β-diketonate Eu^{III} complexes shown incomplete or complete energy transfer from ligand to Eu^{III} ion. Solvatochromism study of DPA based complex leads to balancing of the primary RGB colors to obtain single molecule white emission. The temperature dependent PL study indicates that the DPA based complex could be used as ratiometric temperature sensor (color changes from blue to yellowish-red via white). In addition, the Eu-complex conjugated with near UV LED shown white emission with 0.34, 0.33 CIE coordinates. In the case of CBZ functionalized bipolar ligand and its corresponding β-diketonate Eu^{III} complex shown efficient energy transfers from the ligand to Eu^{III} center metal ion and emits narrow band red emission with apt CIE color gamut. TD-DFT calculations were performed to know the energies of the singlet (^1S) and triplet (^3T) levels for the bipolar ligand and shown good overlap between the ligand triplet level and Eu^{III} excited level. The PLQY is found to be 44.4 %, whereas the DPA based complex shown comparatively less QY (supports the inefficient energy transfer). HOMO and LUMO energy levels energies (redox reaction) were calculated from the electrochemical analysis for the Eu-complexes. The synthesized Eu^{III} complex was doped in PMMA with different percentage ratio and found to be concentration variation influence on emission intensity and symmetry. The CBZ-Eu-complex conjugated with near UV LED (395 nm) shown red emission with CIE color coordinates of 0.66, 0.33 and hence could find potential application in white LEDs.

Key words: Carbazole; bipolar ligand; Eu complex; DFT; white emission

5.1 Introduction:

The new single organic molecule or molecular complex based white light emitting sources are attractive owing to their potential applications in full-color smart displays and lighting sources (including white OLEDs and solid state lighting (LEDs)) [1]. In general, white light can be realized by mixing of three primary colors, in order to cover the entire visible spectrum. Although there are several organic fluorophores that are capable of emitting individual red-blue-green (RGB) color are known; however, white light generated by single molecule (single-component approach) have several advantages than that of simple RGB mixing (multi-component emitters) [2]. The benefit includes improved stability; stable commission International de I'Eclairage (CIE) color coordinates as well as simple fabrication process [3]. Stable white photo and electroluminescence released in a single molecule dyad have been documented [4]. White light creation by aggregated induced emission in single organic molecule has also been reported [5]. Iridium-based molecular complex, which are emits white light (all the way from 440 to 800 nm in the spectral window) [6]. By utilizing the sensitizing/energy harvesting capability of Ir^{III} ion to lanthanides, the Ir-Eu dyad has used to release the white light (bluish green emission from the Ir^{III} emissive center and red emission from the Eu^{III} metal center) [7]. Although, generate white light emission from the single molecular complex is still a huge challenge. The demand of the cumulative global energy crisis is reducing the energy sources and it can be overcome by high energy efficient lighting systems (solid state lighting (SSL)) that can help to conserve energy and reduce overall lighting costs [8].

5.2 White light emissive DPA based Europium complex:

5.2.1 Outline of the Present Study:

Recently, the ligand-based incomplete/partial ET to Eu^{III} metal center leads to white light generation becomes attractive research task [9]. The known white emissive lanthanide complex is limited to solution phase. White emissive lanthanide complex is scarcely reported. In the previous chapter, triphenylamine (TPA) functionalized imidazole-phenanthroline based new bipolar ligand for monochromatic red light emitting Eu^{III} complex was explored [10]. In addition, to get highly efficient monochromatic red light emission and analyze the functionalization (extended TPA moiety with diphenylamine (DPA)) effect on the photoluminescence (PL) emission of the bipolar ligand by means of ET to Eu^{III} metal ion, the DPA decorated phenanthroline-fluorene-TPA bipolar ligand, Phen-Fl-TPA-DPA and its corresponding β-diketonate Eu^{III} complex, $Eu(TTA)_3$Phen-Fl-TPA-DPA have been synthesized. The designed strategy assumption is that the fluorene can improve the morphological and photostability of the Eu^{III} phosphors, because of its strong π-π* absorption. The presence of diphenyl amine moieties in the neutral or bipolar ligand, widen the absorption outline and act as light-harvesting units. TTA can act as an antenna and it is well documented that the presence of fluorine in the ligand can decrease the vibrational quenching and increase the decay time at room temperature [11]. In Eu^{III} complex, ET to center metal ion from neutral ligand, as well as the antenna, is expected in the presently studied Eu^{III} complex (Figure 5.1). The ligand not only plays a role as a sensitizer for the Eu^{III} ion through antenna effect, it is also a

yellow emitting source. It is familiar that the emissions of Eu^{III} metal ions were commonly employed as a structural probe to investigate the coordination and local environment around the cations.

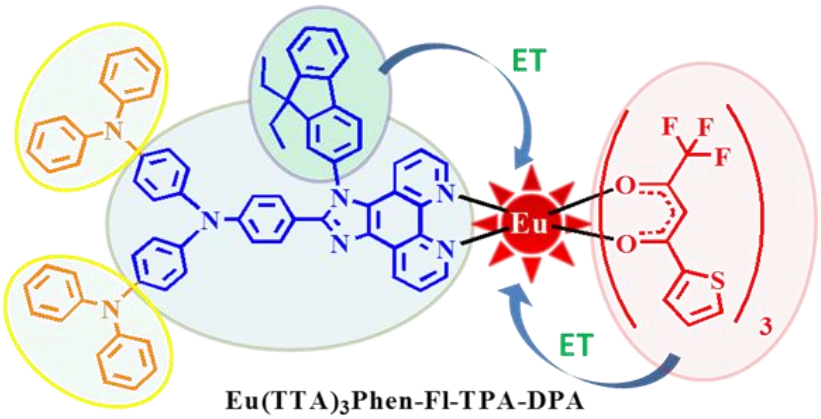

Figure 5.1 The chemical structure of synthesized Eu^{III} complex.

5.2.2 Experimental:

5.2.2.1 Materials and general Information for synthesis:

The details of starting materials for the synthesis and electrolyte materials used in the CV were included in the previous Chapters 2 (2.2.2) and 3.

5.2.2.2 Measurements:

The detailed measurement techniques that are used for the characterization of ligands and respective complexes were mentioned in the previous Chapters 2 (2.2.2, Experimental section). NMR and Mass spectra is given in Figure 5.S1 – 5.S4.

5.2.2.3 Synthesis:

The compounds 4-(diphenylamino)benzaldehyde (1-1), 4-(bis(4-iodophenyl)amino) benzaldehyde (1-2) [12], and 4-(bis(4-(diphenylamino)phenyl)amino) benzaldehyde (1-3) were synthesized by reported references [13, 14]. Synthesis of 1,10-phenanthroline-5,6-dione, 9,9-diethyl-9H-fluoren-2-amine (Fl) and the metal compound tris(thenoyltrifluoroacetone)europium (III) ($Eu(TTA)_3{\cdot}2H_2O$) was explained in Chapter 2.

5.2.2.3.1 *Synthesis of N^1-(4-(diphenylamino)phenyl)-N^1-(4-(1-(9,9-diethyl-9H-fluoren-2-yl)-1H-imidazo[4,5-f][1,10]phenanthrolin-2-yl)phenyl)-N^4,N^4-diphenylbenzene-1,4-diamine (Phen-Fl-TPA-DPA)*:

9,9-diethyl-9H-fluoren-2-amine (Fl) (0.75 g, 3.171 mmol) was added to a stirred solution of 1-3 (1.75g, 2.883 mmol) in glacial acetic acid (30 mL) at room temperature. To this reaction mixture subsequently ammonium acetate (2.2 g, 28.83 mmol) and dione (0.60 g, 2.883 mmol) was added. Then the resulting mixture was stirred for 12 hrs at 110 °C. The progress of the

reaction was monitored by TLC (MeOH in chloroform 1:9, Rf-0.2). The reaction mixture was pour into minimum amount of water and then ammonium hydroxide solution was added. Then the formed solid was filtered and dissolved in dichloromethane, followed by dried with anhydrous sodium sulphate and the solvent was evaporated to get crude compound 3g. The resultant compound was purified with column chromatography by using silica gel (100-200 mesh), eluent with 5% methanol in chloroform and the solvent was evaporated and dissolved in minimum amount of THF solution added excess of hexane solvent, the pale yellow color solid was formed. After settling of solid, decantation was done and this process repeated to get compound 1g (51.1%) as a pale yellow solid. ^{1}H-NMR Data ($CdCl_3$, 400 MHz): δ (in ppm) 9.21-9.16 (m, 2H), 9.03 (d, 1H), 7.91 (d, 1H), 7.87-7.76 (m, 3H), 7.62-7.45 (m, 8H), 7.25-7.16 (m, 9H), 7.14-7.06 (m, 11H), 7.01-6.96 (m, 11H) 2.05 (q, 4H), 0.42 (t, 3H), 0.24 (t, 2H). ^{13}C-NMR Data ($CdCl_3$, 100 MHz): δ (in ppm) 152.6, 150.2, 147.8, 147.6, 143.7, 139.8, 136.5, 130, 129.3, 129.2, 128.5, 127.4, 126, 124.9, 124.2, 124.1, 123.9, 123.6, 123.2, 123.1, 122.8, 122.6, 122.2, 121.4, 120.4, 56.7, 32.7, 8.3. EI-MS: m/z = 1018.82 $[M + H]^+$.

5.2.2.3.2 *Synthesis of Eu(TTA)$_3$ Phen-Fl-TPA-DPA*:

The procedure of Phen-Fl-TPA-DPA was coordination with $Eu(TTA)_3.2H_2O$ and followed previous procedure from Chapter 2 (section 2.2.2.9) to synthesis of $Eu(TTA)_3$ Phen-Fl-TPA-DPA. CHNS Analysis%: Anal. Calc. for: $C_{96}H_{67}EuF_9N_7O_6S_3$; C, 62.88; H, 3.68; N, 5.35; S, 5.25%. , Found: C, 62.96; H, 3.88; N, 5.25; S, 5.45. EI-MS: m/z = 1831.97 $[M - H]^+$.

5.2.2.4 Characterization of the complex:

The detailed synthesis of Eu^{III} complex is summarized in Scheme 5.1.

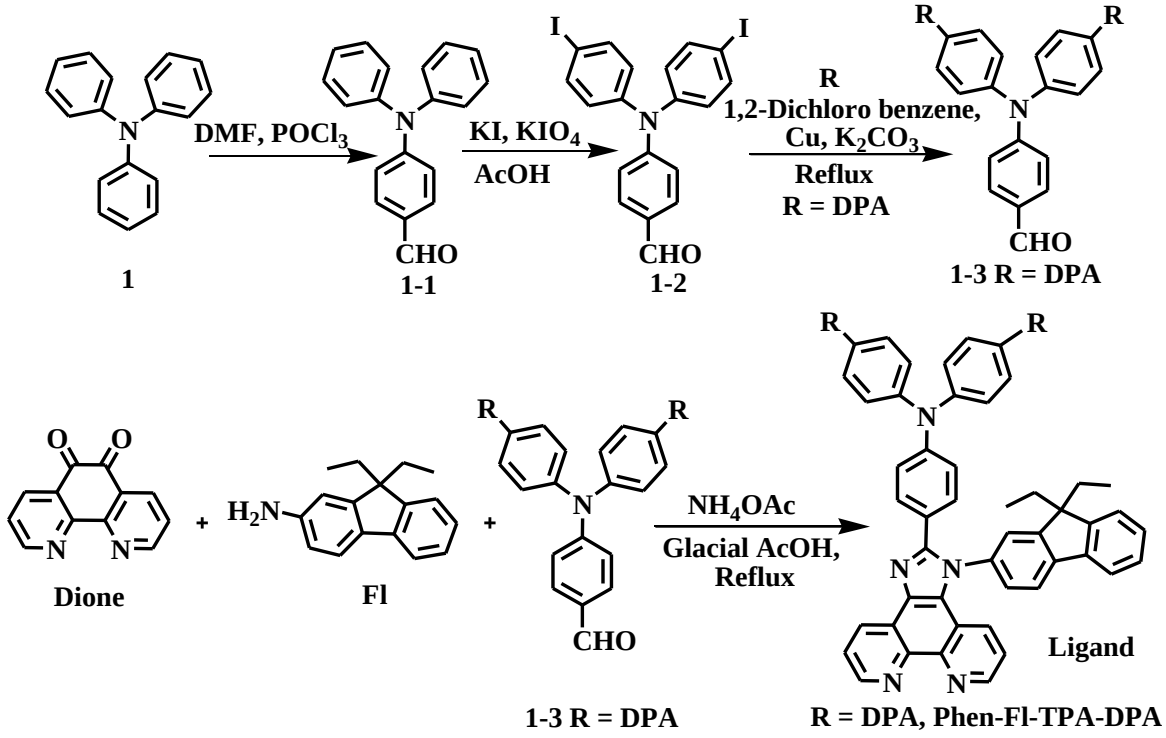

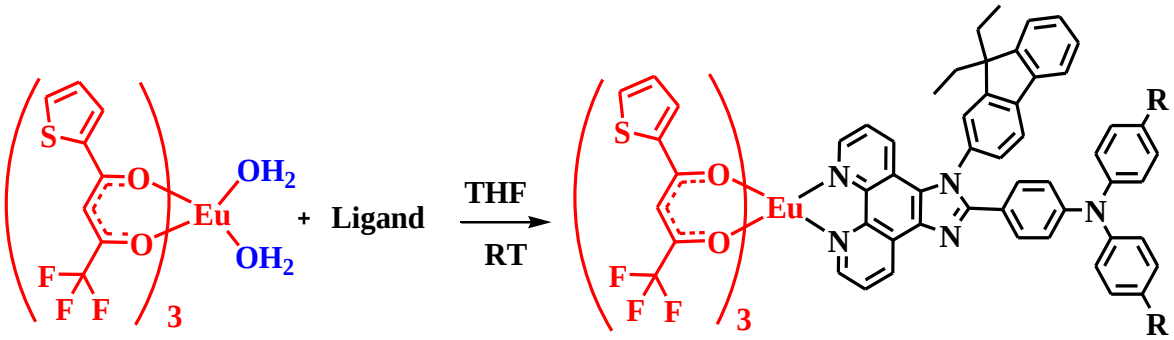

Eu (TTA)$_3$ .2H$_2$O **R = DPA, Eu(TTA)$_3$Phen-Fl-TPA-DPA**

Scheme 5.1 Synthetic route of triphenyl functional-DPA based ligand and corresponding β-diketonate Eu^{III} ternary complex.

5.2.2.5 FT-Infrared spectroscopy:

The FT-IR spectra of the Eu(TTA)$_3$.2H$_2$O complex shown strong carbonyl (C=O) stretching frequency at 1610 cm^{-1} and the same is shifted to 1598 cm^{-1} for the Eu(TTA)$_3$Phen-Fl-TPA-DPA (Figure 5.2). The change in the stretching frequency is an indirect evidence to that the β-diketonate (Eu(TTA)$_3$·2H$_2$O) compound is coordinated with the synthesized neutral ligand. The vibration frequency due to C=N appears at 1589 cm^{-1} for free ligand Phen-Fl-TPA-DPA. After metalation of ligand, the C=N peaks is shifted towards the lower wavenumber (1536 cm^{-1}).

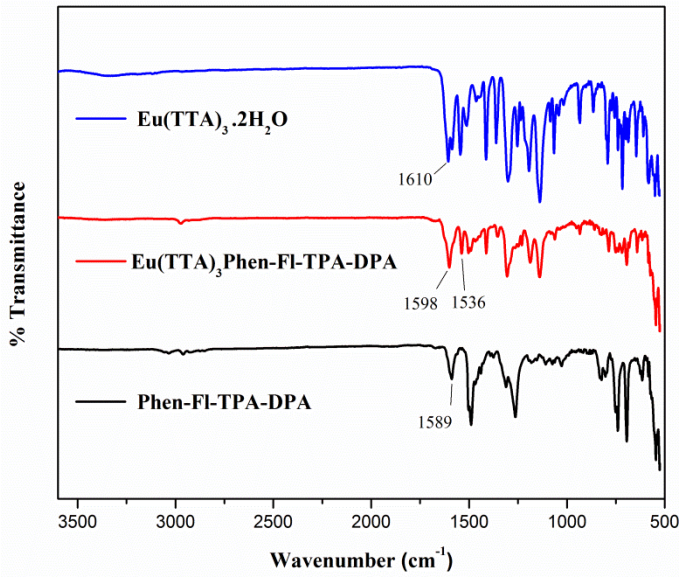

Figure 5.2 FT-IR spectra of the ligand, corresponding Eu^{III}-complex and Eu(TTA)$_3$·2H$_2$O.

5.2.3 Results and Discussion:

5.2.3.1 Thermal properties and Powder X-ray diffraction (PXRD) studies:

To study the thermal stabilities of the bipolar ligand (Figure 5.3, left) and Eu^{III} complex (Figure 5.3, right), thermogravimetric analysis (TGA) and differential scanning calorimetry (DSC) were performed (powder samples) under nitrogen atmosphere from

ambient temperature to 650 °C. The TG analyses were shown that the thermal decomposition occurs above 250 °C for Eu-complex.

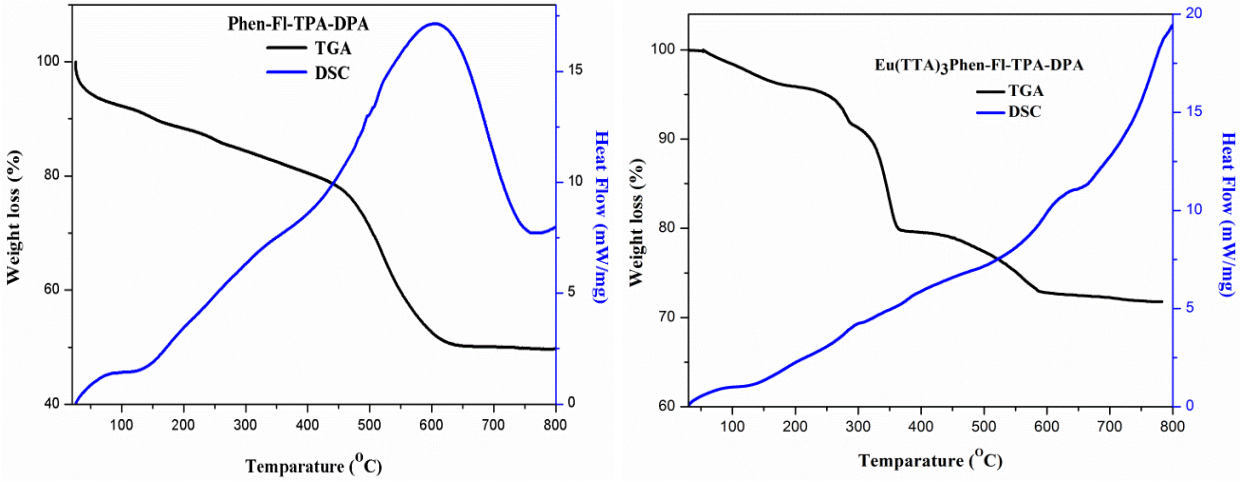

Figure 5.3 DSC-TG analysis curves for the ligand (left) and Eu^{III} complex (right).

Thermal decomposition of $Eu(TTA)_3$Phen-Fl-TPA-DPA shown 271, 336, 503 °C. When compare the thermal decomposition of ligand, Phen-Fl-TPA-DPA (> 350 °C) with Eu^{III} metal complex, ligand was shown less thermal decomposition. It is expected that due to elimination and/or decomposition of ligands, it means the presence of TTA moiety and additional DPA, fluorine groups in the Eu^{III} complex. These results are suggesting that the $Eu(TTA)_3$Phen-Fl-TPA-DPA have good thermal stability above 250 °C which is good for fabrication of the device.

The powder XRD pattern of the Eu complex was executed to find the crystalline or amorphous nature of the Eu^{III} complex and the X-ray pattern is shown in Figure. 5.4. The observed pattern clearly indicates that the complex is in amorphous nature, and this could be useful in fabrication of OLEDs using this Eu^{III} complex as an emission material.

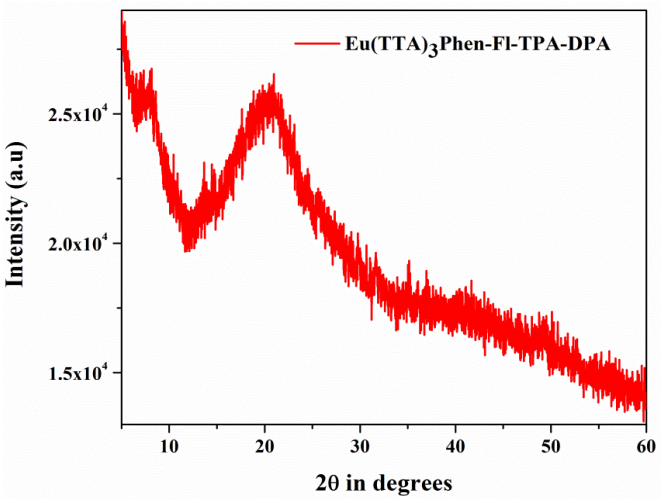

Figure 5.4 PXRD data plot of the Eu^{III} complex

5.2.3.2 Photophysical properties:

5.2.3.2.1 UV-Visible absorption and diffuse reflectance spectral studies:

The UV-Visible absorption spectra of the ligand and Eu^{III} complex were carried out in solution ($CHCl_3$, 1.0×10^{-4} mol L^{-1}), thin film and the solid state (Figure 5.5, left). The absorption spectrum of ligand shows absorption from 240 to 450 nm with λ_{max} values are 306, 280 nm (attributed to the $\pi \rightarrow \pi^*$ transitions of aromatic moieties). The same was verified theoretically by the TD-DFT method, which supports the experimental findings (Figure 5.5, right). The band gap for the Phen-Fl-TPA-DPA ligand (Figure 5.6, left) and corresponding Eu^{III} complex (Figure 5.6, right) calculated from diffuse reflectance spectra and found both ligand and the complex shows similar band gap values (2.6 eV, Table 5.1). Similarly, the absorption studies of Eu^{III} complex and $Eu(TTA)_3 \cdot 2H_2O$ shows the peaks maxima at 340, 296 nm and 340, 275 nm, respectively.

The Eu^{III} complex shown similar peaks which are observed for the ligand as well as $Eu(TTA)_3$ and it is suggesting that the presence of the ligand in the corresponding Eu^{III} complex. The thin film absorption study of Eu^{III} complex shown peaks at 312, 378 nm, whereas the solid (diffuse reflectance spectra, DRS) shown a wide absorbance from 250 to 440 nm. Ligand in solid state was shown peaks maxima at 396, 284 nm. The comparative study of absorption spectra of the Eu^{III} complex in solution, thin film and solid indicates that the absorption maximum shift to longer wavelength for solid phase as compared to that of complex in solution and thin film. The observed bathochromic shift in the absorption spectra is due to the aggregation of the complex in the solid state [9].

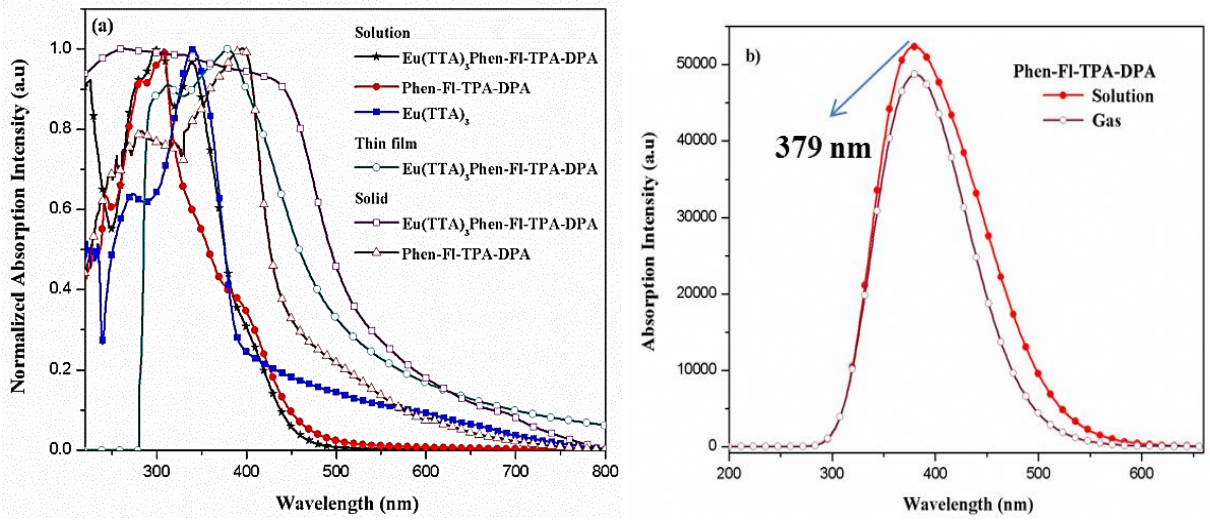

Figure 5.5 The UV-Vis absorption spectra of Eu $(TTA)_3$Phen-Fl-TPA-DPA in chloroform solution and their comparison study in solution as well as thin film (left), The ligand absorption spectra by theoretical analysis in gas as well as solution (right)

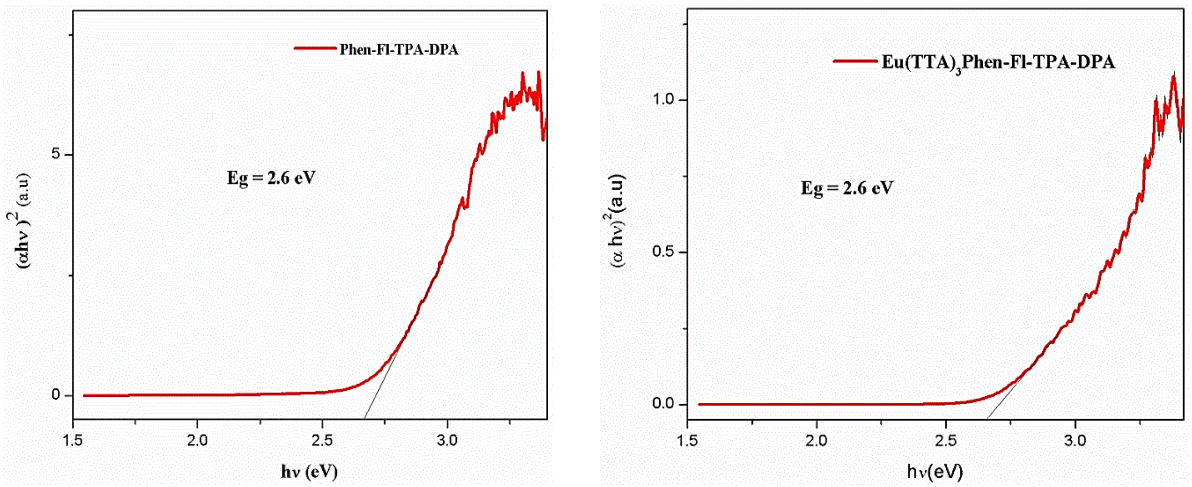

Figure 5.6 The DRS of Phen-Fl-TPA-DPA ligand (left) and corresponding Eu^{III} complex (right).

5.2.3.2.2 Photoluminescence and solvatochromism studies:

The PL emission of the ligand was shown 400 to 700 nm (wide spectral range covering the entire visible spectral window) with a maximum at 517 nm at different excitation wavelengths (285, 305 and 365 nm) in chloroform solution (Figure 5.7, right). To further, understand the broad emission nature of ligand; the same study (PL excitation and emission) was executed in different solvents. Among all the solvents, emission in toluene solution shown distinct behavior. It was kept in mind and stimulated for furthered analysis. The optical properties of the complex in a thin film, as well as solid form (Figure 5.8, left) and their CIE color coordinates (Figure 5.8, right, Table 5.2), are studied. In the case of Eu^{III} complex shown characteristic red emission from Eu^{III} ion at 612 nm, along with that the emission belongs to ligand also been observed ranging from 400 to 600 nm with peak maxima at 517 nm. Based on the above experimental results, it was estimated and attributed that the partial energy transfer from ligand to center metal ion lead to orange-red emission, instead of pure red (Figure 5.10). This is because the intensity ratio (2:1) of red emission is higher than that of yellow emission from the ligand. The CIE color coordinates for the complex in solution (x = 0.34, y = 0.45), solid (x = 0.44, y = 0.40) and thin film (x = 0.59, y = 0.41) refucting the same. Precipitously came to mind about the Latva *et al.,* investigations (i.e) difference between ligand ($^3\pi\pi^*$) and the Eu excited state ($^5D_0$) should be > 2500 cm^{-1} for efficient ET [15]. It is known that the singlet and triplet energy level of the TTA are located at around 25164 (3.12 eV) and 18954 cm^{-1} (2.35 eV) [16], and Eu^{III} metal ion excited $^5D_0$ energy level located at 17500 cm^{-1} [17]. However, to understand the ET in the Eu^{III} complex; it is essential to know the exact location/position of singlet and triplet energy levels of ligand [18].

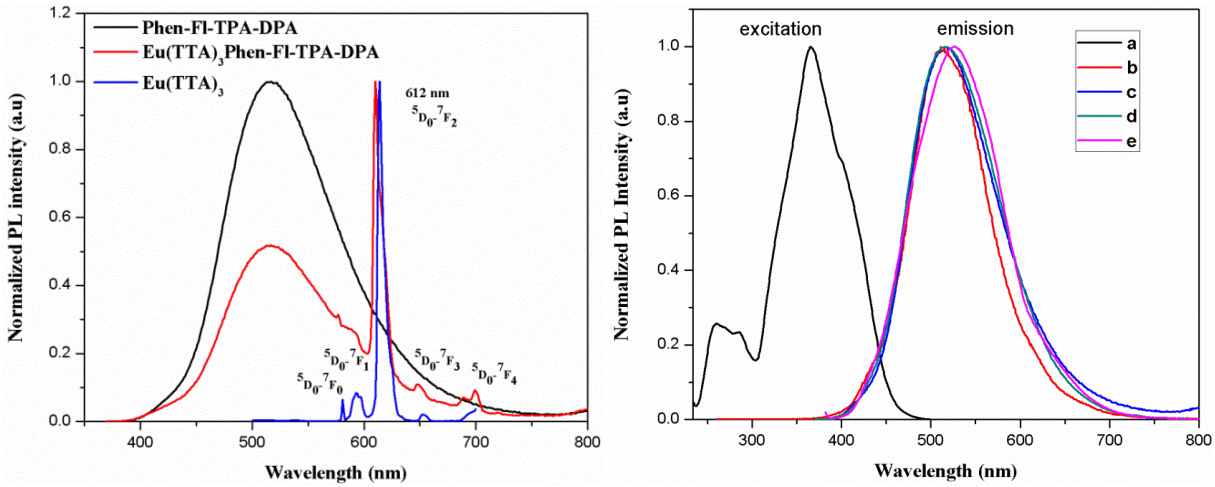

Figure 5.7 The PL emission spectra of ligand (Phen-Fl-TPA-DPA) and Eu metal ion in chloroform solution (left) and the PL excitation and emission spectra of Phen-Fl-TPA-DPA (right). a) excitation (λ_{ex} = 517 nm) and b, c, d, e are emissions at different wavelengths (λ_{em} = 257, 294, 365 and 380, respectively).

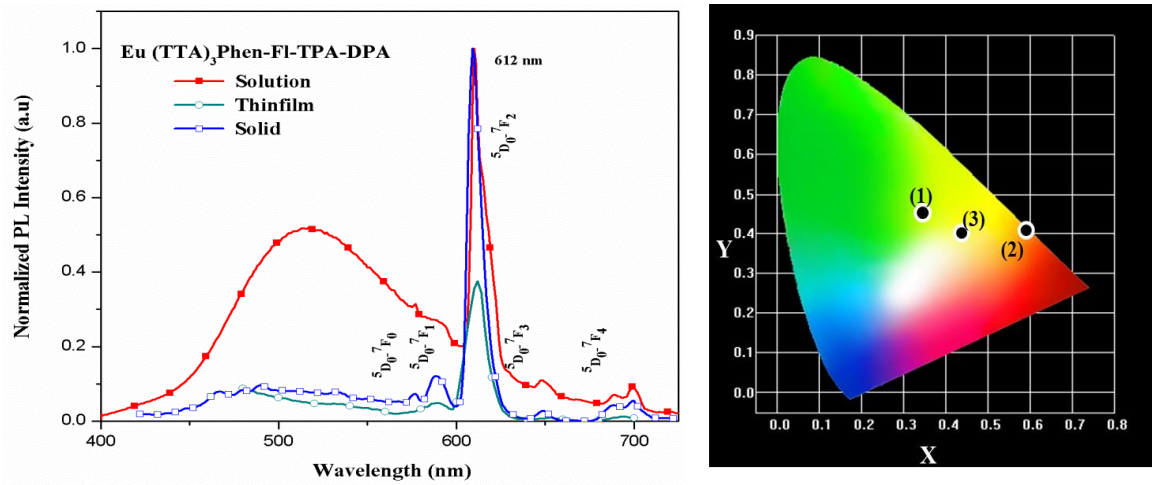

Figure 5.8 The comparison of PL emission spectra of europium metal ion in solution, thin film and solid (left), CIE color coordinates of the Eu^{III} complex in solution, thin film and solid (right).

Synthesized Eu^{III} complex and ligand under UV lamp ($Eu(TTA)_3$Phen-Fl-TPA-DPA, $Eu(TTA)_3$ and Phen-Fl-TPA-DPA) in different solvents shown in Figure 5.9. The solvatochromism is necessary to understand solvent-dependent PL emission of the ligand. The PL emission of the ligand was performed in different solvents, such as toluene, dichlorobenzene (DCM), tetrahydrofuran (THF), acetone, ethylacetate (EtOAc), chloroform ($CHCl_3$), methanol (MeOH), dimethylformamide (DMF), and dimethylsulphoxide (DMSO) and measured their stoke's shift values (Figure 5.10). The obtained results for ligands (from emission spectra) interpreted in terms of Lippert-mataga equation. Based on the increasing the polarity of the solvent, there is a spectral shift observed towards high wavelength and shown red / batho chromic shift. The obtained results and calculations are incorporated in Table 5.2.

Table 5.1. The UV-absorption, PL emission and CIE color coordinates data of synthesized Eu^{III}-complex and corresponding ligand.

S. No.	Compound	λ_{max} (abs) [nm] Solution (a)(b)	Thin film (c)	λ_{ex} (a) [nm]	λ_{em} (a) (d) [nm]	PL QY [%]
1	**$Eu(TTA)_3$Phen-Fl-TPA-DPA**	276, 304, 340	311, 378	276, 304, 365	517, 580, 592, 612, 652, 703	15.3
2	**Phen-Fl-TPA-DPA**	280, 306, 382	--.--	275, 294, 365, 380, 390, 400	517	--.--
3	**$Eu(TTA)_3$**	273, 340	--.--	275, 340	580, 592, 612, 652, 703	--.--

a) measured in chloroform solution, b) absorption peaks from the UV-absorption spectra, c) thin film made on glass substrate, d) emission peaks from photoluminescence emission spectra.

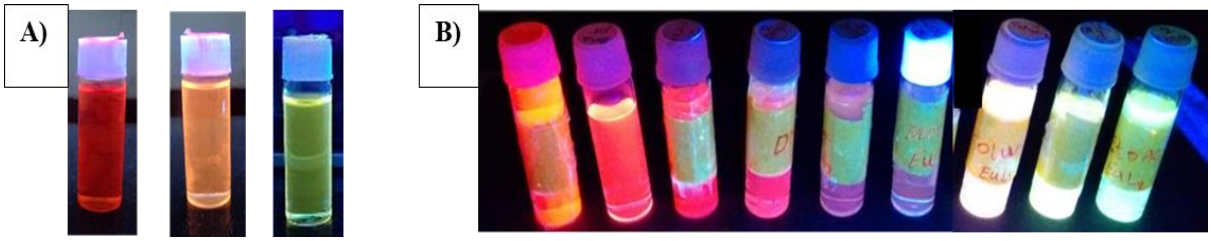

Figure 5.9 Synthesized Eu^{III} complex and ligand under UV lamp. A) $Eu(TTA)_3$Phen-Fl-TPA-DPA (middle), $Eu(TTA)_3$ (left) and Phen-Fl-TPA-DPA (right). B) In different solvents from left to right are ACN, Acetone, MeOH, DMSO, DMF, DCM, Toluene, THF, EtOAc.

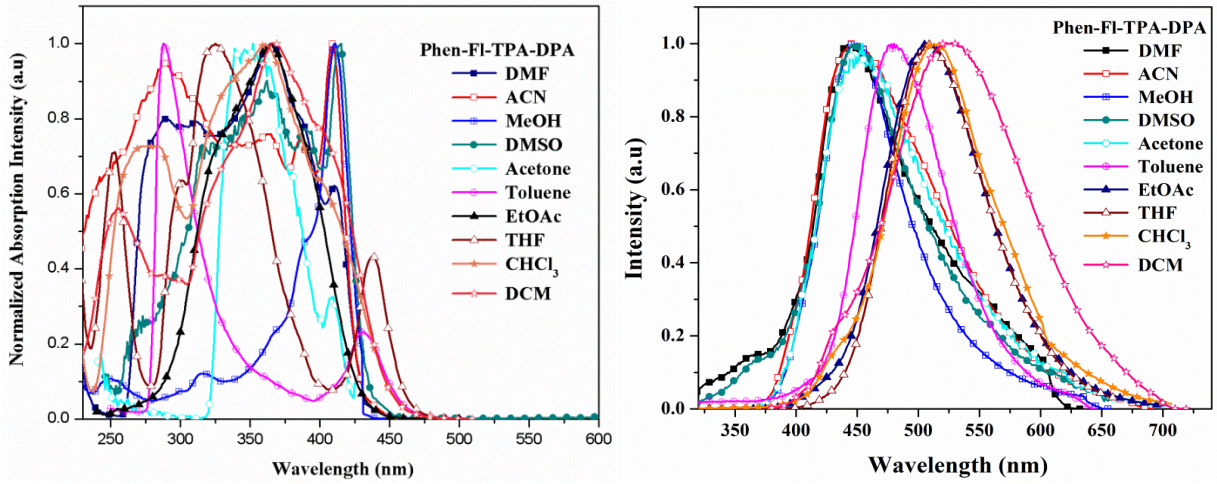

Figure 5.10 The solvent effect of Phen-Fl-TPA-DPA of PL excitation (left) and emission (right) spectra in different solvents.

The following equations (equation 2.11, 2.12) of Lippert−Mataga describes the solvatochromic stokes shift $\Delta\bar{\nu}$ (expressed in wavenumbers) as a function of the change of the dipole moment $\Delta\mu_{ge} = \mu_e - \mu_g$ of the dye. The several solvents are performed with dissimilar dielectric constants (ε) and refractive indices (n) and the plot of $\Delta\bar{\nu}$ as a function of Δf (Figure 5.11) indicating that the linear relationship [correlation coefficient r = 0.72] of the Stokes shift

for the 9 solvents of DPA ligand. The linear fitting of the ligand shown in Figure 5.11 with incorporated with their slope and intercept (cm^{-1}).

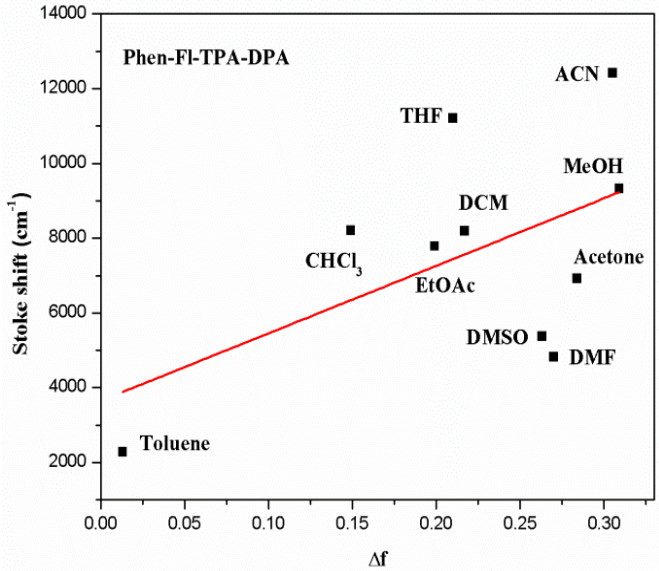

Figure 5.11 The linear stoke's shift vs Δf fitting of Phen-Fl-TPA-DPA.

Table 5.2 PL spectral data of ligands in various solvents.

Phen-Fl-TPA-DPA	λ_{abs} (max) (nm)	λ_{em} (max) (nm)	Stoke's shift (Δν) (cm^{-1})
Toulene	428	480	2336
DCM	367	525	8200
THF	335	509	10204
$CHCl_3$	399	517	5569
EtOAc	364	508	7787
MeOH	316	448	9324
Acetone	346	455	6924
ACN	290	440	11755
DMF	314	443	9273
DMSO	348	448	6414

5.2.3.2.3 Theoretical study:

To understand the reason behind the complete or partial ET, calculated the excited energy states of the ligand were calculated by employing TD-DFT methodology embedded in G09 programme [19]; which was shown great supportive results of the singlet and triplet energy levels located at 23,256 (2.88 eV) and 19,960 cm^{-1} (2.47 eV), respectively (Figure 5.12, left). The difference between the triplet excited state and Eu^{III} metal ion excited $^5D_0$ energy level is shown less than 2500 cm^{-1} and also excited singlet shown less than 25,000 cm^{-1}. The ligand singlet and triplet state energy level, ΔE ($^1\pi\pi^*$–$^3\pi\pi^*$) difference is 3296 cm^{-1}, which is less than 5000 cm^{-1}. These lower energy levels of ligand were suggested that the energy can back transfer from Eu^{III} excited state ($^5D_0$) to the ligand is reversible [20]. It is a very clear indirect indication that the PL emission of Eu^{III} complex shows both ligand (yellow) and Eu^{III} ion (red) emission. The optimized

structure of the ligand (Blue: N) shown in Figure 5.13, right. To calculate the triplet energy of the ligand, the emission spectrm was recorded for the corresponding Gd-complex at 77 K (Figure 5.13). From the phosphorescence spectra, the triplet energy level was found to be at 20,408 cm^{-1}, and the slight deviation was observed for experimental and theoretical study of the triplet level. The above strategy was supported to made idea to get white light emission by a single molecule. If balance the ligand broad (BG) emission and Eu^{III} (R) emission can white light generate. Foremost analyzed emission spectra for Eu^{III} complex with different concentrations (1, 10, 20 and $75x10^{-5}$ mmol) in chloroform solution.

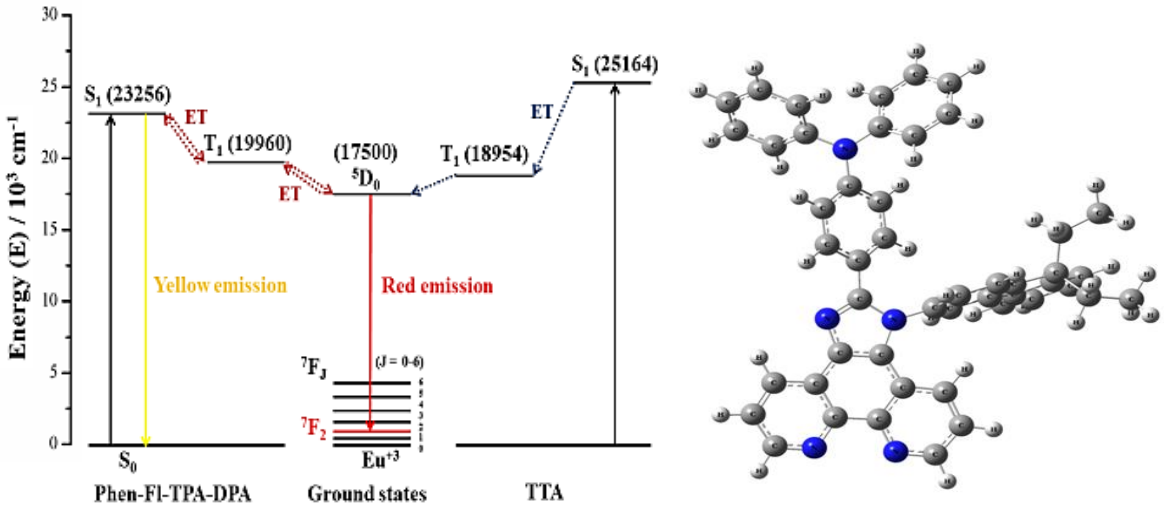

Figure 5.12 Energy transfer process from the ligand to Eu^{III} metal ion (left), the optimized structure of the ligand (Blue: N).

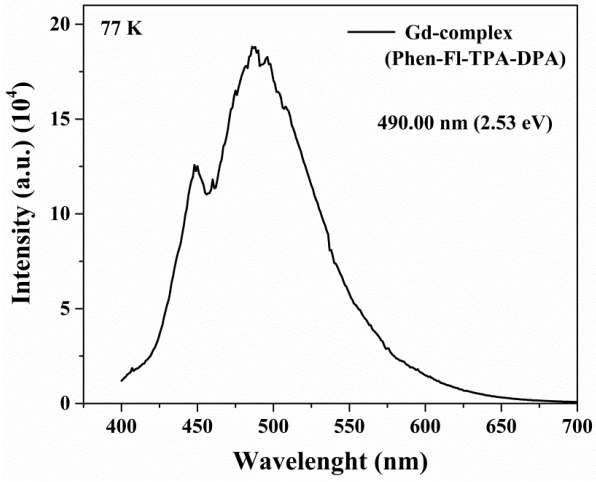

Figure 5.13 The phosphorescence spectrum of DPA based Gd-complex at 77K.

However, no distinguished result was observed from the emission spectrum. On the other hand, red shift, as well as an increase in the emission intensity, was observed (ligand emission) by exciting with different excitation wavelengths for the Eu^{III} complex (Figure 5.14, left). The results, emission ratio of the ligand and Eu^{III} complex depicted in

the bar graph (Figure 5.14, right) as well as CIE coordinates also been given (Figure 5.15, left). So further, based on the above explanation of ligand emission strategy in different solvents; so it has been carried for the Eu^{III} complex in different solvents and the strange response results were perplexed. Perplex to perfection made extremely a white emission with appropriate CIE (0.31, 0.32; correlated color temperature (CCT) = 6558 K, Figure 5.16, right, Table 5.3) color gamut observed from the toluene (Figure 5.16, inset) due to the proper balance between primary colors. CIE color coordinates of the Eu^{III}-complex in different solvents shown in Figure 5.15 right.

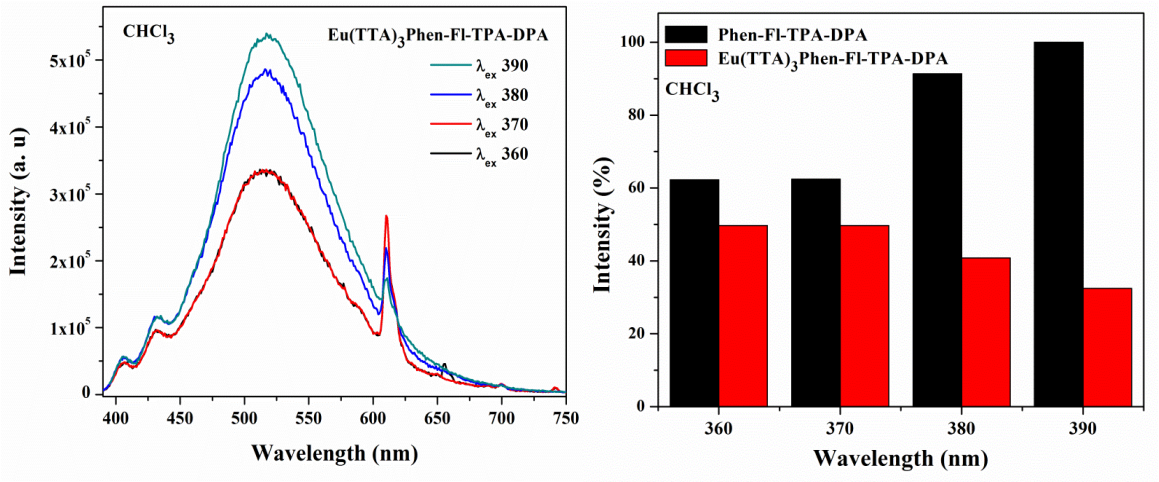

Figure 5.14 Exciting with different excitation wavelengths for the Eu^{III} complex in chloroform solution (left), the emission intensity ratio of the ligand and Eu^{III} ion in the bar graph for the Eu^{III} complex in chloroform solution (right).

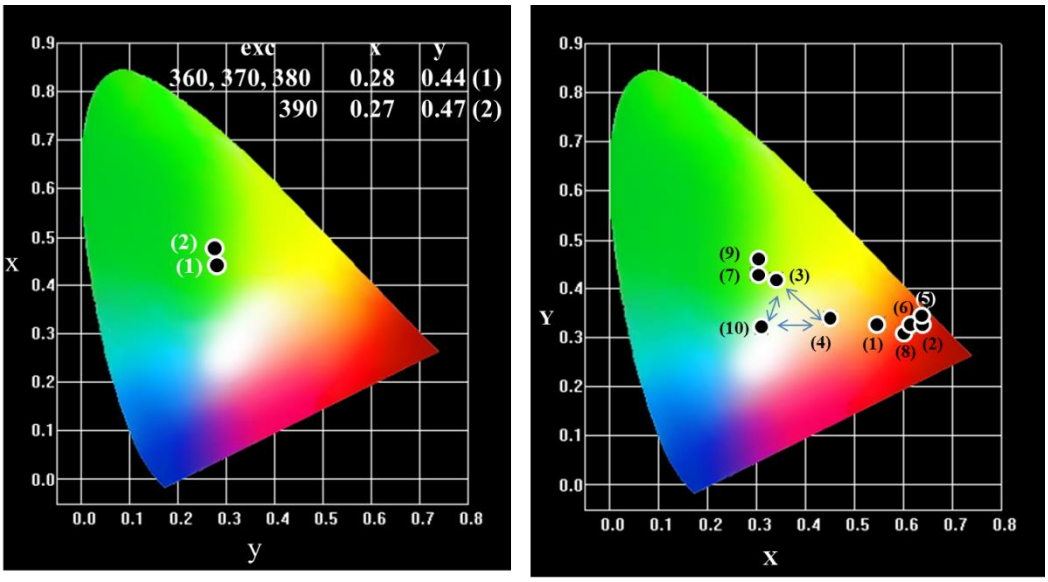

Figure 5.15 CIE coordinates for Eu complex in different excitation wavelengths (chloroform solution) (left), CIE color coordinates of the Eu^{III}-complex in different solvents (right).

Table 5.3 The CIE coordinates data of Eu^{III} complex (CCT – correlated color temperature).

S. No.	$Eu(TTA)_3Phen$-Fl-TPA-DPA	CIE Coordinates		CCT
		x	y	
1	**Acetone**	0.55	0.33	1623
2	**Acetonitrile**	0.64	0.33	2699
3	**Chloroform**	0.34	0.42	5134
4	**Dichloromethane**	0.45	0.34	2083
5	**DMF**	0.64	0.35	2214
6	**DMSO**	0.62	0.33	2359
7	**Ethyl acetate**	0.30	0.43	6377
8	**Methanol**	0.61	0.32	2401
9	**THF**	0.30	0.45	6130
10	**Toluene**	0.31	0.32	6417

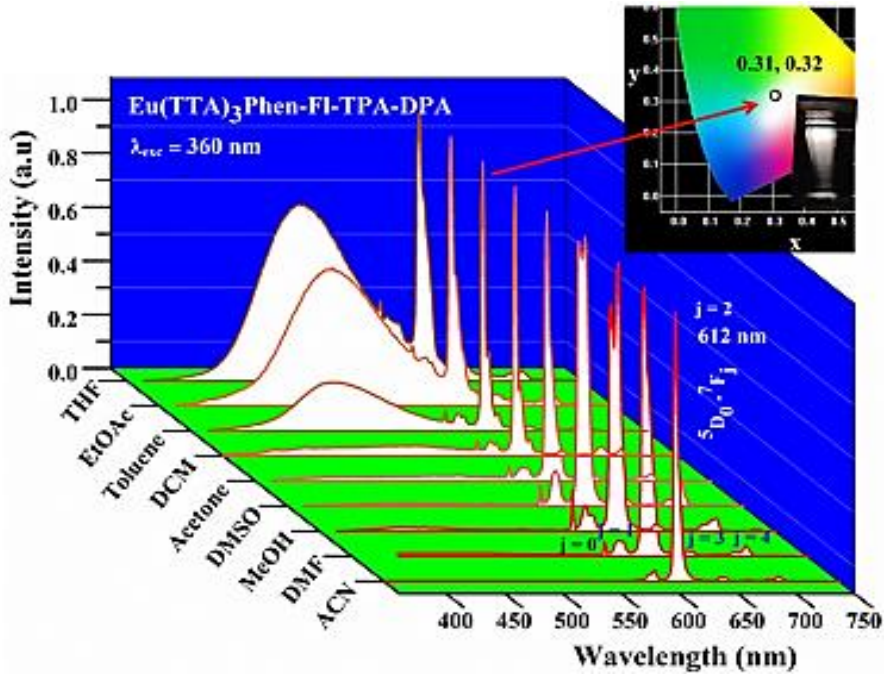

Fig. 5.16 Tthe Eu^{III} complex emission in different solvents and the white light emission in toluene with CIE color gamut (inset).

In addition, from solvatochromism analysis, it was found that the presently synthesized Eu^{III} complex acting as a single component white-light-emitting as well as tunable emission color by changing the solvent. The aromatic ring in toluene is more important. An antenna (ligand) present in the complex is responsible for partial sensitization to obtain white emission. It is due to less difference between the triplet state and Eu^{III} excited state. It was expected to be that the free rotation of phenyl rings of DPA molecule are sufficient in a less polar solvent (less density), which leads to the decrease of the energy level of the excited states of the ligand. In addition, to supporting the same, theoretical analysis has been carried to obtain the knowledge about the energy levels by arresting the C-C bond of DPA (CBZ). It is clear that the optimized CBZ moiety

consisted ligand shown high singlet (25,707 cm^{-1}, 3.18 eV) as well as triplet (21,277 cm^{-1}, 2.63 eV) energy levels, which was greater than DPA ligand. More polar solvents like ACN, DMF, DMSO, which was shown almost pure red emission reveals the sufficient energy gap (complete energy transfer). It is clearly indicating that the solvent plays a major role and the aromatic ring in toluene more preferable for white emission. Moreover to get the very close bright white emission (CIE, x = 0.33, y =0.33), different excitation spectral wavelength analysis were carried out and the results showed that the white emission at 380 nm is better (0.34, 0.33; CCT = 5152 K, Figure 5.17) than that of 360 nm excitation. For well understanding, CIE (Figure 5.18, left), as well as the emission ratio of the ligand and Eu^{III}, the complex has also been depicted in the bar graph (Figure 5.18, right).

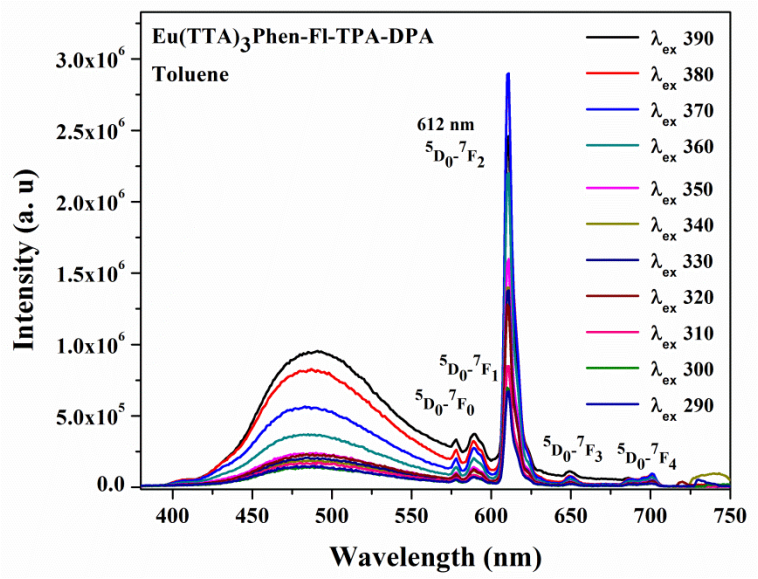

Figure 5.17 Different excitation spectral wavelength analysis of the Eu^{III} complex in toluene.

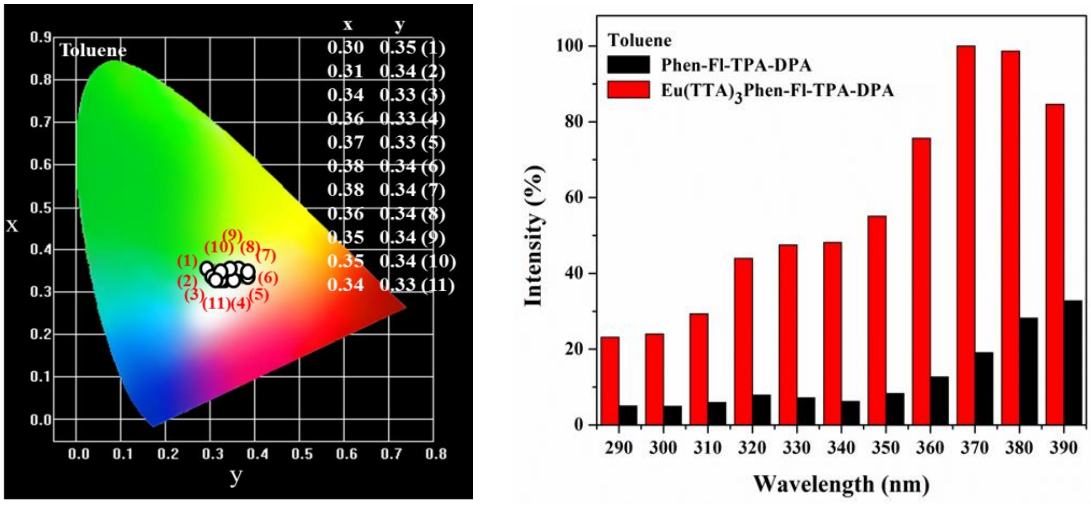

Figure 5.18 CIE for the different excitation spectral wavelength analysis of the Eu^{III} complex in toluene (left), the emission ratio of the ligand and Eu^{III} ion in bar graph for Eu^{III} complex in toluene (right).

Further understand the polar and less polarity solvent effect on white light emission, PL emission spectra were recorded by mixture of solvents (polar (ACN, pure Eu^{III} emission) and less polar (toluene, both ligand, and Eu^{III} emission)) by different ratios from 90 : 10 to 10 : 90, respectively (Figure 5.S5). The intensity of the Eu^{s}, 612 nm emission peak increased from toluene-ACN: 90-10 to 10-90 and the broad emission at 450-600 nm range decreases. The intense Eu^{III} emission (612 nm) shown higher in the pure solvent as compare to that of a mixture of solvents. The corresponding CIE color coordinates were also investigated (Table 5.ST1). It has also been observed that the decrease of intensity of Eu^{III} peak emission as well as increase the ligand emission by mixing of the toluene-EtOAc: 90-10 to 10-90 (Figure 5.S6), respectively and respective CIE coordinates are interpreted (Table 5.ST2). The above study plainly indicates that the solvent polarity plays a vital role.

5.2.3.2.4 Temperature dependent PL study:

Since the Eu^{III} complex was show dual characteristic (bluish-green and red) emission in solution. The temperature sensing application was explored for the presently standard Eu^{III} complex. The PL measurements were done 283-358 °C temperature range. The Eu^{III} complexes with organic ligands also showed high-temperature sensitivity, particularly with β-diketonates [21]. In the present study, when the temperature increasing, the ligand emission from the complex was enhanced as well as 612 nm (characteristic emission of the Eu^{3+} ion) peak intensity decreases and the emission color changed from orange-red (283K) → near white (303K) → green (358K) (Figure 5.19). Obtained temperature dependent PL emission color tuning will certainly give direction to use the presently studied Eu-complex as a temperature sensor. The details of the emission in different wavelength at with specific temperatures and respective CIE color coordinates were investigated (Figure 5.S7). Figure 5.20 shows the intensity ratio between the ligand and Eu^{III} emission (left) as well as the ED and MD transition ratios (right).

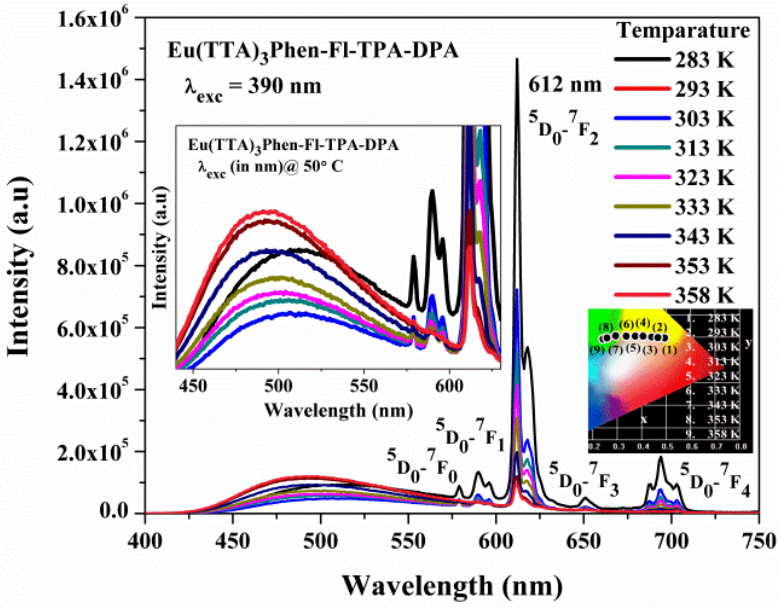

Figure 5.19 Eu^{III}-complex with different temperatures and in onset, ligand emission from Eu^{III} complex.

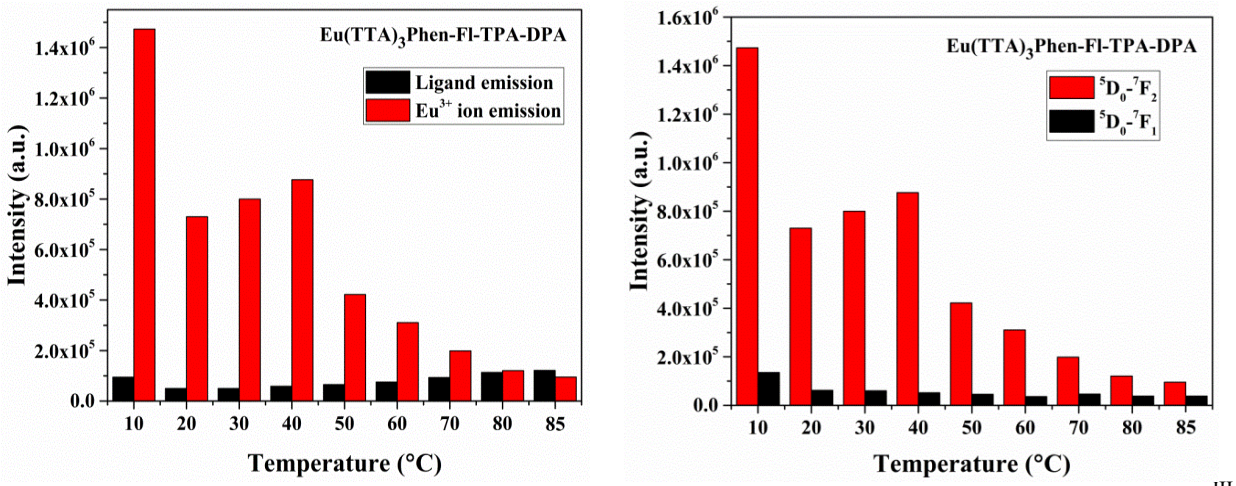

Figure 5.20 The bar graph of the ratio of the ligand emission and 612 nm emission from the Eu^{III} complex in different temperature with different excitation from 300-400 nm in toluene (left) and the bar graph for Eu complex with its intensity ratio (I_2/I_1) in different temperatures at 390 nm in toluene (right).

In addition, it is worth to note that the without DPA functionalization on Phen-Fl-TPA ligand in toluene was shown emission at 380 to 530 nm with 423 nm maxima (blue region) [9]. When DPA was connected, the emission shifted to be from 300 to 630 nm with a maximum at 480 nm (blue-green). However, the addition of Eu^{III} metal ion to DPA ligand the emission spectrum covered from 410 to 630 nm broad range (blue to red) (Figure 5.21). It is also observed in other solvents (THF, EtOAc, DCM, $CHCl_3$). Although primary RGB color balance was observed in only toluene, which leads to white light. To the best of our knowledge white light emission from the Eu^{III} complex with imidazole based neutral ligand observed for the first time. It is also notable that, in the above-mentioned strategy was also influence the PLQY of the Eu^{III} complex was shown 15.3%. The PLQY indirectly supports the partial ET from ligand to center Eu^{III} metal ion.

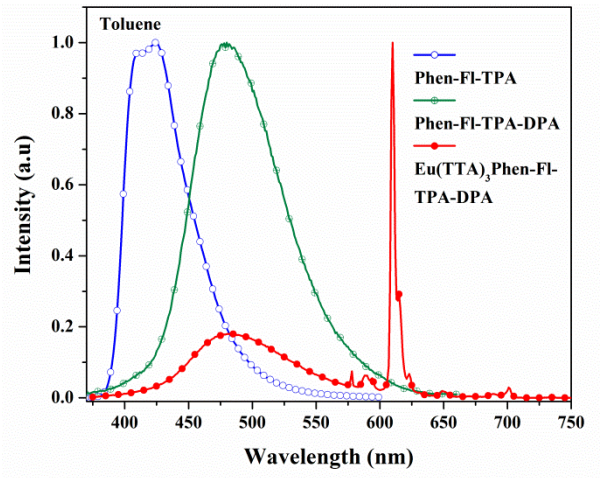

Figure 5.21 The emission of ligand before and after addition of DPA and corresponding DPA connected Eu^{III} complex (370 nm) in toluene.

5.2.3.2.5 PL Lifetime study:

From the lifetime measurement, it was assessed that the incomplete energy transfer influenced on lifetime decay time. Due to this, the solid was shown less lifetime (75.5 μS) than the solution. The succession was followed as DMF (458 μS) > Acetone (261 μS) > DCM (244 μS) > THF (224 μS) > $CHCl_3$ (205 μS) > solid under 360 nm excitation (Figure 5.22).

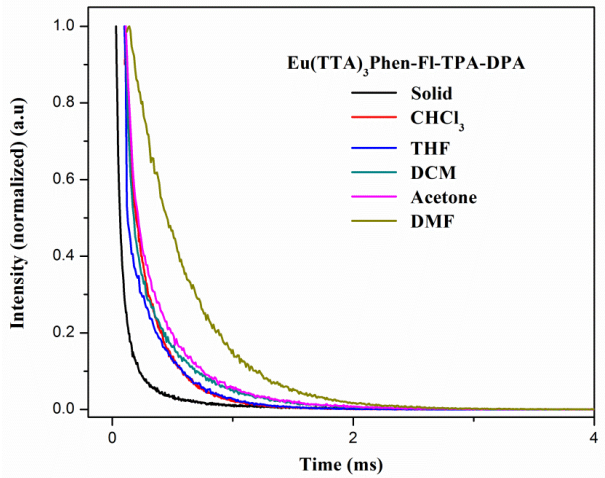

Figure 5.22 Lifetime of the Eu^{III}-complex in solid and in different solvents (λ_{exc} =360 nm).

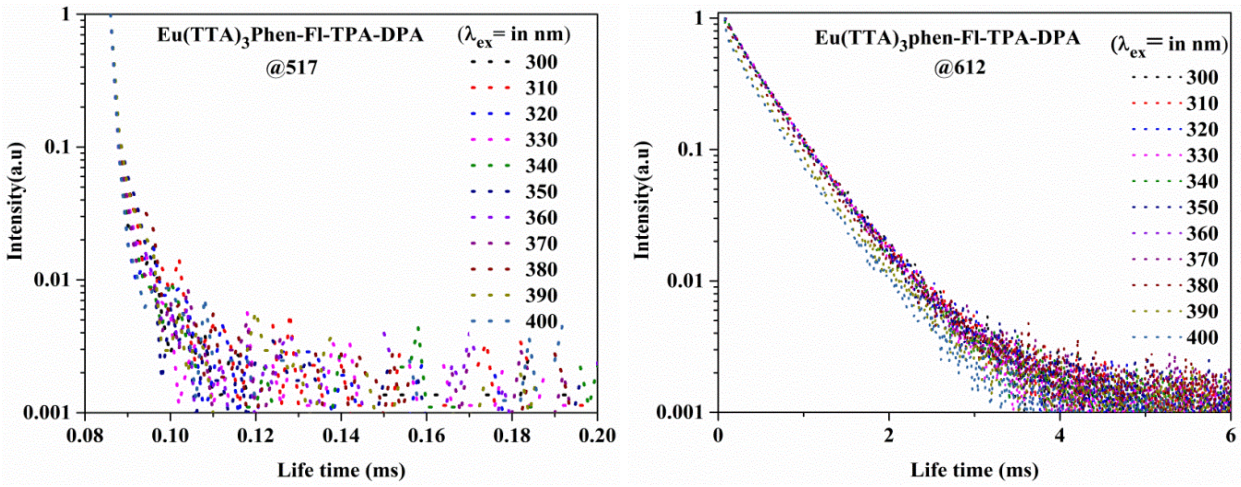

Figure 5.23 The lifetime of the Eu^{III} complex at 517 (left) and at 612 nm (right) as emission barrier and excited with different excitation source from 300-400 nm in solution phase.

In order to further understand the energy transfer process and emission contribution (ligand and Eu^{III} ion), the PL lifetime measurements with different monitoring wavelength were executed. In addition, different excitation wavelengths (spectral window, 300 – 400 nm with the interval of 10 nm) have also been used to measure the lifetime with the monitoring wavelengths 517/500 nm (solution/solid) ligand and 612 nm Eu^{III} emissions in the complex. The lifetime of the complex in solution with 517 nm as a monitoring wavelength was shown similar outcomes. However, in the case of 612 nm as a monitoring wavelength; from 300 to 360 nm excitation shown similar results, however beyond which the lifetime started decreasing and finally at 390 nm shown very

less contribution (shown in Figure 5.23 and 5.24 (bar graphs are shown in inset). In the case of solid, the contribution from 612 nm as a monitoring wavelength is more than 500 nm PL lifetime (Figure 5.25, 5.26).

The obtained lifetime results (Table 5.4) are clearly supporting that the ligand as well as Eu^{III} emission observed in solution, while in the case of solid, little ligand emission contribution along with Eu^{III} red emission. The ligand exhibits distinct excited-state rotation conformation in different polarity solvents, which might be quite common in polarity-dependent fluorophores. Therefore, the white-light emission in toluene may come from the mixture of either several excited states or even ground states.

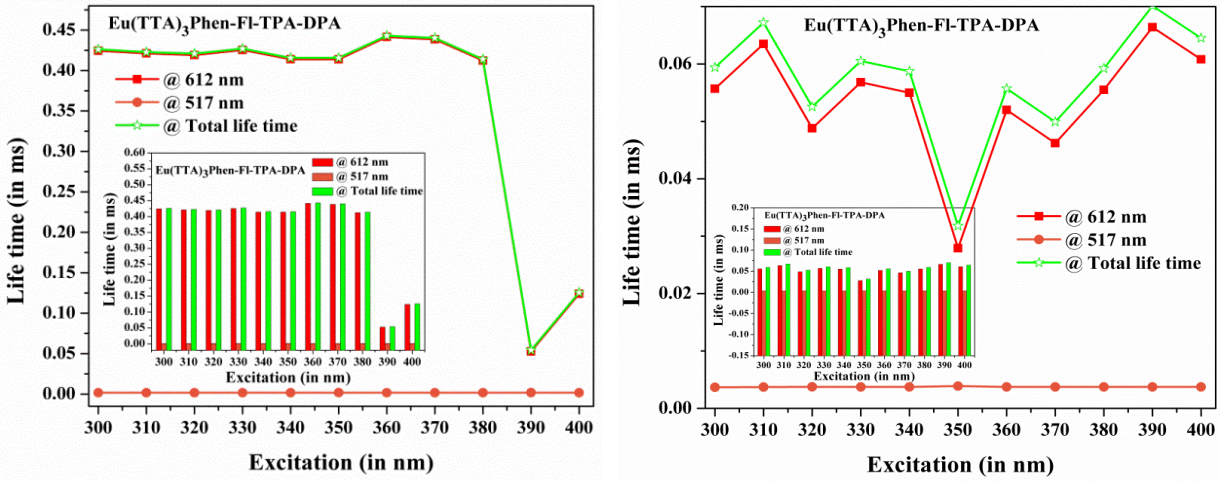

Figure 5.24 The pictorial view of the excitation source verses lifetime of the Eu^{III} complex at 517 and at 612 nm as an emission barrier with different excitation source from 300-400 nm in solution phase. The inset of the image indicates that the ratio of lifetime contribution from 517 as well as from 612 and its resulting lifetime from 300-400 nm excitation source in solution (left) and solid (right).

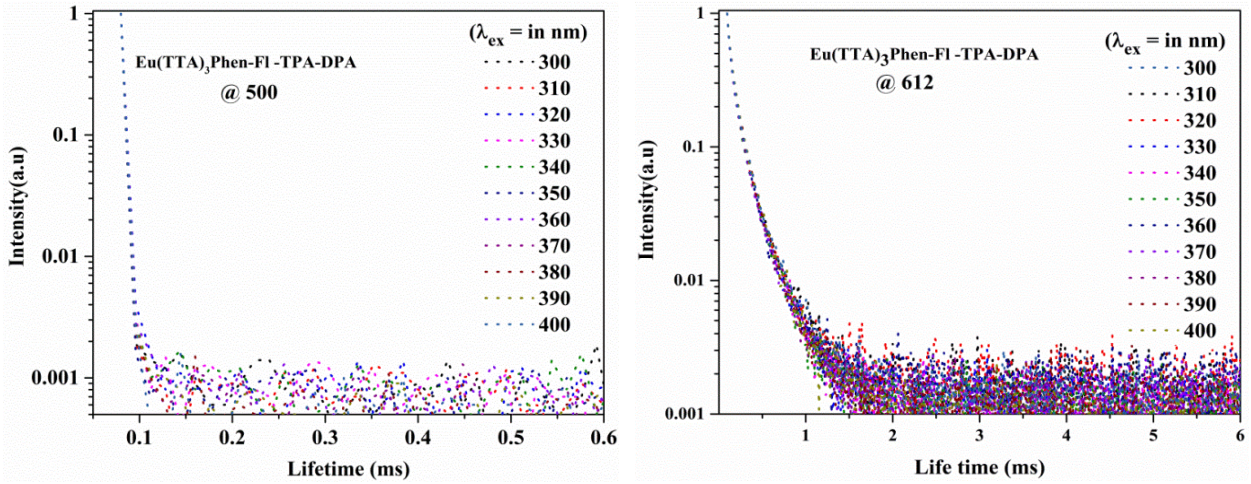

Figure 5.25 The lifetime of the Eu^{III} complex at 500 (left) and at 612 nm (right) as emission barrier; excited with different excitation source from 300-400 nm in the solid phase.

Table 5.4 The calculated lifetime of the Eu^{III} complex at 500, 612 nm and 517, 612 nm as an emission barrier and excited with different excitation source from 300-400 nm in solid phase as well as solution form and their total lifetime contribution (from 500, 612 nm and 517, 612 nm).

S. No.	$Eu(TTA)_3$ Phen-Fl-TPA-DPA	@ 612 nm	@ 575 nm	Total Lifetime	$Eu(TTA)_3$ Phen-Fl-TPA-DPA	@ 612 nm	@ 500 nm	Total Lifetime
		(solution) (in ms)				(solid) (in ms)		
1	300 nm	0.42448	0.00168	0.42616	300 nm	0.0557	0.00368	0.05938
2	310 nm	0.42115	0.00168	0.42283	310 nm	0.0635	0.00370	0.0672
3	320 nm	0.41922	0.00164	0.42086	320 nm	0.0488	0.00374	0.05254
4	330 nm	0.42541	0.00165	0.42706	330 nm	0.0568	0.00372	0.06052
5	340 nm	0.41398	0.00166	0.41564	340 nm	0.0550	0.00373	0.05873
6	350 nm	0.4139	0.00171	0.41561	350 nm	0.0279	0.00389	0.03179
7	360 nm	0.4414	0.00167	0.44307	360 nm	0.0520	0.00372	0.05572
8	370 nm	0.4386	0.00168	0.44028	370 nm	0.0462	0.00372	0.04992
9	380 nm	0.4122	0.00169	0.41389	380 nm	0.0555	0.00372	0.05922
10	390 nm	0.0527	0.00170	0.0544	390 nm	0.0664	0.00372	0.07012
11	400 nm	0.1240	0.00167	0.12567	400 nm	0.0608	0.00372	0.06452

5.2.3.3 Electrochemical analysis:

The furthered supportive outcomes were perceived from the electrochemical analysis for Eu^{III} complex, as well as ligand and which are shown HOMO energy level is -5.65, -5.72; LUMO energy level is -3.13, -3.08; respectively (Table 5.5). The short HOMO/LUMO difference between Eu^{III} complex and ligand reveals the above elucidated strategy. The Eu^{III}-complex projected narrow type energy gap is 2.52 eV and slightly higher for the ligand (i.e) 2.64 eV (Figure 5.26). Figure 5.27 shows the HOMO and LUMO calculated by DFT calculation of the ligand (Phen-Fl-TPA-DPA) in eV. Table 5.6 shows the HOMO and LUMO energy levels of the ligand with their respective band gap as well as singlet and triplet energy levels.

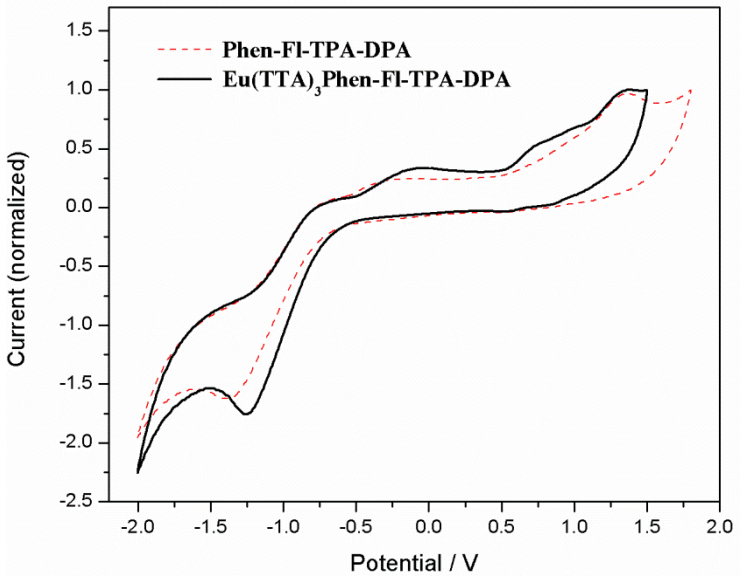

Figure 5.26 Cyclic voltammogram of Eu^{III}-complex and ligand.

Table 5.5 Electrochemical properties of the Eu^{III}-complex and ligand.

S. No.	Compound	Voltage$^{Oxi}_{onset}$ [V] (E_{HOMO} [eV])	Voltage$^{Red}_{onset}$[V] (E_{LUMO} [eV])	$\lambda_{onset,}$ [nm]	Band gap E_g^{Opt}, [eV] (a)
1	**Eu(TTA)$_3$Phen-Fl-TPA-DPA**	1.25 (-5.65)	-1.27 (-3.13)	467	2.65 (2.52)
2	**Phen-Fl-TPA-DPA**	1.32 (-5.72)	-1.32 (-3.08)	466	2.66 (2.64)

a) Calculated the onset wavelength of optical absorption (onset) in the solid-state film (DRS spectra). In bracket, mentioned their energy difference (HOMO and LUMO) value calculated by cyclic voltammogram.

Table 5.6 The HOMO and LUMO energy levels of the ligand with their respective band gap as well as singlet and triplet energy levels.

Molecule	HOMO	HOMO-1	LUMO	LUMO+1	E_g	S1	T1
	in electron volts (eV)						
Phen-Fl-TPA-DPA	-4.56	-5.12	-1.39	-1.17	3.17	2.88	2.47
Eu^{III} metal ion	--.--	--.--	--.--	--.--	--.--	$^5D_0$ level = 2.17	

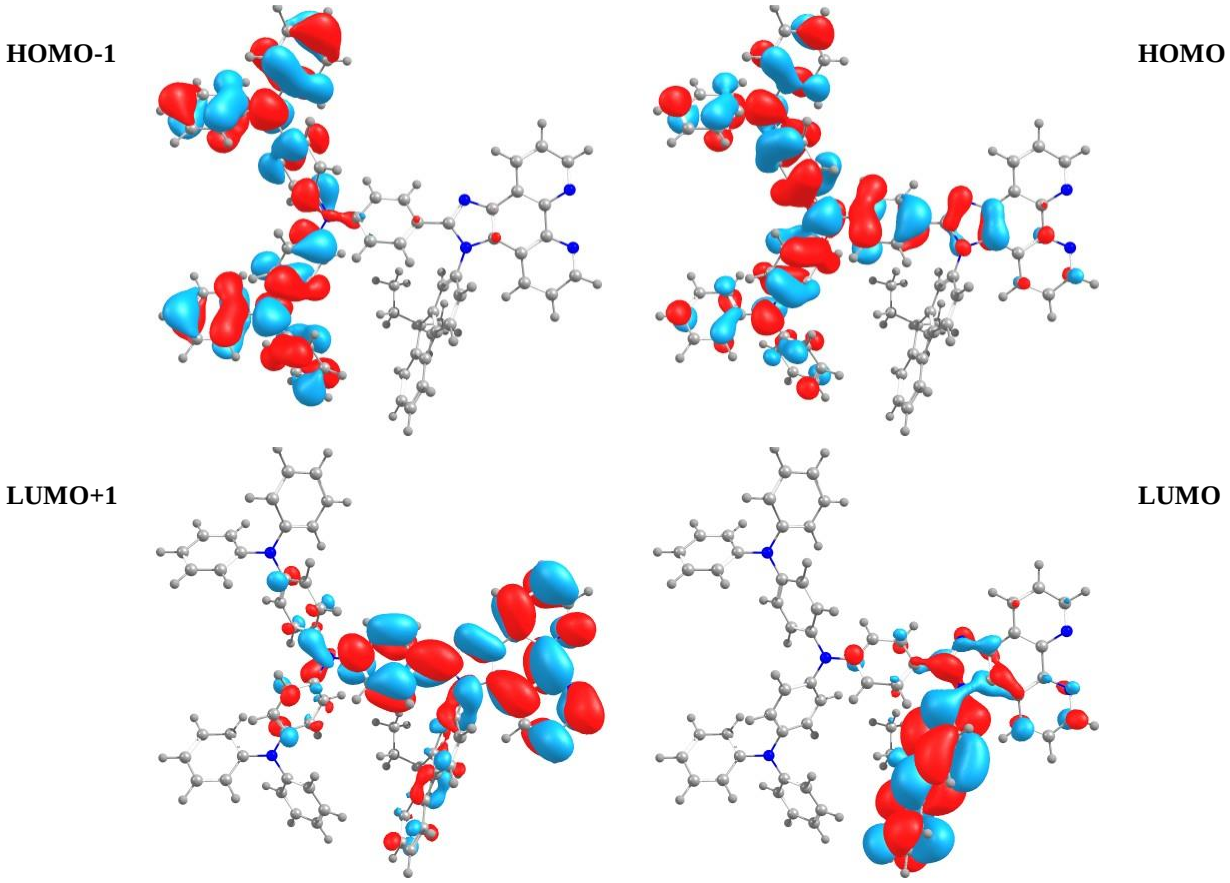

Figure 5.27 The frontier molecular orbitals of HOMO and LUMO calculated by DFT calculation of the ligand, Phen-Fl-TPA-DPA.

5.2.3.4 White LED fabrication using DPA based Eu-complex:

Fortunately, the weak emission observed from the complex in solid form was taken as an advantage to fabricate the white LED. The white LED was fabricated by complex integrated with 395 nm emitted LED (InGaN) chips under 20 mA forward-bias current (Figure 5.28). The excitation source from LED was fully observed by the complex shown in different concentrations (1:10 and 1:50 (Eu^{3+}:PMMA)). The LED show white emission with x = 0.34, y = 0.33 CIE chromaticity coordinates, which are close to the National Television Standard Committee (NTSC) standard value.

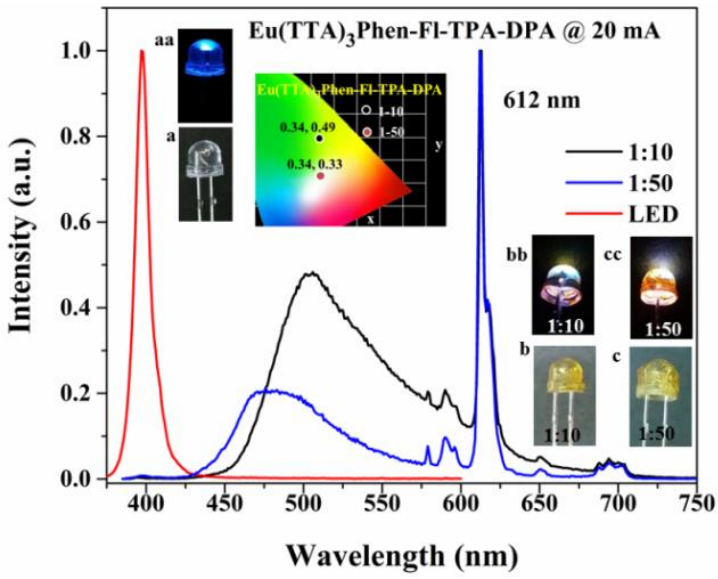

Figure 5.28 White emission from the LED (395 nm). **a** is LED without coating and **aa** is with forward bias. b (1:10) and c (1:50) are Eu^{III} complex coated LEDs and bb, cc is in forward bias.

5.3. Carbazole functionalized new bipolar ligand for monochromatic red light emitting Eu^{III} complex: combined experimental and theoretical study:

5.3.1 Outline of the present study:

In the previous section, diphenylamine was integrated with Phen-Fl-TPA ligand and studied their complexation behavior with the Eu^{III} metal ion. The complex shown incomplete energy transfer from ligand to Eu^{3+} ion leads to single molecular white emissive complex. Here, the introduction of carbazole moiety in place of diphenylamine in the complex and their influence on photophysical properties of corresponding Eu-complex by means of ET from ligand to Eu^{III} metal ion was studied. The synthesized CBZ decorated TPA-phenanthroline-fluorene bipolar ligand is Phen-Fl-TPA-CBZ and the corresponding β-diketonate Eu^{III} complex is $Eu(TTA)_3$Phen-Fl-TPA-CBZ (Phen-Fl-TPA-CBZ = N,N-bis(4-(9H-carbazol-9-yl)phenyl)-4-(1-(9,9-diethyl-9H-fluoren-2-yl)-1H imidazo[4,5f][1,10]phenanthrolin-2-yl)benzenamine, TTA = Thenoyltrifluoroacetone), respectively. The photophysical and electrochemical studies of the bipolar ligand and its corresponding Eu complexes were studied in details. The CIE color coordinates were calculated for the complex and it showed NTSC (National Television Standards

Committee) standard values. The synthesized bipolar ligand and its corresponding Eu^{III} complex structures are represented in Figure 5.29.

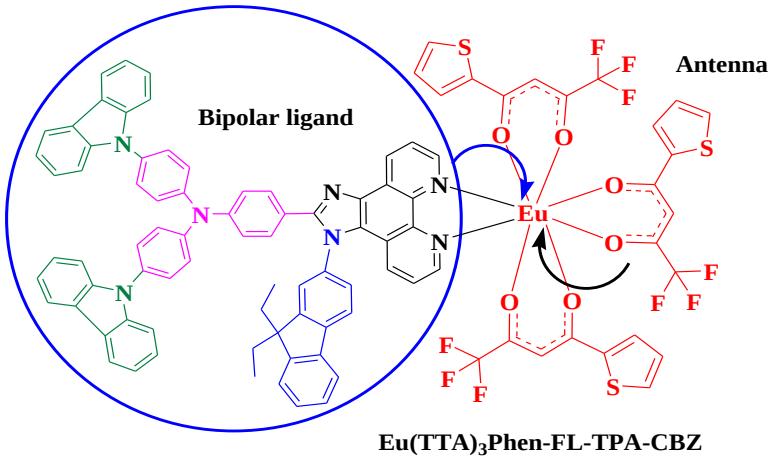

Figure 5.29 Chemical structure of β-diketonate connected bipolar ligand based Eu^{III} complex.

5.3.2 Experimental section:

5.3.2.1 General information for synthesis:

The general information for the synthesis is given in Chapter 2.

5.3.2.2 Measurements:

The physical measurements that are used for characterisation is mentioned in Chapters 2 (2.2.2).

5.3.2.3 Synthesis:

The compound synthesis details for 9,9-diethyl-9H-fluoren-2-amine (1-3), 1,10-phenanthroline-5,6-dione (2-1) and metal complex tris(thenoyltrifluoroacetone) europium(III) ($Eu(TTA)_3(H_2O)_2$) is given in Chapter 2. 4-(bis(4-(9H-carbazol-9-yl)phenyl)amino)benzaldehyde (3-3) [22] was synthesized by reported literature. The synthesis scheme for the ligand and the complex is given in scheme 5.2.

5.3.2.3.1 *Synthesis of N,N-bis(4-(9H-carbazol-9-yl)phenyl)-4-(1-(9,9-diethyl-9H-fluoren-2yl)-1H-imidazo[4,5f][1,10]phenanthrolin-2-yl)benzenamine (Phen-Fl-TPA-CBZ):*

Fl (0.751 g, 3.169 mmol) was added to a stirred solution of dione (0.605 g, 2.880 mmol) in glacial acetic acid (30 mL) at room temperature. To this reaction mixture subsequently, ammonium acetate (2.218 g, 28.80 mmol) and 2-3 (1.74 g, 2.880 mmol) were added. Then the total resulting mixture was stirred for 12 hrs at 110 °C. The progress of the reaction was monitored by TLC (MeOH in Chloroform 1:9, Rf-0.2). The reaction mixture was pouring into the minimum amount of water and then ammonium hydroxide solution was added. The formed solid was filtered off and dissolved in dichloromethane, followed by dried over anhydrous sodium sulphate and the solvent was evaporated to get 2.0 g crude compound. The resultant compound was purified by column

chromatography by using silica gel (100-200 mesh), eluent with 4% methanol in chloroform and the solvent was evaporated and dissolved in minimum amount of THF solution added an excess of hexane solvent, the pale yellow color solid was formed. After settling of solid, decant and repeated this process three more times and get compound-4 (51.7%) solid. ^{1}H-NMR Data (400 MHz, $CDCl_3$): δ (in ppm) 9.23-9.18 (m, 2H), 9.05 (dd, 1H), 8.15 (t, 3H), 7.99 (d, 1H), 7.87-7.85 (m, 1H), 7.78 (dd, 1H), 7.71 (d, 1H), 7.63-7.60 (m, 4H), 7.50-7.36 (m, 16H), 7.31-7.29 (m, 4H), 7.26-7.23 (m, 3H), 7.19-7.16 (m, 2H), 7.13-7.07 (m, 3H). ^{13}C-NMR Data ($CDCl_3$, 100 MHz): δ (in ppm) 152.5, 150.1, 146.7, 146.1, 145.8, 143.6, 140.8, 136.5, 130.5, 130.1, 129.5, 128, 127.8, 127.4, 125.8, 125.5, 125.3, 124.1, 123.1, 123, 122.5, 121.3, 120.4, 120.2, 119.9, 119.7, 109.6, 56.7, 32.7, 8.3. EI-MS: m/z exp (calc). 1014.22, m/z found 1015.10 $[M + H]^+$.

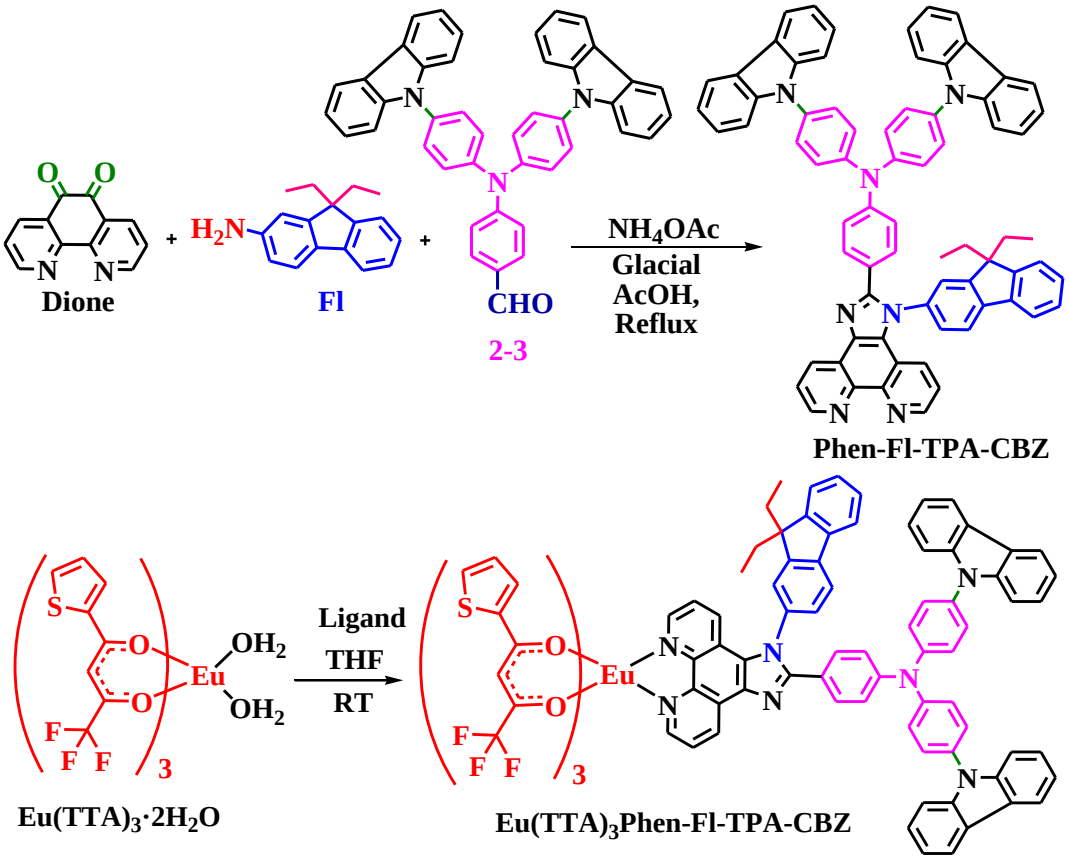

Scheme 5.2 Synthetic route of CBZ attached triphenyl functionalized ligand and the corresponding β diketonate Eu^{III} ternary complex.

5.3.2.3.2 *Synthesis of Eu(TTA)$_3$Phen-Fl-TPA-CBZ*:

Taken a 50 mL of two neck round bottom flask with nitrogen balloon contained adaptor and poured $Eu(TTA)_3(H_2O)_2$ (83 mg, 0.098 mmol, 1eq) dissolved in dry THF (5 mL). The ligand (100 mg, 0.098 mmol, 1eq) dissolved in THF (10 mL) and added to stirred solution of reaction mixture then stirred for 12 hrs at 70 °C. The resulting mixture was concentrated and dissolved in minimum amount of THF and added an excess of hexane to get a solid product. After settled of solid, decant and repeated the process for

several times and dried to get pale yellow color solid with 100 mg (56.1 %). Elemental Analysis: Anal. Calc. for. $C_{96}H_{63}EuF_9N_7O_6S_3$; C, 63.02; H, 3.47; N, 5.36; S, 5.26%, Found: C, 63.22; H, 3.82; N, 5.86; S, 5.22 %. EI-MS: m/z exp (calc). 1829.72, m/z found 1848.31 $[M + H_2O]^+$.

5.3.3 Results and Discussion:

5.3.3.1 Characterization of the complex:

The method of Eu^{III} complex synthesis is summarized in Scheme 1 (synthesis direction of intermediates were given in scheme S1). The compounds are characterized by nuclear magnetic resonance spectroscopy (^1H and ^{13}C NMR, Figure 5.S8-5.S10), LC-MS analysis (Figure 5.S11) Fourier transforms infrared spectroscopy (FT-IR) and elemental analysis. All the measurements were done at room temperature.

5.3.3.1.1 FT-Infrared spectroscopy:

The FT-IR spectrum of ligand and its corresponding Eu^{III}-complex was measured in the range of 500 - 4000 cm^{-1} (Figure 5.30). The FT-IR spectra of the $Eu(TTA)_3(H_2O)_2$ complex shown strong carbonyl (C=O) stretching frequency at 1610 cm^{-1} and the same is shifted to 1597 for the $Eu(TTA)_3$Phen-Fl-TPA-CBZ complex. The change in the stretching frequency is an indirect evidence to that the β-diketonate ($Eu(TTA)_3(H_2O)_2$) compound coordinated with the neutral ligand [23, 24].

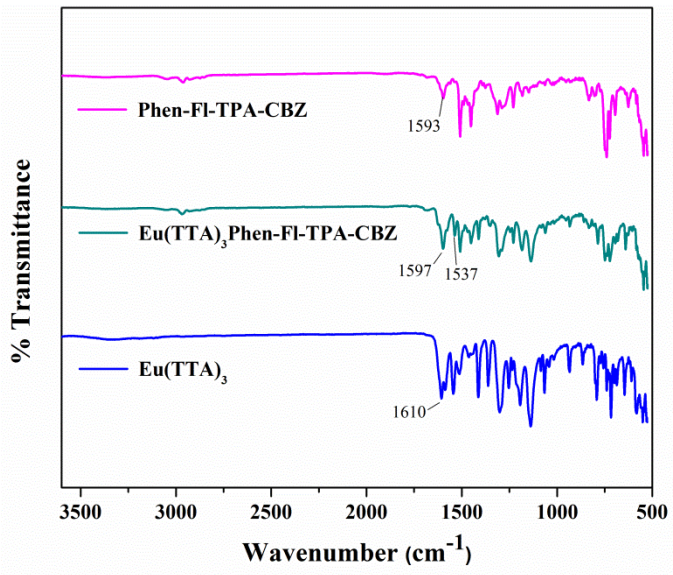

Figure 5.30 FT-IR spectra of the ligand, corresponding Eu^{III}-complex and $Eu(TTA)_3(H_2O)_2$.

The vibration frequency due to C=N appears at 1593 cm^{-1} for free ligand Phen-Fl-TPA-CBZ. After the complex formation by using the phen ligand, the C=N peak is shifted towards lower wavenumber (1537 cm^{-1}) and the same is listed out in Table 5.7. These consequences are signifying that the N atoms in ligand are also coordinates with $Eu(TTA)_3(H_2O)_2$ [25]. Compared with the free ligand, the C-H bending vibration peaks of phenanthroline derivative in Eu^{III} complex shifted towards the higher wavenumber [26-

28] All the above strategies are suggesting that the Eu metal ion was coordinated with a ligand molecule.

Table 5.7 The foremost Infrared frequencies (wavenumber in cm^{-1}) at room temperature for free ligand, its corresponding Eu^{III}-complex and $Eu(TTA)_3(H_2O)_2$.

(Wavenumber in cm^{-1})	**$Eu(TTA)_3$Phen-Fl-TPA-CBZ**	**Phen-Fl-TPA-CBZ**	**$Eu(TTA)_3(H_2O)_2$**
ν (C=O)	1597	--.--	1610
ν (C=N)	1537	1593	--.--
ν (C-N)	1231	1227	--.--
ν (C-F)	1303	--.--	1298
ν (C-CF_3)	1137	--.--	1133
ν (C-H phen)	833, 723	830, 737	--.--

5.3.3.2 Thermal properties and Powder X-ray diffraction studies:

To find the thermal stability and glass transition temperature, DSC-TG analysis was carried out for the synthesized ligand and its corresponding europium complex. The DSC-TGA of ligand and Eu^{III} complex were measured under a nitrogen atmosphere at the range of room temperature to 800 °C and the heating rate was maintained 10 °C for min. TG analysis of ligand shown major thermal decomposition at 435°C. However, Eu^{III} complex shown three stage thermal decomposition at 240, 291, 439°C (Figure 5.31, left). The Eu^{III} complex is shown thermal decomposition above 240°C with gradual decrease and it is due to peripheral molecules. Weight loss with 5% is observed at 235 and 162 for ligand and complex, respectively. The good thermal stability of the Eu^{III} complex is expected, it may be due to the presence of polarized M–O bond [29]. When compare the thermal decomposition of the ligand with Eu^{III} metal complex, a ligand as shown better thermal stability (> 435°C). However, it is less than TPA alone ligand and Eu^{III} complex also shown less [30]. It is expected due to elimination and/or decomposition of ligand in the Eu^{III} complex (which may have been caused by loss of the free ligand from the europium complex), it means the presence of TTA moiety and additional TPA, CBZ groups in the Eu^{III} complex. The obtained specific heat or glass transition temperature of the ligand and Eu^{III} complex are at 137 and 125°C, respectively from the DSC curves (Figure 5.31, left corner). This is due to the sample undergoing a change in heat capacity without change the formal phase. These results are suggesting that the $Eu(TTA)_3$Phen-Fl-TPA-CBZ have good thermal decomposition and it can be used for furthered low thermal founded analysis.

The amorphous nature of the ligand and corresponding Eu^{III} complex are studied by Powder X-ray diffraction (Figure 5.31, right). The PXRD diffraction studies were carried out to evaluate the crystalline or amorphous nature of the ligand and corresponding Eu^{III} complex. The PXRD results of the Eu^{III} complex shows the amorphous structure. The interplanar distances (d) of $Eu(TTA)_3$Phen-Fl-TPA-CBZ complex is shifted to higher value as compare to that of ligand. These changes are indicating that the ligand metal coordination presents in the complex.

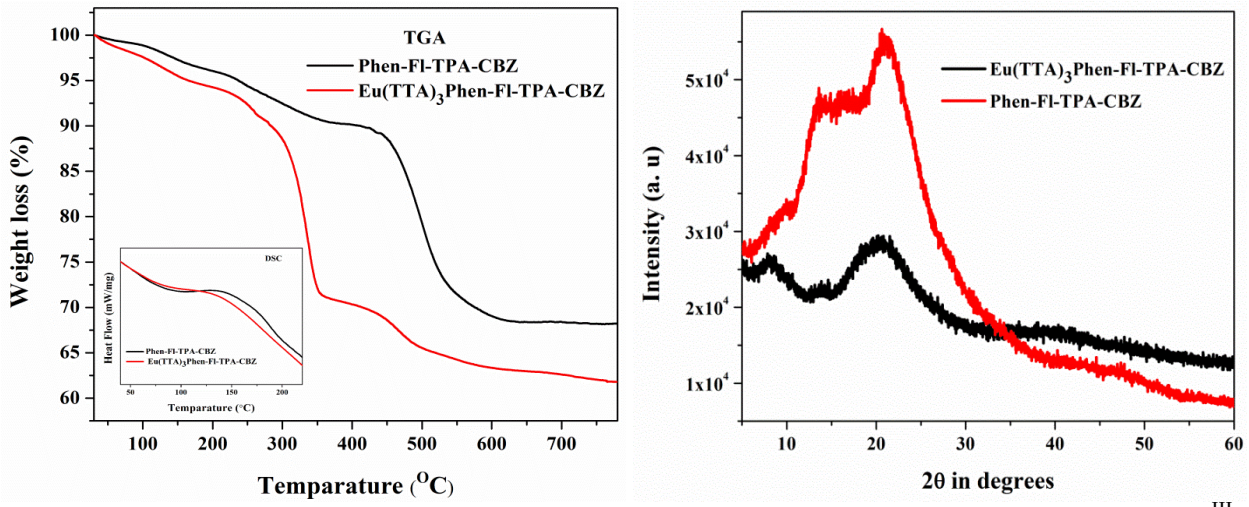

Figure 5.31 DSC-TG (left) and PXRD (right) analysis of the ligand and its corresponding Eu^{III} complex.

5.3.3.3 Photophysical properties:

5.3.3.3.1 UV-Visible absorption and DRS studies:

Figure 5.32, left shows UV-Visible absorption spectra of the ligand and its corresponding Eu^{III} complex was carried out in solution (chloroform solution conc. 1.0×10^{-4} mol L^{-1}). The absorption spectrum of ligand in chloroform solution shows absorption from 240 to 450 nm with λ_{max} values are 307, 280 and 241 nm for Phen-Fl-TPA-CBZ; these bands are attributed to the $\pi \rightarrow \pi^*$ transitions of the ligand. Theoretically calculated UV-spectra in gas and solvent phase also support the experimental findings (Figure 5.32, right). Similarly, the absorption studies of $Eu(TTA)_3$Phen-Fl-TPA-CBZ and $Eu(TTA)_3(H_2O)_2$ shows the peak maxima at 342, 271 nm and 340, 275 nm, respectively. The Eu^{III} complexes shown similar peaks which are observed for the ligand as well as $Eu(TTA)_3(H_2O)_2$. It is suggesting that the presence of the ligands in the corresponding Eu^{III} complexes, which are listed out in Table 5.8. The study of absorption spectra of the Eu^{III} complex in thin film shown peaks at 296, 384 nm (instrumental artefact) and solid shown a wide absorbance from 250 to 440 nm and its ligand is shown peaks maxima at 381, 282 nm, respectively (Figure 5.33, right).

The comparative study of absorption spectra of the Eu^{III} complexe in solution, thin film and solid indicates that the absorption maximum shifts to longer wavelength for solid phase as compared to that of complex in solution and thin film. The observed bathochromic shift in the absorption spectra is due to the aggregation of the complex in the solid phase [31, 32]. The immersed excitation spectrum is differing from the absorption spectra. The peak of the ligand in different solutions has shown a red shift with compare to that of absorption and the peak intensity at ~411 nm is also depends on the polarity of solvent (Figure 5.35, left). The similar peak is also observed in the Eu^{III} complex in $CHCl_3$. It could be that the molar extinction coefficient is much smaller in the n-π^* compares to that of π-π^* (high energy) transition and it can lead to the spectral shift towards shorter wavelength. The similar observations were also been reported [33, 34].

The band gap for all the compounds were calculated by using the DRS with the help of kubelka-munk function. The acquired data from the DRS is converted to Kubelka-Munk function and α is substituted with $F(R_\infty)$ ($\alpha = F(R_\infty)$) (2.1). The $(\alpha h\nu)^2$ (y-axis) was plotted against the hν (x-axis) in eV (electron volts) (Figure 5.33) and the calculated band gap values are listed out in Table 5.12.

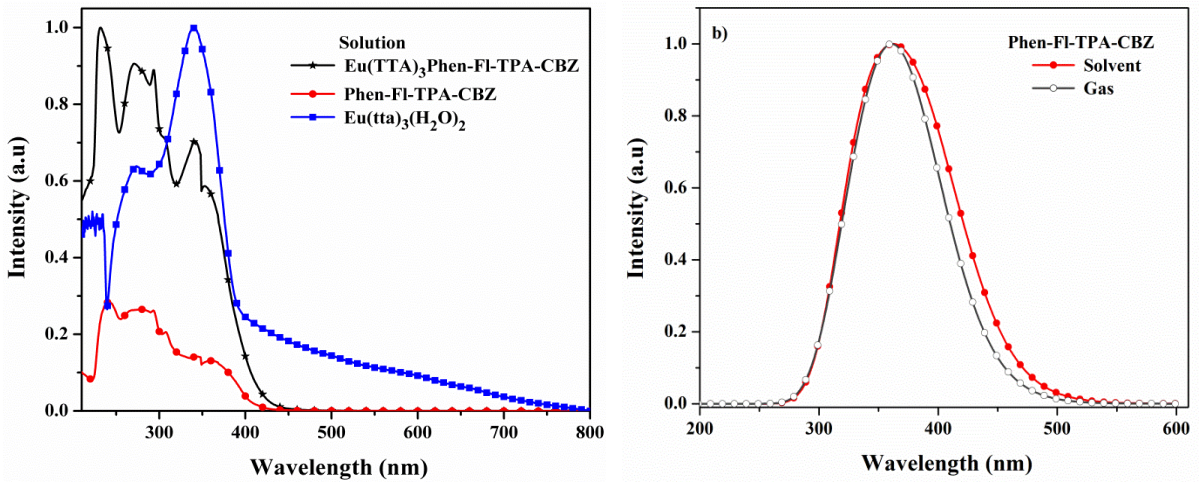

Figure 5.32 The UV-Vis absorption spectra of $Eu(TTA)_3$Phen-Fl-TPA-CBZ and its ligand in chloroform solution (left), The ligand absorption spectra theoretically calculated.

Table 5.8 The UV-absorption and PL emission data of synthesized Eu^{III} complexes and ligands.

S. No	Compound name	UV λ_{max} (abs) [nm] Solution (a)(b)	Thinfilm(b)	Solid(b)	λ_{ex} (d) [nm]	PL λ_{em} (a) [nm]	PLQY (a)[%]
1.	**$Eu(TTA)_3$ Phen-Fl-TPA-CBZ**	232, 271, 293, 307, 342	296, 384	251,327, 409	271 (23,902 ε/ cm^{-1} M^{-1})(e) 342, 394, 401	579, 592, 612, 652, 702	44.4
2.	**Phen-Fl-TPA-CBZ**	241, 280, 293, 307, 342, 362	--.--	282, 339, 381	258 (33,773 ε/ cm^{-1} M^{-1})(e), 271, 360	430, 548(c)	--.--
3.	**$Eu(TTA)_3(H_2O)_2$**	273, 340	--.--	--.--	275, 340	580, 592, 612, 652, 703	

(a) Measured in chloroform solution at 298 K, (b) absorption peaks from the UV-absorption spectra, (c) emission peak from solid PL, (d) wavelengths are taken to get the emission of ligands and Eu^{III} complexes, (e) The calculated molar absorption coefficient.

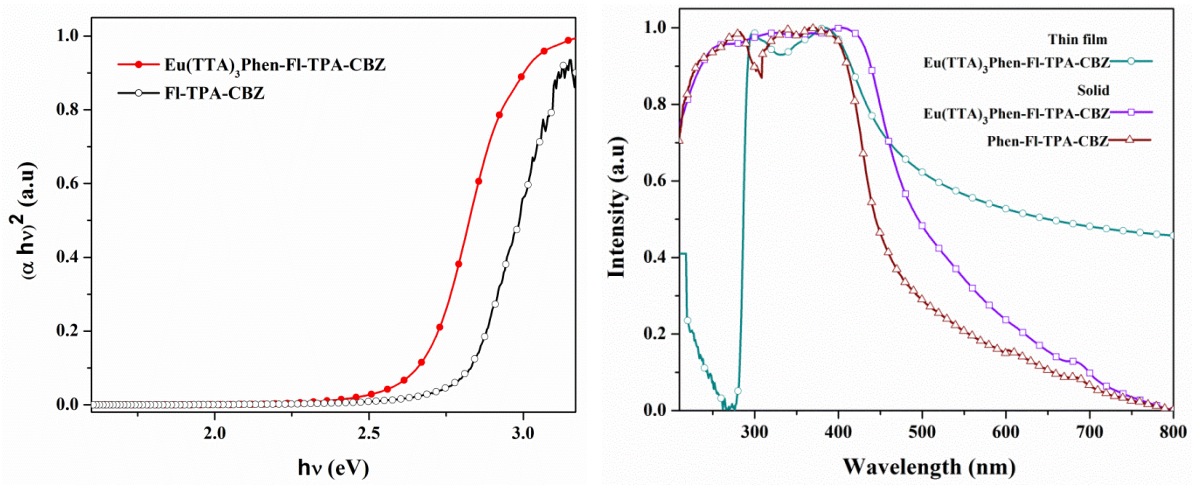

Figure 5.33 The band gap for the ligands and their corresponding Eu^{III} complexes are calculated from diffuse reflectance spectra (left), the UV-Vis absorption spectra of $Eu(TTA)_3$Phen-Fl-TPA-CBZ and its ligand in thin film and solid (right).

5.3.3.3.2 Photoluminescence studies (PL):

In general, Eu^{III} complex emission depends on their ligand triplet state population as well as the excited state of the Eu^{III} complex energy levels. In the present study ligand, Phen-Fl-TPA-CBZ show emission at 430 nm under excitation wavelengths 258, 272 and 360 nm (Figure 5.34, left) in solution. The same is used as monitoring wavelength (430 nm) and shown absorption peak at 272 nm. The ligand in the solid state show emission at 548 nm and the same is used as excitation source. In the case of solid, the ligand emission was shifted towards red shift (Figure 5.34, right) is expected due to aggregation.

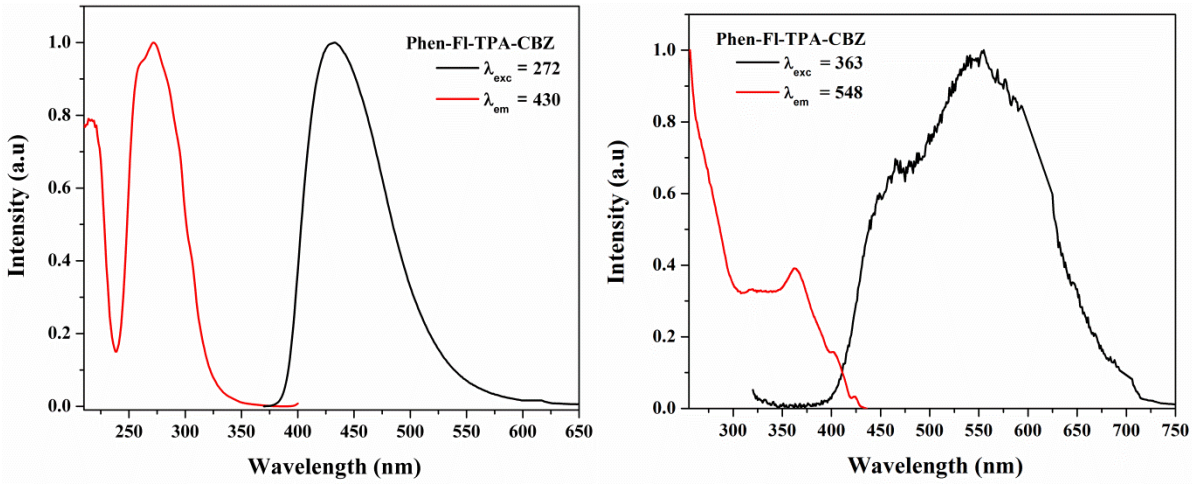

Figure 5.34 The PL excitation and emission spectra of the ligand, Phen-Fl-TPA-CBZ in chloroform (left) and solid (right).

5.3.3.3.3 Solvatochromism study:

The solvatochromism of ligands emission spectra interpreted in terms of Lippert-mataga equation. It defines the stoke's shift in terms of the changes in dipole moment which occur upon excitation. According to the increasing the polarity of the solvent, there is a shift observed towards high wavelength is called red / batho chromic shift, which are showed in Figure 5.35 (left and right). The equations 2.2, 2.3 of Lippert−Mataga describes the solvatochromic Stokes shift $\Delta\bar{\nu}$ (expressed in wavenumbers) as a function of the change of the dipole moment $\Delta\mu_{ge} = \mu_e - \mu_g$ of the dye. The several solvents are performed by eq-2.2 with dissimilar dielectric constants (ε) and refractive indices (n) and by plotting $\Delta\bar{\nu}$ as a function of Δf. Figure 5.35 (left and right) were represents the Lippert−Mataga plot for Phen-Fl-TPA-CBZ in the solvents listed in Table 5.9. The Figure 5.36 indicating that the linear relationship [correlation coefficient r = 0.218, slope = (29.494) × 10^3 cm^{-1}, intercept = (5.010) × 10^3 cm^{-1}] of the Stoke's shift plotting $\Delta\bar{\nu}$ verses Δf for the 10 solvents of CBZ ligand.

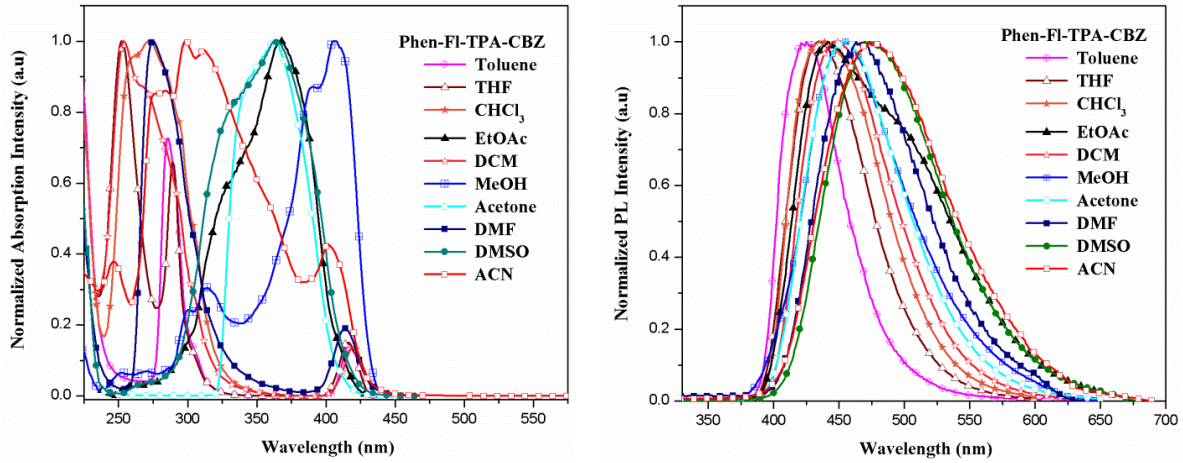

Figure 5.35 The solvent effect of Phen-Fl-TPA-CBZ of PL excitation (left) and emission (right) in different solvents.

Emission of the ligand is shown wavelength fluctuating towards a red shift in the solution with increasing solvent polarity (toluene to acetonitrile). It could be explained as dipole of the excited state is high in polar solvents and it induces peak shift. The emission of the Eu-complex observed under different excitation wavelengths shown intense emission peak at 612 nm, attributed to $^5D_0 \rightarrow {}^7F_2$ transition (electrical dipole). The $Eu(TTA)_3$Phen-Fl-TPA-CBZ shown characteristic red emission at 612 nm under various (271, 342, 394 and 401 nm) excitations. The PL spectrum of CBZ moiety connected Eu^{III} complex was also measured in thin film and solid phase. The thin film of the Eu^{III} complex shown red emission at 612 nm under 385 nm and in the solid phase also shows red emission at 612 nm under 283 and 365 nm (Figure 5.37). These the systems were shown only intense red emission (no ligand emission) and compared with the solid-state; no great differences in the emission spectra for Eu^{III} complex in $CHCl_3$ solution were observed, except the emission intensity.

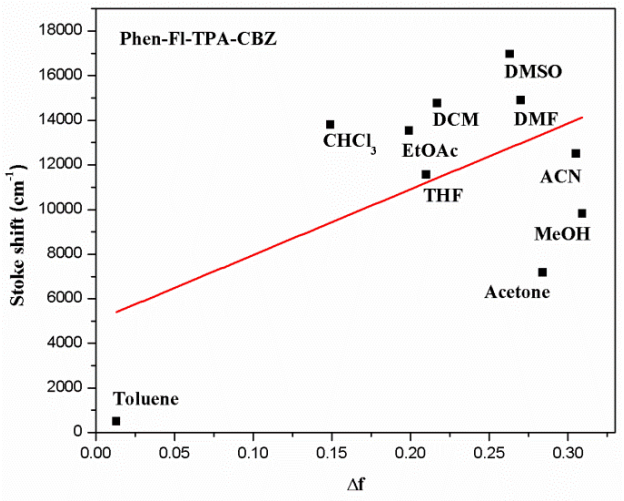

Figure 5.36 Stoke's shift $\Delta\bar{\nu}$ of Phen-Fl-TPA-CBZ (right) versus the Lippert solvent parameter $\Delta f = f(\varepsilon) - f(n^2)$ (The numbers refer to the solvents in Table S1). The straight line represents the linear fit to the 10 data points.

Table 5.9 PL spectral data of ligands in various solvents.

Phen-Fl-TPA-CBZ	**λ_{abs} (max) (nm)**	**λ_{em} (max) (nm)**	**Stoke's shift ($\Delta\nu$) (cm^{-1})**
Toluene	416	425	509
DCM	270	449	14765
THF	289	434	11561
$CHCl_3$	273	438	13799
EtOAc	255	441	13540
MeOH	314	454	9821
Acetone	343	455	7176
ACN	298	475	12518
DMF	275	466	14904
DMSO	263	475	16970

In detail, the Eu^{III} complexes in solution, thin solid film spin coated on a glass and solid show characteristic emission peaks, which are attributed to the intraconfigurational $^5D_0 \rightarrow {}^7F_J$ (J = 0 - 4) transitions. When use the ligand emission wavelength to excite the Eu^{III} complex, emission appears at 579, 592, 612, 652 and 702 nm and these emission lines are corresponding to f-f transitions of $^5D_0 \rightarrow {}^7F_0$, $^5D_0 \rightarrow {}^7F_1$, $^5D_0 \rightarrow {}^7F_2$, $^5D_0 \rightarrow {}^7F_3$ and $^5D_0 \rightarrow {}^7F_4$, which indirectly indicates that there is energy transfer L to M (Eu^{III} ion). The emission of the europium metal ion transitions are observed in the emission spectrum via two main mechanisms (transition): electric dipole (ED) and magnetic-dipole (MD). The $^5D_0 \rightarrow {}^7F_0$ transition at 579 nm (single peak) in the emission spectra indicates that the all Eu^{3+} ions occupy a site of the same symmetry. The $^5D_0 \rightarrow {}^7F_0$, $^5D_0 \rightarrow {}^7F_3$ transitions are forbidden both in magnetic and electric dipole systems [35] and its respective wavelengths 579 nm and 652 nm emission bands are weak. The 592 nm emission band is stronger because of magnetic character of the $^5D_0 \rightarrow {}^7F_1$ transition is independent of the coordinate environment. The observed transition $^5D_0 \rightarrow {}^7F_2$ at 612 nm is most intense induced electronic dipole transition and clearly indicates that the Eu^{III} occupies site without inversion centre. The calculated narrow FWHM for solid is 5, the solution is 10 and thin film is 13 nm, respectively.

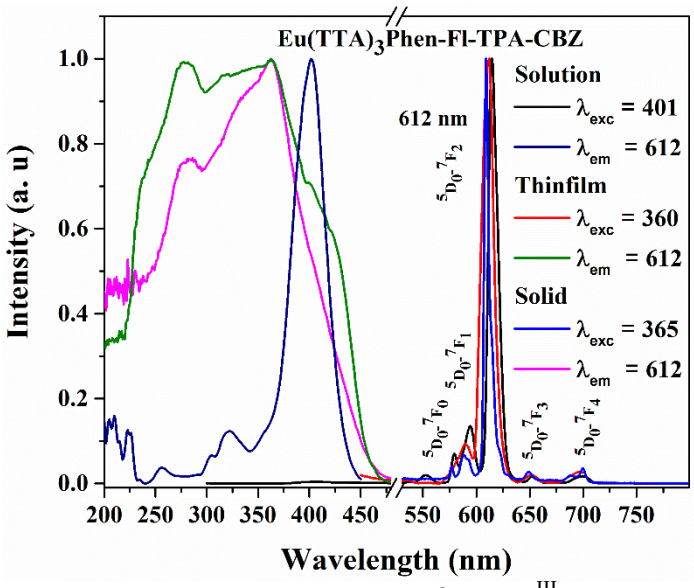

Figure 5.37 The PL excitation and emission spectra of the Eu^{III} complex in solution form, thin film, and solid phase.

The symmetry ratio of the Ln coordination sphere processed by the intensity ratio of the electric dipole transition ($^5D_0 \rightarrow {}^7F_2$) and the magnetic dipole transition ($^5D_0 \rightarrow {}^7F_0$). The I_2/I_1 (I_{7F2}/I_{7F1}) ratio of the $Eu(TTA)_3$Phen-Fl-TPA-CBZ in solution, Thin film and solid were 16.6, 9.07 and 17.5, respectively. The high I_{7F2}/I_{7F1} indicates that the symmetry of the coordination sphere is low [36]. These results are suggesting that the CBZ consisted Eu^{III} complex have a characteristic efficient red emission. The asymmetric ratios of the Eu^{III} complex in solution, solid shown high value compare to that of thin film. It is due to a number of europium ions occupying in solid (constricted padding of metal ions) is high compare to the thin film. It is because of observed photons is become less in thin film results decrease in intensity of the hypersensitive $^5D_0 \rightarrow {}^7F_2$ transition in complex and leads to high symmetry. In addition, asymmetric ratios of the thin film of the complex are high with compare to doped PMMA leads to indicating that the numbers of Eu^{III} metal ions are less by doping. It is more representative to consider the high polarizability of the chelating β-diketonate ligands is tools to enhancing the intensity. From this, it could be expected that the coordination structure of the complex responsible for intensity and leads to variation in the symmetry of the complex.

5.3.3.3.4 Energy transfer mechanism (L to Eu^{III} ion in Eu^{III} complex):

To understand the reason behind the fully or partial energy transfer, we have calculated the singlet and triplet energy states for the bipolar ligand (Figure 5.38) by the computational study (DFT and TD-DFT). The theoretical data of the Phen-Fl-TPA-CBZ, singlet, and triplet energy levels are shown at 25,707 (3.18 eV) and 21,277 cm^{-1} (2.63 eV). The singlet energy of the ligand Phen-Fl-TPA-CBZ also been calculated from the experimental data (the intercept of the absorption and fluorescence spectra, Figure 5.41) and found 25,316 cm^{-1}. It is also well known that the singlet and triplet energy level of the TTA located at around 25,164 (3.12 eV) and 18,954 cm^{-1} (2.35 eV). The synthesized Eu^{III} complexes in the present study have energy transfer to center metal ion from both the

ligand and TTA. It is well known that the Eu^{III} metal ion excited $^5D_0$ energy level located at 17,240 cm^{-1}. The energy level of the triplet state is higher than $^5D_0$ energy level of the Eu^{III} complex which is around 4,037 cm^{-1}. It is suggested that this energy gap (ΔE) between triplet state of the ligand ($^3\pi\pi^*$) and the Eu^{III} excited state ($^5D_0$), facile the energy transfer from ligand to Eu^{III} ion. It means that the triplet state located higher than 19,740 cm^{-1}. It is also supportive according to the Latva et al., investigations [15]. In addition, the energy gap between singlet and triplet states, ΔE ($^1\pi\pi^*$–$^3\pi\pi^*$) is above 5000 cm^{-1} (singlet state should be > 24,740 cm^{-1}). These details are indicating that the efficient energy transfer from the ligand excited singlet to triplet excited state through ISC occurs and subsequently transfer to $^5D_0$ excited level of the Eu^{III} ion. The comparative analysis of singlet and triplet levels were made and found that the presently studied complex have higher energy levels (^1S (83 cm^{-1}) and ^3T (404 cm^{-1})) than that of TPA based Eu^{III}-complex [33]. This clearly indicates that the inclusion of the CBZ molecule facilitates to increase the efficiency by enhanced suitable energy levels through intra molecular energy transfer.

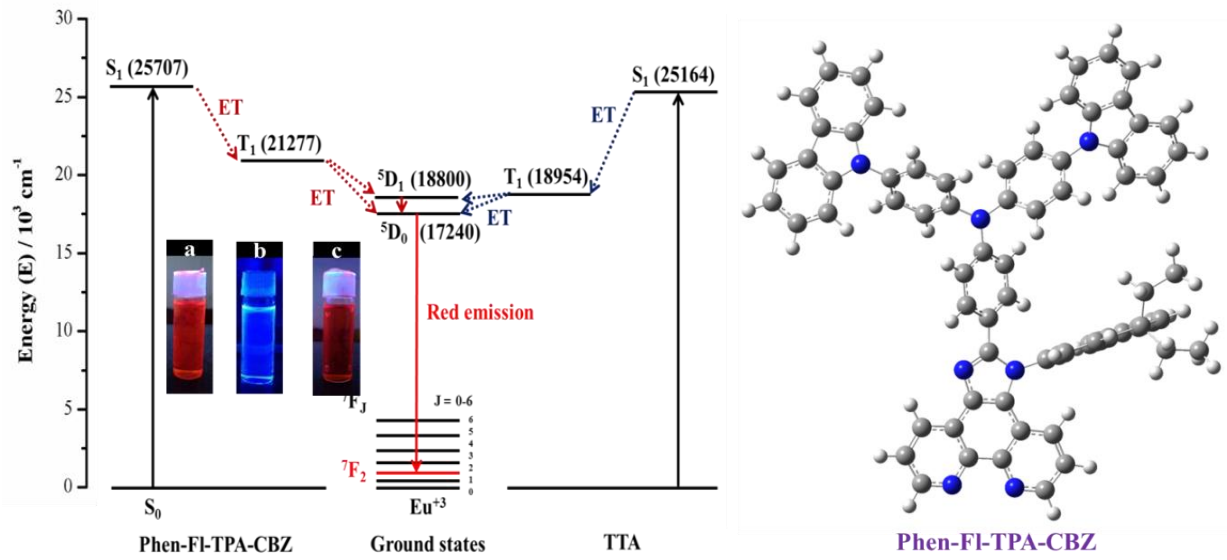

Figure 5.38 The energy transfer diagram for the Eu $(TTA)_3$Phen-Fl-TPA-CBZ and with TTA molecule (dotted line is non-radiative, normal line is radiative, S = singlet, T = triplet, ET = energy transfer) (left), inset (a) Eu $(TTA)_3$Phen-Fl-TPA-CBZ, (b) Phen-Fl-TPA-CBZ and (c) $Eu(tta)_3(H_2O)_2$ in under UV (365 nm) respectively; ground state optimized structures of the ligand (right).

In addition, solvent polarity also may play an important role in the energy transfer process. Since, the ligand energy levels could vary depends on the solvent polarity and appropriate location of the excited levels of the ligand is more important to achieve efficient energy transfer from ligand to Eu^{III} ion. Further, analysis of ligand emission in the different solvent made and found the energy gap decreases (leads to red shift) with increasing the polarity (toluene to acetonitrile). It indicates that the more polar solvents could be suitable to achieve better energy transfer [37]. It is also been documented that the ligand charge transfer state could act as a bridging between the triplet level and Eu^{III} excited level in the energy transfer process. Finally, reach the ground state as radiative red

emission ($^5D_0 \rightarrow {}^7F_2$). The similar type of energy transfer pathway also been investigated and reported with brief particulars [38-41]. The optical properties are investigated after six months and no significant changes were observed. It is clearly indicating that the complex is air stable one. The ligand and its corresponding Eu^{III} complex are observed under normal light and UV-lamp (365 nm) (Figure 5.38, onset).

Ligand showed blue emission and respective Eu^{III} complex was shown red color, respectively. The ground state optimized structure of ligand is shown in Figure 5.38, right. An investigation of complex luminescence properties showed that the characteristic luminescence of the corresponding Eu^{III} occurs through intramolecular energy transfer. In detail that the effective energy transfer between the ligating moieties (Phen-Fl-TPA-CBZ, TTA) occur due to the effective overlap between the absorption spectrum of TTA and emission spectrum of ligand, Phen-Fl-TPA-CBZ (Figure 5.39). In general, the overlap between the emission spectrum of the donor and the absorption spectrum of the acceptor is necessary for effective energy transfer.

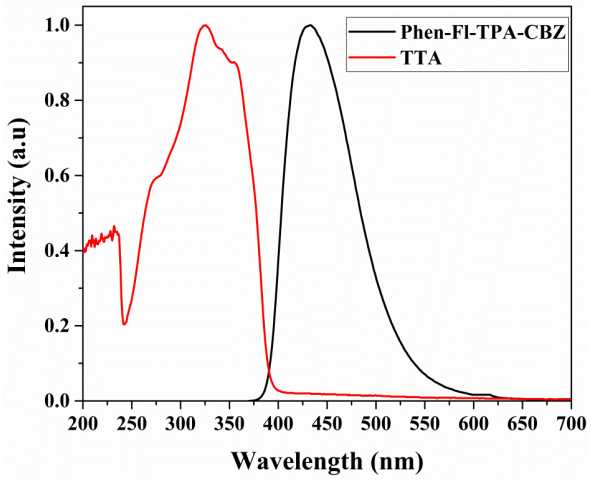

Figure 5.39 The emission of the ligand (Phen-Fl-TPA-CBZ) and UV-vis absorption spectra of TTA at room-temperature.

5.3.3.3.5 Photoluminescence quantum efficiency (PLQY) and PL Lifetime:

By using the following formulas (2.2 and 2.3) the quantum efficiency (φ) can be obtained. PLQY was measured in chloroform solution. The PLQY of the $Eu(TTA)_3$Phen-Fl-TPA-CBZ was shown 44.4 % (error ±3.879), which is higher than that of recently reported without CBZ decorated Eu^{III} complex ($Eu(TTA)_3$Phen-Fl-TPA). In addition, the PLQY of the solid was found be higher (15.0 %) than that of TPA based Eu complex ($Eu(TTA)_3$Phen-Fl-TPA) (~12.1 %). The results of PLQY in solution as well solid were supporting the efficient energy transfer from ligand to center Eu^{III} metal ion. It means that the carbazole moiety influence more compared to that of only TPA moiety in the Eu^{III} complex for the increment of the PLQY. The obtained results were shown better than tri nuclear Eu^{III} complex such as $Eu_3(TTA)_9$trisphen and also than $Eu(TTA)_3$imidazophen [42].

The measured lifetime data was fitted with the single exponential function (Figure 5.40) given by the equation, $I(t) = I_0 + A_1 \exp\left(\frac{-t}{\tau}\right)$; where A_1 is the scalar quantity

obtained from the curve fitting, t is the time in ms, $I_0 = 0$ is the offset value and τ is the decay time value for the exponential component. Luminescence decay curves of the $^5D_0$ excited state were measured at 298 K by monitoring the most intense emission lines ($^5D_0 \rightarrow {}^7F_2$) of the Eu-ion center at 612 nm and at 360 nm excitation. Further to understand the solvent influence; the lifetime was investigated in various solvents (Acetone, DCM, DMF, THF) with different polarity and exhibited mono exponential behaviour reveals the presence of a single chemical environment around the europium ion. The luminescent lifetime values (τ) of Eu^{III} complex found to be 0.53 ms (in $CHCl_3$ solution) and 0.218 ms (in solid state, bi-exponential), respectively. It indicates that the non-radiative relaxation is high in the case of solid. The lifetime of the ligand is also calculated and found to be $1.7x10^{-3}$ ($CHCl_3$ solution). The lifetime changes were observed in different solvents and shown decreased in the order of DMF (0.46) > THF (0.44) > DCM (0.39) > Acetone (0.38) for Eu^{III} complex. In liquid systems the quenching of lifetime is due to non-radiative relaxation via vibronic coupling and it is less in the case of the $CHCl_3$ solution. It could be C-H vibrational oscillators frequency is less compare to that of O-H and N-H.

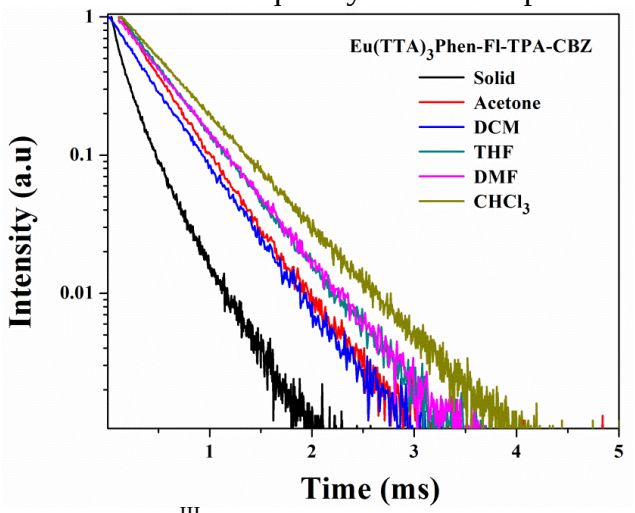

Figure 5.40 The lifetime of the Eu^{III} complex in different solvents and in the form of solid.

5.3.3.3.5 J-O- Spectral parameters:

The calculated Judd-Ofelt (J-O) parameters of the complex showed Ω_2 and Ω_4 are 8.95 and 0.90, respectively. The obtained value of intensity parameter, Ω_2 ($^5D_0 \rightarrow {}^7F_2$) is more sensitive to the symmetry and reveals covalent bonding environment between Eu^{III} ion and the surrounding ligand moiety. In fact, it is higher than that of the calculated J-O for $Eu(TTA)_3$Phen-Fl-TPA. In addition, the symmetry ratio also improved in the presently studied Eu^{III}-complex. The overall quantum yield ($\Phi_{overall}$) for a Eu^{III} complex delights the system as a "black box", in which the internal process is not explicitly considered. The overall QY ($\Phi_{overall}$), intrinsic quantum yield (Φ_{Ln}) are explained d in the Chapter 2 (section 2.2.3.2.4). The experimental branching ratio ($\beta_{1\text{-}3}$) of the Eu^{III} was also been determined from the relative areas of the $^5D_0$–^7F_J emission transitions, which associates with the already predicted Judd–Ofelt theory. The obtained Φ_{Ln} and energy transfer efficiency (Φ_{sen}) indicates that the currently studied ligand is efficient sensitizer for Eu^{III} ion. In addition, the Φ_{sen} is higher than the TPA based Eu-complex. All the calculated parameters are tabulated in Table 5.10 and 5.11.

Table 5.10 Intensity ratio (I_2/I_1), J-O parameters (Ω_2 and Ω_4) and their experimental branching ratios (β_{1-3}) of the complex.

S. No.	Complex name	A_{0-1}	A_{0-2}	A_{0-4}	I_2/I_1	Ω_2 (10^{-20} cm^2)	Ω_4 (10^{-20} cm^2)	β_1	β_2	β_3
1.	$Eu(TTA)_3Phen$-Fl-TPA-CBZ	50	759.42	36.11	14.7	8.95	0.90	5.91	89.81	4.27
2.	$Eu(TTA)_3Phen$-Fl-TPA	50	244.43	39.95	4.88	3.36	0.44	14.95	73.09	11.94

Table 5.11 The Radiative (A_{RAD}) and nonradiative (A_{NR}) decay rates, $^5D_0$ lifetime (t_{obs}), intrinsic quantum yield (Φ_{Ln}), energy transfer efficiency (Φ_{sen}) and overall quantum yield ($\Phi_{overall}$) for complex.

S. No.	Complex name	A_{RAD} (S^{-1})	A_{NR} (S^{-1})	τ_{obs} (ms)	τ_{RAD} (ms)	Φ_{Ln} (%)	Φ_{Sen} (%)	$\Phi_{Overall}$ (%)
1.	$Eu(TTA)_3Phen$-Fl-TPA-CBZ	845.53	374	0.218	1.18	18.47	81.21	15.0
2.	$Eu(TTA)_3Phen$-Fl-TPA	334.38	118	0.660	2.99	22.0	55.0	12.1

5.3.3.3.6 Electrochemical Properties:

Cyclic voltammetry analysis gives significant redox properties to understand the energy levels (HOMO and LUMO) of the Eu^{III}-complex and ligand molecule. The Eu^{III}-complex onset potential is 1.32; its ligand potential is 1.23, respectively (Figure 5.41, left). The reduction wave with onset potentials data was listed in Table 5.12. The HOMO and LUMO energy levels were calculated by using equation 2.9 and 2.10. The HOMO and LUMO energy level of the CBZ consisted Eu^{III}-complex is -5.72 and -3.08. The Eu^{III}-complex projected energy gap is around 2.64 eV. Compared with the reported HOMO and LUMO of the $Eu(TTA)_3Phen$ [43], the E_{HOMO} of the complex increases 0.56 eV. These are one of the interesting results for TTA and Phen contained Eu^{III} complex.

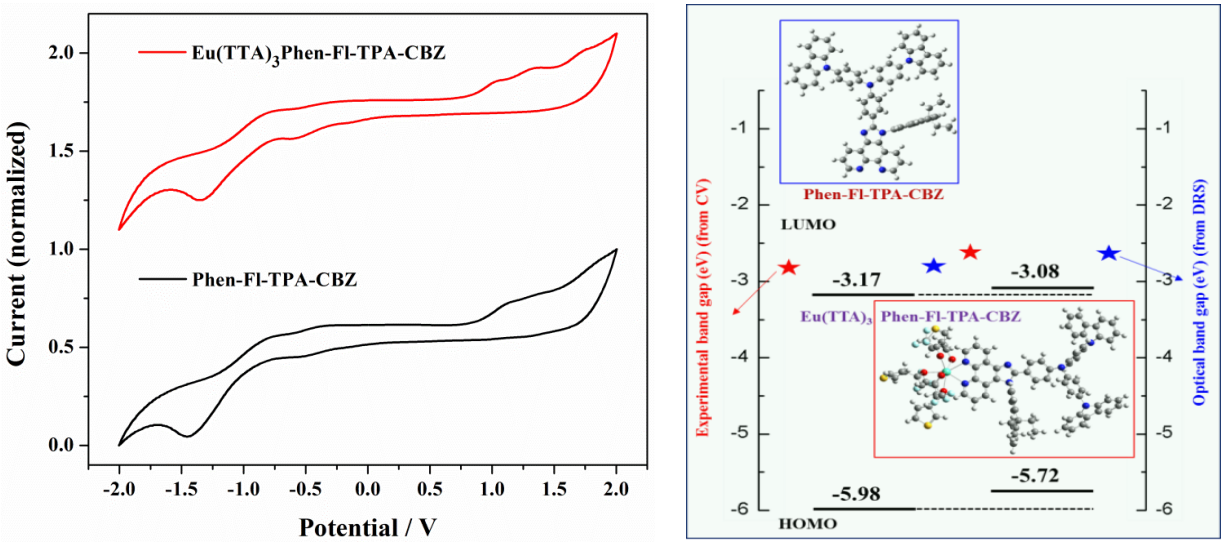

Figure 5.41 Cyclic voltammogram of ligand and its corresponding Eu^{III} complex (left), the energy levels of the ligand as well as Eu^{III} complex arrangement (right).

In the presently studied ligand, each redox reaction involves a reversible one-electron transfer and which is responsible by the presence of phenanthromidazole (phen and imidazole), fluorine and TPA-CBZ moieties. The electron deficient phenanthroimidazole moiety receives the reduction reaction (cathodic active) and electron rich TPA-CBZ moiety (anodic active) receives the oxidation reaction. In addition, it is also worth to note that the DFT analysis showed the existence of electron density on the fluorine moiety in LUMO (Figure 5.42). It is indicating that the fluorine is receiving the reduction reaction. The redox potentials are in the cyclic voltammogram shown not only high peak area waves as well as minor (very less waves) peaks around -0.5 V. The reported TPA based complex shown a similar type of two reduction potentials; in which one is major another one is minor [30].

In the case of currently studied CBZ complex also observed the similar behavior with positive shifting. It is clear that the minor peaks could be attributed to TPA ligand and not related to CBZ moiety in the present complex. In addition, the minor peak is presented in both ligand and complex representing that the peak belongs to the ligand only. In detail, the wave at -0.5 V is expected due to the presence of phenanthromidazole (phen and imidazole) and fluorine moiety. The computational study of optimization is also supporting the same by electron density located on phen and fluorine (LUMO). Each redox reaction involves a reversible one-electron transfer, and each is attributed to a ligand-based redox process. The energy levels of the ligand as well as Eu^{III} complex arrangement has been shown in Figure 5.41, right).

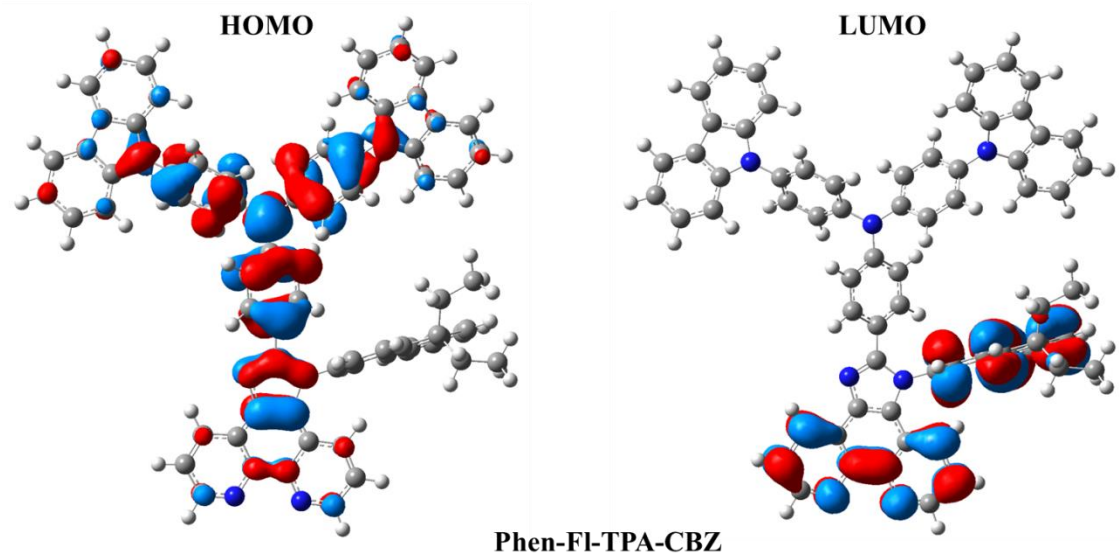

Figure 5.42 The obtained HOMO-LUMO of the ligand.

Table 5.12 Electrochemical properties of the ligands and respective Eu^{III}-complex.

S. No.	Compound Name	$Voltage^{Oxi}_{onset}$[V] (E_{HOMO} [eV])	$Voltage^{Red}_{onset}$[V] (E_{LUMO} [eV])	$\lambda_{onset,}$ [nm] (a)	Energy gap E_g^{Opt}, [eV] (b)
1.	**$Eu(TTA)_3$Phen-Fl-TPA-CBZ**	1.342(-5.72)	-1.32 (-3.08)	467.8	2.65 (2.64)
2.	**Phen-Fl-TPA-CBZ**	1.23 (-5.98)	-1.58 (-3.17)	442.8	2.80 (2.81)

(a) Calculated from the optical absorption (DRS spectra), (b) Calculated the onset wavelength of optical absorption (onset) in solid-state film (DRS spectra). The energy differences (HOMO and LUMO) values calculated by cyclic voltammogram are mentioned in bracket.

5.3.3.3.7 CIE Chromaticity coordinates:

CIE chromaticity coordinates were calculated for ligands and its Eu^{III} complex from emission spectral data's. The CIE color coordinates shown x = 0.61, y = 0.37 and x = 0.66, y = 0.33 for $Eu(TTA)_3$Phen-Fl-TPA-CBZ and $Eu(TTA)_3(H_2O)_2$ (Figure 5.43), respectively. In addition, calculated the CIE coordinates for the relevant ligands also, which are shown in Figure 5.43. Further, the CIE calculated values for the Eu^{III} complex in solid and thin film results are mentioned in Table 5.13. The CBZ connected Eu^{III} complex results exhibited red color in the CIE gamut color space in three phases and close to NTSC (National Television System Committee) standards.

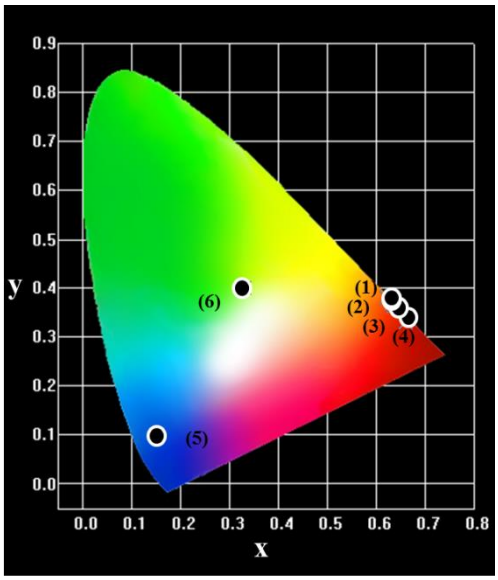

Figure 5.43 The CIE chromaticity coordinates for $Eu(TTA)_3$Phen-Fl-TPA-CBZ in [1) solution, 2) thin film, 3) solid, 4) $Eu(TTA)_3(H_2O)_2$ in solution and ligand in 5) solution, 6) solid].

Table 5.13 The CIE color coordinates for the ligands and Eu^{III} complexes.

S. No.	Compound Name	Solution (a)(b)		Thin film (b)		Solid (b)	
		x	Y	x	y	x	y
1	**$Eu(TTA)_3$Phen-Fl-TPA-CBZ**	0.61	0.37	0.63	0.36	0.64	0.36
2	**Phen-Fl-TPA-CBZ**	0.15	0.10	----	----	0.33	0.40
3	**$Eu(TTA)_3(H_2O)_2$**	0.66	0.33	----	----	----	----

(a) Measured in chloroform solution at 298 K, (b) Emission peaks from PL emission spectra.

5.3.3.3.8 PMMA film of Eu^{III} complex:

We investigated the optical properties of Eu-complex incorporated in PMMA matrix and the corresponding PL spectra shown in Figure 5.44. The digital photographs under 365 nm also shown in the inset of Figure 5.44. The calculated CIE shows good color saturation. It is observed that with increase the percentage of Eu^{III} complex doping with PMMA, emission intensity increased as well as the CIE color coordinates (0.1 %, x = 0.54, y = 0.42; 0.5 %, x = 0.55, y = 0.42 and 1 %, x = 0.61, y = 0.37) move towards

pure or saturated red emission. The asymmetric intensity ratio of (I_2/I_1) Eu^{III} complex doped in PMMA shown 0.1, 0.5 and 1% are 5.98, 6.07 and 8.85, respectively. In addition, when thin film made doping with PMMA in different ratios; the color intensity as well as asymmetric ratio also increases with increasing the doping ratio. It is signifying that the concentration of the Eu^{III} complex is influencing on the same. It can be supported by asymmetric ratios of the pure thin film is high. The number of observed photons is less in doped PMMA results decrease in intensity of the complex and leads to high symmetry.

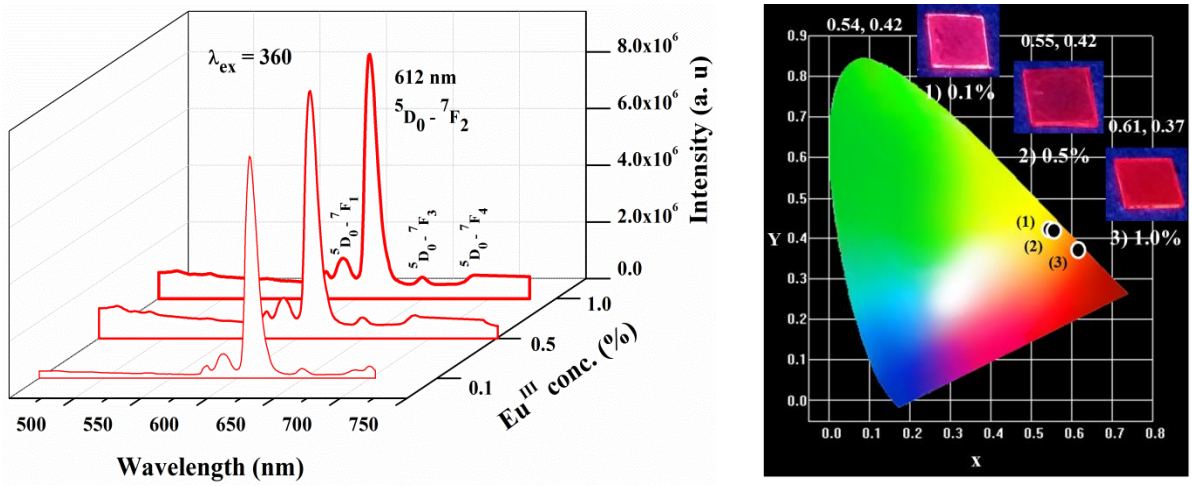

Figure 5.44 The emission spectra of Eu^{III} complex doped PMMA in different percentage ratio (left) and its CIE color coordinates as well as their thin film patterns (right).

5.3.3.3.9 LED fabrication using CBZ based Eu-complex:

The Eu-complex was conjugated with the InGaN UV LED (395 nm) shown in the Figure 5.45. The fabricated LED with 1-10 ratios (Eu-PMMA) was shown orange red emission and 1-50 ratio shown yellowish white emission. The increasing the concentration of the Eu-complex, increasing of the broad band emission in the region of 420-550 nm in the Eu-complex was observed. The broad emission in the Eu-complex is attributed to the ligand emission and it is leads to deviating from the red emission. To support the same, the thin film of the Eu-complex was also shown less intensive ligand emission from the complex by increasing the concentration of the Eu-complex. Furthered, it can also achieve the white emission by balancing the ligand as well as Eu^{III} ion emission.

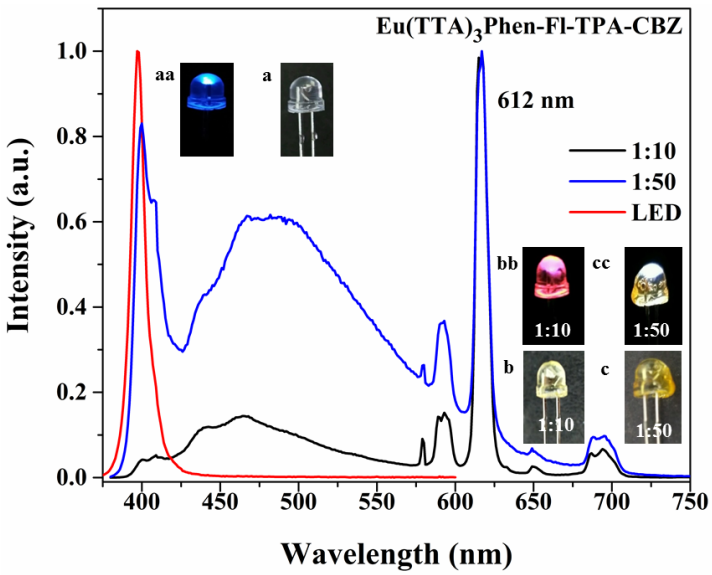

Figure 5.45 LED (395 nm) congugated with Eu-complex. **a** is LED without coating and **aa** is with forward bias. b (1:10) and c (1:50) are Eu^{III} complex coated LEDs and bb, cc is in forward bias.

5.4 Summary and conclusion:

In conclusion, the newly synthesized DPA based Eu^{III} complex acting as a single component white-light-emitter and it is due to balancing the primary RGB colors in toluene. Whereas, the CBZ based Eu-complex shows red emission due to complete energy transfer from ligand to Eu^{III} metal ion. The TD-DFT calculations on singlet and triplet excited states and PL lifetime studies also support the energy transfer mechanism. The temperature dependent PL emission color tuning will certainly give direction to use the presently studied DPA based Eu-complex as a temperature sensor. In addition, the same conjugated with LED (395 nm) shown bright white light emission with appropriate CIE coordinates. In contrast, CBZ based Eu-complex shows red emission from the fabricated LED. The PLQY showed better improvement in $Eu(TTA)_3$Phen-fl-TPA-CBZ (44.4%). The TGA-DSC analysis was showed good thermal decomposition, is above 270°C. The electrochemical analysis was shown HOMO and LUMO energy levels for the Eu^{III}-complex is around 5.72 and 3.08 eV, respectively. All the experimental findings supports that the currently synthesized complexes could be useful in white LEDs and ratiometric temperature sensor.

5.5 References:

[1] (a) S. Li, G. Zhong, W. Zhu, F. Li, J. Pan, W. Huang and H. Tian, *J. Mater. Chem.*, 2005, **15**, 3221; (b) J. D. Furman, A. Y. Warner, S. J. Teat, A. A. Mikhailovsky and A. K. Cheetham, *Chem. Mater.*, 2010, **22**, 2255–2260; (c) S. Reineke, F. Lindner, G. Schwartz, N. Seidler, K. Walzer, B. Lussem and K. Leo, *Nature*, 2009, **459**, 234; (d) A. H. Shelton, I. V. Sazanovich, J. A. Weinstein and M. D. Ward, *Chem. Commun.*, 2012, **48**, 2749; (e) K. T. Kamtekar, A. P. Monkman and M. R. Bryce, *Adv. Mater.*, 2010, **22**, 572; (f) G. Shao, H. Yu, N. Zhang, Y. He, K. Feng, X. Yang, R. Cao and M. Gong, *Phys. Chem. Chem. Phys.*, 2014, **16**, 695–702; (g) Z. Wang, H. Yang, P. He, Y. He, J. Zhao and H. Tang, *Dalton Trans.*, 2016, **45**, 2839–2844; (h) S. Liu, P. He, H. Wang, J. Shi and M. Gong, *Inorg. Chem. Commun.*, 2009, **12**, 506–508.

[2] J. B. H. Kwon, H. S. Jang, H. S. Yoo, S. W. Kim, D. S. Kang, S. Maeng, D. S. Jang, H. Kim and D. Y. Jeon, *J. Mater. Chem.*, 2011, **21**, 12812.

[3] Q. Wang and D. Ma, *Chem. Soc. Rev.*, 2010, **39**, 2387.

[4] S. Park, J. E. Kwon, S. H. Kim, J. Seo, K. Chung, S. Y. Park, D. J. Jang, B. M. Medina, J. Gierschner and S. Y. Park, *J. Am. Chem. Soc*., 2009, **131**, 14043.

[5] Z. Xie, C. Chen, S. Xu, J. Li, Y. Zhang, S. Liu, J. Xu and Z. Chi, *Angew. Chem.Int. Ed.*, 2015, **54**, 7181.

[6] H. J. Bolink, F. D. Angelis, E. Baranoff, C. Klein, S. Fantacci, E. Coronado, M. Sessolo, K. Kalyanasundaram, M. Gratzel and Md. K. Nazeeruddin, *Chem. Commun.*, 2009, 4672.

[7] (a) P. Coppo, M. Duati, V. N. Kozhevnikov, J. W. Hofstraat and L. De Cola, *Angew. Chem. Int. Ed.*, 2005, **44**, 1806; (b) D. Sykes, I. S. Tidmarsh, A. Barbieri, I. V. Sazanovich, J. A. Weinstein and M. D. Ward, *Inorg. Chem.*, 2011, **50**, 11323.

[8] (a) J. P. Duan, P. P. Sun and C. H. Cheng, *Advances in Technology of Materials and Materials Processing*, 2004, **6**, 95-102; (b) W. Centennial, *Coordination chemistry of the lanthanide elements–one hundred years of development and understanding*, 1967, **62**, Chapter 21, pp. 306–317; (c) J. C. G. Bunzli and A. S. Chauvin, in Handbook on the Physics and Chemistry of Rare Earths, ed. J. C. G. Bunzli and V. K. Pecharski, *Elsevier Science Publishers*, Amsterdam, 2014, **44**, pp. 169–281.

[9] (a) A. Kar, S. Kundu and A. Patra, *RSC Adv.*, 2012, **2**, 4879; (b) R. Wang, J. Peng, F. Qiu, Y. Yang and Z. Xie, *Chem. Commun*., 2009, 6723; (c) G. He, D. Guo, C. He, X. Zhang, X. Zhao and C. Duan, *Angew. Chem. Int. Ed.*, 2009, **48**, 6132; (d) A. H. Shelton, I. V. Sazanovich, J. A. Weinstein and M. D. Ward, *Chem. Commun.*, 2012, **48**, 2749; (e) J. Zhang, H. Li, P. Chen, W. Sun, T. Gao and P. Yan, *J. Mater. Chem. C*, 2015, **3**, 1799.

[10] B. Rajamouli, P. Sood, S. Giri, V. Krishnan and V. Sivakumar, *Eur. J. Inorg. Chem.*, submitted.

[11] (a) Y. Zheng, J. Lin, Y. Liang, Q. Lin, Y. Yu, Q. Meng, Y. Zhou, S. Wang, H. Wang and H. Zhang, *J. Mater. Chem.*, 2001, **11**, 2615; (b) C. R. De Silva, R. Wang and Z. Zheng, *Polyhedron*, 2006, **25**, 3449.

[12] H. Xia, J. He, P. Peng, Y. Zhou, Y. Li and W. Tian, *Tetrahedron Letters*, 2007, **48**, 5877.

[13] L. Ji, Q. Fang, M. Yuan, Z. Liu, Y. Shen and H. Chen, *Organic letters*, 2010, **12**, 5192.

[14] Z. Ning, Z. Chen, Q. Zhang, Y. Yan, S. Qian, Y. Cao and H. Tian, *Adv. Funct. Mater*, 2007, **17**, 3799.
[15] M. Latva, H. Takalo, V. M. Mukkala, C. Matachescu, J. C. Rodriguez-Ubis and J. Kankare, *J. Lumin.*, 1997, **75**, 149.
[16] H. Xu, L. H. Wang, X. H. Zhu, K. Yin, G. Y. Zhong, X. Y. Hou and W. Huang, *J. Phys. Chem. B*, 2006, **110**, 3023.
[17] (a) M. Shi, F. Li, T. Yi, D. Zhang, H. Hu and C. Huang, *Inorg. Chem.*, 2005, **44**, 8929; (b) T. Li, W. Shang, F. Zhang, L. Mao, C. Tang, M. Song, C. Du and Y. Wu, *Engineering*, 2011, **3**, 301.
[18] C. Yang, L. M. Fu, Y. Wang, J. P. Zhang, W. T. Wong, X. C. Ai, Y. F. Qiao, B. S. Zou and L. L. Gui, *Angew. Chem. Int. Ed.*, 2004, **43**, 5010–5013.
[19] D. A. Anthony, E. G. Moore, G. Szigethy, J. Xu and N. R. Kenneth, *Inorg. Chem.*, 2009, **48**, 9316.
[20] R. Pavithran, M. L. P. Reddy, S. A. Junior, R. O. Freire, G. B. Rocha and P. P. Lima, *Eur. J. Inorg. Chem.*, 2005, 4129.
[21] (a) S. W. Allison and G. T. Gillies, *Rev. Sci. Instrum.*, 1997, **68**, 2615; (b) B. Zelelow, G. E. Khalil, G. Phelan, B. Carlson, M. Gouterman, J. B. Callis and L. R. Dalton, *Sensors and Actuators B: Chemical*, 2003, **96**, 304-314; (c) S. M. Borisov and O. S. Wolfbeis, *Anal. Chem.*, 2006, **78**, 5094–5101.
[22] Z. Ning, Z. Chen, Q. Zhang, Y. Yan, S. Qian, Y. Cao and H. Tian, *Adv. Funct. Mater.*, 2007, **17**, 3799.
[23] C. Pettinari, F. Marchetti, A. Cingolani, A. Drozdov, I. Timokhin, S. I. Troyanov, V. Tsaryuk and V. Zolin, *Inorg. Chim. Acta*., 2004, **357**, 4181.
[24] C. Yang, J. Luo, J. Ma, D. Zhu, L. Miao, Y. Zhang, L. Liang and M. Lu, *Synth. Met*., 2012, **162**, 1097.
[25] J. Bao, H. Tian and R. Tang, *Inorg. Chim. Acta*., 2013, **401**, 19.
[26] C. J. Xu, F. Xie, X. Z. Guo and H. Yang, *Spectrochimica Acta Part A*., 2005, **61**, 2005.
[27] C. H. Chang, M. H. Yun and W. J. Choi, *Synth. Met.*, 2004, **145**, 1.
[28] S. L. Liu, C. L. Wen, S. S. Qi and E. X. Liang, *Spectrochimica Acta Part A.*, 2008, **69**, 64.
[29] Q. G. Wu, M. Esteghamatian, N. X. Hu, Z. Popovic, G. Enright, Y. Tao, M.D. Iorio and S. N. Wang, *Chem. Mater*., 2000, **12**, 79.
[30] B. Rajamouli, P. Sood, S. Giri, V. Krishnan and V. Sivakumar, *Eur. J. Inorg. Chem*., 2016, 3900.
[31] T. Li, W. Shang, F. Zhang, L. Mao, C. Tang, M. Song, C. Du and Y. Wu, *Engineering*., 2011, **3**, 301.
[32] A. V. Kharchevaa, A. V. Ivanovb, N. E. Borisovab, T. P. Kaminskayaa, S. V. Patsaevaa, V. V. Popova and V. I. Yuzhakov, *Proc. of SPIE*, 2014, 9448.
[33] Zhang, B. Li, B. Lei, Z. Hong and W. Li, *J. Lumin.*, 2008, **128**, 67.
[34] Zhang and B. Li, *J. Lumin.*, 2009, **129**, 1304.
[35] T. Zhu, P. Chen, H. Li, W. Sun, T. Gao and P. Yan, *Phys. Chem. Chem. Phys*., 2015, **17**, 16136.
[36] S. I. Klink, G. A. Hebbink, L. Grave, P. G. B. O. Alink, F. C. J. M. van Veggel and M. H. V. Werts, *J. Phys. Chem. A.*, 2002, **106**, 3681.
[37] T. L. Yang and W. W. Qin, *Indian J. Chem, Sec. A*, 2006, **45**, 2035–2039.

[38] A. D'Aleo, E. G. Moore, G. Szigethy, J. Xu and K. N. Raymond, *Inorg. Chem.*, 2009, **48**, 9316–9324.
[39] F. J. Steemers, W. Verboom, D. N. Reinhoudt, E. B. V. Tol and J. W. Verhoeven, *J. Am. Chem. Soc.*, 1995, **117**, 9408–9414.
[40] G. F. de Sa, O. L. Malta , C. de Mello Donega, A. M. Simas, R. L. Longo, P. A. Santa-Cruz and E. F. da Silva Jr, *Coord. Chem. Rev.*, 2000, **196**, 165–195.
[41] J. H. S. K. Monteiro, A. Bettencourt-Dias and F. A. Sigoli, *Inorg. Chem.*, 2017, **56**, 709−712.
[42] C. Yang, J. Xu, J. Ma, D. Zhu, Y. Zhang, L. Liang and M. Lu, *Photochem. Photobiol. Sci.*, 2013, **12**, 330.
[43] Y. Ohmori, H. Kajii, T. Sawatani, H. Ueta and K. Yoshino, *Thin Solid Films.*, 2001, **393**, 407.

Chapter 6

Mono and binuclear luminescent Eu^{III} molecular complexes for white light emitting diodes: combined Experimental and theoretical study

Abstract

The effect of functionalization of carbazole with spacer in C1 position and fluorine in N1 position in the phenanthroline-imidazole based bipolar ligand has been designed, synthesised, same is utilized to synthesise $Eu(TTA)_3$Phen-Fl-O-CBZ complex and studied their photophysical properties. In addition, phenyl and fluorene functionalization in N1 position of phenanthro-imidazole ring (with alkoxy spacer) and its influence on photophysical properties of their binuclear Eu-complexes were systematically investigated. The mono and binuclear Eu-complexes emission spectra (pure red emission) clearly indicate that the complete energy transfer from ligand (L) to Eu^{III} ion occurs, since there is no emission from ligand was encountered (confirmed by DFT and TD-DFT calculations). It is found that the spacer molecule can decrease the energy gap of HOMO-LUMO energy levels (2.6 eV) with respect to that of without spacer one and increment in the singlet and triplet energy levels was also observed, consequences efficient energy transfer (L to M). The enhanced QY observed by 1% doping with PMMA as compare with other doping concentrations (14.2%). Binuclear Eu show dominant electric dipole transition of Eu^{III} ion ($^5D_0 \rightarrow {}^7F_2$, confirms the Eu^{III} ion in the non-centrosymmetric site). The highest QY (59.5 %, for thin film) obtained for the $Eu_2(TTA)_6$(L2). The binuclear Eu^{III} complexes were combined with InGaN near UV LED, obtained pure red emission with CIE color coordinate values x = 0.65, y = 0.34 and x = 0.66, y = 0.33 for $Eu_2(TTA)_6$(L1) and $Eu_2(TTA)_6$(L2), respectively. The obtained results indicate that the synthesized complexes are potential aspirant for light converting devices.

Key words: Europium; spacer molecule; binuclear complex

6.1 Introduction:

Lanthanide based complexes are attractive due to their own merits such as unique optical properties (4f-4f and 4f-5d electronic transitions), high quantum yield, long luminescent lifetime (μs – ms), low long-term toxicity and structural versatility [1-3]. There are numerous reports are available on luminescent lanthanide complexes for different applications, such as tunable lasers, plastic optical fiber amplifiers (POFA), multi color displays, solar energy convertors, [4, 5] biomedical analyses, optical sensors cell [6], tissue imaging, medical diagnosis and protein labelling [7, 8]. Eu^{III} based complexes are extensively growing attention for medical diagnostics [9], biomarkers [10], electroluminescent materials [11-14], phosphors for white LEDs [15] materials, owing to their simple energy levels of Eu^{III}, as well as efficient line like or narrow band red emission. Eu^{III} and Tb^{III} based complexes exhibit numerous appropriate characteristics, when associated with that of conventional organic fluorophores, which makes them prominent candidate for the biomedical imaging lighting applications. The long excited state lifetimes large energy shift between absorbed and emitted radiations (in the case of ligand sensitization) and very narrow emission bands; these two effects allow the separation of Ln^{III} luminescence and the short-lived background fluorescence [16].

It is well documented that the Eu^{III} based complexes are used as ratiometric optical sensors by monitoring two major emission bands, most commonly the magnetic dipole (MD) $^5D_0 \rightarrow {}^7F_1$ ($\Delta J = 1$) and electric dipole (ED) transition $^5D_0 \rightarrow {}^7F_2$ ($\Delta J = 2$) bands [17-19]. The MD induced $\Delta J = 1$ transition is relatively insensitive to changes in coordination sphere whereas the $\Delta J = 2$ and $\Delta J = 4$ transitions are hypersensitive and generally change substantially upon formation of a new Eu complex. Due to their parity forbidden intra-configurational 4f–4f transitions, the lanthanide ions feature very low absorption coefficients or oscillator strength and hence their direct photoexcitation is inefficient. Therefore, it is necessary to introduce organic chromophoric ligands as sensitizers, which can indirectly populate the higher excited level via energy transfer to boost the emission intensity of lanthanides [20, 21]. The energy transfer or sensitization process usually involves a triplet excited state of a ligand, thus requires efficient intersystem conversion (ISC) in the ligand (facilitated by the heavy metal ion effect) as well as an appropriate alignment of the triplet state energy (T) over that of the accepting lanthanide state(s) [22]. In the case of Eu^{III}, an optimal energy gap (ΔE) should be in the range of ∼2500–3000 cm^{-1}. In proper alignment of triplet energy to the Eu excited levels (lower ΔE values) would enable back energy transfer and thus reduce sensitization efficiency or possibility of obtaining multiple emissions from ligand as well as metal centre [23].

β-diketone based ligands are widely studied and highly represented as one of the important "antennas" for facilitating efficient energy transfers to Eu^{III} ion by ligand sensitization, as a result producing highly harvested emissions in the respective spectral windows [24]. The modification of the ligand structure (β-diketone) on the emission quantum yield of Eu^{III} complexes has been reported [25].

6.2 Mononuclear Europium complex – Effect of carbazole functionalization with spacer moiety in phenanthroimidazole bipolar ligand in Eu^{III} complex on its luminescence properties:

6.2.1 Outline of the Present Study:

In the previous chapter (3 and 5) phenanthroline-TPA based Eu^{III} complex without spacer molecule was designed, synthesised and investigated their photophysical properties [26]. Though a few reports are available related to the functionalization of the phenanthro-imidazole neutral ligand for different applications and especially electroluminescence materials by an employing spacer moieties or molecules are preferred. Arresting the electronic communication between the functional groups with the ligating site is more important, which will give enhanced EL properties in the OLED device [27, 28]. In the present investigation, efforts have been made to separate the electronic communication between the functional moiety to the phenanthro-imidazole and CBZ group by spacer consisting of ether type of molecule (o-alkly group). In general, there are many reports were documented based on carbazole as a hole transporting moiety and straight conjugation (connected at C1 position) with phenanthroline-imidazole. In addition, an alkyl group at N1 position studied often. Straight conjugation is favourable for the low band gap and it is ethical for device applications. Hence, it is capable to get the efficient energy transfer leads to high quantum yields. The ligand and the complex were characterized by routine spectroscopic techniques. The ligand structure was optimized by using DFT calculations. The excited state property of the ligand was studied by time-dependent density functional theory (TD-DFT) calculation. The designed and synthesized bipolar ligand involved Eu^{III} complex structure is represented in Figure 6.1.

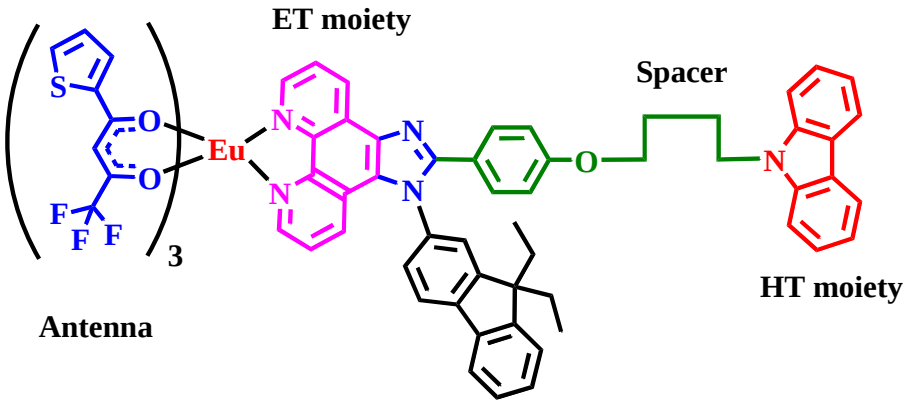

$Eu(TTA)_3$ Phen-Fl-O-CBZ

Figure 6.1 Chemical structure of bipolar ligand based Eu^{III} complex.

6.2.2 Experimental:

6.2.2.1 Materials:

The general information for the synthesis is given in Chapter 2. 1, 4-dibromo butane, 4-hydroxybenzaldehyde, was purchased from Sigma-Aldrich chemicals company.

6.2.2.2 Measurements:

The details of the physical measurement are given in Chapter 2 (2.2.2).

6.2.2.3 Preparation of PMMA thin film:

The Eu^{III} complex was doped with PMMA in 0.1, 0.5 and 1% ratio (PMMA : Eu^{III} = 99.9 : 0.1, 99.95 : 0.5, 99 : 1 in mg) by using chloroform solution with spin coated by two stages were at 500 (20 sec) and 2000 rpm (30 sec), respectively. The prepared thin films were kept under vacuum at 50 °C for 3hrs to get excess solvent evaporation.

6.2.2.4 Synthesis:

The compounds 9,9-diethyl-9H-fluoren-2-amine (Fl, Chapter 2), 4-(4-bromobutoxy)benzaldehyde (1) and 4-(4-(9H-carbazol-9-yl)butoxy)benzaldehyde (2) was synthesized by reported references [29]. Synthesis of 1,10-phenanthroline-5,6-dione and the Eu-complex tris(thenoyltrifluoroacetone)europium(III) ($Eu(TTA)_3.2H_2O$) was mentioned in Chapter 2. Synthesis scheme was shown in Scheme 6.1.

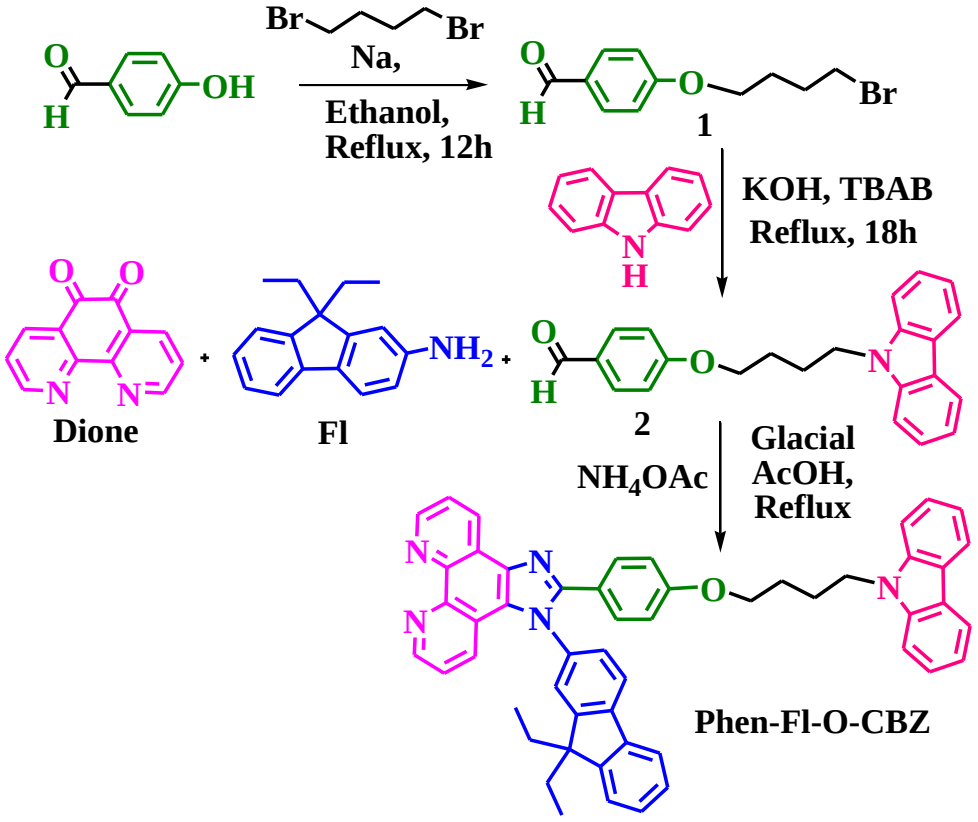

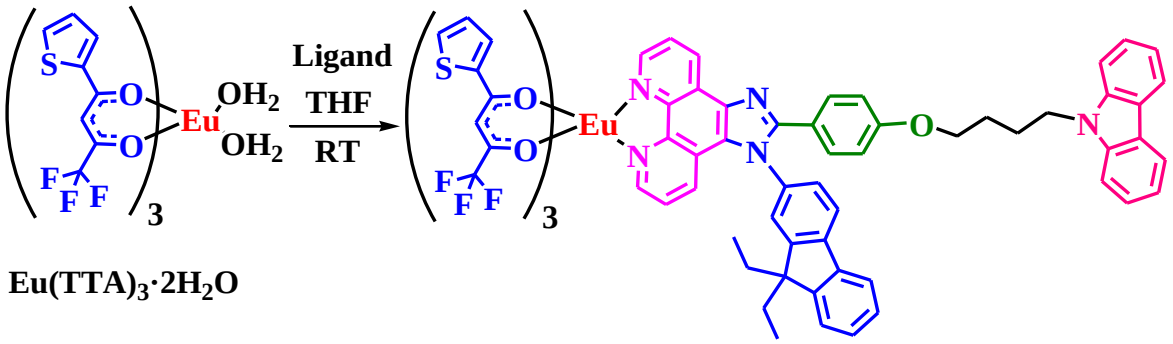

Scheme 6.1 Synthetic route of CBZ attached ether functionalized ligand and the corresponding β- diketonate Eu^{III} ternary complex.

6.2.2.4.1 ***Synthesis of 2-(4-(4-(9H-carbazol-9-yl)butoxy)phenyl)-1-(9,9-diethyl-9H-fluoren-7-yl)-1H-imidazo[4,5-f][1,10]phenanthroline (Phen-Fl-O-CBZ)*:**

2 (0.918 g, 4.373 mmol) was taken in round bottom flask and added 4 (1.5 g, 4.373 mmol) in glacial acetic acid (20 mL) at room temperature. To this reaction mixture subsequently ammonium acetate (3.36 g, 43.73 mmol) and 1 (1.14 g, 4.810 mmol) were added. Then resulting mixture was stirred for 12 hrs at 110 °C. The progress of the reaction was monitored by TLC (MeOH in chloroform 1:9, Rf-0.3). The RM was poured into minimum amount of water and then added ammonium hydroxide solution. The obtained solid was filtered and dissolved in dichloromethane, followed by dried with anhydrous sodium sulphate. The solvent was evaporated to get crude compound (0.5 g). This was purified with column chromatography by using silica gel (100-200 mesh), eluent with 5% methanol in chloroform. The obtained product was dissolved in minimum amount of THF solution added excess of hexane solvent, the pale yellow color solid was formed is 400 mg (58.0%). ^{1}H-NMR Data (400 MHz, DMSO-d_6): δ (in ppm) 9.05-9.04 (m, 1H), 8.97 (d, J = 1.6 Hz, 1H), 8.88 (dd, J_1 = 1.2 Hz, J_2 = 4 Hz, 1H), 8.10 (dd, J_1 = 2.8 Hz, J_2 = 7.8 Hz, 3H), 7.98 (t, J = 6 Hz, 1H), 7.85 (d, J = 1.2 Hz, 1H), 7.85 – 7.79 (m, 1H), 7.61 (dd, J_1 = 1.6 Hz, J_2 = 8.0 Hz, 1H), 7.57 - 7.51 (m, 4H), 7.47 - 7.34 (m, 8H), 7.15 (t, J = 7.2 Hz, 2H), 6.77 (d, J = 8..8 Hz, 2H), 2.06 – 1.96 (m, 4H), 1.84 (t, J = 7.2 Hz, 2H), 1.65 (t, J = 6.4 Hz, 2H), 0.29 (t, J = 7.2 Hz, 3H), 0.12 (t, J = 7.2 Hz, 3H). ^{13}C-NMR Data (100 MHz, DMSO-d_6): δ (in ppm) 159.7, 152.2, 152.1, 150.3, 148.8, 147.8, 144.3, 144.0, 143.3, 140.3, 140.2, 136.9, 135.5, 130.8, 130.1, 128.7, 127.9, 127.7, 126.8, 126.0, 124.3, 124.1, 123.8, 123.4, 122.6, 122.4, 122.1, 121.2, 120.7, 119.8, 119.1, 114.4, 109.6, 67.6, 56.7, 42.2, 32.3, 25.5, 14.4, 9.2. ESI-MS: m/z = 754.56 $[M + H]^+$.

6.2.2.4.2 ***Synthesis of Eu(TTA)$_3$Phen-Fl-O-CBZ*:**

Taken a 50 mL two neck round bottom flask with nitrogen containing balloon adaptor and poured $Eu(TTA)_3$. $2H_2O$ (226 mg, 0.265 mmol, 1 eq) dissolved in dry chloroform ($CHCl_3$) (15 mL). To the above solution added mixture of ligand (200 mg, 0.265 mmol, 1eq) in THF (10 mL) and the reaction mixture (RM) stirred for 12 hrs at room temperature. The resulting product was dissolved in minimum amount of THF and added excess of hexane to get solid product is pale yellow color with 270 mg (65.0%). Elemental analysis: Anal. Calc. for $C_{76}H_{55}EuF_9N_5O_7S_3$:

C, 58.16; H, 3.53; N, 4.46; S, 6.13; Found: C, 57.95; H, 3.82; N, 4.74; S, 6.19%. ESI-MS: m/z = 1569 $[M - H]^+$.

6.2.2.5 FT-IR spectroscopy:

The Fourier transforms (FT-IR) spectrum of the europium complex exhibits the νs(C=O) absorption band due to a strong interaction between oxygen atoms from β-diketone and europium, which leads to stabilization by the resonated chelate ring. As we can see from Figure 6.2, a shift of C=O stretching in Eu^{III} complex is ~1597 cm^{-1}, while in the $Eu(TTA)_3$ is ~1610 cm^{-1}. This observation is important and could take as evidence that the Eu^{III} ion is coordinated through the β-diketone oxygen atoms.

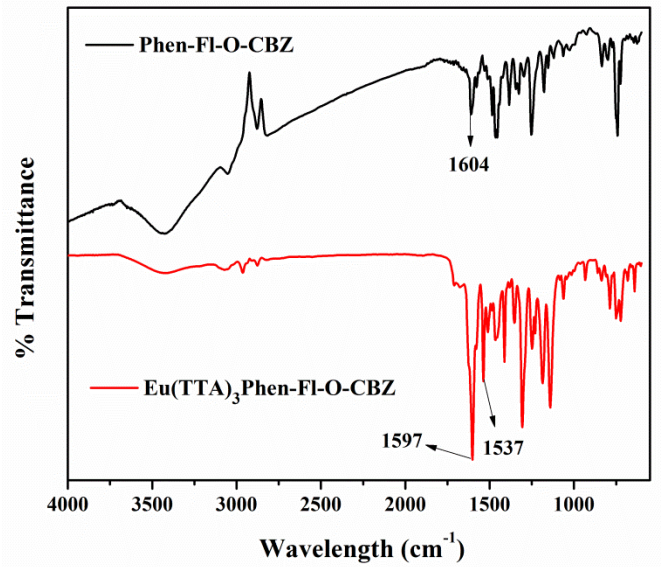

Figure 6.2 FT-IR spectra of the ligand and corresponding Eu^{III}-complex.

In addition, C=N stretching of the ligand also changed from 1604 cm^{-1} (Phen-Fl-O-CBZ only) to 1537 cm^{-1} ($Eu(TTA)_3$Phen-Fl-O-CBZ). All the vibration frequencies are listed in Table 6.1. The perceived peak at 3432 cm^{-1} is due to water molecules present in the $Eu(TTA)_3 \cdot 2H_2O$, which was also observed in the Phen-Fl-O-CBZ as well as $Eu(TTA)_3$Phen-Fl-O-CBZ (comparatively less). It is due to absorbed moisture in the KBr palette. However, in the case of $Eu(TTA)_3$Phen-Fl-O-CBZ was shown very less intensive peak at ~3409 cm^{-1} (Figure 6.2) and it clearly suggesting that the water molecules in the $Eu(TTA)_3 \cdot 2H_2O$ are replaced by bidentate Phen-Fl-O-CBZ.

Table 6.1 The foremost Infrared stretching frequencies (wavenumber in cm^{-1}) for free Phen-Fl-O-CBZ, its corresponding $Eu(TTA)_3$Phen-Fl-O-CBZ complex and $Eu(TTA)_3$.

(Wavenumber in cm^{-1})	**$Eu(TTA)_3$Phen-Fl-TPA-CBZ**	**Phen-Fl-TPA-CBZ**	**$Eu(TTA)_3$**
ν (C=O)	1597	--.--	1610
ν (C=N)	1537	1604	--.--
ν (C-N)	1252	1248	--.--
ν (C-F)	1305	--.--	1298
ν (C-CF_3)	1141	--.--	1133
ν (C-H phen)	837, 750	832, 742	--.--

6.2.3 Results and Discussion:

The results and discussion part briefly emphasises the synthesis of $Eu(TTA)_3$Phen-Fl-O-CBZ and their photophysical/luminescent properties in detail. The effect of the carbazole functionalization of the ligand (Phen-Fl-O-CBZ) and the complexation the same has been achieved. The synthesised ligand and complex were characterized by using multiple spectroscopic techniques (nuclear magnetic resonance spectroscopy (^{1}H and ^{13}C NMR (Figure 6.S1-6.S2), ESI-Mass spectrometry (Figure 6.S3), Elemental analysis, FT-IR, etc).

6.2.3.1 Powder X-ray diffraction (PXRD) studies and Thermal Properties:

The powder X-ray diffraction of ligand and the corresponding complex is shown in Figure 6.3 (left). The complex as well as ligand shows amorphous nature in PXRD analysis. It is observed that the d (angle) of the Eu^{III} complex is decreases as compare to that of ligand molecule. The shifting of the d (angle) to lower value may refer to the formation of the metal ligand bond in the complex. In accordance with that the twisting architecture of the molecule may be responsible for the same.

To study the thermal stabilities of the bipolar ligand and complex, thermogravimetric analyses (TGA) and differential scanning calorimetry (DSC) were performed (powder samples) under nitrogen atmosphere from ambient temperature to 650 °C (Figure 6.3). The ligand was shown major thermal decomposition at 344 °C with slender decreasing of weight loss. However, the decomposition of the Eu^{III} complex was shown with 2 stages, which are 276, 322 °C. The 5% thermal decomposition of the ligand and complex are shown at 280 and 274 °C, respectively. The first stage is belongs to the TTA and further decomposition is attributed to presence of peripheral groups such as fluorene, CBZ moieties. The decomposition of the Eu^{III} complex showed less gradual decreasing than the ligand counterpart. It is observed that the thermal decomposition is less for ligand than that of complex, which is due to presence of TTA and ligand ternary molecules. The DSC of the ligand as well as Eu^{III} complex also been carried out and found the glass transition (Tg) temperature 233 and 120 °C. The reduced Tg of the complex is attributed to mobility of the complex (Fl, CBZ, Phen and TTA) up on heating.

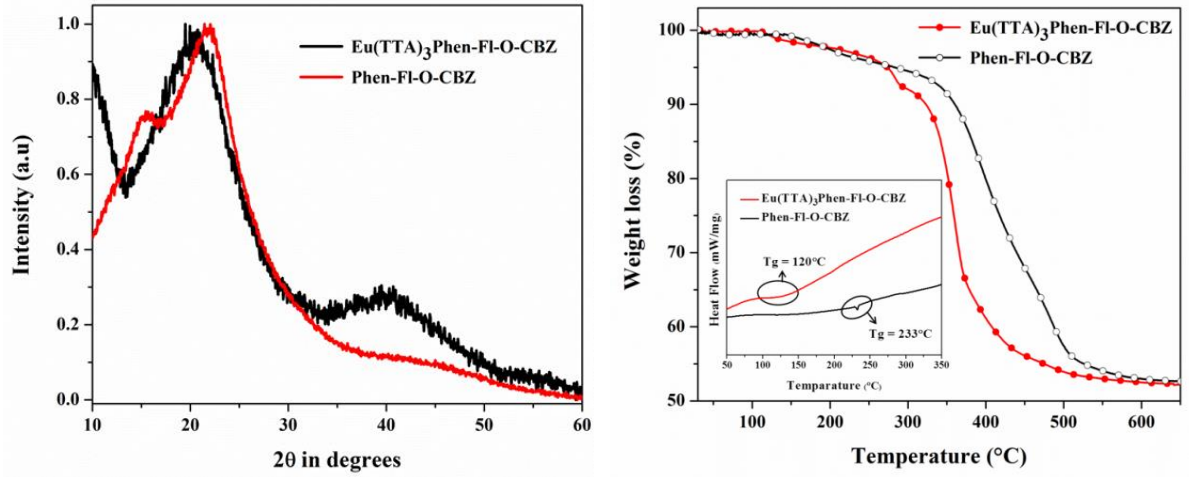

Figure 6.3 PXRD of the ligand and corresponding Eu^{III} complex (left), TG analysis curves for the ligand and its corresponding Eu^{III} complex and in onset mentioned their DSC curves (inset).

6.2.3.1 Photophysical properties:

6.2.3.1.1 UV-Visible absorption and diffuse reflectance spectral studies:

Luminescent europium complexes considered as a light conversion molecular devices by absorbing ultraviolet (UV) radiation and by emitting photons in the visible red spectral region. The UV absorption of the ligand and the corresponding Eu^{III} complex are measured in chloroform solution (10^{-4} mol/Lt, Figure 6.4).

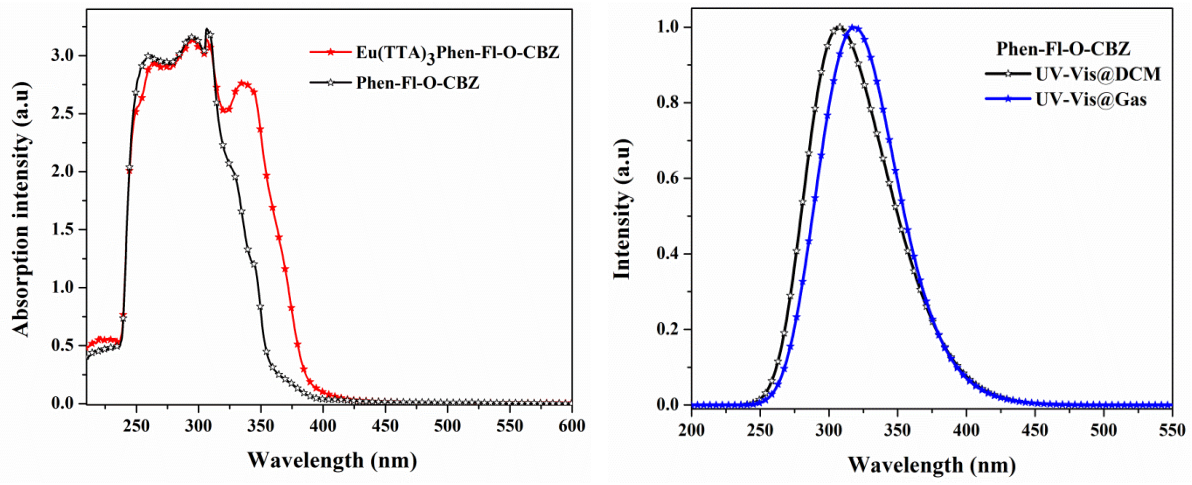

Figure 6.4 The UV absorption spectra of the ligand and respective complex (left); UV-Vis absorption spectra of ligand in DCM/gas (right).

The ligand shown absorption bands at 259, 294, 308, 327, 345 nm and respective complex was shown at 263, 294, 304, 336 nm, respectively (Table 6.2). The peak at ~290 and 350 nm are belongs to the π–π* transition of the ligand and TTA molecule. Consisting of $Eu(TTA)_3$ absorption (273, 340) bands in the $Eu(TTA)_3$Phen-Fl-O-CBZ, indicating that the $Eu(TTA)_3$ existence in the complex (Figure 6.4, left). In order to gain more information regarding the absorption, the ligand structure was first optimized and then UV-absorption of the ligand was calculated in the gas as well in dichloromethane (DCM) by DFT calculation (Figure 6.4, right). The gas as well as in DCM shown absorption at 318, 307 nm, respectively; which are almost similar to that of experimental out comes. The energy gap calculation from the DRS and optimized structure of the Phen-Fl-O-CBZ are shown in Figure 6.5.

Table 6.2 The UV-absorption and PL emission data of synthesized Eu^{III} complexes and ligands.

S. No.	Compound name	UV λ_{max} (abs) [nm] Solution (a) (b)	λ_{ex} (d) [nm]	PL λ_{em} (c) [nm]	FWHM [nm]	I_2/I_1 ratio
1.	**$Eu(TTA)_3$Phen-Fl-O-CBZ**	263, 294, 304, 336	360, 374(d)	580, 592, 612, 652, 702	4.02, 4.14(d)	17.1, 14.6(d)
2.	**Phen-Fl-O-CBZ**	259, 294, 308, 327, 345	365, 360(d)	425, 502 (d)	--.--	--.--
3.	**$Eu(TTA)_3$**	273, 340	275, 340	580, 592, 612, 652, 703	~ 6	~11

(a) measured at 298 K in chloroform solution, (b) absorption peaks from the UV-absorption spectra, (c) emission peaks from PL emission spectra, (d) values of compounds in solid.

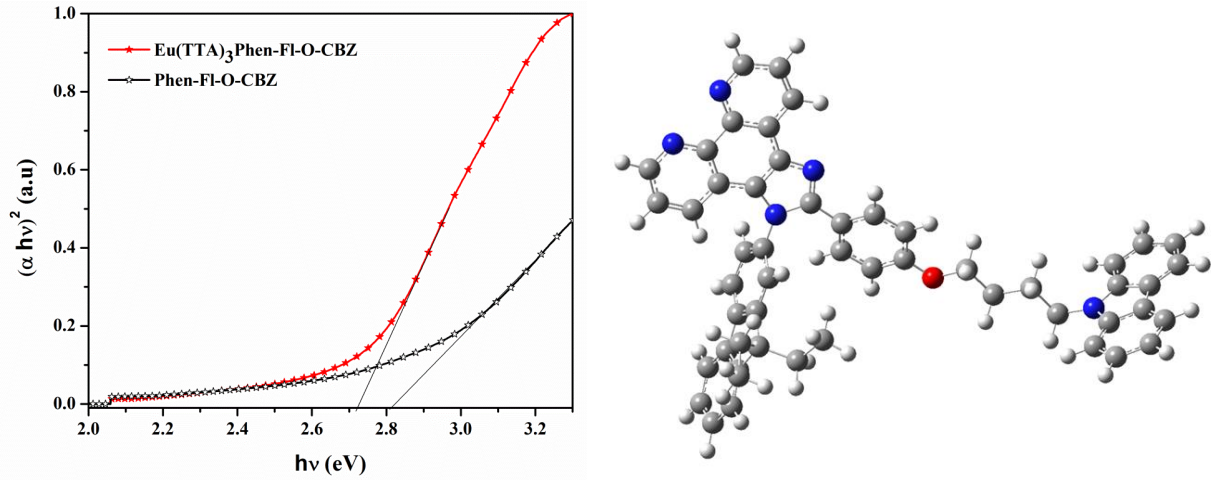

Figure 6.5 The energy gap calculation from the DRS (left); optimized structure of the Phen-Fl-O-CBZ (right).

6.2.3.1.2 PL studies and energy transfer mechanism:

The photoluminescence excitation and emission spectrum in solution as well as solid of Phen-Fl-O-CBZ is shown in Figure 6.6. The emission spectrum of the ligand was shown emission in the region of blue with peak wavelength at 425 nm in solution and shown 502 nm in solid under excitation wavelength at 365 and 360 nm, respectively. Red shift was observed for the emission of ligand moving from solution to solid and it could be attributed aggregation of the complex in the solid state (Figure 6.6, right). However, solid state emission spectrum of ligand shown broad spectrum with peak multiple maxima around at 450, 502 and 610 regions. These peaks are belonging to the primary colors (blue, green and red), and leads to nearly white light emission. It was also reflecting in the CIE color coordinates (Figure 6.13).

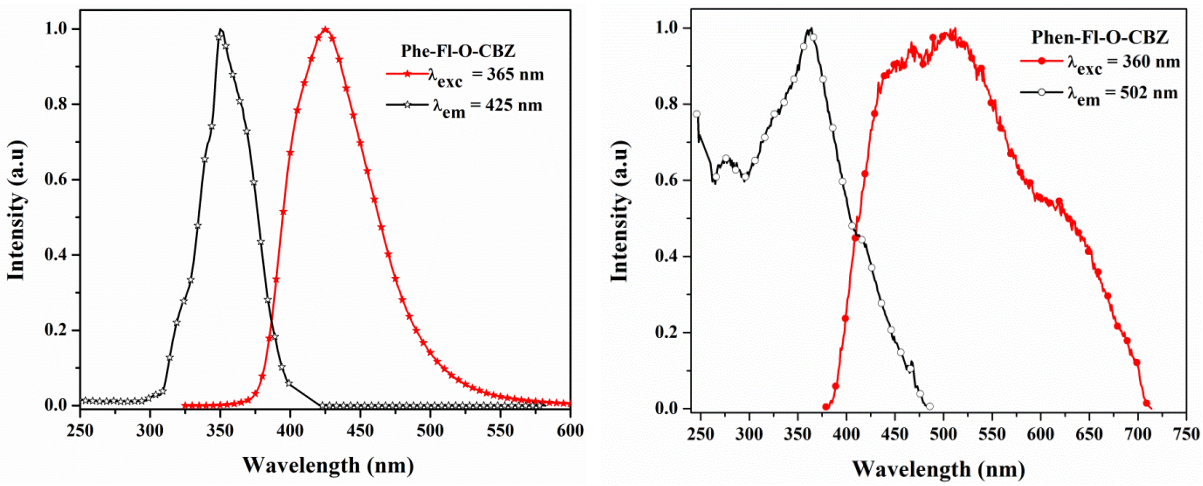

Figure 6.6 The PL excitation and emission spectra of the ligand in solution (left) and solid (right).

The excitation and emission spectra of complex in solution and solid is shown in Figure 6.7, with different wavelength excitations in Figure 6.8. The deactivation of

europium complex of the excited state of $^5D_0$ to the ground states ^7F_J (J=0−4) gives typical Eu^{III} emission bands at ~581, 593, 614, 654, and 702 nm. The excitation spectrum was recorded by monitoring the $^5D_0$-$^7F_2$ transition of Eu^{3+} emission line (electric dipole (ED) transition). The spectrum consisted board band absorption from 275 to 425 nm spectral region. There is Eu^{3+} excitation lines ($^7F_0 \rightarrow {}^5L_6$ (394 nm), $^7F_0 \rightarrow {}^5D_2$ (465 nm)), were not clearly observed probably it may be overlapped with ligand absorption band, other words no Eu^{III} centered excitation bands are seen, pointing to an efficient antenna effect [30]. The emission spectrum was recorded by 374 (solution) and 360 nm (solid) excitation (ligand absorption). The emission of the complex was also checked by using different excitation wavelength (300 - 450 nm) in chloroform as well as solid state. The intensity of the complex was reached as high as up to 380 nm in both cases and afterwards reduced. Except intensity variation, couldn't found any other key deviations from the normal emission lines of Eu^{III} ion (Figure 6.S12 – 6.S13). In addition, the thin film of the complex was analysed (Figure 6.S9). The emission spectrum consists majorly with the Eu^{3+} transition. The spectra are mainly contributed by the dominating hypersensitive $^5D_0 \rightarrow {}^7F_2$ (612 nm) transition as well as relative $^5D_0 \rightarrow {}^7F_1$ (592 nm) and $^5D_0 \rightarrow {}^7F_4$ (702 nm) transitions (Figure 6.7). The fluorescence that is belongs to ligand virtually absent in the spectrum which indirectly indicating that energy that is absorbed by the ligand has completely transferred to the Eu^{III} metal centre. In addition, the PL excitation spectrum corresponds to the ligand absorption, further indicating the sensitized luminescence character of the europium emission.

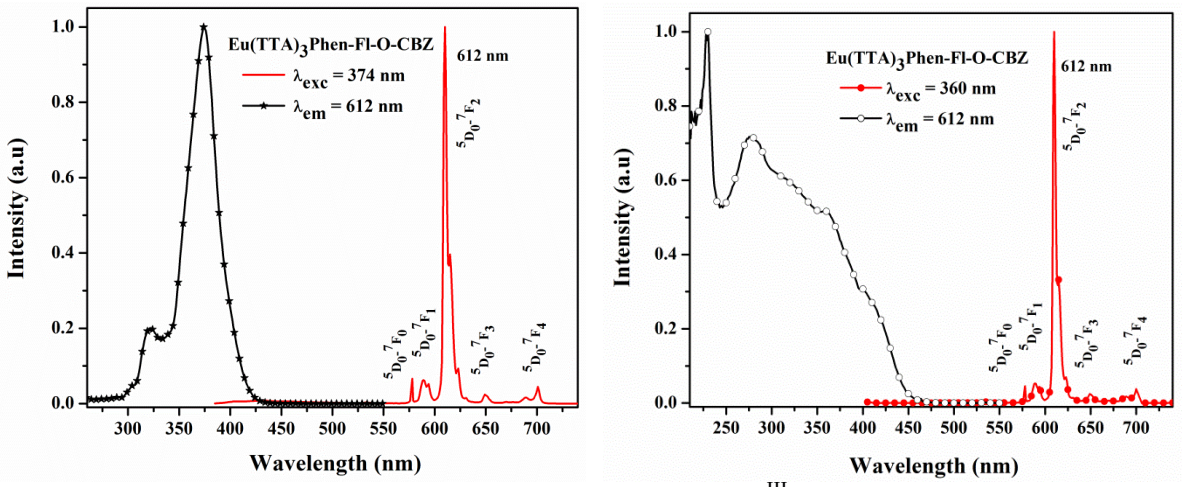

Figure 6.7 The PL excitation and emission spectra of the Eu^{III} complex in solution form (left) and solid (right).

The appearance of $^5D_0$-$^7F_0$ line in the spectra also with no splitting in the 0-0 transition, regardless of symmetry, is expected for a single-site occupation of Eu^{III} ion in the unit cell [31]. Although the magnetic dipole (MD) $^5D_0 \rightarrow {}^7F_1$ transition emission intensity is not hypersensitive (does not depend on the chemical environment around the luminescence centre), even then splitting of this transition into many stark components tells about the site symmetry around Eu^{III} ion. The presence of stark components in this transition, of the present Eu complex, favours a single low symmetry site around Eu^{III} ion. Moreover, the intensity ratio of this forced ED transition to the MD transition R = $I(^5D_0 \rightarrow {}^7F_2)/I(^5D_0 \rightarrow {}^7F_1)$, in which I is integrated intensities of the ED and MD transitions.

It is related to the presence or absence of an inversion centre (covalent nature of local site symmetry) in the coordination sphere. In the present case, the intensity ratio is found to be 4.14 in solution and 4.02 in solid. The value is very high and suggests a highly low symmetric coordination environment around the Eu^{III} ion in the complex is confirmed. The full width half maximum (FWHM) of the complex shown very less value (4.02 (solution), 4.14 (solid)), which is suitable for mono chromatic pure red emission.

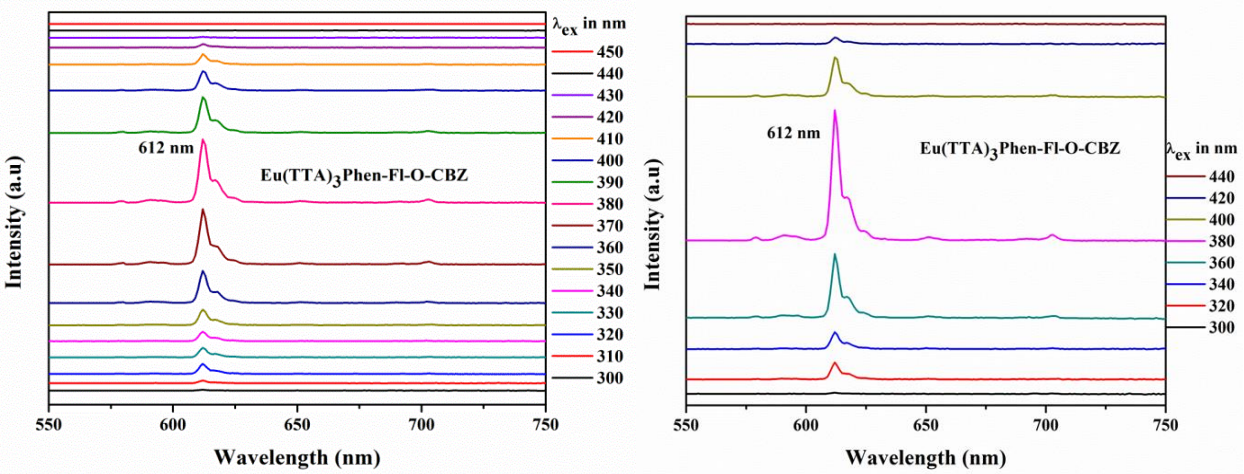

Figure 6.8 The emission spectra of Eu^{III} complex under different wavelengths (300 - 450 nm) in chloroform solution (left), in solid (right).

In general, the energy transfer process pathway in europium luminescent complexes involves of photoexcitation of the ligands energy to Eu^{III} ion through their triplet (T_1) states by means of internal conversion; finally, the Eu^{III} ion emits when transition to the ground state occurs. The excited states of the Eu^{3+} ion were located at $^5D_3$ (24,800 cm^{-1}), $^5D_2$ (21,500 cm^{-1}), and $^5D_1$ (19,100 cm^{-1}), to $^5D_0$ (17,500 cm^{-1}) becomes feasible by internal conversion. Consequently, the energy level's match of the triplet state of the ligands to $^5D_0$ of Eu^{III} is one of the key factors, which action of effect influence on luminescent properties of the Eu-complex. It is well known that TTA energy levels located at 25,164 (singlet) and 18,954 (triplet) [32]. The calculated singlet (S_1) and triplet (T_1) energy levels of the Eu^{III} complex by DFT and TD-DFT analysis were located at 28,025 (3.47 eV) and 22,309 cm^{-1} (2.76 eV) shown in Figure 6.9. The ligand excited energies are capable to transfer the energy fully from the triplet state of the ligand to $^5D_0$ of Eu^{3+} metal ion. As mentioned previously, according to the Leva *et al.*, calculations (($\Delta E = E(T_1) - E(^5D_0)$ is 2500 - 4000 cm^{-1}; singlet above 25,000 (3.09 eV) and triplet above 20,000 cm^{-1} (2.47 eV)). These results are supporting the PL emission of the presently studied Eu^{III} complex. There is no reversible emission possible (due to back transfer) from the complex and the same was reveals in the PL emission spectra (no emission in the rage of 400 to 550 nm was observed for ligand). The Eu^{III} complex, which consist of without spacer have shown less energy singlet level and slight decrease the triplet state was observed (Figure 6.9, right).

These results are suggesting that the spacer molecule can influence on the excited energy levels and can also increase the energy transfer process efficiently. To understand furthered, the similar ligand structure which consist of alkyl chain (ethyl) instead of fluorine molecule at N_1 position also been optimized. The calculated singlet and triplet levels of the complex by DFT and TD-DFT were shown at 28,357 cm^{-1} and 22,896 cm^{-1}, respectively. It is clear that the observed increment in both singlet and triplet energy level in ethyl connected ligand is due to the influence

of ethyl moiety present in the N1 position of the imidazole ring. However, in the case of fluorene connected ligand also have ethyl moiety (different position), but reduced singlet and triplet observed compared to that of ethyl connected ligand. It is indicating that the direct connection of ethyl at N1- in the imidazole can influence (increase) on the energy levels. It could be expected that the fluorene in the complex affects the flexibility of the ligand. This may considerably change the predominantly framework leads to sensitization boosted by decrease of vibronic quenching effect. Therefore, it supports the consideration of stronger sensitization of the synthesized complex than the ethyl based ligand because of the larger energy gap between the ligand triplet and the excited states ($^5D_0$) of europium ion. The similar observations also been reported by employing the chain in between the phenyl rings [33].

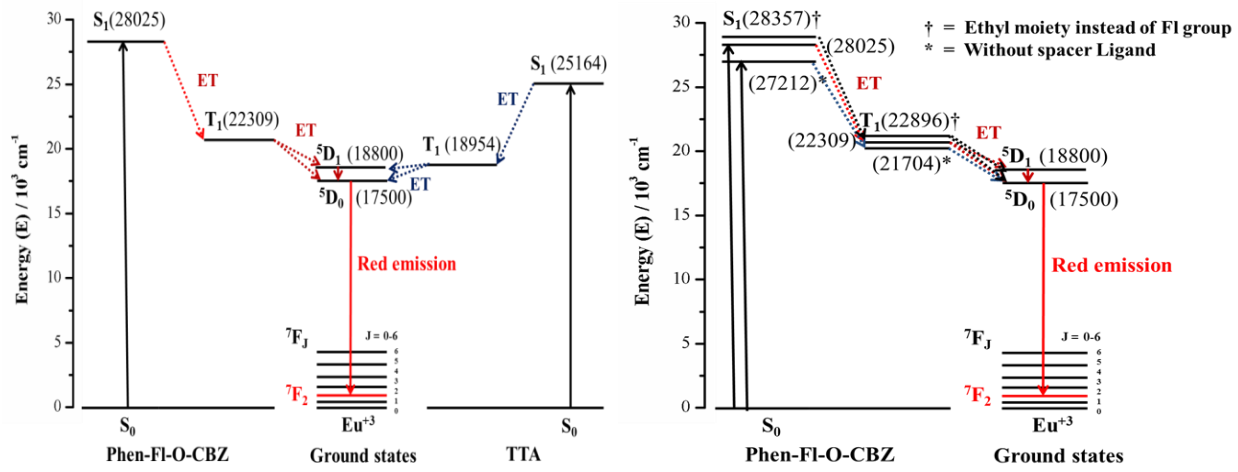

Figure 6.9 The energy transfer diagram for the Eu(TTA)$_3$Phen-Fl-TPA-CBZ and with TTA molecule (dotted line is non-radiative, normal line is radiative, S = singlet, T = triplet, ET = energy transfer) (left), The energy transfer mechanism for the presently studied ligand compared with no spacer ligand and ligand with ethyl moiety instead of fluorine group (right).

The blue color emission was observed from the ligand under UV lamp, whereas the corresponding Eu complex shown red emission at 365 nm. The Eu(TTA)$_3$ also shows red color, and the digital photographs under UV lamp is shown in Figure 6.10.

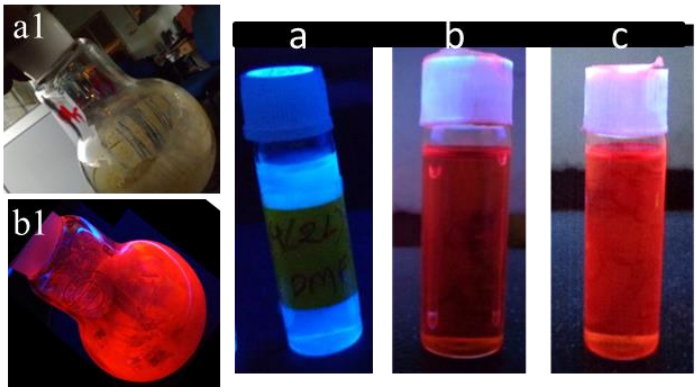

Figure 6.10 Ligand and corresponding Eu^{III} complex under normal light are (a) Phen-Fl-O-CBZ; (b) Eu(TTA)$_3$; (c), (b1) Eu (TTA)$_3$Phen-Fl-O-CBZ (under UV-lamp, 365 nm) and (a1) Eu (TTA)$_3$Phen-Fl-O-CBZ (under normal light).

The QY of luminescence can described as the ratio of the number of photons emitted over the number of photons absorbed. PLQY of the complex was measured in chloroform solution by means of quinine sulfate as a reference in 1M H_2SO_4 (φ = 54.6%) at room temperature [10]. Overall QY were calculated according to the well-known equation (6.1),

$$\varphi_{overall} = \frac{n^2\, A_{ref}\, I}{n_{ref}^2 A I_{ref}} \varphi_{ref} \qquad (6.1)$$

Here, I is absorbance at the excitation wavelength, A is area of the emission spectrum, n is refractive index of solvent, $\varphi_{overall}$ is the QY of the sample and φ_{ref} is the quantum yield of the standard quinine sulfate solution, respectively. The calculated relative PLQY of the Eu complex is 30% (±5%) at 358 nm as an excitation wavelength. These outcomes were shown slight higher to that of TPA based Eu^{III} complex [26] and results are suggesting that the increasing radiative path way by reducing non radiative transition.

The absolute quantum yield (measured by integration sphere) of the complex also calculated by the equation 2.9 and 2.10. The absolute quantum efficiency (measured by integration sphere) of the complex was carried out in solution as well as solid and the obtained values are 11.5 and 5%, respectively. The thin film of the complex was shown less quantum efficiency 1.32%. In addition to understand the QY of the complex by doping with PMMA also were calculated and found those to be 10.7 (0.1%), 14.0 (0.5%) and 14.2 (1%), respectively. It is also found that reducing the quantum yield by doping with excess of complex with PMMA (8.02 (5%)). So these results are signifying that the 1% doping is applicable to get high efficiency.

6.2.3.1.3 Judd-Ofelt and Lifetime analysis:

The Judd-Ofelt parameters were calculated form the PL emission spectra of the Eu^{III} complex by well reported literatures method and the details are also been mentioned in the previous chapters [26, 34]. The calculated value has been tabulated in Table 3 and the Ω_2, Ω_4 values are 10.5, 0.75 (10^{-20} cm^2), respectively. To get faster Eu^{III} radiative rates, it is necessary to design asymmetrical Eu^{III} complexes with larger Ω_2. The increment of the Ω_2 value was observed in the presently studied complex with respective to TPA functionalized Eu^{III} complex. It indicates that there exists lower symmetry in currently stuided complex. The determination of luminescent decay profiles ($^5D_0$ lifetimes (τ_{obs})) for the complex by fitting with mono-exponential curves in different solvents as well as solid are done at room temperature (Figure 6.11). The values are proposing the presence of a single chemical environment around the emitting Eu^{3+} ion and compiled in Table 6.3.

The single exponential function given by the equation $I(t) = I_0 + A_1 \exp\left(\frac{-t}{\tau}\right)$, where I_0 = 0 is the offset value, A_1 is the scalar quantity (from curve fitting), t is the time in ms and τ is the decay time value for the exponential module. The lifetime variations was observed in altered solvents and the following order was followed $CHCl_3$ (0.62) > DCM (0.61) > Acetone (0.60) > THF (0.55) > DMF (0.47) > solid (0.28 ms) at 360 nm. The ligand lifetime values were also been calculated and interpreted in Table 6.3 with different excitations. In general, the primary process that quenches $^5D_0$ excited state of Eu^{3+} in liquid systems by non-radiative relaxation via vibronic coupling [35]. The excited state lifetime of $^5D_0$ (Eu^{3+}) level is usually comparatively long (μs to ms scale) [36], which enable energy transfer to high frequency vibrational oscillators such as O−H, N−H, and C−H. As a result, the existence of these groups in the close proximity of the central metal ion favours quenching of the luminescence. As an according to the obtained results, the C-H vibrational oscillators frequency is less compare to that of O-H and N-H. As of this the $CHCl_3$ and DCM are shown better results.

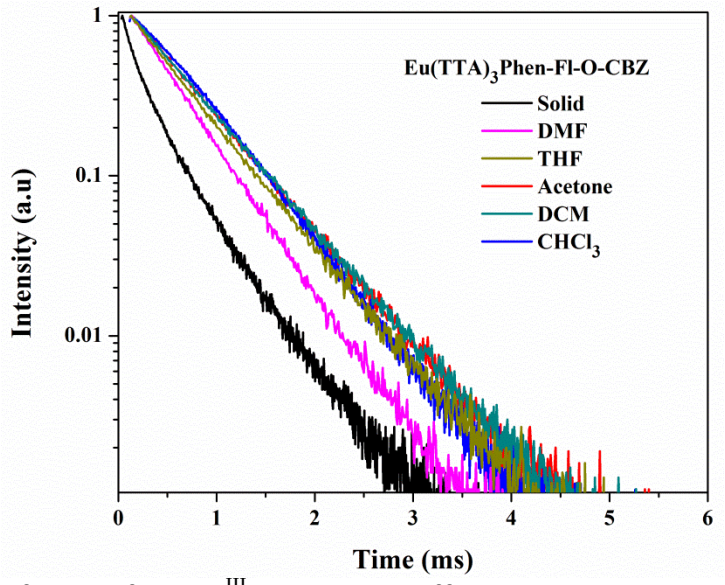

Figure 6.11 The lifetime of the Eu^{III} complex in different solvents and in the form of solid.

Table 6.3 The Judd-Ofelt and lifetime analysis of the Eu - complex.

Compound	Intensity parameters (10^{-20} cm^2)		τ / ms [a]					
	Ω_2	Ω_4	Solid	$CHCl_3$	DMF	THF	DCM	Acetone
$Eu(TTA)_3$Phen-Fl-O-CBZ	10.5	0.75	0.28	0.62	0.47	0.55	0.61	0.60
Phen-Fl-O-CBZ (10^{-3} ms) 280nm	---.--	--.--	1.84	1.91	2.08	2.44	2.47	1.74
Phen-Fl-O-CBZ (10^{-3} ms) 360nm	--.--	--.--	2.29	22.86	25.18	26.19	25.77	22.7

[a] The decay curves were found to be mono-exponential for the β-diketonate Eu^{III} complex and its ligand.

6.2.3.2 Electrochemical Properties:

The electrochemical properties were calculated for the complex as well as for the ligand. The oxidation potentials of the ligand and complex are 1.47 and 1.32 eV, respectively (Fig. 6.12). The obtained oxidation potentials and other values were inferred in Table 6.4. The oxidation potential of the complex was decreases compare to that of ligand. However, similar reduction potential was observed. The equation 2.9 and 2.10 [37] was used to calculate the HOMO and LUMO energy levels.

The arrangement of the energy levels of ligand and its corresponding Eu^{III} complex were interpreted in Figure 6.12 (right). The band gap of the complex and ligand were calculated by DRS spectral analysis (Figure 6.5 left). The energy gap of the complex as well as ligand have less compared to that of without spacer consisted TPA complex [22]. In addition, it is also have less band gap compared to that of without spacer CBZ ligand. These results are suggesting that the spacer arrangement can decrease the energy gap of the complex and leads to the efficient energy transfer to get the high quantum efficiency. The theoretically calculated HOMO-LUMO energy levels are shown similar observations

of experimental results (calculated from optimized structure, Figure 6.S2). The electron density of the ligand is located on phenanthro-imidazole ring and on Fluorene moiety for HOMO and LUMO, respectively. The HOMO-LUMO of the ligand (electron density picture) is mentioned in Table 6.5 and their respective values were mentioned in Table 6.6.

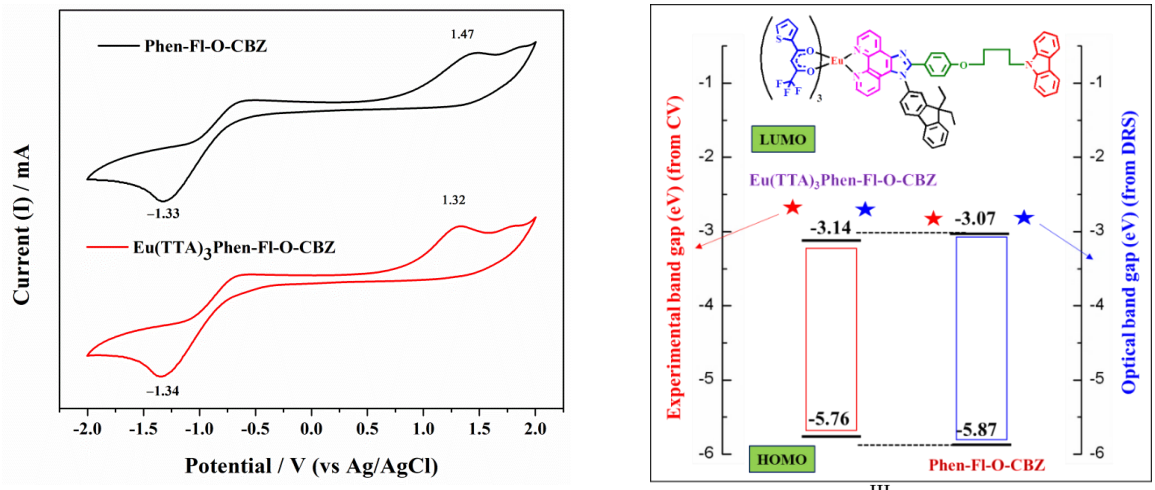

Figure 6.12 Cyclic voltammogram of ligand and its corresponding Eu^{III}-complex (left) and the energy levels of the ligand as well as Eu^{III} complex arrangement (right).

Table 6.4 Electrochemical properties of the ligands and respective Eu^{III}-complex.

S. No.	Compound Name	$Voltage^{Oxi}_{onset}$[V] (E_{HOMO} [eV])	$Voltage^{Red}_{onset}$[V] (E_{LUMO} [eV])	$\lambda_{onset,}$ [nm] (a)	Energy gap E_g^{Opt}, [eV](b)
1	**$Eu(TTA)_3$Phen-Fl-O-CBZ**	1.32 (-5.76)	-1.34 (-3.14)	464	2.67 (2.62)
2	**Phen-Fl-TPA-CBZ**	1.47 (-5.87)	-1.33 (-3.07)	441	2.81 (2.80)

[a] Calculated from the optical absorption (DRS spectra), [b] Calculated the onset wavelength of optical absorption (onset) in solid-state film (DRS spectra). The energy differences (HOMO and LUMO) values calculated by cyclic voltammogram are mentioned in bracket.

Table 6.5 The HOMO and LUMO energy levels of the ligand.

Phen-Fl-O-CBZ	
HOMO-1	**HOMO**
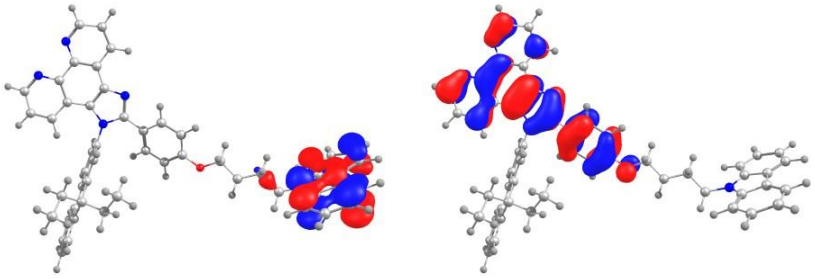	

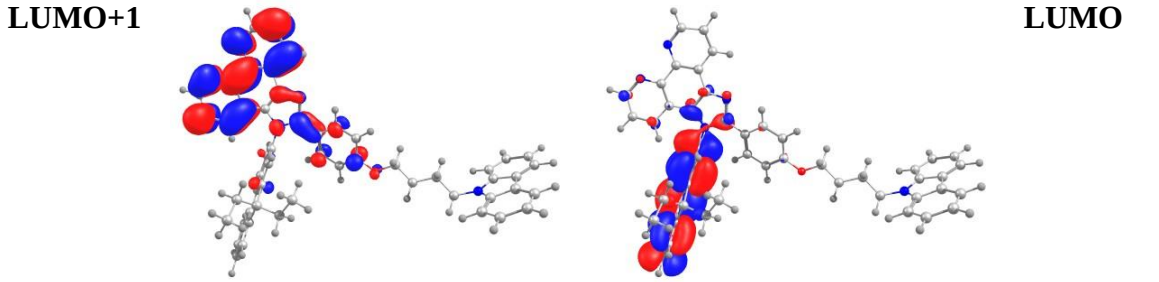

Table 6.6 The HOMO and LUMO energy levels of the ligand.

Molecule	HOMO	HOMO-1	LUMO	LUMO+1	E_g	S1	T1
	in electron volts (eV)						
Phen-Fl-O-CBZ	-5.29	-5.43	-1.38	-1.13	3.91	3.47	2.76
$Eu(TTA)_3$Phen-Fl-O-CBZ	--.--	--.--	--.--	--.--	--.--	$^5D_0$ level = 2.17	

6.2.3.3 CIE Chromaticity coordinates:

The Commission Internationale de l´Eclairage (CIE) values of the ligand and the respective complex was calculated from PL emission spectra in solution as well as solid (Figure 6.13). The obtained results are illustrated in Table 6.7. The ligand shown blue emission in solution but in the case of solid phase, it was shifted towards white emission. By engineering the molecular structure by changing the substitutes, it is possible to generate single molecular white emitters. The complex was shown red emission with appropriate CIE values. These are almost near to the NTSC standard for pure red emission.

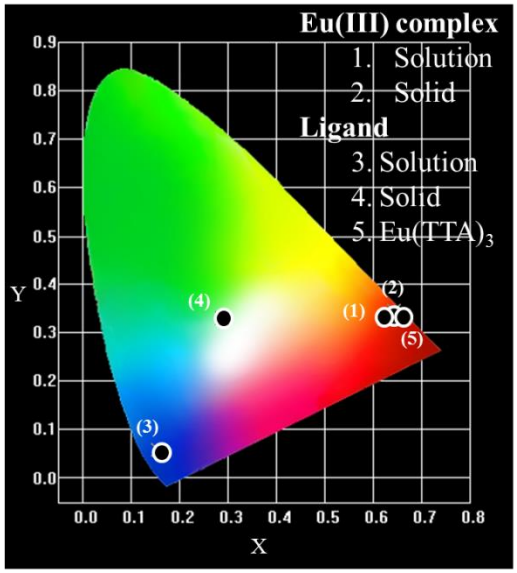

Figure 6.13 The CIE chromaticity coordinates for ligand and $Eu(TTA)_3$Phen-Fl-O-CBZ in solution and solid.

Table 6.7 The CIE color coordinates for the ligand and Eu^{III} complex.

S. No.	Compound Name	Solution (a)(b)		Solid (b)	
		x	y	x	y
1	**$Eu(TTA)_3Phen$-Fl-O-CBZ**	0.623	0.327	0.643	0.343
2	**Phen-Fl-O-CBZ**	0.155	0.05	0.288	0.332
3	**$Eu(TTA)_3.2H_2O$**	0.66	0.33	----	----

(a) Measured in chloroform solution at 298 K, (b) Emission peaks from PL emission spectra.

6.2.3.4 PMMA film of Eu^{III} complex:

To understand the optical properties of Eu-complex in a matrix, the complex was also incorporated in PMMA matrix and the corresponding PL emission spectra respective digital photographs are shown in Figure 6.14. The PL emission of the complex in pure condition, shown less intensive peak compared to that of doped PMMA. The CIE also reflecting the same and 0.1% shown pure emission color coordinates. It is observed that with increase the percentage of Eu^{III} complex doping with PMMA up to 1%, the intensity is varying and the CIE color coordinates are deviating from red emission. Thus, the 0.1% complex with PMMA is superlative for this complex (but relatively quantum efficiency is high for 1%). The calculated CIE coordinates are for 0.1 %, x = 0.64, y = 0.35; 0.5 %, x = 0.58, y = 0.39 and 1 %, x = 0.60, y = 0.38 and their asymmetric intensity ratio of (I_2/I_1) shown 20.4, 12.9 and 15.5, respectively. In addition, the FWHM of the complex shown below 4.2 nm, this is highly necessary to obtain pure narrow emission.

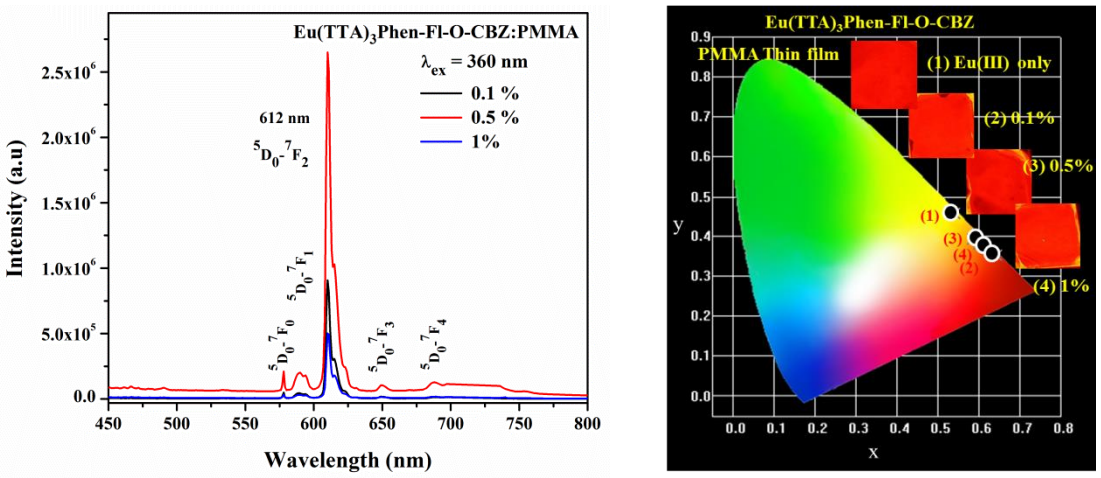

Figure 6.14 The emission spectra of Eu^{III} complex doped with PMMA (different percentage ratio) as well as pure Eu^{III} complex (left) and its CIE color coordinates as well as their thin film patterns (right).

The Eu-complex thin film excitation and emission spectrum is shown in Figure 6.15 (A-D). In order to find the variation in the red emission intensities of the complex (0.1, 0.5, 1% and 5%), the complex was excited from 300-400 nm and were represented in Figure 6.15. In addition, the molar absorption coefficients values were calculated generally for solution by using the Beer-Lamberts law. However, the absorbance coefficient of the thin film calculated by using this equation. Absorption coefficient (α) =

2.303 A/t, where (A) is absorbance and (t) is thickness of thin film [38-40]. The absorption coefficient of the pure film (59.889 cm^{-1}) as well as 0.1% doped complex with PMMA shown almost similar results (41.644 cm^{-1}). The detailed analyses of remaining have been given in below. The absorption coefficient values are tabulated in Table 6.8. Thin film of the complexes were studied with different excitation from 300-400 nm and shown in Figure 6.16. Maxima of the intensity at 612 nm emission peak observed at 240 – 260 nm excitation.

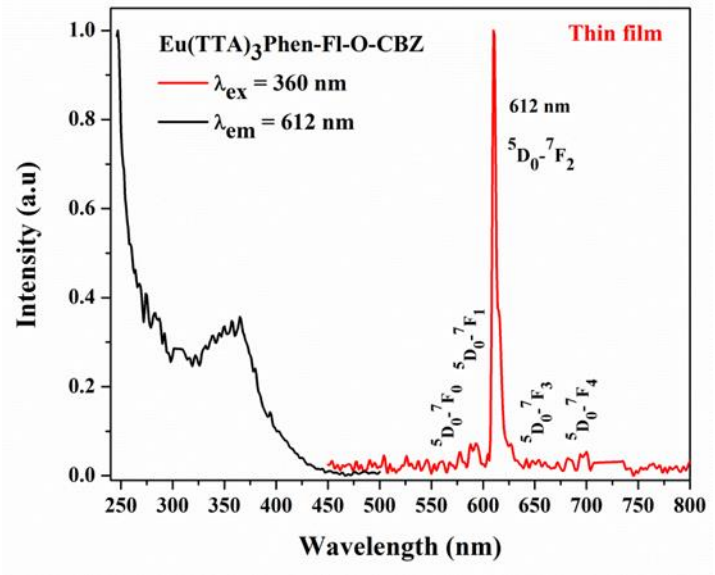

Figure 6.15 The excitation and emission spectra of the Eu-complex in the form of thin film.

Table. 6.8 The molar absorption coefficients calculation values.

Concenration (w/w %)	Absorbance (a.u.)	Thickness of film (cm)	Absorption coefficient (cm^{-1})
Pure/ 100 %	0.5201	0.02	59.889
0.1 %	0.7233	0.04	41.644
0.5 %	0.20464	0.04	11.782
1 %	0.34074	0.04	19.618
5 %	0.410639	0.04	23.643

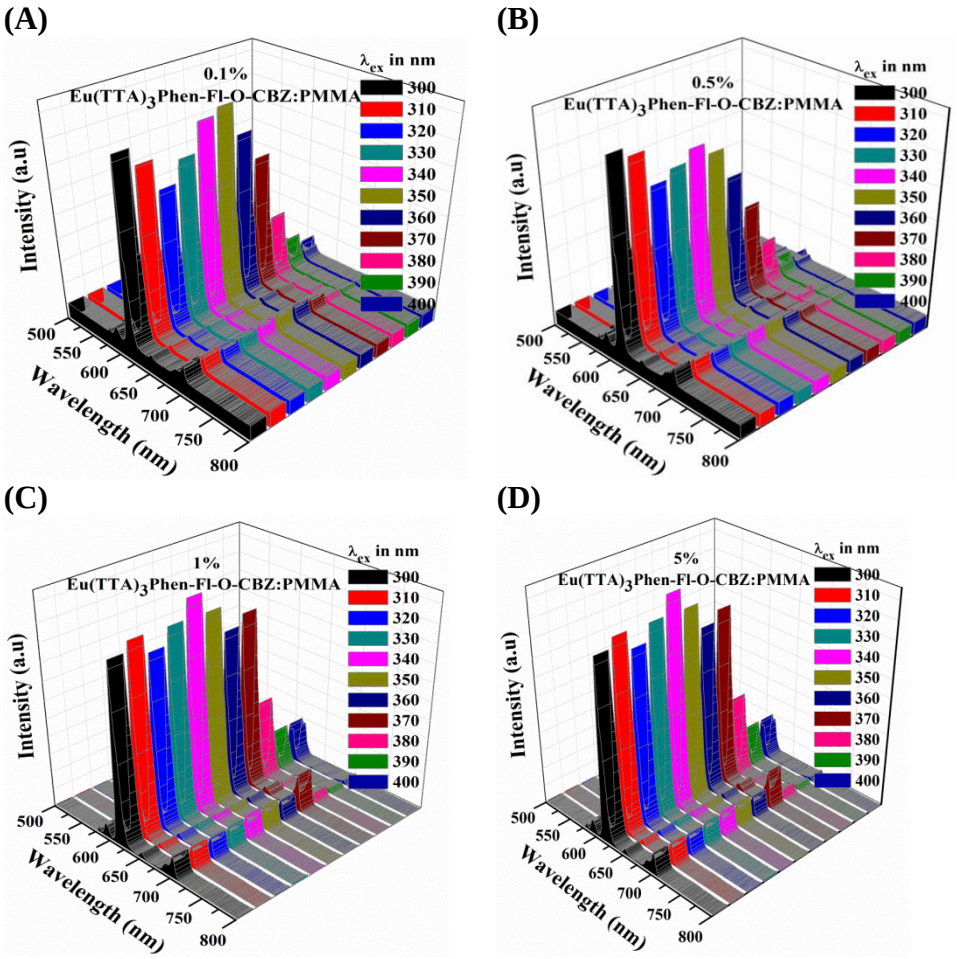

Figure 6.16 The thin film of the complex doped with PMMA at 0.1% (A), 0.5% (B) and 1% (C), The thin film of the complex doped with PMMA at 5% (D).

6.2.3.5 Fabrication of red LED with Eu^{III} complex:

The mononuclear complex was integrated with InGaN LED chip to explore the possibility of using the complex in warm white LEDs. The obtained results are shown red emission and the CIE values are x = 0.65, y = 0.34 in both the ratio (1-10 and 1-50).

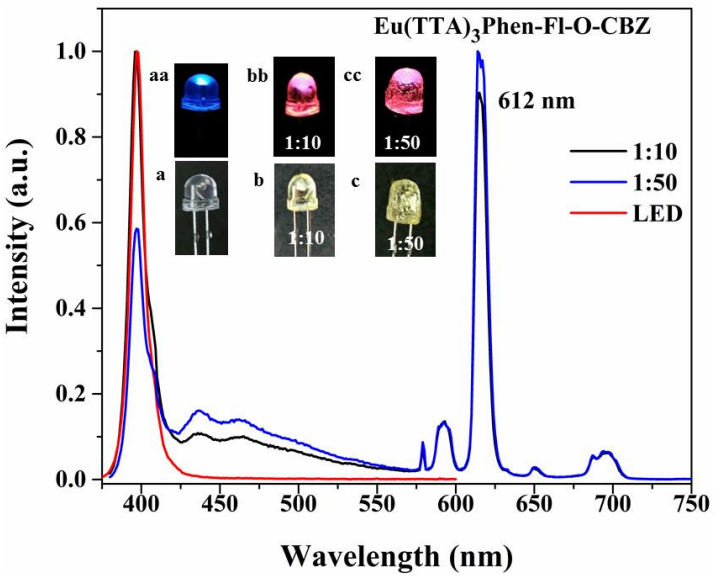

Figure 6.17 The spectra of Eu^{III} complex coated on the 395 nm emitted LED (InGaN) chip. In inset **a** is the original 365 nm emitted LED chip, **aa** is under forward bias. **b** and **c** are coated with binuclear Eu^{III} complex and **bb** and **cc** are with forward bias, respectively.

6.3 Bi-nuclear luminescent Eu^{III} molecular complexes:

6.3.1 Outline of the present study:

In the previous part, phenanthroimidazole-CBZ based bipolar ligand for Eu^{III} complex with ethoxy spacer molecule was explored [41]. In the present investigation, design and synthesis two new phenanthroline based ancillary ligands (two phenanthroimidazole rings separated by phenyl and ethoxy chain, factionalized in the N1 position with phenyl and fluorene group) and used for the synthesis of binuclear Eu-complexes was investigated. The luminescent europium site isolation (can prevent concentration quenching effect) can be achieved by using the long ethoxy chain (O-C_4H_8-O) along with phenyl (Ph) group. We show that the new two binuclear Eu-complex, thereafter labeled $Eu_2(TTA)_3$(L1), $Eu_2(TTA)_3$(L2) allows both PL and EL show characteristic red emission. As compared with mono nuclear complex, dinuclear complex presented better thermal stability and achieve stronger luminescence, which makes it a promising light-conversion molecular device [42-44]. Some of the literature works [45-49] shown that the quantum efficiencies of the bi and trinuclear europium complexes are higher (about 10%) than mononuclear one, and their lifetimes of these europium complexes were longer than the mononuclear ones.

The chosen phenanthroline moiety is a rigid planar, hydrophobic, electron-accepting hetero aromatic system, whose nitrogen atoms are exquisitely placed to act cooperatively in cation binding for Eu-metal ion. In addition, it can reduce the non-radiative decay of the excited states of the europium ion, improve the stability of the europium complexes, and increase the ET efficiency from the ligands to the europium ion. It can also benefit to improve the thermal stability of the complex [50]. The chosen flexible alkyl spacer molecule (C-C bond) can make the flexible nature in the complex

and can lead to getting high thermal stability [51] It can also help to arrested communication between the two phenanthroimidazole moieties to get efficient emission from the Eu emissive centre in the complexes [41, 51, 52].

Both the ligands and their binuclear Eu-complexes were characterized by various spectroscopic techniques (NMR, FT-IR, Mass and elemental analysis). The ligands structures were optimized by using DFT calculations and their excited state photophysical properties were evaluated by time-dependent density functional theory (TD-DFT) calculation. The designed and synthesized ancillary ligands (L1 and L2) and the corresponding binuclear Eu^{III} complex ($Eu_2(TTA)_3(L1)$, $Eu_2(TTA)_3(L2)$) molecular structure is depicted in Figure 6.18.

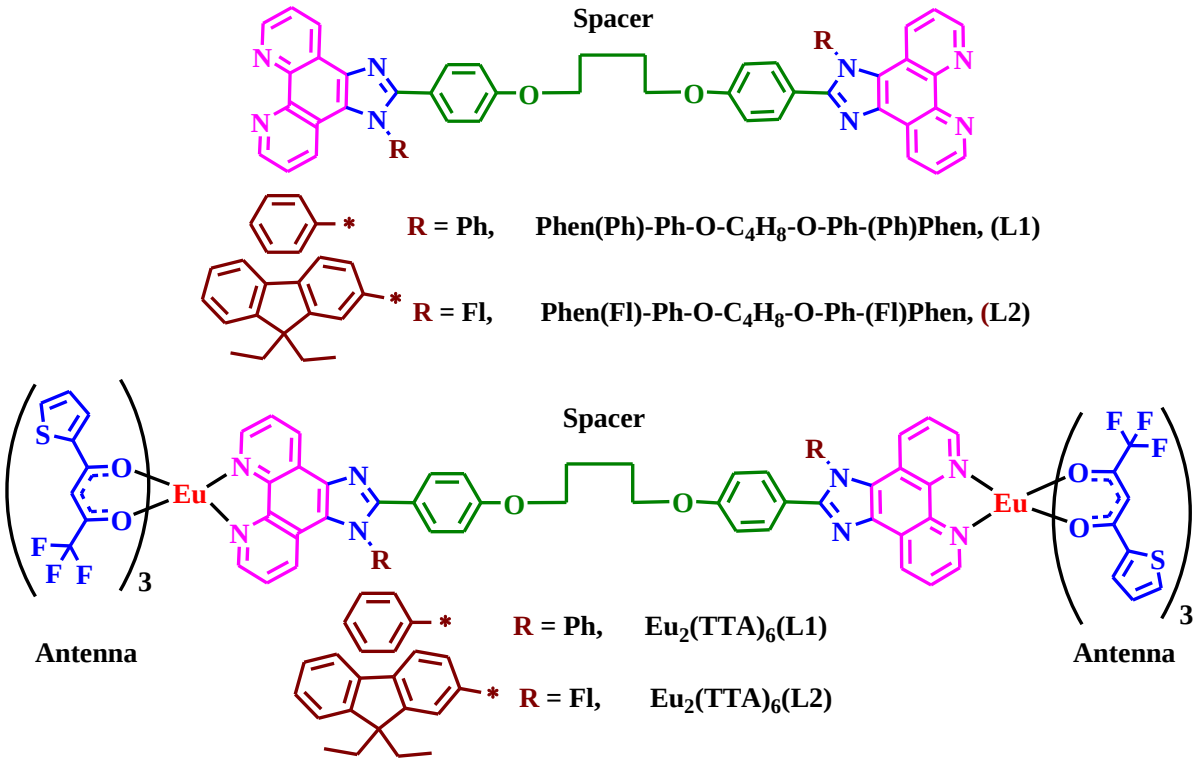

Figure 6.18 Chemical structure of bipolar ligand and the corresponding binuclear $Eu(TTA)_3$ complex.

6.3.2 Characterization of the Eu-complexes:

The detailed synthetic condition and reactions of ligands and their binuclear Eu^{III} complexes are summarized in Scheme 6.2.

6.3.3 Experimental

6.3.3.1 Materials:

The details are given Chapter 2 (2.2.2) experimental sections.

6.3.3.2 Measurements: The instruments details are used in this study given in Chapter 2 (2.2.2)

6.3.3.3 Synthesis:

The synthsis of intermediates were followed previous Chapter 2.

6.3.3.3.1 *Synthesis of di-aldehyde (dial) compound*:

4-hydroxybenzaldehyde was taken in round bottom flask and added acetonitrile (CH_3CN) solution. To this reaction mixture added potassium carbonate base and stirred for 10 minutes then added 1, 4-dibromo butane. The resulting reaction mixture was stirred for 48 h at 85 °C under nitrogen atmosphere. The resulting of the reaction mixture of was checked by TLC (ethyl acetate (EtOAc) in pet ether 2:8, Rf-0.3). The resulting of the compound was filtered to remove the excess of the base from the reaction mixture. After that, the reaction mixture was extracted with ethyl acetate and followed by dried with anhydrous sodium sulphate. The solvent was evaporated to get crude compound (8 g). The obtained crude was purified by column chromatography by using silica gel (100-200 mesh), eluent with 15 % ethyl acetate in pet ether. The obtained pale yellow color solid was 6.1 g (50.0 %). ^{1}H-NMR Data (400 MHz, DMSO-d_6): δ (in ppm) 9.88 (s, 2H), 7.83 (d, 4H, *J* = 8.8 Hz), 7.00 (d, 4H, *J* = 8.4 Hz), 4.14 (br-s, 4H), 2.04-2.03 (m, 4H). ^{13}C-NMR Data (100 MHz, DMSO-d_6): δ (in ppm) 190.8, 163.9, 132.0, 131.5, 129.9, 114.7, 114.0, 67.7, 67.54, 25.8, 25.7, 25.4.

6.3.3.3.2 *Synthesis of 2-(4-(4-(4-(1-phenyl-1H-imidazo[4,5-f][1,10]phenanthrolin-2-yl)phenoxy)butoxy)phenyl)-1-phenyl-1H-imidazo[4,5-f][1,10]phenanthroline* (L1):

The aniline (0.1.22 mL, 13.42 mmol) was taken in round bottom flask and added dial compound (2.0 g, 6.771 mmol) in glacial acetic acid (30 mL) at room temperature. To this reaction mixture subsequently, ammonium acetate (5.16 g, 67.11 mmol) and diketo compound (2.81 g, 13.42 mmol) were added. Then resulting mixture was stirred for 12 hrs at 110 °C under nitrogen atmosphere. The resulting of the reaction mixture of was monitored by TLC (MeOH in Chloroform 1:9, Rf-0.4). The RM was poured into the minimum amount of water and then added ammonium hydroxide solution to neutralize the reaction mixture (pH ~7). The solid was filtered and dissolved in dichloromethane, followed by dried with anhydrous sodium sulphate. The solvent was evaporated to get crude compound (3.50 g). The obtained crude was purified by column chromatography by using silica gel (100-200 mesh), eluent with 4% methanol in chloroform. The purified product was dissolved in minimum amount of THF solution added an excess of hexane solvent, the pale yellow color solid was formed is 400 mg (55.0%). ^{1}H-NMR Data (400 MHz, DMSO-d_6): δ (in ppm) 9.08 (dd, 2H, *J* = 2 Hz, *J* = 4.4 Hz), 9.01 (dd, 2H, *J* = 1.6 Hz, *J* = 8 Hz), 8.94 (dd, 2H, *J* = 1.6 Hz, *J* = 4 Hz), 7.87-7.84 (m, 2H), 7.75-7.69 (m, 10H), 7.51 (d, 4H, *J* = 8.8 Hz), 7.48-7.45 (m, 2H), 7.33 (dd, 2H, *J* = 1.2 Hz, *J* = 8.4 Hz), 6.91 (d, 4H, *J* = 8.8 Hz), 4.04 (br-s, 4H), 1.85 (br-s, 4H). Elemental analysis: Anal. Calc. for $C_{54}H_{38}N_8O_2$: C, 78.05; H, 4.61; N, 13.49; Found: C, 77.99; H, 4.58; N, 13.55 %. EI-mass: m/z, Cal. 830.93; found 831.52 (M+1).

6.3.3.3.3 *Synthesis of 2-(4-(4-(4-(1-(9,9-diethyl-9H-fluoren-7-yl)-1H-imidazo[4,5-f][1,10]phenanthrolin-2-yl)phenoxy)butoxy)phenyl)-1-(9,9-diethyl-9H-fluoren-7-yl)-1H-imidazo[4,5-f][1,10]phenanthroline* (L2):

The same procedure which is followed for the L1 was carried out to synthesis of the ligand L2. NMR Data (400 MHz, DMSO-d_6): δ (in ppm) 9.07 (m, 1H), 9.01 (d, 1H, *J* = 8 Hz), 8.91 (d, 1H, *J* = 4 Hz), 8.17-8.10 (m, 1H), 7.99-7.97 (m, 1H), 7.89-7.87 (m, 2H), 7.68-7.62 (m, 1H), 7.55 (d, 2H, *J* = 9.2 Hz), 7.49-7.47 (m, 2H), 7.42-7.38 (m, 3H), 6.81 (dd, 2H, *J* = 2.4 Hz, *J* = 8.8 Hz), 3.95 (br-s, 2H), 3.80-3.79 (m, 1H), 3.68-3.65 (m, 1H), 2.03-2.00 (m, 4H), 0.32-0.28 (m, 3H), 0.16-0.11 (m, 3H). ^{13}C-NMR Data (100 MHz, DMSO-d_6): δ (in ppm) 165.0, 159.7, 152.3, 152.2, 150.3, 148.8, 147.9, 144.1, 143.3, 140.1, 136.9, 135.5, 130.9, 130.1, 128.7, 128.0, 127.8, 127.7, 126.9, 124.3, 124.2, 123.8, 123.4, 122.6, 122.4, 122.1, 121.2, 119.9, 114.5, 97.6, 82.9, 68.7, 67.6, 66.1, 56.75, 33.6, 32.3, 25.5, 23.7, 8.74, 8.51. Elemental analysis: Anal. Calc. for $C_{76}H_{62}N_8O_2$: C, 81.55; H, 5.58; N, 10.01; Found: C, 81.49; H, 5.50; N, 10.11 %. EI-mass: m/z, Cal. 1118.5; found 1120.24 (M+1).

6.3.3.3.4 *Synthesis of $Eu_2(TTA)_6$(L1)*:

Taken two neck round bottom flask (50 mL) with nitrogen containing balloon adaptor and poured $Eu(TTA)_3.2H_2O$ (205 mg, 0.240 mmol, 1 eq) dissolved in dry chloroform ($CHCl_3$) (15 mL). To this solution, added mixture of compound L1 (200 mg, 0.240 mmol, 1eq) in chloroform (10 mL) and the reaction mixture (RM) stirred for 12h at 60 °C temperature. The resulting product was dissolved in minimum amount of THF and excess of hexane added to get a solid product. The obtained final pale yellow color product was 414 mg (70.0 %). Elemental analysis: Anal. Calc. for $C_{102}H_{62}Eu_2F_{18}N_8O_{14}S_6$: C, 49.76; H, 2.54; N, 4.55; S, 7.81; Found: C, 49.70; H, 2.48; N, 4.62; S, 7.89%.

6.3.3.3.5 *Synthesis of $Eu_2(TTA)_6$(L2)*:

The same procedure which is followed for the $Eu_2(TTA)_6$(L1) was carried out to the synthesis of the ligand L2. Elemental analysis: Anal. Calc. for $C_{124}H_{86}Eu_2F_{18}N_8O_{14}S_6$: C, 54.15, H, 3.15, N, 4.07, S, 7.00; Found: C, 54.01, H, 3.10, N, 4.00, S, 6.95%.

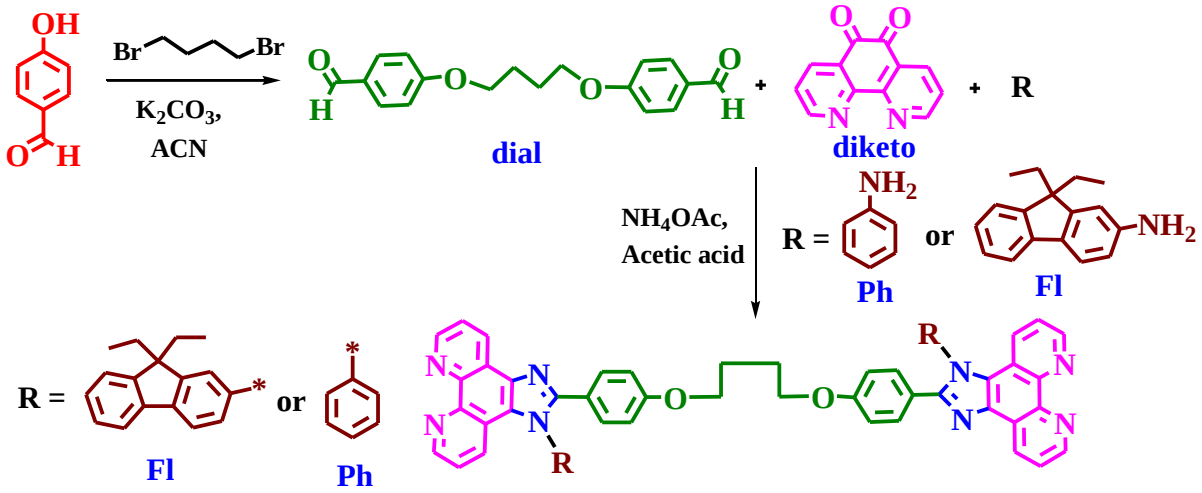

R = Ph, Phen(Ph)-Ph-O-C_4H_8-O-Ph-(Ph)Phen, (L1)
R = Fl, Phen(Fl)-Ph-O-C_4H_8-O-Ph-(Fl)Phen, (L2)

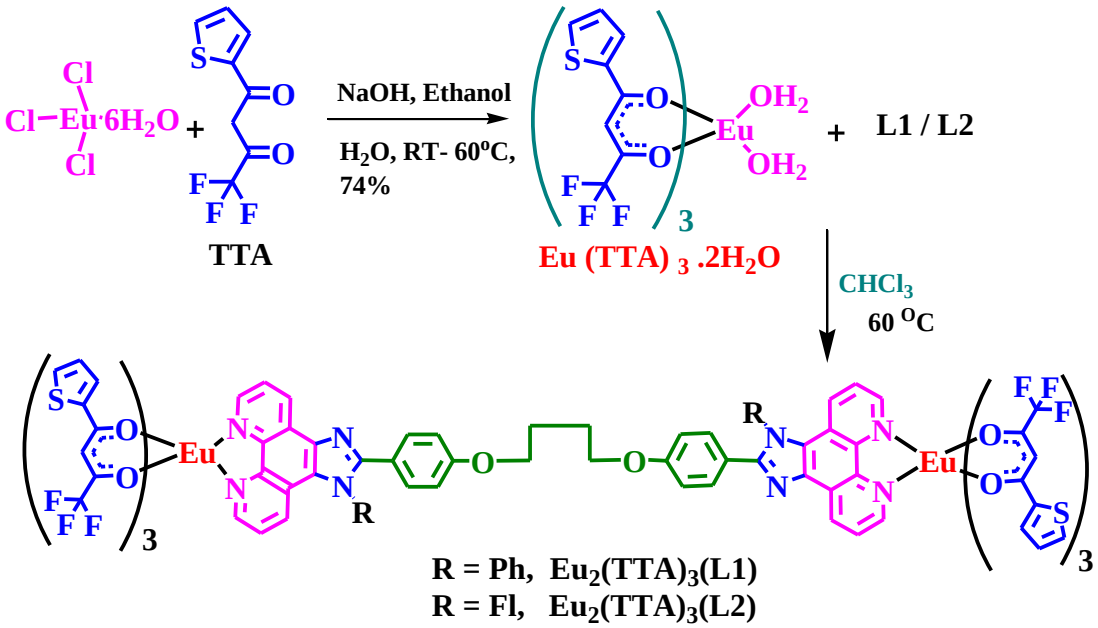

Scheme 6.2 Synthetic route of the spacer (ether) attached and N1-functionalized phenthroimadazole ligand and the corresponding β- diketonate Eu^{III} ternary binuclear complex.

6.3.3.4 FT-Infrared spectroscopy:

The infrared spectra of the ligands and their binuclear Eu-complexes were measured at room temperature in the spectral window of 500 - 4000 cm^{-1}. The observed major strong carbonyl (C=O) stretching frequency functional group of $Eu(TTA)_3.2H_2O$ complex found to be at 1614 cm^{-1} and which is further shifted to 1601 cm^{-1} for the $Eu_2(TTA)_6(L1)$ and 1599 cm^{-1} for the $Eu_2(TTA)_6(L2)$, respectively (Figure 6.17).

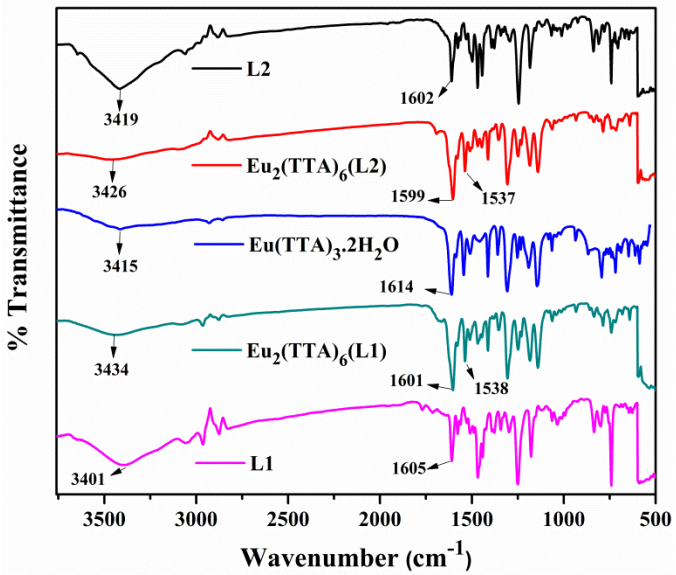

Figure 6.17 FT-IR spectra of the ligands and corresponding Eu^{III}-complexes as well as comparison with $Eu(TTA)_3$.

These stretching frequency deviations in the IR spectra, are the evidence that the β-diketonate ($Eu(TTA)_3$) is coordinated with ligating (N,N) phenanthroline group in the ligands (L1 and L2), respectively. It leads to the formation of the C=N bond and is converted into a structure of C=N–Eu-O bond in the final binuclear Eu-complexes. In addition, the vibrational frequency of C=N appears at 1605 cm^{-1} (L1) and 1602 cm^{-1} (L2) in the ligands were shifted to 1538 and 1537 cm^{-1} in the complexes, respectively. These major functional groups changing in the spectra are indicated that the ligand coordinated with Eu^{III} ion in the binuclear complexes. Further, it was also supported by remaining functional groups varying from ligand to Eu-complex, which are tabulated in the Table. 6.9. These obtained results are concluding that the N atom in ligand coordinates with $Eu(TTA)_3$ complex.

Table 6.9 The Infrared frequencies (wavenumber in cm^{-1}) at room temperature (RT) for free ligands and its corresponding $Eu_2(TTA)_3(L1)$, $Eu_2(TTA)_3(L2)$ complex and $Eu(TTA)_3$.

(Wavenumber in cm^{-1})	**$Eu_2(TTA)_3(L1)$**	**$Eu_2(TTA)_3(L2)$**	**L1**	**L2**	**$Eu(TTA)_3$**
ν (C=O)	1601	1599	--.--	--.--	1614
ν (C=N)	1538	1537	1605	1602	--.--
ν (C-N)	1249	1250	1247	1245	--.--
ν (C-F)	1307	1306	--.--	--.--	1300
ν ($C-CF_3$)	1142	1140	--.--	--.--	1137
ν (C-H phen)	832, 786	835, 785	836, 742	839, 740	--.--

6.3.4 Results and Discussion:

The synthesis of binuclear Eu-complexes ($Eu_2(TTA)_6(L1)$ and $Eu_2(TTA)_6(L1)$) and their photophysical properties were discussed in detail in the results and discussion part. The effect of N1 functionalization of the ligand by phenyl and fluorene moiety (L1 and L2) and the binuclear Eu complexation by the same has been accomplished. The synthesized ligands and their corresponding binuclear Eu-complexes were characterized by using various spectroscopic techniques (nuclear magnetic resonance spectroscopy (^1H and ^{13}C NMR, Figure 6.S4-S6), ESI-Mass spectrometry (Figure 6.S7), Elemental analysis, Fourier transforms infrared spectroscopy (FT-IR), etc.). Coordination of the ligand and the complex confirmation made by FT-IR and elemental analysis confirmed the presence of elemental compositions (C, H, N) in the molecular Eu-complex. The thermal decomposition and morphological study of the ligands as well as the corresponding binuclear Eu complexes also been discussed. The synthesized binuclear Eu^{III} complexes were imbedded in a PMMA matrix with different Eu^{III} complex concentrations and studied their photophysical properties. The detailed PL excitation and emission spectra express the essential information regarding the spectral characteristics of the attached chromophoric ligating group and the site symmetry with respect to Eu^{III} ion in the complex. The theoretical calculations were performed by using density functional theory (DFT) frame work using B3LYP/6-31G (d, p) level of theory, to estimate the energy levels to support the mechanistic pathway of energy transfer from ligand to Eu ion in the complex.

6.3.4.1 Thermal Properties and Powder X-ray diffraction (PXRD) studies:

The thermal behaviour of the ligand (L1 and L2) and the corresponding binuclear Eu-complex ($Eu_2(TTA)_6(L1)$ and $Eu_2(TTA)_6(L2)$) under a nitrogen atmosphere were examined by means of thermogravimetric analysis (TGA). The general profile of the weight loss for the ligands and the binuclear Eu-complexes are displayed in Figure 6.18. The TGA of the complexes, $Eu_2(TTA)_6(L1)$ and $Eu_2(TTA)_6(L2)$ shown 10 % decomposition at 283 and 279 °C, respectively. The TGA of the complexes, $Eu_2(TTA)_6(L1)$ and $Eu_2(TTA)_6(L2)$ are shown first minor mass loss of approximately 6.01 % in the range of 110 to 165 °C, which corresponds to the elimination of coordinated water and solvent molecules in the structure. The major second decomposition observed for the complexes ($Eu_2(TTA)_6(L1)$ and $Eu_2(TTA)_6(L2)$) at 320 °C (lost 12.1 % and reached to 87.8 %) and 316 °C (lost 11.8 % and reached to 88.1 %), respectively. This corresponds to the degradation of the TTA ligand in the molecular structure. The third decomposition undergoes at 438 (lost 54 % and reached to 64 %) and 404 °C (lost 61 % and reached 38.9 %) and the final decomposition undergoes at 651 and 545 °C, respectively. This is corresponds to the decomposition of the ancillary ligands (presence of fluorene, Phenyl, phenanthroline groups).

The ligand (L1 and L2) thermal decomposition temperature is high as compared to that of the corresponding binuclear Eu-complexes. The first minor decomposition of ligands (L1 and L2) shown at 184 and 170 °C belongs to the water molecules and major decomposition at 403 (lost 8.26 % and reached to 91.7 %) and 417 °C (lost 14.1 % and reached to 85.8 %), respectively. The temperature at 442 and 225 °C observed 10 % weight loss, which could be attributed to the decomposition of ligand fragments (fluorene, Phenyl, phenanthroline groups) presence in the ligand moieties.

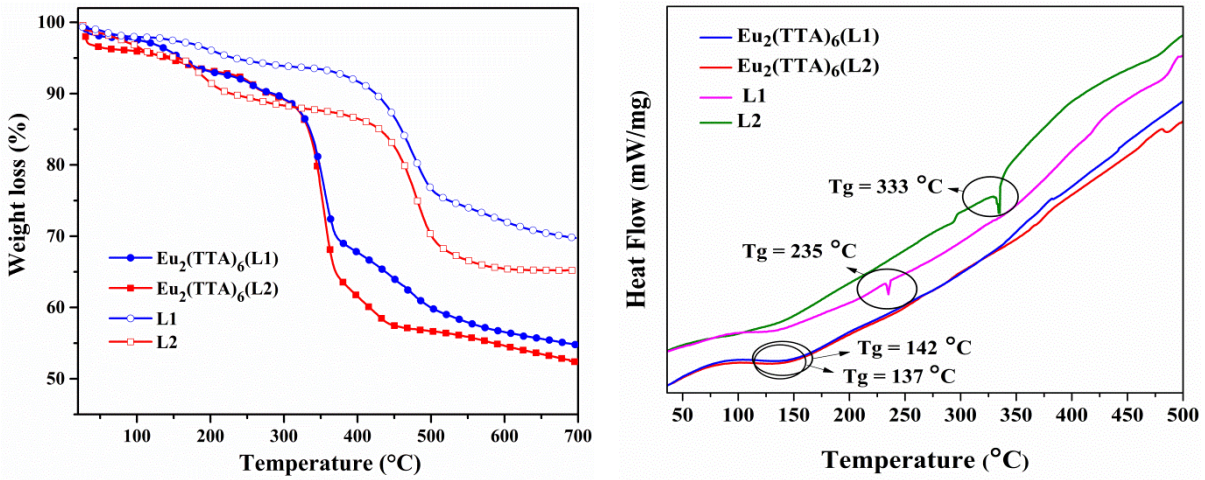

Figure 6.18 TG analysis curves for the ligands (L1 and L2) and its corresponding binuclear Eu^{III} complexes (($Eu_2(TTA)_6(L1)$ and $Eu_2(TTA)_6(L1)$) and in onset mentioned their DSC curves.

The DSC studies of the ligands and the corresponding binuclear complexes show the glass transition temperature (T_g) ranging from 137 to 333 °C. The ligand moieties are shown good T_g values as compare to that of corresponding Eu complexes (the same is marked in the DSC curve in Figure 6.18 right). The T_g of the ligands L1 and L2 are 333

and 235 °C as well as respective complexes, $Eu_2(TTA)_6(L1)$ and $Eu_2(TTA)_6(L2)$ shown 142 and 137 °C, respectively. The PXRD analysis of the complexes was shown broad diffraction peaks and is indicating that the amorphous nature of the complexes (Figure 6.19).

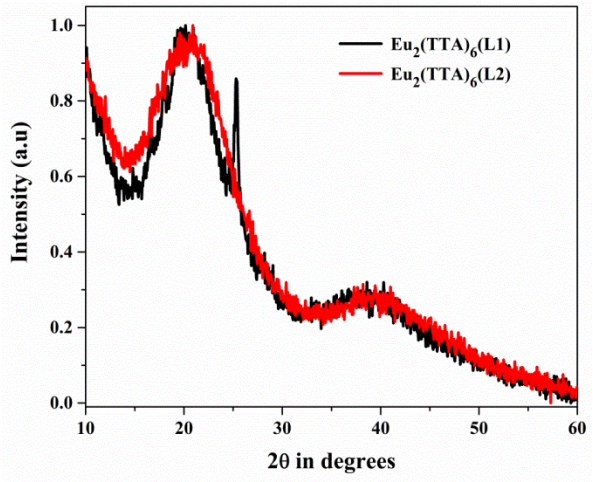

Figure 6.19 The PXRD analysis of the complexes, $Eu_2(TTA)_6(L1)$ and $Eu_2(TTA)_6(L2)$.

6.3.4.2 Photophysical properties:

6.3.4.2.1 UV-Visible absorption and Diffuse Reflectance Spectral studies:

The absorption spectrum of the ligands (L1 and L2) and the corresponding binuclear Eu-complexes is shown in Figure 6.20, left. Both the ligands and Eu complexes show similar absorption spectral profiles, however, the absorption edge of the Eu complex is slightly shifted towards near UV region (extending to a longer wavelength from 350 to 400 nm).

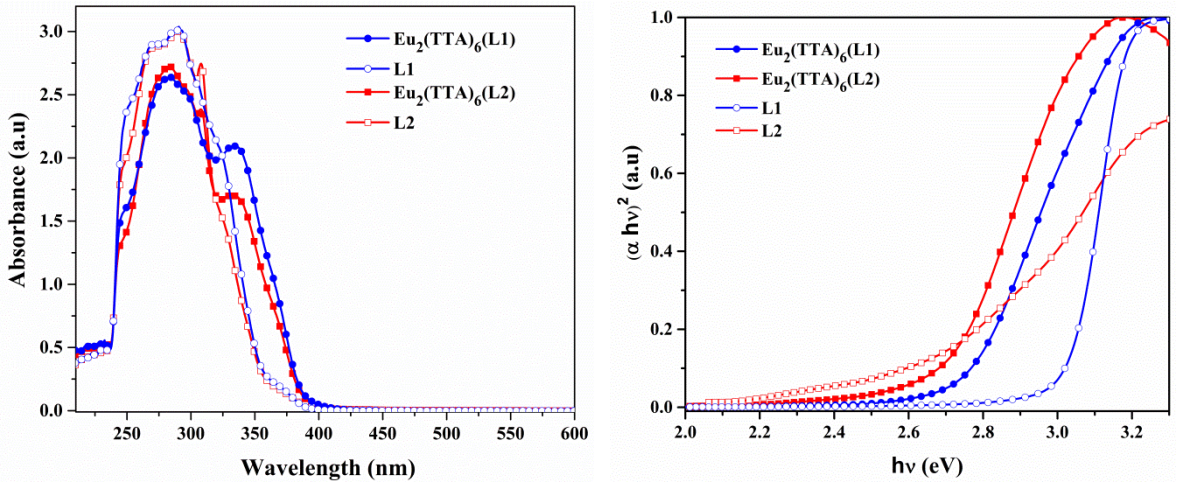

Figure 6.20 UV absorption spectra of the bipolar ligands and binuclear Eu-complexes (left); band gap calculations from the UV-absorption spectra (right).

In addition, the absorption peak consists shoulder in the near UV region, which is not present in the case of ligands. The strong absorption in the UV to near UV region is due to strong π to π* transition of aromatic chromophores present in the complex as well as ligand moieties.

The occurrence or coordination of the bipolar ligand not only enhances the absorption intensity but also fulfills the high coordination number of the central metal Eu^{III} ion. Thus improves the coordination saturation as well as thermal stabilities of binuclear Eu-complexes. The calculated absorptions peaks are tabulated in Table 6.10. The band gap was calculated for all the compounds by converting the UV-visible data (Figure 6.20, right) into Kubelka-Munk function. The acquired spectrum is converted to Kubelka-Munk function ($\alpha = F(R_\infty)$, equation 2.1) [53].

Table 6.10 The UV-absorption and PL emission data of synthesized binuclear Eu^{III} complexes and ligands.

S. No.	Compound name	UV λ_{max} (abs)[nm] Solution (a) (b)	λ_{exc} [nm] Solution/solid	PL λ_{em} (c) [nm]	FWHM [nm]	I_2/I_1 ratio
1	**$Eu_2(TTA)_6(L1)$**	246, 284, 335	321, 374 /272, 230, 426(d)	580, 592, 612, 652, 702	4.31/ 4.43(d)	14.2/ 13.8(d)
2	**$Eu_2(TTA)6(L2)$**	245, 285, 335	320, 365/270, 230, 438(d)	580, 592, 612, 652, 702	4.78/ 6.26(d)	16.0/ 10.2(d)
3	**L1**	249, 269, 290, 324	347/275, 320, 365(d)	425/448(d)	--.--	--.--
4	**L2**	248, 271, 289, 326	352/276, 315, 365(d)	425,/521(d)	--.--	--.--
5	**$Eu(TTA)_3$**	273, 340	275, 340	580, 592, 612, 652, 703	~ 6	~11

(a) Measured at 298 K in chloroform solution, (b) absorption peaks from the UV-absorption spectra, (c) emission peaks from PL emission spectra, (d) values of compounds in solid.

6.3.4.2.2 Photoluminescence studies:

The binuclear Eu^{III} complexes PL excitation spectra in solution state in chloroform solvent, $c = 1 \times 10^{-5}$ M were recorded at room temperature and are displayed in Figure 6.21 (left). The ligands, L1 and L2 in solution form are shown emission at a blue region which is 425 nm at excitation wavelength 347 and 352 nm, respectively. However, the ligands, L1 and L2 in the solid state shown emission at 448 and 521 nm with excitation wavelength 365 nm, respectively (Figure 6.21, right). The spectral shifting (bathochromic shift) from the solution to solid was observed and attributed to the aggregation of the molecule in the solid state (well documented). In case of binuclear Eu-complexes the excitation spectral profile was taken by monitoring the high intense $^5D_0 \rightarrow {}^7F_2$ (612 nm) electric dipole transition of the Eu^{III} ion. The spectra consist of broad absorption in the UV to near UV region (broad band between 275 and 425 nm), which can be assigned to the π–π^* electronic transition of the aromatic moieties present in the ligand. The absence of 4f–4f electronic transitions of the Eu^{III} ion in the absorption spectrum evidence that the luminescence sensitization via the excitation of the ligand. It is effective in the presently studied binuclear Eu-complexes.

The PL emission of the binuclear complexes and ligands were studied in solution as well as in solid state (Figure 6.22). The emission bands are observed for Eu^{III} complexes at around 579, 592, 612, 650 and 695 nm, and are attributed to the $^5D_0$–^7F_J (f–f transitions) with J = 0, 1, 2, 3 and 4, respectively. The $^5D_0 \rightarrow {}^7F_0$ transition is weak and situated at 579 nm (single peak) due to $^5D_0$-$^7F_0$ transition indicates that all Eu^{III} ions in the structure occupy a site of the same symmetry and experience the similar

crystal field perturbation in the complex. The moderately strong $^5D_0 \rightarrow {}^7F_1$ transition is indicated when Eu^{III} ion occupies the center of the symmetric site and this MD transition is independent of the coordinate environment. The hypersensitive ED $^5D_0 \rightarrow {}^7F_2$ transition consists of a strong emission at 612 nm. It leads to red luminescence and the local environment of the Eu^{III} ion sense to be more non-symmetrical. The observed broad peaks at about 650 as well as 695 nm correspond to the $D_0 \rightarrow {}^7F_3$ and $^5D_0 \rightarrow {}^7F_4$ transitions, respectively. It was noted that the absence of a broadband in the 380–530 (solution) and 380-700 nm region corresponding to the ligand emission in the emission spectra highlights that efficient ligand-to-metal energy transfer happens in the presently studied binuclear Eu-complexes.

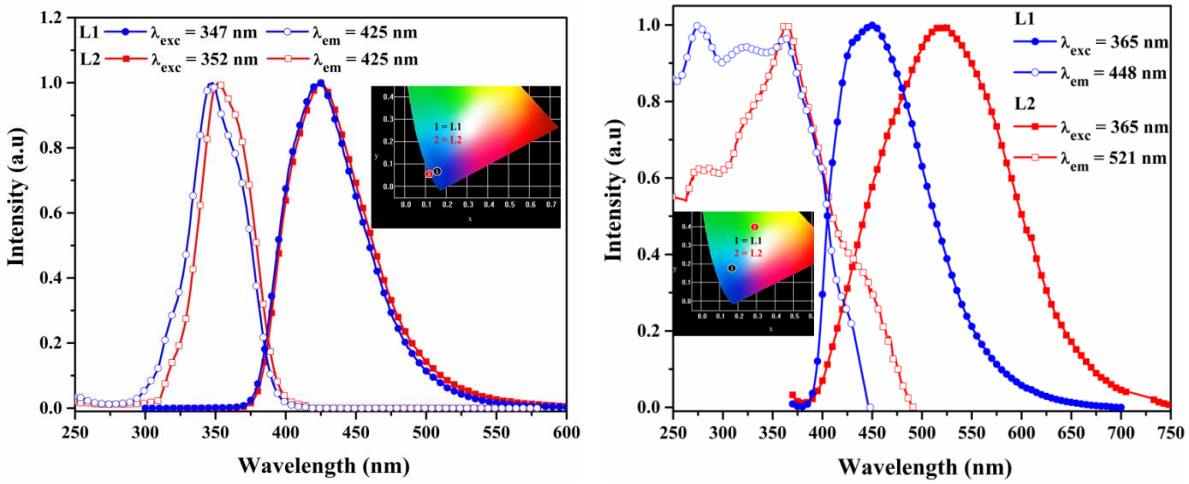

Figure 6.21 The PL excitation and emission spectra of the ligands (L1 and L2) in solution (left) and solid state (right).

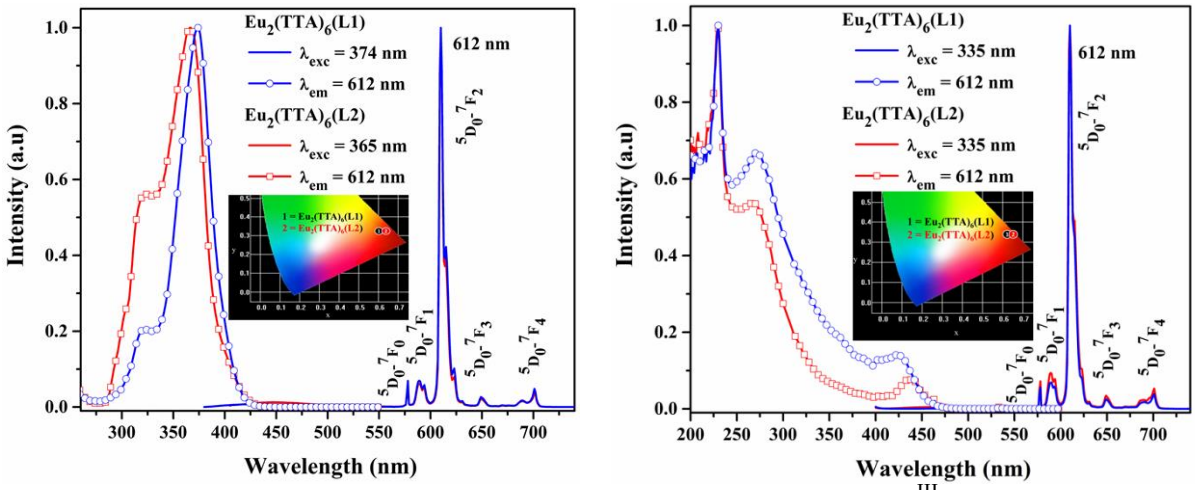

Figure 6.22 The PL excitation and emission spectra of the binuclear Eu^{III} complex in solution (left) and solid state (right).

The emission intensity of the electric dipole transition is more intense and it reaches the characteristic red emission. The europium ion site symmetry or asymmetric ratio was calculated from the integrated emission intensity ratio of the $^5D_0$-$^7F_2$ transition to $^5D_0$-$^7F_1$ transition (I_2/I_1) from the PL emission spectra of the complexes in solution as well as solid state. The intensity

ratio (I_2/I_1) of the Eu^{III} complex, $Eu_2(TTA)_6(L1)$ in solution and solid are 14.2 and 13.8; $Eu_2(TTA)_6(L2)$ in solution and solid are 16.0 and 10.2; respectively. The intensity ratio of the solution was found to be higher than that of solid. It is also signifying that the Eu^{III} ion occupied non-centre of symmetry site in the complex. In addition, it was clear that the Eu^{III} ion and ligand have strong coordination interaction. As compared with the intensity ratio (I_2/I_1) of $Eu(TTA)_3$ was around 11.5 which is indicating that the current synthesized Eu-complexes are in high-intensity ratio than $Eu(TTA)_3$ in solution. The calculated full width at half maximum (FWHM) values are 4.31 and 4.78 nm (solution); 4.43 and 6.26 nm (solid) for $Eu_2(TTA)_6(L1)$ and $Eu_2(TTA)_6(L2)$, respectively. The less value of FWHM for the complexes is indicating that the narrow emission intensive characteristic band is very much suitable to achieve the efficient red emission.

It is generally believed that the energy transfer process proceeds through triplet (^1T) pathway in the europium luminescent molecular complexes. Understanding the energy transfer process from ligand to center metal ion is very much necessary, thus it is necessary to gain and understand the excited energy levels of Eu^{III} ion as well as the ligand. Since the energy transfer from the organic part towards metal ions occurs efficiently by two different pathways. In which the first one, described by Forster, It takes into an account of multipolar interactions between distinct oscillating centers [54]. The second one is Dexter's mechanism, postulates energy transfer through the electron exchange between the organic chromphoric ligand and lanthanide ion in the complex [55, 56]. The similar nature of this process requires an overlap of the emission spectra of the donor (ligand) and the absorption spectra of the acceptor. Based on this criteria it was examined by the overlap between the emission spectrum of the ligand (L1 and L2) and absorption spectra of the TTA (acceptor). The overlap observed in the region of 375-450 nm. It is clearly indicating that the energy transfer process can appear through ligand triplet level to TTA triplet excited state through intra molecular energy transfer [57, 58]. The process implicates the photoexcitation of the ligand (antenna or organic chromophore) energy to Eu^{III} ion via their triplet (^3T) states by means of internal conversion; finally, the Eu^{III} ion emits photons to ground state from first excited levels ($^5D_0$). It is also well documented that the Eu^{III} excited levels were located at $^5D_3$ (24,800 cm^{-1}), $^5D_2$ (21,500 cm^{-1}), and $^5D_1$ (19,100 cm^{-1}), to $^5D_0$ (17,500 cm^{-1}) feasible by internal conversion (thermal activation) [59].

The energy level matching is the key factor one need to consider for efficient energy transfer from ligands to Eu^{III} ion in the complex. Thus, the energy level's match of the triplet state of the ligands to $^5D_0$ of Eu^{III} is one of the vital factors, which directly influence the PLQY of the Eu complex. It is also well known that anionic ligand (TTA) energy levels located at 25,164 (singlet) and 18,954 (triplet) [26]. The presently calculated singlet (^1S) and triplet (^3T) energy levels of the Eu^{III} complex by DFT and TD-DFT analysis of L1 and L2 were located at 29,013 (3.59 eV), 27,172 (3.36 eV) cm^{-1} (singlet) and 22,173 (2.74 eV), 22,152 cm^{-1} (2.74 eV) (triplet), shown in Figure 6.23. These obtained outcomes are showing capable of transferring the energy from the triplet state of the ligand to $^5D_0$ of Eu^{III} metal ion efficiently. These results were also supported according to the Latva *et al.,* calculations [22] (($\Delta E = E(T_1) - E(^5D_0)$ is 2500 - 4000 cm^{-1}; singlet above 25,000 (3.09 eV) and triplet above 20,000 cm^{-1} (2.47 eV)). Since the energy difference between the ^3T and $^5D_0$ level is comparatively high and hence there is no reversible emission possible (due to back energy transfer) from the complex. The same was reveals in the PL emission spectra (no emission was observed in the rage of 400 to 550 nm for ligand moieties). It could be expected that the fluorene in the complex sensitization boosted by decrease the vibronic quenching effect. Previous studies reveal that the fluorene molecule at the

N_1 position in the ligand is better sensitizer than consist of the alkyl chain (ethyl) [41]. The observed complete energy transfer process was also been supported by Reinhoudt's empirical rule [60]. In addition, it was also discussed that in this energy transfer mechanism TTA excited singlet and triplet state can act as a transitional state between the singlet to triplet excited states of the ligand as well as triplet excited state to the excited $^5D_0$ level of Eu^{III} ion, respectively. The effective overlap between the ligating moieties and the absorption spectrum of TTA showed that the characteristic luminescence of the corresponding Eu^{III} occurs through intramolecular energy transfer which is shown in pictorial view in Figure S8.

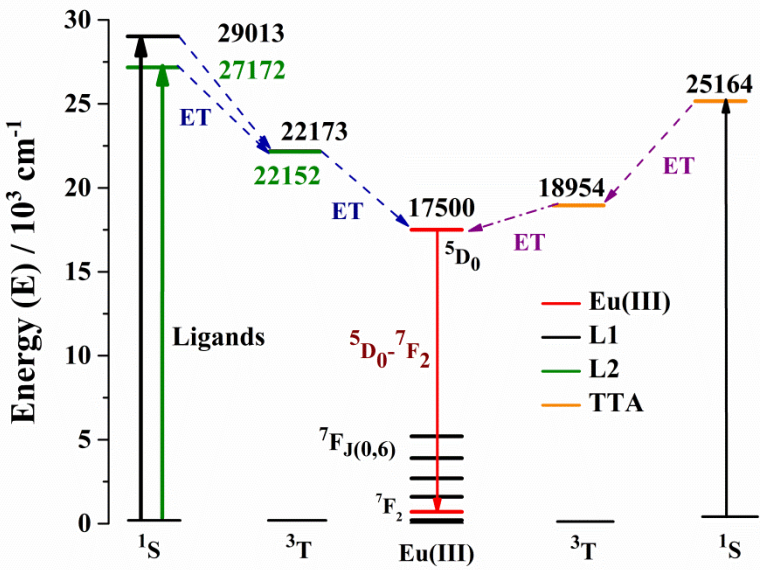

Figure 6.23 The energy transfer diagram for the complexes and energy transfer to Eu^{III} ion from ligand as well as TTA molecule (S = singlet, T = triplet, ET = energy transfer).

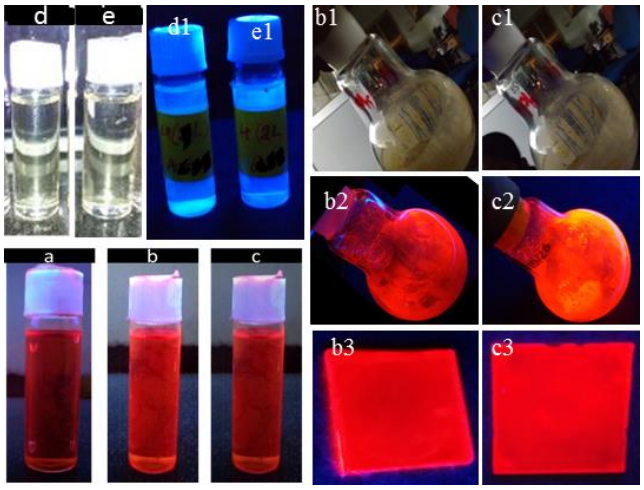

Figure 6.24 Ligands and corresponding Eu^{III} complexes under UV (365 nm) light are (a) $Eu(TTA)_3$, (b) $Eu_2(TTA)_6(L1)$, (c) $Eu_2(TTA)_6(L2)$; (b1) (c1) are under normal light; (b2) (c2) are under UV light; (b3((c3) are thin films; (d) (e) are L1 and L2 under normal light (d1) (e1) are under UV light.

The digital photograph of the compound (ligands and complexes are in solution, thin film and solid form) in the natural light and under UV lamp (365 nm) are shown in Figure 6.24. The blue color emission was observed from the ligand under UV lamp, whereas the corresponding Eu complex shown red emission at 365 nm excitation. The respective thin films of the complexes are also shown bright red color. In addition, $Eu(TTA)_3$ complex digital photograph also given for reference and shown red color.

The measured PLQY were compared with the unimolecular Eu-complex [41] shown higher QY in the solution state and similar in the case of solid, respectively. The obtained results are clearly indicating in solution state, the radiative path way increasing by reducing non-radiative transition in the complex. However, in case of solid state there is no significance effect was found. The detailed absolute quantum efficiency (measured by integration sphere) calculations of the Eu-complex by using the already reported procedure [26, 41]. The absolute quantum efficiency (measured by integration sphere) of the complex was carried out in solution as well as solid by monitoring the higher electric dipole transition (612 nm). The obtained absolute QY for the binuclear Eu-complex in solution is found to be are 40.7 and 30.0 %, respectively. Whereas, the complexes are in solid state show 31.8 and 32.4 %, respectively. In addition, QY of the complexes doping with PMMA thin film was also measured and shown 52.7 and 59.5 %. The observed QY is higher than that of the solution and solid. It indicates that the complex dispersed in PMMA leads to efficient energy transfer via reducing the non-radiative transitions. It is also worth to note that the presence of PMMA matrix leads to closer the acceptor and donor. In addition, QY of the thin film of $Eu_2(TTA)_6(L2)$ is found to be higher than that of $Eu_2(TTA)_6(L1)$. It is expected due to the presence of fluorene molecule in the complex, $Eu_2(TTA)_6(L2)$ leads to increase the efficient energy transfer to central Eu^{III} metal via ligand. The similar observations also found in the case of solid. These results can also supported by the theoretical calculations of the singlet and triplet energy levels location and singlet energy level (L1) is near to the triplet level as compared with L1. So it may efficiently transfer the energy in L2 than L1 via singlet to triplet energy level. As compared with the reported phenanthroline with spacer consisted complex (solution and solid are 11.5 and 5%) [41], currently synthesized complexes were shown improved QY (solution above 3 times, solid above 6 times). These results are suggesting that the fluorene with spacer molecule in binuclear complexes (2 Eu metal ions) extensively increase the energy transfer process leads to high QY.

6.3.4.2.3 Judd-Ofelt and Lifetime analysis:

The Judd-Ofelt parameters were essential to understand the physical implication of the symmetric/asymmetric and covalent/ionic bonding environment between Eu^{III} ion and the surrounding ligand moiety. Since these calculations were initials to calculate the sensitization energy transfers process and other spectral parameters. The J-O parameters were calculated for binuclear Eu^{III} complexes from the PL emission spectra by well-reported method from literature [57, 61, 62] and the details are given in chapter 2. The calculated value has been tabulated in Table 6.11 and the Ω_2, Ω_4 values are 1.79, 0.23 (10^{-20} cm^2) ($Eu_2(TTA)_6(L1)$) and 2.44, 0.244 (10^{-20} cm^2) $Eu_2(TTA)_6(L2)$, respectively. To achieve the best Eu^{III} radiative rates, it is necessary to design asymmetrical Eu^{III} complexes with having larger Ω_2. Intensity parameter Ω_4 ($^5D_0 \rightarrow {}^7F_2$) is less sensitive to the coordination sphere than Ω_2 in the complex and reflects chemical environment rigidity surrounding the Eu^{III} ion. The most importantly isolated magnetic dipole is $^5D_0$ to $^7F_1$ (J=1) transition and it has no electric dipole involvement, which is practically independent

of the ion's chemical environment. Based on these criteria it is used as a reference for calculating of J–O intensity parameters.

The lifetime of the ligands as well as complexes were measured in different solvents and in solid form which are interpreted in the Figure 6.25. The lifetime of luminescent decay profiles ($^5D_0$ lifetimes (τ_{obs})) for the complexes and ligands was best fitted with mono-exponential curves and measured at room temperature. The observed luminescence decay profile corresponds to a single exponential function, thus implying the presence of only one emissive Eu^{III} centre. The single exponential function is given by the equation $I(t) = I_0 + A_1 \exp\left(\frac{-t}{\tau}\right)$, where $I_0 = 0$ is the offset value, A_1 is the scalar quantity (from curve fitting), t is the time in ms and τ is the decay time value for the exponential module. The values are suggesting the presence of a single chemical environment around the emitting Eu^{III} ion and compiled in Table 6.11. The lifetime variations was observed in different solvents and the following order was followed $CHCl_3$ (0.67) > Acetone (0.62) > DCM (0.60) > THF (0.59) > DMF (0.50) > solid (0.43 ms) for $Eu_2(TTA)_6(L1)$ and $CHCl_3$ (0.68) > Acetone (0.64) > DCM (0.62) > THF (0.61) > DMF (0.49) > solid (0.42 ms) for $Eu_2(TTA)_6(L2)$ at 360 nm. Both the complexes were followed same trend in the solution form towards decreasing of the lifetime.

The highest lifetime of the solution ($CHCl_3$) as compared with solid indicates that the non-radiative transition decreases via reducing the vibrational coupling and leads ratiative transition enhancement. In addition, the primary process that quenches $^5D_0$ excited state of Eu^{III} in solution form by non-radiative relaxation via vibronic coupling. The excited state lifetime of $^5D_0$ (Eu^{3+}) level (μs to ms scale) was enable energy transfer by high frequency vibrational oscillators such as O−H, N−H, and C−H and leads to favours quenching of the luminescence. According to the gained results, the C-H vibrational oscillator frequency is less as compare to that of O-H and N-H and $CHCl_3$ and DCM are shown enhanced results.

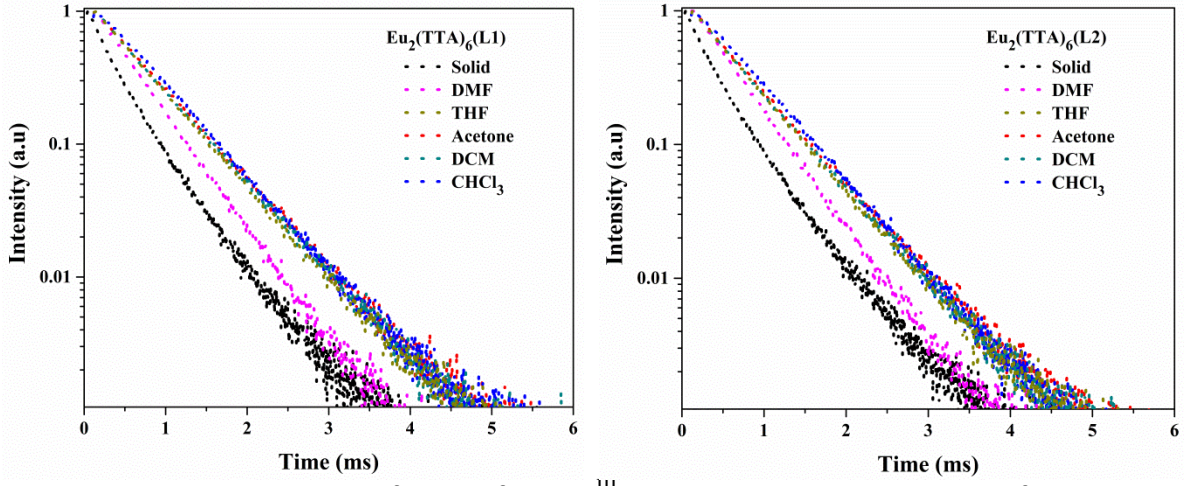

Figure 6.25 The lifetime of the Eu^{III} complexes, $Eu_2(TTA)_6(L1)$ (left) and $Eu_2(TTA)_6(L2)$ (right) in different solvents and in the form of solid.

The intrinsic lanthanide quantum yield (Φ_{Ln}) rationalization in coordination complexes depends on the Judd-Ofelt theory, which considers an odd number of crystal-field contributions. The $\Phi_{Ln,}$ experimental branching ratio ($\beta_{1\text{-}3}$), stimulated emission cross section ($_{\sigma 1\text{-}3}$), radiative (A_{RAD}), nonradiative (A_{NR}) decay rates, $^5D_0$ lifetime (t_{obs}) and energy transfer efficiency (Φ_{sen}) parameters were calculated by reported literature [63-67, 57, 41]. The obtained intrinsic quantum

yield (Φ_{Ln}) and energy transfer efficiency (Φ_{sen}) indicates that the currently studied ligand is an efficient sensitizer for Eu^{III} ion in the complexes. The Φ_{sen} is higher for $Eu_2(TTA)_6(L2)$ is 91.81 than the complex $Eu_2(TTA)_6(L1)$ is 85.14. The obtained higher sensitization is leads to efficient energy transfer and it reveals the higher QY of the $Eu_2(TTA)_6(L2)$. The detailed calculated parameters are tabulated in Table 6.12 and Table 6.13.

Table 6.11 The Judd-Ofelt and lifetime analysis of the complexes and ligands in solid form as well as in different solvents.

S. No.	Compound	Intensity Parameters (10^{-20} cm^2)		τ / ms [a]					
		Ω_2	Ω_4	Solid	$CHCl_3$	DMF	THF	DCM	Acetone
1	$Eu_2(TTA)_6(L1)$	1.78	0.23	0.43[b]	0.67	0.50	0.59	0.60	0.62
2	$Eu_2(TTA)_6(L2)$	2.44	0.24	0.42[b]	0.68	0.49	0.61	0.62	0.64
3	L1 (10^{-3} ms) λ_{exc} 280 nm	--.--	--.--	2.11	1.62	1.71	2.10	2.55	1.76
4	L1 (10^{-3} ms) λ_{exc} 360 nm	--.--	--.--	4.33	11.5	12.0	21.9	23.0	26.8
5	L2 (10^{-3} ms) λ_{exc} 280 nm	---.--	--.--	1.70	1.85	2.52	1.71	2.51	1.72
6	L2 (10^{-3}ms) λ_{exc} 360 nm	--.--	--.--	1.92	21.8	24.5	20.6	23.0	20.8

[a] The for the β-diketonate Eu^{III} complex and its ligand. [b] decay curves were best fitted with bi-exponential curves.

Table 6.12 Experimental branching ratios (β_{1-3}) and stimulated emission cross section (σ_{1-3}) of the complex.

S. No.	Complex name	σ1	σ2	σ3	β_1	β_2	β_3
1.	$Eu_2(TTA)_6(L1)$	0.520	6.935	0.336	7.92	86.65	5.42
2.	$Eu_2(TTA)_6(L2)$	0.505	1.117	0.329	5.96	89.82	4.24

Table 6.13 The Radiative (A_{RAD}) and nonradiative (A_{NR}) decay rates, $^5D_0$ lifetime (t_{obs}), intrinsic quantum yields (Φ_{Ln}), energy transfer efficiency (Φ_{sen}) and overall quantum yield ($\Phi_{overall}$) for the complex.

S. No.	Complex name	A_{RAD} (S^{-1})	A_{NR} (S^{-1})	τ_{obs} (ms)	τ_{RAD} (ms)	Φ_{Ln} (%)	Φ_{Sen} (%)	$\Phi_{Overall}$ (%)
1.	$Eu_2(TTA)_6(L1)$	630.681	170	0.43	1.59	27.04	85.14	31.8
2.	$Eu_2(TTA)_6(L2)$	838.937	154	0.42	1.19	35.29	91.81	32.4

6.3.4.3 Electrochemical Properties:

The electrochemical properties were carried out for the newly synthesized ligands and the corresponding binuclear complexes and shown in Figure 6.26. From the voltammogram, the oxidation potentials of the ligands (L1 and L2) and complexes ($Eu_2(TTA)_6(L1)$ and $Eu_2(TTA)_6(L2)$) were found to be 1.38, 1.27 and 1.45, 1.39 eV, respectively. The obtained oxidation potentials from the CV analysis and other values are tabulated in Table 6.14. The obtained oxidation potentials of the complexes were

decreases as compare to that of ligand. Similarly in case of reduction potential the same trend was observed. The equation 2.1 and 2.11 [37] used to calculate the HOMO and LUMO energy levels.

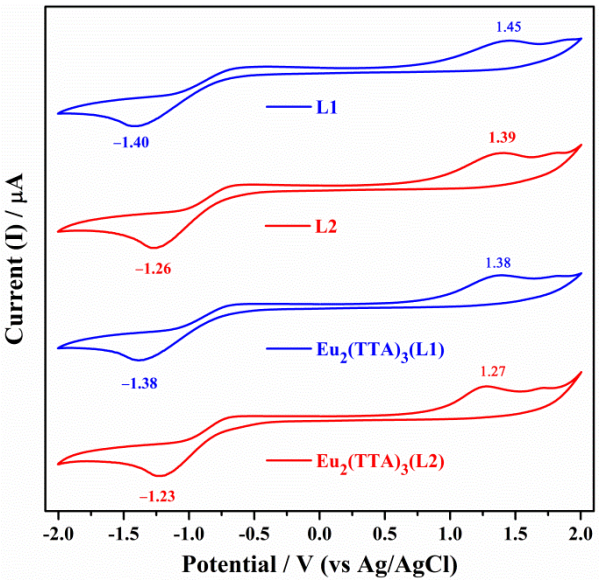

Figure 6.26 Cyclic voltammogram of ligands and its corresponding binuclear Eu^{III}-complexes.

Table 6.14 Electrochemical properties of the ligands and respective binuclear Eu^{III}-complexes.

S. No.	Compound Name	Voltage$^{Oxi}_{onset}$ [V] (E_{HOMO} [eV])	Voltage$^{Red}_{onset}$ [V] (E_{LUMO} [eV])	$\lambda_{onset,}$ [nm] (a)	Energy gap E_g^{Opt}, [eV] (b)
1	**$Eu_2(TTA)_6$(L1)**	1.38 (-5.78)	-1.38 (-3.02)	452.4	2.74 (2.76)
2	**$Eu_2(TTA)_6$(L2)**	1.27 (-5.67)	-1.23 (-3.17)	459.2	2.70 (2.50)
3	**L1**	1.45 (-5.85)	-1.40 (-3.00)	411.9	3.01 (2.85)
4	**L2**	1.39 (-5.79)	-1.26 (3.14)	454.1	2.73 (2.65)

(a) Calculated from the optical absorption (DRS spectra), (b) Calculated the onset wavelength of optical absorption (onset) in solid-state film (DRS spectra). The energy differences (HOMO and LUMO) values calculated by cyclic voltammogram are mentioned in bracket.

The calculated optical energy gap (DRS spectral analysis) of the ligands as well as complexes was similar to that of the results obtained from the electrochemical analysis. The overall band gap of the complexes was less as compared with the respective ligands. The TPA based complex energy gap is slightly higher than that of currently synthesized complexes [26]. These results are suggesting that the spacer arrangement can be a better choice to get suitable energy difference between the ligand excited triplet level and Eu $^5D_0$ level. The L2 consist less energy gap than L1 ligand and it is suitable to harvest the efficient energy from the Eu-complex. Similarly, the complex ($Eu_2(TTA)_6$(L2)) gained less energy gap and more suitable to get efficient energy transfer. Since the efficient energy transfer process needs acceptor ($^5D_0$) energy level should be lesser than donor (ligand). This criteria very much can full filled by $Eu_2(TTA)_6$(L2) complex. The energy gap (obtained from DRS) and HOMO-LUMO values (obtained from CV) are well matched with the theoretical calculations by DFT calculations (calculated from the

optimized structure, Figure 6.27) [68-71]. The calculated frontier molecular orbitals of the ligands L1 and L2 electron density is located on phenanthro-imidazole ring and on Ph/Fluorene (some of the electron density was transferred to imidazole moiety) moiety for HOMO and LUMO, respectively (Table 6.14) and their respective values were mentioned in Table 6.15. In addition, the computed vertical transitions as well as their oscillator strengths and configurations of ligands (L1 and L2) were also incorporated in the Table 6.S2.

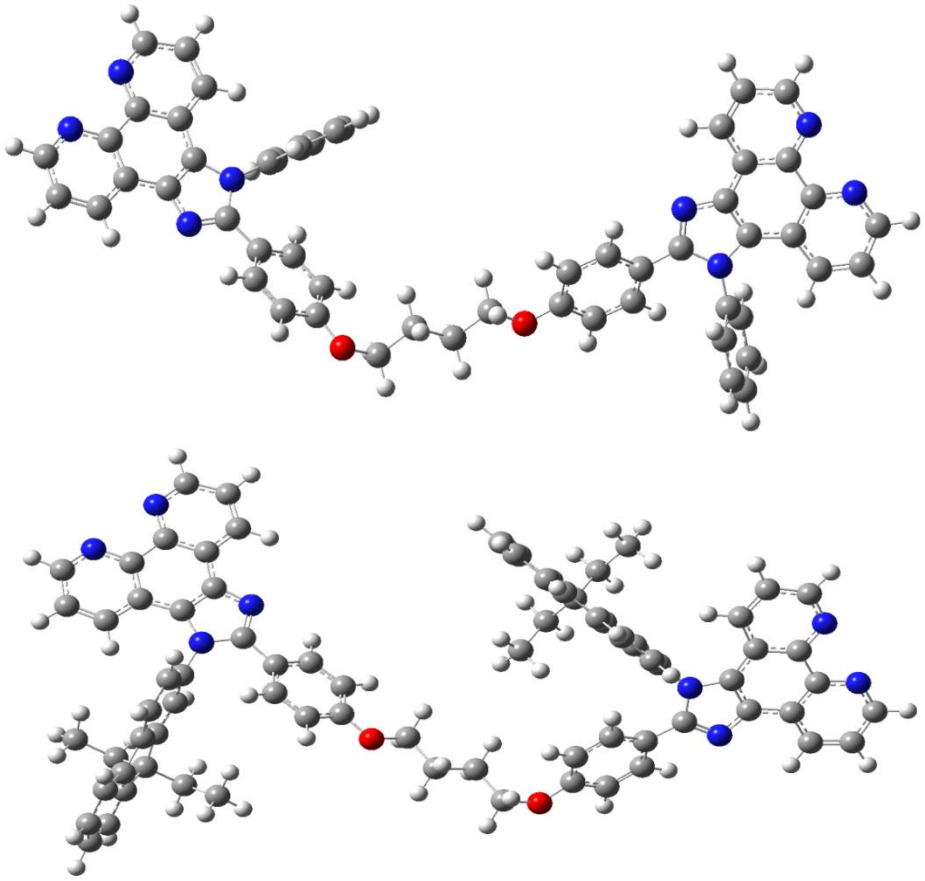

Fig. 6.27 The optimized ligands, L1 (up) and L2 (down) structures by theoretical analysis.

Table 6.14 The HOMO and LUMO energy levels of the ligands.

L1	
HOMO-1	**HOMO**
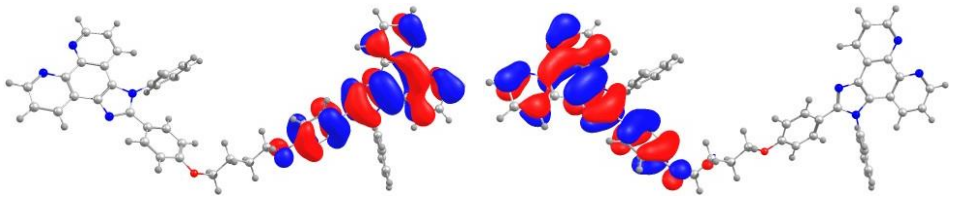	

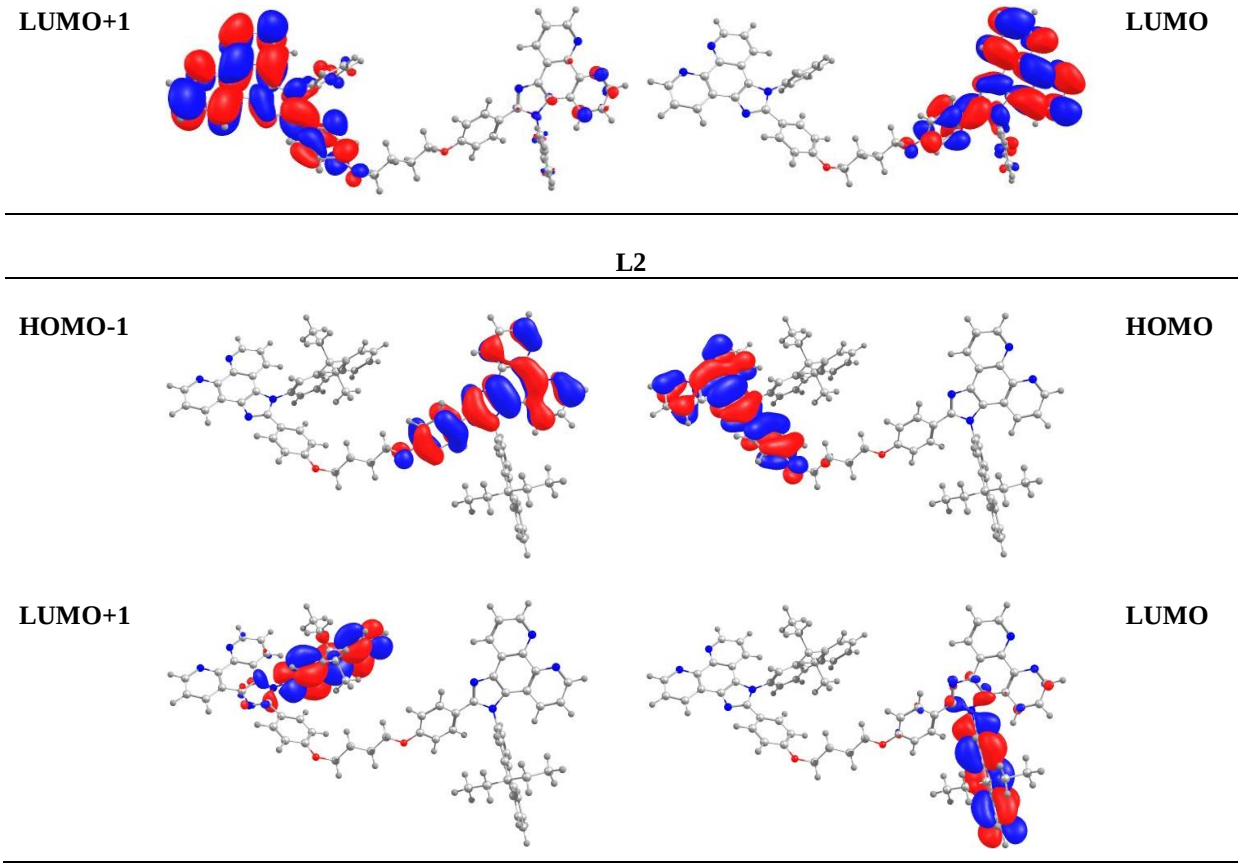

Table 6.15 The HOMO and LUMO energy levels of the ligands.

Molecule	HOMO	HOMO-1	LUMO	LUMO+1	E_g	S1	T1
	in electron volts (eV)						
L1	-5.40	-5.35	-1.22	-1.18	4.13	3.59	2.75
L2	5.31	5.36	1.43	1.42	3.87	3.36	2.74
$Eu_2(TTA)_6$(L1)	--.--	--.--	--.--	--.--	--.--	$^5D_0$ level = 2.17	
$Eu_2(TTA)_6$(L2)							

6.3.4.4 CIE Chromaticity coordinates:

The Commission Internationale de l´Eclairage (CIE) values of the ancillary ligands and their respective binuclear complexes were calculated from the PL emission spectra in solution as well as solid state (Figure 6.28). The calculated CIE values are tabulated in Table 6.16. The ligand shown blue emission in solution but in the case of the solid state, it was shifted towards sky blue and greenish white emission. By molecular structure engineering (by functionalizing or changing the substitutes in the back bone of the ligand), it is possible to generate white light emissive from single molecular emitters. The complexes was shown red emission with apt CIE color coordinate values and almost identical to the CIE value of the pure red emission designated by the national television standers committee (NTSC). The optimizations of the ligand structures are in progress in our laboratories, to obtain pure white (near) emissions.

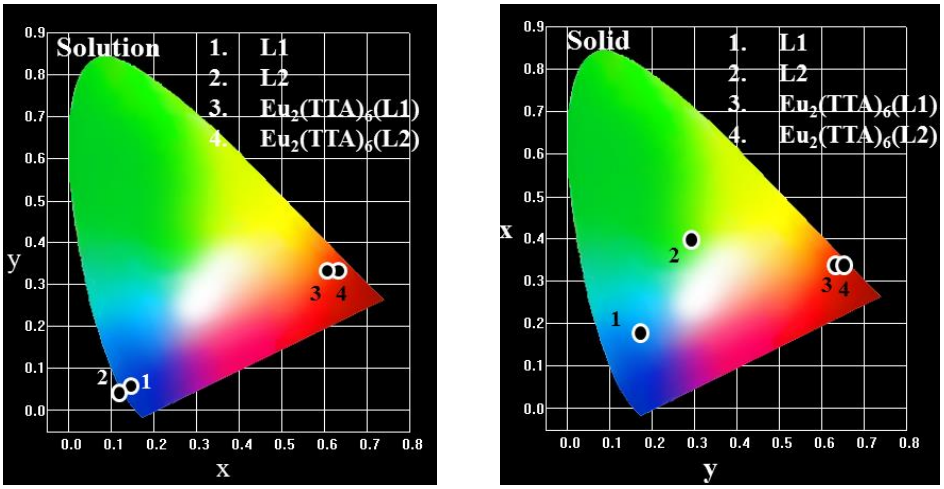

Figure 6.28 The CIE chromaticity coordinates for bipolar ligands and binuclear Eu complexes in solution (left) and solid (right).

Table 6.16 The CIE color coordinates for the bipolar ligands and binuclear Eu^{III} complexes.

S. No.	Compound Name	Solution (a)(b)		Solid (b)	
		x	y	x	y
1	**$Eu_2(TTA)_6(L1)$**	0.61	0.33	0.63	0.33
2	**$Eu_2(TTA)_6(L2)$**	0.63	0.33	0.65	0.34
3	**$Eu(TTA)_3.2H_2O$**	0.66	0.33	0.65	0.33
4	**L1**	0.16	0.06	0.17	0.18
5	**L2**	0.11	0.05	0.29	0.40

(a) Measured in chloroform solution at 298 K, (b) Emission peaks from PL emission spectra.

6.3.4.5 PMMA film of binuclear Eu^{III} complexes:

In order to gain more information about the optical properties of Eu-complex in a matrix, the complex was also dispersed in PMMA matrix and their PL emission spectra, respective digital photographs are shown in Figure 6.29. The PL emission of the thin film was made in different concentrations which are 0.1, 0.5, 1 and 5 % doping of complex with PMMA. As compared with the complex in the pure situation on a glass substrate shown less intensity peaks then PMMA doped thin films. However, all the percentage of the thin films was shown best characteristic pure red emission and satisfying the NTSC standards (x = 0.66, y = 0.33). In addition, the FWHM and intensity ratios were also calculated to understand the emission as well as the symmetry of the complexes (Table 6.ST1). The FWHM of the complexes was found to be very narrow (almost 4 nm). It is better as compared to that of complexes in solution and solid state. The calculated intensity ratios of complexes were shown approximately 20 (I_2/I_1), which is clearly indicating that the Eu metal ion occupied non-centre of symmetry and experienced more unsymmetrical. Thin film intensity parameter value is higher than that of the complex in solution and solid, which also signifying that the currently synthesized complexes are better achiever to get the efficient pure red luminescence. It is also worth to note that the thin film of the QY was also improved than that of solution and solid. The detailed calculated CIE, FWHM and intensity ratios were incorporated in the Table 6.ST1. These

obtained outcomes signifying that the energy transfer from the ligand to Eu^{III} metal ion is very efficient in the presently discussed binuclear complexes. The pictorial view of the CIE color coordination location in the CIE color grout is shown in Figure 6.S9, left.

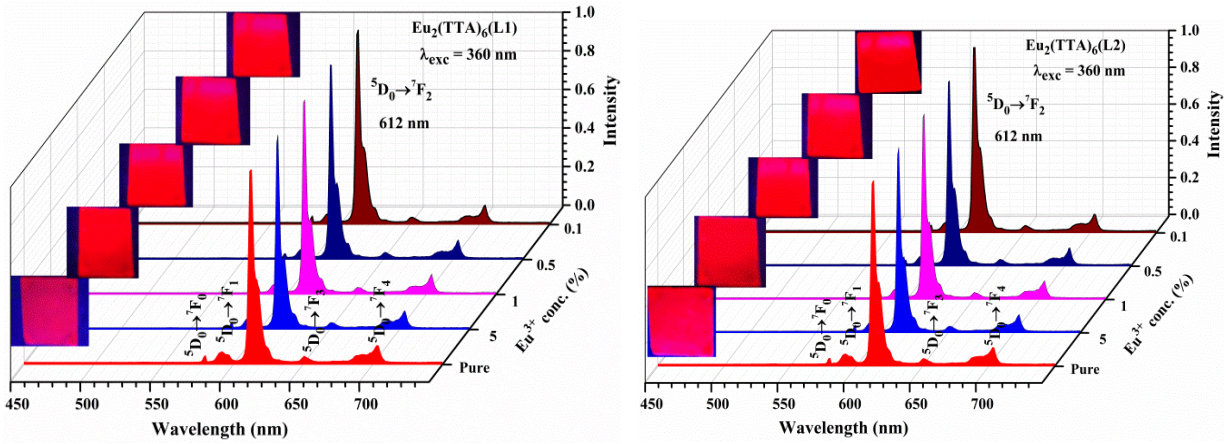

Figure 6.29 The emission spectra of Eu^{III} complexes (left-L1, right-L2) doped with PMMA (different percentage ratio) as well as pure Eu^{III} complex.

6.3.4.6 Fabrication of LED with Eu complexes:

The combination of a 395 nm emitting InGaN chip with the complexes in different ratios like 1:10 and 1:50 (Eu^{III} complex: PMMA) are made to use light-emitting diodes for the complexes. The fabricated LEDs were glowing under 20 mA forward-bias current. The emission of the complexes was shown intensive red emission peaking wavelength at 612 nm. The excitation source of the LED is almost transferred to the complex, $Eu_2(TTA)_6(L2)$ and it is less in the former complex (Figure 6.30). However, both the complexes are shown efficient red emission with CIE are x = 0.65, y = 0.34 (1:10) (for complex 1); x = 0.66, y = 0.34 (1:50) and for complex 2, the CIE values are x = 0.66, y = 0.33 (1:10); x = 0.66, y = 0.33 (1:50), respectively. These results are indicating that the presently synthesized complexes are best materials for red emitting LEDs. The LED CIE color coordinates for the Eu^{III} complexes in different ratio were shown in Figure 6.S9, right.

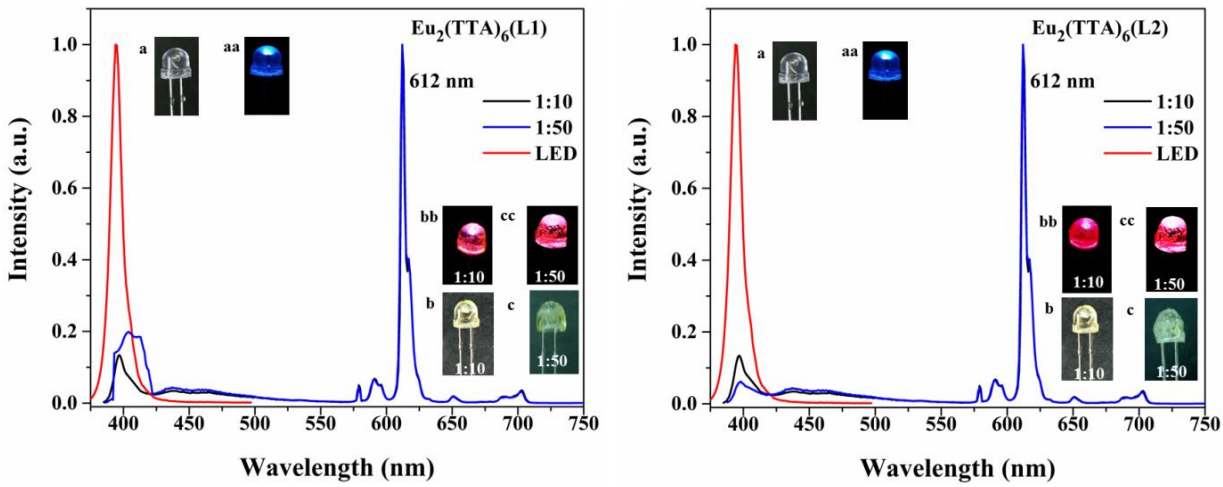

Fig. 6.30 The spectra's of Eu^{III} complexes coated on the 395 nm emitted LED (InGaN) chip. In inset **a** is the original 365 nm emitted LED chip, **aa** is under forward bias. **b** and **c** are coated with binuclear Eu^{III} complexes and **bb** and **cc** are with forward bias, respectively.

6.4 Summary and Conclusion:

In summary, new bipolar ligand with spacer moiety was synthesized and used the same for Eu^{III} complex. The PL emission spectra of the complex clearly indicates that the fully energy transfer is happening; the same was also confirmed by DFT and TD-DFT calculations. The spacer molecule can decrease the energy gap of HOMO-LUMO energy levels. In other words, it was increases singlet and triplet energy levels results efficient energy transfer. The improved intensity ratios as well as FWHM were shown better for the complex. The absolute quantum efficiency of the complex showed 11.5% and enhanced quantum efficiency observed by 1% doping of complex in PMMA. The complex has shown worthy thermal decomposition. In addition, we have designed and synthesised two ancillary ligands (in the ligand structure the two phenanthroline moiety connected through phenyl ethoxy spacer (N1 fuctionlized by phenyl and fluorene) and using this corresponding binuclear Eu-complexes was synthesized successfully. The isolation of the luminescent Eu core was achieved (reduce the concentration quenching effect through non-radiative energy transfer among the Eu ion in the complex). The PL emission spectral study of the ligands shown blue to greenish yellow (solution to solid) and their respective complexes showed efficient characteristic red emission. No additional emission in the region of 400-550 nm indicates the efficient energy transfer (confirmed by DFT and TD-DFT calculations). The calculated spectral parameters shown currently synthesized ligands are good sensitizers for Eu^{III} metal ion. The suppression of radiationless transitions caused by vibrational relaxation or non-radiative energy migration is reduced comparatively significant in the thin film of the complex $Eu_2(TTA)_6(L2)$ compare to that of complex $Eu_2(TTA)_6(L1)$ leads to highest QY (59.5 %), fluorene sensitization also plays a vital role. The fabricated LED conjugated with Eu-complex shown efficient red emission. These observations are indicating that the presently synthesized complexes are potential in lighting applications.

6.5 References:

[1] J. C. G. Bunzli and S. V. Eliseeva, *J. Rare Earths*, 2012, **28**, 824–842.

[2] J. C. G. Bunzli and A. S. Chauvin, in Handbook on the Physics and Chemistry of Rare Earths, ed. J. C. G. Bünzli and V. K. Pecharski, Elsevier Science Publishers, Amsterdam, 2014, ch. 261, vol. **44**, pp. 169–281.

[3] X. Huang, S. Han, W. Huang and X. Liu, *Chem. Soc. Rev.*, 2013, **42**, 173–201.

[4] H. Liang, Q. Zhang, Z. Zheng, H. Ming, Z. Li, J. Xu, B. Chen and Hui Zhao, *Optics Letters*, 2004, **29**, 477–479.

[5] J. Hwan Oh, H. M. Song, Y. K. Eom, J. H. Ryu, M. J. Ju and H. K. Kim, *Bull. Korean Chem. Soc.*, 2011, **32**, 2743–2750.

[6] F. Piccinelli, M. Bettinelli, A. Melchior, C. Grazioli and M. Tolazzi, *Dalton Trans.*, 2015, **44**, 182–192.

[7] X. Zhou, X. Zhao, Y. Wang, B. Wu, J. Shen, L. Li and Q. Li, *Inorg. Chem.*, 2014, **53**, 12275–12282.

[8] J. Feng and H. Zhang, *Chem. Soc. Rev.*, 2013, **42**, 387–410.

[9] G. Han, Y. Deng, J. Sun, J. Ling and Z. Shen, *Exp Ther Med.*, 2015, **9**, 1561–1566.

[10] C. Yang, J. Xu, Y. Zhang, Y. Li, J. Zheng, L. Liang and M. Lu, *J. Mater. Chem. C*, 2013, **1**, 4885–4901.

[11] J. C. G. Bunzli, *Chem. Rev.*, 2010, **110**, 2729–2755; K. S. Kumar, B. Schafer, S. Lebedkin, L. Karmazin, M. M. Kappes and M. Ruben, *Dalton Trans.*, 2015, **44**, 182–192.

[12] Y. Liu, Y. Wang, H. Guo, M. Zhu, C. Li, J. Peng, W. Zhu and Y. Cao, *J. Phys. Chem. C*, 2011, **115**, 4209–4216.

[13] Y. Liu, J. Wang, Y. Wang, Z. Zhang, M. Zhu, G. Lei, W. Zhu, *Dyes and Pigments*, 2012, **95**, 322–329.

[14] Y. Liu, Y. Wang, J. He, Q. Mei, K. Chen, J. Cui, C. Li, M. Zhu, J. Peng, W. Zhu and Yong Cao, *Organic Electronics*, 2012, **13**, 1038–1043.

[15] G. Shao, H. Yu, N. Zhang, Y. He, K. Feng, X. Yang, R. Cao and M. Gong, *Phys. Chem. Chem. Phys*., 2014, **16**, 695–702.

[16] C. P. M. Montgomery, S. Benjamin, J. N. Elizabeth, R. Pal and D. Parker, *Acc. Chem. Res.*, 2009, 925–937.

[17] E. J. New, D. Parker, D. G. Smith and J. W. Walton, *Curr. Opin. Chem. Biol.*, 2010, **14**, 238–246.

[18] J. Hammell, L. Buttarazzi, C. H. Huang and J. R. Morrow, *Inorg. Chem.*, 2011, **50,** 4857–4867.

[19] S. I. Weissman, *J. Chem. Phys.*, 1942, **10**, 214–217.

[20] C. Yang, L. M. Fu, Y. Wang, J. P. Zhang, W. T. Wong, X. C. Ai, Y. F. Qiao, B. S. Zou and L. L. Gui, *Angew. Chem. Int. Ed.*, 2004, **43**, 5010–5013.

[21] Y. M. Luo, Z. Chen, R. R. Tang, L. X. Xiao, H. J. Peng, *Spectrochimica Acta Part A: Molecular and Biomolecular Spectroscopy*, 2008, **69**, 513–516.

[22] M. Latva, H. Takalo, V. M. Mukkala, C. Matachescu, J. C. Rodriguez-Ubis and J. Kankare, *J. Lumin.* 1997, **75**, 149–169.

[23] S. V. Eliseeva and J. C. G. Bunzli, *Chem. Soc. Rev.*, 2010, **39**, 189–227.

[24] C. Freund, W. Porzio, U. Giovanella, F. Vignali, M. Pasini and S. Destri, *Inorg. Chem*., 2011, **50**, 5417–5429.

[25] T. Pagnot, P. Audebert and G. Tribillon, *Chem. Phys. Lett.*, 2000, **322**, 572–578.
[26] B. Rajamouli, P. Sood, S. Giri, V. Krishnan and V. Sivakumar, *Eur. J. Inorg. Chem.* 2016, 3900–3911.
[27] M. R. Anoop, P. S. Binil, S. Suma and M. R. Sudarsanakumar, *J. rare earths*, 2012, **30**, 709–715.
[28] S. Dehn, K. W. K. Tong, R. G. C. Clady, D. M. Owen, K. Gaus, T. W. Schmidt, F. Braet and P. Thordarson, *New J. Chem.*, 2011, **35**, 1466–1471; S. Li, G. Zhong, W. Zhu, F. Li, J. Pan, W. Huang and H. Tian, *J. Mater. Chem.*, 2005, **15**, 3221-3228.
[29] S. Raphael, M. L. P. Reddy, K. V. Vasudevan and A. H. Cowley, *Dalton Trans.*, 2012, **41**, 14671; D. Q. Y. Feng, H. Wang, X. Bao, Y. Guo, Y. Cheng and L. Wang, *Inorg. Chem. Commun.*, 2010, **13**, 613–617.
[30] S. Biju, R. O. Freire, Y. K. Eom, R. Scopelliti, J. C. G. Bunzli, and H. K. Kim., *Inorg. Chem.*, 2014, **53**, 8407−8417.
[31] Z. Assefa, G. S. Me, H. H. Patterson and R. Reynolds., *Inorg. Chem.*, 1994, **33**, 2187–2195.
[32] H. Xu, H. L. Wang, X. H. Zhu, K. Yin, G. Y. Zhong, X. Y. Hou and W. Huang, *J. Phys. Chem. B*, 2006, **110**, 3023–3029.
[33] X. Zhou, Y. Guo, Z. Shi, X. Song, X. Tang, X. Hu, Z. Zhu, P. Li and W. Liu, *Dalton Trans.*, 2012, **41**, 1765–1775.
[34] T. Zhu, P. Chen, H. Li, W. Sun, T. Gao and P. Yan, *Phys. Chem. Chem. Phys.*, 2015, **17**, 16136–16144.
[35] G. R. Choppin and D. R. Peterman, *Coord. Chem. Rev.*, 1998, **174**, 283−299.
[36] E. G. Moore, A. P. S. Samuel and K. N. Raymond, *Acc. Chem. Res.*, 2009, **42**, 542−552.
[37] (a) F. Wei and G. X. Yu, *J. Lumin.*, 2013, **134**, 710–717; (b) D. M. de Leeuw, M. M. J. Simenon, A. R. Brown, R. E. F. Einerhand, *Synth. Met.*, 1997, **87**, 53–59.
[38] Triloki, R. Rai, and B. K. Singh, *Proceedings of the DAE Symp. on Nucl. Phys.* 2013, 58.
[39] W. B. Salih, *J. of university of anbar for pure science*, 2010, 4.
[40] J. H. Nahida, *International Journal of Basic and Applied Sciences* (IJBAS-IJENS), 2012, **12**, 58.
[41] B. Rajamouli and V. Sivakumar, *New J. Chem.*, 2017, **41**, 1017-1027.
[42] X. F. Zhang, C. J. Xu and J. Wan, *Monatsh Chem*, 2014, **145**, 1913–1917.
[43] H. Jang, C. H. Shin, B. J. Jung, D. Kim, H. K. Shim and Y. Do, *Eur. J. Inorg. Chem.*, 2006, 718–725.
[44] T. Cardinaels, K. Driesen, T. N. Parac-Vogt, B. Heinrich, C. Bourgogne, D. Guillon, B. Donnio and K. Binnemans, *Chem. Mater.*, 2005, **17**, 6589-6598.
[45] A. P. Bassett, S. W. Magennis, P. B. Glover, D. J. Lewis, N. Spencer, S. Parsons, R. M. Williams, L. De Cola and L. Pikramenou, *J. Am. Chem. Soc.*, 2004, **126**, 9413–9424.
[46] M. Irfanullah and K. Iftikhar, *Inorg. Chem. Commun.*, 2009, **12**, 296–299.
[47] C.-L. Yang, J.-X. Luo, J.-Y. Ma, L.-Y. Liang and M.-G. Lu, *Inorg. Chem. Commun.*, 2011, **14**, 61–63.
[48] C.-L. Yang, J.-X. Luo, J.-Y. Ma, M.-G. Lu, L.-Y. Liang and B.-H. Tong, *Dyes Pigm.*, 2012, **92**, 696–704.
[49] C. Yang, J. X. Jianying Ma, D. Zhu, Y. Zhang, L. Liang and M. Lu, *Photochem. Photobiol. Sci.*, 2013, **12**, 330.
[50] H. Xu, Q. Sun, Z. An, Y. Wei and X. Liu, *Coord. Chem. Rev.*, 2015**, 293–294**, 228–249.

[51] S. Dehn, K. W. K. Tong, R. G. C. Clady, D. M. Owen, K. Gaus, T. W. Schmidt, F. Braet and P. Thordarson, *New J. Chem.*, 2011, **35**, 1466–1471.
[52] S. Li, G. Zhong, W. Zhu, F. Li, J. Pan, W. Huang and H. Tian, *J. Mater. Chem.*, 2005, **15**, 3221-3228.
[53] K. Singh and S. Vaidyanathan, *RSC Advances*, 2016, **6**, 98652–98662.
[54] C. B. Murphy, Y. Zhang, T. Troxler, V. Ferry, J. J. Martin and W. E. Jones, *J. Phys. Chem. B*, 2004, **108**, 1537–1543.
[55] D. L. Dexter, *J. Chem. Phys.*, 1953, **21**, 836–850.
[56] E. Nakazawa, in *Phosphor Handbook*, ed. S. Shionoya, W. M. Yen and H. Yamamoto, CRC Press, Boca Raton, 2007, 2nd edn.
[57] A. R. Ramya, M. L. P. Reddy, A. H. Cowley and K. V. Vasudevan, *Inorg. Chem*. 2010, **49**, 2407–2415.
[58] E. G. Moore, A. P. S. Samuel and K. N. Raymond, *Acc. Chem. Res.*, 2009, **42**, 542.
[59] K. Binnemans, *Coord. Chem. Rev.*, 2015, **295**, 1–45.
[60] F. J. Steemers, W. Verboom, D. N. Reinhoudt, E. B. V. Tol and J. W. Verhoeven, *J. Am. Chem. Soc.* 1995, **117**, 9408–9414.
[61] B. Rajamouli, C. S. D. Viswanath, S. Giri, C. K. Jayasankar and V. Sivakumar, *New J. Chem.*, 2017, **41**, 3112–3123.
[62] S. J. L. Ribeiro, R. E. O. Diniz, Y. Messaddeq, L. A. Nunes and M. A. Aegerter, *Chem. Phys. Lett.* 1994, **220**, 214.
[63] J.-C. G. Bunzli, A. –S. Chauvin, H. K. Kim, E. Deiters and S. V. Eliseeva, *Coord. Chem. Rev.*, 2010, **254**, 2623–2633.
[64] W. T. Carnall, In *Handbook on the Physics and Chemistry of Rare Earths*, Eds. K. A. Gschneidner and L. Eyring, North-Holland Publishing Co., Amsterdam, 1979, **3**, 171–208.
[65] A. Aebischer, F. Gumy and J.-C. G Bunzli, *Phys. Chem. Chem. Phys.*, 2009, **11**, 1346–1353.
[66] C. G. Walrand and K. Binnemans, In *Handbook on the Physics and Chemistry of Rare Earths*, Eds. K. A. Gschneidner and L. Eyring, Elsevier Science: Amsterdam, 1998, **25**, 101–264.
[67] C. Reinhard and H. U. Gudel, *Inorg. Chem.*, 2002, **41**, 1048–1055.
[68] H. Li and Y. Wang, K. Yuan, Y. Tao, R. Chen, C. Zheng, X. Zhou, J. Li and W. Huang, *Chem. Commun*., 2014, **50**, 15760.
[69] M. M Nolasco, P. D. Vaz and L. D. Carlos, *New J. Chem*., 2011, **35**, 2435.
[70] S. Yoo, X. C. Zeng and S. S. Xantheas, *J. Chem. Phys.*, 2009, **130**, 221102(1-4).
[71] B. Komjati, A. Urai, S. Hosztafi, J. Kokosi, B. Kovats, J. Nagy and P. Horvath, *Spectrochimica Acta Part A: Molecular and Biomolecular Spectroscopy*, 2016, **155**, 95–102.

Chapter 7

Designing of ancillary ligands / organic chromophores and study their excited photophysical properties for Eu^{III} complexes – a theortical approach

Abstract

A series of organic chromophores or ancillary ligands (based on phenanthroimidazole) conjugated with triphenylamine or carbazole moieties were designed with and without spacer and studied their excited state photophysical properties by density functional theory and time-dependent density functional theory. The UV absorption analysis shown maxima around λ_{max} 288, which is belongs to the π-π^* transition of the ligands. The excited state photophysical properties reveal that the location of the triplet level found among three (1a-f, 2a-f, 3a-f) series 3a-f shown better energy matching with the excited state ($^5D_0$) of Eu^{III} ion and could facilitate the energy transfer from ligand to Eu ion very efficient. In addition, the substituted phenyl moiety (mCF_3 and pCF_3) at N1-position in the phenanthro-imidazole ligand give additional benefits by reducing the triplet energy comparatively with other substitution that leads to efficient energy transfer from L to Eu ion in the complex could be expected. In addition, HOMO and LUMO calculations given lead that some of the designed ligands can also serve as host materials for triplet dopant in OLEDs. The systematic theoretical study is certainly leads to synthesis of best ligand molecules for Eu complexes.

Key words: Ancillary ligand; organic chromophore; DFT; TD-DFT; energy transfer; Eu-complex; OLEDs

7.1 Introduction:

Lanthanide based coordination complexes have gained much attention (both academia and industry) due to their unique spectral features (the shapes of the emission spectra are very sharp, the emission wavelengths are independent of the ligand environment, and only the emission intensities are sensitive to the surroundings) and emerging technological applications [1]. Open-shell 4f electrons of Ln^{3+} are shielded from the environment by the closed-shell 5s and 5p electrons. Thus, the excitation energies of $4f^n$ excited states are independent of the chemical surroundings. Since, the 4f-4f electronic transition is forbidden in nature, in order to gain high intense emission, the excited energy levels of lanthanides need to be populated by means of sensitization (antenna effect) [2]. In order to gain efficient emission from the lanthanides (due to low absorption strength/coefficients of lanthanide ions), one need to consider the excitation level population; however the lanthanide electronic transitions are forbidden one. Hence, indirect population of the excited state is highly necessary to gain better quantum yield. In organo-lanthenide complexes, in coordinated organic chromophore groups are getting excited and transfer their excited energy to the higher level of lanthanide ions (from ligand/ chromophore triplet level to lanthanide excited level, well accepted energy transfer mechanism).

According to Lava *et al.,* [3] the chromophore triplet energy level should be higher than that of the lanthanide excited levels to facilitate efficient energy transfer. For example, in the case of Eu complex the $^5D_0$ level is located at 17,500 cm^{-1} and the ligand should have above 20,000 cm^{-1} (triplet state) and above 25,000 cm^{-1} (singlet state) to gain efficient red emission [4, 5]. Thus, the location of triplet levels plays vital role to achieve the red emission or mixing of chromophore emission (blueish- green with red) to get white emission from the Ln-complex. Triplet energies of the well-known ligands are 2-Thenoyltrifluoroacetone (tta, 18,800 cm^{-1}), hexafluoroacetylacetonate (hfa, 22,000 cm^{-1}), benzoyltrifluoroacetylacetonate (bfa, 21,400 cm^{-1}), dibenzoylmethane (dbm, 20,600 cm^{-1}), 1,10-phenanthroline (phen, 21,480 cm^{-1}) and tetra azatriphenylene (aza, 23,800 cm-1) [6-10].

Ln^{III} coordination complexes are widely used in OLEDs, optoelectronics bioprobes in medicine and biology [11-14]. The developments of Ln complexes as efficient emitters become an important role in coordination chemistry. In this context, the theoretical strategy has proven to be successful in the design of efficient luminescent lanthanide complexes for different applications like OLED, light conversion molecular devices (LCMDs) [15, 16]. Last two decades, organometallic complexes based on Ir, Ru, Os and Re etc., was gained much attention due to their capability of harvesting the triplet exciton to the ground state by heavy metal ion effect [17]. The pursuit to design stable triplet harvesters based on luminescent organo-lanthanide complexes with conjugated organic ligands (chromophores) continues to stimulate ever increasing technological applications (smart displays, OLEDs). Although many lanthanide emitters have been developed for green and blue emitting OLEDs [18, 19], the molecular design for efficient red emitters is not very clear and a systematic plan for rational molecular design is highly desirable. Among all lanthanides, Eu^{3+} based organo-lanthanide complex is known to emit in the red spectral region, due to electric dipole transition. The ED transition is highly hypersensitive in nature and it is strongly structural dependent (used as a structural probe) [20]. In particular, to achieve inexpensive OLEDs for commercial applications, there is an urgent need for highly efficient red emitting materials to overcome the weakness of the currently existing red emitting Eu^{III} complexes.

Therefore, it is important to understand the mechanisms of energy transfer upon photoexcitation of these complexes to find the best ligand−lanthanide pairs to improve the efficiency and sensitivity of luminescence behavior. In energy transfer mechanism of lanthanide complexes, ligand plays a vital role for the selection of ligand to synthesize lanthanide complex. Because the triplet level of the ligand should match with the Ln excited state, otherwise there is no energy transfer from the ligand to Ln, and finally there is no efficient emission from the Ln ions. The mechanism of energy transfer (probable luminescence mechanism) from the ligand triplet state to the $^5L_6$ and $^5D_1$ excited state of Eu^{III} ion shown in Figure 7.1 (Jablonski diagram). The W_{ET} and W_{BT} symbols represent the energy transfer and back-transfer rates. The Φ and k symbols represent the non-radiative decay rates. Typical values of the remaining transfer rates were assumed to be identical to those found for coordination compounds, namely, $\Phi = 10^4$, $\Phi^{(1)} = 10^6$, $\Phi^{(2)} = 10^8$, and $\Phi^{(3)} = 10^5$ s^{-1} [21]. Thus, the Ln^{3+} emission is directed by the virtual position of the triplet (^1T) and singlet (^1S) excited states of the coordinated ligands and the resonant levels of the lanthanide ion.

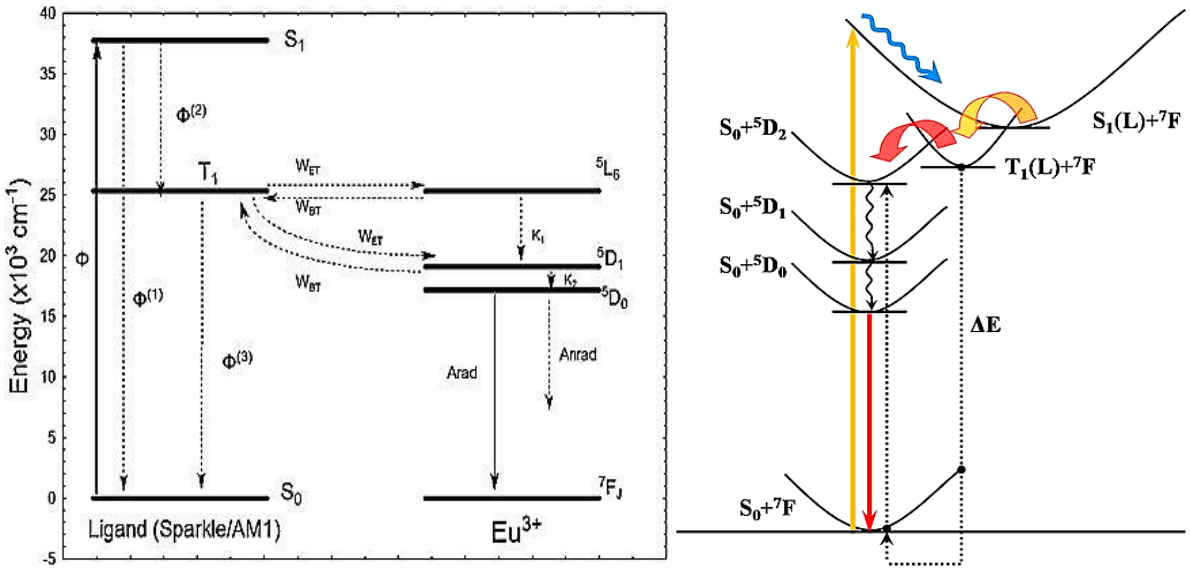

Figure 7.1 Schematic representation of the energy transfer mechanism [22] and configurational coordinate diagram and the energy transfer process in Eu complex [23].

In early sixties (1960), a number of experimental studies have been performed on the absorption and emission spectra of europium complexes by DeShazer and Diecke [24] and Carnall [25, 26] and the energy levels of trivalent europium ion from these early experiments have been assigned to $^{2S+1}L_J$ multiplets by Wybourne [27], Ofelt [28] and Judd [29] to mention only some well known authors [30]. $Eu(TTA)_3.2H_2O$ and $Eu(DBM)_3.2H_2O$ is well studied as red emitting complexes, however, the replacement of coordinated water molecule in the coordination sphere is necessary to enhance the PLQY and reduce the vibrational deactivation of excited energy by O-H stretching in the coordinated environment. There are several class of ancillary ligands synthesized to saturate the coordination sphere of the Eu-complex as well as enhance the overall PLQY. The classes of ligands are such as benzimadazole, bipyridine, phenanthroimidazole, phosphor-ligand [24–30]. The ancillary ligand function is two fold: one it can enhance the overall red emission of Eu^{III} ion by energy harvesting and second one it can be easily functionalized for specific applications, for example, to increase the solubility of the

complexes by functionalization of polar groups and electron rich moiety functionalization leading to enhancement in the charge (hole and electron) transporting properties and increase the overall performance of the device.

7.2 Design and photo physical study of ancillary ligands by theoretical approach:

7.2.1 Objective of the present study:

In the previous chapters, a series of phenanthro-imidazole based ancillary ligands were designed and synthesized for $Eu(TTA)_3$ complexes and explored their application in lighting devices as well as temperature sensing by understanding their photophysical properties. In the present study, several ancillary ligands were designed and studied their excited state photophysical properties by computational methods (DFT and TD-DFT). The design strategy of the ancillary ligand is:

The electron deficient phenanthro-imidazole group functionalized with electron rich (triphenylamine and carbazole) molecule and different N1-functinoalization with spacer and without spacer. Further, the highest occupied molecular orbital (HOMO)/lowest unoccupied molecular orbitals (LUMO), optimized geometries, frontiers orbitals, optical properties (UV-Vis spectrum in gas and solvent) for the designed ancillary ligands were also been systematically investigated. More specifically, the ideal simple molecular design of ancillary ligands for Eu^{III} complexes consisting of a 1,10-phenanthroline-imidazole as core and different electron accepting units (m-CF_3, p-CF_3) and donating units like (CH_3, O-CH_3, fluorene, triphenylamine and carbazole). Based on these functional group/moieties, a three series of ligands (Figure 7.2, 7.3 and 7.4) were designed and theoretically investigated all the ligands, and compared the energy levels of ligand with Eu^{III} metal ion for understanding the ET and further investigation.

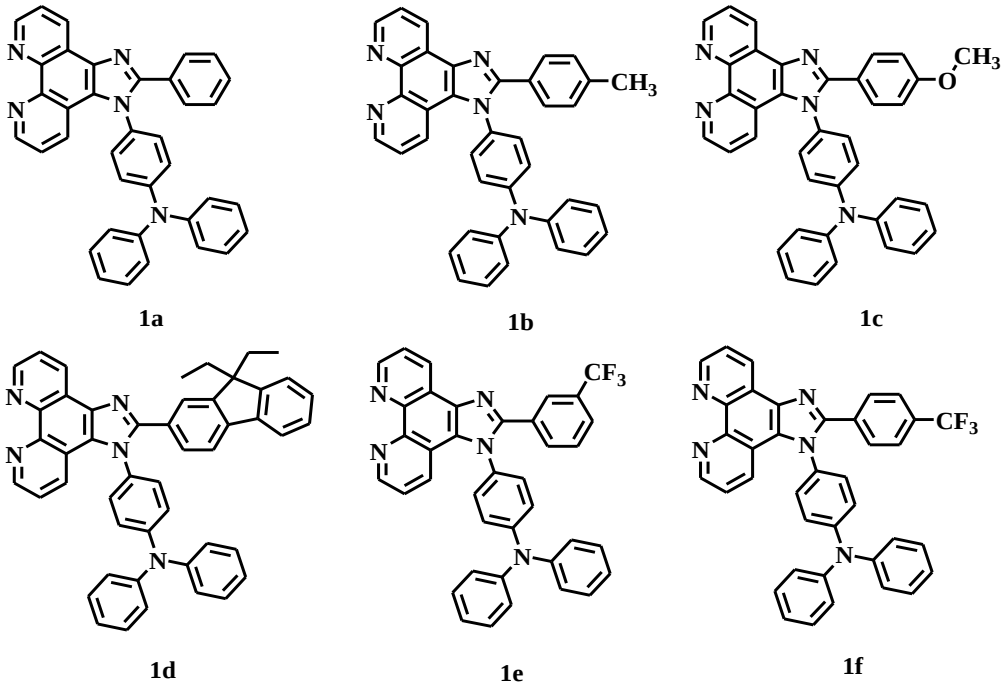

Figure 7.2 The chemical structure of phenanthro-imadzole without spacer.

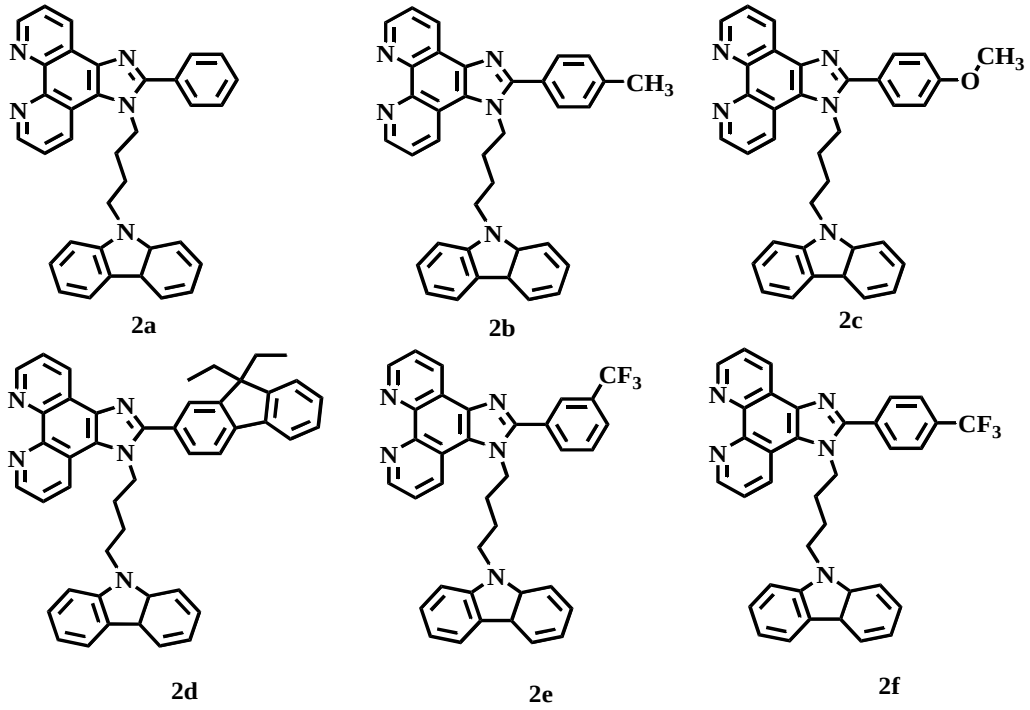

Figure 7.3 The chemical structure of phenanthro-imadzole with spacer.

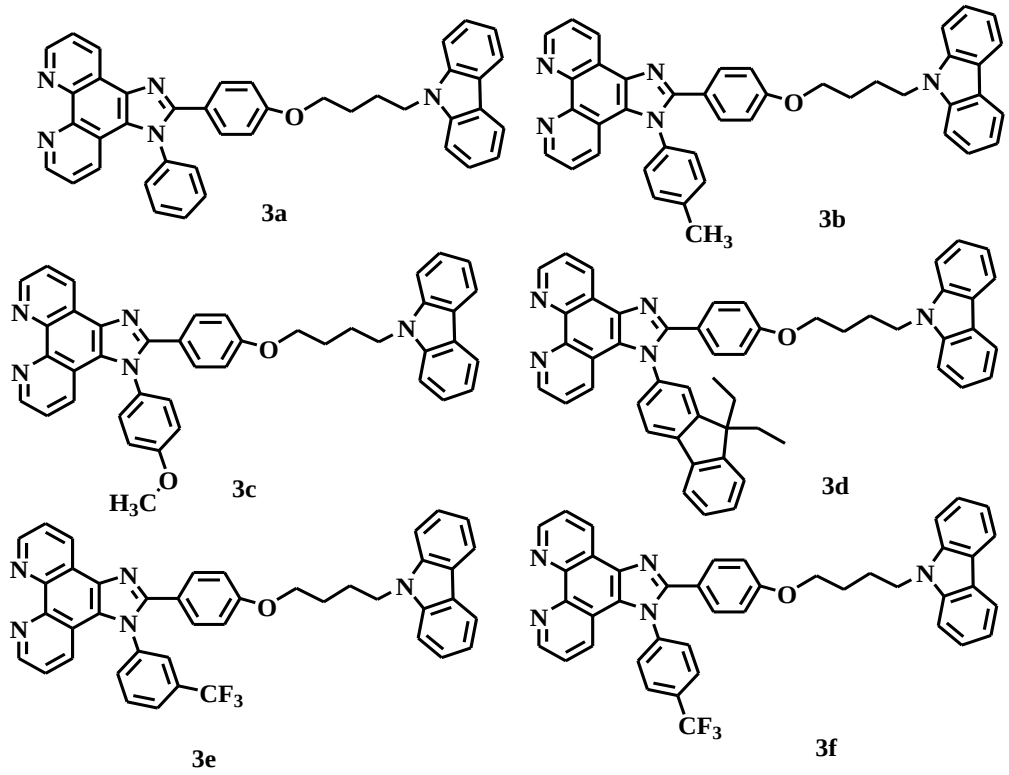

Figure 7.4 The chemical structure of phenanthro-imadzole without spacer.

7.2.2 Computational details:

Theoretical calculations were carried out using the density functional theory (DFT) method with the Gaussian 09 package [31]. Geometry optimizations were performed in gas phase and without symmetry constraints by using B3LYP hybrid functional, which combines Becke's three-parameter functional (B3) [32] with the Lee–Yang–Parr (LYP) correlation functional [33], in combination with Pople basis sets (6-311+G*) [34]. The minimum energies of the optimized structures were checked by frequency analysis at the same level of theory. On the basis of the optimized structures of the ground and excited states, the absorption and emission properties in dichloromethane (CH_2Cl_2) and gas medium were calculated by TDDFT [35, 36] and associated with the polarized continuum model (PCM) [37]. Taking into consideration that the geometry of the molecule might change in solvent phase the optimization of the geometries under solvent phase was also carried out. No prominent change in the geometries of the molecule was observed. All the calculations were carried out using Gaussian09 W and Gaussian view suite of programs.

7.2.3 Optimized structures:

All the designed ancillary ligand structures were optimized and the geometries are depicted in Figure 7.5, 7.6 and 7.7.

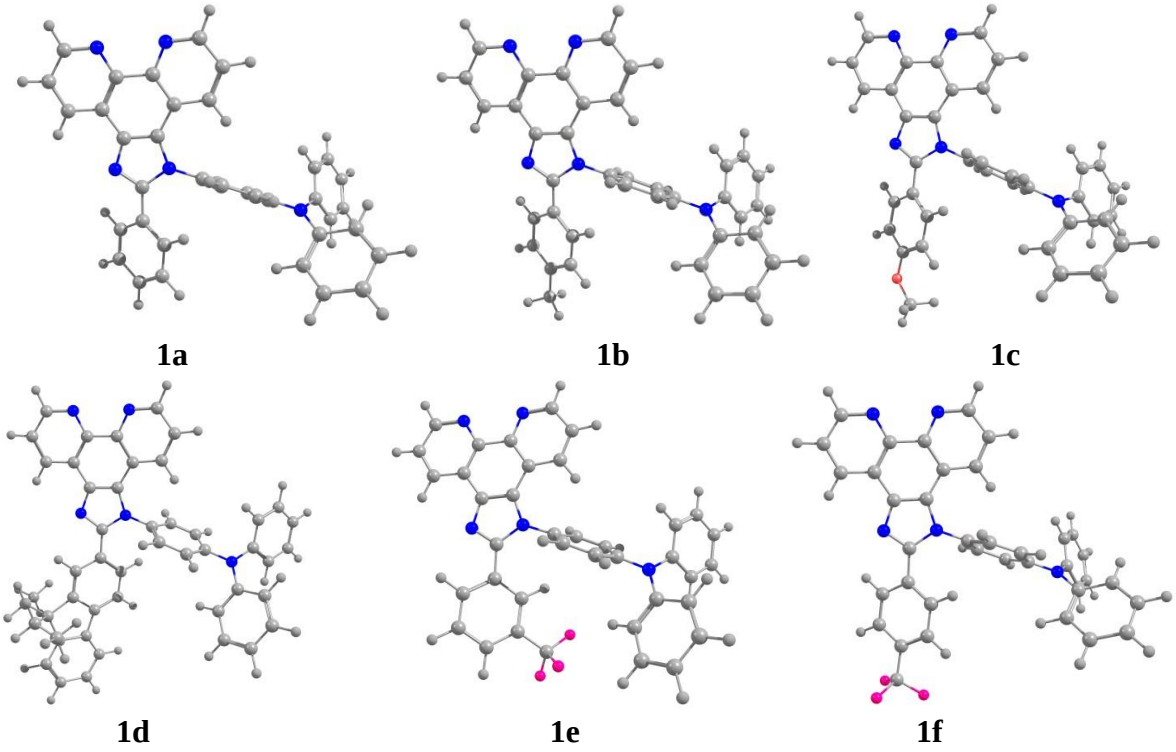

Figure 7.5 Optimized structures of ancillary ligands (1a-1f)

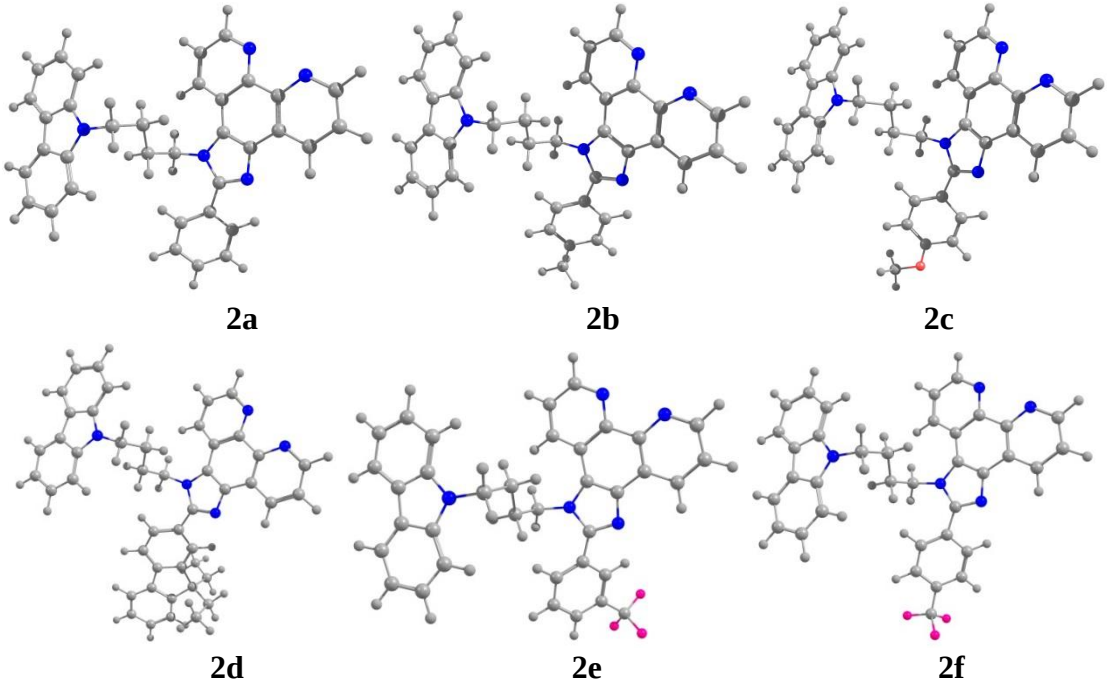

Figure 7.6 Optimized structures of ancillary ligands (2a-2f).

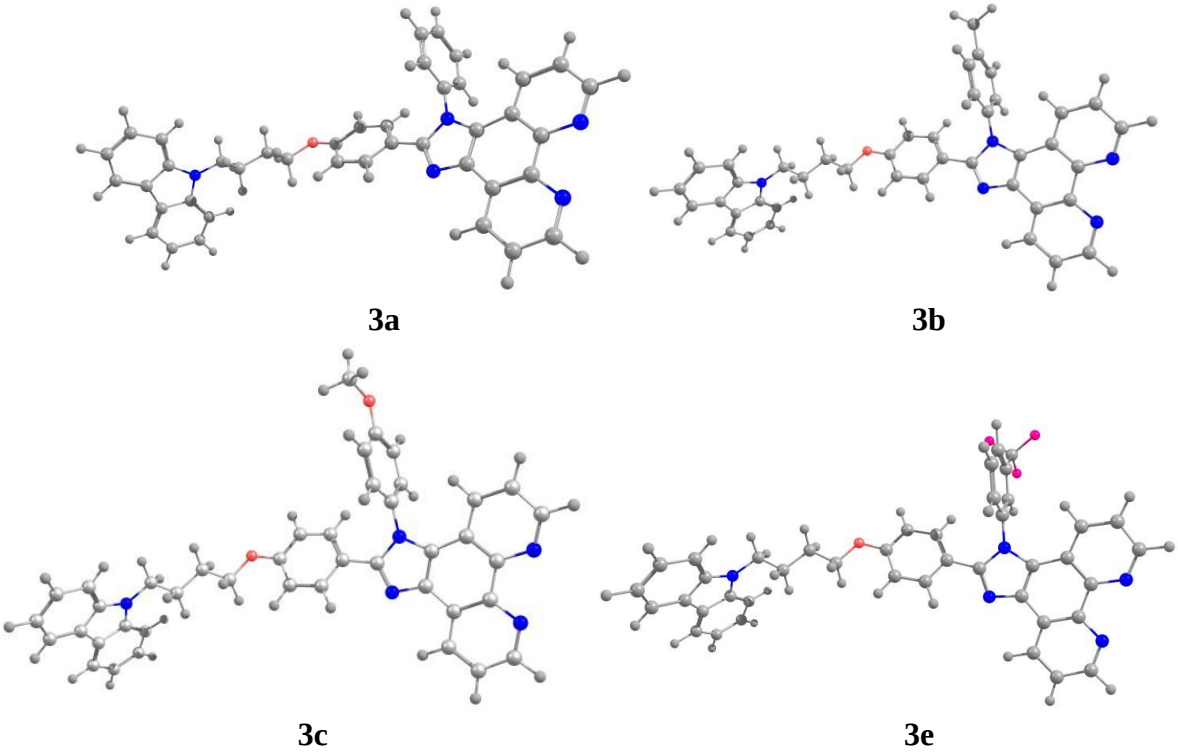

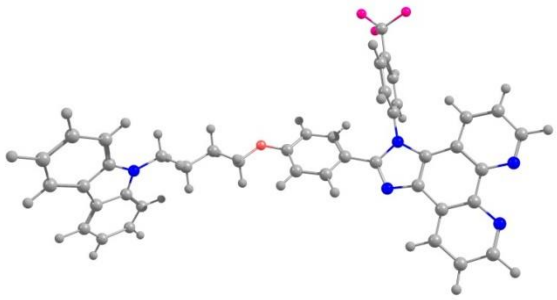

3f

Figure 7.7 Optimized structures of ancillary ligands (3a-3f).

7.2.4 Results and discussion:

7.2.4.1 Understanding of frontier molecular orbitals of ancillary ligands:

To demonstrate the photophysical properties of the designed ancillary ligands, the frontier molecular orbital energies, as well as the contour plots of HOMO and LUMO of investigated ancillary ligands were plotted in Figure 7.8 - 7.10. The calculated energy levels and components of frontier molecular orbitals (FMOs) are collected and tabulated in Table 7.1-7.3. The HOMO of 1a-1f is mainly located in 1,10-phenantroline imidazole moiety (Figure 7.8 and Table 7.1), with a small contribution from the phenyl ring and very tiny contribution from the central nitrogen atom in triphenylamine group were observed. Nevertheless, in the case of 1a molecule the HOMO contribution from the triphenylamine moiety is more as compare with the phenyl ring in the ligand structure. The LUMOs are mainly distributed in the electron-accepting 1, 10-phenonatroline moiety, also with a small contribution from the phenyl group in 1a and 1b molecule. In case of 1c-1f, tiny contribution in phenyl ring of the triphenylamine moiety was observed. Thus, the change in substitution of molecules with different groups there is a considerable effect was observed in LUMO compare to that of HOMO (almost no change). The complete spatial separation of HOMOs and LUMOs in p-type and n-type units for all these molecules implies their bipolar charge transporting features. These molecules reveal great difference in molecular geometries, which should be responsible for their different physical properties such as the triplet energy and amorphous stability.

The calculated HOMO and LUMO energies, HOMO–LUMO energy gaps, of the 1a-1f molecules were shown in Table 7.4. The substituents to the phenanthro-imidazole core with donating and accepting units destabilizes HOMO energy levels and stabilizes the LUMO energy levels of the parent molecule (1a), as shown in Figure 7.8. The HOMO destabilizations and LUMO stabilizations were calculated to be almost with 0.02–0.16 eV and 0.04–0.34 eV variation, respectively. The HOMO and LUMO energy levels of all molecules lie at −5.24 to −5.40 and −1.10/−1.53 eV respectively. The calculated energy gaps in the range of 3.88 to 4.21 eV. HOMO of 1a-1F compound, the HOMO increment was observed in the following order: 1f < 1a < 1e < 1b < 1d < 1c. The HOMOs for most of the 1b-1e (except 1f) are slightly higher (0.05–0.16 eV) than that of 1a, indicating that the hole transporting and injection abilities can be improved by the introduction of substituents (electron donating and withdrawing groups). For ligand (1f), the HOMO is decreased compare with 1a by 0.12 eV, this can be ascribed, the different conjugated interaction between the CF_3 and the core molecule. The LUMOs of 1d-1f gradually decrease as follows: 1a >1d >1e > 1f. but in the case of 1b and 1c LUMO increases

slightly, suggesting that the LUMOs of 1b and 1c were determined predominately by the introduction of bridging heteroatoms of C and O, can generally enhance the electron-transport and injection abilities of the material with the decreased LUMO.

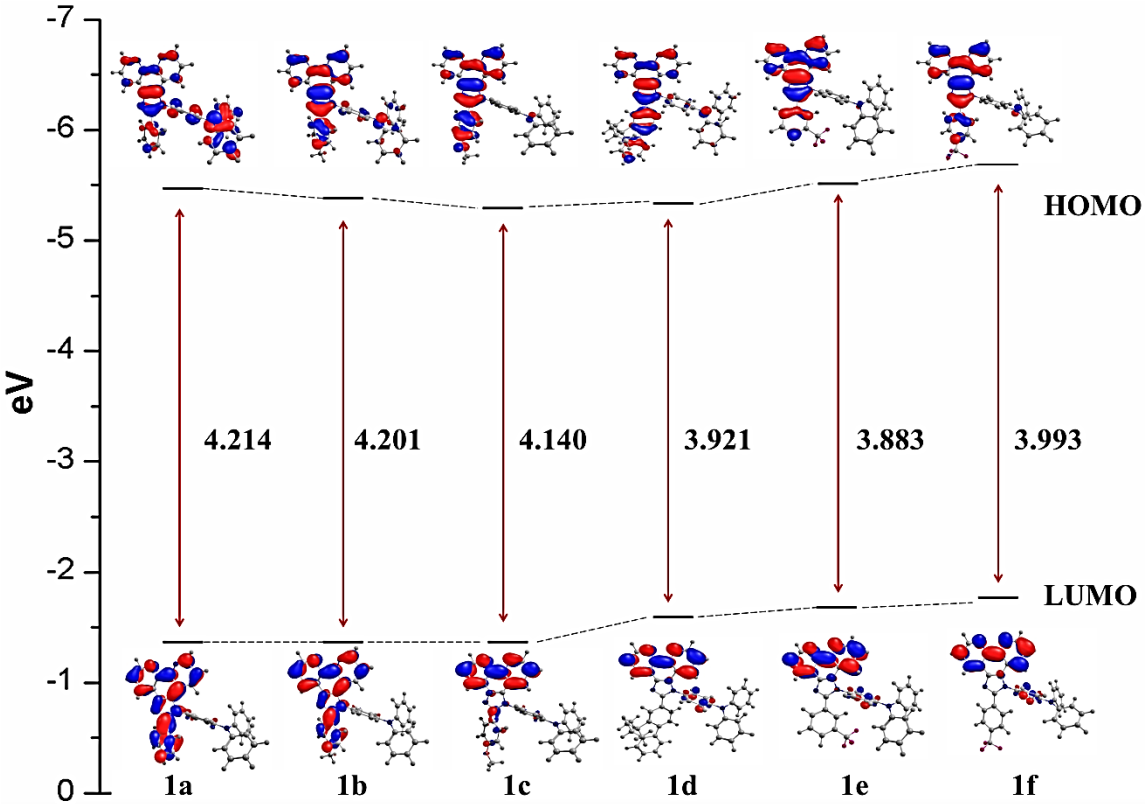

Figure 7.8 Energy level diagram of ancillary ligands (1a-1f).

Table 7.4 Computed orbital energies and band gaps of the ancillary 1a-1f ligands.

Compound	HOMO (eV)	LUMO (eV)	HOMO-1 (eV)	LUMO+1 (eV)	Band gap (eV)
1a	-5.4066	-1.1921	-5.4752	-1.1292	4.214
1b	-5.3527	-1.1513	-5.4428	-1.1012	4.201
1c	-5.2412	-1.1012	-5.4439	-1.1062	4.140
1d	-5.2951	-1.3733	-5.4266	-1.1341	3.921
1e	-5.3840	-1.5001	-5.6390	-1.2517	3.883
1f	-5.5320	-1.5388	-5.6496	-1.2577	3.993

Table 7.2 reveals that, HOMO of the compounds are mainly located on electron donating carbazole molecule and the LUMO is located mainly on 1, 10 phenantroline moiety. As the substitution of different groups on the molecules leads to small change in the LUMO level but no change was observed in HOMO. In the case of 2a, 2b, 2e and 2f the LUMO located on both 1,10 phenantholine imidazole and phenyl ring, but in case of 2c, 2d, it is only located on 1,10 phennathroline moiety. In 2a-2f series the calculated HOMO and LUMO energies, HOMO–LUMO energy gaps, of 1a-1f molecules were shown in Table 7.5. The substituent to the core with donating and accepting units destabilizes HOMO energy levels and stabilizes the LUMO energy levels as compared to that of parent molecule (2a), (Figure 7.9). The HOMO

destabilizations and LUMO stabilizations were calculated to be almost with 0.01–0.09 eV and 0.04–0.34 eV variation, respectively. The HOMO and LUMO energy levels of all molecules lie at −5.43 to −5.60 and −1.10/−1.53 eV respectively, and the obtained energy gaps in the range of 3.91 to 4.21 eV. In second series (2a-2f), HOMOs gradually increase in the following order: 1e < 1f < 1c < 1b < 1f < 1c, The HOMO's for most of the 2b, 2c and 2d are slightly higher (0.01-0.09 eV) than that of 2a. Indicating that the hole transport and injection abilities have been improved by the introduction of substituents (electron donating groups). For 2e and 2f of the HOMO is decreased compare with 2a by 0.06, 0.07 eV, this can be ascribed to the different conjugated interaction between the CF3 and the core molecule. The LUMOs of 2b-2d gradually decreases and the trend is as follows: 2f >2e >2d > 2a. But in the case of 2b and 2c LUMO slightly increases, suggesting that the LUMOs of 2b and 2c were determined predominately by the introduction of bridging heteroatoms of C and O, can generally enhance the electron-transport and injection abilities of the material with the decreased LUMO.

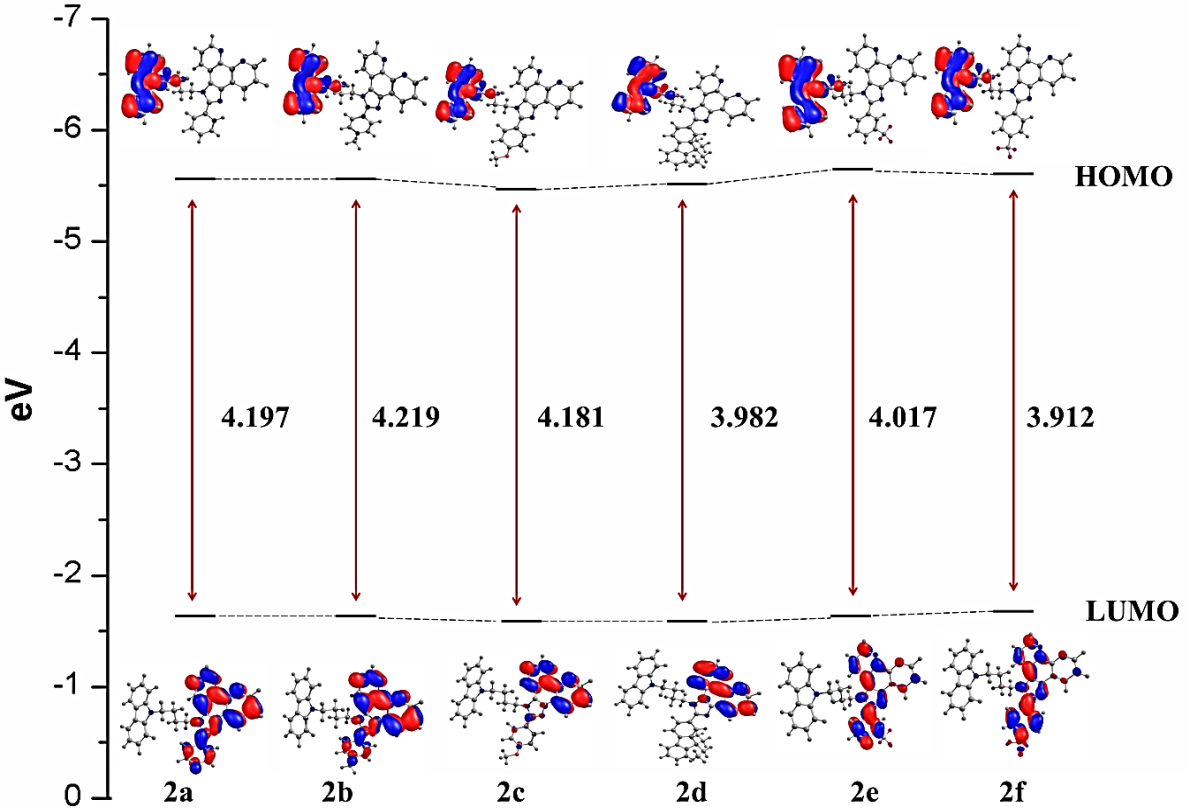

Figure 7.9 Energy level diagram of ancillary ligands (2a-2f).

Table 7.5 Computed orbital energies and band gaps of the ancillary 2a-2f ligands.

Compound	HOMO (eV)	LUMO (eV)	HOMO-1 (eV)	LUMO+1 (eV)	Band gap (eV)
2a	-5.5359	-1.3388	-5.6311	-1.2683	4.197
2b	-5.5209	-1.3015	-5.5596	-1.2340	4.219
2c	-5.4387	-1.2574	-5.5383	-1.1793	4.181
2d	-5.4673	-1.4846	-5.5163	-1.2737	3.982
2e	-5.6066	-1.5894	-5.8064	-1.3973	4.017
2f	-5.5966	-1.6843	-5.8357	-1.4245	3.912

In 3a-3f series, the HOMO – LUMO energy levels, band gap values are tabulated in Table 7.3 and 7.6. Ligand 3d synthesis and the theoretical study was executed and discussed in Chapter-6. Figure 7.3 reveals that, the HOMO is mainly located on electron donating carbazole moiety and the LUMO is located in different position depending on the functional groups. In the case of 3a, 3b, 3c LUMO contribution mainly on 1,10 phenantroline groups and tiny contribution on the imidazole moiety was observed. In case of 3e and 3f, the LUMO contribution mainly on electron deficient CF_3 substituted phenyl ring.

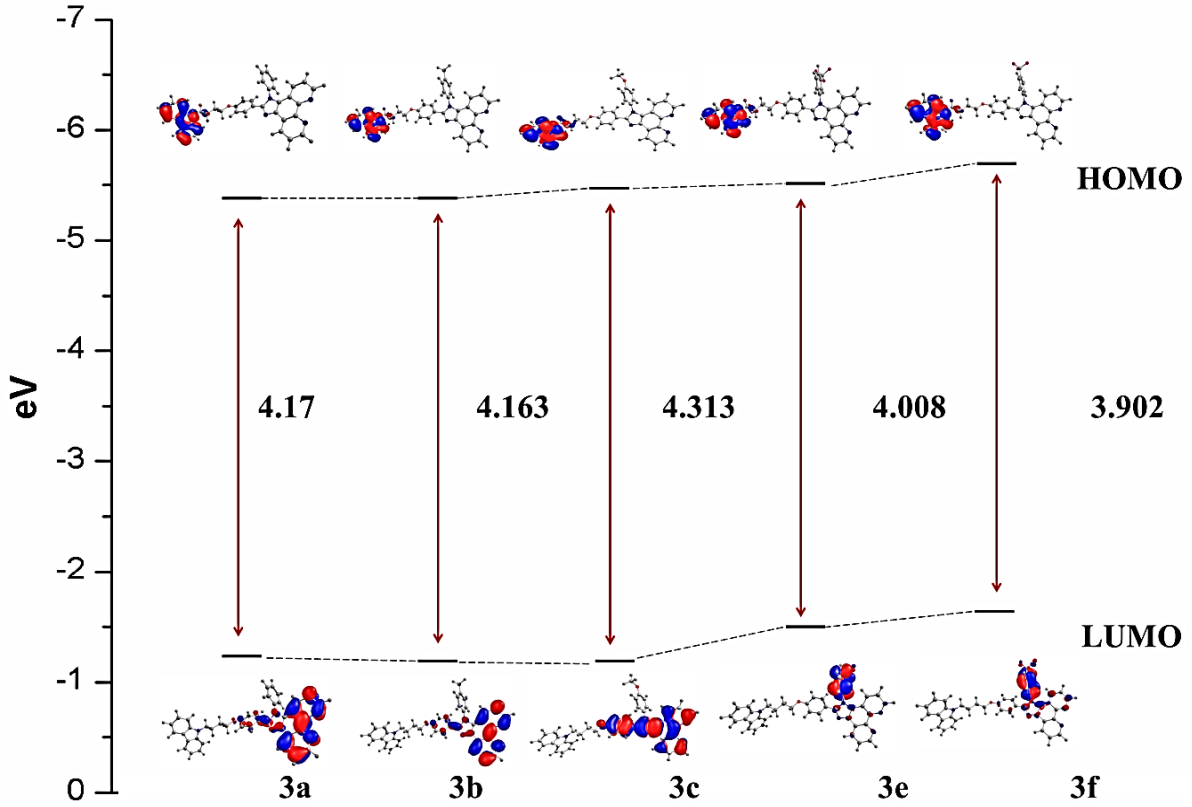

Figure 7.10 Energy level diagram of ancillary ligands (3a-3f).

Table 7.6 Computed orbital energies and band gaps of the ancillary ligands 3a-3f.

Compound	HOMO (eV)	LUMO (eV)	HOMO-1 (eV)	LUMO+1 (eV)	Band gap (eV)
3a	-5.3438	-1.1722	-5.4376	-1.1442	4.171
3b	-5.3095	-1.1458	-5.4333	-1.1001	4.163
3c	-5.4594	-1.1451	-5.4741	-1.3608	4.313
3d	-5.4594	-1.4510	-5.4741	-1.3608	4.008
3e	-5.4589	-1.5567	-5.4981	-1.3067	3.902

The substituents to the core with e- donating and accepting units destabilizes HOMO energy levels and stabilizes the LUMO energy levels of the parent ligand (3a), (as shown in Figure 7.10). The variation HOMO destabilizations and LUMO stabilizations were calculated to be almost with 0.03–0.11 eV and 0.02–0.38 eV respectively. The HOMO and LUMO energy levels of all ligands lie at −5.30 to −5.45 and −1.14/−1.55 eV, respectively. The calculated energy gaps are in the range of 3.91 to 4.31 eV. For all these ligands HOMOs gradually increase

in the following order: 3c = 3e < 3f < 3a < 3b. The HOMO of 3b slightly higher (0.03 eV) than 3a, indicating that the hole injection and transport abilities could be improved by the introduction of substituents (electron donating groups). For 3c, 3e and 3f of the HOMO is decreased compare with 3a by 0.11 eV, this can be ascribed to the different conjugated interaction between the OCH_3 and CF_3 and the core molecule. The LUMOs of 3e and 3f gradually decreases and the trend is: 3f > 3e > 3a. But, in the case of 3b and 3c LUMO increases slightly, it is suggesting that the LUMOs of 3b and 3c were determined predominately by the introduction of bridging heteroatoms of C and O can generally enhance the electron-transport and injection abilities of the material with the decreased LUMO. The ligand 3d HOMO and LUMO of the complexes were explained in Chapter 6 (section 6.2.3.2) [38].

7.2.4.2 Host materials- ancillary ligands:

The designed ligands furthered can serve as host materials for triplet dopant in phosphorescent OLEDs. The ligand 1e shown nearby similar HOMO and LUMO of the 4,4 ,4-tris(3-methylphenyl phenylamino)-triphen (m-MTDATA (5.1 and 1.9 eV). m-MTDATA as a common hole-injection material for devices. It indicates that the designed ligand 1e can act as a hole injection material. The HOMO of the ligands (1a-e) are around at 5.2-5.4 eV, which is almost similar to at of most of the hole transporting materials such as TPD (5.1 eV), NPB (5.2 eV), PEDOT:PSS (5.2 eV), CuPc (5.3 eV), α-NPB (5.4 eV), PTPD (5.4 eV), α-NPD (5.4 eV) [39-41]. In case of spacer at N1 position ligands (2e and 2f) are shown highest HOMO energy level and it is shown similar result of hole transporting nature of polyvinyl carbazole PVK (5.8 eV) material. Among all the ligands, third series ligands have shown almost similar or less HOMO energy levels. It is due to presence of spacer at C1 position and leads to arrest the communication between the hole and electron transporting moieties as well as help to increase the overall performance of the device.

Table 7.1 The HOMO, LUMO, HOMO-1 and LUMO+1orbitals of the ancillary ligands (1a-f).

	HOMO	LUMO	HOMO-1	LUMO+1
1a	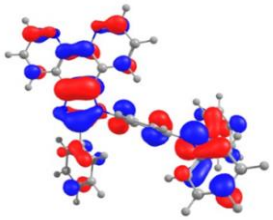	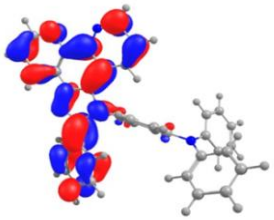	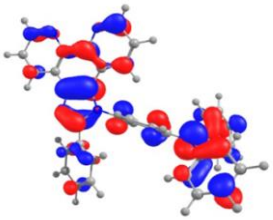	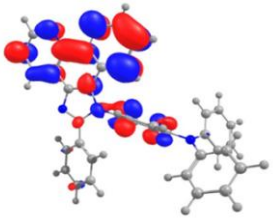
1b	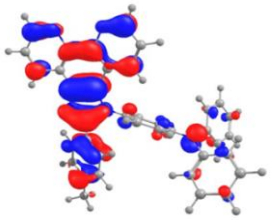	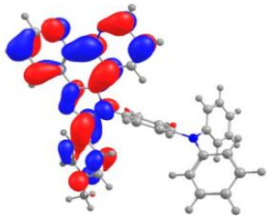	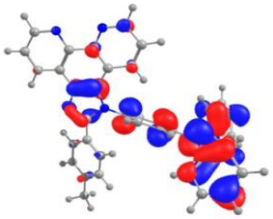	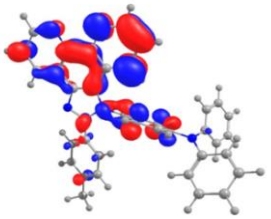
1c	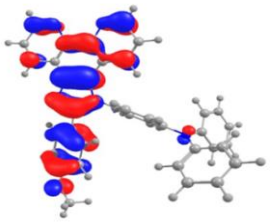	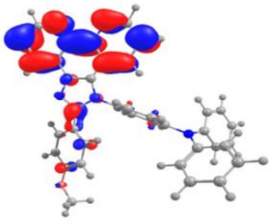	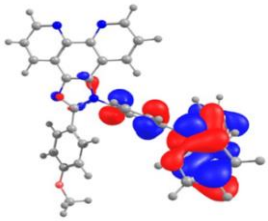	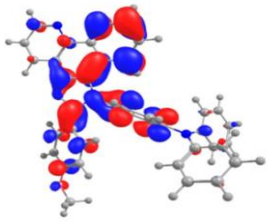
1d	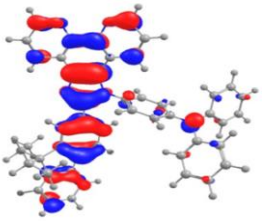	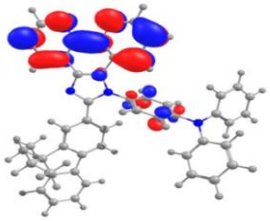	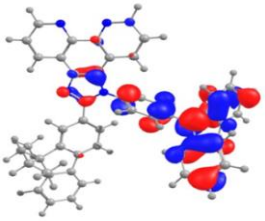	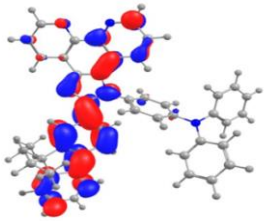
1e	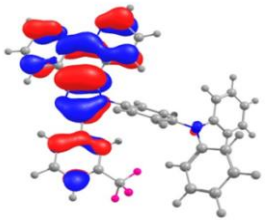	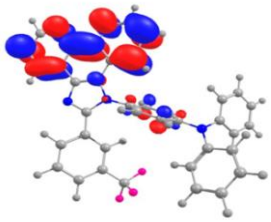	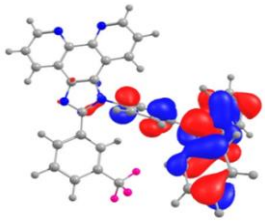	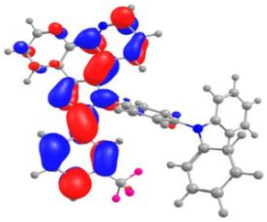
1f	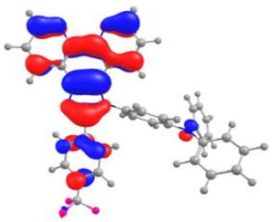	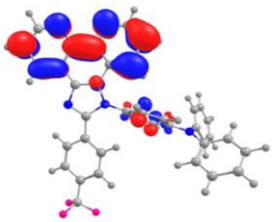	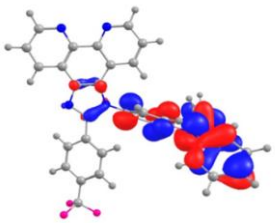	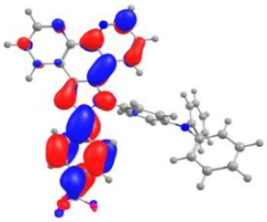

Table 7.2 The HOMO, LUMO, HOMO-1and LUMO+1 orbitals of the ancillary ligands (2a-f).

	HOMO	LUMO	HOMO-1	LUMO+1
2a	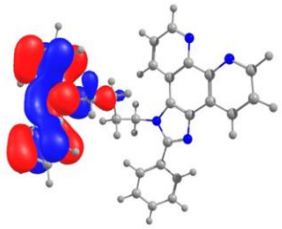	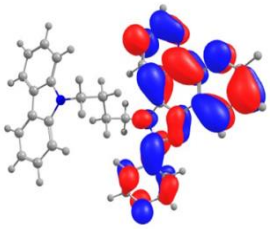	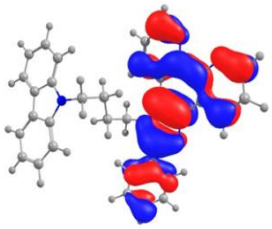	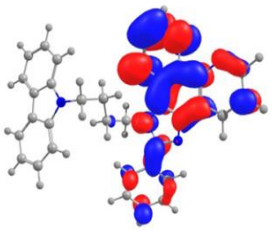
2b	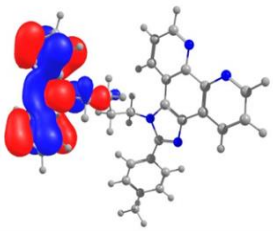	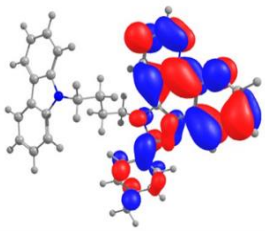	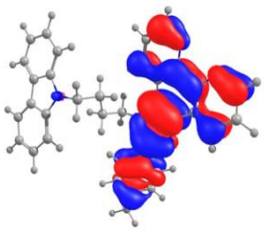	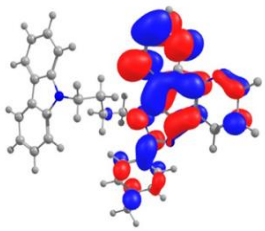
2c	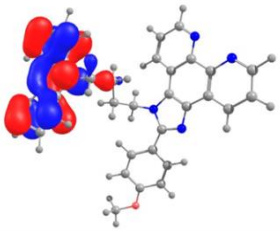	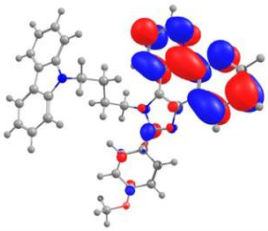	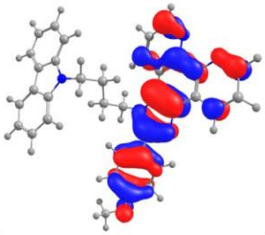	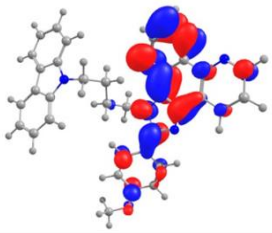
2d	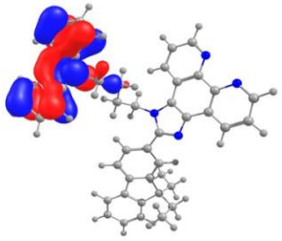	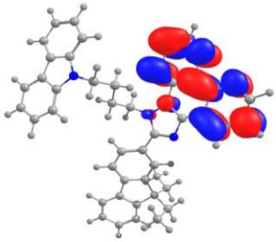	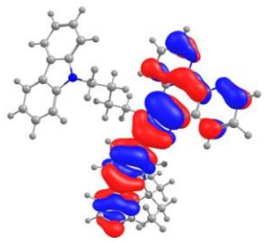	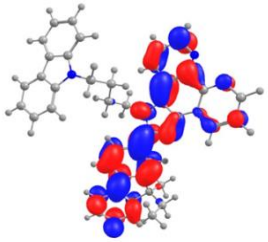
2e	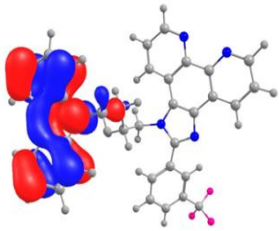	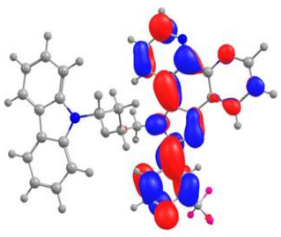	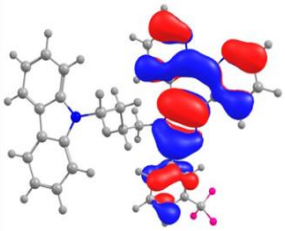	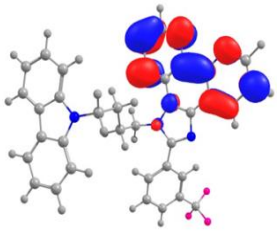
2f	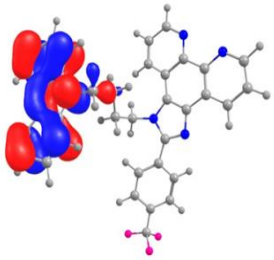	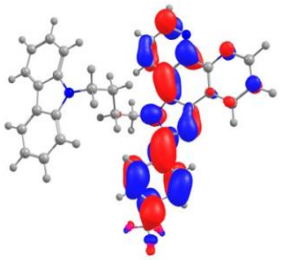	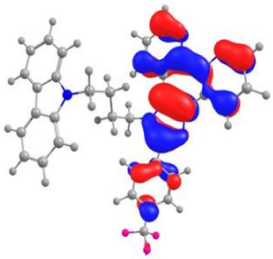	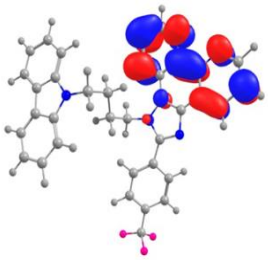

Table 7.3 The HOMO, LUMO, HOMO-1 and LUMO+1 orbitals of the ancillary ligands (3a-f).

	HOMO	LUMO	HOMO-1	LUMO+1
3a	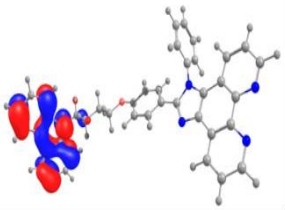	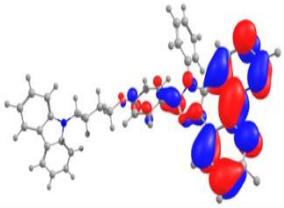	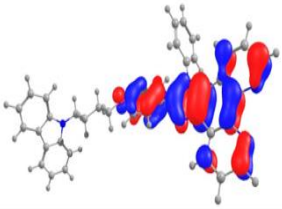	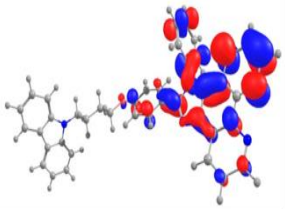
3b	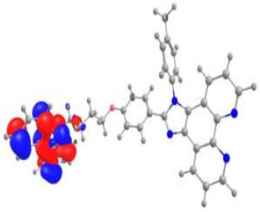	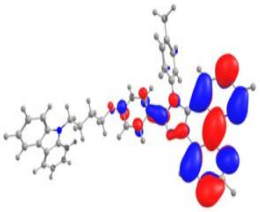	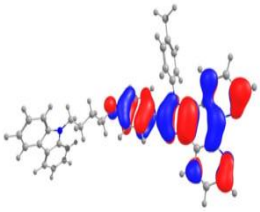	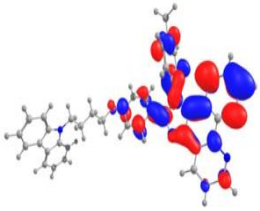
3c	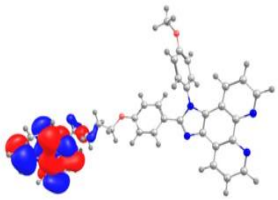	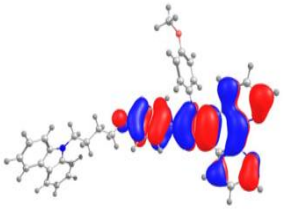	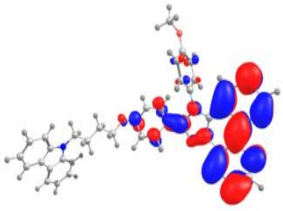	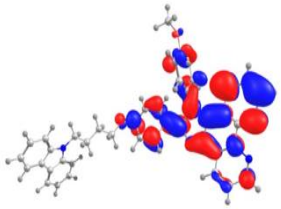
3e	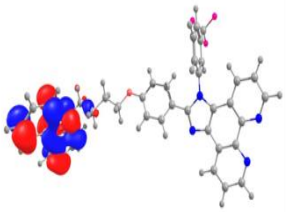	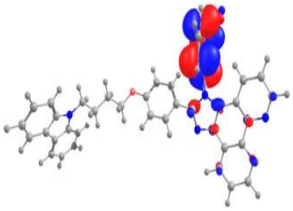	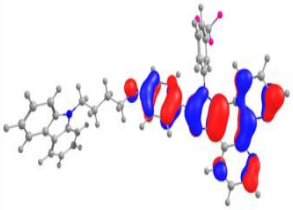	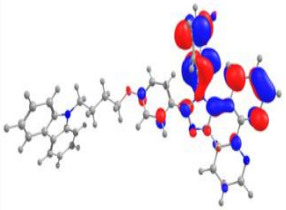
3f	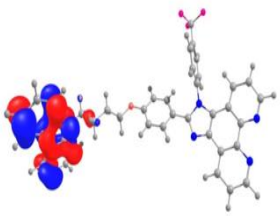	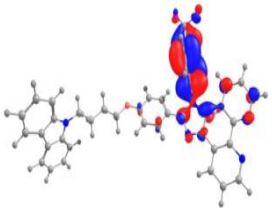	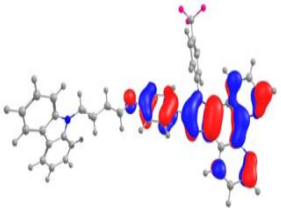	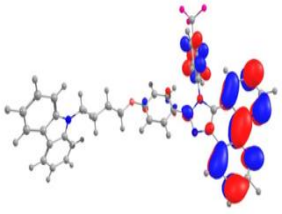

7.2.4.3 Absorption spectral studies of the ancillary ligands (1a-f, 2a-f and 3a-f):

Over the years, time dependent density functional theory (TD DFT) calculations have been used extensively for the prediction of absorption and emission spectra [42]. Therefore, the TDDFT gas phase calculations have been performed at the B3LYP/6-311+G (d,p) level of theory on the optimized ground state geometries. The resultant vertical transition energies (E in eV) oscillator strength (f_0) and the compositions and percentage contributions of the various configurations are summarized in Table 7.7-7.9. Table 7.7 reveals the TPA series of the molecules (1a-1f) having absorption bands ranging from 320 to 350 nm, and the most intense absorption bands along with their transitions are given in Table 7.7. In all the molecules, the S_0-

S_1 electronic transitions are predominant with high oscillator strengths. Triplet electronic transition (S_0-T_1) is allowed in the range 440 to 470 nm.

Figure 11 explains the absorption spectra of 1a-1f in gas and DCM phase. Table 8 reveals the second series of the ligands (2a-2f) absorption bands ranging from 310 to 340 nm. The most intense absorption bands along with their transitions are given in Table 7.8. Triplet electronic transitions (S_0-T_1) are allowed in the range 440 to 470 nm. Table 7.9 reveals the third series of the ligands (3a-3f), absorption bands ranging from 320 to 350 nm, and the intensity of the absorption bands along with their transitions are given in Table 7.9. Among all the ligand the 1d is found to have the highest λ_{max} with 353 nm, which has oscillator strength of 0.6218. This transition is due to 68% contributions from the HOMO-LUMO and arises mainly due to intramolecular charge transfer (ICT) along with π - π^* transitions. The second best based on λ_{max} is 1c with 333 nm, which has an oscillator frequency 0.2396, this transition is due to 60.5% contribution from HOMO-LUMO+1. Compare to all 1f is having highest excitation energy (3.77 eV) and 1d having lowest excitation energy (3.50 eV). It is interesting to note that, while introducing fluorine moiety the λ_{max} increased to 23 nm corresponding to 1a molecule. Surprisingly, all the molecules are showing almost same excitation wavelengths (328-333 nm) except 1d (353 nm).

In second series of ligands (2a-2f), among all 2d is found to have the highest λ_{max} with 347 nm, which has oscillator strength of 0.5945. This transition is due to 61% contributions from HOMO-LUMO level. In comparison, 2a is having highest excitation energy (3.89 eV) and 2d having lowest excitation energy (3.56 eV). All ligands are showing excitation wavelengths in same region (315-324 nm), except 2d (347 nm) and 2f (333 nm). It is worth to note that, while introducing fluorine (CF_3) moiety the λ_{max} increased to 32 nm corresponding to 2a ligand. In third series of ligands, 3a is found to have the highest λ_{max} with 331 nm, which has oscillator strength of 0.30. This transition is due to 36% contributions from HOMO - LUMO and 53% contribution from HOMO - LUMO+1. In comparison 3c is having highest oscillator strength 0.4153 which is due to HOMO – LUMO+1 with 62% contribution. Compare to all ligands 3e is having highest excitation energy (3.89 eV) and 2a having lowest excitation energy (3.73 eV). In comparing with all compounds 3e and 3f are showing excitation wavelengths in same region (318-329 nm) and 3a, 3b and are showing in same region at 326-331 nm. In compare with all the series of the ligands 1d and 2d is found to have highest λ_{max} with 353, and 347 nm, which has oscillator strength of 0.6218 & 0.5945, respectively.

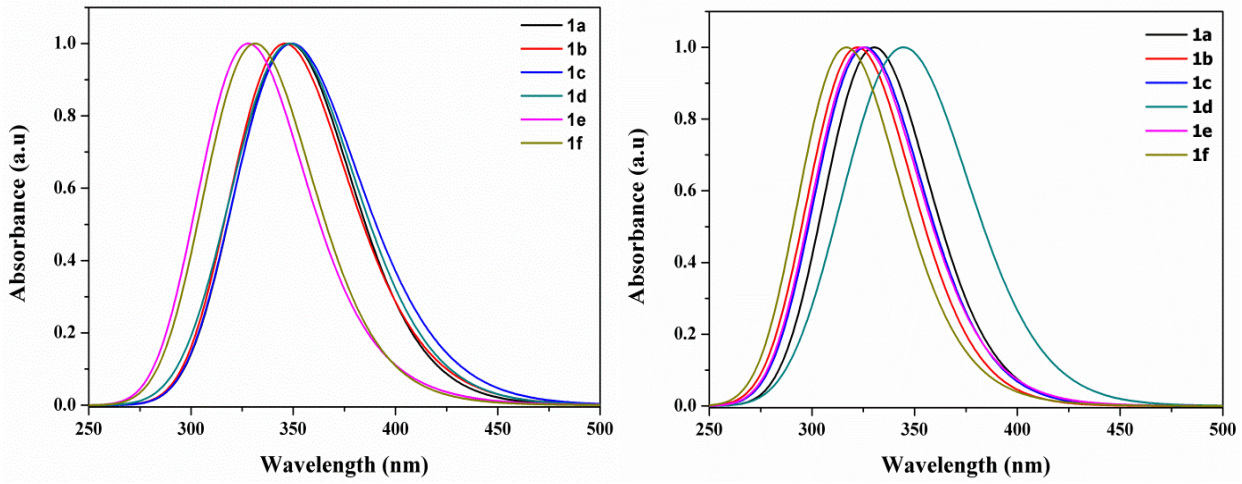

Figure 7.11 UV-Vis spectrum of series of 1a-1f compounds in DCM (left) and gas (right) phase.

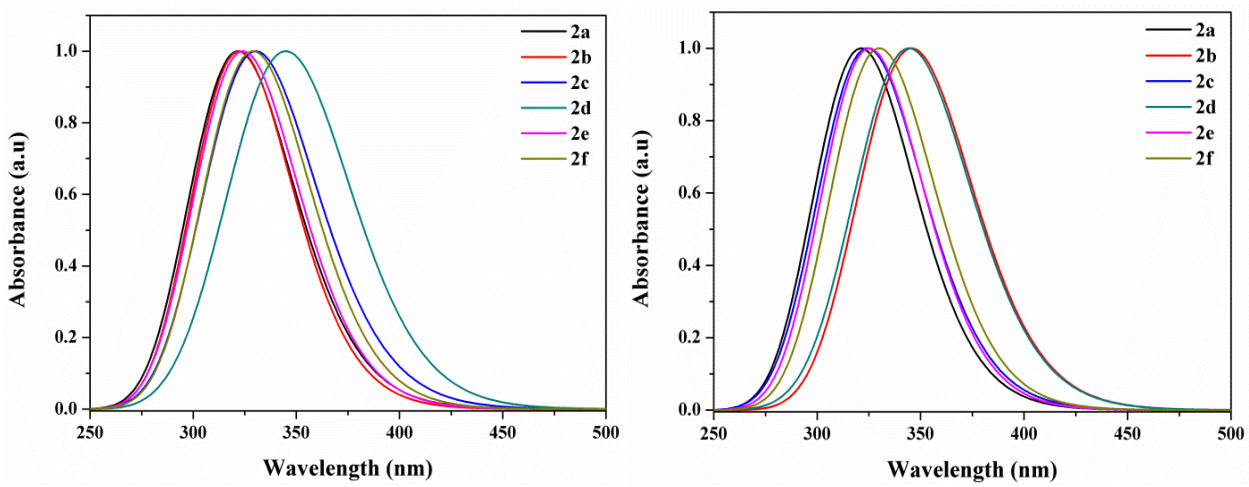

Figure 7.12 UV-Vis spectrum of 2a-2f compounds in DCM (left) and gas (right) phase.

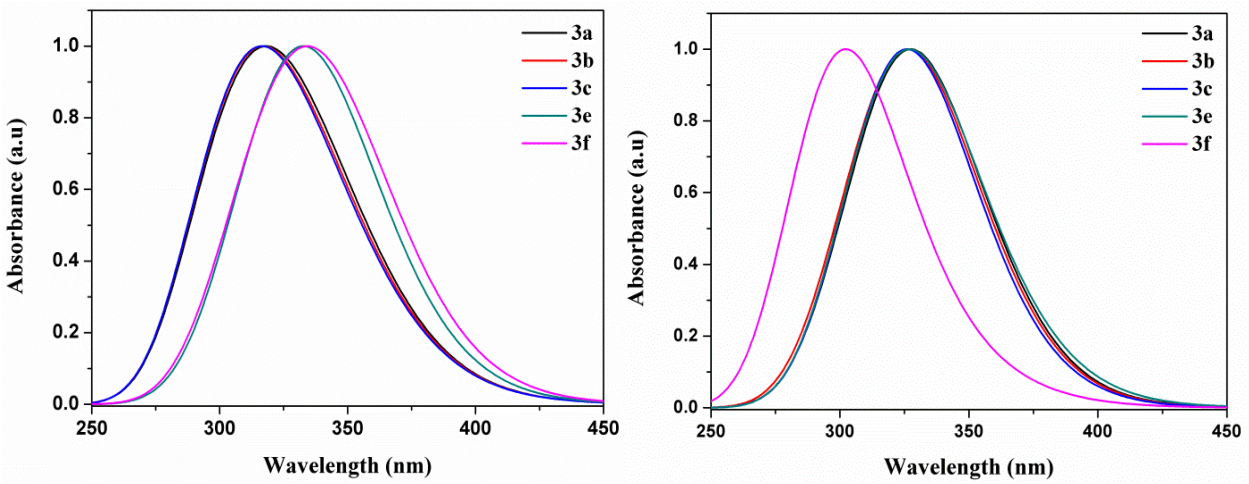

Figure 7.13 UV-Vis spectrum of 3a-3f compounds in DCM (left) and gas (right) phase.

7.2.4.4 Energy transfer mechanism:

In general, in ligand sensitized emission of Eu complexes requires careful consideration of the organic chromophore molecular structure. In order to define the excitation wavelength, maximize absorbance strength at this wavelength and facilitate intramolecular energy transfer to populate the Eu^{III} excited state levels ($^5D_1$ or $^5D_0$). The designed molecular structures of the organic chromophore or ancillary ligands are optimized and predicted their ground and excited state photophysical properties. In order to verify the potentiality of using the designed ancillary ligands (1a-1f, 2a-2f and 3a-3f), we have proposed the schematic energy transfer diagram (ET mechanism) for Eu complex along with the TTA (β-diketone based ligand) energy levels (Figure 7.14, 7.15 and 7.16). The N1 functionalization of the ligand with TPA molecule (1a-f) is shown singlet levels at 27777, 27868, 27770, 26817, 26342, 26198 cm^{-1} and triplet level at 22589, 22514, 22349, 21334, 22355, 21994 cm^{-1}, respectively. The 1a, 1b and 1c ligands are shown similar singlet energy level. In fact 1c have slight lower singlet energy than 1a and 1b, due to presence of oxygen linkage in between the methyl and phenyl ring. The oxygen atom contains two lone pairs of electrons when it is attached to a side chain ((Ph-OCH_3), it can cause a +ve mesmeric effect (M) on the side chain. Although, oxygen itself very electronegative and also

exerts an –ve inductive effect (I). The electrons can delocalize into the ring and leads to be a -OCH_3 group more electron donating than a -CH_3 group. The significant electronegativity of the trifluomethyl group was often described as existence intermediate between the electronegativities of fluorine and chlorine [43].

However, in case of the strong electron withdrawing groups the singlet energy levels as well as triplet energy level are reduced and it was clearly indicating that the fluorination can leads to reduce the excited energy levels of the ligands to facilitate the efficient energy transfer to Eu^{3+} ion. The N1 functionalization of the ligand with spacer connected CBZ molecule (2a-f) is shown singlet levels at 29192, 28864, 28235, 28115, 28810, 28192 cm^{-1} and triplet level at 22930, 22790, 22630, 22593, 22795, 22332 cm^{-1}, respectively. The fluorene moiety connected 2d ligand shown less singlet energy level as compare to at of rest of the ligands (2 a- b, e, f) and triplet energy also shown less. However, the fluorination on ligand 2f (p-CF_3) shown less triplet energy level as compare to 2e (p-CF_3). Among meta and para CF_3 groups, para CF_3 connection leads to decreases the singlet and triple energy levels. It is indicating that the p-CF_3 has better energy level matching with the Eu^{3+} excited ($^5D_0$) state. The C1 functionalization of the ligand with spacer connected CBZ molecule (3a-f) is shown singlet levels at 28126, 28064, 28036, 28025, 28275, 28297 cm^{-1} and triplet level at 22398, 22228, 22392, 22309, 22334, 22336 cm^{-1}, respectively. The 3e and 3f ligands were shown better improved singlet state than 3a-d and these both have similar triplet energy level. At C1 functionalization of the ligand (m and p-CF_3) with spacer no much effect on the singlet and triplet level was observed. However, these ligands have singlet level above 25000 cm^{-1} and their triplet energy levels have above 20000 cm^{-1}. In addition, the difference between excited triplet and Eu^{3+} ion ($^5D_0$) levels (2500 cm^{-1}) and the difference between ligand excited singlet and triplet are well sufficient to transfer the energy from ligand to Eu^{3+} ion in the Eu-complexes.

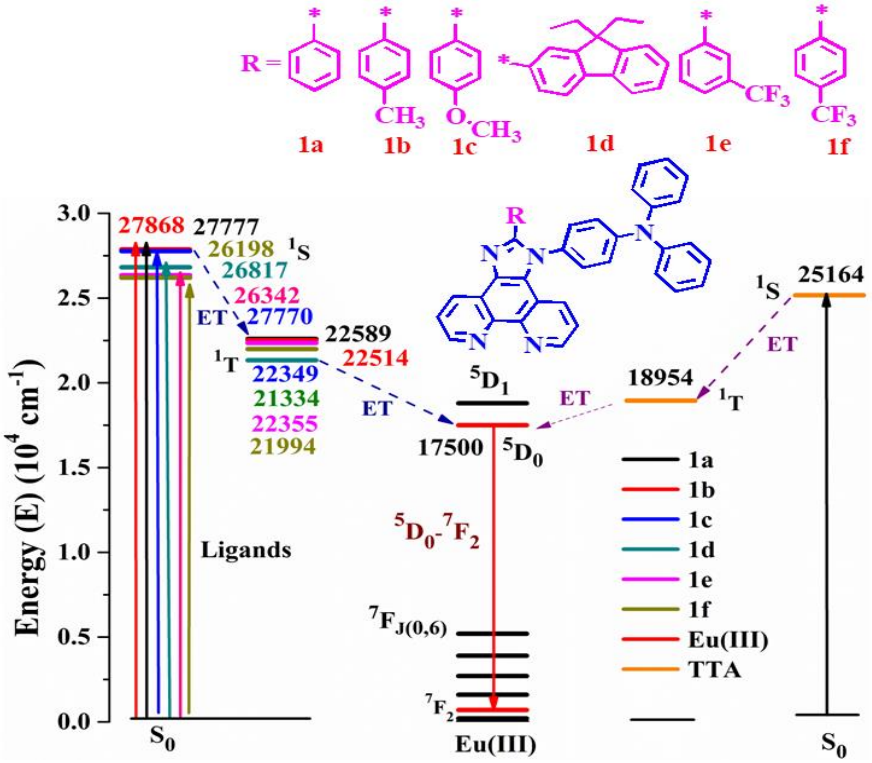

Figure 7.14 The proposed energy transfer mechanism of 1a-1f ligand and TTA to Eu energy levels in Eu complex.

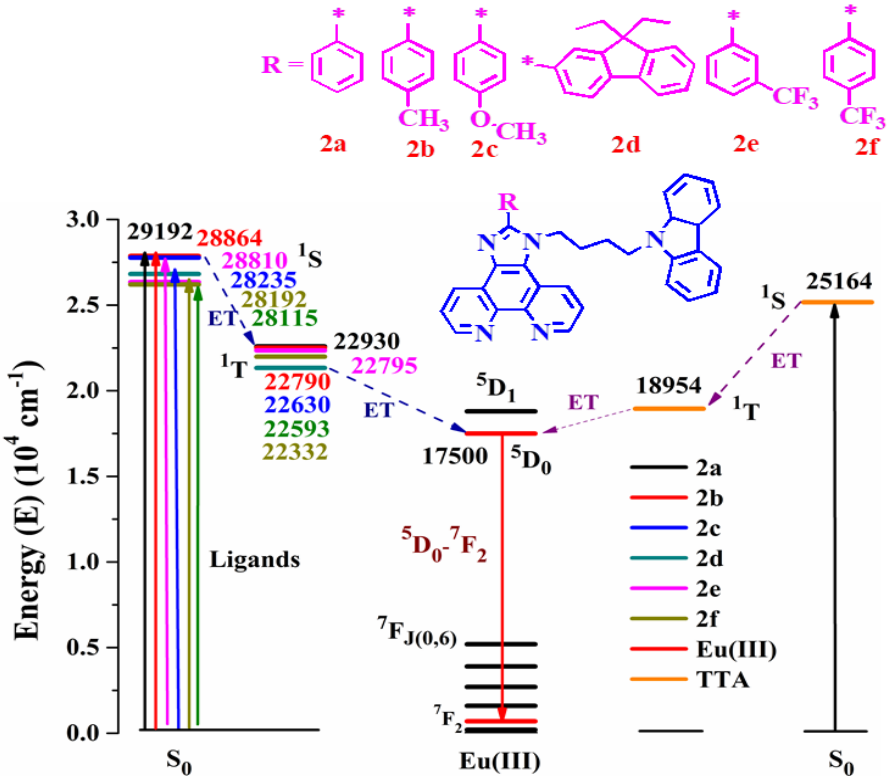

Figure 7.15 The proposed energy transfer mechanism of 2a-2f ligand and TTA to Eu energy levels in Eu complex.

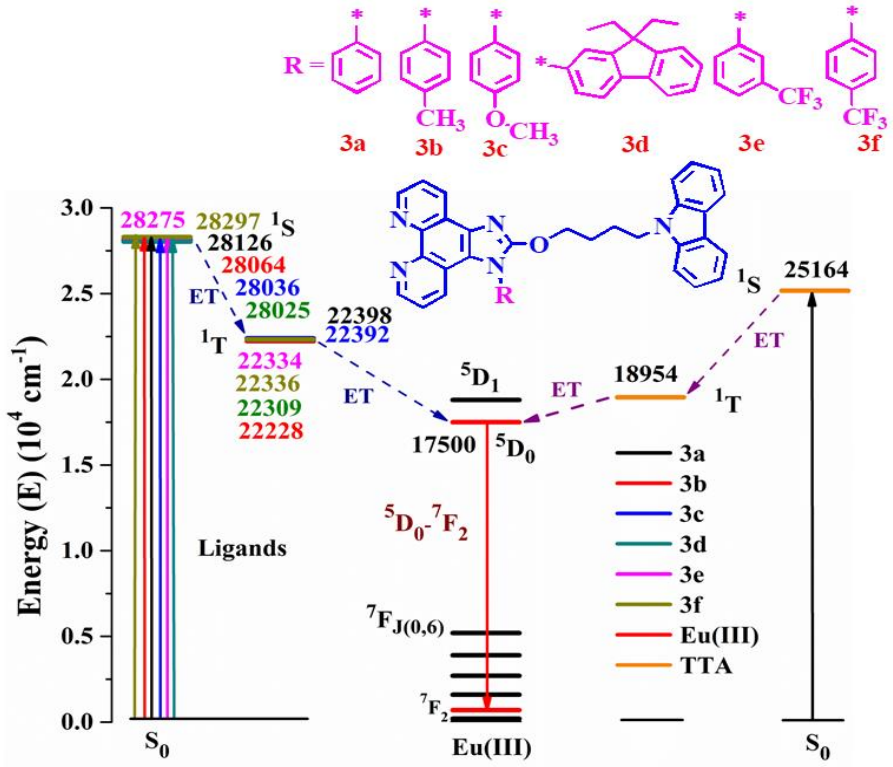

Figure 7.16 The proposed energy transfer mechanism of 3a-3f ligand and TTA to Eu energy levels in Eu complex.

The designed ligands can use not only as an antenna for red emission from the Eu^{3+} ion; it can also be used for Tb^{3+} ion to get the green emission. Since the triplet energy of the all the designed ligands are located more than 22,000 cm^{-1}. The Tb^{3+} excited state ($^5D_4$) located at 20,430 cm^{-1}, which are well suited for the energy transfer to Tb^{III} ion [44].

Table 7.7: Computed vertical transitions and their oscillator strengths and configurations[a] of 1a-1f compounds.

Compound	State	Energy (eV)	λ_{max} nm	*f*	Configuration
1a Singlet	Gas	3.6723	337.62	0.0409	HOMO-1 → LUMO (18.80%). HOMO → LUMO+1 (46.67%).
		3.7541	330.26	0.1467	HOMO-1 → LUMO (18.06%). HOMO-1 → LUMO+1 (16.49%). HOMO → LUMO (51.03%). HOMO → LUMO+1 (38.50%). HOMO → LUMO+3 (12.40%).
	DCM	3.444	359.95	0.0103	HOMO → LUMO (66.16%). HOMO → LUMO+1 (22.45%).
		3.6137	343.10	0.077	HOMO-1 → LUMO (66.17%).
Triplet	Gas	2.7788	446.18	0	HOMO-2 → LUMO+1 (12.83%). HOMO-1 → LUMO+3 (11.12%). HOMO → LUMO (40.38%). HOMO → LUMO+1 (18.68%).
	DCM	2.8098	441.26	0	HOMO-2 → LUMO (18.41%). HOMO-1 → LUMO (31.14%). HOMO-1 → LUMO+1 (53.73%).
1b Singlet	Gas	3.6375	340.85	0.0434	HOMO-1 → LUMO+1 (16.49%). HOMO-2 → LUMO (10.96%). HOMO → LUMO+1 (50.63%).
		3.7615	329.61	0.2291	HOMO → LUMO (45.47%). HOMO → LUMO+1 (42.39%). HOMO → LUMO+3 (12.39%).
		3.9471	314.12	0.1297	HOMO-3 → LUMO+1 (16.05%). HOMO-1 → LUMO+1 (37.13%). HOMO-1 → LUMO+2 (32.40%). HOMO → LUMO (13.02%). HOMO → LUMO+3 (24.34%).
		3.9782	311.66	0.1267	HOMO → LUMO+2 (49.33%). HOMO → LUMO+3 (44.65%).
	DCM	3.4552	358.84	0.0087	HOMO → LUMO (68.18%).
		3.8058	325.78	0.3118	HOMO-2 → LUMO (18.97%). HOMO-1 → LUMO (12.91%). HOMO-1 → LUMO+1 (63.87%).
		3.9337	315.18	0.5411	HOMO → LUMO+3 (66.76%).
Triplet	DCM	2.7915	444.15	0	HOMO-2 → LUMO (17.12%). HOMO-1 → LUMO (28.20%). HOMO-1 → LUMO+1 (55.50%).

	Gas	2.7628	448.77	0	HOMO-4 → LUMO+4 (11.07%). HOMO-2 → LUMO (13.70%). HOMO-1 → LUMO (21.51%). HOMO-1 → LUMO+1 (12.02%). HOMO → LUMO (47.62%). HOMO → LUMO+1 (29.69%).
1c Singlet	Gas	3.5677	347.52	0.0391	HOMO → LUMO (63.46%).
		3.7200	333.29	0.2396	HOMO → LUMO (23.09%). HOMO → LUMO+1 (60.58%). HOMO → LUMO+3 (19.19%).
		3.8896	318.76	0.1581	HOMO → LUMO+2 (56.80%). HOMO → LUMO+6 (10.38%).
	DCM	3.4431	360.09	0.047	HOMO → LUMO (55.32%).
		3.7360	331.86	0.3017	HOMO-2 → LUMO (16.72%). HOMO-1 → LUMO+1 (66.8%).
		3.9288	315.58	0.5036	HOMO → LUMO+2 (13.8%). HOMO → LUMO+3 (65.81%).
Triplet	Gas	2.7505	450.77	0	HOMO-4 → LUMO+5 (10.48%). HOMO-2 → LUMO (15.02%). HOMO → LUMO (26.67%). HOMO → LUMO+1 (52.65%).
	DCM	2.7710	447.43	0	HOMO-2 → LUMO (13.32%). HOMO-1 → LUMO (22.98%). HOMO-1 → LUMO+1 (55.75%).
1d Singlet	Gas	3.5075	353.48	0.6218	HOMO-1 → LUMO (11.41%). HOMO → LUMO (67.95%).
		3.6362	340.97	0.277	HOMO-1 → LUMO (66.08%). HOMO → LUMO+1 (16.84%).
		3.8824	319.35	0.2007	HOMO → LUMO+2 (62.97%).
	DCM	3.3249	372.89	0.0961	HOMO → LUMO (67.28%). HOMO → LUMO+1 (19.08%).
		3.4969	354.63	0.5039	HOMO-1 → LUMO (62.03%). HOMO → LUMO+1 (21.86%).
		344.07	3.0034	0.5066	HOMO-1 → LUMO (23.90%). HOMO-1 → LUMO+1 (63.48%).
Triplet	Gas	2.6451	468.73	0	HOMO-2 → LUMO (12.61%). HOMO → LUMO (59.37%).
	DCM	2.6451	468.73	0	HOMO-2 → LUMO+2 (17.54%). HOMO-1 → LUMO (55.27%). HOMO-1 → LUMO+1 (26.26%). HOMO → LUMO (15.16%).
1e Singlet	Gas	3.4285	361.63	0.0415	HOMO → LUMO (69.90%).
		3.7266	332.70	0.2219	HOMO-1 → LUMO (54.84%). HOMO-1 → LUMO+1 (30.16%). HOMO → LUMO+3 (10.84%).

		3.7791	328.08	0.1221	HOMO-1 → LUMO+1 (42.30%).
					HOMO → LUMO+4 (25.97%).
		3.8337	323.40	0.1358	HOMO-1 → LUMO+1 (32.47%).
					HOMO → LUMO+2 (41.32%).
		3.9203	316.27	0.3565	HOMO → LUMO+1 (13.91%).
					HOMO → LUMO+3 (66.61%).
	DCM	3.2661	379.61	0.0338	HOMO → LUMO (67.61%).
		3.6517	339.52	0.1722	HOMO-1 → LUMO (55.14%).
					HOMO-1 → LUMO+1 (40.18%).
		3.8037	325.95	0.3701	HOMO-1 → LUMO+1 (52.28%).
					HOMO → LUMO (10.50%).
		3.8578	320.38	0.2509	HOMO → LUMO+2 (26.17%).
					HOMO → LUMO+3 (57.94%).
					HOMO → LUMO+4 (13.05%).
Triplet	Gas	2.7302	454.12	0	HOMO-2 → LUMO (10.47%).
					HOMO-2 → LUMO+1 (12.71%).
					HOMO-1 → LUMO (59.71%).
					HOMO-1 → LUMO+2 (14.17%).
					HOMO → LUMO (12.15%).
	DCM	2.7717	441.32		HOMO-2 → LUMO (13.72%).
					HOMO-2 → LUMO+1 (10.06%).
					HOMO-1 → LUMO (55.6%).
					HOMO-1 → LUMO+2 (13.65%).
1f Singlet	Gas				
	DCM	3.2482	381.70	0.0131	HOMO → LUMO (69.21%).
		3.6497	339.71	0.2998	HOMO-1 → LUMO (57.23%).
					HOMO-1 → LUMO+1 (37.94%).
		3.775	328.21	0.3160	HOMO-1 → LUMO+1 (55.20%).
					HOMO → LUMO+2 (13.99%).
		3.8091	325.50	0.1007	HOMO-1 → LUMO (12.88%).
					HOMO → LUMO+2 (64.99%).
Triplet	Gas	2.7272	454.61	0	HOMO-2 → LUMO (10.47%).
					HOMO-2 → LUMO+1 (12.56%).
					HOMO-1 → LUMO (58.57%).
					HOMO-1 → LUMO+3 (11.51%).
					HOMO-1 → LUMO+4 (12.77%).
	DCM	2.7683	447.87	0	HOMO-2 → LUMO (12.73%).
					HOMO-2 → LUMO+1 (11.16%).
					HOMO-1 → LUMO (58.30%).
					HOMO-1 → LUMO+2 (16.92%).

[a]Orbital contributions below 10% are omitted

Table 7.8: Computed vertical transitions and their oscillator strengths and configurations[a] of 2a-2f compounds.

Compound	State	Energy (eV)	λ_{max} nm	*f*	Configuration
1a Singlet	Gas	3.6938	335.65	0.0366	HOMO-1 → LUMO (52.3%)
		3.8913	318.62	0.1631	HOMO-4 → LUMO (14.68%)
					HOMO-1 → LUMO (35.67%)
					HOMO-1 → LUMO+1 (40.09%)
					HOMO → LUMO+1 (37.71%)
	DCM	3.6194	342.55	0.062	HOMO-1 → LUMO (66.36%)
					HOMO → LUMO (12.34%)
		3. 8711	320.28	0.2563	HOMO-3 → LUMO (23.74%)
					HOMO-1 → LUMO (13.36%)
					HOMO-1 → LUMO (64.34%)
Triplet	Gas	2.8136	440.66	0	HOMO-3 → LUMO (18.41%)
					HOMO-1 → LUMO (44.30%)
					HOMO-1 → LUMO+1 (42.74%)
	DCM	2.843	436.11		HOMO-7 → LUMO+2 (10.48%)
					HOMO-3 → LUMO (20.75%)
					HOMO-1 → LUMO (26.76%)
					HOMO-1 → LUMO+1 (55.75%)
2b Singlet	Gas	3.6612	338.64	0.0392	HOMO-1 → LUMO (56.50%)
		3.8671	320.62	0.2643	HOMO-1 → LUMO (33.38%)
					HOMO-1 → LUMO+1 (52.13%)
					HOMO → LUMO (14.21%)
					HOMO → LUMO+1 (19.08%)
	DCM	3.5787	346.45	0.069	HOMO-1 → LUMO (67.69%)
Triplet	Gas	2.7981	443.10	0	HOMO-6 → LUMO+3 (12.19%)
					HOMO-3 → LUMO (18.10%)
					HOMO-1 → LUMO (39.33%)
					HOMO-1 → LUMO+1 (47.74%)
	DCM	2.8257	438.78	0	HOMO-3 → LUMO (19.26%)
					HOMO-1 → LUMO (25.07%)
					HOMO-1 → LUMO+1 (56.98%)
2c Singlet	Gas	3.5986	344.54	0.0370	HOMO → LUMO (65.59%)
		3.822	324.38	0.2716	HOMO-4 → LUMO (20.98%)
					HOMO → LUMO (19.55%)
					HOMO → LUMO+1 (63.35%)
	DCM	3.5007	354.17	0.0694	HOMO-1 → LUMO (68.29%)
		3.7635	329.44	0.2817	HOMO-3 → LUMO (19.51%)
					HOMO-1 → LUMO+1 (65.92%)
Triplet	Gas	2.7847	445.23	0	HOMO-3 → LUMO (17.12%)
					HOMO → LUMO (23.43%)
					HOMO → LUMO (57.79%)
	DCM	2.8058	441.88	0	HOMO-3 → LUMO (14.92%)

					HOMO-1 → LUMO (21.57%)
					HOMO-1 → LUMO+1 (57.37%)
2d Singlet	Gas	3.5648	347.80	0.5945	HOMO → LUMO (61.10%)
					HOMO → LUMO+1 (32.36%)
		3.6471	339.96	0.2872	HOMO-3 → LUMO+1 (10.18%)
					HOMO → LUMO+1 (59.4%)
	DCM	3.4859	335.68	0.4528	HOMO-1 → LUMO (63.85%)
					HOMO-1 → LUMO+1 (24.43%)
		3.6176	342.73	0.6509	HOMO-1 → LUMO+1 (62.94%)
		3.8933	318.46	0.1335	HOMO-1 → LUMO+2 (65.28%)
Triplet	Gas	2.6485	468.14	0	HOMO-3 → LUMO+2 (15.42%)
					HOMO → LUMO (61.37%)
	DCM	2.6773	463.09	0	HOMO-1 → LUMO (54.19%)
2e Singlet	Gas	3.8482	339.85	0.0015	HOMO → LUMO (70.27%)
		3.7381	331.68	0.1076	HOMO-1 → LUMO (40.57%)
					HOMO-1 → LUMO+1 (53.35%)
		3.8382	323.03	0.2669	HOMO-3 → LUMO+1 (14.02%)
					HOMO-1 → LUMO (53.51%)
	DCM	3.5721	347.09	0.0022	HOMO → LUMO (69.33%)
		3.666	338.19	0.1030	HOMO-1 → LUMO (54.82%)
					HOMO-1 → LUMO+1 (32.99%)
					HOMO → LUMO+1 (25.08%)
		3.8492	322.10	0.3686	HOMO-1 → LUMO+1 (57.83%)
Triplet	Gas	2.7867	444.92	0	HOMO-3 → LUMO (12.51%)
					HOMO-3 → LUMO+1 (15.34%)
					HOMO-1 → LUMO (58.20%)
					HOMO-1 → LUMO+2 (19.15%)
	DCM	2.8263	438.69	0	HOMO-3 → LUMO (18.04%)
					HOMO-2 → LUMO (48.12%)
2f Singlet	Gas	3.5461	349.63	0.0006	HOMO → LUMO (70.52%)
		3.7185	333.43	0.2573	HOMO-1 → LUMO (54.66%)
					HOMO-1 → LUMO+1 (40.05%)
		3.8036	325.96	0.1959	HOMO-1 → LUMO+1 (52.08%)
					HOMO → LUMO+1 (14.77%)
	DCM	3.4954	354.70	0.0011	HOMO → LUMO (70.10%)
		3.6586	338.89	0.1575	HOMO-1 → LUMO (47.45%)
					HOMO-1 → LUMO+1 (32.98%)
					HOMO → LUMO+1 (37.73%)
		3.8037	325.96	0.3739	HOMO-1 → LUMO+1 (56.05%)
Triplet	Gas	2.7688	447.78	0	HOMO-3 → LUMO (12.01%)
					HOMO-3 → LUMO+1 (14.58%)
					HOMO-1 → LUMO (58.85%)
					HOMO-1 → LUMO+2 (20.57%)
		2.8089	441.40	0	HOMO-3 → LUMO (15.24%)
					HOMO-3 → LUMO+1 (12.08%)

					HOMO-1 → LUMO (55.11%)
					HOMO-1 → LUMO+2 (20.04%)

[a]Orbital contributions below 10% are omitted.

Table 7.8: Computed vertical transitions and their oscillator strengths and configurations[a] of 3a-3f compounds**.**

Compound	State	Energy (eV)	λ_{max} nm	*f*	Configuration
3a Singlet	Gas	3.5932	345.05	0.0298	HOMO → LUMO (56.93%)
		3.7363	331.84	0.3007	HOMO → LUMO (36.19%)
					HOMO → LUMO+1 (53.72%)
		3.9400	314.68	0.1211	HOMO-3 → LUMO (16.50%)
					HOMO → LUMO (11.35%)
					HOMO → LUMO+1 (16.18%)
					HOMO → LUMO+2 (62.79%)
	DCM	3.4873	355.53	0.082	HOMO-1 → LUMO (68.71%)
		3.7307	332.34	0.3998	HOMO-3 → LUMO (16.85%)
					HOMO-1 → LUMO+1 (67.38%)
		4.0657	304.95	0.4432	HOMO-3 → LUMO (16.75%)
					HOMO-1 → LUMO+2 (66.48%)
Triplet	Gas	2.7559	449.89	0	HOMO-3 → LUMO (14.42%)
					HOMO → LUMO (36.04%)
					HOMO → LUMO+1 (49.27%)
					HOMO → LUMO+2 (16.56%)
	DCM	2.777	446.46	0	HOMO-3 → LUMO (13.41%)
					HOMO-1 → LUMO (22.82%)
					HOMO-1 → LUMO+1 (57.63%)
3b Singlet	Gas	3.5881	345.54	0.0375	HOMO → LUMO (61.31%)
		3.7633	329.46	0.3594	HOMO-3 → LUMO (13.19%)
					HOMO → LUMO (29.87%)
					HOMO → LUMO+1(54.26%)
	DCM	3.4796	356.31	0.0837	HOMO-1 → LUMO (68.77%)
		3.7317	332.25	0.3946	HOMO-3 → LUMO (17.27%)
					HOMO-1 → LUMO+1 (67.33%)
		4.0644	305.05	0.4918	HOMO-3 → LUMO (16.37%)
					HOMO-1 → LUMO+2 (66.78%)
Triplet	Gas	2.7560	449.87	0	HOMO-3 → LUMO (14.93%)
					HOMO → LUMO (32.64%)
					HOMO → LUMO+1 (52.57%)
					HOMO → LUMO+3 (10.28%)
	DCM	2.7768	446.49	0	HOMO-3 → LUMO (13.44%)
					HOMO-1 → LUMO (26.2%)
					HOMO-1 → LUMO+1 (57.57%)
3c Singlet	Gas	3.5871	345.64	0.0443	HOMO → LUMO (63.72%)
		3.8011	326.18	0.4183	HOMO-3 → LUMO (16.88%)

					HOMO → LUMO (25.28%)
					HOMO → LUMO+1 (62.27%)
	DCM	3.4761	356.68	0.0845	HOMO-1 → LUMO (68.80%)
		3.7362	331.84	0.3861	HOMO-4 → LUMO (13.90%)
					HOMO-1 → LUMO+1 (67.23%)
		4.0617	305.23	0.5072	HOMO-4 → LUMO (11.37%)
					HOMO-1 → LUMO+2 (66.68%)
Triplet	Gas	2.7594	449.32	0	HOMO-3 → LUMO (15.19%)
					HOMO → LUMO (31.10%)
					HOMO → LUMO+1 (54.50%)
	DCM	2.7763	446.26	0	HOMO-1 → LUMO (23.50%)
					HOMO-1 → LUMO+1 (57.44%)
3e	Gas	3.4367	360.77	0.009	HOMO-1 → LUMO (69.52%)
Singlet					
		3.6866	336.31	0.1843	HOMO-1 → LUMO+1 (18.59%)
					HOMO-1 → LUMO+2 (59.69%)
		3.8909	318.65	0.2515	HOMO-3 → LUMO+2 (19.61%)
					HOMO-1 → LUMO+1 (13.69%)
					HOMO-1 → LUMO+2 (22.16%)
					HOMO-1 → LUMO+3 (60.26%)
	DCM	3.5057	353.66	0.0711	HOMO-1 → LUMO (68.34%)
		3.6905	335.95	0.3135	HOMO-3 → LUMO (13.02%)
					HOMO-1 → LUMO (10.61%)
					HOMO-1 → LUMO+1 (65.45%)
					HOMO-1 → LUMO+2 (17.35%)
Triplet	Gas	27449	451.68	0	HOMO-5 → LUMO+5 (10.73%)
					HOMO-3 → LUMO+2 (13.82%)
					HOMO-1 → LUMO (24.44%)
					HOMO-1 → LUMO+1 (36.26%)
					HOMO-1 → LUMO+2 (32.42%)
					HOMO-1 → LUMO+3 (30.07%)
	DCM	2.7691	447.74	0	HOMO-3 → LUMO (12.92%
					HOMO-1 → LUMO (22.13%)
					HOMO-1 → LUMO+1 (56.62%)
3f	Gas	3.3526	364.81	0.0307	HOMO-1 → LUMO (69.46%)
Singlet					
		3.7623	324.55	0.1302	HOMO-1 → LUMO+2 (54.63%)
		3.8826	319.34	0.2631	HOMO-3 → LUMO+1 (20.83%)
					HOMO-1 → LUMO+1 (14.73%)
					HOMO-1 → LUMO+2 (36.26%)
					HOMO-1 → LUMO+3 (53.02%)
	DCM	3.5084	353.39	0.0502	HOMO-1 → LUMO (67.72%)
		3.6087	343.57	0.2482	HOMO-1 → LUMO (13.67%)
					HOMO-1 → LUMO+1 (65.57%)
					HOMO-1 → LUMO+2 (20%)
		3.8526	321.82	0.2631	HOMO-1 → LUMO+2 (65.77%)

Triplet	Gas	2.7415	452.26	0	HOMO-5 → LUMO+5 (10.29%). HOMO-3 → LUMO+1 (14.08%). HOMO-1 → LUMO (37.54%). HOMO-1 → LUMO+1 (21.61%). HOMO-1 → LUMO+2 (39.01%). HOMO-1 → LUMO+3 (25.45%).
	DCM	2.7694	447.70		HOMO-3 → LUMO (13.59%) HOMO-1 → LUMO (16.47%). HOMO-1 → LUMO+1 (54.29%).

[a]Orbital contributions below 10% are omitted.

7.3 Summary and conclusion:

In summary, numerous ligands were designed and studied their excited state photophysical properties by theoretical study. The systematic study of the excitation window by DFT method revealed strong π-π* transition of the ligands due to presence of aromatic rings. The triplet level location also been calculated by using TD-DFT method and found that among three (1a-f, 2a-f, 3a-f) series a-f shown better energy matching with the excited state ($^5D_0$) of Eu^{III} ion and could facilitate the efficient energy transfer from ligand to Eu ion. In addition, the substituted phenyl moiety (mCF_3 and pCF_3) at N1-position in the phenanthro-imidazole ligand give additional benefits by reducing the triplet energy comparatively with other substitution that leads to efficient energy transfer from L to Eu ion in the complex could be expected. The systematic theoretical is certainly leads synthesis the best ligand molecules for Eu complexes. In addition, some of the ligands can also serve as host materials for triplet dopant.

7.4 References:

[1] J. C. G. Bunzli and S. V. Eliseeva, *J. Rare Earths*, 2012, **28**, 824–842.
[2] S. I. Weissman, J. Chem. Phys., 1942, **10**, 214.
[3] M. Latva, H. Takalo, V. M. Mukkala, C. Matachescu, J. C. Rodriguez-Ubis and J. Kankare, *J. Lumin.*, 1997, **75**, 149–169.
[4] N. Sabbatini, M. Guardigli and J. M. Lehn, *Coord. Chem. Rev.*, 1993, **123**, 201.
[5] N. Sabbatini, M. Guardigli, I. Manet, R. Ungaro, A. Casti, R. Ziessel, G. Ulrich, Z. Asfari and J. M. Lehn, *Pure Appl. Chem.*, 1995, **67**, 135.
[6] T. Yayamura, S. Iwata, S. lwamaru and H. Tomiyasu, *J. Chem. Soc. Faraday Trans.*, 1994, **90**, 3253–3259.
[7] J. Feng and H. Zhang, *Chem. Soc. Rev.*, 2013, **42**, 387–410.
[8] J. C. G. Bunzli, *Chem. Rev.*, 2010, **110**, 2729–2755.
[9] K. S. Kumar, B. Schafer, S. Lebedkin, L. Karmazin, M. M. Kappes and M. Ruben, *Dalton Trans.*, 2015, **44**, 182–192.
[10] Y. Liu, Y. Wang, H. Guo, M. Zhu, C. Li, J. Peng, W. Zhu and Y. Cao, *J. Phys. Chem. C*, 2011, **115**, 4209–4216.
[11] H. Xu, Q. Sun, Z. An, Y. Wei and X. Liu, *Coord Chem Rev.*, 2015, 293–294, 228–249.
[12] C. Spangler and M. Schaaferling, Lanthanide luminescence: Photophysical, analytical and biological aspects; Eds: P. Haanninen and H. Haarma, Springer series fluorescence, 2011, Vol. 7, pp 235−262.
[13] J. C. G. Bunzli, *Chem. Rev.*, 2010, **110**, 2729−2755.
[14] (a) S. V. Eliseeva and J. C. G. Bunzli, *Chem. Soc. Rev.*, 2010, **39**, 189−227; (b) J. C. G. Bunzli, *Coord. Chem. Rev.*, 2015, **293−294**, 19−47.
[15] R. O. Freire, F. R. G. Silva, M. O. Rodrigues, M. E. Mesquita, N. B. C. Junior, *J. Mol. Model.*, 2005, **12**, 16–23.
[16] R. O. Freire, R. Q. Albuquerque, S. A. Junior, G. B. Rocha, M. E. Mesquita, *Chem. Phys. Lett.*, 2005, **405**, 123–126.
[17] (a) M. A. Baldo, D. F. O'Brien, Y. You, A. Shoustikov, S. Sibley, M. E. Thompson and S. R. Forrest, *Nature*, 1998, **395**, 151–154; (b) M. A. Baldo and S. Lamaneky, *Appl. Phys. Lett.*, 1999, **4**, 75-77; (c) E. Holder, B. M. W. Langeveld and U. S. Schubert, *Adv. Mater.*, 2005, **17**, 1109–1121.
[18] S. Heer, O. Lehmann, M. Haase and H. U. Gudel, *Angew. Chem. Int. Ed.*, 2003, **42**, 3179–3182.
[19] (a) A. B. Dias, *J. Am. Chem. Soc.*, 2011, **133**, 19566–19566; (b) A. R. Ramya, Sunil Varughese and M. L. P. Reddy, Dalton Trans., 2014, **43**, 10940.
[20] (a) H. Xu, Q. Sun, Z. An, Y. Wei and X. Liu, *Coord. Chem. Rev.*, 2015, **293–294**, 228–249; (b) H. Xu, R. Chen, Q. Sun, W. Lai, Q. Su, W. Huang and X. Liu, *Chem. Soc. Rev.*, 2014, **43**, 3259–3302.
[21] O. L. Malta, F. R. G. Silva, R. L. Longo, *Chem. Phys. Lett.*, 1999, **307**, 518–526.
[22] J. D. L. Dutra, I. F. Gimenez, N. B. Costa Junior and R. O. Freire, *J. Photochem. Photobiol. A: Chemistry*, 2011, **217**, 389–394.
[23] K. A. Romanova, A. Y. Freidzon, A. A. Bagaturyants and Y. G. Galyametdinov, *J. Phys. Chem. A*, 2014, 118, 11244–11252.
[24] L. G. D. Shazer and G. H. Dieke, *J. Chem. Phys.*, 1963, **38**, 2190– 2199.

[25] W. T. Carnall, G. L. Goodman, K. Rajnak and R. S. A. Rana, *J. Chem. Phys.*, 1989, **90**, 3443– 3457.
[26] W. T. Carnall, In Energy level structure and transition probabilities in the spectra of the trivalent lanthanides in LaF_3; Eds.; W. T. Carnall, H. Crosswhite and H. M. Crosswhite, Department of Physics, the John Hopkins University: Baltimore, MD, 1978.
[27] B. G. Wybourne, Spectroscopic properties of the rare earths; J. Wiley and Sons Inc., New York, 1965.
[28] G. S. Ofelt, *J. Chem. Phys.*, 1963, **38**, 2171–2180.
[29] B. R. Judd, *J. Chem. Phys.*, 1966, **44**, 839–840.
[30] C. Holzer, A. M. Wernbacher, J. M. Senekowitsch, K. Gatterer and A. M. Kelterer, *J. Phys. Chem. A*, 2014, **118**, 11499–11511.
[31] F. Jensen, Introduction to computational chemistry, 2nd ed.; John Wiley & Sons, inc., England, 2007.
[32] M. J. Frisch, G. W. Trucks, H. B. Schlegel, G. E. Scuseria, M. A. Robb, J. R. Cheeseman, G. Scalmani, V. Barone, B. Mennucci, G. A. Petersson, H. Nakatsuji, M. Caricato, X. Li, H. P. Hratchian, A. F. Izmaylov, J. Bloino, G. Zheng, J. L. Sonnenberg, M. Hada, M. Ehara, K. Toyota, R. Fukuda, J. Hasegawa, M. Ishida, T. Nakajima, Y. Honda, O. Kitao, H. Nakai, T. Vreven, J. A. Montgomery, Jr., J. E. Peralta, F. Ogliaro, M. Bearpark, J. J. Heyd, E. Brothers, K. N. Kudin, V. N. Staroverov, R. Kobayashi, J. Normand, K. Raghavachari, A. Rendell, J. C. Burant, S. S. Iyengar, J. Tomasi, M. Cossi, N. Rega, J. M. Millam, M. Klene, J. E. Knox, J. B. Cross, V. Bakken, C. Adamo, J. Jaramillo R. Gomperts, R. E. Stratmann, O. Yazyev, A. J. Austin, R. Cammi, C. Pomelli, J. W. Ochterski, R. L. Martin, K. Morokuma, V. G. Zakrzewski, G. A. Voth, P. Salvador, J. J. Dannenberg, S. Dapprich, A. D. Daniels, Ö. Farkas, J. B. Foresman, J. V. Ortiz, J. Cioslowski and D. J. Fox, Gaussian 09, Revision A.1, Gaussian, Inc., Wallingford CT, 2009.
[33] A. D. Becke, *Phys. Rev. A*, 1988, **38**, 3098–3100.
[34] C. T. Lee, W. T. Yang and R. G. Parr, *Phys. Rev. B: Condens. Matter*, 1988, **37**, 785–789.
[35] R. Krishnan, J. S. Binkley, R. Seeger and J. A. Pople, *J. Chem. Phys.*, 1980, 72, 650–654.
[36] R. E. Stratmann, G. E. Scuseria and M. J. Frisch, *J. Chem. Phys.*, 1998, **109**, 8218–8224.
[37] (a) N. N. Matsuzawa, A. Ishitani, D. A. Dixon and T. Uda, *J. Phys. Chem. A*, 2001, **105**, 4953–4962; (b) M. E. Casida, C. Jamorski, K. C. Casida and D. R. Salahub, *J. Chem. Phys.*, 1998, **108**, 4439–4449.
[38] M. Cossi, G. Scalmani, N. Regar and V. Barone, J. Chem. Phys., 2002, 117, 43–54. V. Barone, M. Cossi and J. Tomasi, J. Chem. Phys., 1997, 107, 3210–3221.
[39] B. Rajamouli and V. Sivakumar, *New J. Chem.*, 2017, **41**, 1017–1027.
[40] P. Strohriegl, D. Wagnera, P. Schrögela, S. T. Hoffmannb, A. Kohlerb, U. Heinemeyerc and I. Munster, Proc. of SPIE, 2013, **8829**, 882906.
[41] H. Mu, W. Li, R. Jones, A. Steckl and D. Klotzkin, *J. Lumin.*, 2007, **126**, 225–229.
[42] S. I. Ahn, W. K. Kim, S. H. Ryu, K. J. Kim, S. E. Lee, S. H. Kim, J. C. Park and K. C. Choi, *Organic Electronics*, 2012, **13**, 980–984.

[43] (a) R. V. Solomon, P. Veerapandian, S. A. Vedha and P. Venuvanalingam, *J. Phys. Chem. A*, 2012, **116**, 4667–4677; (b) R. V. Solomon, R. Jagadeesan, S. A. Vedha and P. Venuvanalingam, *Dyes pigm.*, 2014, **100**, 261–268.

[44] J. E. True, T. D. Thomas, R. W. Winter and G. L. Gard, *Inorg. Chem*. 2003, **42**, 4437–4441.

[45] S. B. Meshkova, A. V. Kiriyak, Z. M. Topilova and A. M. Andrianovm, *Russ. J. Inorg. Chem.*, 2007, **52**, 556.

Chapter 8

Summary and Conclusions

The present works deals with molecular designing and synthesis of novel class bipolar or ancillary ligand for europium complexes and explore the possibility of using the same in white LEDs, temperature sensor and OLED applications. The observations and the conclusions derived from the present investigations are summarized in this chapter.

8.1 Effects of electron withdrawing groups in imidazole-phenanthroline ligands and their influence on photophysical properties of Eu^{III} complexes for white light emitting diodes

The designed ancillary ligands were synthesized and two of them structurally characterized. Their corresponding Eu-complexes were also been synthesized successfully and studied their photophysical properties syatamatically. The excited energy of the ligand is fully transferring to the Eu-metal ion in the complexes, 1Eu, 2Eu and 3Eu confirmed from the PL emission analysis. However, fluorene integrated with phenthroimazolde show white light emission and the corresponding mono nuclear Eu^{III} complex tris-β-diketones shown red emission. The QY of the complex, 2Eu was shown higher value (39.4 %) indicating that the presence of m-CF_3 leads to improve the efficiency and $Eu(TTA)_3$Phen-pCF_3-Ph showed 78.7 % (thin film). The analysis from the InGaN-based LED (395 nm) also supported the same. The consumption of the emission from the source is higher in m-CF_3 connected complex than remained complexes. The calculated CIE color coordinates for the complexes are shown bright red emission in solution, solid, thin film and LEDs. These are indicating that the fluorine moieties could reduce the non-radiative transition and leads to enhancement in the red emission. The white emissive fluorene based ligand combined with near UV LED show yellowish green emission with CIE color coordinates of x = 0.26, y = 0.36 (1-10) and sky blue, x = 0.20, y = 0.29 (1-50), whereas the Eu complex integrated with near UV LED show red color emission with CIE color coordinates of x = 0.66, y = 0.34, respectively. White emission from LED was obtained from the mixing of ligand and the complex (host guest system) combined with near UV LED. This work demonstrates that the potential usage of the ligand and the complex can give complement color to produce white emission. The prominent results are indicating that the synthesized complexes are efficient and applications to novel organic Eu^{III} devices, like organic liquid lasers, plastic lasers, and optical fibers.

8.2 Design and synthesis of new bipolar ligands based on phenanthroimidazole for tunable emissive Eu^{III} complexes: combined experimental and theoretical study

Successful incorporation of Ph, mCF_3, pCF_3 and Fl moiety in phenanthroimidazole ligands were achieved and their efficient β-diketonate Eu^{III} complexes have been synthesized, spectroscopically characterized. The photophysical, electrochemical properties have been investigated, to know the effect of the substitution in the ligand. All the ligands and complexes show similar UV-Visible absorption behaviour (π - π^*, at ~270, ~360 nm). DFT calculations were supportive of the experimental outcomes. Eu-complexes and its ligands PL study were carried out in solution form as well as in solid and thin film. The study indicates that the Eu-complex emits tunable emission due to incomplete/partial energy transfer (white (solution), red (solid)), whereas fluorene decorated Eu-complex shows narrow band red emission with

appropriate CIE color gamut. The calculated asymmetric ratio (I_2/I_1) clearly indicates that the Eu^{III} ion located in the non-centro symmetric site or the local chemical environment is asymmetric in nature. The obtained PL emission clearly indicates that the efficient energy transfer encountered in case of fluorene based complex. The energy transfer mechanism for all the Eu-complexes was proposed based on combined experimental and theoretical study (DFT, TD-DFT). The PL lifetime of the Eu^{III} complexes also supports the emission behaviour. The calculated band gap of the complex by DRS and CV are almost similar. The Judd–Ofelt spectral intensity parameters, electrochemical study and absolute QY (mCF_3 based Eu-complex shows better QY of 75.9 %) of the Eu-complexes were also been investigated. White and red LED was fabricated using these complexes with near UV LEDs (395 nm). These promising properties are suggesting that the synthesized Eu^{III} molecular complex is a potential red emitters for white LEDs and can be used a ratiometric temperature sensor.

8.3 Carbazole and fluorene functionalized phenanthro-imidazole ancillary ligand based Eu-complexes for leds: detailed photophysical and theoretical study

Two bipolar ligands and their corresponding Eu^{III} complexes were designed and successfully synthesized. DSC-TGA showed good thermal stability and decomposition, which is good for furthered solicitations and good glass transition temperature as well. The PL analysis indicates that all complexes showed pure red emission at around 612 nm, which is due to electric dipole transition of Eu^{III} ion present in the complex. In addition, there is no ligand emission in complex which clearly indicates that the complete energy transfer from the ligand to Eu^{III} metal ion occurs. To support the same, the energy transfer mechanism by computational study (DFT and TD-DFT) also been executed. The obtained absolute QY found to be superior (77.3%) to that of the reported complexes. The Judd–Ofelt theory to the emissive properties of Eu^{III} complexes were investigated and the lifetime found better in $Eu(TTA)_3$Phen-Fl-CBZ complex was to be 0.64 ms. The calculated HOMO-LUMO band gap of the complexes was good for furthered analysis. The fabricated red LED (Eu complexes with 395 nm emitted LED) shown pure red emission and the CIE color coordinates are x = 0.66, y = 0.33. The obtained results indicating that the presently studied complexes may potential application in white LEDs.

8.4 Controlled energy transfer from ligand to Eu^{III} ion: A unique strategy to obtain bright white/red light emission and their versatile applications

The newly synthesized DPA based Eu^{III} complex acting as a single component white-light-emitter and it is due to balancing the primary RGB colors in toluene. Whereas, the CBZ based Eu-complex shows red emission due to complete energy transfer from ligand to Eu^{III} metal ion. The TD-DFT calculations of singlet and triplet excited states and PL lifetime studies also support the energy transfer mechanism. The temperature dependent PL emission color tuning will certainly give direction to use the presently studied DPA based Eu-complex as a temperature sensor. In addition, the same conjugated with LED (395 nm) shown bright white light emission with appropriate CIE coordinates. In contrast, CBZ based Eu-complex shows red emission from the fabricated LED. The PLQY showed better improvement in $Eu(TTA)_3$Phen-fl-TPA-CBZ (44.4%). The TGA-DSC analysis was showed good thermal decomposition, is above 270°C. The electrochemical analysis was shown HOMO and LUMO energy levels for the Eu^{III} complex is around 5.72 and 3.08 eV,

respectively. All the experimental findings supports that the currently synthesized complexes could be useful in white LEDs and ratiometric temperature sensor.

8.5 Mono and binuclear luminescent Eu^{III} molecular complexes for white light emitting diodes: combined Experimental and theoretical study

A new bipolar ligand with spacer moiety was synthesized and used the same for Eu^{III} complex. The PL emission spectra of the complex clearly indicates that the fully energy transfer is happening; the same was also confirmed by DFT and TD-DFT calculations. The spacer molecule can decrease the energy gap of HOMO-LUMO energy levels. In other words, it was increases singlet and triplet energy levels results efficient energy transfer. The improved intensity ratios as well as FWHM were shown better for the complex. The absolute quantum efficiency of the complex showed 11.5% and enhanced quantum efficiency observed by 1% doping of complex in PMMA. The complex has shown worthy thermal decomposition. In addition, we have designed and synthesised two ancillary ligands (in the ligand structure the two phenanthroline moiety connected through phenyl ethoxy spacer (N1 fuctionlized by phenyl and fluorene)) and using this corresponding binuclear Eu-complexes was synthesized successfully. The isolation of the luminescent Eu core was achieved (reduce the concentration quenching effect through non-radiative energy transfer among the Eu ion in the complex). The PL emission spectral study of the ligands shown blue to greenish yellow (solution to solid) and their respective complexes showed efficient characteristic red emission. No additional emission in the region of 400-550 nm indicates the efficient energy transfer (confirmed by DFT and TD-DFT calculations). The calculated spectral parameters shown currently synthesized ligands are good sensitizers for Eu^{III} metal ion. The suppression of radiationless transitions caused by vibrational relaxation or non-radiative energy migration is reduced comparatively significant in the thin film of the complex $Eu_2(TTA)_6(L2)$ compare to that of complex $Eu_2(TTA)_6(L1)$ leads to highest QY (59.5 %), fluorene sensitization also plays a vital role. The fabricated LED conjugated with Eu-complex shown efficient red emission. These observations are indicating that the presently synthesized complexes are potential in lighting applications.

8.6 Designing of ancillary ligands / organic chromophores and study their excited photophysical properties for Eu^{III} complexes – A theoretical approach

Numerous ligands were designed and studied their excited state photophysical properties by theoretical study. The systematic study of the excitation window by DFT method revealed strong π-π^* transition of the ligands due to presence of aromatic rings. The triplet level location also been calculated by using TD-DFT method and found that among three (1a-f, 2a-f, 3a-f) series a-f shown better energy matching with the excited state ($^5D_0$) of Eu^{III} ion and could facilitate the efficient energy transfer from ligand to Eu ion. In addition, the substituted phenyl moiety (mCF_3 and pCF_3) at N1-position in the phenanthro-imidazole ligand give additional benefits by reducing the triplet energy comparatively with other substitution that leads to efficient energy transfer from L to Eu ion in the complex could be expected. The systematic theoretical is certainly leads synthesis the best ligand molecules for Eu complexes. In addition, some of the ligands can also serve as host materials for triplet dopant.

8.7 Scope for future work

1. The synthesized potential Eu-complexes to be screened for OLED applications with suitable device structure.
2. Temperature dependent PL study of the dual emissive europium complexes to be carried out for possible application colorimetric or ratiometric temperature sensor.
3. Tailoring the bipolar or ancillary ligand and utilize the same for the synthesis of Eu-complexes obtain single molecule white emissive Europium complexes.
4. Theoretically screened ambipolar ancillary ligands to be used to synthesize terbium (Tb) and europium (Eu) complexes.
5. N1 substitution with different functional groups can be executed in the phenanthro-imidazole binuclear Eu-complexes.

Publications:

1. **B. Rajamouli**, P. Sood, S. Giri, V. Krishnan and V. Sivakumar, "New dual characteristic bidentate ligand for ternary mono nuclear europium(III) molecular complex: synthesis, photophysical, electrochemical and theoretical study'' *Eur. J. Inorg Chem.*, 2016, 24, 3900-3911.
2. **B. Rajamouli** and V. Sivakumar, "Effect of carbazole functionalization with a spacer moiety in the phenanthroimidazole bipolar ligand in a Europium(III) complex on its luminescence properties: combined experimental and theoretical study'' *New J. Chem.,* 2017, 41, 1017-1027.
3. **B. Rajamouli,** C. S. Dwaraka Viswanath, S. Giri, C. K. Jayasankar and V. Sivakumar, "Carbazole functionalized new bipolar ligand for monochromatic red light emitting Europium(III) complex: combined experimental and theoretical study"- *New J. Chem.*, 2017, 41, 3112-3123.
4. **B. Rajamouli** and V. Sivakumar, "Carbazole and fluorene functionalized phenanthro-imidazole ancillary ligand based Eu(III) complexes for LEDs: Detailed photophysical and theoretical study'' *Chemistry Select*, 2017, 2, 4138–4149.
5. **B. Rajamouli,** Rachna Devi, Abhijeet Mohanty, Venkata Krishnan and V. Sivakumar, "Effects of electron withdrawing groups in imidazole-phenanthroline ligands and their influence on photophysical properties of Eu^{III} complexes for white light emitting diodes'' *New J. Chem.*, 2017, 41, 9826–9839.
6. S. Kasturi, **B. Rajamouli** and V. Sivakumar, "Versatile luminescent Europium(III)–β-diketonate-imidazo-bipyridyl complexes intended for white LEDs: A detailed photo-physical and theoretical study" *Inorg. Chem.*, 2017, 56, 9376–9390.
7. **B. Rajamouli** and V. Sivakumar, "White light emissive bipolar ligand and their Eu^{III} complex for white/red light emitting diodes'' *Journal of Photochemistry and Photobiology A: Chemistry*, 2017, *J. Photochem. Photobio. A*, 2017, 347, 26-40.
8. **B. Rajamouli**, S. Kasturi, S. Giri and V. Sivakumar, "Controlled energy transfer from ligand to Eu(III) ion: A unique strategy to obtain bright white light emission and their versatile applications" *Inorg. Chem.*, 2017, 56, 10127–10130.
9. **B. Rajamouli** and V. Sivakumar, "Bi-nuclear luminescent Europium(III) molecular complexes for white light emitting diodes: Experimental and theoretical study'' *Photochemical & Photobiological Sciences,* 2017 (submitted).
10. S. Kasturi, **B. Rajamouli,** K. Aravind Babu, S. Giri, M. J. Allen and V. Sivakumar, "Effect of N-conjugation in imidazo-bipyridyl ancillary ligands, their energy transfer impact on Eu(III)–β-diketonate complexes for white LEDs", *Inorg. Chem.*, 2017 (submitted).
11. **B. Rajamouli,** S. Nayak and V. Sivakumar, Effects of N1-subtitution in imidazole-phenanthroline ancillary ligands on photophysical properties for Eu(III) complexes (to be communicated).
12. **B. Rajamouli,** and V. Sivakumar, White light emissive Eu(III) complex for white LEDs (to be communicated).
13. **B. Rajamouli,** and V. Sivakumar, Functionalized phenanthro-imidazole based Eu^{III} complex for temperature and colorimetric sensing and white LED applications (to be communicated).
14. **B. Rajamouli,** and V. Sivakumar, A theoretical approach – manipulating the ligand excited state to obtain white emission and estimate the energy transfer process (to be communicated).

Book Chapter:

1. V. Sivakumar and **B. Rajamouli**, Molecular designing of Luminescent Europium Metal Complexes for OLEDs: An Overview, 2017, Pan Stanford Publishing, Singapore.

Papers Presented in Conference Proceedings:

In National Conference Proceeding:

1) **B.Rajamouli** and V.Sivakumar, "Synthesis and photo physical studies of multifunctional Europium molecular complex for OLEDs" in NCLA 2014 February 5 - 7, Rani Durgavati University, Jabalpur, M.P – Poster presentation.
2) **B. Rajamouli** and V. Sivakumar, ''Tunable luminescent Europium molecular complexes for lighting applications: Experimental and theoretical study'', in RSW, Feb 21 – 23, 2017, NIT Rourkela, Odisha – Poster presentation.
3) **B. Rajamouli** and V. Sivakumar, ''Carbazole consequences in Europium complexes for phosphorescent OLEDs'' in RSW, Feb 12-14, 2016, NIT Rourkela, Odisha – Poster presentation.
4) **B. Rajamouli** and V.Sivakumar, ''Synthesis of binuclear nuclear Eu^{III} complex and their photophysical study for phosphorescent OLEDs'', in NCLA, Feb 18-20, 2016, Nagpur, India – Poster presentation.
5) **B. Rajamouli** and V.Sivakumar, ''New ternary Europium (III) molecular complex for OLEDs: combined experimental and theoretical study'', in NCLA, Jan 9-11, 2017, IICT, CSIR laboratory, Hyderabad – Poster presentation.

In International Conference Proceeding:

1) **B.Rajamouli** and V.Sivakumar, "Synthesis of multifunctional Europium molecular complex for phosphorescent OLEDs" in The International Conference on Luminescence, 13-18 july 2014, Wroclaw, Poland – Poster Presentation.
2) **B.Rajamouli** and V.Sivakumar, "Design and synthesis of bipolar ligands for Eu molecular complexes and their photophysical study" in 8th Singapore International Chemistry Conference 2014 (SICC8), 14-17 Dec 2014, University Town Campus, Singapore – Oral presentation.
3) **B.Rajamouli** and V.Sivakumar, "Synthesis of carbazole derivatives of Europium molecular complexes for phosphorescent OLEDs" in ICLA 2015 February 9-12, Dr. M.R. Doreswamy Auditorium, PES University, Bangalore, K.P. – Poster presentation.
4) **B.Rajamouli** and V.Sivakumar, "Smart red radiating Eu(III) molecular materials for energy efficient phosphorescent OLEDs'' in Sustainable Energy Technology for Smart and Clean Cities (SETS & CC – 2016), July 27-29, 2016, Amara Raja Auditorium, Karkambadi, Tirupathi, Andhrapradesh – Oral presentation.
5) Rachana Devi, **B. Rajamouli** and V. Sivakumar, "Experimental and theoretical investigation of bi and tri nuclear EuIII complexes for red/white emitting LEDs" in 8th East Asia Symposium on Functional Dyes and Advanced Materials (EAS8), September 20-22, 2017, CSIR-NIIST, Thiruvananthapuram, Kerala, India.

CURRICULUM VITAE

RAJAMOULI BODDULA,
Ph. D Scholar, Dept. of Chemistry,
NIT Rourkela, Odisha, INDIA.
Email: rajamouliboddula@gmail.com
Mobile no: 7735011605, 9704245340.

Ph. D., Department of Chemistry (Inorganic Chemistry), National Institute of Technology, Rourkela, Odisha, India, 2013-2017 (submittion on May 2017).

M. Sc., Chemistry (Organic Chemistry), Smt. Jaasti Bullammai P.G. College, Andhra University, Andhra Pradesh (A. P.), India, 2010 (CGPA 7.1, First Class)

B. Sc., Chemistry with Botany and Zoology, Masterji Degree & P.G. Coleege, Kakathiya University, Warangal, Andhra Pradesh, India, 2008 (68.1 %, First Class).

Intermediate (10+2) Chemistry with Botany, Zoology and Physics, Board of Intermediate Education, Sriharsha Junior College, Andhra Pradesh, India, 2005 (62.5 %, First Class).

SSC (10^{th}), Kakatiya Vidyalayam, Board of Secondary Education, Andhra Pradesh, India, 2003 (80.5 %, Distinction).

Thesis Title:

Luminescent Eu^{III} complexes based on phenanthro-imidazole ligands for white LEDs/OLEDs and temperature sensors: combined experimental and theoretical investigations.

Area of Study: Lanthanide based luminescenct materials, experimental, theoretical study and their LED/OLEDs applicatios as well as sensing applications

Advisor: Dr. V. Sivakumar,

Assistant Professor,

Department of Chemistry

National Institute of Technology, Rourkela, Odisha, India, 769008.

Email: vsiva@nitrkl.ac.in, siva.vai@gmail.com,

Ph: 0661-2462654 (O), 0661-2463654 (R).

Research & Professional Experience

- Senior Research Fellow, National Institute of Technology Rourkela (NITR), Odisha, India – Sep 2015 to May 2017.
- Senior Research Fellow, Board of Research in Nuclear Sciences (BRNS), DAE, India –Jan 2015 to Aug 2015.
- Junior Research Fellow, Board of Research in Nuclear Sciences (BRNS), DAE, India –Jan 2013 to Dec 2014.
- Senior chemist in GVK BIO & CO., Hyderabad, India from July 2012- Dec 2012 in R&D Department.
- Junior chemist in GVK BIO & CO., Hyderabad, India from July 2011- July 2012 in R&D Department.
- Lecturer in Masterji Degree & P.G. College, Warangal, Telangana, India, from July 2010-July 2011.

Technical Skills (Experimental and Theoretical)

- Familiar with modern methods of organic synthesis and also capable of doing multi step synthesis in mg to gm level.
- Maintaining perfect documentation and performing good laboratory standard operating procedures **(SOP).**
- Handled reagents such as oxidising agents, reducing agents, pyrophoric agents, protection groups, hazardous reagents.
- Characterization of compounds through interpretation of NMR, Mass (LCMS and GCMS), Elemental analysis, FT-IR spectroscopy and HPLC.
- Photophysical study such as UV-absorption, Photoluminescence (QY, lifetime and J-O parameters (solution, solid and thin film)) and CIE color coordinates.
- Electrochemical experiments such as cyclic voltammetry anlysis.
- LED fabrication and their photophysical characterization.
- Computational study (DFT and TD-DFT with the Gaussian 09 package), Becke's three-parameter functional (B3) with the Lee–Yang–Parr (LYP) correlation functional in combination with Pople basis sets (6-311+G*).

COMPUTER AWARENESS

PGDCA (Microsoft Office), Chemcraft, Chemdraw, Origin, Scifinder, Reaxys, Matlab, Mercury, Dimand, Gassian (DFT), Ortep, etc

Honours and Affiliation:

- Received (exceptional performance) outstanding achievement award in GVK BIO & CO., Hyderabad, 2012.
- Qualified in Graduate Aptitude Test in Engineering (GATE) in Chemistry, 2011.
- Best and active participant in schools (appreciation) as well as in college level.

Personal Profile:

Name	:	RAJAMOULI BODDULA
Father's name	:	BHADRAIAH
Date of birth	:	12-06-1988
Marital Status	:	Married
Nationality	:	Indian
Languages known	:	Telugu, Hindi and English (reading and writing)
Permanent address	:	C/o Boddula Kistaiah, Vill: Peddampally, Mdl: Regonda (post), Dist: Warangal, Telangana state, INDIA, Pin: 506 348.

Annexure I
(Chapter 2)

Effects of electron withdrawing groups in imidazole-phenanthroline ligands and their influence on photophysical properties of Eu^{III} complexes for white light emitting diodes

Contents

27. **Figure 2.S14.** The triplet state energy level calculation from the phosphorescence emission spectra of the Gd^{III} coordinated ligand at 77K (left), the PL emission spectra of the ligand and UV-absorption spectra of the TTA at room temperature (right).
28. **Table 2.ST13.** The ligand and corresponding Eu^{III} complex CIE color coordinates in thin film.
29. **Figure 2.S15.** The lifetime of the ligand in different excitation from 300-420 nm in solid form.

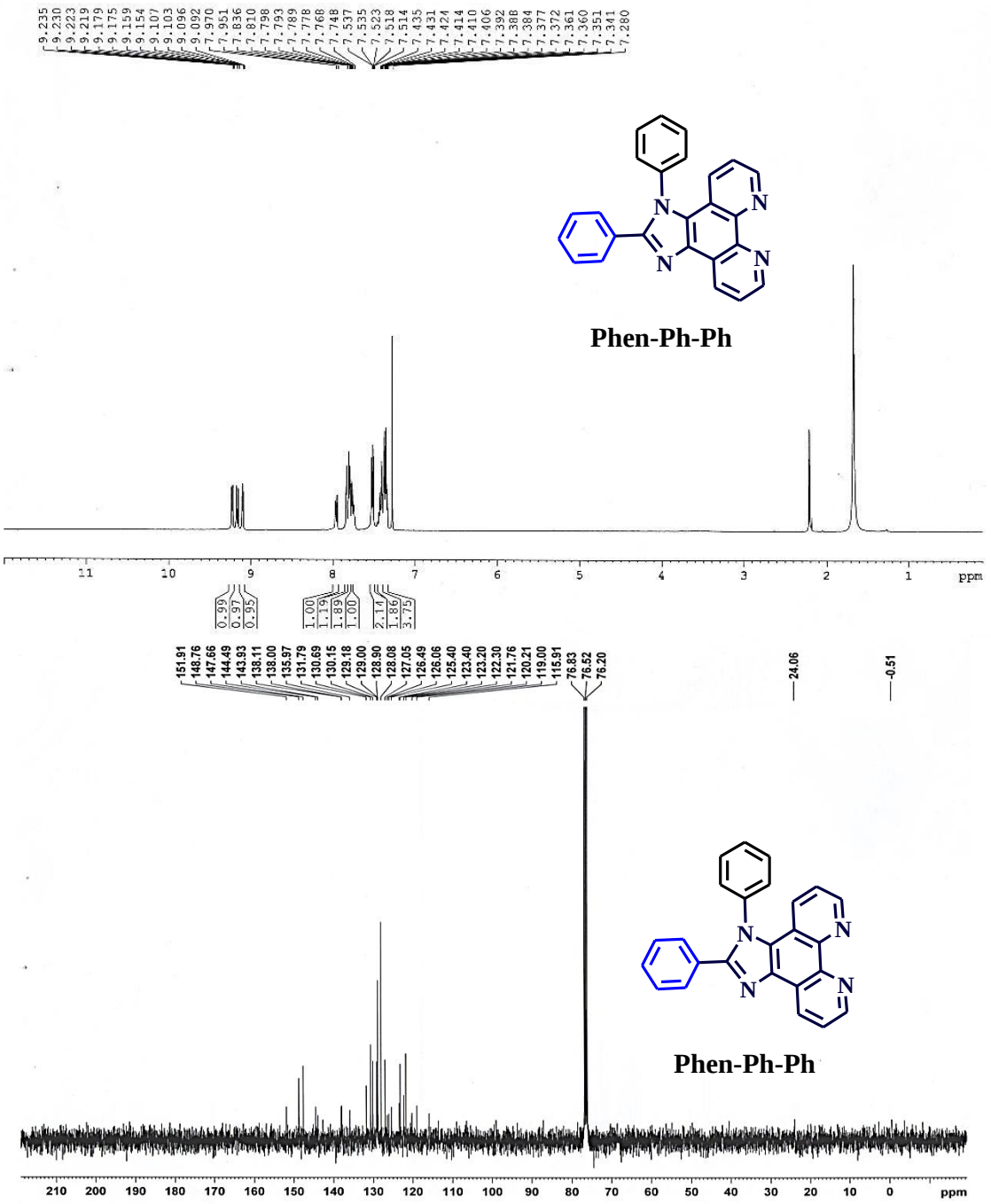

Figure 2.S1 The ^{1}H (top) and ^{13}C (bottom) NMR of the 1L ligand.

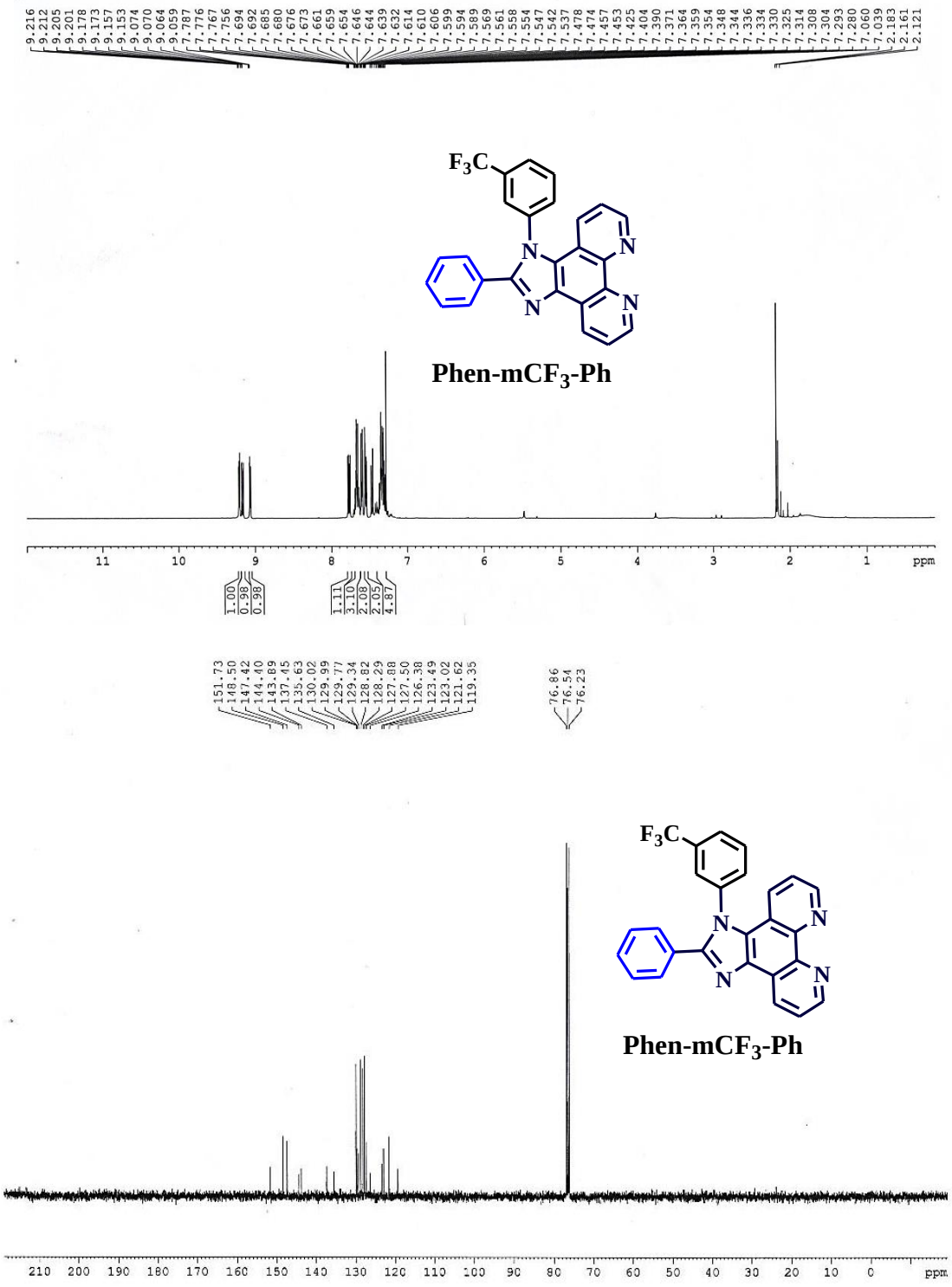

Figure 2.S2 The ^{1}H (top) and ^{13}C (bottom) NMR of the 2L ligand.

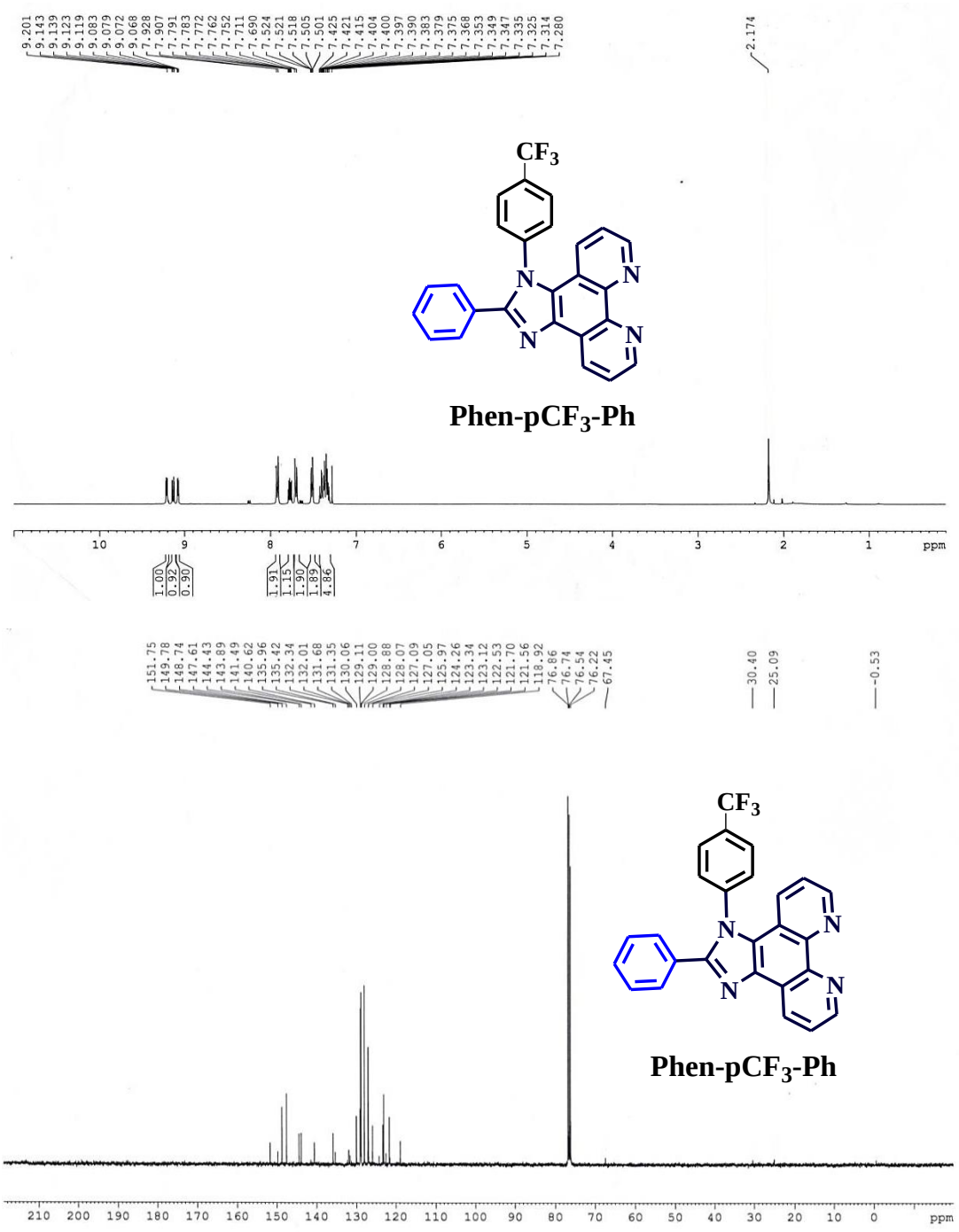

Figure 2.S3 The ^{1}H (top) and ^{13}C (bottom) NMR of the 3L ligand.

Table 2.ST1 The PL intensity of the magnetic and electric dipole transitions of the complexes and their ratio of the Eu^{III} complexes in solution form as well as solid form.

S.No.	Complex name	$^5D_0$-$^7F_1$ (a.u.)	$^5D_0$-$^7F_2$ (a.u.)	Ratio
		Solution Phase		
1.	**$Eu(TTA)_3$Phen-Ph-Ph**	280058.74	3505695.0	12.52007
2.	**$Eu(TTA)_3$Phen-mCF_3-Ph**	1629022.00	2274303.8	13.961201
3.	**$Eu(TTA)_3$Phen-pCF_3-Ph**	1097453.91	16787376.4	15.2967
		Solid Phase		
1.	**$Eu(TTA)_3$Phen-Ph-Ph**	8280000	531000000	6.41304
2.	**$Eu(TTA)_3$Phen-mCF_3-Ph**	3940000	41800000	10.6091
3.	**$Eu(TTA)_3$Phen-pCF_3-Ph**	723554.76	11400000	15.756

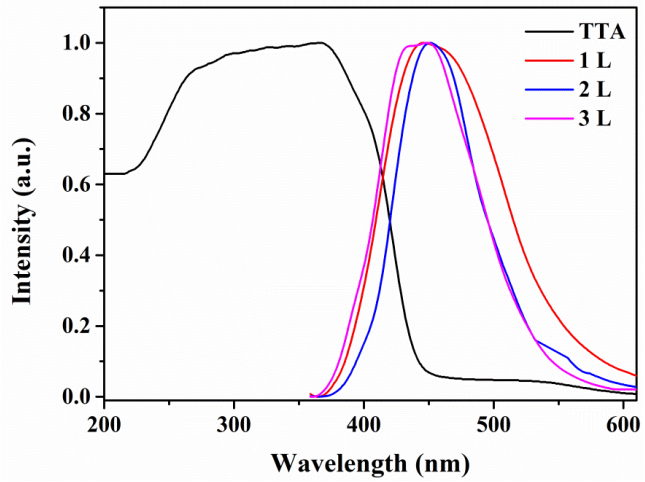

Figure 2.S4 The emission spectrum of ligands, 1L, 2L and 3L and UV-vis absorption spectra of the TTA at room-temperature.

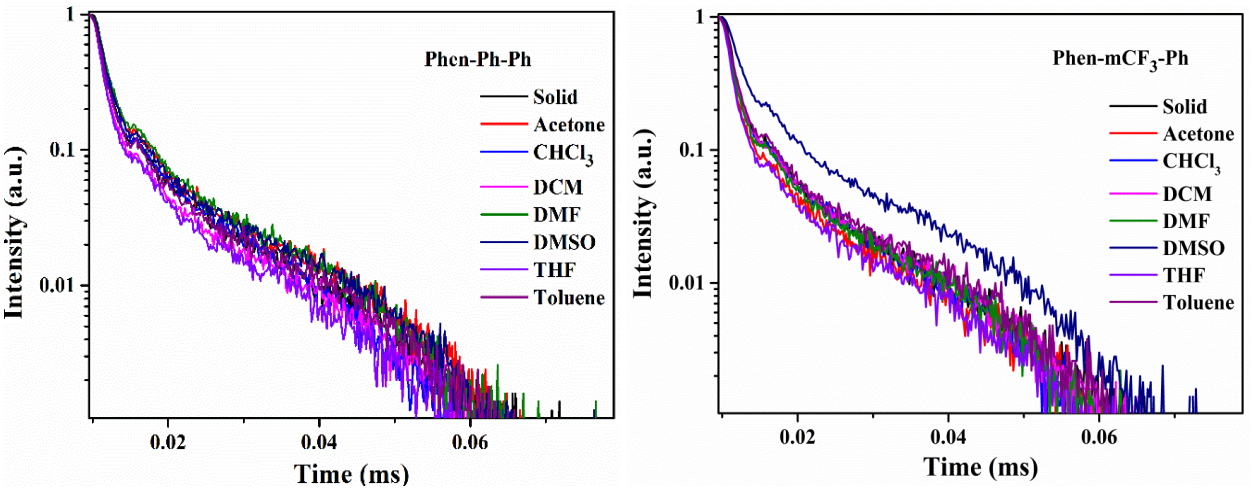

Figure 2.S5 The lifetime of the ligand, Phen-Ph-Ph in different solvents, the lifetime of the ligand, Phen-mCF_3-Ph in different solvents.

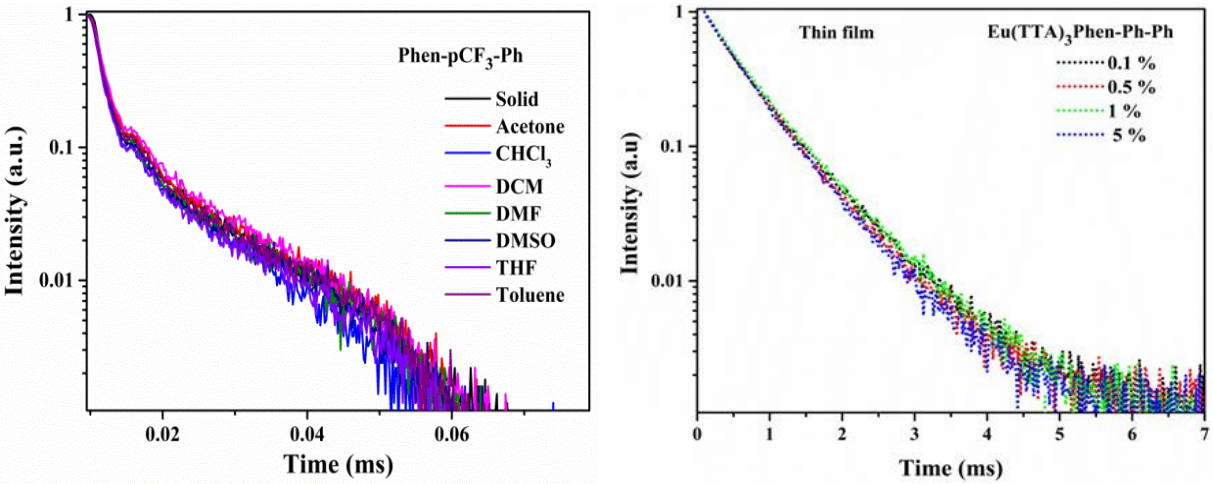

Figure 2.S6 The lifetime of the ligand, Phen-pCF_3-Ph in different solvents, the lifetime of thin film of the Eu-complex, Eu(TTA)$_3$Phen-Ph-Ph in different concentrations.

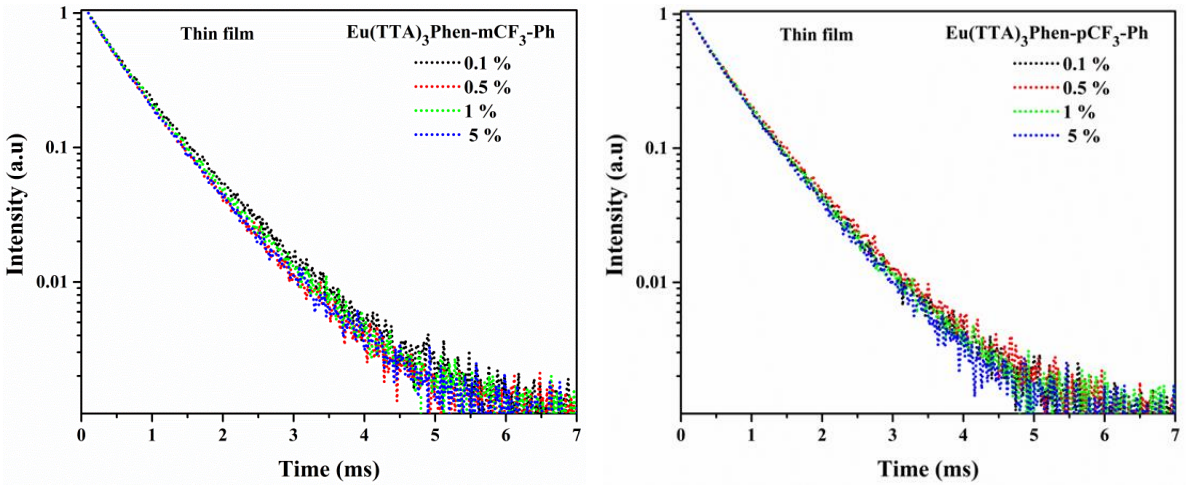

Figure 2.S7 The lifetime of thin film of the Eu-complex, Eu(TTA)$_3$Phen-mCF_3-Ph (right) and Eu(TTA)$_3$Phen-pCF_3-Ph (left) in different concentrations.

Table 2.ST2 The calculated experimental branching ratios ($\beta_{1\text{-}3}$) of the complexes.

S. No.	Compound	β_1	β_2	β_3
1.	**1Eu, Solution**	6.68	88.30	4.83
2.	**Solid**	12.52	80.47	7.27
3.	**Thin film, 0.1%**	15.93	72.47	11.58
4.	**0.5 %**	14.32	76.05	9.61
5.	**1 %**	19.41	69.9	10.68
6.	**5 %**	25.1	61.09	13.80
7.	**2Eu, Solution**	5.62	90.45	3.91
8.	**Solid**	8.21	85.37	6.41
9.	**Thin film, 0.1%**	15.47	73.47	11.05
10	**0.5 %**	19.09	70.19	10.70
11.	**1 %**	19.16	68.58	12.25
12.	**5 %**	23.67	65.80	13.52

13.	**3Eu, Solution**	6.16	89.49	4.33
14.	**Solid**	5.86	88.30	5.83
15.	**Thin film, 0.1%**	14.23	72.06	13.70
16.	**0.5 %**	22.21	67.22	10.56
17.	**1 %**	15.71	70.01	14.26
18.	**5 %**	24.21	62.26	13.51

Table 2.ST3 The CIE color coordinates calculated out comes of the Eu^{III} complexes and their intensity ratios in thin film.

Complex	**Thin film**			
	Asym. Ratio	**CIE**		**FWHM**
		x	y	
1Eu 0.1%	9.15	0.619	0.379	9.42
0.5%	8.17	0.633	0.365	10.58
1.0%	5.16	0.637	0.361	13.63
5.0%	2.63	0.6341	0.365	17.91
2Eu 0.1%	7.50	0.617	0.381	10.37
0.5%	5.32	0.625	0.373	13.50
1.0%	4.56	0.633	0.365	14.19
5.0%	2.94	0.637	0.361	17.13
3Eu 0.1%	9.45	0.575	0.421	9.56
0.5%	7.69	0.579	0.417	10.68
1.0%	4.74	0.582	0.415	13.91
5.0%	3.09	0.586	0.411	16.89

Table 2.ST4 The CIE color coordinates calculated results from the PL emission spectra of the Eu^{III} complexes in solution at different excitation source.

Solution				
Compounds	**x**	**y**		**λ_{ex} (nm)**
$Eu(TTA)_3Phen$-Ph-Ph	0.625007	0.325309		291
	0.625347	0.338608		372
$Eu(TTA)_3Phen$-mCF_3-Ph	0.59976	0.316711		273
	0.641875	0.332231		340
	0.6418866	0.332868		371
$Eu(TTA)_3Phen$-pCF_3-Ph	0.644295	0.333256		342
	0.631659	0.327631		374

Table 2.ST5 The CIE color coordinates calculated results from the PL emission spectra of the ligands in solution form at different excitation source.

Solution				
Compounds	**x**	**y**		**λ_{ex} (nm)**
Phen-Ph-Ph	0.218529	0.138168		246
	0.159785	0.0395788		329
	0.180163	0.0745647		271

Phen-mCF$_3$-Ph	0.176331	0.0675948		290
	0.159286	0.0410187		340
Phen-pCF$_3$-Ph	0.171973	0.0610895		271
	0.160165	0.0393145		321

Table 2.ST6 The CIE color coordinates calculated results from the PL emission spectra of the Eu^{III} complexes in solid form at different excitation source.

SOLID				
Compounds	**x**	**y**	**colour**	**λ_{ex} (nm)**
Eu(TTA)$_3$Phen-Ph-Ph	0.639333	0.341546		270
	0.644392	0.348862		360
Eu(TTA)$_3$Phen-mCF$_3$-Ph	0.632984	0.342448		270
	0.648876	0.34382		360
Eu(TTA)$_3$Phen-pCF$_3$-Ph	0.589598	0.34419		270
	0.642717	0.342321		360

Table 2.ST7 The CIE color coordinates calculated results from the PL emission spectra of the ligands in solid form at different excitation source.

Solution				
Compounds	**x**	**y**		**λ_{exc} (nm)**
Phen-Ph-Ph	0.166401	0.175981		339
	0.165785	0.179578		380
Phen-mCF$_3$-Ph	0.162099	0.135490		349
	0.162286	0.1360187		380
Phen-pCF$_3$-Ph	0.151671	0.112979		353
	0.156015	0.113045		380

Table 2.ST8 The HOMO-LUMO and singlet triplet calculations of the ligands.

Ligands	**HOMO**	**LUMO**	**Band gap**	**S1 (eV)**		**T1 (eV)**	
		(eV)		**gas**	**dcm**	**gas**	**dcm**
Phen-Ph-Ph	5.742	1.516	4.226	3.488	3.613	2.774	2.807
Phen-mCF$_3$-Ph	5.894	1.877	4.017	3.510	3.629	2.768	2.803
Phen-pCF$_3$-Ph	5.918	1.901	4.017	3.489	3.638	2.767	2.804

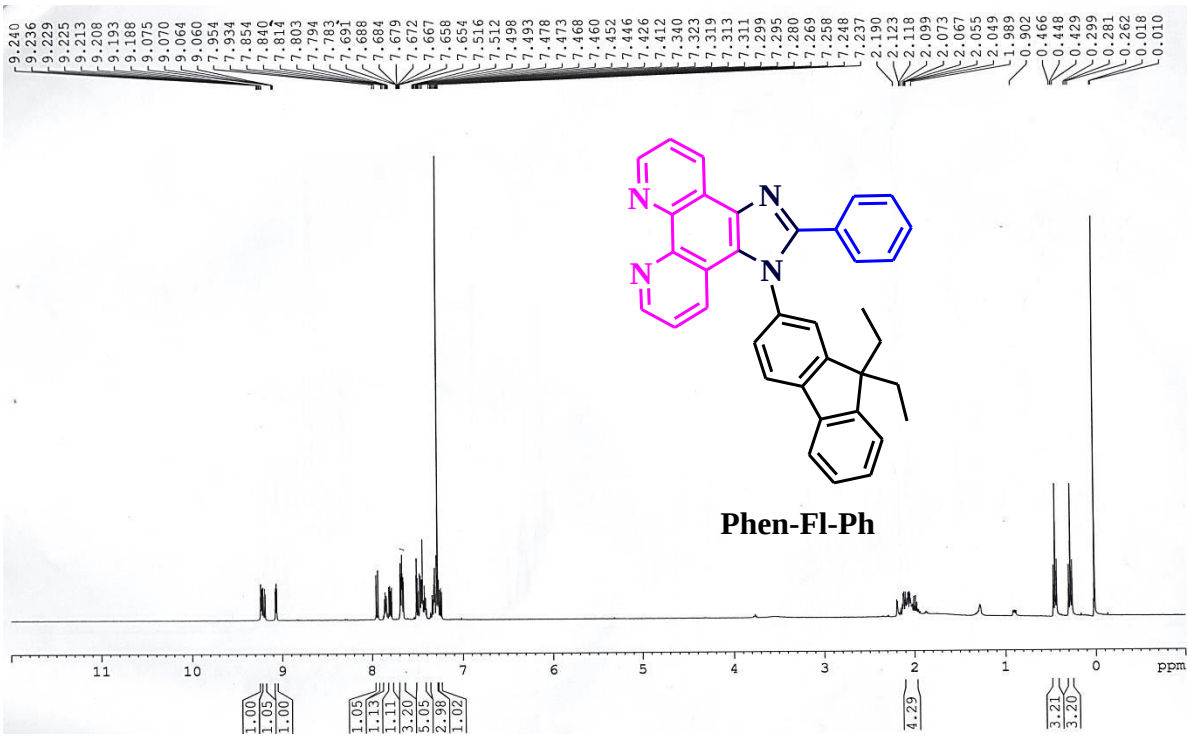

Figure 2.S8 The ^{1}H-NMR of the ligand, Phen-Fl-Ph.

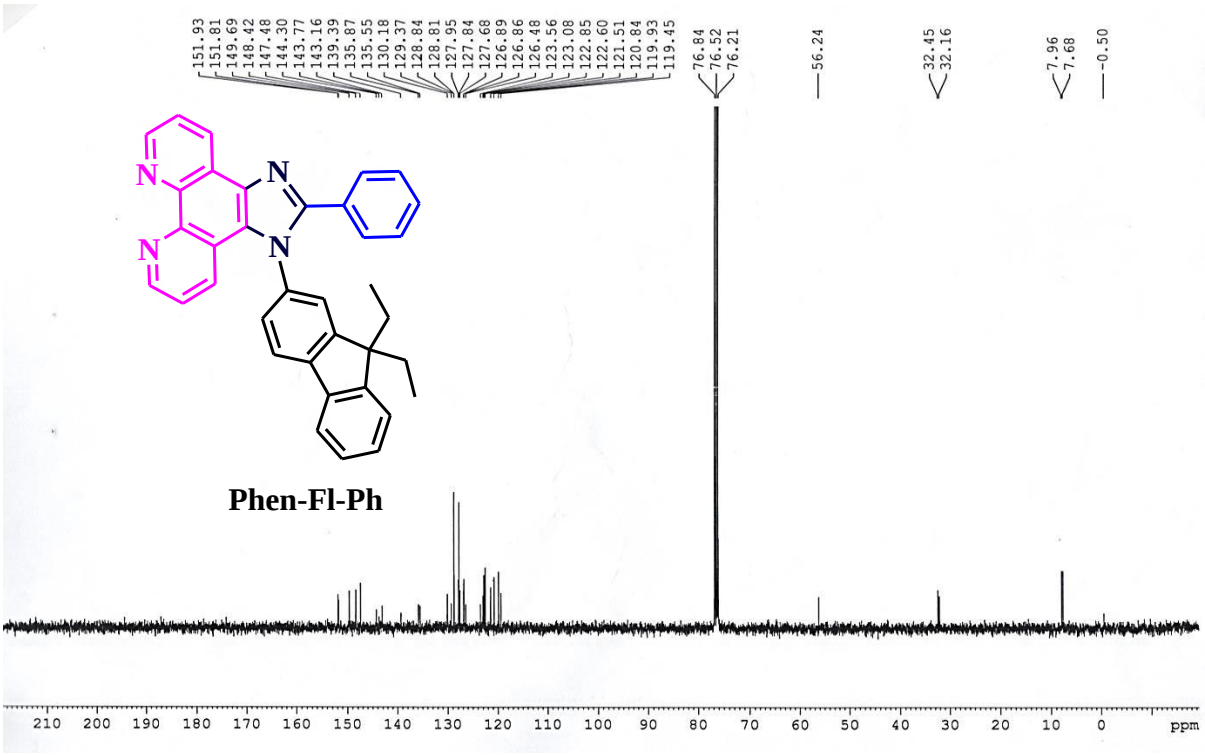

Figure 2.S9 The ^{13}C-NMR of the ligand, Phen-Fl-Ph.

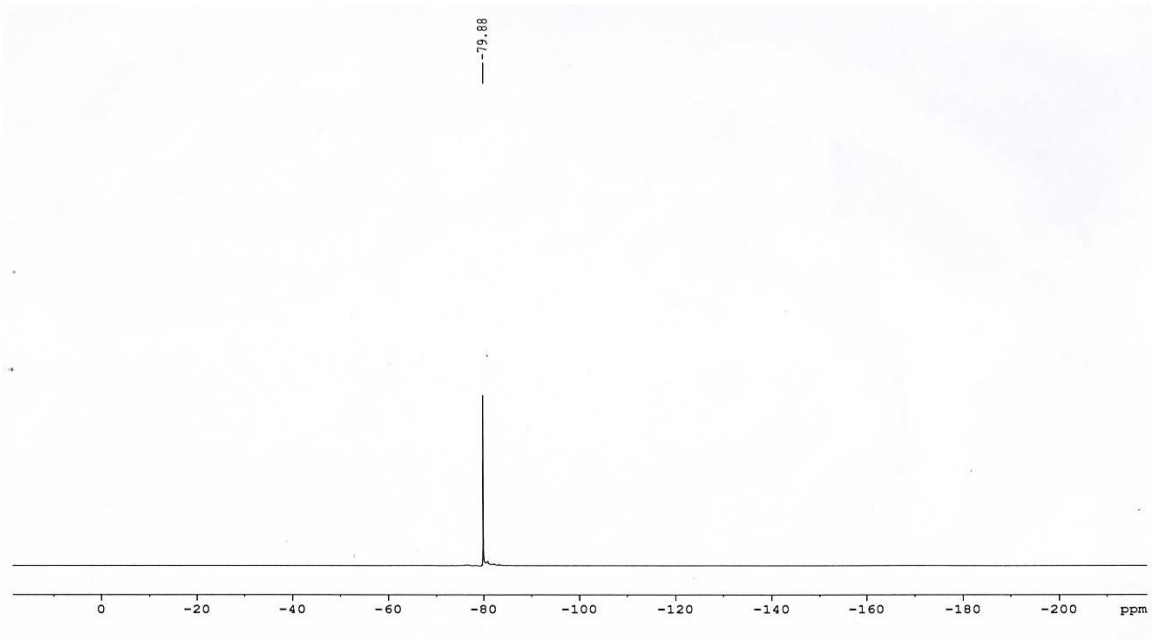

Figure 2.S10 The ^{19}F-NMR spectra of the complex, Eu(TTA)$_3$Phen-Fl-Ph.

Eu(TTA)$_3$.2H$_2$O characterization:

To know the structure formation of Eu(TTA)$_3$. 2H$_2$O, the complex have been characterized by FT-IR, Elemental analysis and ^{1}H-NMR analysis. The FT-IR spectra of TTA ligand shows C=O ($\nu_{c=o}$) stretching frequency at 1663 cm^{-1} and the corresponding Eu(TTA)$_3$ shows C=O ($\nu_{c=o}$) stretching frequency at 1609 cm^{-1}, respectively. The difference (54 cm^{-1}) between these two frequencies were clearly supports the formation of Eu(TTA)$_3$ complex. In FT-IR spectra, the peak appeared at 3409 cm^{-1} for Eu(TTA)$_3$ is attributed to the water molecule. Similarly, TTA molecule also shows the same peak, it is due to the presence of moisture in the KBr pellet. However the broadness and % of transmittance is more for Eu(TTA)$_3$. 2H$_2$O. Elemental analysis: Anal. Calc. for $C_{24}H_{16}EuF_9O_8S_3$: C, 33.85; H, 1.89; S, 11.30. Found: C, 33.60; H, 1.38; S, 10.89%. ^{1}H-NMR Data (400 MHz, DMSO-d$_6$): δ 7.45 (S, 3H), 6.37 (d, 6H), 3.59 (s, 3H).

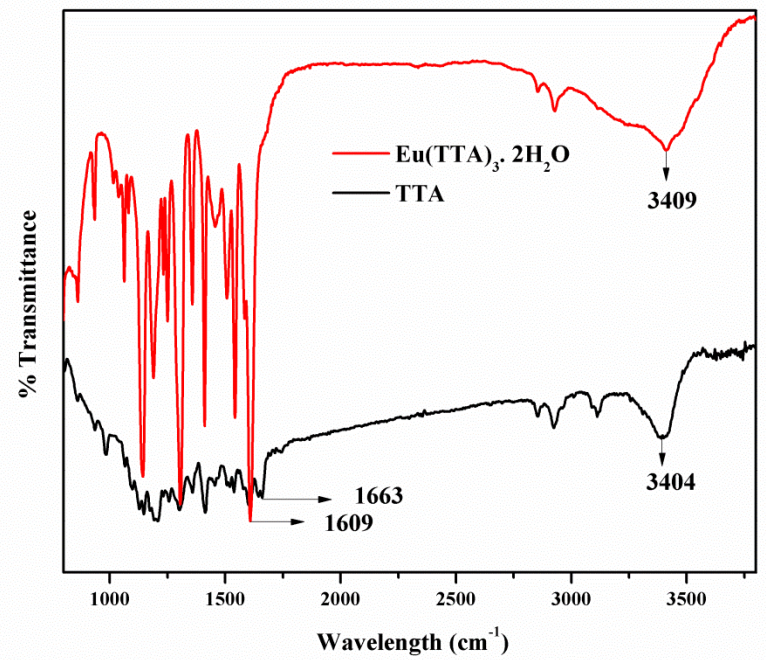

Figure 2.S11 The comparison FT-IR spectra of the TTA and $Eu(TTA)_3.2H_2O$.

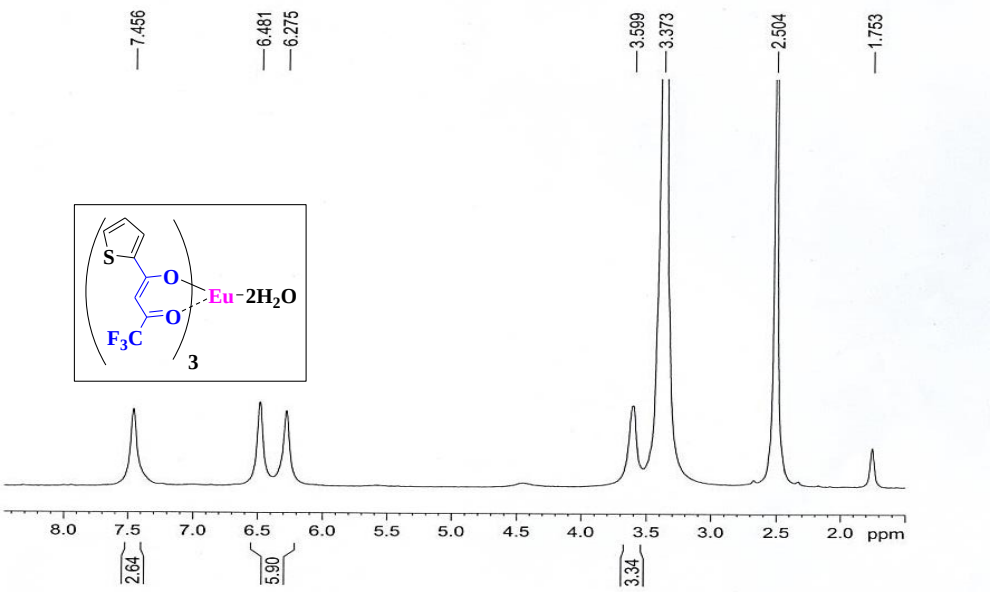

Figure 2.S12 The 1H-NMR spectra of the $Eu(TTA)_3.2H_2O$.

Table 2.ST9 PL spectral data of ligands in various solvents.

Phen-Fl-Ph	λ_{abs} (max) (nm)	λ_{em} (max) (nm)	Stoke's shift ($\Delta\nu$) (cm^{-1})
Toulene	343	400	4154
DCM	344	412	4797
THF	340	407	4841
$CHCl_3$	340	409	4961

EtOAc	341	404	4573
MeOH	367	476	6239
Acetone	340	419	5545
DMF	343	419	5288
DMSO	341	419	5459

Table 2.ST10 The CIE color coordinates of the ligand in different solvent.

S. No.	Phen-Fl-Ph (λ_{exc} in nm)	Solid, CIE	
		x	y
1	**Acetone**	0.1610	0.0720
2	**$CHCl_3$**	0.1634	0.0585
3	**DCM**	0.1675	0.0733
4	**DMF**	0.1620	0.0806
5	**DMSO**	0.1596	0.0731
6	**EtOAC**	0.1662	0.0709
7	**MeOH**	0.2301	0.0288
8	**THF**	0.1632	0.0642
9	**Toluene**	0.1655	0.0513

Table 2.ST11 The CIE color coordinates for the ligand in different excitation source from 300-400 nm.

S. No.	Phen-Fl-Ph (λ_{exc} in nm)	Solid, CIE	
		x	y
1	300	0.3030	0.3371
2	310	0.302909	0.337281
3	320	0.30031	0.337477
4	330	0.300472	0.337939
5	340	0.29995	0.337515
6	350	0.298368	0.336104
7	360	0.297848	0.334295
8	370	0.295492	0.328957
9	380	0.332399	0.385680
10	390	0.382114	0.445974
11	400	0.407202	0.479914

Table 2.ST12 CIE color coordinates for the ligand and the complex in solution and solid phase.

Compounds	x	y	Colours	λ_{ex} (nm)
		Solution		
Phen-Fl-Ph	0.172794	0.00674089		277
	0.159757	0.046403		330
$Eu(TTA)_3$Phen-Fl-Ph	0.641257	0.332481		342
	0.599967	0.31926		291
	0.6310	0.3288		376
		Solid		
Phen-Fl-Ph	0.261269	0.338822		280
	0.30031	0.337477		320

$Eu(TTA)_3Phen$-Fl-Ph	0.638551	0.34138		270
	0.648061	0345129		360

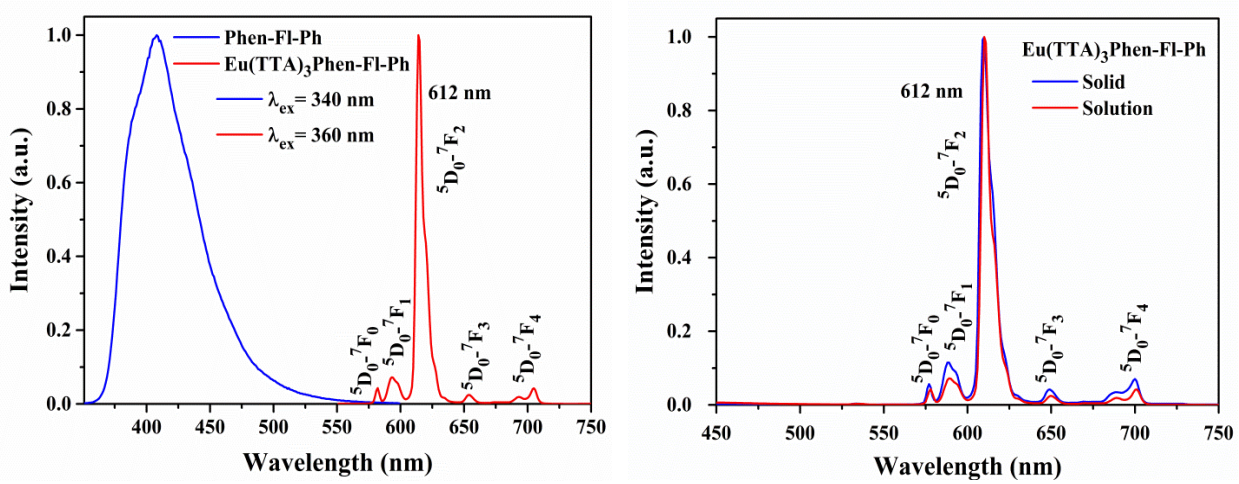

Figure 2.S13 The PL spectra of the ligand (left) and the combined emission spectra of the complex and the ligand (right) in chloroform solution.

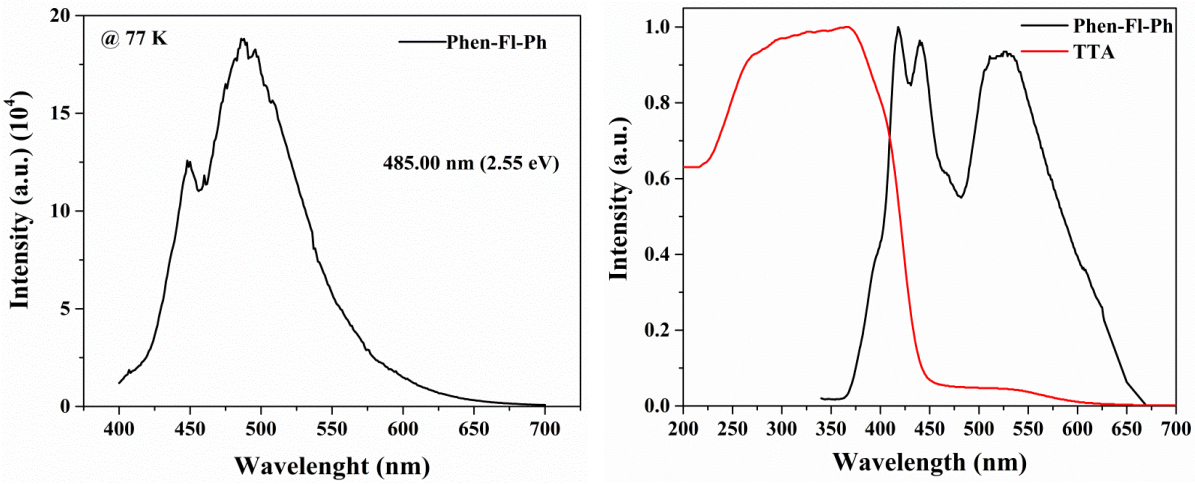

Figure 2.S14 The triplet state energy level calculation from the phosphorescence emission spectra of the Gd^{III} coordinated ligand at 77K (left), the PL emission spectra of the ligand and UV-absorption spectra of the TTA at room temperature (right).

Table 2.ST13 The ligand and corresponding Eu^{III} complex CIE color coordinates in thin film.

Complex	**Thin film CIE**		**FWHM**
	x	**y**	
	Eu complex		
0.1%	0.66	0.34	11.4
0.5%	0.66	0.34	14.0
1.0%	0.66	0.34	14.0
5.0%	0.65	0.34	17.9
Ligand			

0.1%	0.20	0.18	NA
0.5%	0.20	0.20	NA
1.0%	0.20	0.19	NA
5.0%	0.20	0.19	NA
Pure	0.30	0.43	NA

NA = not applicable

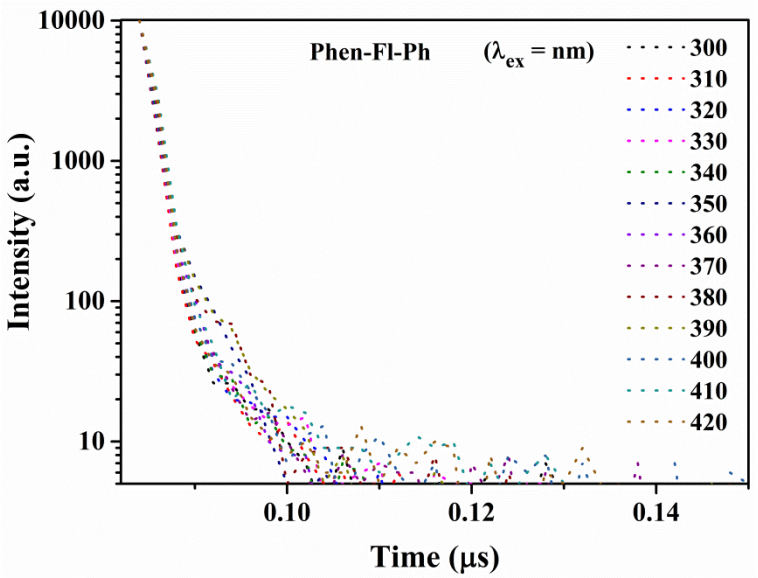

Figure 2.S15 The lifetime of the ligand in different excitation from 300-420 nm in solid form.

Annexure II
(Chapter 3)

Design and synthesis of new bipolar ligands based on phenanthroimidazole for tunable emissive Eu^{III} complexes: combined experimental and theoretical study

Contents:

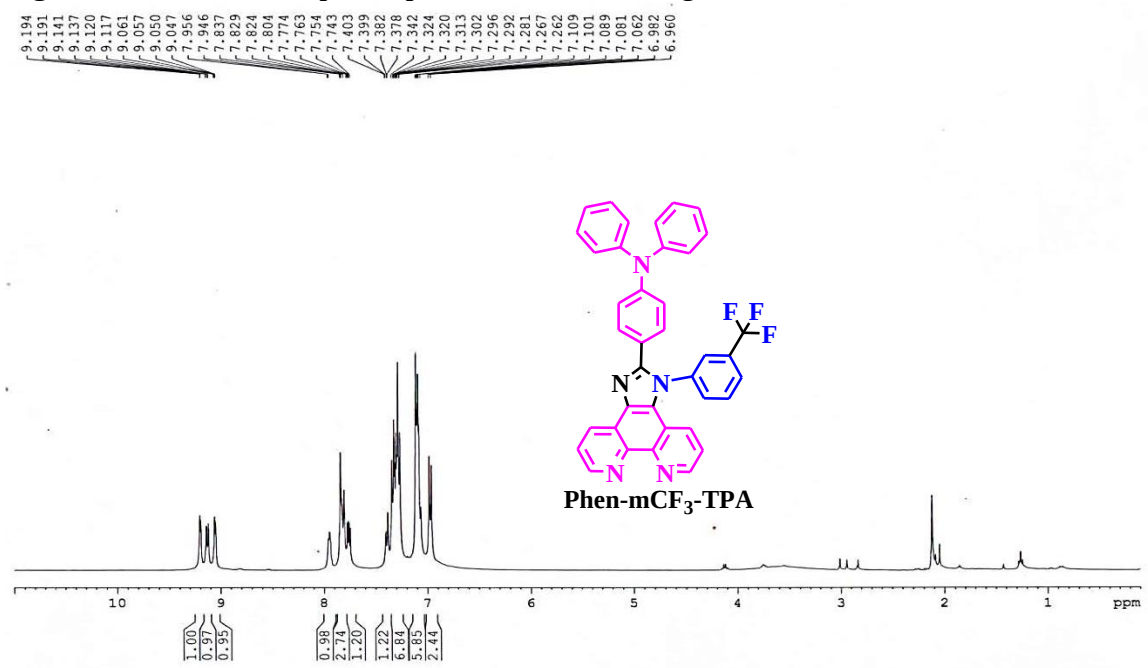

Figure 3.S1 The ^{1}H-NMR spectra of the ligand, Phen-mCF_3-TPA.

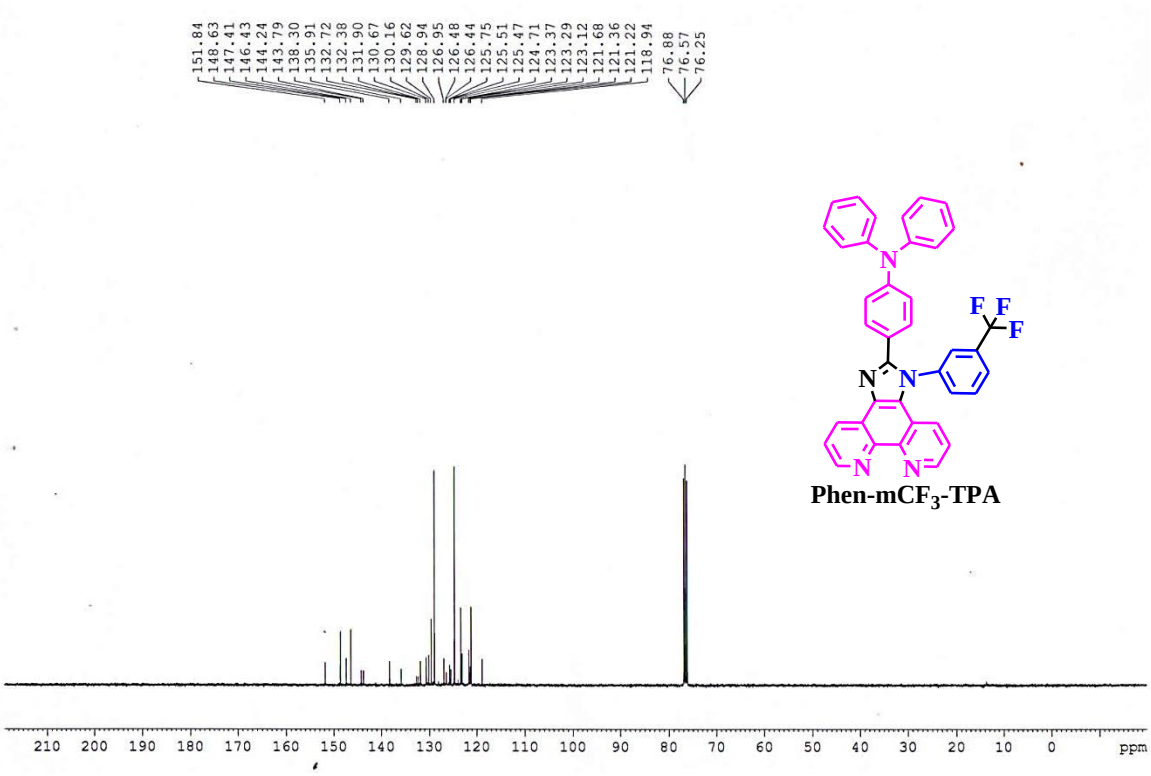

Figure 3.S2 The ^{13}C-NMR spectra of the ligand, Phen-mCF$_3$-TPA.

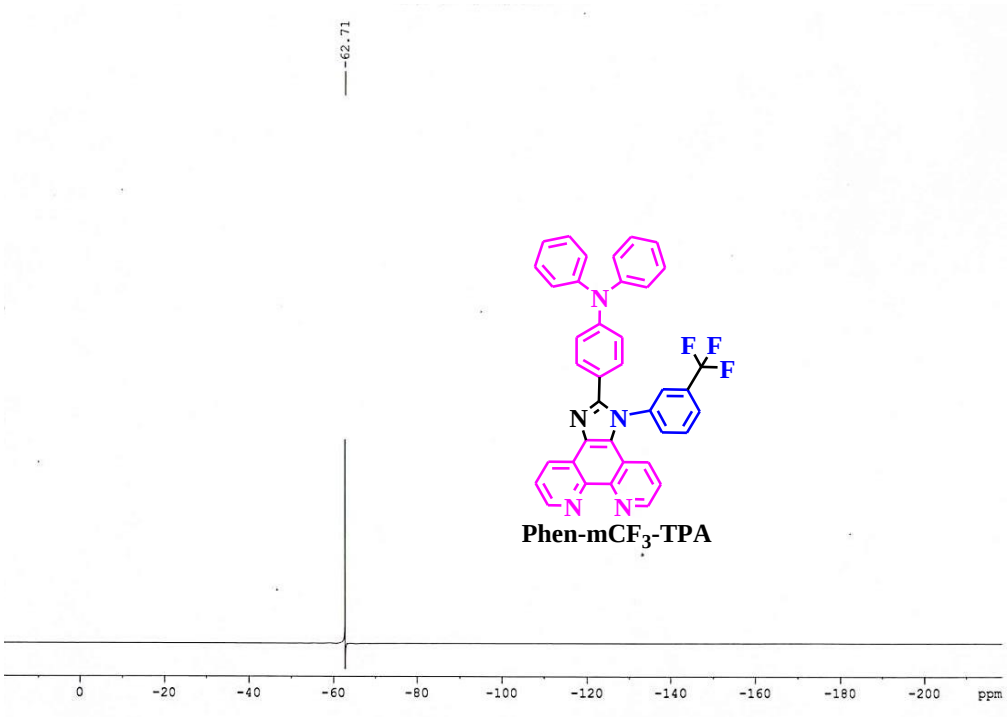

Figure 3.S3 The ^{19}F-NMR spectra of the ligand, Phen-mCF$_3$-TPA.

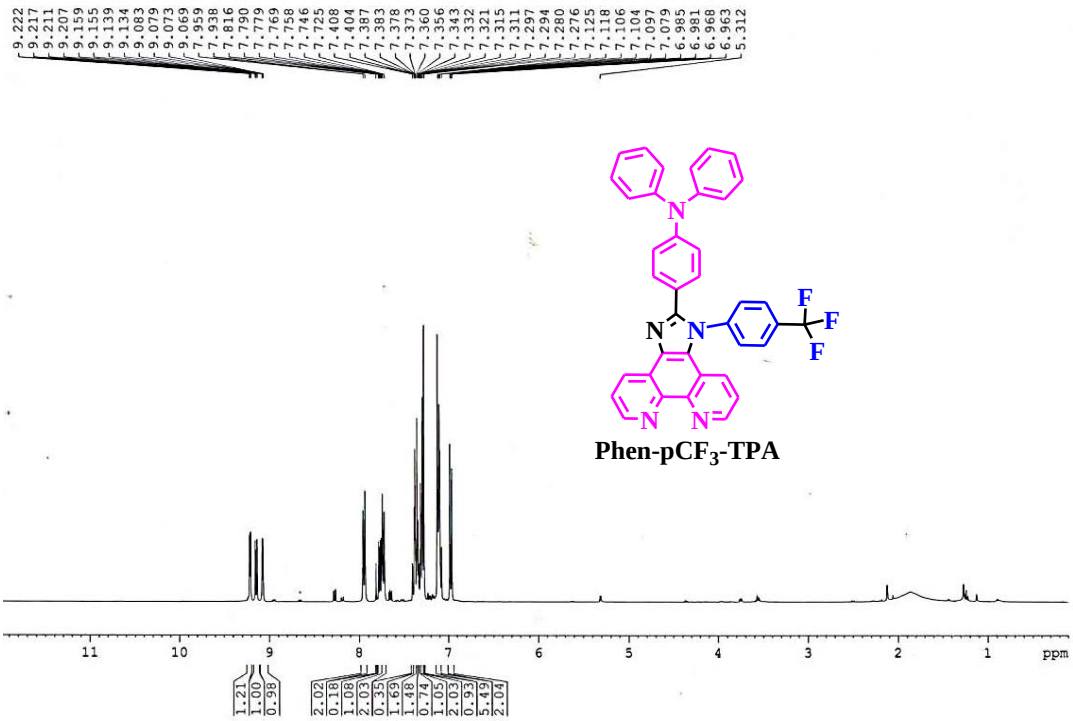

Figure 3.S4 The ^{1}H-NMR spectra of the ligand, Phen-pCF_3-TPA.

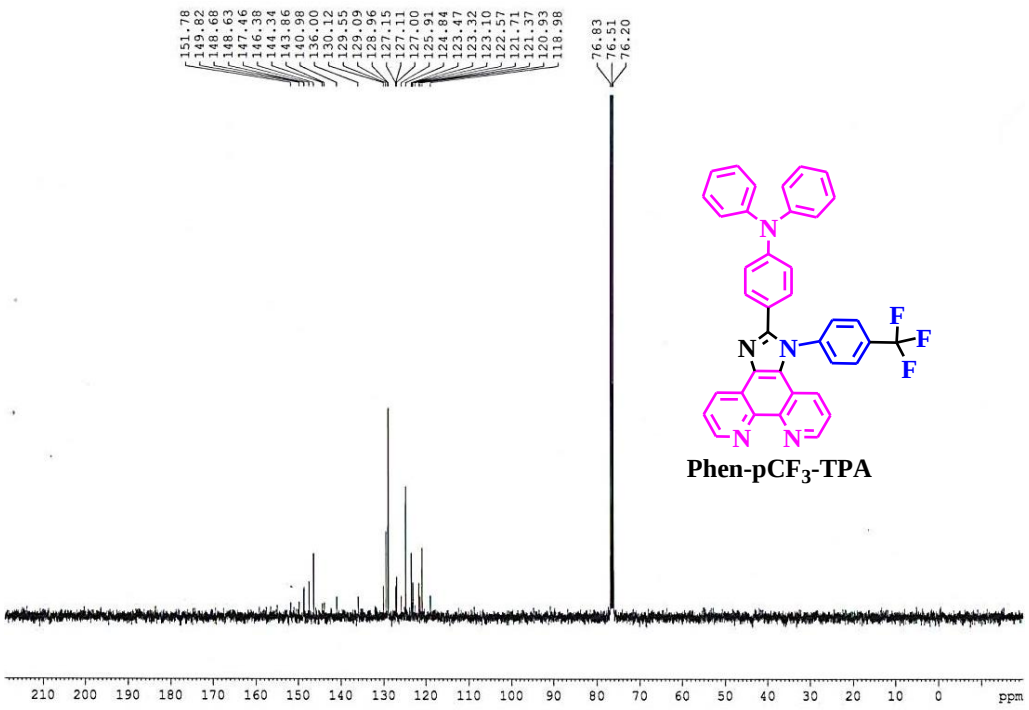

Figure 3.S5 The ^{13}C-NMR spectra of the ligand, Phen-pCF_3-TPA.

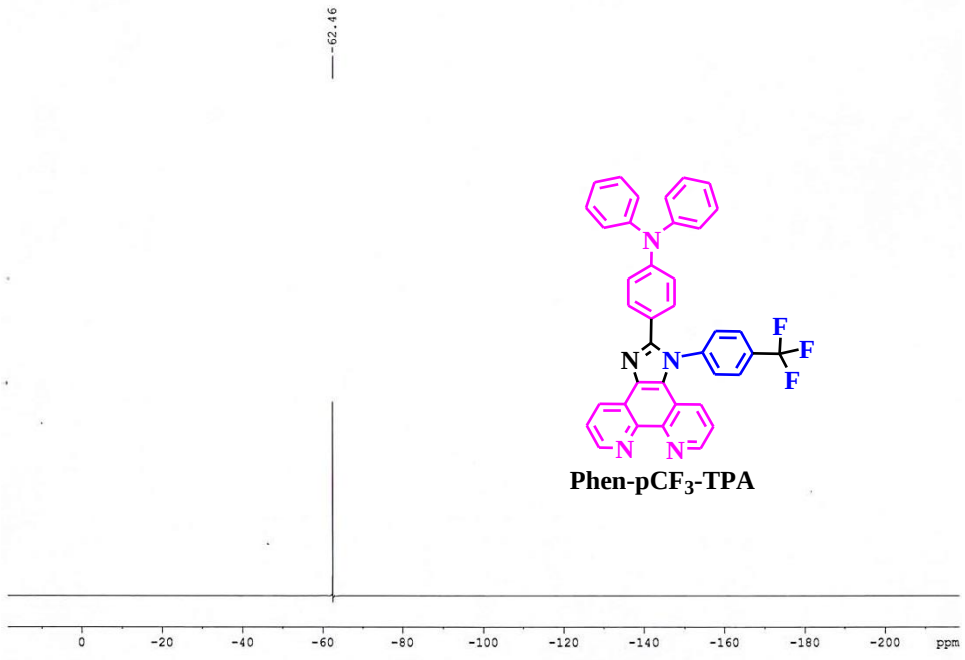

Figure 3.S6 The ^{19}F-NMR spectra of the ligand, Phen-pCF_3-TPA.

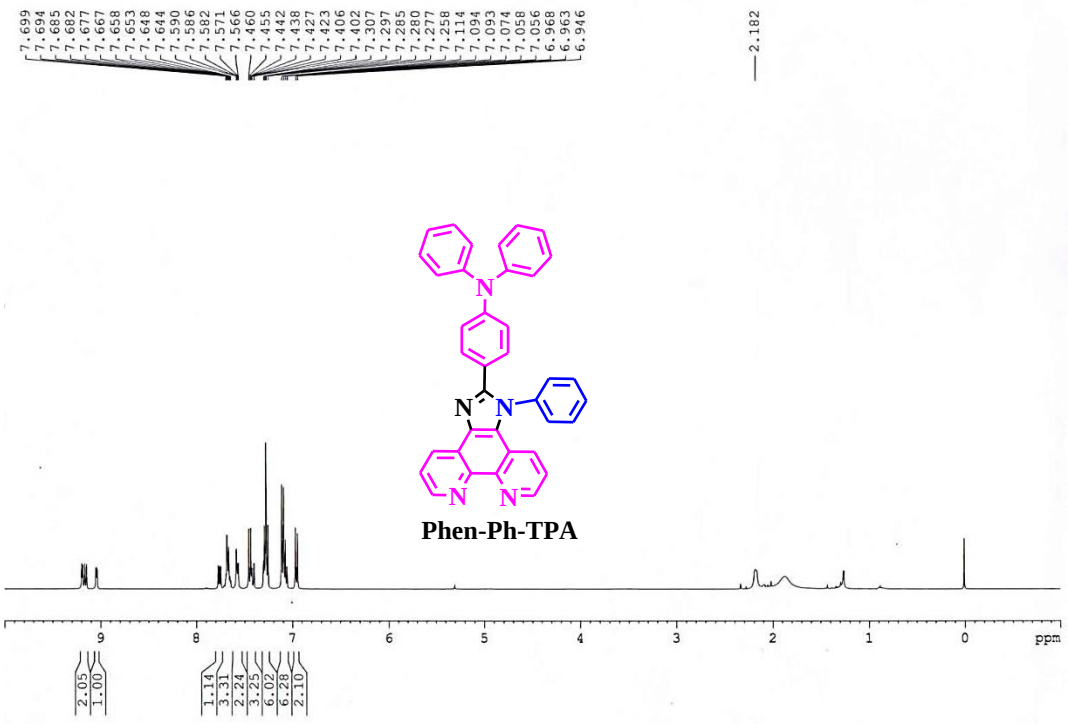

Figure 3.S7 The ^{1}H-NMR spectra of the ligand, Phen-Ph-TPA.

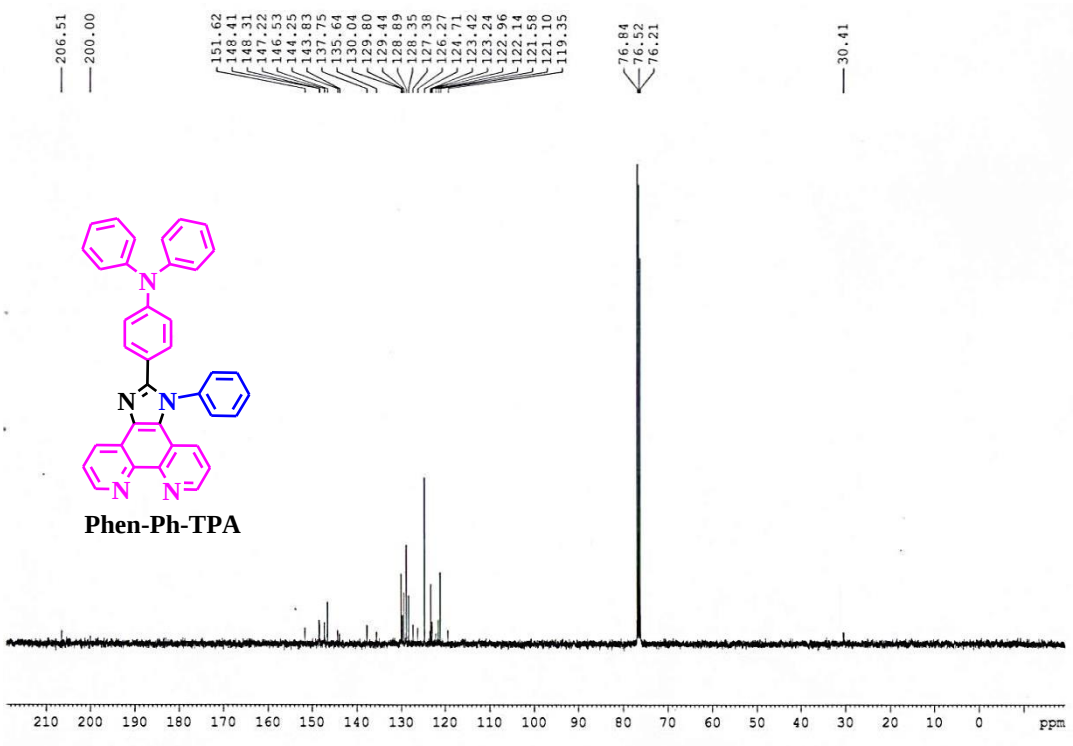

Figure 3.S8 The ^{13}C-NMR spectra of the ligand, Phen-Ph-TPA.

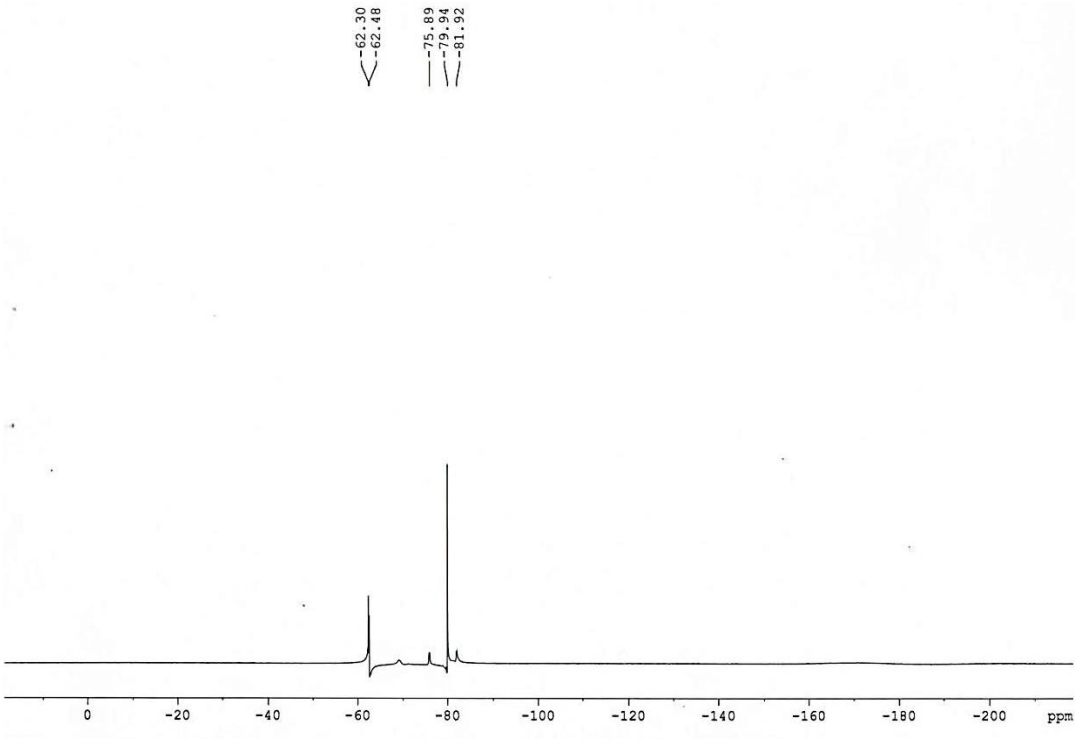

Figure 3.S9 The ^{19}F-NMR spectra of the Eu-complex, Eu(TTA)$_3$Phen-mCF_3-TPA.

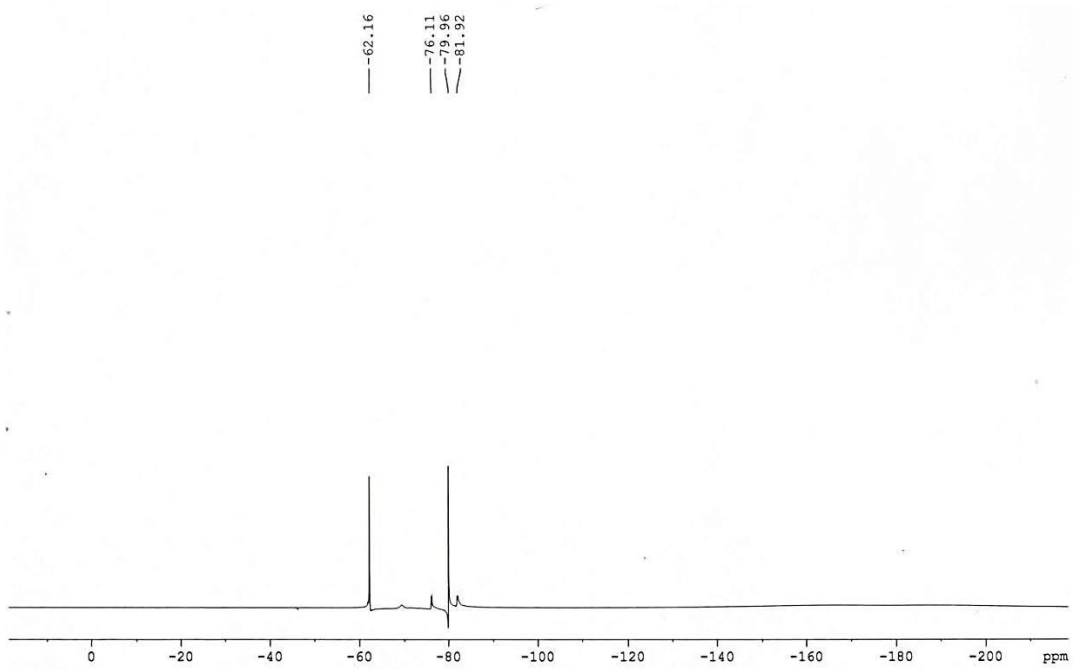

Figure 3.S10 The ^{19}F-NMR spectra of the Eu-complex, Eu(TTA)$_3$Phen-pCF_3-TPA.

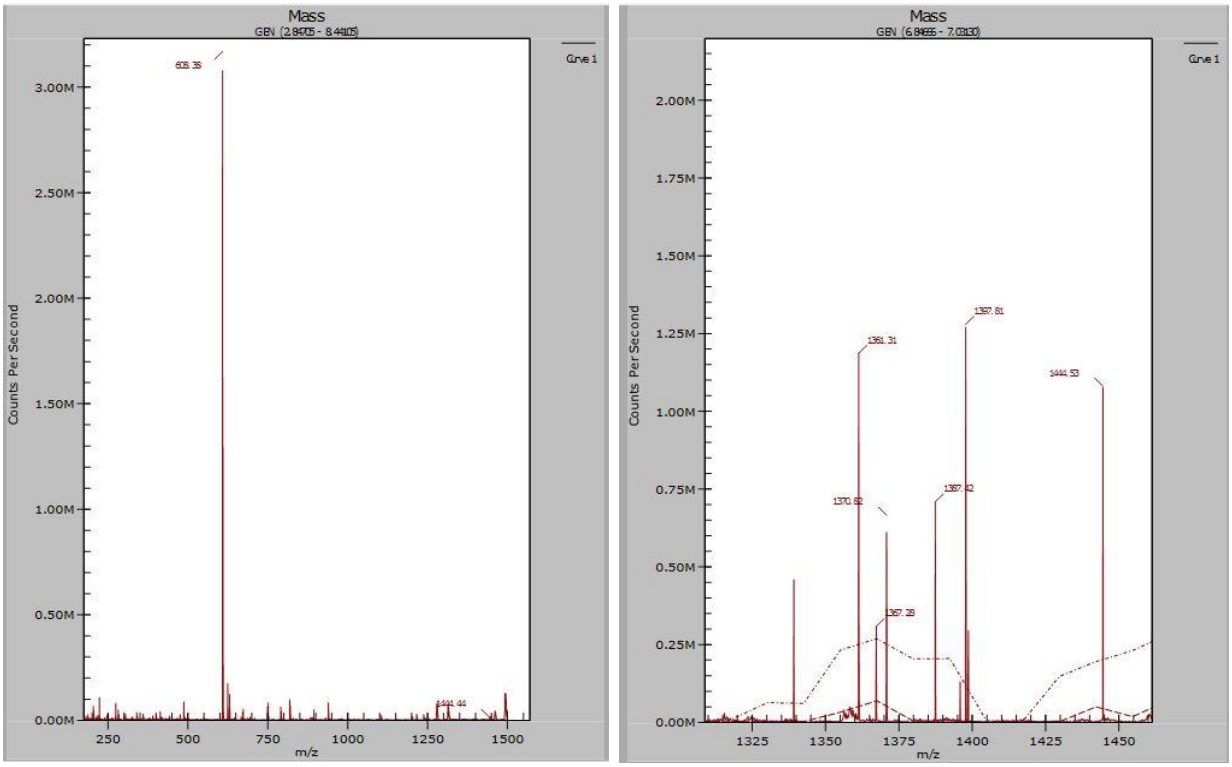

Figure 3.S11 The mass spectra of the ligand (left) and Eu-complex, Eu(TTA)$_3$Phen-mCF_3-TPA (right).

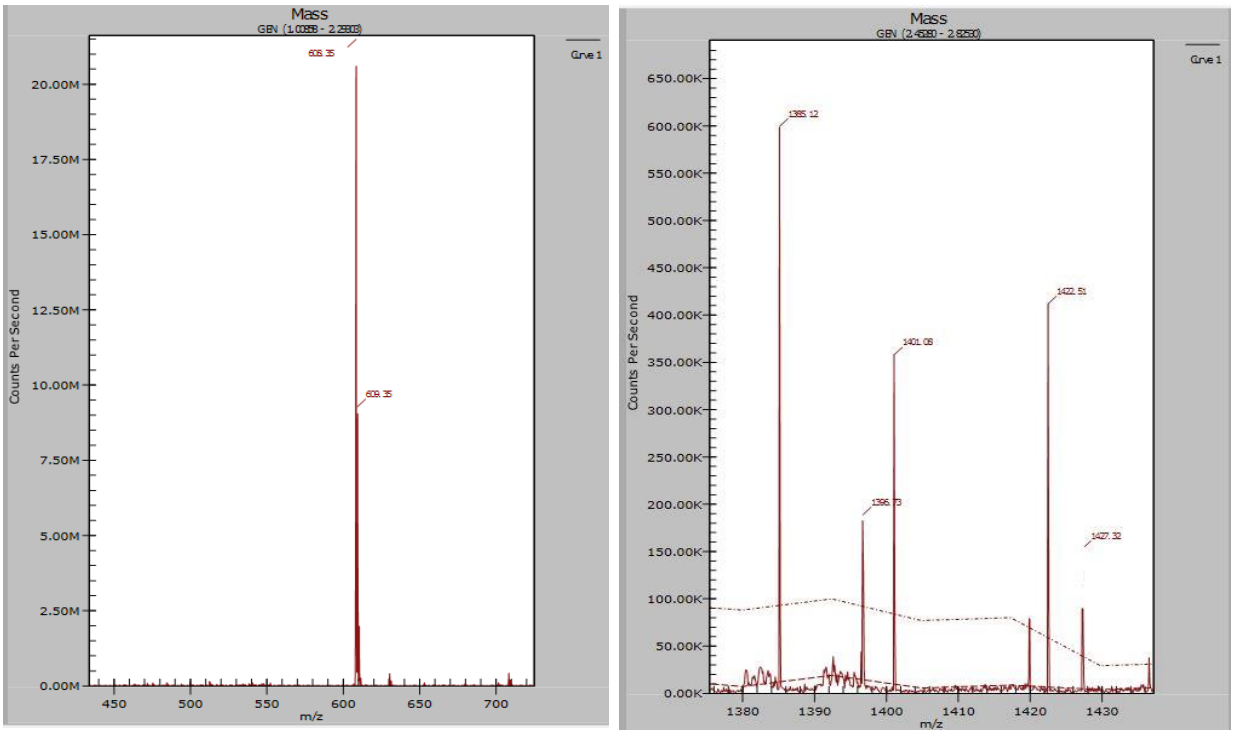

Figure 3.S12 The mass spectra of the ligand (left) and Eu-complex, Eu(TTA)$_3$Phen-pCF$_3$-TPA (right).

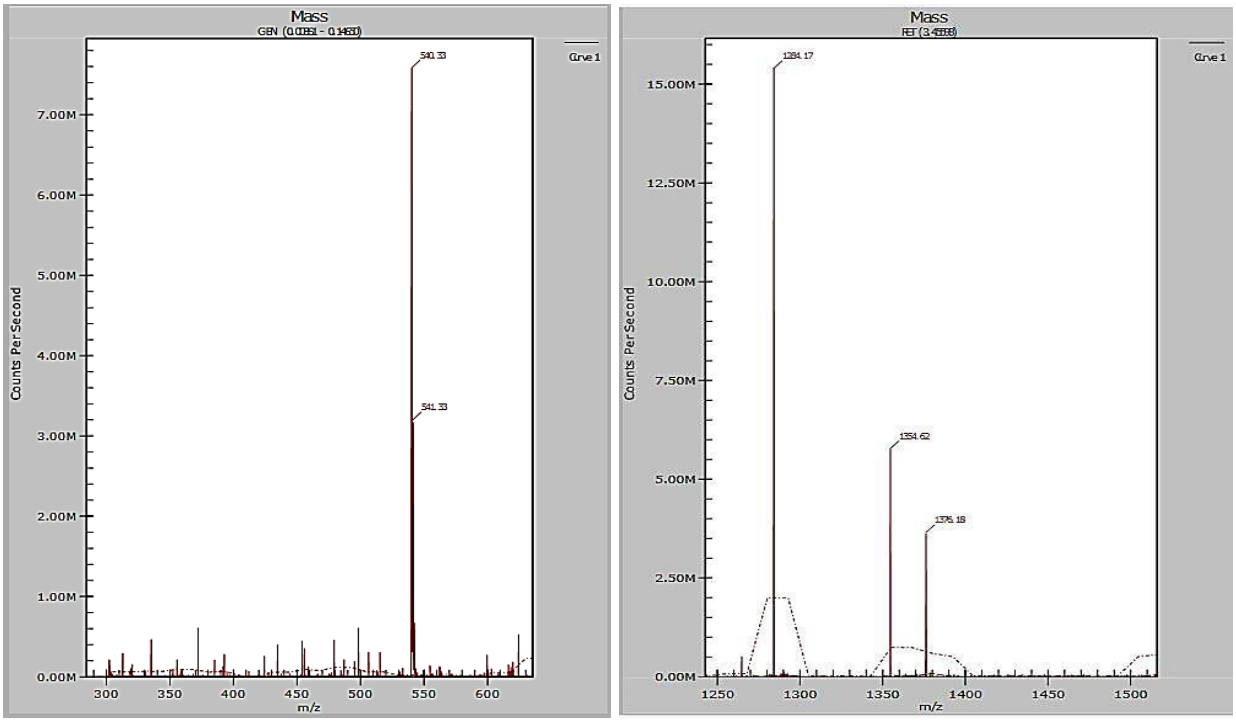

Figure 3.S13 The mass spectra of the ligand (left) and Eu-complex, Eu(TTA)$_3$Phen-Ph-TPA (right).

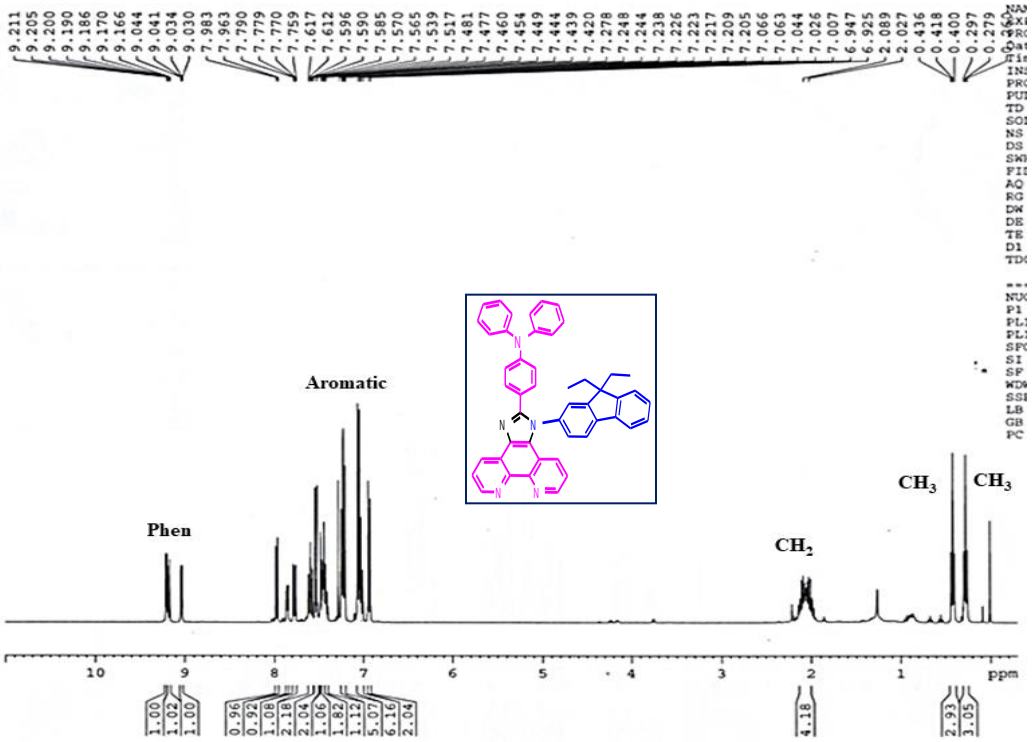

Figure 3.S14 The ^{1}H-NMR spectra of the ligand (Phen-Fl-TPA).

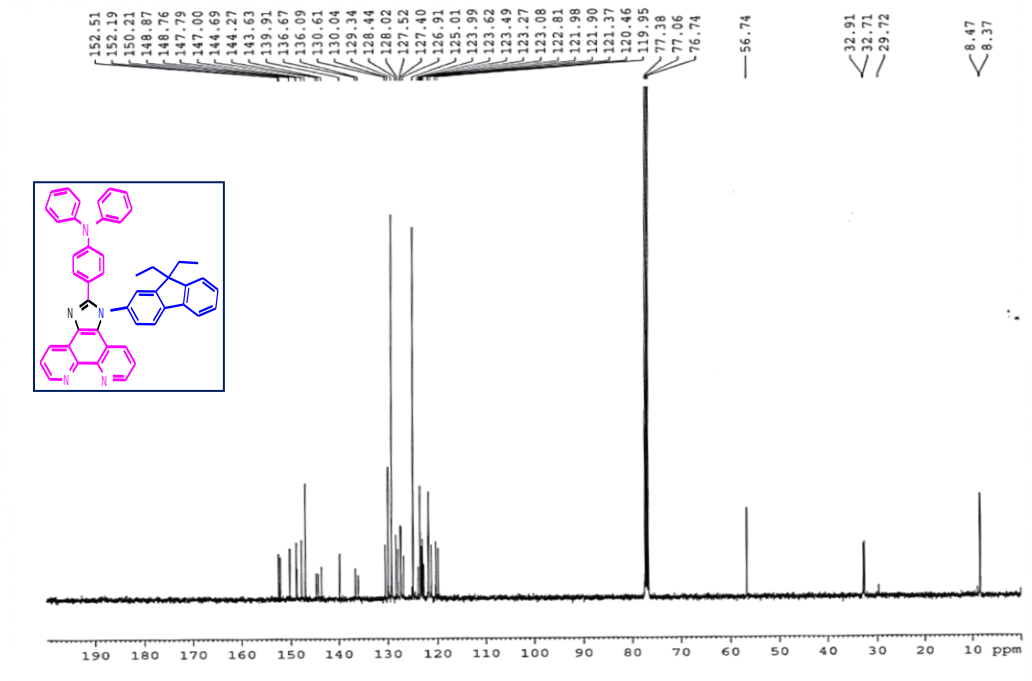

Figure 3.S15 The ^{13}C-NMR spectra of the ligand (Phen-Fl-TPA).

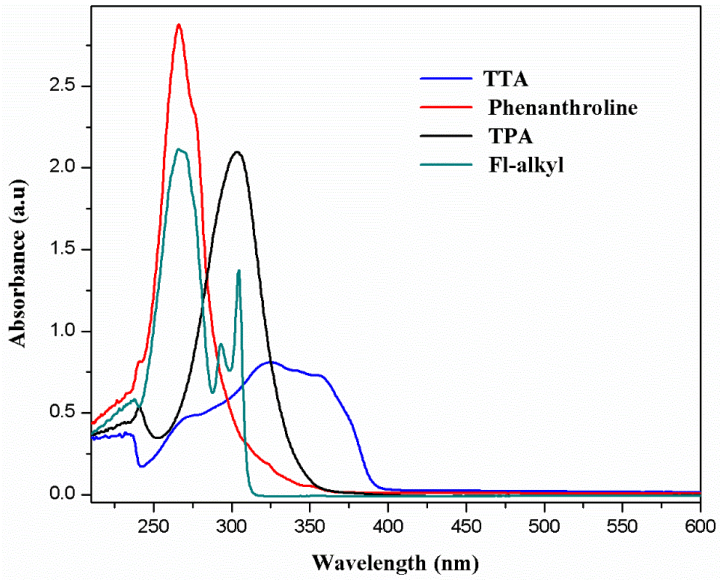

Figure 3.S16 The absorption spectrum of the starting materials in chloroform solution.

Annexure-III
(Chapter 4)

Carbazole and fluorene functionalized phenanthro-imidazole ancillary ligand based Eu^{III} complexes for leds: detailed photophysical and theoretical study

Contents:

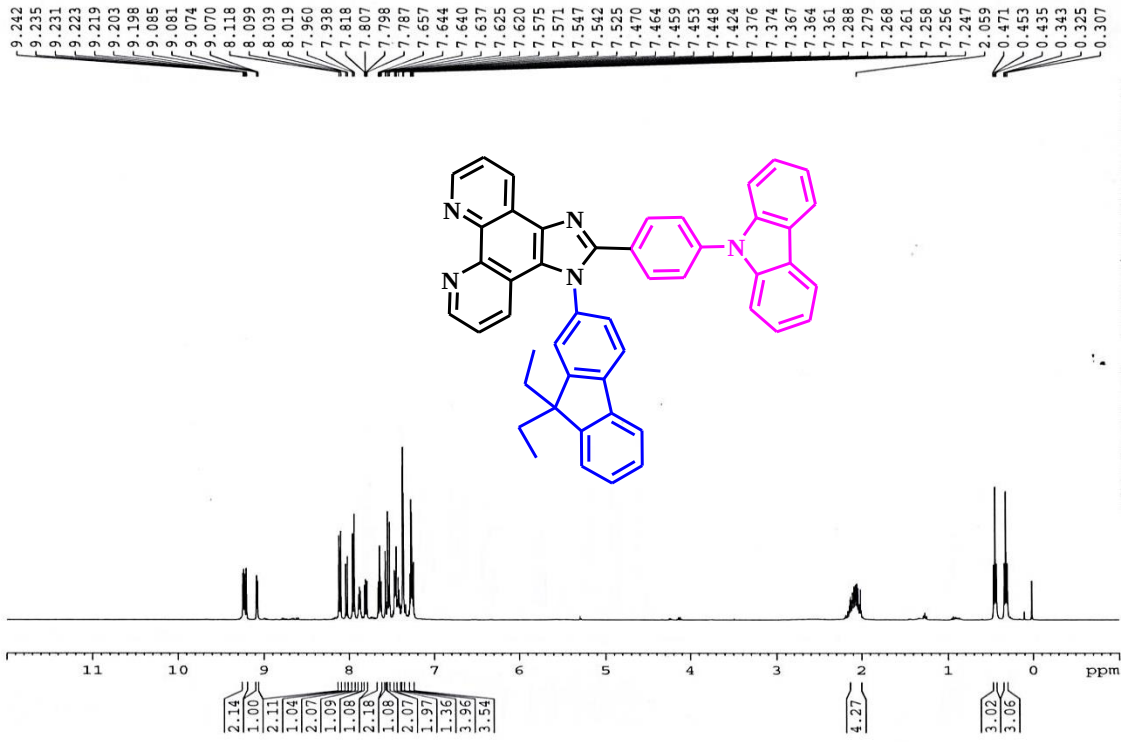

Figure 4.S1 The ^{1}H-NMR spectra of the ligand, 1L.

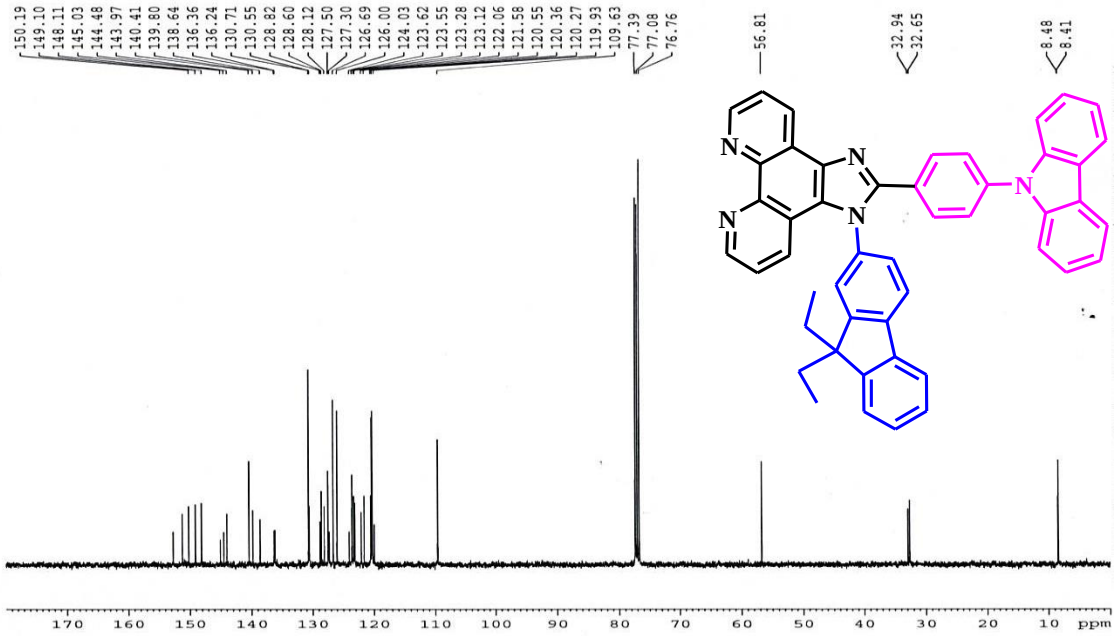

Figure 4.S2 The ^{13}C-NMR spectra of the ligand, 1L.

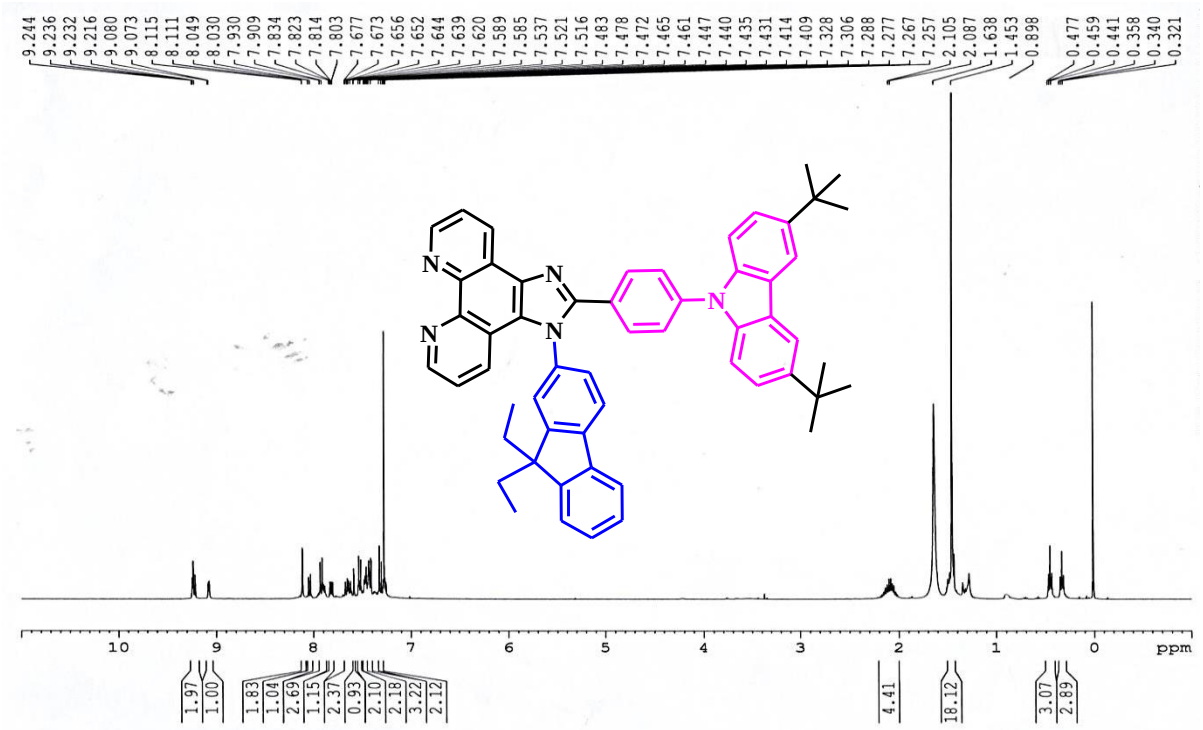

Figure 4.S3 The ^{1}H-NMR spectra of the ligand, 2L.

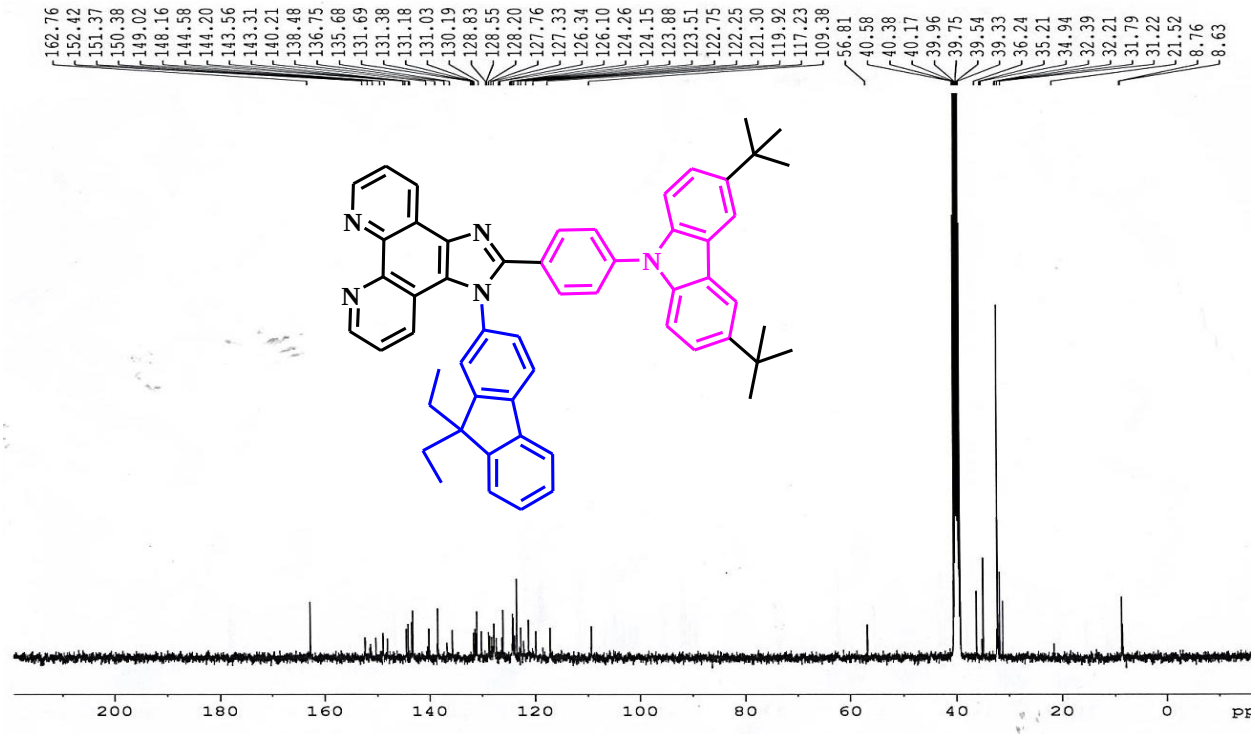

Figure 4.S4 The ^{13}C-NMR spectra of the ligand, 2L.

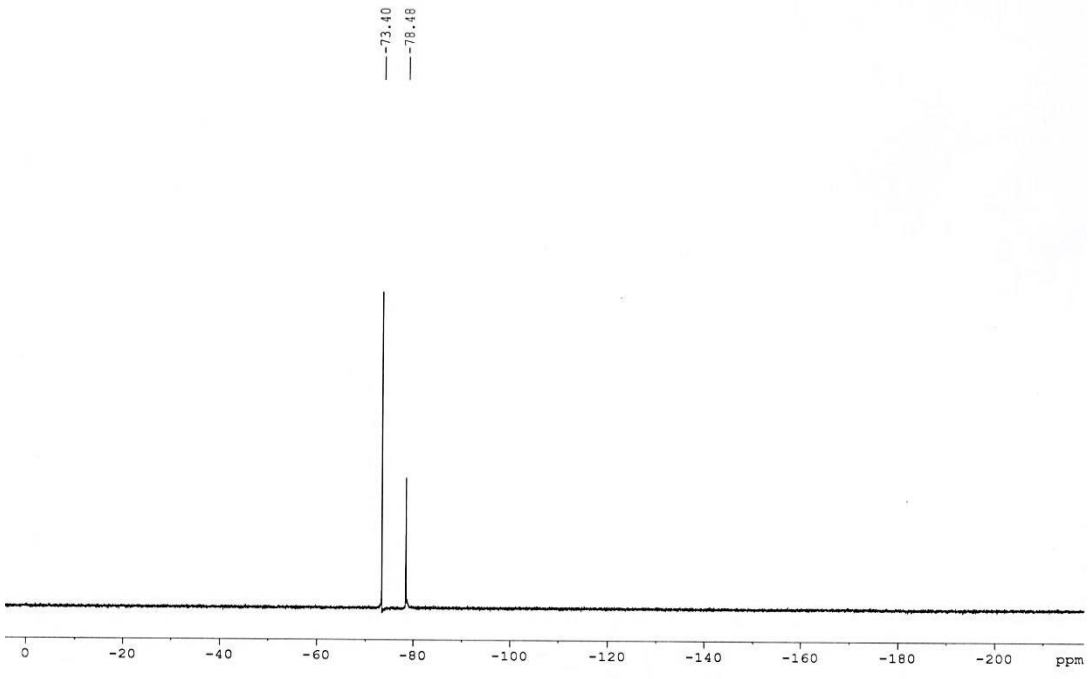

Figure 4.S5 The ^{19}F-NMR spectra of the Eu(TTA)$_3$Phen-Fl-CBZ.

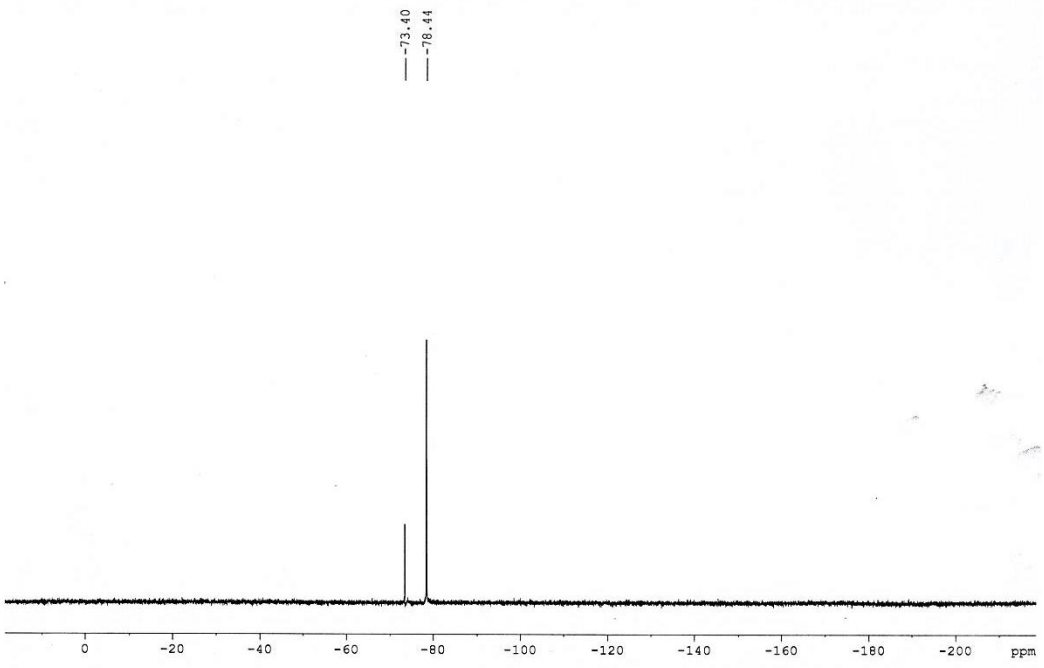

Figure 4.S6 The ^{19}F-NMR spectra of the Eu(TTA)$_3$Phen-Fl-t-but CBZ.

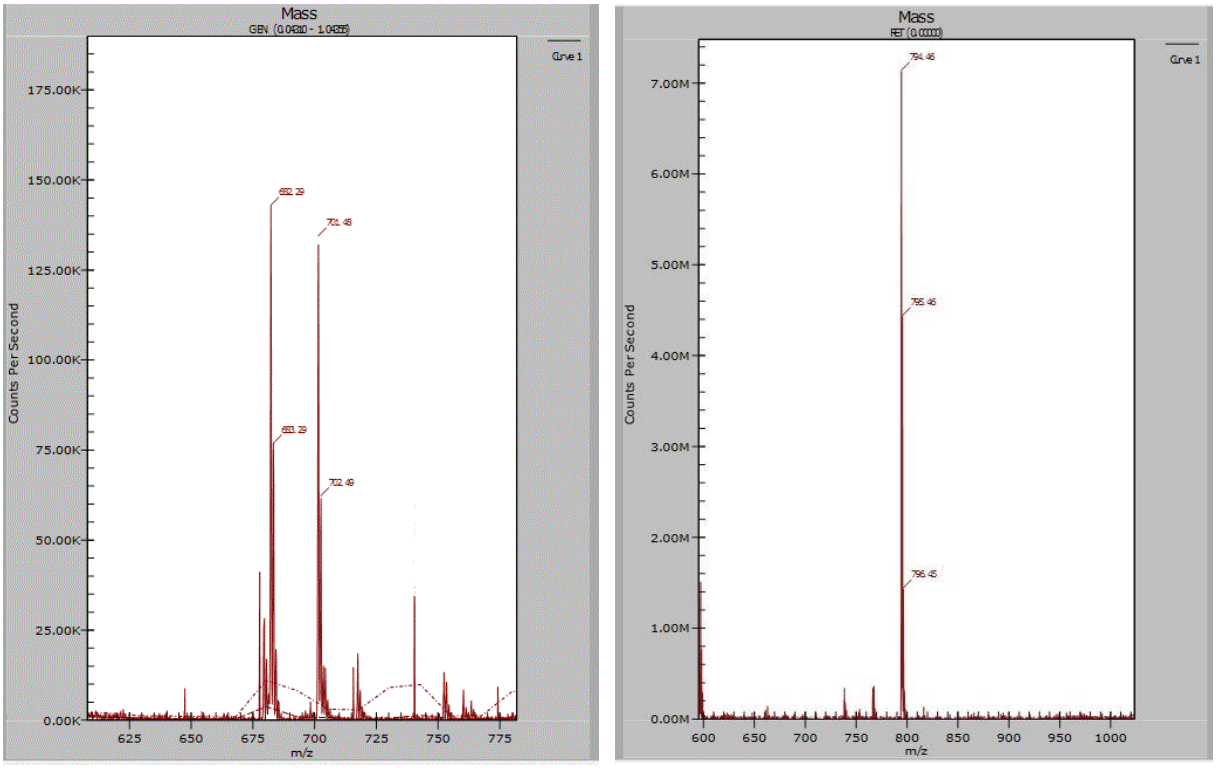

Figure 4.S7 The Mass spectrometry (LC-MS) analysis of the ligand, Phen-Fl-CBZ (left) and ligand, Phen-Fl-t-but CBZ (right).

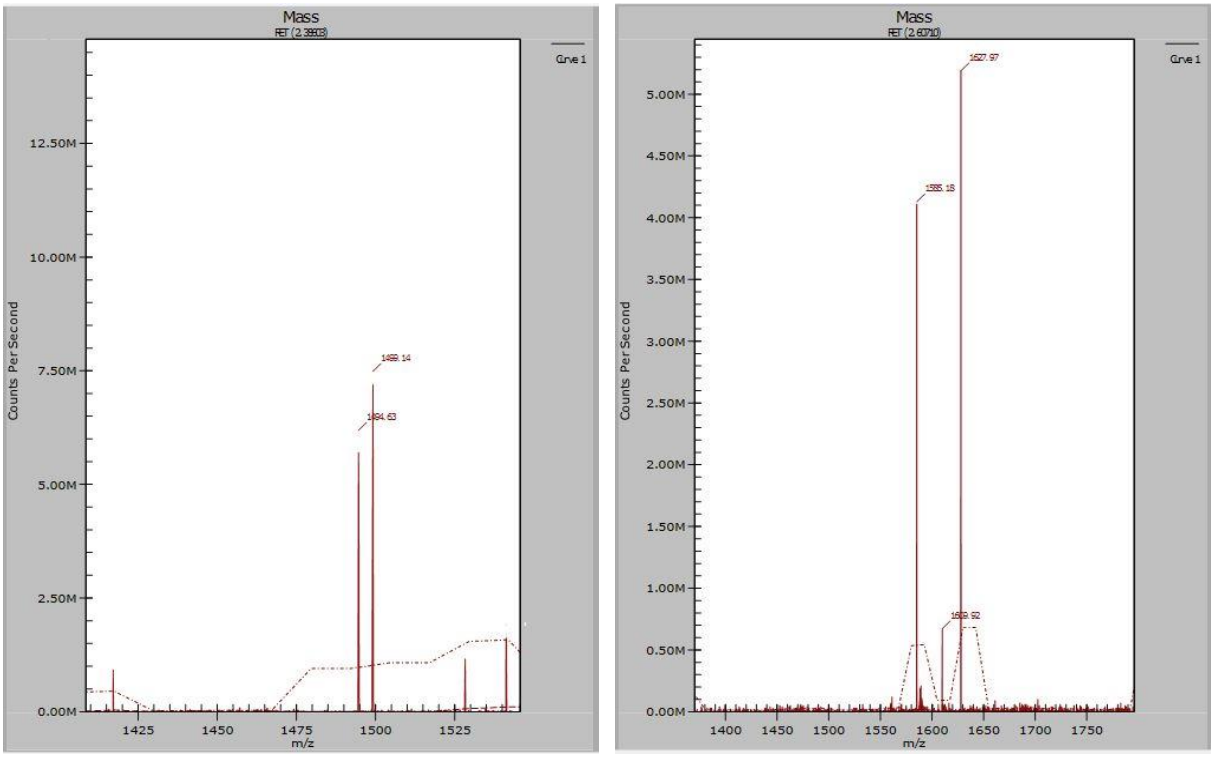

Figure 4.S8 The Mass spectrometry (LC-MS) analysis of the Eu^{III} complex, $Eu(TTA)_3$Phen-Fl-CBZ (left) and Eu^{III} complex, $Eu(TTA)_3$Phen-Fl-t-but CBZ (right).

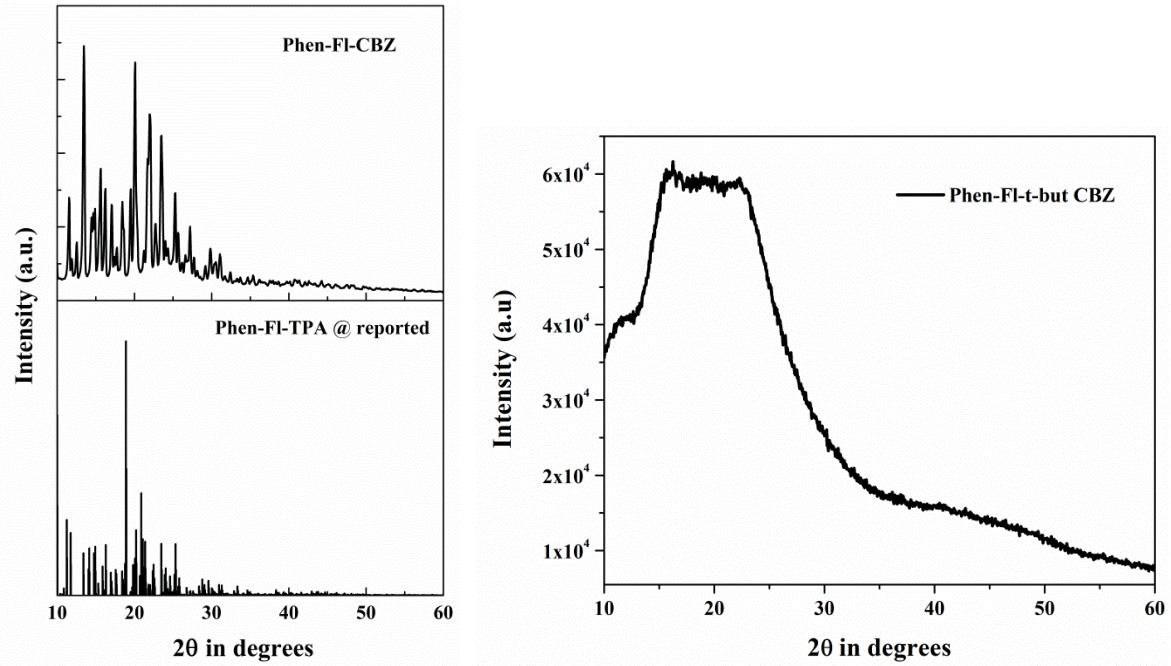

Figure 4.S9 The PXRD of the ligands, 1L (left) and 2L (right). The ligand, 1L comparison with already reported Phen-Fl-TPA ligand.

Annexure IV
(Chapter 5)

Controlled energy transfer from ligand to Eu^{III} ion: A unique strategy to obtain bright white/red light emission and their versatile applications

Contents

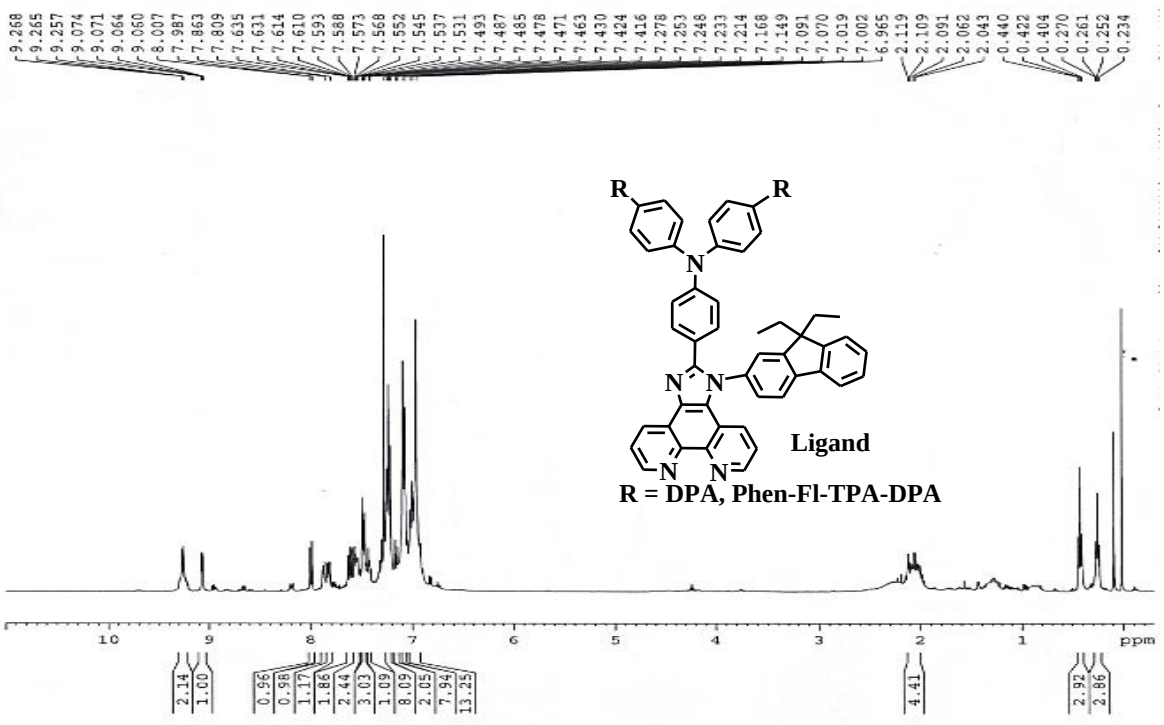

Figure 5.S1 The ^{1}H NMR spectra of the Phen-Fl-TPA-DPA ligand.

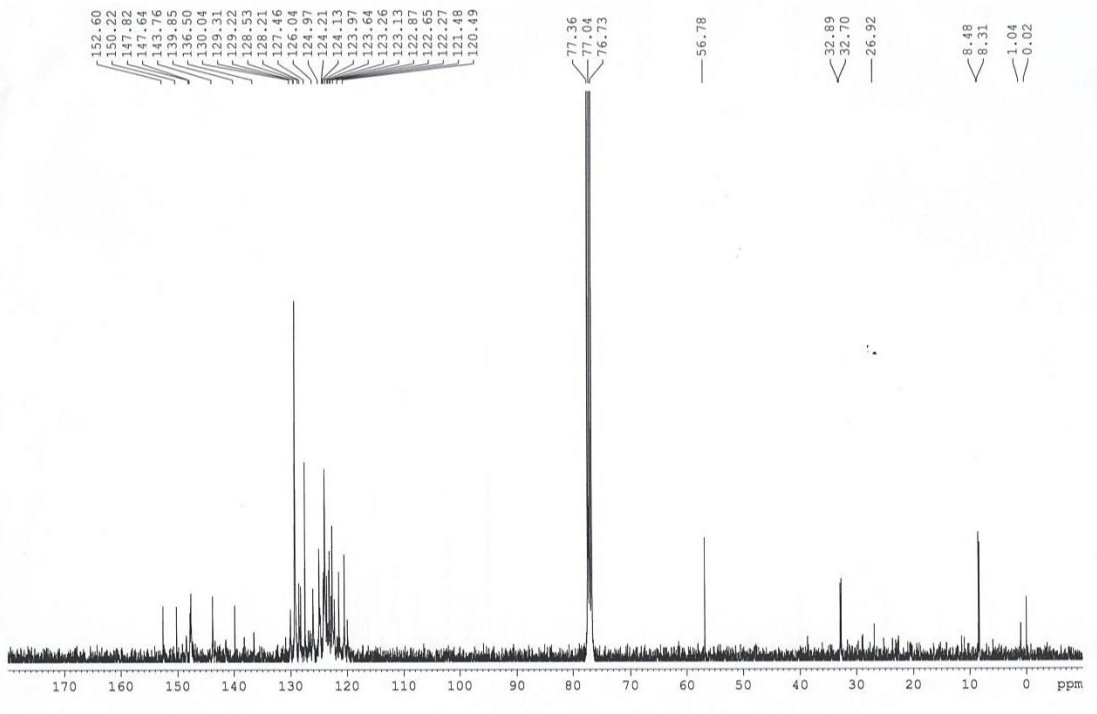

Figure 5.S2 The ^{13}C NMR spectra of the Phen-Fl-TPA-DPA ligand.

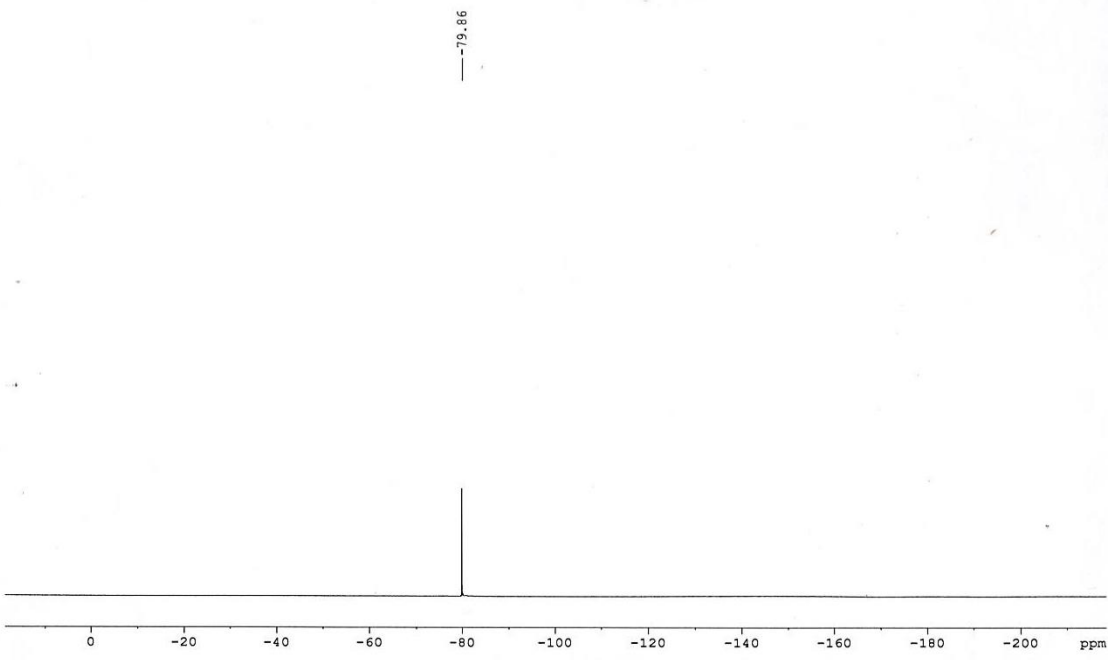

Figure 5.S3 The ^{19}F-NMR spectra of the of the Eu^{III} complex ($Eu(TTA)_3$Phen-Fl-TPA-DPA).

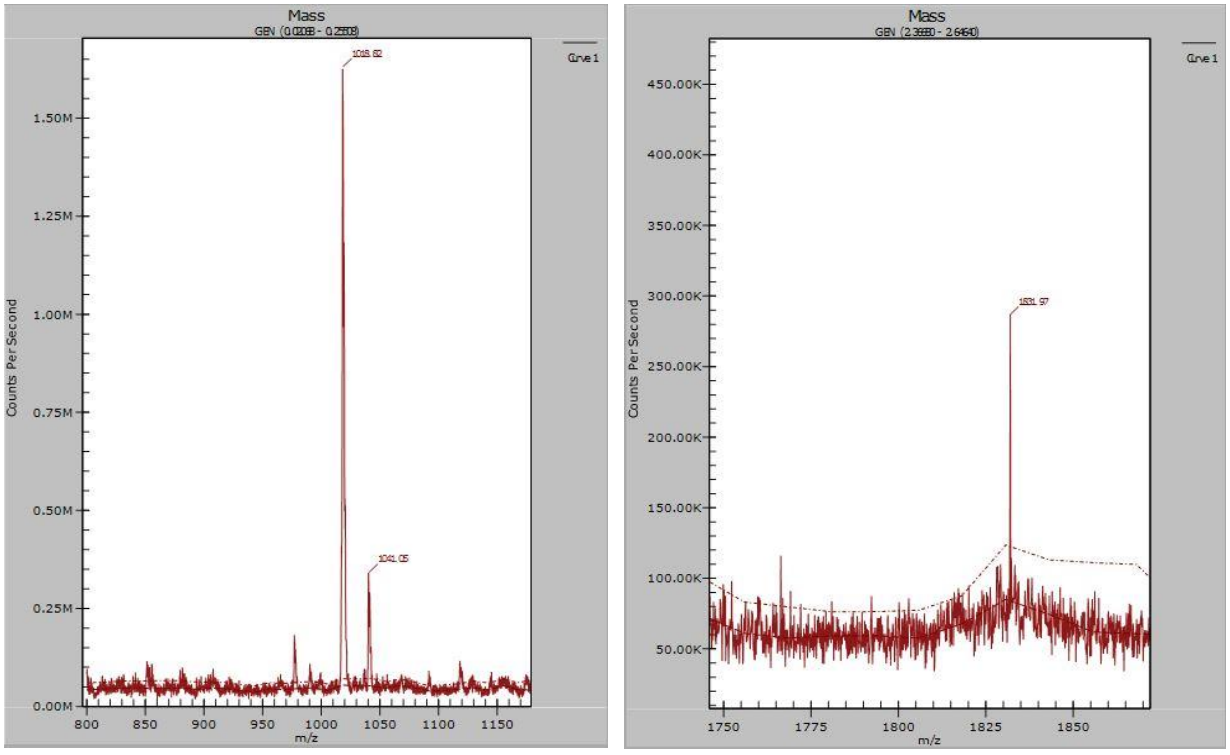

Figure 5.S4 The mass spectra of the Phen-Fl-TPA-DPA ligand (left), the mass spectra of the Eu^{III} complex ($Eu(TTA)_3$Phen-Fl-TPA-DPA).

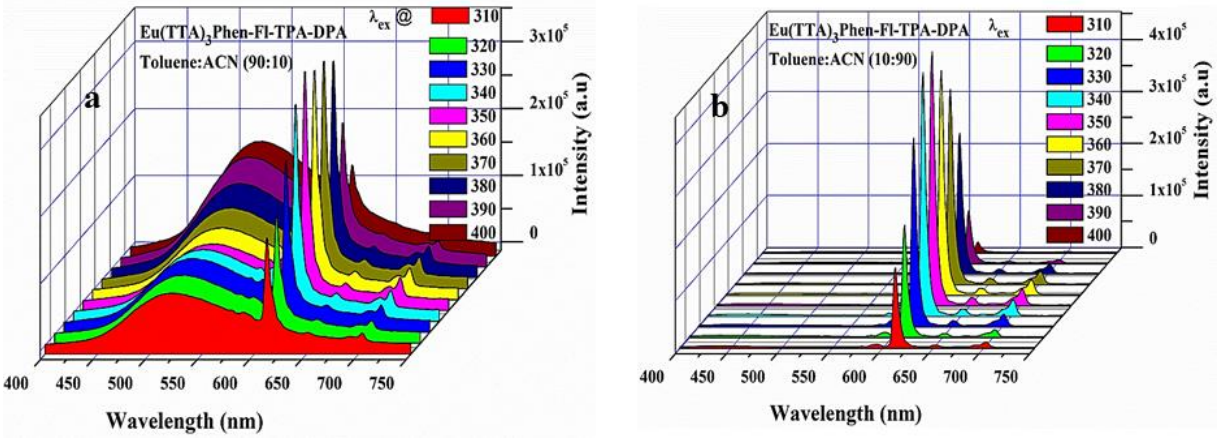

Figure 5.S5 The Eu^{III} complex in mixture of toluene and acetonitrile (ACN) solution with different concentration ratios from 10-100 (a, b) at different excitation wavelength source from 310 – 400 nm.

Table 5.ST1 CIE coordinates of the Eu^{III} complex in mixture of toluene and acetonitrile (ACN) solution with different concentration ratios at different excitation wavelength source from 300 – 420 nm.

Wavelength (λ_{max})	**CIE Coordinates Tol (90):(10) ACN**		**I (Lum)**	**CIE Coordinates Tol (10):(90) ACN**		**I (Lum)**
	x	**y**		**x**	**y**	
300	0.34280	0.46542	1.173E+004	0.53713	0.30013	1.197E+003
310	0.34172	0.46565	1.331E+004	0.55671	0.30435	1.580E+003
320	0.35378	0.46036	1.514E+004	0.59083	0.31180	2.474E+003
330	0.36766	0.45436	1.515E+004	0.61088	0.31657	3.083E+003
340	0.37831	0.45000	1.430E+004	0.61842	0.31888	3.188E+003
350	0.37096	0.45306	1.525E+004	0.61636	0.31941	2.863E+003
360	0.36107	0.45551	1.703E+004	0.61374	0.32059	2.506E+003
370	0.34972	0.46017	1.971E+004	0.60277	0.32144	1.881E+003
380	0.33033	0.47125	2.235E+004	0.54312	0.32058	8.369E+002
390	0.32323	0.48066	2.321E+004	0.39810	0.31310	3.338E+002
400	0.32789	0.48699	2.176E+004	0.32835	0.31807	2.107E+002
410	0.33734	0.49431	1.819E+004	0.29449	0.28914	1.716E+002
420	0.35321	0.50107	1.332E+004	0.28764	0.28771	1.393E+002

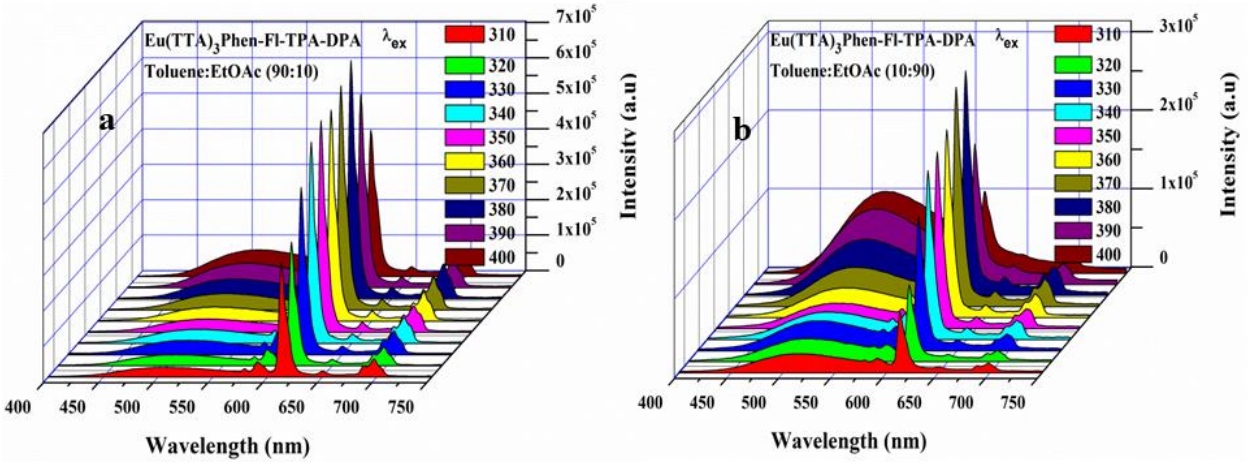

Figure S6 The Eu^{III} complex in mixture of toluene and EtOAc solution with different con^{c}. ratios from 10-100 (a, b) at different excitation wavelength source from 310 – 400 nm.

Table 5.ST2 CIE coordinates of the Eu^{III} complex in mixture of toluene and ethyl acetate (EtOAc) solution with different concentration ratios at different excitation wavelength source from 300 – 420 nm.

Wavelength (λ_{max})	**CIE Coordinates Tol(90):(10) EtOAc**		**I (Lum)**	**CIE Coordinates Tol (10):(90) EtOAc**		**I (Lum)**
	x	**y**		**x**	**y**	
300	0.45687	0.38146	5.632E+003	0.36203	0.43711	3.587E+003
310	0.44997	0.38321	6.364E+003	0.36403	0.43549	4.454E+003
320	0.45335	0.38442	8.482E+003	0.38732	0.42725	6.185E+003
330	0.47202	0.37972	9.130E+003	0.41302	0.41868	6.220E+003
340	0.48469	0.37672	8.979E+003	0.42518	0.41491	5.887E+003
350	0.47944	0.37766	9.292E+003	0.41772	0.41812	6.739E+003
360	0.46998	0.37942	1.034E+004	0.40622	0.42322	8.627E+003
370	0.45711	0.38343	1.182E+004	0.37966	0.43518	1.147E+004
380	0.41784	0.39772	1.251E+004	0.33558	0.45777	1.395E+004
390	0.39113	0.41313	1.258E+004	0.31825	0.47119	1.477E+004
400	0.38391	0.42595	1.231E+004	0.32111	0.47893	1.431E+004
410	0.38303	0.44042	1.133E+004	0.33180	0.48500	1.236E+004
420	0.38525	0.45721	9.509E+003	0.34745	0.49042	9.278E+003

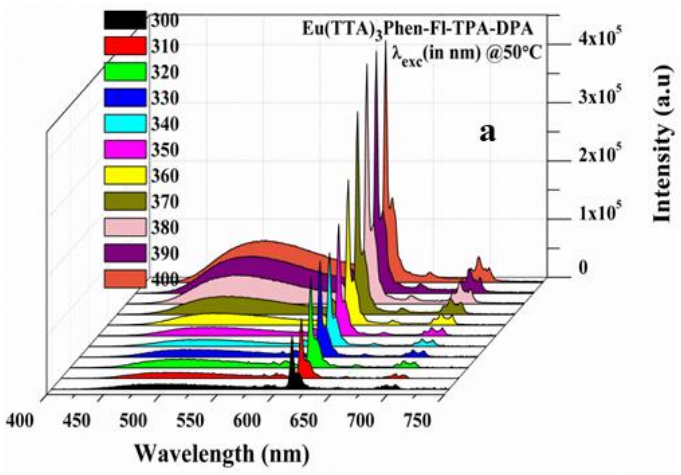
Eu(TTA)3Phen-Fl-TPA-DPA
λexc(in nm) @50°C
a
300
310
320
330
340
350
360
370
380
390
400
4x10^5
3x10^5
2x10^5
1x10^5
0
Intensity (a.u)
400 450 500 550 600 650 700 750
Wavelength (nm)

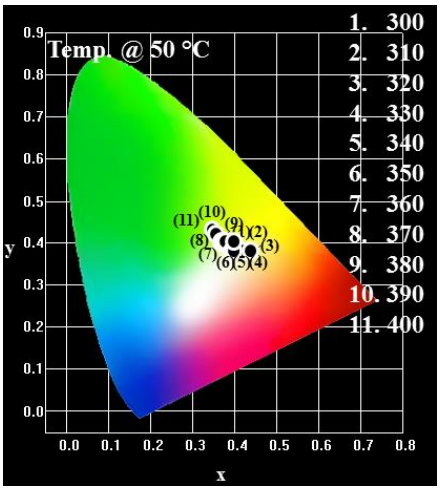
Temp. @ 50 °C
1. 300
2. 310
3. 320
4. 330
5. 340
6. 350
7. 360
8. 370
9. 380
10. 390
11. 400
x
y

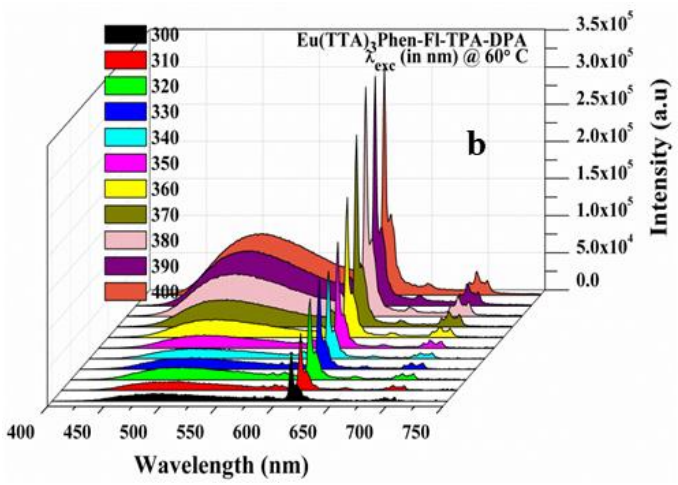
Eu(TTA)3Phen-Fl-TPA-DPA
λexc (in nm) @ 60° C
b
300
310
320
330
340
350
360
370
380
390
400
3.5x10^5
3.0x10^5
2.5x10^5
2.0x10^5
1.5x10^5
1.0x10^5
5.0x10^4
0.0
Intensity (a.u)
400 450 500 550 600 650 700 750
Wavelength (nm)

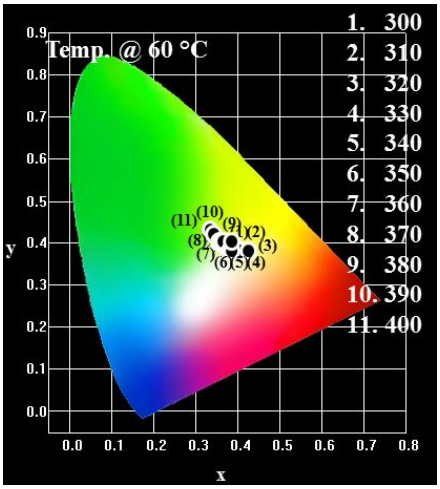
Temp. @ 60 °C
1. 300
2. 310
3. 320
4. 330
5. 340
6. 350
7. 360
8. 370
9. 380
10. 390
11. 400
x
y

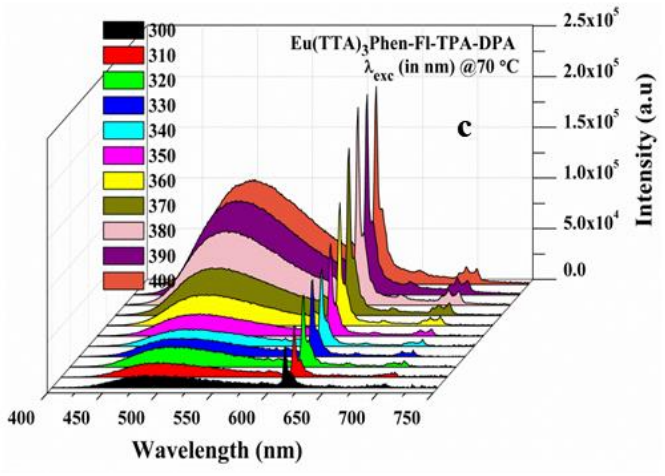
Eu(TTA)3Phen-Fl-TPA-DPA
λexc (in nm) @70 °C
c
300
310
320
330
340
350
360
370
380
390
400
2.5x10^5
2.0x10^5
1.5x10^5
1.0x10^5
5.0x10^4
0.0
Intensity (a.u)
400 450 500 550 600 650 700 750
Wavelength (nm)

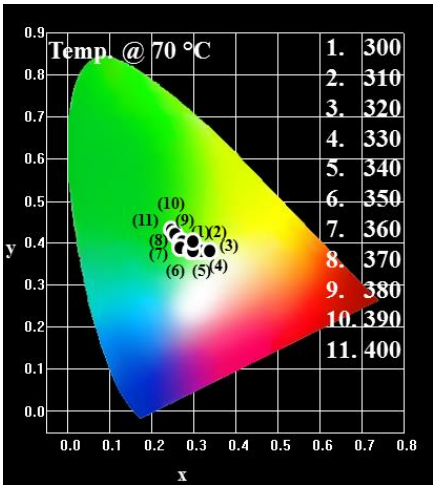
Temp. @ 70 °C
1. 300
2. 310
3. 320
4. 330
5. 340
6. 350
7. 360
8. 370
9. 380
10. 390
11. 400
x
y

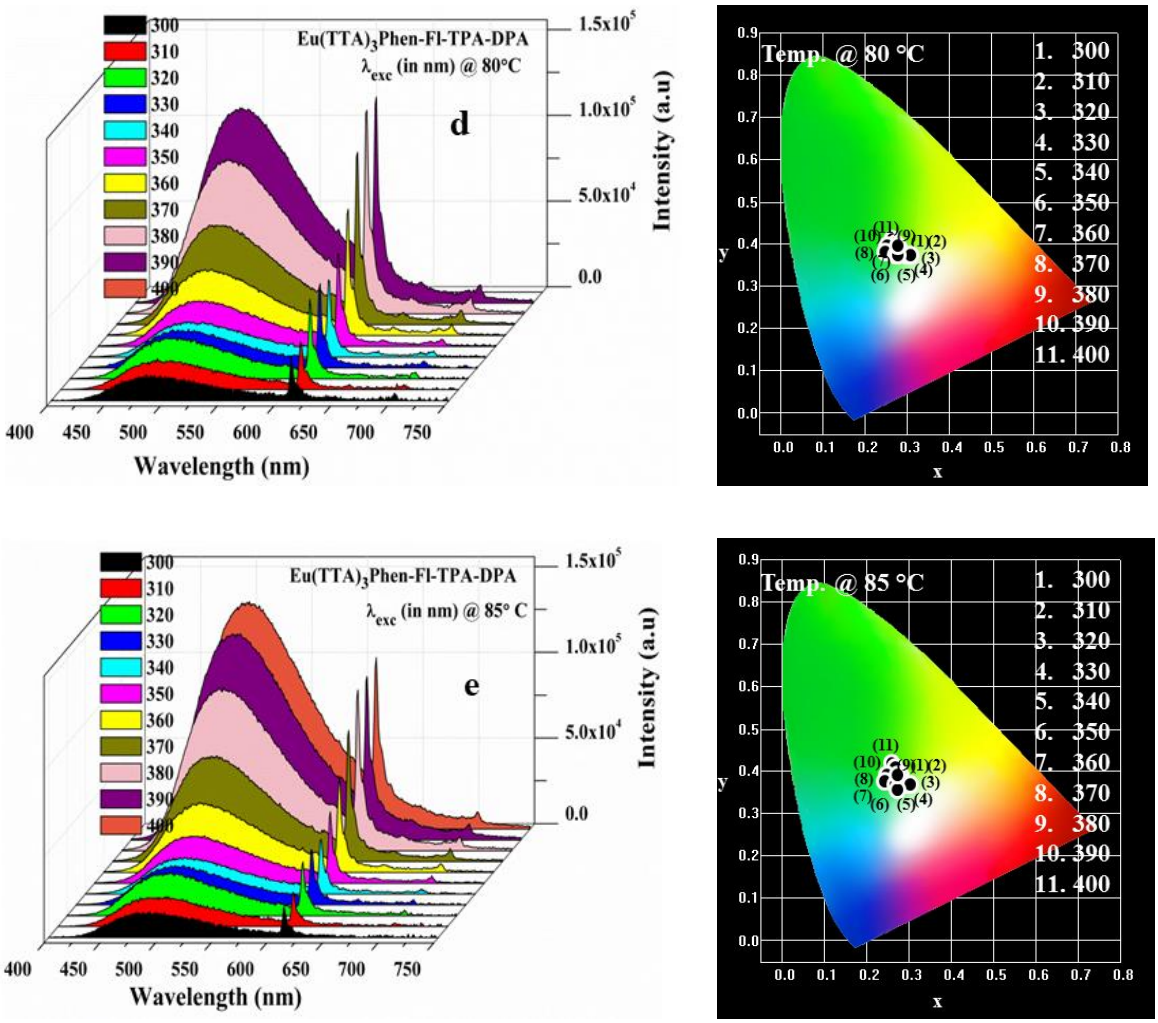

Figure 5.S7 The emission of Eu^{III} complex in different temperature with different excitation from 300-400 nm and their respective CIE color coordinates toluene (a-e).

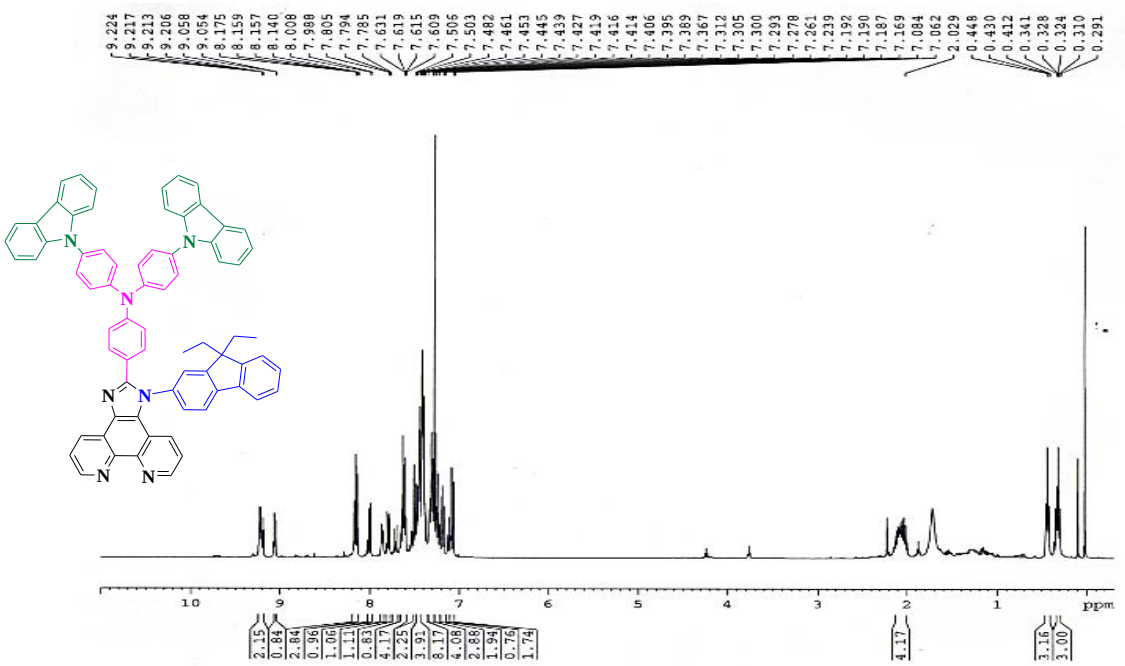

Figure 5.S8 ^{1}H-NMR of Phen-Fl-TPA-CBZ ligand.

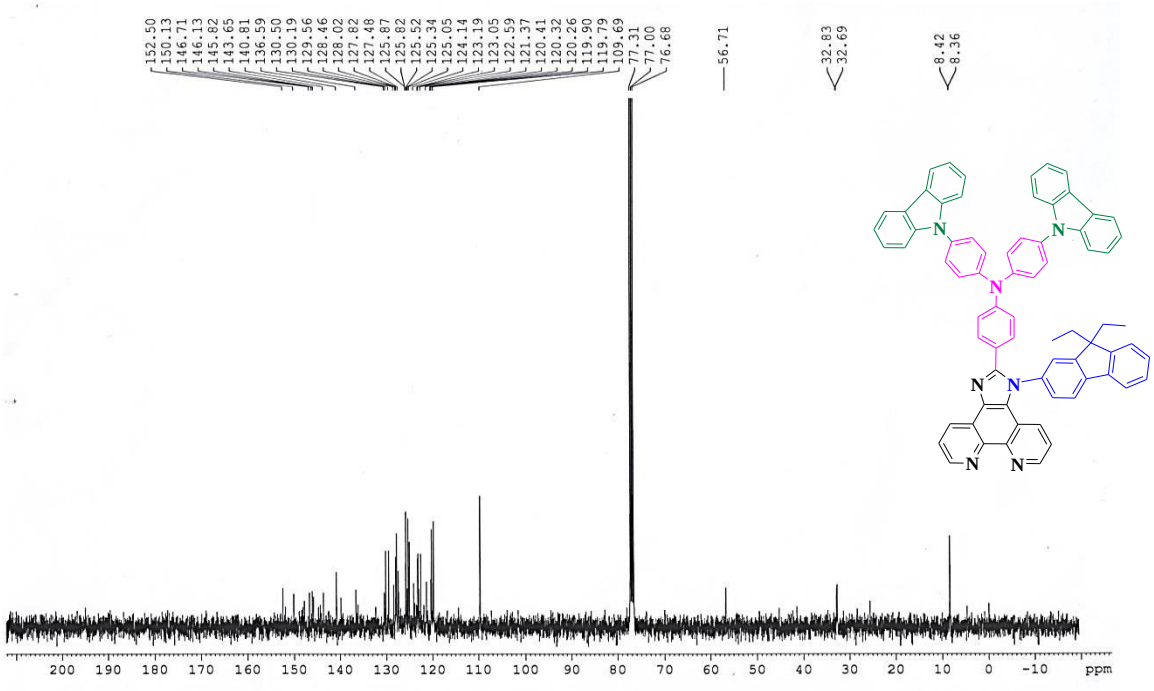

Figure 5.S9 ^{13}C-NMR (down) of Phen-Fl-TPA-CBZ ligand.

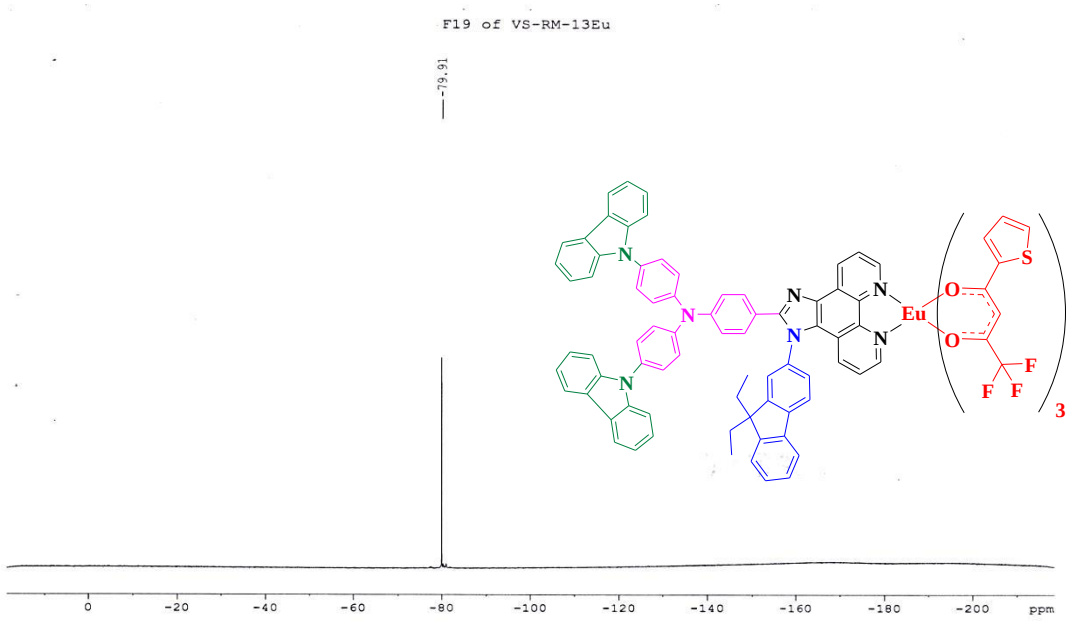

Figure 5.S10 ^{19}F-NMR of Phen-Fl-TPA-CBZ ligand.

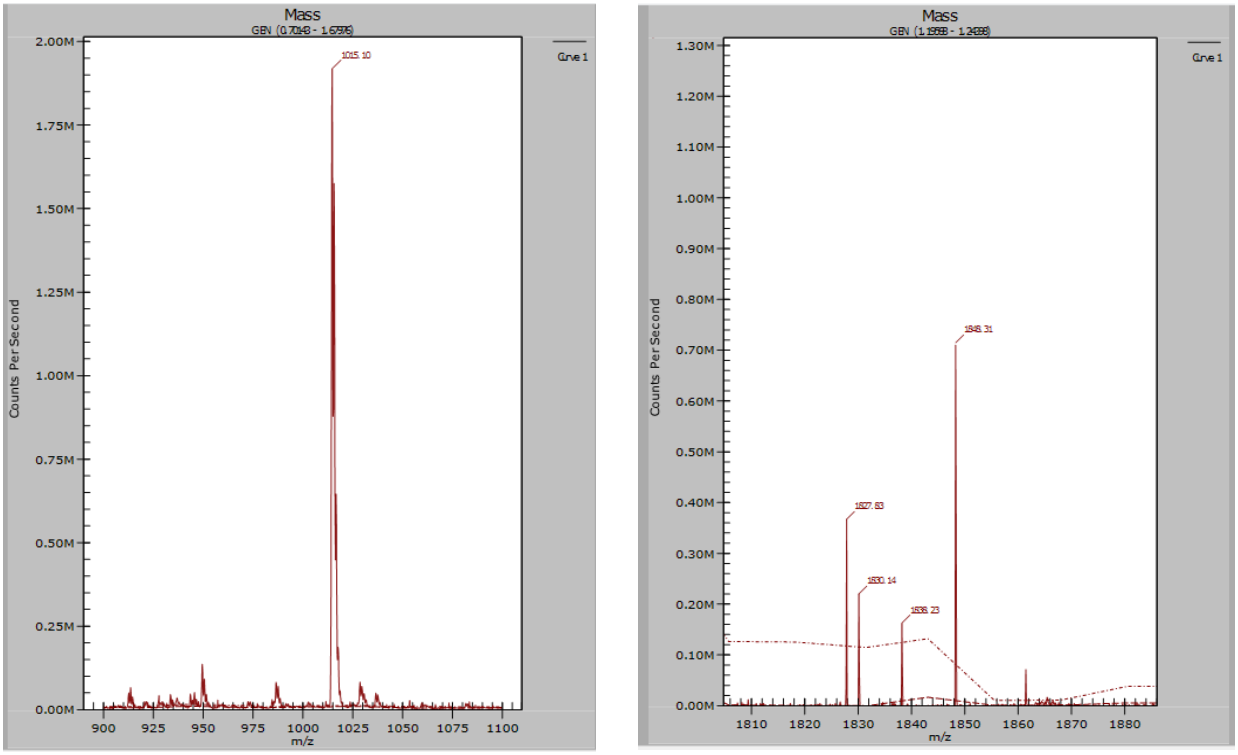

Figure 5.S11 The mass spectrum of the ligand, Phen-Fl-TPA-CBZ (right), the mass spectrum of the complex, Eu(TTA)$_3$Phen-Fl-TPA-CBZ (Left).

Annexure V
(Chapter 6)

Mono and binuclear luminescent Eu^{III} molecular complexes for white light emitting diodes: combined Experimental and theoretical study

Contents

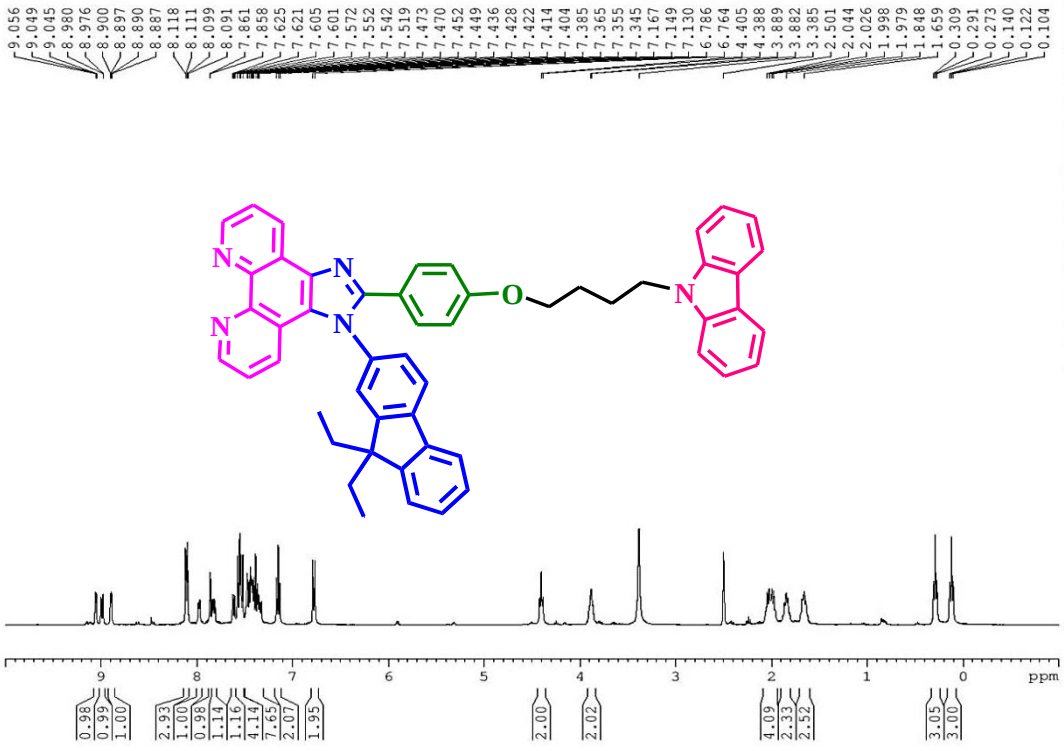

Figure 6.S1 The ^{1}H and ^{13}C NMR spectra are of the Ligand.

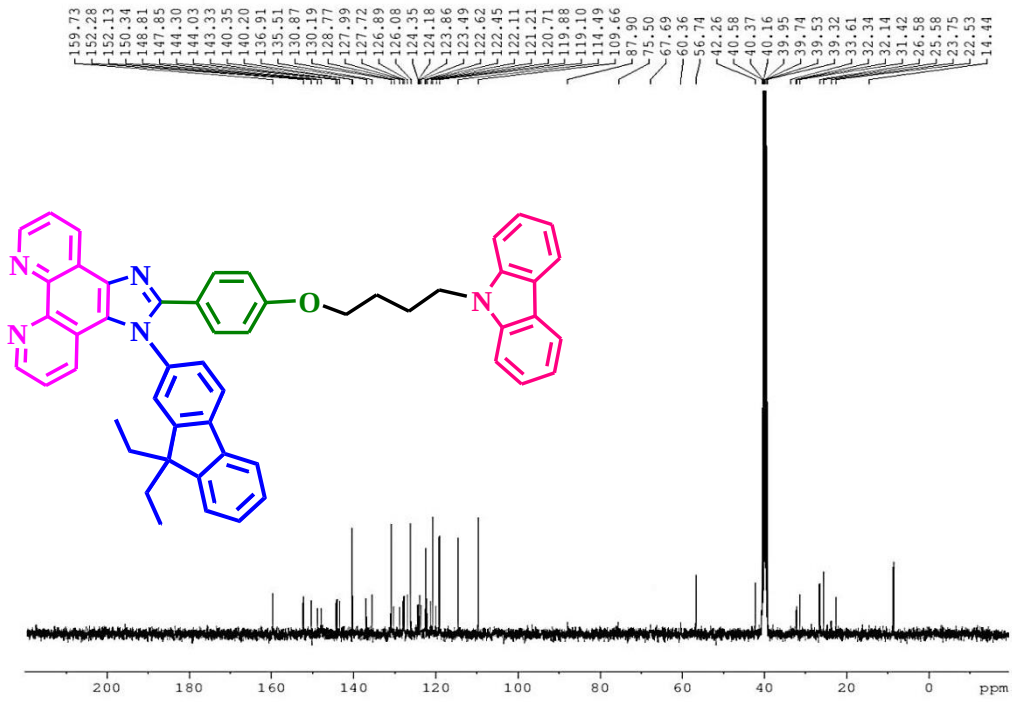

Figure S2 The ^{1}H and ^{13}C NMR spectra are of the Ligand.

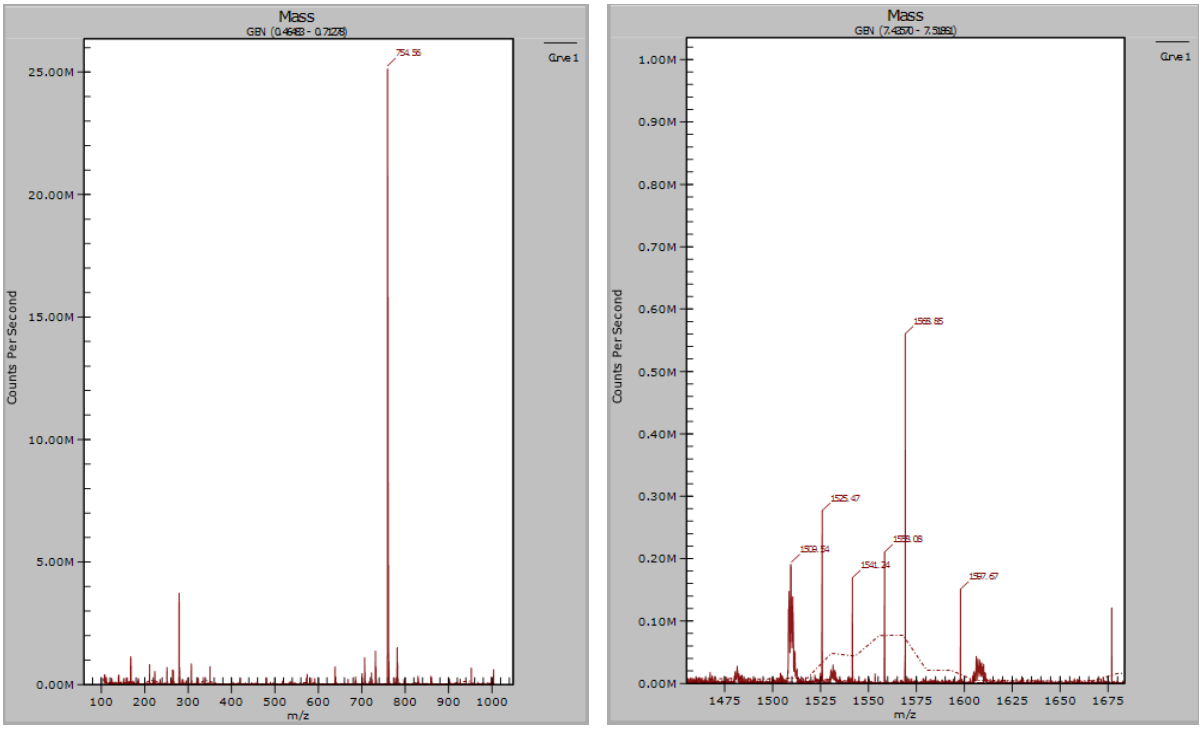

Figure 6.S3 The Mass spectrum of the Ligand (left) and corresponding Eu(TTA)^{3}Phen-Fl-O-CBZ complex (right).

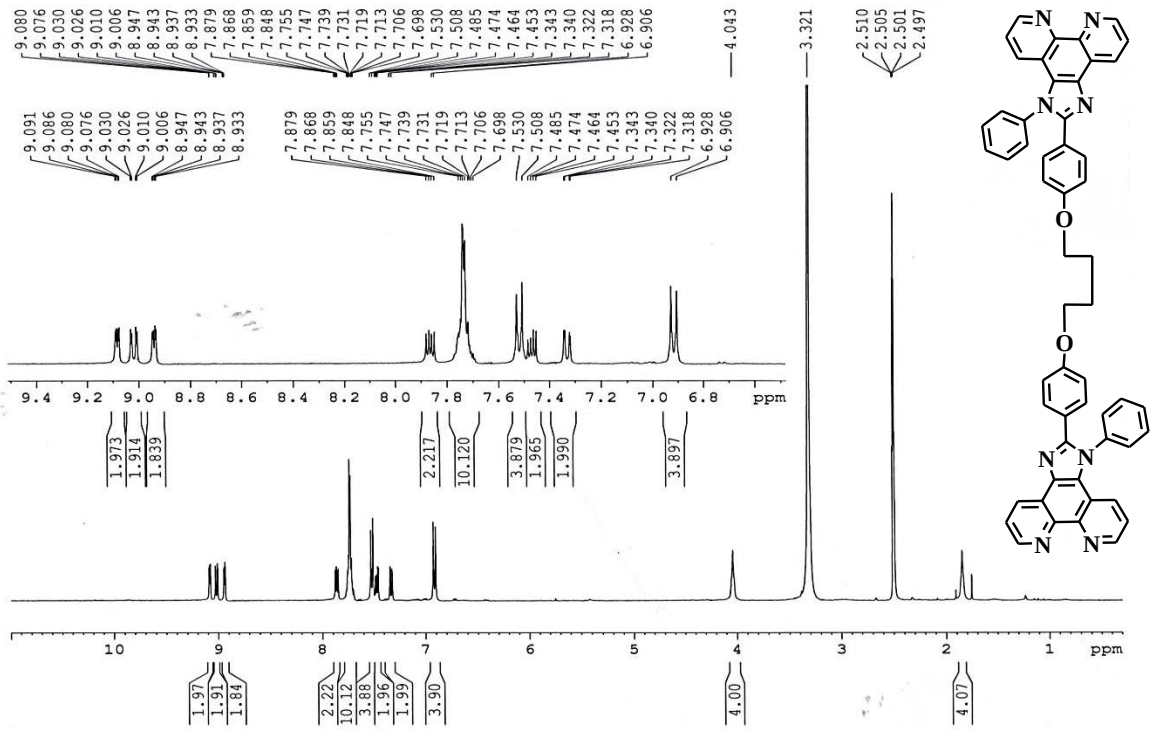

Figure 6.S4 The ^{1}H-NMR of the ligand L1.

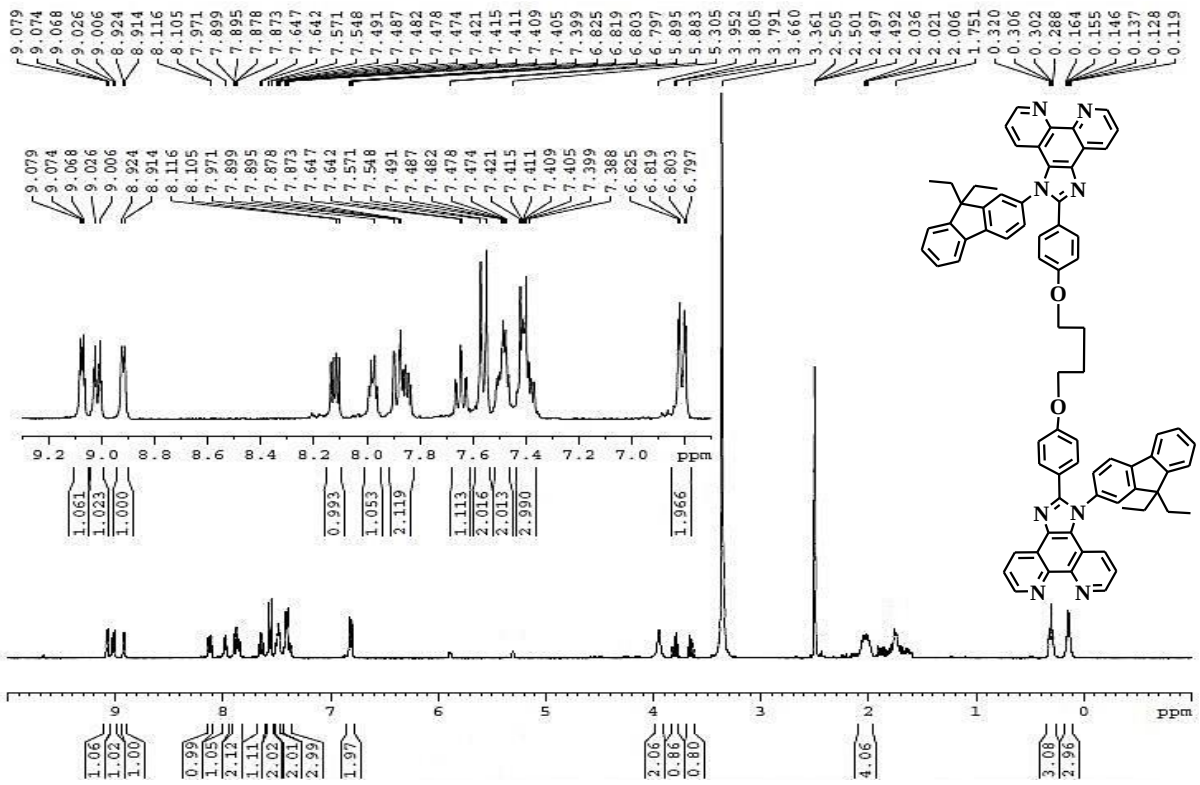

Figure 6.S5 The ^{1}H-NMR of the ligand L2.

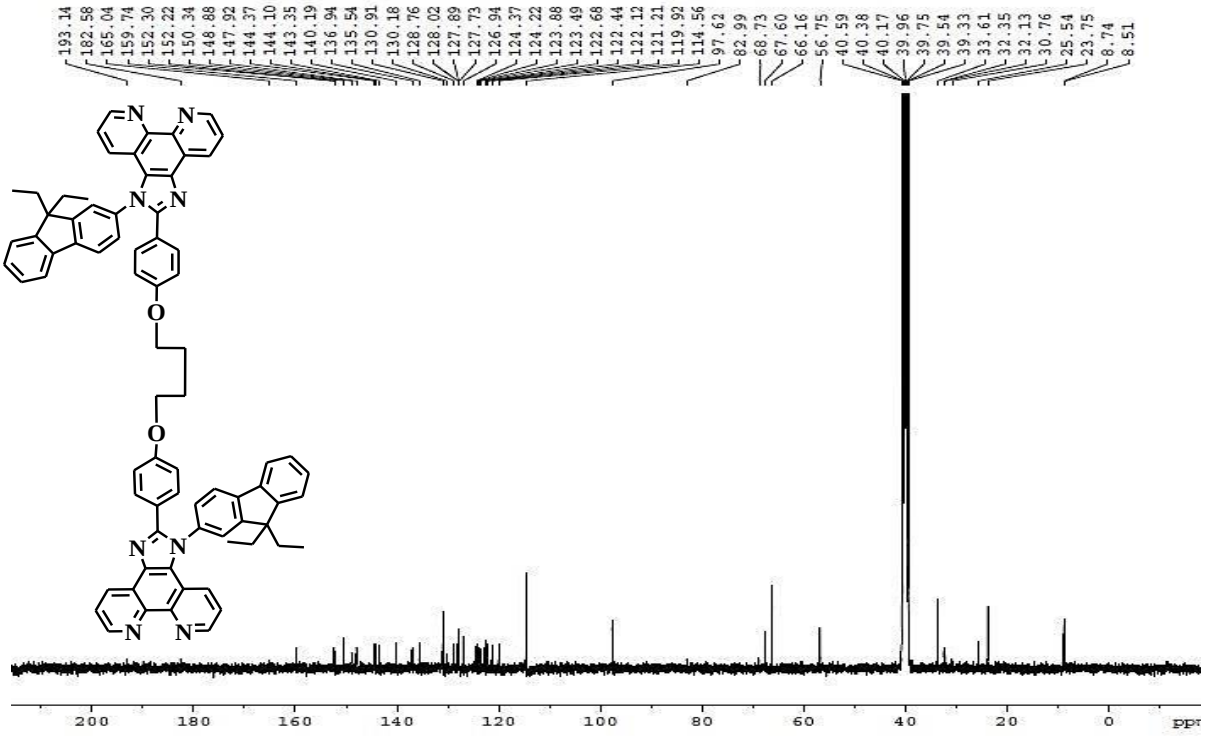

Figure 6.S6 The ^{13}C-NMR of the ligand L2.

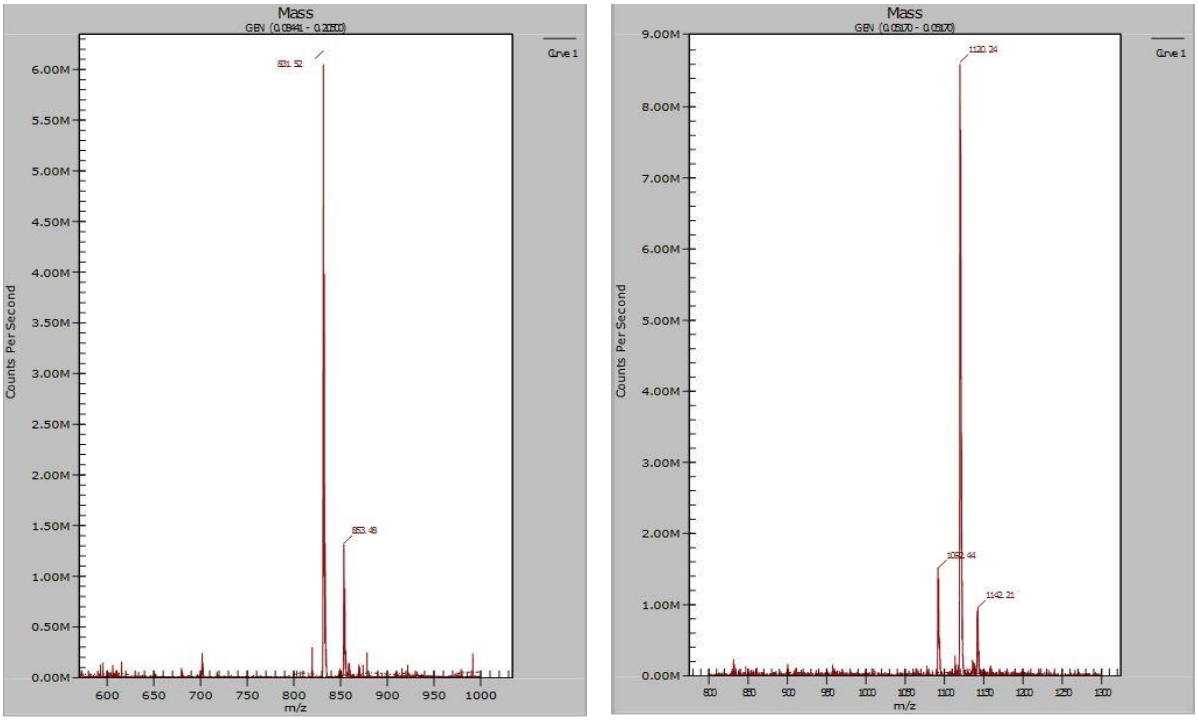

Figure 6.S7 The mass spectrum of the ligand L1 (left) and ligand L2 (right).

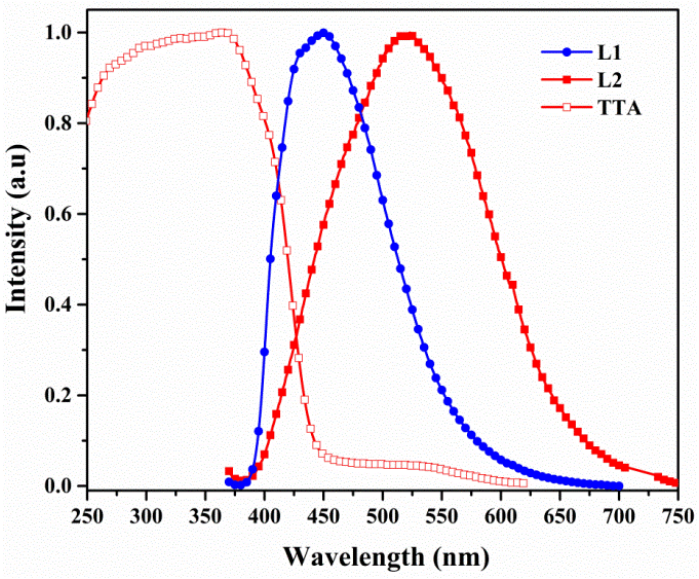

Figure 6.S8 The PL emission spectra of the ligands, L1 and L2, overlap with the TTA UV absorption spectra under room temperature.

Table 6.ST1 The Eu^{III} complexes CIE color coordinates in thin film.

$Eu_2(TTA)_6(L1)$	**Thin film**			
	CIE		**FWHM**	**I_2 / I_1**
	x	**y**		
0.1%	0.661	0.330	3.80	20.74
0.5%	0.663	0.330	3.97	20.96
1.0%	0.664	0.330	3.80	22.37
5.0%	0.666	0.331	3.18	21.27
Pure	0.661	0.333	4.14	18.14
$Eu_2(TTA)_6(L2)$				
0.1%	0.645	0.329	3.83	20.66
0.5%	0.655	0.330	4.03	21.31
1.0%	0.663	0.332	4.02	21.33
5.0%	0.663	0.332	4.17	21.83
Pure	0.662	0.335	4.21	17.72

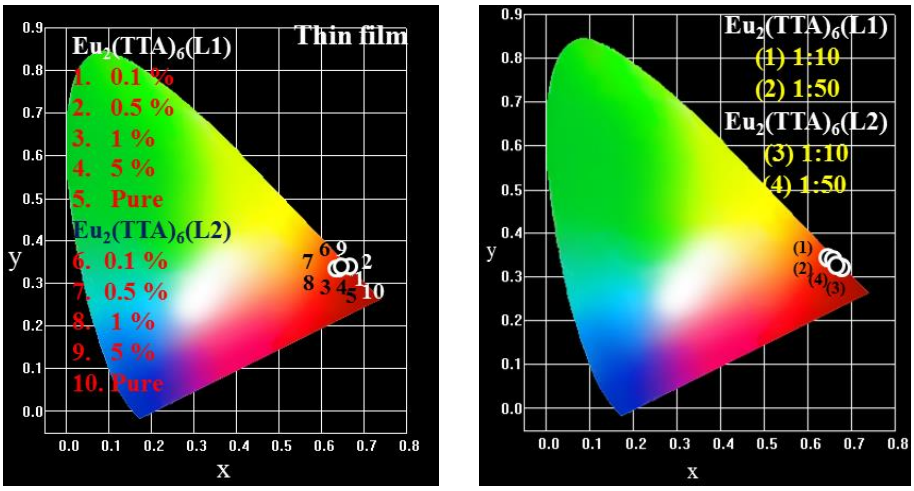

Figure 6.S9 The Eu^{III} complexes CIE color coordinates in thin film (left) and LED CIE color coordinates for the Eu^{III} complexes in different ratio (right).

Table 6.S2 Computed vertical transitions and their oscillator strengths and configurations of ligands (L1 and L2).[a]

Compound		State	Energy(eV)	λ_{max}nm	*f*	Configuration
L1	**(S1)**	Gas	3.5972	344.67	0.0411	HOMO → LUMO+1 (51.8%)
	(S2)		3.6112	343.33	0.0323	HOMO-1 → LUMO (54.7%)
	(S3)		3.7319	332.23	0.3496	HOMO → LUMO+1 (37.8%)
						HOMO → LUMO+3 (46.9%)
Triplet	**(T1)**	Gas	2.7492	450.98	-	HOMO-2 → LUMO+1 (13.2%)
						HOMO → LUMO+1 (41.4%)
						HOMO → LUMO+3 (44.4%)
						HOMO → LUMO+4 (15.8%)
	(T2)		2.7642	448.53	-	HOMO-3 → LUMO (14.4%)
						HOMO-1 → LUMO (39.9%)
						HOMO-1 → LUMO+2 (45.3%)
	(T3)		3.1644	391.81	-	HOMO-2 → LUMO+3 (13.8%)
						HOMO → LUMO+1 (45.0%)
						HOMO → LUMO+9 (24.9%)
L2	**(S1)**	Gas	3.3690	368.02	0.0098	HOMO → LUMO+1 (70.2%)
	(S2)		3.4171	362.83	0.0204	HOMO-1 → LUMO (70.1%)
	(S3)		3.7025	334.87	0.00	HOMO-1 → LUMO+1 (70.6%)
Triplet	**(T1)**	Gas	2.7465	451.42	-	HOMO-2 → LUMO+3 (13.8%)
						HOMO → LUMO+3 (32.8%)
						HOMO → LUMO+5 (50.41%)

(T2)	2.7607	449.10	-	HOMO-9 → LUMO+8 (10.1%) HOMO-3 → LUMO+2 (13.2%) HOMO-1 → LUMO (21.9%) HOMO-1 → LUMO+2 (28.4%) HOMO-1 → LUMO+4 (51.0%)
(T3)	2.9833	415.60	-	HOMO-35→LUMO+17 (10.3%) HOMO-6 → LUMO+1 (39.6%) HOMO-4 → LUMO+1 (37.8 %) HOMO → LUMO+1 (10.9%)

[a]Orbital contributions below 10% are omitted.